Brest
29, 30 november 2000

actes de colloques 32

Editors
Michel Olagnon
Gerassimos Athanassoulis

Rogue waves 2000

32

Ifremer

ROGUE WAVES 2000

M. Olagnon and G.A. Athanassoulis
Editors

Proceedings of a Workshop
organized by Ifremer
and held in Brest, France
29-30 November 2000
within the Brest SeaTechWeek 2000

Ifremer

Preface

Rogue waves have repeatedly been damaging offshore oil and gas production facilities for the last decades as severely as they have been sinking ships and taking a hard tribute of human lives ever since man has been going to sea. Whether they should be called *Rogue waves*, *Freak waves*, or *Extreme Storm Waves* is sometimes a subject of discussion between scientists who have different views on their generating mechanisms, but damage to offshore structures and ship losses are a clear evidence of the existence of such waves. It has, thus, become urgent that more measurements, more studies and an active co-operation of all implied parties should be developed and put together in order to reach the ability to understand, predict and forecast such unexpected, giant waves, and thus, ensuring safer conditions for those who work and sail at sea.

Several accidents, that have recently occurred at offshore platforms and FPSOs, triggered discussions in the International Ship and Offshore Structure Congress 1997, and motivated research on the subject of waves which are uncommonly high and severe with respect to sea state conditions prevailing at the time of incident. At the present stage, application of this research to the prediction and the forecasting of the associated risks can be envisioned. In this connection, and after discussing the matter with a number of scientists and engineers who were to become members of the Scientific Committee, we decided to hold a workshop on the subject. The goal of this workshop is to assess the state of the art concerning the conditions of occurrence of waves or groups of waves of unexpected severity, and to establish a "road map" concerning the research actions and collaborations needed to improve the prediction and forecasting abilities in this domain.

The sessions of this workshop have been organized as a sequence of questions, as follows:

1. What problems are rogue waves facing us with ?
2. What would we have been expecting from the State of the Art ?
3. What do we actually observe ?
4. How could we explain these observations ?
5. How can we model and numerically simulate rogue waves ?
6. Can we reproduce them in testing tanks ?
7. What are our statistical prediction and our detection abilities ?
8. Where should we go from now ?

The participants have partly answered these questions, and indicated promising directions to work on. We hope that the material included in the present Proceedings will be useful to those who need and/or want to improve further our knowledge and understanding on this important and demanding subject.

The workshop brought together a large group of willing persons, from the academia and the industry of many nations. Whether we will now sail forward only a cable's length or many a mile, we cannot say. Yet we know for sure that, together, we cannot but make some progress towards the avoidance of the casualties provoked by rogue waves.

This volume contains most of the papers presented in the workshop, that is, all papers sent by the authors to the editors up to March 2001. The papers appear in the volume according to the order of presentation in the workshop. An author index can be found in page 377.

At the end of the volume we have added a collective list of references appearing in all papers included herewith, and an additional list of recently published (mainly after the workshop) works on rogue waves.

All figures in the main part of the volume are in black-and-white (b&w), although many authors submitted coloured versions of them. The transformation to b&w proved to be successful in some cases and deteriorating in other cases. To cope with the latter problem, an Appendix has been prepared containing some of the figures/photos in their original coloured version. The reader is informed that a (b&w) figure in the main part of the volume appears also as a coloured plate at the end of the volume (in the Appendix), by the declaration: [See also Appendix CP], which is added in figure's legend.

September 2001

Michel Olagnon & Gerassimos Athanassoulis
Editors of the Proceedings
on behalf of the Scientific Committee
ROGUE WAVES 2000

Scientific Committee

Gerassimos Athanassoulis	National Technical University of Athens (Greece)
Alain Cariou	IRCN[1] (France)
David J.T.Carter	Satellite Observing Systems (UK)
Günther Clauss	Technische Universität Berlin (Germany)
George Z. Forristall	Shell (USA & The Netherlands)
Sverre Haver	Statoil (Norway)
Harald E. Krogstad	Norwegian University of Science and Technology (Norway)
Georg Lindgren	Lund University (Sweden)
Dag Myrhaug	Norwegian University of Science and Technology (Norway)
Arvid Næss	Norwegian University of Science and Technology (Norway)
Michel Olagnon	Ifremer (France)
Edward J. Powers	University of Texas (USA)
Marc Prevosto	Ifremer (France)
Igor Rychlik	Lund University (Sweden)
Don Smith[2]	Health and Safety Executive (UK)
Martin J. Sterndorff	DHI Water & Environment (Denmark)
Rodolfo Tedeschi	Università degli studi di Genova (Italy)
Hiroshi Tomita	Ship Research Institute[3] (Japan)

[1] IRCN became Principia-Marine in 2001.
[2] Now with OGP – International Association of Oil and Gas Producers.
[3] SRI became National Maritime Research Institute in 2001.

Acknowledgements

ROGUE WAVES 2000 was organized by the Metocean Group of Ifremer (Institut Français de Recherche pour l'Exploitation de la Mer), in cooperation with IRCN (Institut de Recherches de la Construction Navale), and benefitted from the support of the Communauté Urbaine de Brest, of the Conseil Général du Finistère, and of the Région Bretagne.

It was one of the events of the Brest SeaTechWeek 2000, a week devoted to exchanges between research and industry in marine science and technology.

The cover photograph was taken by Philippe Lijour when he served as first mate on the *Esso Languedoc* in the eighties. Philippe Lijour is now in charge of nautical affairs at *Centre d'Etudes Techniques Maritimes Et Fluviales* in Brest.

The difficult task of collecting the presented papers, uniformising the style, and compiling this volume of Proceedings was carried out by the Sea Waves Study Group of NTUA (National Technical University of Athens), with the collaboration of the Metocean Group of Ifremer.

Our thanks go to all those who supported this workshop by helping to find funding and by volunteering their personal time and efforts, with special mention to this last respect of Alain Lagrange and Sylvie van Iseghem, from Ifremer, and Yannis Georgiou and Eleni Holevas, from NTUA.

Participants

Pierre Ailliot	email Pierre.Ailliot@ifremer.fr
Gerassimos Athanassoulis	email mathan@central.ntua.gr
Sergei Badulin	email bsi@wave.sio.rssi.ru
Nigel Barltrop	email n.barltrop@eng.gla.ac.uk
Jurjen Battjes	email j.battjes@ct.tudelft.nl
Konstandinos Belibassakis	email kbel@fluid.mech.ntua.gr
Nigel Bellamy	email n.bellamy@geos.com
Elzbieta Bitner-Gregersen	email Elzbieta.Bitner-Gregersen@dnv.com
Pierre Bonmarin	email bonmarin@pollux.irphe.univ-mrs.fr
Carlo Brandini	email Brandini@dicea.unifi.it
Bas Buchner	email B.Buchner@marin.nl
Alain Cariou	email A.cariou@ircn.asso.fr
David J.T. Carter	email djc@satobsys.co.uk
Didier Clamond	email didier@math.uio.no
Günther Clauss	email Clauss@ism.tu-berlin.de
Riccardo Codiglia	email codiglia@univ.trieste.it
Giorgio Contento	email contento@univ.trieste.it
Kristian Dysthe	email kristian.dysthe@mi.uib.no
Alan Edwards	email Alan.Edwards@cec.eu.int
Gerhard Ersdal	email Gerhard.Ersdal@npd.no
Douglas Faulkner	fax ++44 141 9565071
Emmanuel Fontaine	email Emmanuel.Fontaine@ifp.fr
Samantha Free	email sfree@nodent.co.uk

Renata Gentile	email renata@diam.unige.it
Richard Gibbs	email richard.gibbs@eng.ox.ac.uk
Chris Graham	email c.graham@siep.shell.com
Colin Grant	email grantck@bp.com
Johannes Guddal	email j.guddal@dnmi.no
Carlos Guedes Soares	email guedess@alfa.ist.utl.pt
Jim Gunson	email jgunson@meto.gov.uk
Sverre Haver	email SVHA@statoil.com
Katerin Hessner	email reichert@oceanwaves.de
Martin Holt	email Mwholt@meto.gov.uk
René Huijsmans	email r.h.m.huijsmans@marin.nl
Morten Huseby	email mhuseby@math.uio.no
Michel Huther	email michel.huther@bureauveritas.com
Sylvie van Iseghem	email svaniseg@ifremer.fr
Alastair Jenkins	email a.jenkins@dnmi.no
Bruce Johnson	email aronj@bellatlantic.net
Olivier Kimmoun	email kimmoun@esim.fr
Peter Kjeldsen	email peter.kjeldsen@c2i.net
Gudmund Kleiven	email Gudmund.Kleiven@hydro.com
David Kriebel	email kriebel@usna.edu
Marc Le Boulluec	email mlb@ifremer.fr
Pierre Liagre	email Pierre-Liagre@tamu.edu
Georg Lindgren	email georg@maths.lth.se
Paul C. Liu	email liu@glerl.noaa.gov
Ulla Machado	email ullam@maths.lth.se
Anne Karin Magnusson	email a.k.magnusson@dnmi.no
Christophe Maisondieu	email christophe.maisondieu@ifremer.fr
Tom Marthinsen	email Tom.Marthinsen@hydro.com
Jaak Monbaliu	email jaak.monbaliu@bwk.kuleuven.ac.be
Valérie Monbet	email valerie.monbet@univ-ubs.fr
Nobuhito Mori	email mori@criepi.denken.or.jp
Raymond Nerzic	email nerzic@optimer.fr
Michel Olagnon	email Michel.Olagnon@ifremer.fr
Efim Pelinovski	email enpeli@hydro.appl.sci-nnov.ru
Marc Prevosto	email Marc.Prevosto@ifremer.fr
Pierre Queffeulou	email Pierre.Queffeulou@ifremer.fr
Valérie Quiniou-Ramus	email vquiniou-ramus@nodent.co.uk
Konstanze Reichert	email reichert@oceanwaves.de
Wolfgang Rosenthal	email rosenthal@gkss.de
Torsten Schlurmann	email schlurma@uni-wuppertal.de
Don Smith	email Don.smith@ogp.org.uk
Carl Trygve Stansberg	email carltrygve.stansberg@marintek.sintef.no
Christopher Swan	email c.swan@ic.ac.uk
Paul Taylor	email paul.taylor@eng.ox.ac.uk
Rodolfo Tedeschi	email tedeschi@dinav.unige.it
Hiroshi Tomita	email Tomita@srimot.go.jp
Karsten Trulsen	email karsten.trulsen@math.sintef.no
Arjan Voogt	email a.j.voogt@marin.nl
Julian Wolfram	email J.Wolfram@hw.ac.uk
Jun Zhang	email Jzhang@civilmail.tamu.edu

CONTENTS

Session 1

Design and Operation Problems Related with Rare or Unexpected Wave Events

Rogue Waves - Defining Their Characteristics for Marine Design

Keynote address by Douglas Faulkner

Emeritus Professor of Naval Architecture and Ocean Engineering,
University of Glasgow, Glasgow, Scotland, UK
Fax: ++44(141)9565071

Abstract. A brief history of the increasing awareness of freak (rogue) waves includes their proposed use for survival design and for forensic investigations of marine accidents. In particular, extreme wave heights which have elevated steep faced crests have been shown to be much more damaging than present design rules and codes allow for. The market and technical trends in trading ships and in offshore installations are outlined. The nature of such extreme abnormal seas is illustrated, including their effect on trading ships and on FPSO/FSU vessels. Design to provide some capability to survive such wave actions is then discussed and some critical operational conditions are suggested for further study. Provisional design criteria are suggested.

1 Introduction

This paper introduces the need for a paradigm shift in thinking for the design of ships and offshore installations to include a Survival Design approach [1,2] additional to current design requirements. At present ship primary structure is designed to withstand length dependent linear waves not exceeding 10.75 m high which are meant to represent a lifetime extreme in North Atlantic winter conditions [3]. Green water pressure loads from class society rules lie in the range 26 to 60 kN/mm^2.

Service experience, advanced analyses and experiments show that these are quite inadequate standards to withstand the actions of realistic large steep elevated waves. Moreover, it seems that most mariners feel that weather routing does not provide adequate protection to cargo ships from these extreme storms by issuing effective weather avoidance actions. Too often decisions are governed by charter dates rather than by ship safety.

1.1 Brief History

Draper first aroused my interest in exceptionally high *freak* waves [4] by suggesting these were not curious and unexplained quirks of nature. He added, their occurrence can be calculated with an acceptable degree of precision, and he identified two aspects of their statistics.

But it was an aircraft engineer, Buckley, who first suggested that ship hull girder design required a new approach [5]. Further research work for the US Navy identified extreme and climatic wave spectra for use in ship structural design [6] followed by his first application of survivability design using first principles [1] because present rules and criteria were inadequate. He was doing no more than transferring aircraft design principles to ships.

These publications, together with the analytical work undertaken for Lord Donaldson's Assessment of the loss of the m.v. *DERBYSHIRE* led me to postulate [6] that a steep elevated *abnormal* wave probably collapsed the forward hatch covers during typhoon ORCHID. This was followed by a more technical paper covering all possible loss scenarios in the light of the final underwater survey of the wreckage [7] and by experiments. The Honourable Mr. Justice Colman's report [8] confirmed the quite inadequate strength requirements of cargo ship hatch covers (which go back to 1966). He also criticised IACS' recent 1998 rules and suggested they too were inadequate. He suggested they should be based on extreme steep elevated waves and ultimate strength criteria, that is, on survival design.

In September 1998 a WMO Conference was held in UNESCO, Paris [9] at which Keynote papers were presented by myself for ships (based on my *DERBYSHIRE* experience) and by C. Grant for offshore installations. The need to characterise abnormal/freak waves for design and operation was accepted and a whitepaper report by the COST 714 Management Committee outlined research needs to achieve this. This was worked up in detail and presented to the European Commission who authorised it as the "MaxWave" Project which was approved and announced at a recent conference in Brest [10].

1.2 Market and Technical Trends

Trading Ships. Recent market projections suggest that by 2012 ship freight may double to about 13 billion tonnes carried over 20% longer voyages of about 5000 nautical miles. Technically, this suggests more larger ships to meet the economies of scale are needed to meet the increasing demands from developing countries. Some of the shorter shipping routes are likely to include faster freight carriers.

Given the present difficulties in finding/producing well trained crew, and in providing effective inspection, maintenance and ship traffic control, it seems reasonable to expect perhaps a three-fold increase in marine accidents and losses.

Offshore Developments. Oil and gas demands will continue to increase, mainly because of increasing living standards in developing countries. Nuclear power is unpopular, we cannot depend on Middle East supplies and other land based exploitation is limited. Inevitably the increased demand is likely to be met mainly from offshore oil and gas installations, much of them in harsher deeper water environments. Again, the risks will become greater even though the industry is generally rapid in responding to increased knowledge.

Safety. The new environmental knowledge arising from MaxWave and other studies could hardly have come at a better time to provide more realistic environmental data for survival design loads. At the same time the use of better fatigue and ultimate strength modelling (which is now available) should ensure the best prospect of limiting severe damage and losses in both industries.

2 The Cruel Sea

Lord Nelson said *"I can commend men and ships, but I cannot command the wind and sea"*. Adlard Coles likened some extremely chaotic seas to a witche's caldron. Most of the illustrations are from his excellent book [11]. The challenge now is to model them sufficiently well so that designers can begin to design marine structures having some capability to survive such seas.

2.1 Survival Seas

Pyramidal waves are usually generated as standing waves which are non-translatory. They usually occur within the circle of maximum wind speed in revolving tropical storms. Figure 1 shows a prize winning photograph of such a wave off south Japan. It is not dissimilar to Hokusai's painting "The Wave" of 1830.

Figure 2 shows breaking interactions between several steep waves. It looks as if it comes from another world with extreme chaos and a near vertical wave crest rising against the background sky. Figure 3 is also from the North Atlantic and shows the sort of near breaking wave front which nearly capsized the QUEEN MARY when carrying 15,000 American troops in WWII. Note the freak wave coming up astern.

Figure 4 shows a deep water wave front breaking without interruption from 200 m to nearly 350 m. Figure 5 shows a boiling following sea which would be bad news from any small ships or boats.

I could not resist including Fig. 6 which is taken from the front cover of Ochi's book [12] which nevertheless deals almost entirely with Gaussian linear waves! A better book for dealing with high asymmetrical waves by Tucker and Pitts is to appear shortly [13]. For recent insights into wave generation physics the book by Komen et al [14] can be recommended. From a bibliography of freak wave observations by mariners and others I select three by Nickersen [15,16,17].

2.2 Effects on Ships

The bibliography of the occurrence of rogue waves and their effect on ships and yachts is extensive. A sample has been given in references [2,6,18].

Fig. 7 is a sketch of a 256,000 dwt VLCC in 1977 meeting an elevated wave generated in the southerly Agulhas current which opposes the prevailing sea. The crest height above the deck could be accurately judged from the bridge as the foremast was totally submerged, and the crows-nest reinforced windows were smashed in. The

estimated wave height was about 30 m, and had the vessel been a bulk carrier laden in dense ore she would not have survived.

Fig. 8 shows a distressed fishing boat struggling to remain hove to in seas described as 40-50 ft. high accompanied by 60-65 knot winds. Fig. 9 also shows a cargo vessel about to encounter a long spilling breaker. Fig. 10 is a remarkable picture of a Great Lakes bulk carrier deluged on the beam by a wide rogue wave. Had her hatches been designed to just meet the 1966 LC requirements this wave would have breached the ship in several holds.

Figs. 11 to 14 show container ships in distress. In Fig. 11 the ship is experiencing fore end slamming and loss of freeboard. The ship is approaching a wall of water at mast height in Fig. 12 and Fig. 13 shows dislodged and smashed containers. In Fig. 14 the large APL China lost 400 containers with 700 or more damaged and a complete hold flooded. Three other 4500 TEU container ships were caught and damaged in the same storm in November 1998 in the NE Pacific. They limped into Seattle and other ports and eventually the total loss of cargo and damage to containers and ships was reported as being about $3 billion.

2.3 Abnormal Waves

Reports of extreme sea states in deep and shallow water frequently refer to a single high wave, or the "wave from nowhere" or sometimes there are several successive high waves, for example, the "Three Sisters". Summaries of observed freak waves are provided by Nickersen [15,16,17]. These include very steep "walls of water" and long generally shallower troughs. Another phrase used by mariners is "holes in the sea". These could well be unusually deep troughs, or perhaps a shallow trough which appears to be deep. For example, as seen from a ship which has mounted a high crest with a steep back face dropping into what might well appear to be a "hole in the sea" even though the trough is shallow.

Abnormal (Freak or Rogue) waves are individual waves of exceptional height and/or abnormal shape. Some put exceptional as $> 2\ H_s$, but there are many waves which exceed this. I prefer a value $> 2.4\ H_s$ (2.5 was used in refs. [2,6]). Although we do not yet know enough about their generation physics they are generally transient and we can perhaps begin to classify them as follows:

A. Extreme waves in stationary seas arising from different frequencies getting into step, as Draper puts it [4], or indeed from non linear superposition and phasing of many wave frequencies.

B. Steep elevated waves which arise from:
   a) wave and opposing current interactions
   b) focussed wave groups and their interactions
   c) refraction around shoals or from inclined seabeds (beach effects)
   d) wave caustics from diffraction at coastlines and around islands
   e) young waves are steep, especially in intensifying winds.

C. Episodic waves in deep water from outlying events. These too can have very steep elevated crests and include the Three Sisters group generally intruding at 30° to 50° from the predominant wave system.

D. Breaking waves (progressive open orbits); it is claimed that high velocity very steep crests which arise are generated from energy overshoot actions. The two categories are *spilling* and *plunging* breakers, but the latter can be ignored in deepwater.

E. Standing waves (no progression) which arise from:
(a) opposing wave trains
(b) crossing wave systems
(c) rapid changes in wind direction, for example, the pyramidal waves which occur within tropical cyclones
(d) coastline diffraction which may lead to wave interference actions.

Previously I have included as a separate category revolving tropical storms (RTS) because the seas generated are significantly different from those observed in other storms. This is because the input energy is rotational which restricts the fetch and at the same time it is advancing at a speed of 5 to 12 knots initially and up to 25 to 30 knots as the RTS recurves northwards (in northern hemispheres). Moreover, the rate of change of wind speeds is generally faster than in other storms and the waves are young and generally very steep, with pyramidal waves inside the radius of maximum wind, as described above. When added to any existing swell and longer fetch wind waves the maximum wave height may well exceed 30 m.

Steep elevated waves with crest amplitudes as high as 0.74 x wave height have been recorded. The crest kinematics are complex, but toward the top of the crest the forward velocity can be twice that at the mean waterline. Weather expert Houghton and wave scientist Judi Wolf [20], in describing the devastation in the 1998 Sydney to Hobart Race, which claimed six lives and sank five boats, recalls: *seas of 15 m were common and 20 m waves were encountered with considerable regularity. Boats were encountering waves of double the expected height and a 300% increase in steepness – lethal by any standards.*

Finally, we should note that real sea is usually 3-dimensional. Although new physics is tackling this it will be some while before it can be reasonably modelled. However, improved 1-dimensional and 2-dimensional models of the sea will surely provide a major step forward even for Survival Sea modelling.

3 Survival Design

This subject was introduced in 1.1. The underlying thinking is that when one examines serious ship damages and losses, as Buckley has done, it becomes clear that in many cases they could not be caused by the normal extreme sea conditions used in present design. We need to look at the effects of individual waves, or sequence of waves, of exceptional height and/or abnormal shape. Then, modelling the actions of

such waves would provide inputs to critical ship conditions (e.g. excessive water on deck, rolling, etc.) for which some relatively low safety factor should be applied in design so the ship has some capability to survive these conditions. This is the essence of survival design [1,2] which would then become a necessary addition to or replacement of present design rules.

3.1 The Survivability Envelope

NOAA has built up an extensive database of hourly wave buoy measurements over an effective measurement period of about 10 years from a wide range of wave climates around the USA coast and trading waters. Buckley has used this to define *operability* and extreme *survivability* envelopes from climatic wave spectra (long term averages) from a wide range of significant wave heights H_s and peak periods T_p. These are shown in Fig. 15 [21]. The upper part of the survivability envelope from points S_1 to S_2 was mainly defined by data from the category 5 hurricane CAMILLE of 1969.

Buckley then went on to include the worldwide data of Hogben et al [22] as shown in Fig. 16. The top of the survivability envelope is split into the northern (1) and southern (2) hemispheres. The southern envelope is more severe because of the severity of the southern seas and the SW Pacific in particular. Its peak value of H_S = 18 m is actually being used by the offshore industry for operations West of Shetland.

Buckley was delighted to find that his left hand envelope of waves of limiting steepness of Fig. 15 corresponded within about 2% with Hogben et al's data. In 1979 Hogben recommended to the ISSC that waves of limiting steepness be defined by:

$$T_p^2 = 13H_s \tag{1}$$

It may be noted that in fetch limited storms Buckley found the JONSWAP spectrum with shape parameters between 1 to 3 gave good spectral modelling. A value of 3.3 is widely used in the North Sea.

Regarding the operability envelopes, the lower regions may be said to approximately correspond to normal extreme design for ships. However, the upper bound points O_1, O_2 and correspond to occurrence levels of H_s of about once a year (according to Buckley). These substantially exceed the maximum wave heights and risk of once in 20 years implicit in ship design – see next section.

3.2 Critical Ship Conditions

A provisional but not comprehensive list of ship design related subjects which have been suggested for Survival Design considerations includes:

(a) Primary hull strength
(b) Hatch cover and coaming strength
(c) Fore end protection
(d) Wave impact on hull and deck structure and fittings, and on bridge fronts
(e) Capsize, especially of small vessels
(f) Cargo shift, cargo damage

(g) Pooping damage
(h) Steering when hove to (inadequate rudder size)
(i) Hatchless container ships

The recommendations from the final *DERBYSHIRE* proceedings [8] should take care of (b) for forward hatch covers in large ships, because the principles of survival design are being applied. But, all hatch covers and coamings are vulnerable, and smaller cargo ships must be included Of the remainder (a) and (d) are perhaps the most important and are now briefly discussed.

Primary Hull Strength. Two independent dynamic simulations for the m.v. *DERBYSHIRE* and for an offshore FPSO typical of those now operating in the northern North Sea and West of Shetland have shown that maximum realistic wave induced bending moments in the hull girder could well exceed present requirements [3], perhaps by as much as:

- 40% in the hogging mode
- 80% in the sagging mode.

This is clearly serious and should be investigated further. In the last four years a large container ship and a medium size bulk carrier have broken their backs, both were maintained in reasonable condition. Two badly maintained tankers broke their backs – the ERICA caused considerable pollution damage off the Brittany coast in October 1999. It is not unreasonable to assume that a first principles survival design approach, of the type illustrated above, would have provided an additional safety margin to minimise if not eliminate such risks.

Wave Impact. A recent FPSP/FSU study for the HSE has shown that whereas present green water design pressures range from 25 to 60 kN/mm^2, whereas those derived from bow damage experienced on SHIEHALLION, operating West of Shetland, have been estimated as being of the order:

- 750 to 1000 kN/m^2 locally
- about 200 kN/m^2 globally.

My own analyses using survival design principles yield values about twice as large. Either way, these results are an order of magnitude greater than present design rules, and the same conclusion was reached from a similar recent study for the HSE [23]. Clearly ship rules need to be changed. Fortunately, the HSE has substantially increased its requirements for offshore installations.

3.3 Provisional Design Suggestions

Engineers are often faced with insufficient data from which to make decisions, for example, relating to design equations. But, designs have to proceed so the best present information should be used, with the hope that the resulting equations are truly provisional until better data and/or analyses can improve them. With this in mind I

have made some survival design suggestions arising from my *DERBYSHIRE* work, as follows:

A. For many ship structural applications the choice of survival H_s should be length dependent, for example I have provisionally suggested:

$$\left.\begin{aligned} H_s &= 16 - (4 - L/100)^2 \\ for\ \ 150m &\le L \le 400m \end{aligned}\right\} \qquad (2)$$

For $L \le 120$, $H_s = L/12$ is suggested, which I believe are/were USCG rules.

B. The associated T_p range to examine should be close to equation (1), and associated wave lengths suggested are:

$$\left.\begin{aligned} \lambda &= 16\ H_s\ \ to\ \ 20\ H_s\ ,\ L \ge 150m \\ &= 11\ H_s\ \ to\ \ 16\ H_s\ ,\ L \le 100m \end{aligned}\right\} \qquad (3)$$

C. Critical extreme waves for a notional $\alpha = 0.01$ probability of exceedance assuming 12 hour exposure and $p_e = 0.4$ times Longuet-Higgins are:

$$\left.\begin{aligned} H_\alpha &= 2.4\ H_s \\ A_c &= 0.65\ H_s\ \ crest\ \ amplitude \\ m &= 0.5\ \ mean\ \ crest\ \ slope \end{aligned}\right\} \qquad (4)$$

D. Pressures for horizontal wave impacts:

$$\left.\begin{aligned} p_i &= 0.5\ C_p\ \ \rho v^2 \\ where\ \ v &= 2\lambda / T\ \ crest\ \ velocity \\ C_p &= 9\ \ locally\ \ (A \le 1m^2) \\ &= 3\ \ globally\ \ (A \le 6.25m^2) \end{aligned}\right\} \qquad (5)$$

E. Structural survival design should use ultimate strength modelling with suggested load factors of 1.0 for plate elements and 1.5 for grillages.

Finally, using derived survival loads and load combinations, a properly validated large amplitude nonlinear motion program, such as LAMP [24], should be used to evaluate motions and internal forces in the ship or structure for component and system design.

4 Acknowledgement and Closure

This paper derives from my work for the *DERBYSHIRE* investigation and for MaxWave, and I thank those who have inspired me in both endeavours. The combination of new wave data and understanding combined with a paradigm addition to design is a challenge where interactions between both communities are essential.

5 Figures

Fig.1. Pyramidal wave off south Japan

Fig. 2. North Atlantic Chaos

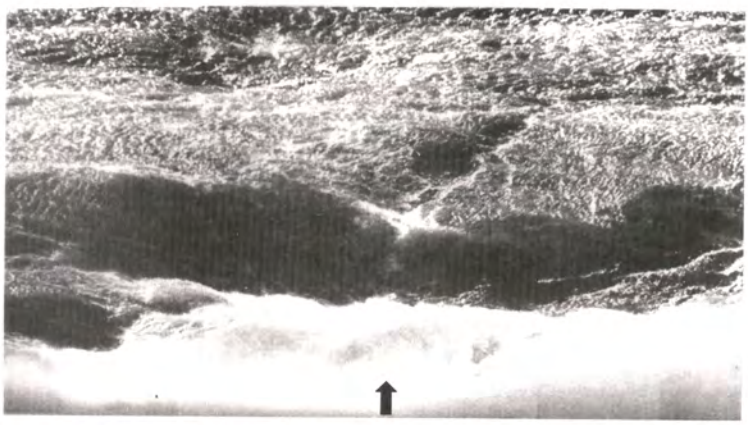

Fig. 3. The ultimate North Atlantic storm

Fig. 4. South Pacific breaking wave front

Fig. 5. A boiling following sea

Fig. 6. Very steep breaking wave crest

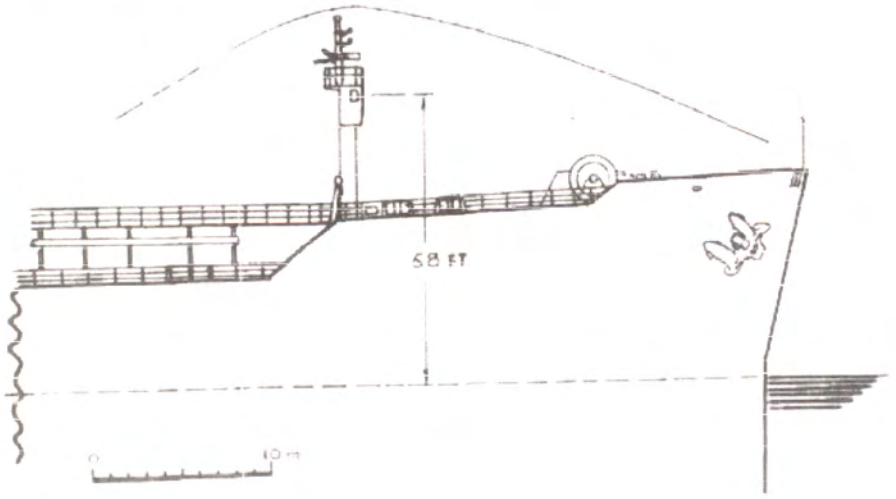

Fig. 7. VLCC ATHENE and a 30 m wave off Port Elizabeth in 1977

Fig. 8. Distressed fishing boat in seas described as 40-50 ft. high

Fig. 9. Cargo ship about to encounter a wall of water

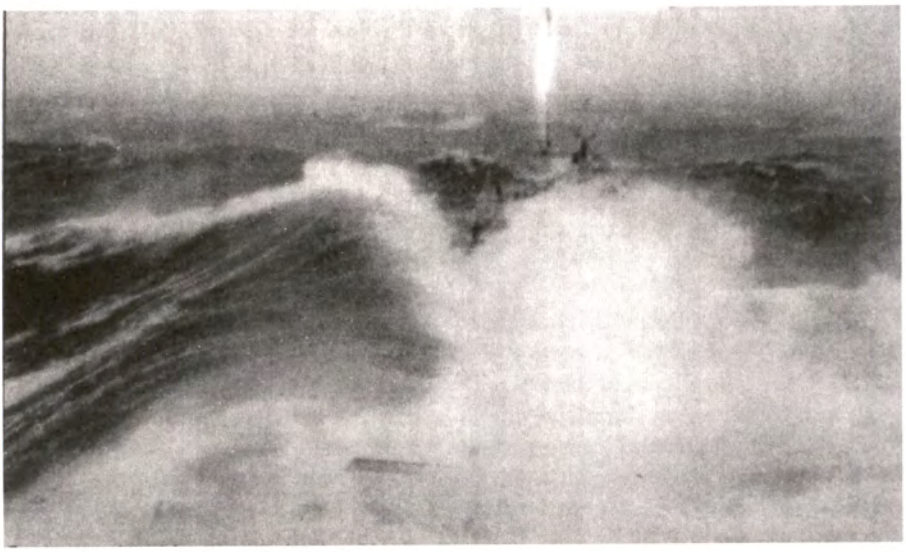

Fig. 10. MV SELKIRK SETTLER encounters a beam on rogue wave in 1977 [See also Appendix CP]

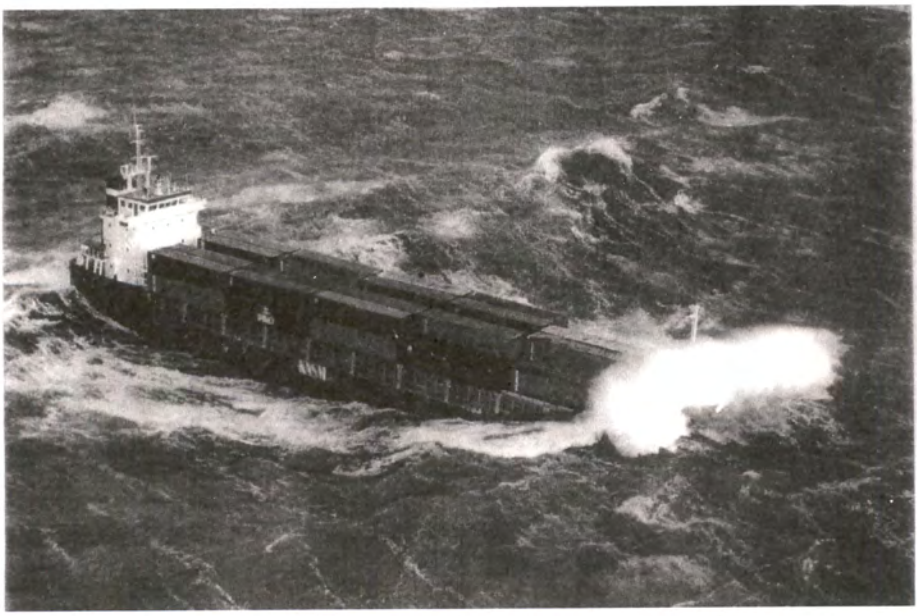

Fig. 11. Container ship plunging into moderate seas [See also Appendix CP]

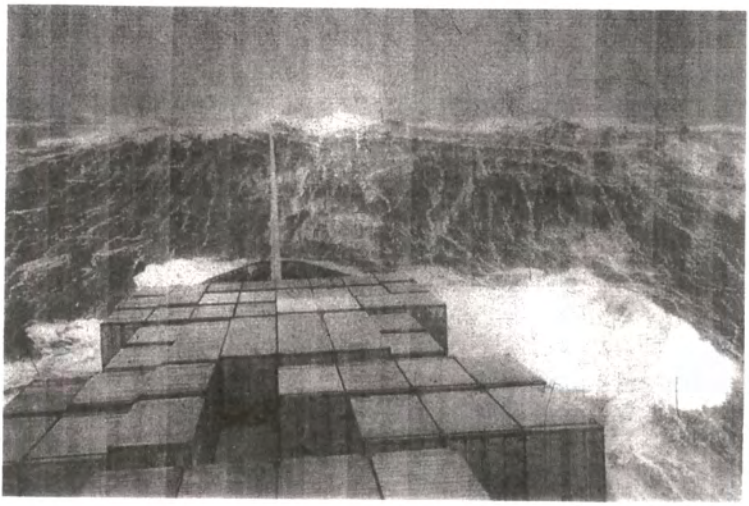

Fig. 12. Container ship about to encounter a wall of water

Fig. 13. Dislodged and smashed containers

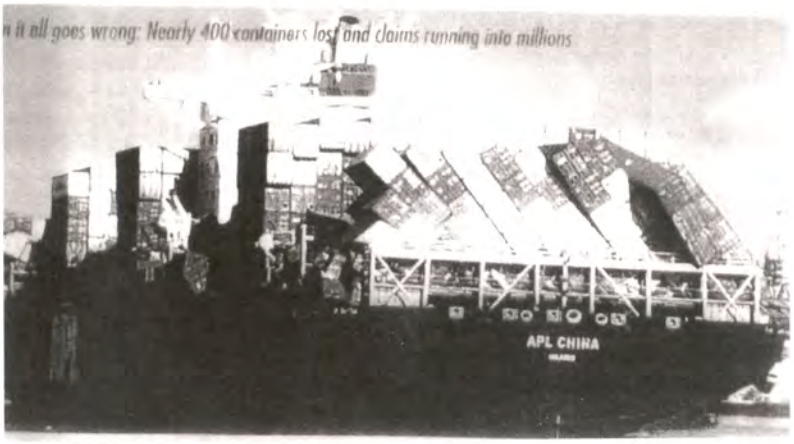

Fig. 14. The APL China with lost and damaged containers

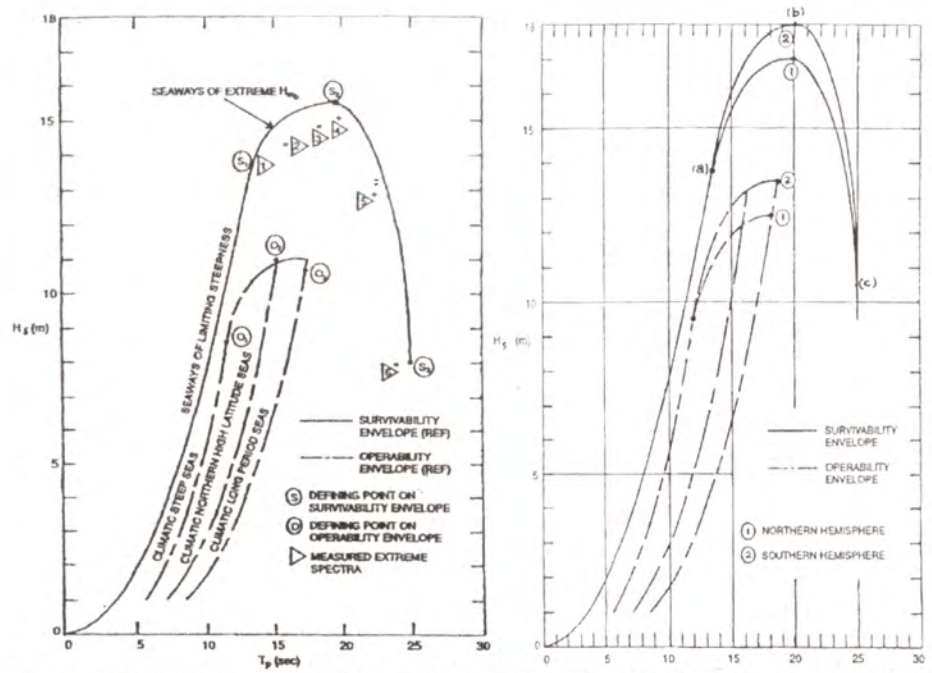

Fig. 15. NOAA baseline Survivability and Operability envelopes for Northern and Southern hemispheres

References

1. Buckley, W.H.: Stability Criteria: Development of a First Principles Methodology. 5th Int. Conf. Stability of Ships and Ocean Vehicles, STAB'94, vol. 3, (Nov. 7-11 1994)

2. Faulkner, D., Buckley, W.H.: Critical Survival Conditions for Ship Design. RINA 1st Int. Conf. Design and Operation for Abnormal Conditions, Glasgow, (21-22 Oct. 1997) 1-25
3. Nitta, A., Arai, H., Magaino, A.: Basis of IACS Unified Longitudinal Strength Standard. Int. J. Marine Structures, vol. 5, no. 1 (1992)
4. Draper, L.: Freak Ocean Waves. Oceanus, vol. 10, no. 4 (1964) (also in Mar. Obsr., London, vol. 35, (1965)
5. Buckley, W.H.: Hull Girder Structural Design – The Case for New Loading Conditions for Extreme Waves. Nav. Eng. J., Feb. (1978)
6. Donaldson, Lord: Assessment (Derbyshire), Annex. Cm 3120, London: HMSO (1995) 37-60
7. Faulkner, D.: An Independent Assessment of the Sinking of the M.V. *DERBYSHIRE*. Trans. SNAME (1999) *(later published by RINA as paper W218 (1999) which will appear with full discussion in RINA Trans., 2001)*
8. Colman, A.D.: Report on the Re-Opened Formal Investigation into the Loss of the MV *DERBYSHIRE*. Treasury Solicitors Office publication (2000)
9. WMO: Provision and Engineering/Operational Application of Ocean Wave Data. Conf. Report WMO/TD-No. 938, Marine Meteorology and related Oceanographic Activities, Report No. 42, UNESCO (1998)
10. IFREMER: Rogue Waves 2000. Int. Conf. BREST, 29-30 Nov. (2000)
11. Coles, K. Adlard: Heavy Weather Sailing. 4th edn revised by Peter Bruce, Adlard Coles Nautical (1991)
12. Ochi, Michel K.: Ocean Waves – The Stochastic Approach. Ocean Technology Series 6, CUP (1998)
13. Tucker, M.J. and Pitt, E.G.: Waves in Ocean Engineering. Elsevier (2001)
14. Komen, G.J. et al: Dynamics and Modelling of Ocean Waves. CUP (1994)
15. Nickersen, J.W.: Marine Observation Program, Freak Waves and Extreme Storm Waves. Mariners Weather Log, Washington, vol. 29 (1985) 13-17
16. Nickersen, J.W.: "Three Sisters" Marine Historic Voyage. Mariners Weather Log, vol. 30 (1986) 190-196
17. Nickersen, J.W.: Freak Waves! Mariners Weather Log, vol. 37, no. 2 (1993) 13-27
18. Faulkner, D., Corlett, B.J., Romeling, J.U.: Design of Hatch Covers and Coamings for Abnormal Waves. RINA Int. Conf., Watertight Integrity and Ship Survivability, London, 21-22 Nov. (1996)
19. Buckley, W.H.: Extreme and Climatic Wave Spectra for Use in Structural Design of Ships. Naval Engineers J., Sept. (1988)
20. Houghton, D., Wolf, J.: Waves of Destruction. Yachting World, Jan. (2001)
21. Buckley, W.H.: Design Wave Climates for the Worldwide Operation of Ships – Part 1: Establishment of Design Wave Climates. (being published as a SNAME T&R Report)
22. Hogben, N., Dachuna, N.M.C., Oliver, G.F.: Global Wave Statistics. Unwin Brothers (1986)
23. Morrison, W.D.M., Millar, J., Buchner, Bas: Green Water Susceptibility of North Sea FPSO/FSUs. IBC's 15th Conf. on Floating Production Systems, London, 11/12 Dec. (2000)
24. Lin, Woei-Min, Salvesen, Nils: Nine Years of Progress with LAMP – The Large Amplitude Motion Program. Report SAIC-97/1079, Dec. (1979) of the Science Applications International Corp., 134 Holiday Court, Annapolis, MD, 21401, USA.

A Sudden Disaster – in Extreme Waves

Peter Kjeldsen

Trondheim Maritime Academy,
Ladehammerveien 6. – 7004 Trondheim, Norway
Fax: ++47 73528378, peter.kjeldsen@c2i.net

Abstract. This paper describes establishment of a world data bank related to ship accidents caused by freak waves and rogue waves. Basic relevant definitions for such waves are given together with examples of ship accidents. Laboratory experiments with wave-current interactions leading to coalescing wave groups containing deep water plunging breakers are described. Further experience obtained from capsizing experiments in such waves is given.

1 Introduction

Loss of a large norwegian ship with the entire crew in the middle of the North Atlantic is not a common event. However at a special occasion two large norwegian bulk ships M/S "NORSE VARIANT" and M/S "ANITA" disappeared at the same time at the same location. Both ships passed Cape Henry with only one-hour interval in time on voyages from the U.S.A. to Europe. Both ships came right into the center of a very extreme weather event with a strong low pressure giving 15 m significant wave heights and mean wave periods close to 10 seconds and strong northerly winds with wind velocities near 60 knots. "NORSE VARIANT" had deck cargo that was damaged and moved by water on deck with the result that a hatch cover was broken and left open. The ship took in large amounts of water and sank before an organised evacuation was finished. Only one member of the crew was rescued on a float.

"ANITA" disappeared completely at sea with the whole crew and no emergency call was ever given. The Court of Inquiry then concluded that the loss can be explained by an event in which a very large wave suddenly broke several hatch covers on deck, and the ship was filled with water and sank before any emergency call was given.

2 New Basic Definitions

The wave that caused the loss of "ANITA" was probably a freak or rogue wave. In our research we have defined a freak wave as a wave with a zero-downcross wave height that exceed 2 times the significant wave height. A crucial question is then:

Will the freak or rogue wave that hits the ship be a breaking wave?

It is not possible to characterise the severeness of a particular sea state containing large random waves some of them even breaking using only traditional parameters height and period of the individual waves. Experiences show that accidents occur if there is a quite unique exceedance of critical threshold values for several parameters simultaneously. Wave steepness seems to be a parameter at least as important as wave height, under some special circumstances even more important. Traditionally wave steepness of a random wave has been introduced as a ratio between total wave height and total wave length. However, in a random sea many waves can occur with the same total steepness but different asymmetry, and thus some of them will be breaking others not. The random waves in a severe directional wind generated sea are clearly asymmetric both in the wind direction and in the vertical direction. In order to obtain a better description of freak waves and rogue waves, and in particular to distinguish if they are breaking or not a DATUM and 4 new wave parameters were introduced. Then the mean water level is taken as reference DATUM and crest height, crest front steepness, crest rear steepness and horizontal and vertical wave asymmetries are introduced see [4] and [3].

A freak wave or rogue wave is essentially an abnormal 3-dimensional wave crest and we need some new definitions, that also takes the 3-dimensional aspects of such a wave into account, see Fig. 1. At the top here is shown a photograph by Fukumi Kuriyama of such a wave together with the new definitions we have to introduced.

The seaway is considered to be made up of an infinite sum of component waves from all directions and with all frequencies and the elevation $\eta(t)$ of the sea surface above a fixed point can then be expressed as:

$$\eta(t) = \int_{-\pi}^{\pi} \int_{0}^{\infty} cos\left(2\pi ft + \Theta(f,\alpha)\right) \sqrt{2E(f,\alpha)}\, df d\alpha \quad . \tag{2.1}$$

Here $E(f,\alpha)$ is the directional wave spectrum, which might be the directional wave spectrum from a wind generated sea. However more common is a situation where the resulting directional spectrum is composed of several wave patterns both a wind generated sea from one direction and two or three swells from arbitrary directions.

$$\sqrt{2E(f,\alpha)} \tag{2.2}$$

is then the amplitude, and

$$\Theta(f,\alpha) \tag{2.3}$$

is the phase angle of the component waves coming from direction α with frequency f and t is the time coordinate.

If a freak wave occur it often happens that it comes from a direction that deviates significantly from the main wind direction. It thus suddenly strikes on the ship with another direction than the other waves and this makes the situation particular dangerous during storm conditions if the ship is in a head sea and suddenly goes into an

abnormal roll, because the freak wave strikes 40 degrees off the wind direction. The direction of a single wave is defined as the direction of the projection of the particle velocity vector on the sea surface as Fig. 1 shows.

The crest elevation of the abnormal wave must be compared to the other waves in the sea state, and here is the first problem. Normally the significant wave height has been used as a measure of the severity of the sea state, but the significant wave height might be determined in several ways. We recommend that the moment m_0 determined from the unidirectional wave spectrum is used instead as a reference:

$$m_0 = \int_0^\infty S(f)\,df \ . \tag{2.4}$$

The significant wave height $H_{1/3}$ is then given by

$$H_{1/3} = 4\sqrt{m_0} \ . \tag{2.5}$$

2.1 First Basic Definition

A freak wave can now be defined as a wave that satisfies the following condition:

$$MAX\left(\eta_i(t)\right) > 4\sqrt{m_0} \ . \tag{2.6}$$

In order to define a true appearance of a unique single elevated wave crest, the following additional conditions can be used:

$$MAX\left(\eta_{i-1}(t)\right) < 4\sqrt{m_0} \tag{2.7}$$

$$MAX\left(\eta_{i+1}(t)\right) < 4\sqrt{m_0} \ . \tag{2.8}$$

This implies that wave number (i-1) before the freak wave (i), and wave number (i+1) behind the freak wave (i) are both normal waves.

The crest front steepness in space is then defined in Fig. 1 as:

$$\varepsilon = MAX\left(\eta_i(x)\right)/L \ . \tag{2.9}$$

Experimental investigations [4] of spilling breakers and plunging breakers generated in deep water and analysed by digitalization of high speed films showed the following values for crest front steepness when the breaking inception started :

$$0.32 < \varepsilon < 0.78 \ . \tag{2.10}$$

Spilling breakers entrained air at this point and plunging breakers appeared with a vertical front. The crest front angle Θ then becomes:

$$\Theta = Arc\tan\varepsilon \tag{2.11}$$

and we obtain :

$$17.74 \text{ degrees} < \Theta < 37.95 \text{ degrees} . \tag{2.12}$$

Stokes in [13] assumed that in the region near the crest the water surface could be approximated by two straight lines forming an angle α. Further if wave particle velocity below the crest equals the nonlinear phase speed of the wave then the angle α becomes 120 degrees, and we have a symmetrical spilling breaker. The angle between the wave front and the vertical then becomes 60 degrees, and the angle between the front of the wave and a horizontal line becomes 30 degrees in the region very close to the crest in a spilling breaker. Values of epsilon as given by Eq. (2.10) when inception of breaking takes place are also confirmed by independent experiments performed by [1] and are in reasonable agreement with this theoretical result.

The crest front steepness and the crest front angle can also be estimated from observations in the time domain. The simplest assumption will be that the wave travels with linear phase speed computed corresponding to the zero-downcross wave period. T^I is the time difference between the passage of the zero-upcross point ahead of the crest and the passage of the crest, (corresponding to L^I in space.):

$$\varepsilon = \frac{MAX\left(\eta(t)\right)}{T^I C_0} = \frac{MAX\left(\eta(t)\right) 2\pi}{T^I g T_{ZD}} . \tag{2.13}$$

For steep waves we have used a nonlinear phase speed C_S and obtained a better estimation of the crest front steepness and the crest front angle:

$$\varepsilon = \frac{\eta^I}{T^I C_S} . \tag{2.14}$$

The nonlinear phase speed itself depend on wave steepness and is given by [2] for Stokes waves using Padè approximations to 110^{th} order:

$$C_S = f\left(\frac{2\pi H}{gT^2}\right) . \tag{2.15}$$

We have then used Cokelet`s model to approximate non-linear transient waves before breaking takes place. Experiments presented by [12] confirms that the use of such a nonlinear phase speed is in agreement with observations.

Other experiments have shown that wave impacts on ships increase with increasing crest front steepness. In some cases wave crest front steepness is a much more important parameter for a ship than wave height itself.

Other wave asymmetry parameters are given in Fig. 1 and recommended by IAHR for use in research. Of particular interest is the length of the wave crest in a 3-dimensional breaking wave. The ratio between wave crest length and ship length is one of the important parameters that determine the capsizing potential of such a wave.

2.2 Second Basic Definition

A freak wave can also be defined as a wave that satisfies the following condition:

$$MAX\left(H_i\right) > 8\sqrt{m_0} \quad . \tag{2.16}$$

In this case it is important to check both the zero-downcross and the zero-upcross wave heights, and these will be different. Here we can also include the situation with a coalescing wave group in which 2 or 3 waves following each other all satisfy Eq. (2.16). That is a more dangerous situation for a ship and might in some cases lead to capsizing. If 3 abnormal waves occur together, such an event is called " Three sisters " by ship officers.

2.3 Third Basic Definition

In order to evaluate the risk for a capsizing it is necessary to evaluate if a wave is a freak wave and at the same time is a breaking wave. In order to obtain such a condition we must expect that the wave must be a high wave and at the same time a wave with a large crest front steepness.

Here reference will be given to laboratory experiments developed in order to perform capsizing experiments with ships and platforms, [6]. Steep plunging breakers were generated in deep water from highly nonlinear coalescing wave groups. In these experiments it was found that the wave broke when the nondimensional ratio between the zero-downcross wave height H_{zd} and the zero-downcross wave period T_{zd} became:

$$\frac{2\pi H_{ZD}}{g T_{ZD}^2} = 0.0548 \tag{2.17}$$

corresponding to a value of crest front steepness computed from Eq. (2.13) as:

$$\varepsilon = \frac{\eta^I}{T^I C_O} = \frac{\eta^I 2\pi}{T^I g T_{zd}} = 0.200 \tag{2.18}$$

g is here the acceleration of gravity. The horizontal asymmetry parameter was:

$$\mu = \frac{\eta^I}{H_{ZD}} = 0.770 \ . \tag{2.19}$$

This particular parameter will be very nearly the same when it is measured in the space and in the time domain.

Evaluation and proper analysis of a measured freak wave includes an analysis that indicates if the measured freak wave also could be a breaking wave. Such an evaluation could be made using Eq. (2.18) or Eq. (2.19) as given above. The ratio between wave height and wave length (or period) as in Eq. (2.17) is useless, as many irregular random waves can occur with the same ratio, some of them breaking others not.

3 Summary of Research on Freak Waves Linked to Ship and Offshore Accidents

Accidents including a large number of severe heavy weather damages on ships and offshore structures were collected in a WORLD DATA BANK from 3 sources:

1. *Cargo ships, fishing vessels and passenger liners*
2. *NATO ships operating in the North Atlantic*
3. *Experiences from the offshore industry with FPSO ships, steel jackets and semisubmersible platforms*

Ship capsizings caused by freak waves were mapped, however the actual waves that caused the accidents were normally not recorded. In some cases freak or rogue waves with a capsizing potential were also measured and analysed from some specific places of the world, see Fig. 2. One example is a freak wave measured on the FRIGG-field in Norway Area No 5, see Fig. 3. For this wave the following data were recorded:

$$crest\ height / \left(4\sqrt{m_0}\right) = 1.68 \tag{3.1}$$

$$H_{ZD} / \left(4\sqrt{m_0}\right) = 2.29 \tag{3.2}$$

$$\varepsilon = \frac{\eta^I}{T^I C_0} = \frac{\eta^I 2\pi}{T^I g T_{zd}} = 0.308 \tag{3.3}$$

$$\mu = \frac{\eta^I}{H_{ZD}} = 0.738 \tag{3.4}$$

The sea state had a significant wave height 4.27m. Based on the above it is reasonable to expect that this wave developed further as a plunging breaker. A joint probability density distribution is computed for this case as shown in Fig 3. It is remarkable that this particular wave has not only an abnormal crest height but at the same time an abnormal crest front steepness. This gives this particular wave a large capsizing potential.

None of the available statistical models for crest front steepness can predict this observation. Only in a few unique cases photos of such freak waves have been taken. Fig 3 shows such a scenario with a large norwegian bulk ship heading into an abnormal wave in the Bay of Biscay, Area No 8.

Even more rare is the opportunity to have a ship with recording instruments running into a freak wave. Such a case happened unexpected in Area No 20 the Mediterranean Sea. A 100 m long monohull high speed vessel was running with 40 knots in a sea state with significant wave height 3.5 – 4 m and was suddenly struck by a freak wave. Fig 4 shows the recorded bow acceleration 1.5 g (2.17 times the 10^{th} value), and the recorded strain in the longitudinal beam that was 80 Mpa (5.28 times the 10^{th} value.)

The LEWEX research programme was a large international effort initiated in Area No 1, The Newfoundland banks which are notorious for freak waves. The LEWEX programme had several scientific scopes one of them was to improve design of ships operating in the North Atlantic. Parallel seakeeping trials were here performed with two instrumented ships and directional wave buoys anchored in 4000 m water depth [8]. Fig 5 shows examples of two directional wave spectra measured here. The first one shows two wave patterns dispersing nearly perpendicular to each other.

Analysis of the world data bank show that freak waves often appear in areas where wind waves meets opposing currents. Fig 5 shows also a directional spectrum measured in the Gulf Stream and shows a very complicated combination of several wave patterns refracted by the current. A freak wave was measured in this spectrum with a shipborne sensor.

4 Experiments with Freak Waves on Opposing Currents

Analysis of the data bank showed that freak waves often occur on locations with opposing ocean currents. For this reason a series of extensive model experiments were performed with nonlinear coalescing wave groups focusing into large giant waves on opposing currents. A kinematic model was also established in order to predict both wave kinematics and wave impact forces and global wave forces caused by the wave crests of such giant waves. These kinematic and wave force models were then confirmed by extensive model testing and full scale sea trials.

The experiments with freak waves generated on opposing currents were performed in the large wave tank at the Canada Centre for Inland Waters. This wave flume is shown in Fig. 6. The tank is 100 m long and 4 m wide. It is not the surface elevation but the kinematics in the crests of the freak waves that is important for prediction of wave forces.

The particle velocities were measured with an acoustic Doppler current meter. Fig. 6 shows development of plunging breakers in deep waters with and without an opposing current. It is seen that the plunging breaker on a weak opposing current appears with a larger crest height and a larger crest front steepness. Fig. 6 shows also measured horizontal velocities both in the crest above mean water level and below mean water level.

The kinematics in the wave crests on currents was predicted with a new third order model, see [11]. There is obviously a need to develop an international standard for laboratory experiments with freak waves and breaking waves.

5 Capsizing Experiments

Extensive series of capsizing experiments were performed at Norwegian Hydrodynamic Laboratories in Trondheim. Steep plunging breakers were generated in deep water from highly nonlinear coalescing wave groups, see [6].

Fig. 5 shows an example of a 3-dimensional steep elevated wave crest generated from focusing of 100 individual wave components with different directions over a synoptic angle of 105 degrees. This lead to extreme steep shortcrested breaking waves, called " Pyramidal Breakers ". The wave generated here is similar to the photo of such a wave taken by Fukuri Kuriyama and shown in Fig. 1.

A capsizing experiment is difficult to perform. It is necessary to use high speed film technique in order not only to observe the very fast development of the unstable wave, but in particular to observe the fast ship-wave interaction. When the jet from a high wave crest strikes on the superstructure of the vessel, the ship performs a combined motion in roll, heave and sway and during this the mass moment of inertia is influenced by a rapid changing added mass following the vessel in the capsizing.

It was found that the angle of roll, rolling velocity and rolling acceleration of the ship at the moment the freak wave was striking, are important parameters to consider. Therefore a random wave train was generated with a prescribed wave spectrum and inside this was a coalescing wave group that developed a breaking freak wave. The position of this wave could be shifted slightly in order to hit the superstructure exactly on different positions.

The capsizing event was found to depend on the following wave parameters:

1. *Zero-downcross wave height*
2. *Wave crest height*
3. *Crest front steepness*
4. *Local particle velocities in the plunging jet*
5. *Local particle accelerations in the wave crest*
6. *The crest length of a breaking wave compared to ship length.*

It was also found that heeling forces from the wind on a large superstructure contributed to the development of a capsizing. Thus the wind force including gust effects must always be considered. The dynamic stability of a ship depends on the displace-

ment and the mass moment of inertia. Unfortunately the displacement is not yet included in international rules regulating demands for dynamic stability of ships.

There is thus an obvious need for development of an international standard regarding capsizing experiments.

A development of a numerical ocean basin is initiated [12] and this might also include a numerical simulation of capsizing.

6 Learning from Ship Accidents

The research work related to establishment and analysis of the WORLD DATA BANK, has shown certain patterns and risk elements that should be taken into account by:

1. *Ship officers*
2. *Naval architects and designers.*

Good seakeeping has been a forgotten factor in many cases. For the ship officers there is a need for further education in particular in the following items:

1. *How to avoid the center of severe extra tropical cyclones,*
2. *How to handle a damaged ship in severe waves, and*
3. *What is the right time to evacuate a damaged ship ?*

For naval architects and designers the following items should be considered:

1. *Ship displacement and mass moment of inertia should be taken into account in criteria for dynamic stability*
2. *High impact forces caused by extreme waves breaking on the superstructure should be considered. In particular large windows are weak points*
3. *Pressure from large amounts of water on deck should be considered*
4. *Hatch covers on bulk ships are weak points and should have the same strength as the ship hull*
5. *Extreme freak weather events caused by change of climate, might lead to an increasing number of scenarios containing extreme waves and freak waves*

Thus, it is obvious that there is a great need for further research in this area.

7 Conclusions

- There is a need to increase survivability of modern ships, in such a way that a damaged ship with a heeling angle can sustain impacts from large waves and still maintain a marginal dynamic stability.
- The rules and requirements of ship dynamic stability are clearly insufficient.

Not only the area below the GZ-curve should be taken into account but also the displacement of the ship and the mass moment of inertia given as the radius of gyration. This applies both to intact stability criteria and to criteria for damaged stability.

- High impact forces caused by extreme waves breaking on the superstructure of ships and should be considered. In particular large windows are weak points.
- Dynamic pressures from large amounts of water on deck should be considered.

  Hatch covers on bulk ships are weak points and should have the same strength as the ship hull.
- A world data bank is established indicating the areas where freak waves and rogue waves are measured or reported. The data bank contains also information of ship accidents caused by extreme waves in these areas. Measured freak waves in this data bank shows abnormal values of crest front steepness, clearly very different from the normal population of steep waves. None of the existing models for prediction of joint probability of crest front steepness and wave height contain the potential to predict the steepness of these observed waves.
- An international standard is needed for hydrodynamic laboratories performing capsizing experiments with ships and platforms in breaking waves and extreme non-breaking waves. This standard should be based on laboratory measurements of wave kinematics. Heeling moments caused by the action of wind forces should also be taken into account in capsizing experiments.
- A better education of ship officers is needed. In particular we need a better education in ship handling of intact and damaged ships in severe weather conditions. Better guidelines should be given to ship officers regarding the choice of the right time to evacuate a damaged ship, and the time needed to evacuate in severe wave conditions.
- It is strongly recommended to use maximum expected wave height instead of significant wave height in forecasts to ship officers worldwide. In sea areas where it becomes possible to forecast a probability for freak waves or rogue waves, such a forecast should certainly be distributed.
- The probability to encounter extreme waves, freak waves and rogue waves are linked to wave climate. Now we observe scenarios with extreme weather events on several places on the globe with short time intervals and a global heating is predicted and recorded. These freak weather events with strong winds in both tropical cyclones and in extra tropical cyclones might also lead to an increasing number of scenarios containing freak waves and rogue waves.

8 Figures

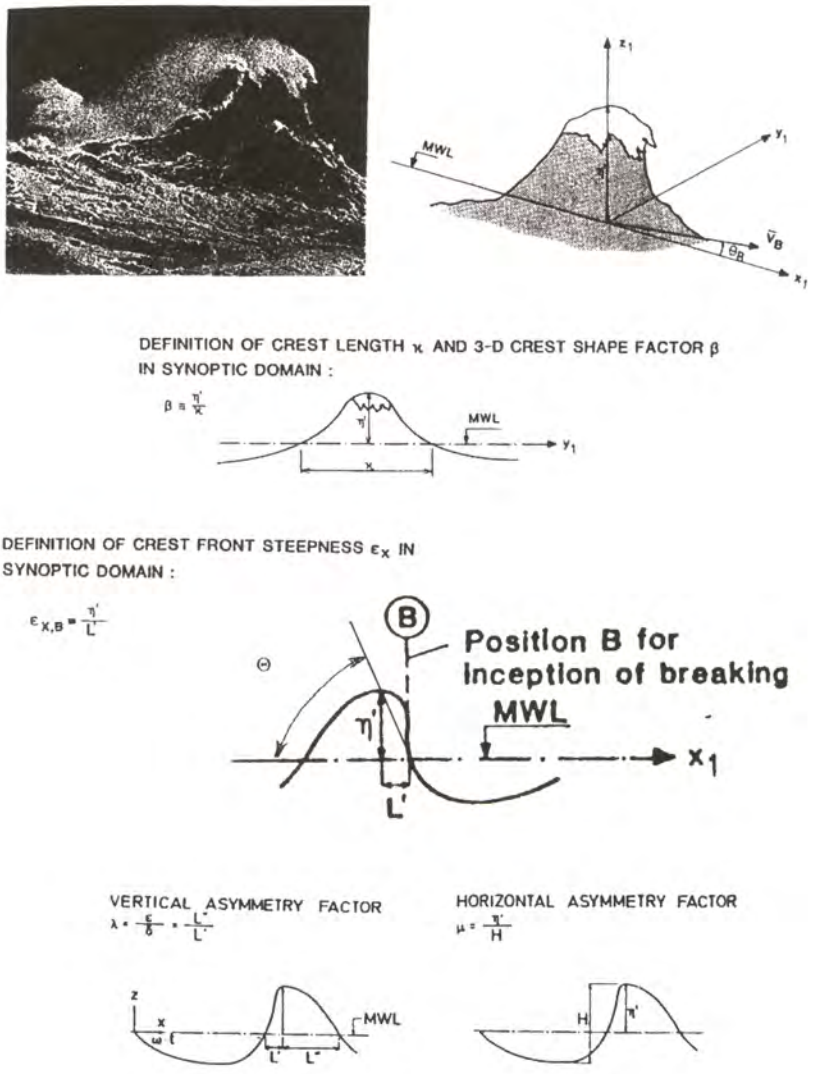

Fig. 1. Basic definitions. Photo by Fukumi Kuriyama

World Data Bank

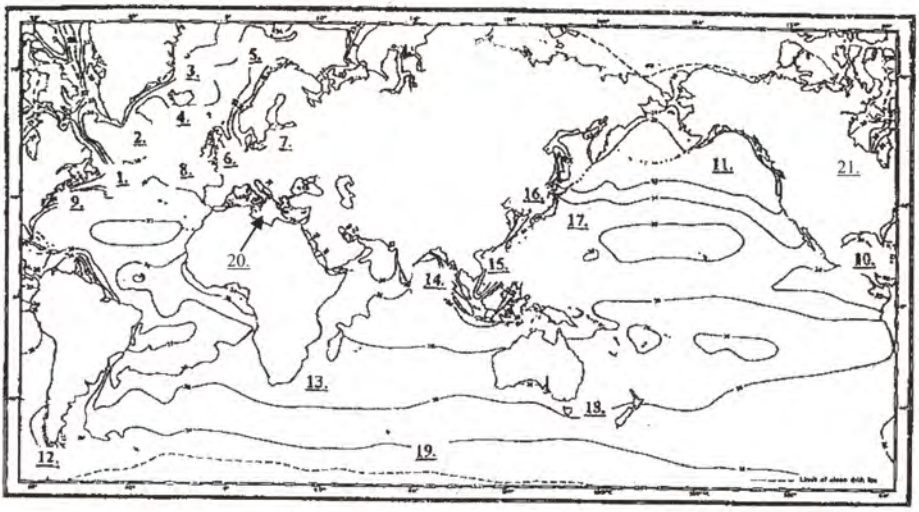

1	Newfoundland Banks	12	The Sea near Cap Horn
2	The Sea south of Greenland	13	Aghulhas current east of South Africa
3	Coastal areas near Iceland	14	The Bengal Sea
4	Coastal areas near Færø Islands	15	The South China Sea
5	Coastal areason the norwegian coast	16	The Japan Sea
6	The North sea	17	The Pacific Sea east of Japan
7	The Baltic Sea	18	Coastal areas near Australia
8	The Biscay Bay	19	Areas south of 40 degr. south
9	Gulf Str on the east coast of USA.	20	Mediterranean Sea
10	The Mexican Gulf	21	Great Lakes
11	The Sea west of British Columbia.		

Fig.2. Dangerous Areas that contain Freak Waves under certain Meteorological Condition (Copyright Peter Kjeldsen/TC. Trondh. Maritime vg. Skole)

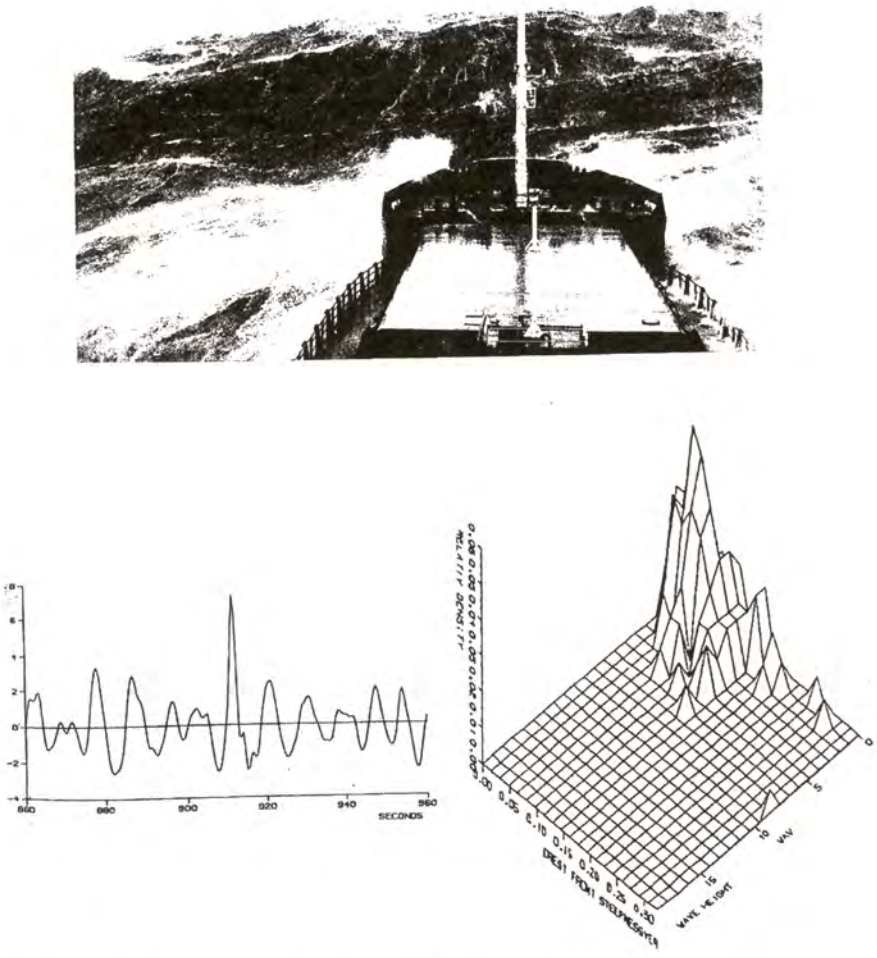

Fig. 3. Above: A Norwegian bulk ship heading into an abnormal wave in area No 8. Below: Example of a freak wave and the corresponding joint probability distribution of wave height and crest front steepness measured in area No 3

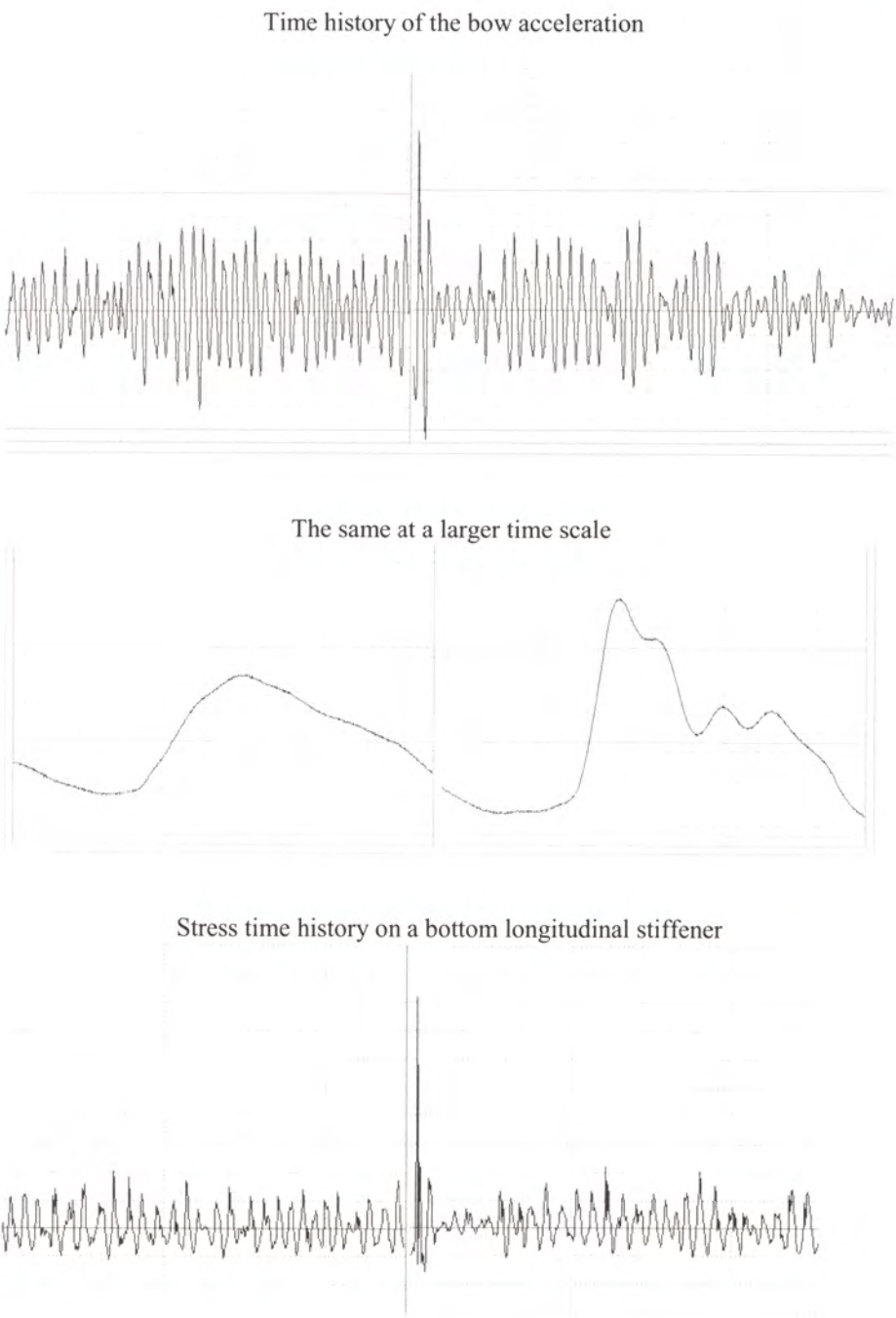

Fig. 4. Example of extreme bow acceleration and stress measured on a high speed ship in Area No 20. The significant wave height was 3.5 – 4 m

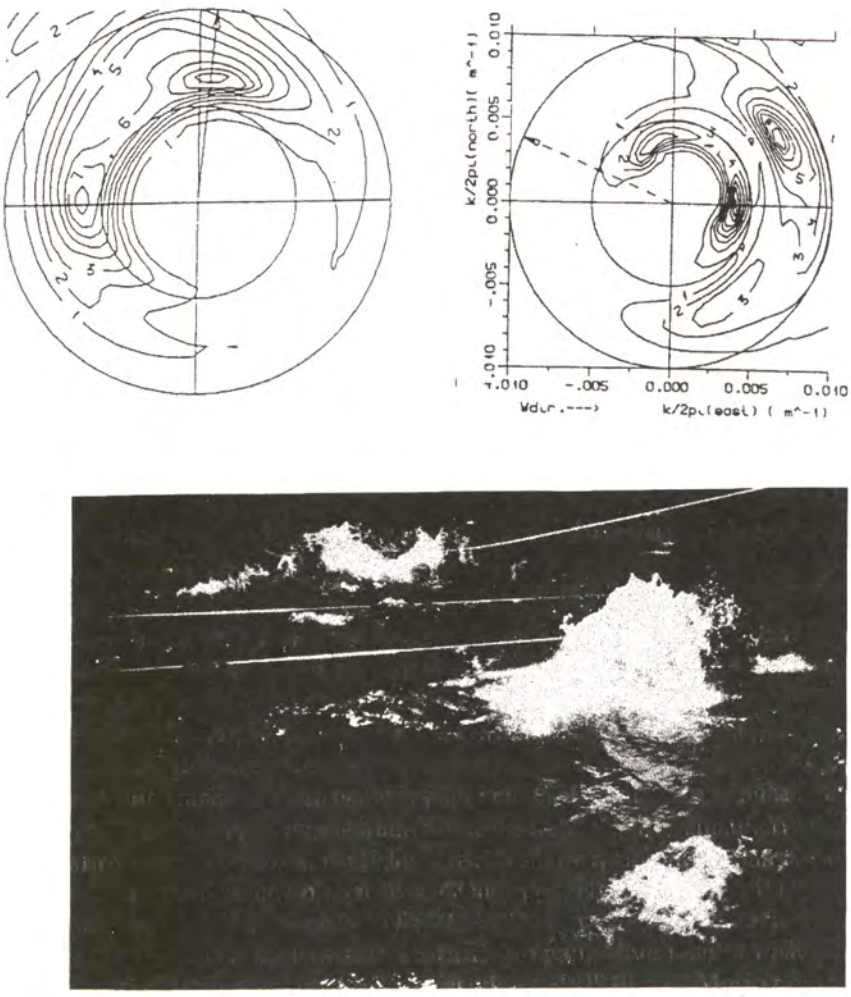

Fig. 5. Above left: A bimodal directional wave spectrum. Right: A directional spectrum showing wave-current refraction in the Gulf Stream.
Below: A 3-dimensional shortcrested freak wave generated in laboratory experiments in order to simulate the wave shown in Fig. 1

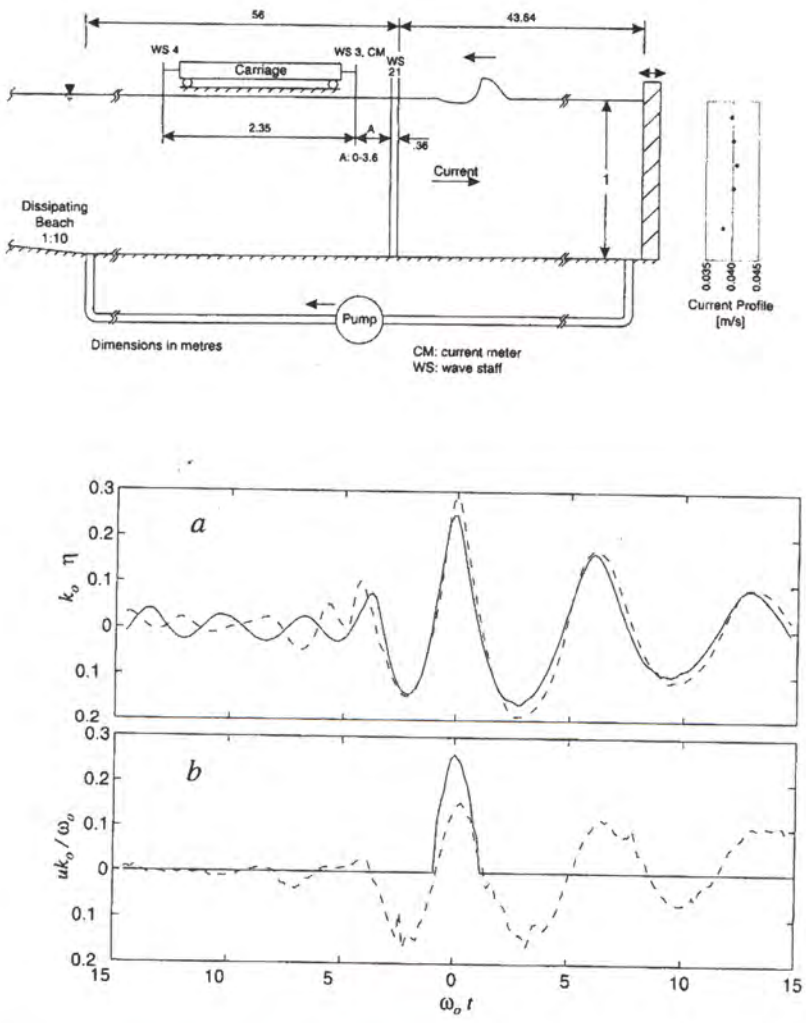

Fig. 6. Above: The CCIW wind wave flume. Below: Examples of surface elevations and horizontal velocities with and without opposing currents.

9 Acknowledgements

We will express our gratitude to Dr. Pierre Bonmarin, Dr. Michel Huther, Dr Michael Skafel, Dr William Drennan, Dr. Hiroshi Tomita and Professor Bruce Johnson. They all contributed in a significant way to this study.

References

1. Bonmarin, P.: Some Geometric and Kinematic Properties of Breaking Waves. Proc. Int. Conf. "ROGUE WAVES 2000" Brest, France (2000)
2. Cokelet, E.D.: Steep Gravity Waves in Water of Arbitrary Uniform Depth. Philosophical Transactions of the Royal Society of London, No 1335 Vol 286. (1977) 183-230
3. I.A.H.R./P.I.A.N.C. List of Sea State Parameters. Supplement to Bulletin No 52." (1986)
4. Kjeldsen, S.P., Myrhaug, D.: Breaking Waves in DeepWaters and Resulting Wave Forces. Proc. 11th Offshore Technology Conference, Paper No. 3646 Houston, Texas (1979)
5. Kjeldsen, S.P., Vinje, T., Myrhaug, D., Brevig, P.: Kinematics of Deep Water Breaking Waves. Proc. 12th Offshore Technology Conference, Paper No 3714. Houston, Texas (1980)
6. Kjeldsen, S.P.: 2- and 3-Dimensional Deterministic Freak Waves. Proc. 18th Int. Conf. on Coastal Engineering . Cape Town, South Africa (1982)
7. Kjeldsen, S.P.: Dangerous Wave Groups. Norwegian Maritime Research, Vol 12, No 2 (1984) 4-16
8. Kjeldsen, S.P.: The Practical Value of Directional Ocean Wave Spectra. In Beal, R.C. (editor): Measuring Modeling, Predicting and Applying Directional Ocean wave Spectra. The Johns Hopkins University Press, Baltimore London (1991)
9. Kjeldsen, S.P.: Examples of Heavy Weather Damages caused by Giant Waves. SNAJ. Bulletin of the Society of Naval Architects of Japan, Vol 828 1997/10 (1997) 744-748
10. Kjeldsen, S.P., Bonmarin, P., Skafel, M.G., Drennan, W.M.: Lagrangian Measurements of Accelerations in the Crest of Breaking and Broken Waves. Proc. 26th International Conference on Coastal Engineering. Copenhagen, Denmark. (1998)
11. Kjeldsen, S.P., Drennan, W.M., Skafel, M.G.: Modelling of Velocities in Giant Waves. The ISOPE-Journal, Vol. 10. No 3 (2000) 170-172
12. Kjeldsen, S.P., Bonmarin, P.: Development of a Numerical Ocean Basin for Simulation of Ringing Effects on Monotower Platforms. ISOPE-2001 Conference. Stavanger, Norway. (2001)
13. Stokes, G.G.: Supplement to a Paper on the Theory of Oscillatory Waves. Mathematical and Physical Papers, Vol 1. Cambridge University Press, London (1880) 314-326

FPSO Bow Damage in Steep Waves

Peter Gorf[1], Nigel Barltrop[2], Barbaros Okan[2], Trevor Hodgson[3] and Rod Rainey[4]

[1] BP, Chertsey Rd, Sunbury on Thames, Middlesex, TW16 7LN, UK
gorfpk@bp.com
[2] University of Glasgow, NA&OE, Glasgow G12 8QQ, UK
{n.barltrop, bokan}@eng.gla.ac.uk
[3] WS Atkins, Golden Square, Aberdeen AB1 1RD
thodgson@wsatkins.co.uk
[4] WS Atkins, 171 High Holborn, London WC1, 7AA, UK
rctrainey@wsatkins.co.uk

Abstract. The Schiehallion FPSO was damaged by wave impact in November 1998. Research undertaken to better understand the environment and to determine suitable design pressures is described. The research includes calculations, model experiments in the Glasgow wave/towing tank and full scale measurements with a wave buoy and pressure transducers and strain gauges in the Schiehallion bow. Several projects, with UK government, industry and EU funding, are continuing to investigate this problem.

1 Introduction

The turret-moored Schiehallion FPSO is stationed in the Atlantic to the West of the Shetland Isles. A photograph of the vessel is shown in Figure 1:

Particulars:	
Length	245 m
Breadth	45 m
Depth	27 m
Lightship	42,425 mt
Deadweight	152,360 mt (at 20m)
Displacement	194,785 mt (at 20m)
Storage Cap.	950,000 bbls
Water Depth	395m
Flexible Risers	
Wire/Chain Mooring Legs	
Suction Anchors	
180 BOPD Throughput Capacity	

Fig. 1. The Schiehallion FPSO

Fig. 2. The bow damage

1.2 The wave impact incident

During the night of the 9th November 1998, in a sea state estimated as: Hs = 14m, Tp = 15-16 sec, an area of forecastle plating, 20m above the mean water line and above the main deck level, was pushed in by 0.25m. See Figure 2. There was some associated minor plating deformation inside the forepeak (in the main hull below the main deck). There was no damage to the flare tower supports or to any process equipment.

2 Strengthening and Research

Following the damage it was necessary to undertake repairs and strengthening of the bow. This work, based on desk studies to estimate design pressures, was completed in the second quarter of 1999. The studies identified uncertainties in the loading caused both by the uncertainties in the probabilities of the waves that might cause severe impacts and the uncertainties in the impact pressure from a known wave.

BP therefore started a program of follow on research comprising:

- Installation of a bow monitoring system (during December 1999 to January 2000).
- Installation of a wave monitoring data buoy, in February 2001.
- Analysis of hull global bending and shear from wave impact (on both the bow & Forefoot).
- Model tests to evaluate slam loads / pressures.
- Encouraging and participating in the SAFEFLOW EU project/JIP, including more model tests and the analysis of the bow monitoring data. (Project started in January 2001)

3 Full Scale Measurements

3.1 The Bow Monitoring System

The bow monitoring system comprises pressure transducers and strain gauges as shown in Figure 3. The pressure transducers show individual local pressures. The array of pressure transducers and the strain-gauged structure will indicate the degree of correlation. The pressure sensors trigger data collection when the pressure exceeds 3 bar.

Data collection from the monitoring system commenced on the 19th January 2000. To 28th January 2001, twenty four data sets have been collected. These contain peak pressures from three to six bar, but a high pressure has only been found on one pressure sensor in any incident and the strain gauges show small overall forces, so indicating that no significant slam events have occurred so far.

3.2 The Wave Data Buoy

A Triaxys wave monitoring buoy will collect both wave directional spectra and a time history of water surface elevation. The latter will be analyzed to determine probabilities of steep, high waves. These will be used in the SAFEFLOW project and will be input to a bow slam residual risk assessment.

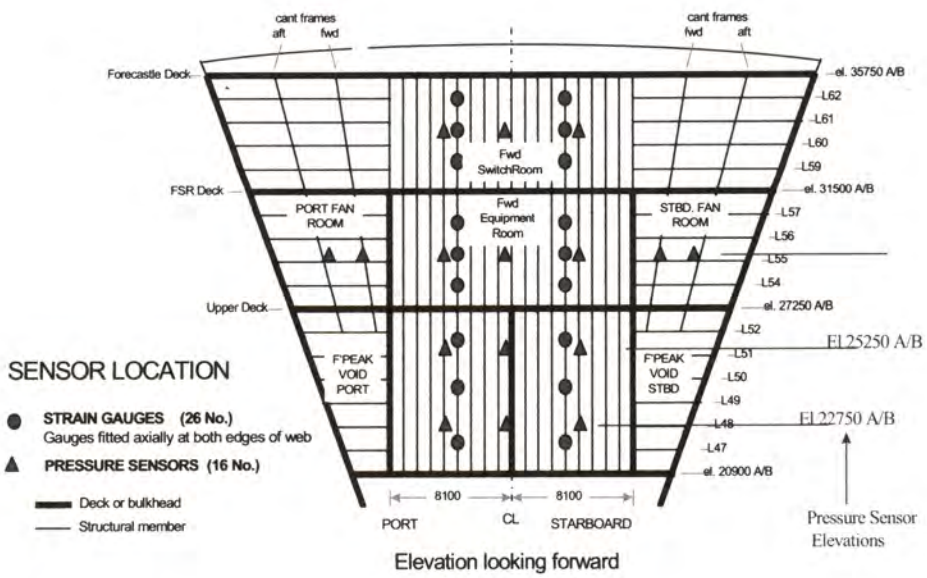

Fig. 3. Bow instrumentation

4 The Model Tests

Glasgow University were asked to investigate the bow loads by building a 1:80 instrumented bow model and testing it in the wave tank. Forces and pressures were measured in a range of waves with the bow fixed at various drafts and trims. (Additional tests with the complete vessel floating will be performed during 2001.) Froude scaling was used. This is required to obtain the correct waves and is expected to give good results for overall loads but may result in poor values for peak pressures where fluid compressibilty and local structural flexibilty may also be important but cannot be scaled properly (unless the more important Froude scaling is abandoned).

4.1 The Bow Model

The model was built at a scale of 1:80 and extended aft from the bow for 90m at full scale. The model was supported on substantial hollow box sections with a screw-jack to change draught and a hinge to change trim. The model is shown, out of the water in Figure 4. The model included pressure transducers, at approximately the same positions as in the prototype bow, and the bow was divided horizontally into three bow sections, each of which was separately supported on strain gauged bars, so allowing both local pressures and overall forces (longitudinal, vertical and moment about a transverse axis) to be measured.

A problem with this type of model is the sealing between the sections. This was anticipated and so the model was designed to operate with or without seals. Initially thin rubber seals were used but the T joint between two bow sections and the aft section was found to be too stiff so the initial work was done without seals. Later a jig was made for prefabricating flexible T joints and a successful low stiffness seal can was made.

Fig. 4. The bow model (without seals and, in the tank, with seals)

4.2 The Model Waves

A range of waves was required for test purposes. After some discussion it was decided to use frequency component focussing to obtain a variety of different waves. All the methods used linear theory to develop the signal for the wave paddle but included calibration in finite height waves, which made some allowance for the change in celerity with wave height, which was important for focussing the different frequency components at the bow of the ship. Several methods were adopted for generating the waves:

1) High waves were produced using New Wave theory [2]. This provides an average highest wave form for any given Hs, Tz and spectrum shape. This is a wave in which the resultant of the frequency components in each narrow frequency band are proportional to the spectral ordinate and are in phase at the high crest.

2) Steep waves were obtained by applying New Wave theory to a truncated steepness spectrum and transforming the results back to water surface elevation. (Truncation was needed because from the theory the steepest waves have negligible height).

3) In error waves were generated using the steepness spectrum but without the intended transformation back to elevation. The result was a severe breaking wave at the target point. These waves were interesting because they produced very much higher loads than the waves intended to be used.

4) A second type of steep wave was produced by taking the highest New Wave amplitude and frequency components but arranging the components to be in phase at a zero up-crossing.

5) Combinations of high and steep waves were also used in the procedure, with phasing to obtain waves with a steep face above the mean water level.

The various methods produced a wide range of waves. Figure 5 shows the theoretical average shapes of the highest waves most likely to be seen in the given sea states and of a typical steep wave. Notice the symmetry in the highest wave and the antisymmetry in the steep wave.

A measured and theoretical (linear theory) highest wave and measured and theoretical breaking wave are shown in Figures 6a and 6b.

As expected, the breaking wave departs significantly from the underlying linear theory than the highest wave.

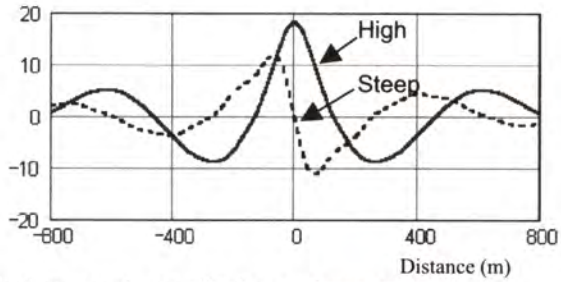

Fig. 5a. Theoretical average shapes of highest and steep waves

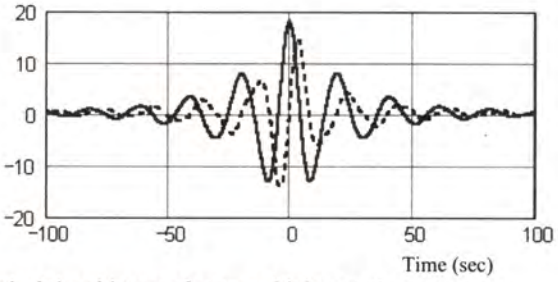

Fig. 5b. Theoretical time history of average highest and steep waves

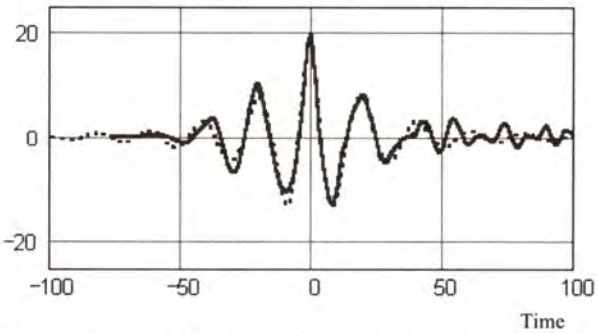

Fig. 6a. Measured highest wave (solid) and linear theory average highest wave (dotted)

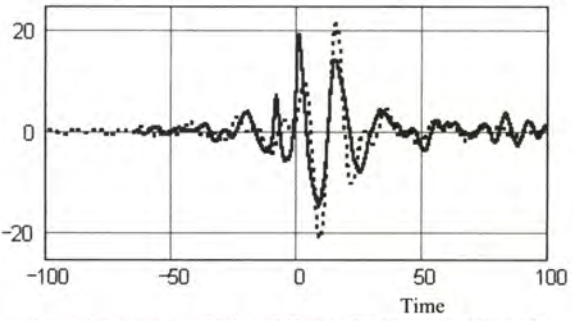

Fig. 6b. Measured breaking wave (solid) and linear theory wave (dotted)

4.3 Model Test Results

Some results from the tests are shown in Figures 7 (forces)and Figure 8 (pressures).

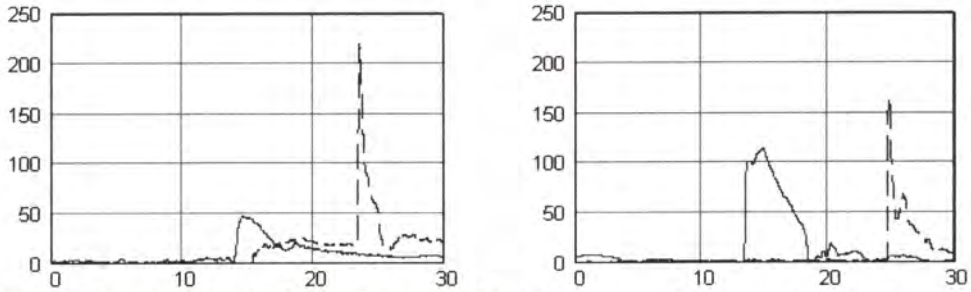

Fig. 7. Force time histories for top (left) and middle (right) segment high waves (solid line) , breaking waves (dashed line)

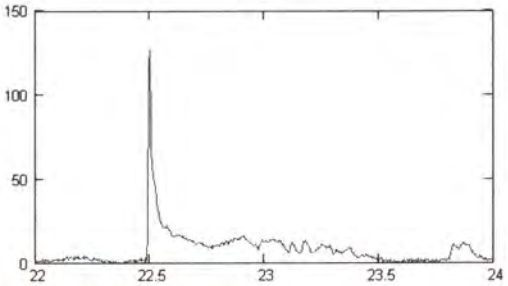

Fig. 8. Pressure time history for breaking waves

Qualitatively, breaking wave slams load large parts of the bow approximately simultaneously and result in much higher pressures, forces and dynamic responses than the 'progressive slam' in a non breaking waves, where the impact moves across the bow.

From the model tests a large table of pressures and forces for different steepness waves, was obtained and this was interpreted in conjunction with full scale wave data.

5 Interpretation of Results

The results were interpreted as follows:

- Determine the probability of occurrence of the different slam events.
- Determine the likely structural response to these loads, including dynamic effects, which may differ from the dynamic response of the model.
- Check local strength, by comparing equivalent static pressures against capacity of bow plating and scantlings. (The equivalent pressures are static pressures which have the same effect as the complicated spatial/time history of the actual dynamic load. The equivalent pressure varies according to the plate or area of stiffened plating being assessed.)

- Check global strength by comparing the total equivalent load on the forecastle structure with its capacity.

Wave front steepness is important for wave slam but there is much less data on wave front steepness than on wave height. The best source found was Myrhaug and Kjeldsen, [1]. They estimate crest front steepness using crest elevation, crest rise time and wave period from the following formulas, which is exact for a regular sinusoidal wave.

$$\varepsilon = \frac{\eta}{\left(\frac{g}{2\pi}\right) \cdot T_{rise} \cdot T} \tag{1}$$

Myrhaug and Kjeldsen, [1], give the joint probability of high and steep fronted waves within a sea state based on wave-rider buoy measurements. However it is clear that more data on extreme wave shapes is needed, owing to the following limitations in the wave front steepness data:

- Data based on wave rider buoy results which is thought to under-predict steepness of extremely steep fronted waves.
- Limited amount of data (6,000 waves) offshore Norway.
- Poor statistical fit for extrapolation to steepness of tank test waves.
- Some reports from mariners suggest that steep faced waves may be more common.

Also crest height, rather than overall wave height would be a more useful parameter.

The probabilities of some of the highest and breaking waves, based on comparison with the Myrhaug and Kjeldsen data, [1], are given in Table 1.

Table 1. Frequency of occurrence of highest and breaking waves

Sea State	Highest Wave		Breaking Wave	
	Steepness(1)	Frequency(2)	Steepness(1)	Frequency(2)
18.0m, 14.4s	1.80	680	3.79	16.6×10^6
14.6m, 11.0s	2.10	9,000	3.76	13.8×10^6
20.2m, 15.3s	1.74	460	5.50	8.7×10^{15}
22.0m, 15.9s	1.48	120	8.21	7.5×10^{31}

Notes: 1) Non-dimensional steepness [1]; 2)Frequency of exceedence once in number of waves shown. (900 corresponds to about 1 in 3 hrs, 120 to about one every 25mins. Data based on extrapolated wave rider buoy records offshore Norway

From the work it has been found that 'progressive' impacts, from non-breaking waves, have a relatively long duration compared with stiffener/plate natural periods and therefore result in a quasi-static response to the load. Breaking waves can lead to

a simultaneous loading over a large area during the impact event and this can cause a significant dynamic response. Fortunately the probability of large breaking waves appears to be very low.

The tank tests included dynamic response, but the scaled natural frequencies were lower than estimated for the prototype. Correcting to the actual period showed that only a moderate dynamic amplification would be expected in likely progressive impact events.

The mass of water in contact with the structure increases natural periods significantly, although the increase is mode shape dependent.

Although waves were run for a number of model pitch angles the pressures were found to relatively insensitive to the angle.

The model was fixed in the tank so the effect of ship motion was allowed for by calculation. The vessel motions were estimated in irregular waves. It was found that the bow motion was much less than wave particle velocities, so the effect of bow velocity was relatively small. However the instantaneous bow draft, affects the relative crest elevation and hence the part of the bow subject to high loads. The bow tends to be pitched up for an impact in longer period, higher waves, but down for an impact in shorter period sea states.

The results of the analysis are shown in Table 2.

Table 2. Pressures on bow plating and scantlings

Component	Peak Pressure(1)	Equivalent Static Pressure(2)	Design Pressure(2)
Longitudinal Scantlings Plating	110 te/m^2	95 te/m^2	100 te/m^2
Upper Bow Stiffeners	110 te/m^2	70 te/m^2	75 te/m^2
Lower Bow Stiffeners	110 te/m^2	60 te/m^2	55 te/m^2
Notes: 1) Peak pressures from progressive slam events; 2) Equivalent pressures over each component allowing for dynamic effects and movement of water surface across structure. (Pressures used when strengthening bow structure.).			

6 Further work

Considerable further work is required to determine a methodology for the prediction of wave impact design pressures and loads. Vessel motion, green sea loading and impact are being considered by the on-going EPSRC and SAFEFLOW projects, with full floating models. For a moving ship, the average profile 'New Wave' approach is less useful than for the fixed bow modelled here because the characteristics of the particular sequence of random waves will affect the ship motion and the resulting loading. Therefore random wave time histories are being used instead. For the EPSRC work these time histories are constrained to have a specified extreme event at a speci-

fied position in the tank so that only short (nearly) random time histories should be required. The results from the EPSRC project will be made available to the SAFE-FLOW project. The SAFEFLOW project will provide design guidance for bow and deck wave impact design. It has a duration of three years from January 2001, but an initial phase of project will be completed in one year.

References

1. Myrhaug D. and Kjeldsen S. P., 1987, *Prediction of occurrences of steep and high waves in deep water*, J. Waterways, Port, Coastal and Ocean Engineering, ASCE, Vol 113, No 2, pp128-138.
2. Tromans P.S., Anaturk A.R. and Hagemeijer P., 1991, *A new model for the kinematics of large ocean waves*, Proc 1st Offshore and Polar Engineering Conference, Edinburgh.

Capsize Resistance and Survivability When Smaller Vessels Encounter Extreme Waves

Bruce Johnson

NAOE Department, U. S. Naval Academy,
Annapolis, MD, USA
telephone: +1 301-262-8519, fax: +1 410-293-2219
aronj@bellatlantic.net

Abstract. The presentation begins with a review of the 1998 Sydney-Hobart Race in which it was reported that "yachts that experienced problems or encountered difficulties and even those that continued racing reported that exceptional waves were responsible for inflicting the damage or causing severe knockdowns. These waves were always a minimum of 20% and up to 100% bigger than the prevailing seas and always came from a direction other than the prevailing wave pattern." [21]
The presentation discussed two capsize modes:

1. Loss of waterplane area (hull form) stability on a wave crest in steep waves and/or spilling breakers, a high risk for improperly designed and or loaded vessels in storms and
2. Wave impact capsize caused by a plunging extreme wave, a lower risk for stable vessels in storms, i.e. being in the wrong place at the wrong time during a low probability event.

Short video clips of small vessel full-scale and model capsizes were included in the presentation.

1 Introduction

The Society of Naval Architects and Marine Engineers (SNAME) is organizing a new ad-hoc panel on fishing vessel operations and safety whose goals include investigating the feasibility of establishing risk-based fishing vessel stability criteria appropriate to the type of vessel and its operating area [11] [15].

1. Identify hazards associated with small vessel capsizes and sinkings and develop guidelines to reduce wave impact damage and personal injuries.
2. Work with NOAA and the international meteorological and oceanographic communities to improve predictions of dangerous local wave conditions
3. Suggest ways to improve survivability for smaller vessels and their crews when they encounter extreme waves.

The IMO voluntary fishing boat safety regulations for vessels > 79 feet (24 m) in length are based on one-size-fits-all criteria derived from computer generated static stability righting-arm curves. The current version is known as the

1993 Torremolinos Protocol and can be found on the IMO web site. (For technical and historical details on its development see [2], [10], [15], [18] and [19]. The Torremolinos Protocol has been criticized 1) for lacking "rational criteria" ([18], [19], [27], [11]) and 2) for promoting capsize resistance at the expense of operational safety conditions on board ([4],[5], [28] and [29]).

Existing voluntary guidelines for fishing vessel stability are intended to provide significant capsize resistance for the vessel during storms that contain few rogue waves. Satisfying the voluntary IMO Torremolinos criteria for fishing vessels longer than 24 meters, for example, does not provide the capability to survive a direct hit by rogue waves or by other extreme (breaking) waves. Capsize resistance criteria for fishing vessels generally do not address or insure crew survivability, which frequently involves escaping from a vessel that is stable while inverted. In addition crew members who abandon a vessel in a major storm can be in danger of life threatening capsizes in many types of life rafts. Of the six men who died in the 1998 Sydney-Hobart sailboat race, three were attempting to survive in a life raft that capsized repeatedly in extreme waves.

2 Capsize and Extreme Wave Research on Smaller Vessels

Most capsize research concerning vessels of all sizes has concentrated on loss of waterplane area (hull form) stability on a wave crest in steep waves and/or spilling breakers. ([16], [3], [11], [28] and [29]. See also an excellent review of the 2000 Stability Conference in [1]).

On the other hand, much yacht capsizing research has concentrated on wave impact capsizes caused by extreme breaking waves, thought to be a primary cause during the 1979 Fastnet Race disaster. ([17], [25], [26], [9], [31]). These studies showed that in beam seas, the location of the vessel relative to the breaking position of the wave is critical. If the vessel is caught in the curl of a plunging breaker, or in the secondary wave created by the jet impact of the plunger, capsize is possible in waves as small as 1.2 times the beam of the vessel. The roll moment of inertia is also an important parameter because a vessel with a large value of this parameter will roll to a smaller angle on impact but expose the deckhouse and work area to the full impact of the plunging wave jet. More recently, experiments on multihull capsizing (Deakin 2001) and the re-righting of sailing yachts in waves ([24]) have been investigated.

Part of the capsize research effort suggests that the experimenter attempt to characterize the asymmetry of the breaking wave by analyzing the wave parameters suggested by Kjeldsen ([22], [6], [7], [14], [32]).

As discussed at the Rogue Wave 2000 Conference ([23]), open ocean rogue waves appear to be short-lived and the probability of measuring one from a single platform record is small. During the 1998 Sydney-Hobart race as reported in [13] from which the adjacent Figure 10 is taken, the Esso Kingfish-B platform located in the Bass Strait measured no waves more than twice the significant

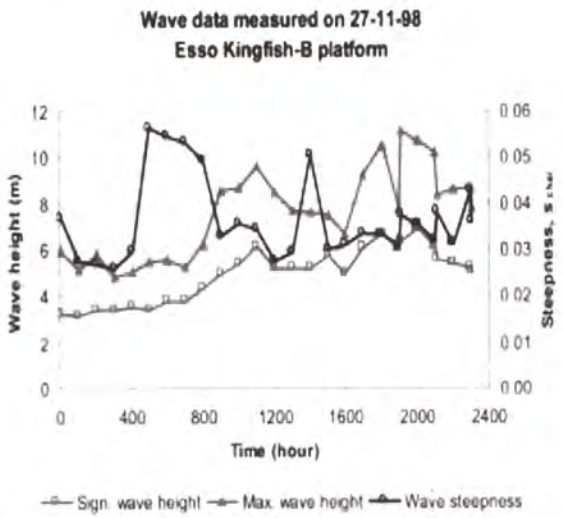

Fig. 1. Wave height (significant and maximum) and direction in eastern Bass Strait [See also Appendix CP]

wave height, even though the participants reported many very large breaking waves during the race (Note that the date is incorrect and should be 27-12-98).

3 Future Work

The long range goal is to create a fishing vessel research program to develop a new set of scalable non-dimensional parameters for designing and building safer fishing vessels ([3], [4], [8]). In order to experimentally determine fishing vessel design parameters, which improve survivability in a severe seaway, a new "free-to-broach" towing rig will be developed. This rig will allow models of a series of existing and proposed new fishing boat designs to be investigated for capsizing resistance while towed under computer control to a region of the tank where computer-generated irregular waves are combined with deterministic steep waves produced by wave energy concentration ([25], [14], [8], [20] and several methods presented at the Rogue Wave 2000 conference). This technique avoids using radio-controlled models which are difficult to position precisely in capsizing wave conditions. It should also be useful for validating attempts to mathematically model the surf-riding phenomenon, [30]. Towing models in quartering seas should shed light on the dynamic stability characteristics of several classes of fishing vessels, improving on the zero-speed beam-sea capsize testing previously done at the Naval Academy on sailing yachts ([26], [31]) and the USCG 44 ft and 47 ft Motor Life Boats, [32].

It is expected that the effects of variations in length, beam, draft, freeboard, sheer line, bulwark and deckhouse arrangements and loading conditions can be

correlated with a new set of design parameters for increasing fishing boat safety in a variety of situations, [4].

References

1. Belenky, Vadim, L.: Seventh International Conference on the Stability of Ships and Ocean Vehicles (STAB' 2000) - A Review, Marine Technology, Vol. 38, No. 1 (January 2001) 1-8
2. Bird, H. and Morrall, A.: Research Towards Realistic Stability Criteria. Proceedings of the International Conference on the Safeship Project: Ship Stability and Safety, RINA, London (9-10 June 1986)
3. Blume, P.: On Capsize Model Testing. Proceedings of the U. S. Coast Guard Vessel Stability Symposium, New London, CT (March 15-17, 1993)
4. Boccadamo, G., Cassella, P, Russo Krauss, G, and Scamardella, A.: Analysis of I.M.O. Stability Criteria by Systematic Hull Series and by Ship Disasters. Proceedings of the 5th International Conference on Stability of Ships and Ocean Vehicles (STAB 94), Melbourne, Fl. USA (1994)
5. Boccadamo, G., Cassella, P., and Scamardella, A.: Stability, Operability and Working Conditions on Board Fishing Vessels. Proceedings of the 7th International Conference on Stability of Ships and Ocean Vehicles (STAB 2000), Launceston, Tasmania, Australia (7-11 February 2000)
6. Bonmarin, P. and Ramamonjiarisoa, A.: Deformation to Breaking of Deep Water Gravity Waves. Experiments in Fluids, vol 2, (1984) 1-6
7. Bonmarin, P.: Some Geometric and Kinematic Properties of Breaking Waves. Rogue Wave 2000 Conference, Brest, France (November 29-30, 2000)
8. Buckley, W.H.: Stability Criteria: Development of a First Principles Methodology. Proceedings of the 5th International Conference on Stability of Ships and Ocean Vehicles (STAB 94), Melbourne, Fl. USA (1994)
9. Claughton, A. and Handley, P: An Investigation into the Stability of Sailing Yachts in Large Breaking Waves. University of Southampton Ship Science Report No. 15 (January 1984)
10. Cleary, W.: The Regulation of Ships Stability Reserve. Proceedings of the U. S. Coast Guard Vessel Stability Symposium, New London, CT (March 15-17, 1993)
11. Dahle, E. A., and Myrhaug, D.: Risk Analysis Applied to Capsize of Fishing Vessels. Marine Technology, Vol. 32, No. 4 (October 1995) 245-257.
12. Deakin, B.: Model Tests to Study Capsize and Stability of Sailing Multihulls. Proceedings of the 15th Chesapeake Sailing Yacht Symposium, Annapolis, MD (January 26-27, 2001)
13. deKat, Jan O: Dynamics of Vessel capsizing in Critical Wave Conditions. Workshop on Safety of Ocean Racing Yachts, Sydney (28 March 1999)
14. Duncan, J.H., Wallendorf, L. A. and Johnson, B.: An Experimental Investigation of the Kinematics of Breaking Waves. Proceedings of the IAWR Seminar on Wave Analysis in Laboratory Basins (1-4 Sept. 1987) 411-422.
15. Dyer, M.G.: Hazard and Risk in the New England Fishing Fleet. Marine Technology, Vol. 37, No. 1 (2000) 30-49
16. Grochowalski, S.: Investigation into the Physics of Ship Capsizing by Combined Captive and Free-Running Model Tests. SNAME Transactions (1989) 169-212
17. Kirkman, K.: On the Avoidance of Inverted Stable Equilibrium. AIAA/SNAME Ancient Interface XIII (1983)

18. Kobylinski, L.: Methodology of the Development of Stability Criteria on the Basis of Risk Evaluation. Proceedings of the 5th International Conference on Stability of Ships and Ocean Vehicles (STAB 94), Melbourne, Fl. USA (1994)
19. Kobylinski, L.: Stability Standards - Future Outlook, Proceedings of the 7th International Conference on Stability of Ships and Ocean Vehicles (STAB 2000), Launceston, Tasmania, Australia (7-11 February 2000)
20. Kriebel, D.L. and Alsina, M.V.: Simulation of Extreme Waves in a Background Random Sea. Proceedings of the Tenth International Offshore and Polar Engineering Conference, Seattle, USA (28 May - 2 June, 2000)
21. Mundle, R.: Fatal Storm: The Inside Story of the Tragic Sydney-Hobart Race. International Marine/McGraw-Hill (1999)
22. Myrhaug, D. and Kjeldsen, P.: Parametric Modeling of Joint Probability Density Distributions for Steepness and Asymmetry in Deep Water Waves. Journal of Coastal Engineering, Amsterdam (1983)
23. Olagnon, M. and van Iseghem, S.: Some cases of observed rogue waves and attempts to characterize their occurrence conditions. Proceedings of the Rogue Wave 2000 Conference, Brest France (29-30 November 2000)
24. Renilson, M., Binns, J. R., and Tuite, A.: The Re-Righting of Sailing Yachts in Waves - A Comparison of Different Hull Forms, Proceedings of the 15th Chesapeake Sailing Yacht Symposium, Annapolis, MD (January 26-27, 2001)
25. Salsich, J.O., Johnson, B., and Holton, C.: A Transient Wave Generation Technique and Some Engineering Applications. Proceedings of the 20th American Towing Tank conference (1983a)
26. Salsich, J. and Zseleczky, J. J.: Experimental Studies of Capsizing in Breaking Waves. AIAA/SNAME Ancient Interface XIII (1983b)
27. Umeda, N., and Ikeda, Y.: Rational Examination of Stability Criteria in the Light of Capsizing Probability. Proceedings of the 5th International Conference on Stability of Ships and Ocean Vehicles (STAB 94), Melbourne, Fl. USA (1994)
28. Umeda, N., Matsuda, A., Hamamoto, M. and Suzuki, S.: Stability Assessment for Intact Ships in the Light of Model Experiments. J. of Marine Science and Technology, SNAJ, Japan, Vol. 4 (1999) 45-57
29. Umeda, N. and Matsuda, A.: Broaching in Following and Quartering Seas - Theoretical Attempts and New Prevention Device. Proceedings of the 7th International Conference on Stability of Ships and Ocean Vehicles (STAB 2000), Launceston, Tasmania, Australia (7-11 February 2000)
30. Vassalos, D. and Maimun, A.: Broaching-To: Thirty Years On, Proceedings of the 5th International Conference on Stability of Ships and Ocean Vehicles (STAB 94), Melbourne, Fl. USA (1994)
31. Zseleczky, J.J.: Evolving Methods for Estimating Capsize Resistance in Breaking Waves. SNAME New England Sailing Yacht Symposium, New England (March 1988)
32. Zseleczky, J.J. and Cohen, S.H.: Model Tests to Evaluate the Capsize Resistance of a Motor Lifeboat in Breaking Waves. 22nd American Towing Tank Conference, St. Johns, Newfoundland (1989)

ONSTREAM JIP: FPSO Design Optimisation through Structural Reliability Analysis Methods

Valerie Quiniou-Ramus and Brian Campbell

Noble Denton Europe Ltd., Noble House, 131 Aldersgate Street,
London EC1A 4EB, UK
Tel: +44 (0)20 7606 4961 - Fax: +44 (0)20 7606 5035
onstream@nodent.co.uk, http://www.nobledenton.com

Abstract. Walk-on discussion for the Rogue Waves 2000 Workshop – Brest, 23-30/11/2000. This paper presents the OnStReAM Joint Industry Project and how it relates to Rogue Waves and to the need for a better knowledge and modelling of the environment.

1 Presentation of the JIP

Noble Denton Europe Ltd is about to launch the ONSTREAM JIP with the support of the Health and Safety Executive (HSE) in the UK. The aim of the JIP is to provide guidance on FPSO design Optimisation through Structural Reliability Analysis Methods.

The project team will benefit from Noble Denton's unique blend of actual floating production project experience (e.g. Roncador, Agbani, Banff, Foinhaven and Schiehallion) together with cutting edge risk, safety and reliability based research. The project team will also include external consultants in order to provide input on issues regarding overall FPSO design and operation, naval architecture and structural reliability analysis.

At present the "fast track" nature of the FPSO developments have meant that "good practice" from a number of specialisms has been brought to bear on the complete system design without having the opportunity to integrate or balance the reliability levels of different sub-systems which combine to produce the FPSO. The ramifications of this lack of integration are amplified by the fact that there is a relatively large number of structural limit states present in FPSO design, when compared to fixed structures, leading to greater difficulty in understanding true safety levels. To name but a few, Hull Midship Section design, Station Keeping design, Bow Structure design against Slamming, Deck and Topsides design against Greenwater, etc.

This lack of integration, at the design stage, and resulting problems are typified by the fact that a number of FPSOs currently operating in the UKCS were not completed either within budget or schedule. If this is not significant enough, even after coming

on stream a number of FPSOs have suffered from either falling short of expectations or experiencing structural damage during operation, leading to production downtime.

As a result, the need has been identified to ascertain the reliability of each critical structural limit state relating to FPSO design and to evaluate the consequences of failure on personnel, environment, production and repair / replacement. This will make it possible to integrate the risks associated with each limit state, and therefore to calculate the overall system reliability of an FPSO and to pin-point the most critical limit states in order to optimise the whole system.

Obvious benefits of this study include an optimisation of the system safety and reliability, together with the enhancement of the system performance and the achievement of a balanced risk throughout the field life of the development. This will induce capital and/or operating cost benefits on FPSO components leading to more efficient designs and a reduction in repair costs and their associated loss of production periods.

2 Assessment of the Probability Distribution Function Associated to the Wave

The reliability assessment of each limit state starts with the identification of all parameters involved in their design, in order to evaluate all possible sources of uncertainty. Major parameters are typically those which are environment related and in particular the wave. When conducting reliability analysis, probability distribution functions are associated to the different variables. Environment distributions are usually derived from metocean data deemed relevant to the locations under consideration. Hindcast environmental data may be supplied for this task. Where appropriate, joint probability models, e.g. linking wind, wave and current events, are developed and applied to the analysis in order to avoid conservatisms. In most cases, an FPSO is designed to withstand a 100-year return environment, and the use of typical wave spectrum (JONSWAP, Pierson-Moskovitch) is a common practice. Nevertheless, exceptional storms and expected wave events are possible: how do they compare with the statistical 100-year return wave event? Are they still predictable using second order wave modelling?

For illustration, let us focus first on hull midship section design. The evaluation of this limit state is a balance between the resistance – the hull midship section's strength – and the load – still water and wave-induced bending moments and shear forces.

For this limit state, the main relevant input parameters are: FPSO main characteristics (L, B, lightship displacement and Centre of Gravity), structural data (steel yield, scantling and stiffener distribution, welds, corrosion), wave data (Tp and Hs, spectrum, direction) and operational data (storage amount and distribution).

Few of the International Rules are tailor-made for the FPSO. It therefore, often becomes necessary to refer to the Rules for Ships (sea-going vessels) or Mobile Offshore Units, which have a larger empirical / historical background and are broadly approved "rules of thumb" but are not always relevant for the issues encountered by FPSOs. They usually provide the engineers with several formulae for the evaluation

of design Wave Bending Moments (hog and sag) and Shear Forces and minimum required section modulus or strength, as a function of an effective wave height which is dependent on the vessel's length only. The Rules also influence the choice of the hull scantling. They give some nominal indications on the plate thickness decreasing with time to make allowances for corrosion. Finally, permissible stresses have to satisfy the Rule requirements (safety factors).

In the document HSE OTO 98164 (Faulkner, [1]), it is claimed that though IACS (International Association of Classification Society) Unified Standard aims to unify the Rules' requirements, there is still a large diversity in the design wave-induced bending loads and in their interpreted reliability. In that document, 8 rules have been compared (see Fig.). For a given probability of exceedance Pe, say 10^{-8}/wave, the ratio of the highest calculated design wave-induced moment Mw to the lowest is 1.8. In addition, for a given Mw, Pe varies by 4 orders of magnitude in sag and 3 orders in hog.

It is worth noticing however that the Rules now offer computer-based design (3D Finite Element Analysis) as an alternative. Use of this direct design in place of the usual rule of thumb, and provided the computer programs are accurately checked, is likely to improve the consistency in the reliability levels achieved through design.

Nevertheless, the reliability level itself could be improved only if the environmental loading is better assessed. This is even more necessary for Bow Structure design against Slamming loads or Deck and Topside design against Greenwater, where the wave height and profile are critical parameters.

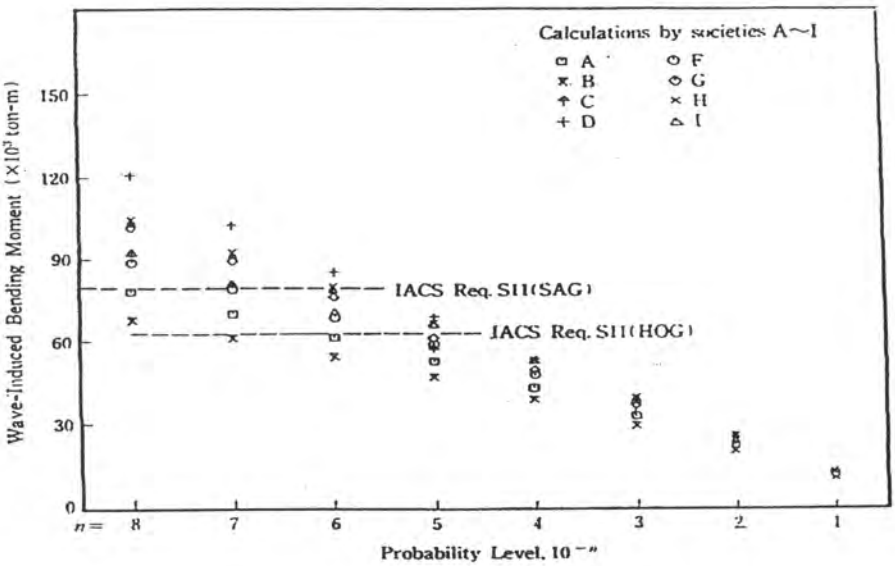

Fig. 1. Eight classification society plots of different wave bending probabilities for the same container ship and route (copied from report HSE OTO 98164)

To cope with the lack of understanding on probability of exceedance of a given sea-state and a given vessel response, Research Institutes and companies in the Oil Industry ought to work together. There is a need to improve our knowledge on these unexpected or "Rogue" waves, to develop adapted joint distribution functions for these events, and to develop design tools to be used when designing an FPSO. This would considerably help in optimising FPSO designs.

References

1. Faulkner, D.: Reliability Based Design and Assessment of FPSO structures. HSE OTO 98164 (November 1998)

Session 2

State-of-the-art Modelling of the Surface Elevation and Near Surface Field Kinematics

Statistics of Wave Crests from Second Order Irregular Wave 3D models

Marc Prevosto

IFREMER Centre de Brest
B.P. 70, F-29280 Plouzané, France
Marc.Prevosto@ifremer.fr
WWW home page: http://www.ifremer.fr/metocean/

Abstract. The statistics of the elevation and kinematics of waves in real seas are very rarely accessible from *in-situ* measurements which induced very high costs. An alternative to the actual waves observation is to derive from the spectral climatology of waves, completed with other environmental data like the wind and the current, the statistics of the individual waves. But this requires accurate models of irregular gravity waves which take into account all the main nonlinearities and interactions with the local wind, current and bathymetry. In a first step, methodologies have been based on second order irregular wave 3D models and have supplied the engineers with new better accurate models of statistics of wave crests. These models do not include yet the complex interactions with wind and current but participate to the improvement of the tools for the design of offshore structures.

1 In-Situ Measurements

The statistics of the elevation and kinematics of waves in real seas have been greatly based for specific site studies on *in-situ* measurements (North-Sea and Gulf of Mexico oil fields). The incomparable great quality of a measurement is that it includes all the physical phenomena, but unfortunately also those which corrupt the actual observation of waves (mooring behavior and transfer function for buoys, fouling effect for plunged or underwater probes, sea foam or spray effect). To this list will be added the problems of spatial integration, calibration and data transformation and transmission. So it becomes difficult to clean the measurements without degrading the extreme or unexpected events. Moreover the wave instruments furnish point measurements and so the instrumentation might be very expensive and long to build accurate statistics, making cost and duration time not always compatible with the constraints of the project on the site. Apart for some very rich data base, measurements will be used to analyze typical situations and to validate or invalidate models.

So the question is: *Is it reasonably possible to build accurate statistics of wave kinematics from wave measurements?* The answer is obviously *No!* Apart for some very extensive data base (e.g. North-Sea and Gulf of Mexico oil fields).

The alternative issue is then: *Is it reasonably possible to build accurate statistics*

of wave kinematics from wave models? This is what attempt to answer a lot of works this last ten years mainly in using nonlinear irregular wave 3D models.

2 Power Spectra versus Wave by Wave

More and more information on waves are restricted to information on energy. The hindcast models use better wind fields and assimilate larger amount of data (e.g. satellite). They use better models of generation, interaction and dissipation and profit by the always increasing power of the computers. The satellites, too, furnish spectral information with the SAR (directional spectrum) or the altimeters (Hs).

The so-called "Wave forecast" of the Meteorological Offices consists in the forecast of sea states (Hs, main direction or directional spectrum) and the step to forecast the corresponding stochastic information on the wave kinematics, is a giant step if we know that we have to collect information and to input in the stochastic models local currents, winds and bathymetry and to take into account complex phenomena, nonlinearities and breaking effects. To take such a giant step, the addition of small steps will be necessary, some of them have been already taken that we describe hereafter.

The advantages of working with the spectral information is that this information i) is available all over the world (limited to the grid of the models or to the time- space sampling of the satellite tracks), ii) has been collected or computed for several years (up to 40 years for the hindcast models and 15 years for the satellites), iii) is available in forecast problems thanks to forecast wind fields as input of wave hindcast models. The difficult passage from spectral to wave by wave information is illustrated in Fig. 1.

3 Methodologies for Statistics

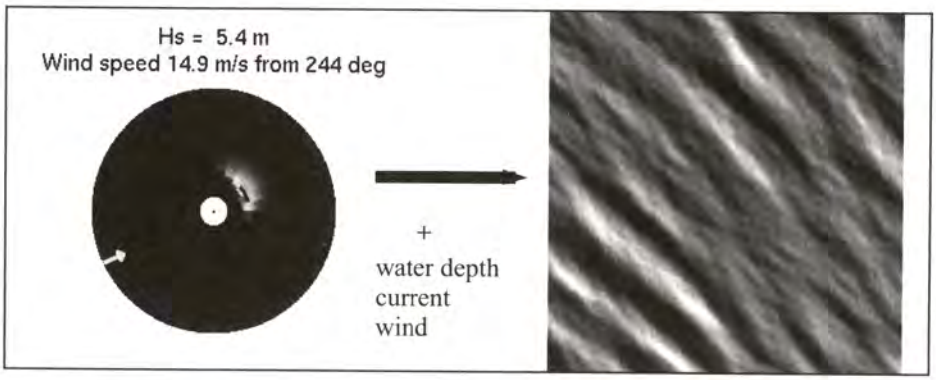

Fig. 1. From directional spectra to wave kinematics [See also Appendix CP]

The methodologies to furnish statistics of waves inside a sea state starting from spectral information are of different kinds. They can be based on Monte Carlo techniques and development of simulators (Forristall [3,10], Prevosto [8,10]), or derived from theoretical considerations: Transformed Gaussian process method (Rychlik [11]), First Order Reliability Method (FORM) (Tromans [13]).

Starting from measurements or from simulation or theoretical methodologies, simplified parameterized models based on a fitting procedure have been proposed as better practical tools for the engineers.

In any case, independently of the methodology, the answers will differentiate from the model of irregular gravity waves taken as starting point.

3.1 Linear Model

The simplest linear model of superposition of Airy waves used the directional spectral density $S(\theta,f)$ as statistical information on the variance of the amplitudes of the components.

$$\eta_i(t) = \sum_{\theta,f}\left[b(\theta,f)sin(2\pi f)+c(\theta,f)cos(2\pi f)\right] = \\ = \sum_{\theta,f}\left[a(\theta,f)sin(2\pi f+\phi(\theta,f))\right] \tag{1}$$

with b and c Gaussian random variables defined by

$$\mathrm{E}\left[b^2(\theta,f)\right] = \mathrm{E}\left[c^2(\theta,f)\right] = S(\theta,f)d\theta df \tag{2}$$

and

$$\mathrm{E}\left[b(\theta_i,f_j)c(\theta_k,f_l)\right] = 0 \tag{3}$$

This model furnishes a Rayleigh law as the law of the crest heights.

$$\mathrm{P}(C>c) = exp\left(-8\frac{c^2}{H_S^2}\right), \text{ with } H_S = 4\sqrt{\iint S(\theta,f)d\theta df} \tag{4}$$

3.2 Non Linear Models

Wave height considered as the crest-trough amplitude (and this definition could be extended to other parameters, e.g. crest-trough pressure, crest-trough velocity as soon as kinematics is studied under the mean water level) are influenced by the steepness nonlinearity at one higher order of magnitude than the crest or trough amplitudes. This explain the good fitting and quality of models of wave heights based on the linear assumption.

But more complicated models have to be considered to take into account the

strong effect of the nonlinearities on the crest amplitudes (or other amplitude of the kinematics), e.g. the hybrid model (Zhang [15]), the Creamer-transformation (Creamer [1]) or the Stokes 5th order correction (Dawson [2]). But as an intermediate way, which take into account the wave spreading, irregular 2nd order 3D models have been extensively used and validated for the last years.

3.3 Stokes 2nd Order Based Models

2nd Order Directional - 3D Wave Model. The 2nd order Stokes expansion based on the linear part (Eq. 1) is

$$\begin{aligned}\eta_2(t) = &\sum_{\theta_i, f_j, \theta_k, f_l} \Big\{ a(\theta_i, f_j)\, a(\theta_k, f_l)\, T^D(\theta_i, f_j, \theta_k, f_l) \times \\ &\times \cos\Big(2\pi\big(f_j - f_l\big) + \big(\phi(\theta_i, f_j) - \phi(\theta_k, f_l)\big)\Big)\Big\} \; + \\ + &\sum_{\theta_i, f_j, \theta_k, f_l} \Big\{ a(\theta_i, f_j)\, a(\theta_k, f_l)\, T^S(\theta_i, f_j, \theta_k, f_l) \times \\ &\times \cos\Big(2\pi\big(f_j + f_l\big) + \big(\phi(\theta_i, f_j) + \phi(\theta_k, f_l)\big)\Big)\Big\} \; - c_{\eta_2},\end{aligned} \tag{5}$$

where $-c_{\eta_2}$ is a constant to ensure that $\mathrm{E}\left[\eta_2(t)\right] = 0$. Moreover, the two second order transfer functions T^S and T^D of course depend of the water depth. Their expressions are given in appendix 1.

2nd Order Uni-Directional - 2D. If now we consider a uni-directional wave train in which all the components propagate in the same direction, we obtain, of course, the same linear part of the elevation

$$\eta_1(t) = \sum_{\theta, f} a(\theta, f)\, sin\big(2\pi f + \phi(\theta, f)\big) = \sum_{f} a_u(f)\, sin\big(2\pi f + \phi_u(f)\big) \tag{6}$$

but a different second order part in applying Eq. 5 with $a(\theta, f) = a_u(f)$, $\phi(\theta, f) = \phi_u(f)$ and $\theta_i = \theta_k = 0$, and calculating $T_u^S\left(f_j, f_l\right)$, $T_u^D\left(f_j, f_l\right)$.

3.4 Crest Height Probability Distribution

Mainly focussed on the aim to produce simple parametric models corresponding to unidirectional or directional sea states and to infinite to intermediate water depths, some authors proposed and fitted crest height probability distribution models based on perturbations of the laws of the linear case. Some used measurements, others the Stokes 2nd order irregular waves models.

Jahns and Wheeler. This model is based on a nonlinear transformation of a Rayleigh law, where the transformation is dependent of the crest height normalized by water depth (Jahns & Wheeler [5]). This model has been fitted later from measurements (Haring & Heideman [4]). It appears clearly wrong in infinite depth where it tends to the Rayleigh law. The fitting used wave staff measurements in the Gulf of Mexico and Waverider measurements in the North Sea.

$$\mathbf{P}\left(C > c \middle| H_s; h\right) = exp\left(-8\frac{c^2}{H_S^2}\left(1 - 4.37\frac{c}{h}\left(0.57 - \frac{c}{h}\right)\right)\right) \tag{7}$$

Derived Narrowband Models. Some other models were derived from a narrowband model of the 2D second order irregular waves model. This model obtained from Eqs 1 and 5, in the 2D case, is valid if the spectral density is sufficiently narrow to consider the 2nd order transfer functions as constant. In this case, $T_u^D\left(f_j, f_\ell\right)$ (resp. $T_u^S\left(f_j, f_\ell\right)$) are considered constant and equal to $T_{nb}^D\left(f_m\right)$, (resp. $T_{nb}^S\left(f_m\right)$), with

$$T_{nb}^D\left(f_m\right) = \lim_{\substack{f_j \to f_m \\ f_\ell \to f_m}} T_u^D\left(f_j, f_\ell\right), \text{ and } T_{nb}^S\left(f_m\right) = \lim_{\substack{f_j \to f_m \\ f_\ell \to f_m}} T_u^S\left(f_j, f_\ell\right) \tag{8}$$

where f_m a mean frequency to be defined. This gives for the second order part

$$\begin{aligned}\eta_2(t) = {} & T_{nb}^D\left(f_m\right)\sum_{f_j, f_\ell} a_u\left(f_j\right)a_u\left(f_\ell\right)cos\left(2\pi\left(f_j - f_\ell\right) + \left(\phi_u\left(f_j\right) - \phi_u\left(f_\ell\right)\right)\right) \\ & + T_{nb}^S\left(f_m\right)\sum_{f_j, f_\ell} a_u\left(f_j\right)a_u\left(f_\ell\right)cos\left(2\pi\left(f_j + f_\ell\right) + \left(\phi_u\left(f_j\right) + \phi_u\left(f_\ell\right)\right)\right) \\ & - T_{nb}^D\left(f_m\right)\sum_{f_j} a_u^2\left(f_j\right) .\end{aligned} \tag{9}$$

If $\eta_1(t)$ is considered as a product of an amplitude and a phase time function, $\eta_1(t) = A(t)cos\left(\Omega(t)\right)$, where the amplitude and instantaneous frequency are slowly varying, the unidirectional narrowband second order part becomes

$$\begin{aligned}\eta(t) = {} & A(t)cos\left(\Omega(t)\right) + \\ & + T_{nb}^D\left(f_m\right)A^2(t) + T_{nb}^S\left(f_m\right)A^2(t)cos\left(2\Omega(t)\right) + \frac{1}{8}H_S^2 T_{nb}^D\left(f_m\right) .\end{aligned} \tag{10}$$

The formulas for T_{nb}^D and T_{nb}^S are given in appendix 2. If we consider that the envelope varies sufficiently slowly, the crest occurs at instant t_c when $\Omega\left(t_c\right) = 0$. Then the crest height given by the linear part is $A\left(t_c\right)$, and the crest height at second order is

$$A_{nonlin}(t_c) = A(t_c) + \left(T_{nb}^{D}(f_m) + T_{nb}^{S}(f_m)\right)A^2(t_c) - T_{nb}^{D}(f_m)\frac{H_S^2}{8}, \quad (11)$$

which links linear to nonlinear crest heights by a quadratic transformation:

$$C = C_{lin} + \left(T_{nb}^{D}(f_m) + T_{nb}^{S}(f_m)\right)C_{lin}^2 - T_{nb}^{D}(f_m)\frac{H_S^2}{8}. \quad (12)$$

Tayfun [12], Tung and Huang [14], Kriebel and Dawson (1991) [6], Kriebel and Dawson (1993) [12] and Prevosto *et al.* [9] proposed models based on such a non-linear quadratic relation:

$$C = C_{lin} + \alpha(f_m;h)C_{lin}^2 + \beta = Q(C_{lin}), \quad (13)$$

and on the Rayleigh law for the distribution of the linear crests:

$$\mathbf{P}(C_{lin} > c|H_s) = exp\left(-8\frac{c^2}{H_S^2}\right) \quad (14)$$

So, in a classical way, the distribution of the nonlinear crests is obtained by applying the inverse nonlinear transformation.

$$\mathbf{P}(C > c|H_s;f_m,h) = exp\left(-\frac{8}{H_S^2}\left(Q^{-1}(c)\right)^2\right) \quad (15)$$

The only solution of the inverse transformation is

$$C_{lin} = Q^{-1}(C) = \frac{-1+\sqrt{1+4\alpha(C-\beta)}}{2\alpha} \quad (16)$$

giving

$$\mathbf{P}(C > c|H_s;f_m,h) = exp\left(-\frac{8}{H_S^2}\left(\frac{-1+\sqrt{1+4\alpha(C-\beta)}}{2\alpha}\right)^2\right) \quad (17)$$

The differences between the parametric models proposed by a number of authors come from different choices of $\alpha(f_m;h)$ and β, and different approximations of $Q^{-1}(C)$. All the previous authors apart Prevosto *et al.* [9] take β equal to zero and coefficient of the transformation from second order *regular* Stokes wave. But unfortunately in finite water depth the irregular narrowband models do not tend to the regular model (due to the difference terms), making the Kriebel and Dawson finite depth model not an exact one (Compare Eq. 20 to the sum of Eq. 36 and Eq. 37). Tung and Huang [14] made an error by taking into account in infinite water depth a low frequency part which in fact does not exist (Eq. 36).

Kriebel and Dawson. The Kriebel and Dawson model is based on the second order regular Stokes wave model in infinite or finite depth, giving

$$C = C_{lin} + \frac{1}{2}\frac{R}{H_S}C_{lin}^2 \rightarrow C_{lin} = \left(1 + \sqrt{1 + 2\frac{R}{H_S}C}\right)\frac{H_S}{R} \tag{18}$$

$$\text{with} \begin{cases} R = kH_s f_2(kd) \\ k \leftarrow T_m = 0.95T_p \end{cases} \tag{19}$$

$$\text{and } f_2(kd) = \frac{\cosh kd\left(2 + \cosh 2kd\right)}{2\sinh^3 kd} - \frac{1}{\sin 2kd} \tag{20}$$

Kriebel and Dawson approximated the inverse transformation $Q^{-1}(C)$, first [6] at second order and later [7] with a corrected third order expansion. This induces a problem in the crest distribution when the steepness is strong. These simplifications are not necessary as we know an analytic form of the inverse transformation (Eq. 16).

In infinite depth the exact Kriebel and Dawson model and the Tayfun model are the same. A difference could exist, which comes from the definition of T_m (Eq. 19).

$$\mathrm{P}\left(C > c \middle| H_s, T_p\right) = exp\left(-\frac{8}{H_S^2 k^2}\left(-1 + \sqrt{1 + 2kc}\right)^2\right) \tag{21}$$

The same technique is used in (Dawson [2]) with a 5th order regular expansion. These models, though based in their principle on narrowband assumptions, do not use an exact narrowband Stokes expansion. This induces errors in the models, apart in infinite depth where harmonic and narrowband expansion are the same.

3.5 New Models

Two new models have been recently proposed and take into account the 3D structure of the waves.

Forristall Model. It is based on a perturbated Weibull law with the two parameters written as steepness and Ursell number polynomials (Forristall [3]). Starting from simulations based on a synthetic directional spectrum data base and different water depths, two different sets of coefficients of the polynomials were fitted from 2D and 3D simulations.

$$\mathrm{P}(C > c) = exp\left(-\left(\frac{c}{\alpha H_S^2}\right)^{\beta}\right) \tag{22}$$

$$\text{with } \alpha = \alpha_1 + \alpha_2 S_1 + \alpha_3 U_r, \quad \beta = \beta_1 - \beta_2 S_1 - \beta_3 U_r + \beta_4 U_r^2, \tag{23}$$

where, $S_1 = \dfrac{2\pi H_s}{g\, T_{01}^2}$ is the steepness and $U_r = \dfrac{H_s}{k_{01}^2 d^3}$ is the Ursell number.

The fit on 2D simulations gave

$$\alpha = \frac{1}{\sqrt{8}} + 0.2892 S_1 + 0.1060 U_r, \quad \beta = 2 - 2.1597 S_1 + 0.968 U_r^2. \tag{24}$$

The fit on 3D simulations gave

$$\alpha = \frac{1}{\sqrt{8}} + 0.2568 S_1 + 0.0800 U_r, \quad \beta = 2 - 1.7912 S_1 - 0.5302 U_r + 0.968 U_r^2. \tag{25}$$

The advantage of this model is its simplicity, but it does not take into account variations in the directional spreading.

Prevosto Model. It is based on a nonlinear transformation of a Rayleigh law, where the transformation is based on the narrowband Stokes expansion (Prevosto [10]). The two parameters Hs and mean wavenumber are perturbed to take into account the spectral bandwidth, the directional spreading and the water depth in Eqs 12-14. It has a unique expression in 2D and 3D case.

$$\tilde{H}_s = \alpha_{H_s}, \ldots \tilde{f}_m = \alpha_{f_m}. \tag{26}$$

In looking at different directional spectrum climatologies and different water depths, the α_{H_s} and α_{f_m} formulations have been determined from simulations and theoretical considerations to be:

$$\alpha_{H_S} = 1 - \frac{1}{2}\left(tanh(kd) - 0.9\right)\sqrt{\frac{2}{1+s}}. \tag{27}$$

where s is the power of the equivalent $\cos^{2s}$ directional distribution at the peak frequency, and

$$\alpha_{f_m} = \frac{1}{1.23} \quad \text{with} \quad f_m = \frac{1}{T_{02}} \tag{28}$$

The formulation of α_{H_s} has been chosen to take into account the fact that the effect of the directional spreading on the crest heights is opposite in deep and shallow water (see [8]). This model has the advantage of furnishing a unique expression both the 2D and 3D cases, and so can be adapted to all intermediate situations.

3.6 Comparison of the Models

These models have been compared to the empirical distribution of crest heights calculated from 1000 hours of simulations (3D second order irregular waves model) of a sea-state with parameters (Hs=5m, T_{02}=7s, s=11). Three different water depths have been used (1000m, 30m, 20m). It is clear that in all the cases (Figs. 2-4), Forristall and Prevosto models give very good results. In the deep water case the Haring (Jahns and Wheeler) model is close to Rayleigh and in shallow water the Kriebel models are not at all accurate.

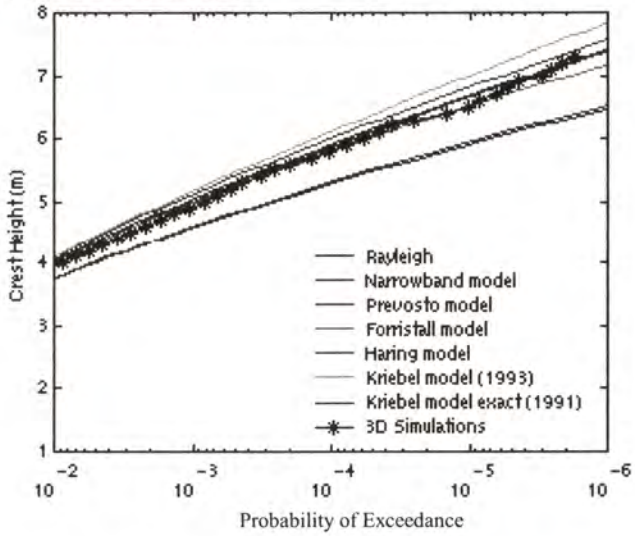

Fig. 2. Water depth 1000 meters [See also Appendix CP]

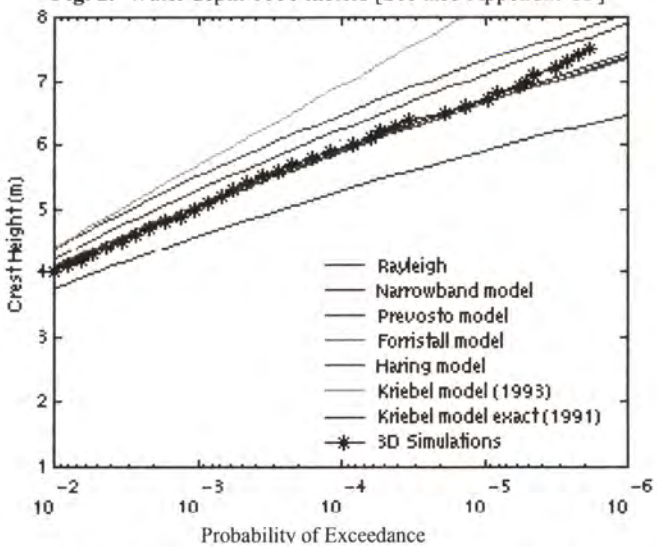

Fig. 3. Water depth 30 meters [See also Appendix CP]

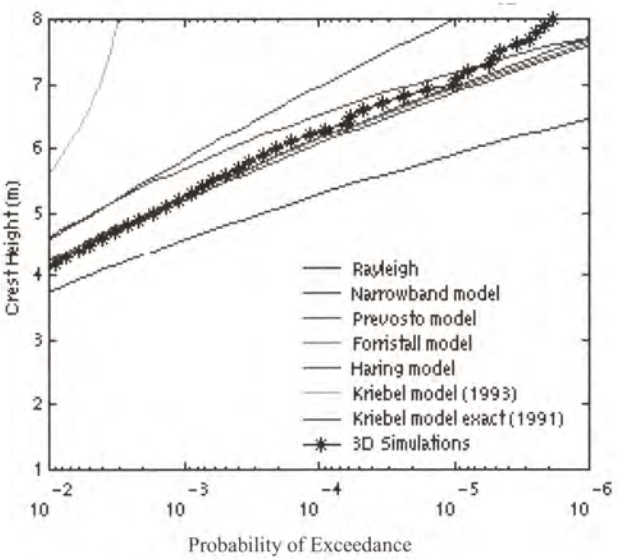

Fig. 4. Water depth 20 meters [See also Appendix CP]

4 Validity of the 2nd Order Models in Extreme Situations

The use of 2nd order models has the advantage to work with simple wave models. If these models are used to calculate design crest heights, their validity has to be proved before using such extreme values.

The biggest crest encountered during the 1000 hours (Fig. 5, red curve), in the 1000 meters water depth case, has a wave height of 12 meters, a crest height of 7.4 meters (1.5 times the Hs), a wave period of 8.5 sec and a crest duration of 4 sec. This wave has a crest shape very close to the breaking limit. In this case the difference between the 2D and 3D models is very small compared to the modification of the shape of the wave due to the 2nd order nonlinearity. If now we consider an harmonic wave with a 5th order expansion giving the same crest height, wave height and crest duration (Fig. 6) we observe that the 2nd order expansion for this very extreme wave is not so far from the higher expansion and that the main improvement in the model is from linear to second order. This, of course, does not validate the distributions based on the 2nd order irregular waves models, but shows that accurate distribution models like the two Forristall and Prevosto models permits in a first step to greatly improve the tools for the design of offshore structures.

A 3D view of this biggest crest is given in Fig. 7, which shows the complexity of the shape and of the slopes of such a wave and so the difficulties to define it as a dangerous or not dangerous wave.

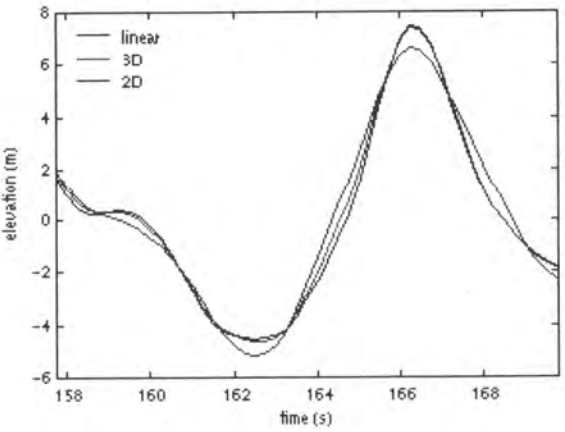

Fig. 5. The biggest crest [See also Appendix CP]

5 Conclusion

As an alternative to the actual waves observation, the use of the spectral information combined with models of irregular gravity waves has permitted to supply the engineers with new better accurate distributions of wave crests. These distributions have been fitted starting from 3D second order irregular waves models. If partly validated for the crest heights, this methodology will not be enough accurate for other parameters of the crest kinematics which ask for higher order expansion. Moreover, the introduction of breaking, local wind and current will introduce certainly modifications in the probability of occurrence of extreme kinematics. But at the moment, to take into account in the irregular wave models local wind and current is a big issue not yet solved, which will be the next step for the improvement of the design tools and to progress in the maritime risk assessment.

References

1. Creamer, D.B., Henyey, F.S., Schult, R., Wright, J.: Improved Linear Representation of Ocean Surface Waves" J. Fluid Mech., **205** (1989) 135-161
2. Dawson, T.H.: Rayleigh Law and Stokes Correction for High Waves in Heavy Seas. US Naval Academy Report (2000) p.11
3. Forristall, G.Z.: Wave Crest Distributions: Observations and Second-Order Theory. Journal of Physical Oceanography, **30**, 8 (2000) 1931-1943
4. Haring, R.E., Heideman, J.C.: Gulf of Mexico Rare Wave Return Periods. Proc. Offshore Technology Conference (1978) 1537–1550, OTC 3230
5. Jahns, H.O., Wheeler, J.D.: Long-Term Wave Probabilities Based on Hindcasting of Severe Storms. J. Pet. Technol. (1973) 473–486

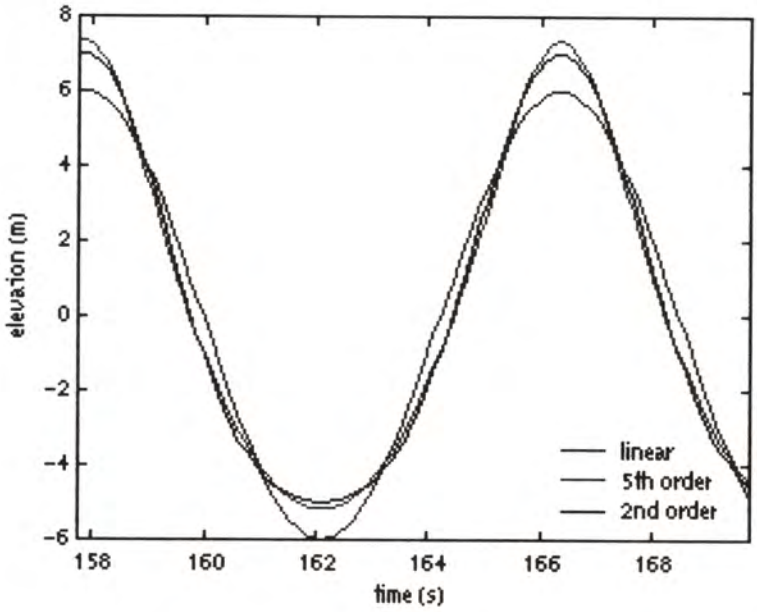

Fig. 6. The equivalent regular wave [See also Appendix CP]

Fig. 7. 3D view of the biggest crest [See also Appendix CP]

6. Kriebel, D.L., Dawson, T.H.: Nonlinear Effects on Wave Groups in Random Seas. J. Offshore Mech. Arctic Eng., no. 113 (1991) 142-147
7. Kriebel, D.L., Dawson, T.H.: Nonlinearity in Wave Crest Statistics. Proc. 2nd Int. Symp. Ocean Wave Measurement and Analysis (1993) 61-75
8. Prevosto, M.: Effect of Directional Spreading and Spectral Bandwidth on the Nonlinearity of the Irregular Waves. Proc. 8th ISOPE Conf., vol. III (1998) 119-123
9. Prevosto, M., Krogstad, H.E., Robin, A.: Probability Distributions for Maximum Wave and Crest Heights. Coastal Engineering, **40** (2000) 329-360
10. Prevosto, M., Forristall, G.Z., (Results of the WACSIS project to be published)
11. Rychlik, I., Johannesson, P., Leadbetter, M.R.: Modelling and Statistical Analysis of

Ocean-Wave Data Using Transformed Gaussian Processes. Marine Structures, **10** (1997) 13-47
12. Tayfun, M.A.: Narrow-Band Nonlinear Sea Waves. J. Geophys. Res., **85**, no. C3 (1980) 1548-1552
13. Tromans, P.S., Taylor, P.H.: The Shapes, Histories and Statistics of Non-Linear Wave Crests in Random Seas. Proc. OMAE Conf. (1998)
14. Tung, C.-C., Huang, N.E.: Peak and Trough Distributions of Nonlinear Waves. Ocean Eng., **12**, no. 3 (1985) 201-209
15. Zhang, J., Yang, J., Wen, J., Prislin, I., Hong, K.: Deterministic Wave Model for Short-Crested Ocean Waves: Part I. Theory and Numerical Scheme. Applied Ocean Research, **21**, no. 4 (1999) 167-188

Appendix 1: Second Order Transfer Functions:

$$T\left(\theta_i f_j, \theta_k f_\ell\right) = \frac{1}{2g}\left(2\left(\omega_j + \omega_\ell\right) D\left(\vec{k}_i, \vec{k}_k\right) + \omega_j\omega_\ell + \omega_j^2 + \omega_\ell^2 - \frac{g^2\,\vec{k}_i\,\vec{k}_k}{\omega_j\omega_\ell}\right) \tag{29}$$

with

$$\vec{k}_i = k_j\,\vec{d}_i,\ k_j = \left|\vec{k}_i\right|,\ \vec{d}_i = \cos\theta_i\,\vec{x} + \sin\theta_i\,\vec{y},\ \left(2\pi f_j\right)^2 = \omega_j^2 = g k_j \tanh\left(k_j h\right) \tag{30}$$

$$\vec{k}_k = k_\ell\,\vec{d}_k,\ k_\ell = \left|\vec{k}_k\right|,\ \vec{d}_k = \cos\theta_k\,\vec{x} + \sin\theta_k\,\vec{y},\ \left(2\pi f_\ell\right)^2 = \omega_\ell^2 = g k_\ell \tanh\left(k_\ell h\right) \tag{31}$$

with h the water depth and

$$D\left(\vec{k}_i, \vec{k}_k\right) = \frac{2\left(\omega_j + \omega_\ell\right)\left(g^2\,\vec{k}_i\cdot\vec{k}_k - \omega_j^2\omega_\ell^2\right) + g^2\left(k_j^2\omega_\ell + k_\ell^2\omega_j\right) - \omega_j\omega_\ell\left(\omega_j^3 + \omega_\ell^3\right)}{2\omega_j\omega_\ell\left(\left(\omega_j + \omega_\ell\right)^2 - g\left|\vec{k}_i + \vec{k}_k\right| \tanh\left(\left|\vec{k}_i + \vec{k}_k\right| h\right)\right)} \tag{32}$$

$$D\left(k\,\vec{d}_i, \omega, k\,\vec{d}_k, -\omega\right) = 0 \tag{33}$$

Appendix 2: Narrow-Band Non Linear Transfer Coefficients

In the formulas below, $\kappa = k_m h$ is the dimensionless water depth, with k_m a mean wavenumber, where

$$\left(2\pi f_m\right)^2 = g k_m \tanh\left(k_m h\right) \tag{34}$$

The expressions for vertical displacement, Eulerian (fixed point) measurements are, in finite or infinite water depth (see [9] for more formulas):

$$T_{nb}^{D}\left(f_m\right) = c_{diff}\left(\kappa\right) k_m, \ldots, T_{nb}^{S}\left(\kappa\right) = c_{sum}\left(\kappa\right) k_m \tag{35}$$

with

$$c_{diff}\left(\kappa\right) = \frac{\Pi\left(\kappa\right) + \kappa\left(1 - \left(\tanh\kappa\right)^2\right)}{\Pi\left(\kappa\right)^2 - 4\kappa \tanh\kappa 2} \qquad c_{diff}\left(\infty\right) = 0 \tag{36}$$

and

$$c_{sum}\left(\kappa\right) = \frac{1}{4}\left(\frac{2 + \left(1 - \left(\tanh\kappa\right)^2\right)}{\left(\tanh\kappa\right)^3}\right) \qquad c_{sum}\left(\infty\right) = \frac{1}{2} \tag{37}$$

where

$$\Pi\left(\kappa\right) = \tanh\kappa + \kappa\left(1 - \left(\tanh\kappa\right)^2\right) \qquad \Pi\left(\infty\right) = 1 \tag{38}$$

A Complete Modal Expansion of the Wave Potential and Its Application to Linear and Nonlinear Water-Wave Problems

G.A. Athanassoulis and K.A. Belibassakis

Department of Naval Architecture and Marine Engineering,
National Technical University of Athens,
PO Box 64033 Zografos, 15710 Athens, GREECE
mathan@central.ntua.gr

Abstract. Under the assumptions of incompressibility and irrotationality, the problem of evolution of water waves over a variable bathymetry region admits of at least two different variational formulations. A *Hamiltonian* one, proposed by Petrov (1964) and exploited further by Zakharov (1968), and an *unconstrained* one, proposed by Luke (1967). The present development is based on *Luke's variational principle*, in which the admissible fields are free of essential conditions, except for smoothness and completeness prerequisites. A complete local-mode series expansion of the wave potential is constructed, which represents exactly the vertical structure of the wave field. This series contains the usual propagating and evanescent modes, plus two *additional modes*, called the *free-surface mode* and the *sloping-bottom mode*, introduced in order to consistently treat the non-vertical end-conditions at the free-surface and the bottom boundaries, respectively. Using this expansion, in conjunction with the variational principle, the original problem is reformulated as a *non-linear coupled-mode system* of second-order differential equations in the propagation (horizontal) space, fully accounting for the effects of non-linearity and dispersion. The main features of this approach are: (i) Various standard models of water-wave propagation are recovered by appropriate simplifications of the coupled-mode system. Among them are included the mild-slope equation(s), the second-order Stokes solutions, and the Boussinesq equation. (ii) In all cases examined, a small number of modes (up to 5 or 7) are enough for the precise numerical solution, provided that the two new modes (the free-surface and the sloping-bottom ones) are included in the local-mode series.

1 Introduction

The interaction of water waves with an uneven bottom topography requires, in principle, the solution of a complicated, nonlinear, free-boundary value problem. A well-known specific feature of this problem is that the propagation space does not

coincide with the physical space. While the latter is the whole liquid domain (an irregularly shaped horizontal strip, in the case of a shallow-sea environment), the former is only the horizontal plane.

Direct numerical solutions of this problem are possible with or without the consideration of viscous effects. The numerical treatment in the framework of Navier-Stokes equations has recently become possible (see, e.g., [7]), being, however, extremely demanding computationally. Usually, the problem is treated in the framework of potential flow [23]. Even under the latter assumption, the complete numerical solution to the non-linear free-surface problem exhibits great difficulties. Several time-domain numerical methods have been developed by various authors. See, e.g., [11], [24], [19], and the survey by Tsai and Yue [23]. In order to improve efficiency, Wang *et al.* [25] proposed a multi-subdomain approach, and Kennedy and Fenton [8] introduced a local polynomial approximation, satisfying the Laplace equation within each subdomain. Still, however, considerable computer requirements limit the use of the above fully non-linear models in practical applications.

On the other hand, there is a vast literature of simplified model wave equations, mainly based on the assumptions of *weak free-surface non-linearity* and *slowly varying bathymetry*. These model equations have more conventional form, permitting the development of relevant theoretical results, and they are more efficient computationally, within the range of their applicability. For example, combining appropriate asymptotic treatment with depth integration, a class of *Boussinesq-type* models is derived, accounting for the effects of weak non-linearity and weak dispersion for shallow water waves. Improved versions of these models with enhanced dispersion characteristics, extending the range of applicability to larger depths and/or variable bathymetry, have been reported by many authors; see, e.g., [13], [18], [10], [9], and the references cited therein. In general, however, these models cannot be relied on as the depth increases, or the bathymetry is not slowly varying. Another important example is a class of models that can be considered as weakly non-linear generalizations of the *mild-slope* equation, e.g., the models developed by Beji and Nadaoka [3], [17], and Tang and Ouellet [22]. These models can describe combined refraction-diffraction of weakly non-linear water waves, but still suffer from the assumption of slowly varying bathymetries.

Our main concern herewith is to develop a non-linear theory for the case of a smooth, generally shaped bathymetry, without imposing any mild-slope type assumptions neither on the free-surface nor on the bottom boundary. Under the assumptions of incompressibility and irrotationality, the problem of evolution of water waves over a variable bathymetry region admits of at least two different variational formulations: A *Hamiltonian* one, constrained on the below-the-surface kinematics proposed by Petrov in 1964 [20] and further developed by Zakharov [27] and his associates; and an *unconstrained* one, proposed by Luke in 1967, [12]. See also [26] and [14]. The present development is based on *Luke's variational principle*, in which the admissible fields are free of essential conditions, except, of course, for the smoothness and completeness (compatibility) prerequisites. The vertical structure

of the wave field is exactly represented by means of a local-mode series expansion of the wave potential. This series contains the usual propagating and evanescent modes, plus two *additional modes*, called the *free-surface mode* and the *sloping-bottom mode*, introduced in order to consistently treat the non-vertical end-conditions at the free-surface and the bottom boundaries, respectively. A similar technique has been successfully applied to the solution of the linearised, [1,2], and the second-order, [4], problems, over variable bathymetry regions, in the frequency domain.

Using the local-mode expansion, in conjunction with the variational principle, the original problem is reformulated as an infinite, non-linear, coupled-mode system of second-order differential equations in the propagation (horizontal) space, fully accounting for the effects of non-linearity and dispersion. Various simplified equations, like *Boussinesq-type* models, in shallow water depth, and *non-linear mild-slope* models, in intermediate depth, can be obtained as limiting forms.

Numerical solutions are presented for the linearised and the second-order coupled-mode system, as a first step towards the numerical treatment of the fully nonlinear problem. The discrete equations are obtained by truncating the local-mode series into a finite number of terms, and by using finite differences for the discretisation of the equations on the horizontal plane. Results for the case of a smooth underwater shoaling with a steep bottom slope, show that the rate of decay of the modal-amplitude functions with respect to the mode number is very fast. This means that a small number of modes (up to 5 or 7) are sufficient to accurately calculate the potential field and its spatial derivatives throughout the liquid domain, justifying the inclusion of the two additional modes into the expansion.

2 Variational Formulation of the Problem

Under the assumptions of incompressibility and irrotationality, the problem of evolution of water waves, propagating over a variable bathymetry region, can be reformulated as a variational equation by means of Luke's variational principle [12]. The admissible fields are free of essential conditions, except, of course, for the smoothness and completeness (compatibility) prerequisites. All the analysis presented in this work can be generalized to $N+1$ spatial dimensions, in short $(N+1)D$, where $(N+1)D = ND\left(\begin{matrix}propagation\\space\end{matrix}\right)+1D\left(\begin{matrix}cross\\space\end{matrix}\right)$. Cf. Friedman and Shinbrot [5,6]. For simplicity, in the sequel, we shall restrict ourselves to the $(1+1)D$ case.

Luke's functional, modeling the homogeneous, nonlinear, water-wave problem, reads as follows:

$$\mathscr{F}_{Luke}[\Phi,\eta] = \int_{t_1}^{t_2}\int_{x_1}^{x_2} dx dt \int_{z=-h(x)}^{z=\eta(x,t)} \left\{ \frac{\partial \Phi}{\partial t} + \frac{1}{2}\left\{ \left(\frac{\partial \Phi}{\partial x}\right)^2 + \left(\frac{\partial \Phi}{\partial z}\right)^2 \right\} + gz \right\} dz \,, \qquad (1)$$

where x is the horizontal and z is the vertical (positive upwards) co-ordinates, $\Phi = \Phi(x,z,t)$ is the velocity potential, and $\eta = \eta(x,t)$ is the free surface elevation. If there is an applied pressure distribution $\bar{p}(x,t)$ on the free surface, and a prescribed (outward) normal velocity $\bar{v}_n(x,t)$ on the bottom surface, then we have to add to Luke's functional (1) the following, forcing-implied functional

$$\mathscr{F}_{forc.}[\Phi,\eta] = \int_{t_1}^{t_2}\int_{x_1}^{x_2} dxdt\, \bar{P}(x,t)\,\eta(x,t) - \int_{t_1}^{t_2}\int_{x_1}^{x_2} dxdt\, \bar{U}\Phi(x,-h,t)\,, \qquad (2)$$

where $\bar{P} = \bar{p}/\rho$, and $\bar{U} = \bar{v}_n\sqrt{1+(\partial h/\partial x)^2}$. The non-homogeneous, nonlinear, water-wave problem is then modeled by requiring the stationarity of the functional

$$\mathscr{F}[\Phi,\eta] = \mathscr{F}_{Luke}[\Phi,\eta] + \mathscr{F}_{forc.}[\Phi,\eta]\,. \qquad (3)$$

More precisely, the variational equation

$$\delta_{\Phi}\mathscr{F} = 0 \;\Leftrightarrow\; \left\{ \begin{array}{ll} \Delta\Phi = 0, & x_1 < x < x_2,\ -h(x) < z < \eta(x;t) \\ \dfrac{\partial\Phi}{\partial x}\dfrac{\partial\eta}{\partial x} - \dfrac{\partial\Phi}{\partial z} + \dfrac{\partial\eta}{\partial t} = 0, & x_1 < x < x_2,\ z = \eta(x;t) \\ \dfrac{\partial\Phi}{\partial x}\dfrac{\partial h}{\partial x} + \dfrac{\partial\Phi}{\partial z} = -\bar{U}, & x_1 < x < x_2,\ z = -h(x) \end{array} \right\}, \qquad (4)$$

models the *water-wave kinematics*, while the variational equation,

$$\delta_{\eta}\mathscr{F} = 0 \;\Leftrightarrow\; \left\{ \frac{1}{2}\left(\frac{\partial\Phi}{\partial x}\right)^2 + \frac{1}{2}\left(\frac{\partial\Phi}{\partial z}\right)^2 + \frac{\partial\Phi}{\partial t} + g\eta = -\bar{P},\ x_1 < x < x_2,\ z = \eta(x;t) \right\}, \qquad (5)$$

models the *water-wave dynamics* (Bernoulli's integral). We shall now proceed with the construction of a complete, local-mode representation of the wave potential, which, in conjunction with the variational equations (4) and (5) can provide us with a coupled-mode system of differential equations with respect to the unknown modal amplitudes and the unknown free-surface elevation.

3 Local-mode Representation of the Wave Potential

Consider a generally-shaped (non-uniform) strip D, extending to infinity in both directions $x \to \pm\infty$, and bounded by the graphs of the functions $z = -h(x)$ ("lower" boundary, sea bed), and $z = \eta(x,t)$ ("upper" boundary, sea surface):

$$D = D[h,\eta] = \{(x,z) : -\infty < x < +\infty,\ -h(x) < z < \eta(x,t)\}. \tag{1}$$

See Fig. 1. The functions $h(x)$ and $\eta(x,t)$ are assumed to be continuously differentiable with respect to x. The free-surface elevation $\eta(x,t)$ is also continuously differentiable with respect to time t, ranging either over the half-line $t \geq t_0$, or over the whole t-axis. The functions h and η satisfy the inequality $-h(x) < \eta(x,t)$, for all $x \in \mathbb{R}$ and all $t \in I$, which ensures the connectedness of the set D.

Let $\Phi(x,z;t)$ be a function defined on $D \times I$, which, for each $t \in I$, is two times continuously differentiable in D, with continuous first derivatives up to and including the boundary of D. Moreover, $\Phi(x,z;t)$ is continuously differentiable with respect to $t \in I$, for $(x,z) \in \bar{D}$. We now state (without proof) the following:

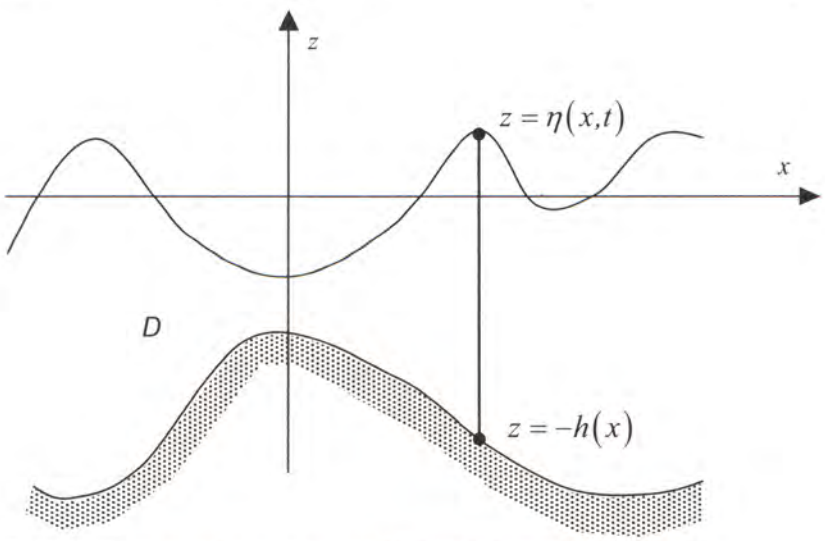

Fig. 1. Water waves propagating over a generally-shaped (non-uniform) strip D.

Theorem 1 [Modal expansion of a smooth function in a non-uniform strip]: Any function $\Phi(x,z;t)\in C^2(D\times I)\cap C^1(\bar{D}\times I)$ admits of the following, uniformly convergent, series expansion:

$$\Phi(x,z;t)=\sum_{n=-2}^{\infty}\varphi_n(x,t)\cdot Z_n\big(z;h(x),\eta(x,t)\big),\qquad (x,z;t)\in D\times I\,, \tag{2}$$

where

$$Z_{-2}(z)=\frac{\mu_0h_0+1}{2(\eta+h)h_0}\cdot(z+h)^2\;-\;\frac{\mu_0h_0+1}{2h_0}\cdot(\eta+h)\;+\;1\,, \tag{3a}$$

is called the *free-surface mode,*

$$Z_{-1}(z)\;=\;\frac{\mu_0h_0-1}{2h_0(\eta+h)}\cdot(z+h)^2\;+\;\frac{1}{h_0}(z+h)\;+\;\frac{2h_0-(\eta+h)(\mu_0h_0+1)}{2h_0}\,, \tag{3b}$$

is called the *sloping-bottom mode,* and

$$Z_0(z;h,\eta)=\frac{cosh\big[k_0(z+h)\big]}{cosh\big[k_0(\eta+h)\big]}\,,\qquad Z_n(z;h,\eta)=\frac{cos\big[k_n(z+h)\big]}{cos\big[k_n(\eta+h)\big]}\,,\qquad n=1,2,3,\ldots\,. \tag{3c,d}$$

The z-independent quantities $k_n=k_n(h,\eta)$, $n=0,1,2\ldots$, appearing in Eqs. (3c,d), are defined as the roots of the transcendental equations

$$\mu_0-k_0\cdot tanh\big[k_0(h+\eta)\big]=0\,,\qquad \mu_0+k_n\cdot tan\big[k_n(h+\eta)\big]=0\,,\qquad n=1,2,3,\ldots\,, \tag{4}$$

where μ_0, $h_0>0$ are positive constants, not subjected to any a priori restrictions.

If, in addition, the depth function $h(\bullet)\in C^1(\mathbb{R})$ and the free-surface elevation $\eta(\bullet,\bullet)\in C^1(\mathbb{R}\times I)$, then, series (2) can be differentiated term-by-term with respect to x, z, and t, leading to series expansions for the corresponding derivatives.

4 The Coupled-mode System

4.1 The Nonlinear Coupled-mode System

The series expansion (3.2) permits us to obtain series representations for the variation $\delta\Phi$ of the wave potential Φ, with respect to the modal amplitudes φ_n and the free surface elevation η. The general form of the total variation of Φ is

$$\delta\Phi(x,z;t)=\sum_{n=-2}^{\infty}\Big(\delta\varphi_n(x;t)Z_n(z;h,\eta)+\varphi_n(x;t)\delta Z_n(z;h,\eta)\Big). \qquad \textbf{(1a)}$$

Since $Z_n = Z_n(z;h,\eta)$ is independent of φ_n, we have, in general,

$$\delta Z_n(z;h,\eta)=W_n(z;h,\eta)\delta\eta, \qquad \textbf{(1b)}$$

where $W_n(z;h,\eta)=\partial Z_n(z;h,\eta)/\partial\eta$. Especially on the free surface, the vertical modes $Z_n = Z_n(z=\eta;h,\eta)$ take the constant value 1. Thus, $\delta Z_n = 0$, on the free surface. Furthermore, the series expansions of the partial derivatives of $\Phi(x,z;t)$, permit us to obtain modal series expansions for all expressions appearing in the right-hand side of Eqs. (2.4,5). Introducing the above series expansions in the variational equation $\delta\mathcal{F}[\Phi,\eta]=0$, and using standard arguments of the calculus of variations, we eventually arrive at the following:

Theorem 2 [The nonlinear coupled-mode system]: Under the additional assumption that $\varphi_n(x;t)$ are twice continuously differentiable with respect to x, the problem (2.4,5) is equivalent with the following coupled-mode system

$$\frac{\partial\eta}{\partial t}+\sum_{n=-2}^{\infty}\left(A_{mn}(\eta)\frac{\partial^2\varphi_n}{\partial x^2}+B_{mn}(\eta)\frac{\partial\varphi_n}{\partial x}+C_{mn}(\eta)\varphi_n\right)=\bar{U}[Z_m]_{z=-h},$$
$$m=-2,-1,0,1,2\ldots, \qquad \textbf{(2a)}$$

$$g\eta+\sum_{n=-2}^{\infty}\left(\frac{\partial\varphi_n}{\partial t}+[W_n]_{z=\eta}\varphi_n\frac{\partial\eta}{\partial t}-\bar{U}[W_n]_{z=-h}\varphi_n\right)-$$
$$-\sum_{\ell=-2}^{\infty}\sum_{n=-2}^{\infty}\left(a_{\ell n}^{(0,2)}(\eta)\varphi_\ell\frac{\partial^2\varphi_n}{\partial x^2}+a_{\ell n}^{(1,1)}(\eta)\frac{\partial\varphi_\ell}{\partial x}\frac{\partial\varphi_n}{\partial x}+b_{\ell n}(\eta)\varphi_\ell\frac{\partial\varphi_n}{\partial x}+c_{\ell n}(\eta)\varphi_\ell\varphi_n\right)=-\bar{P}. \qquad \textbf{(2b)}$$

The matrix-coefficients $A_{mn}(\eta)$, $B_{mn}(\eta)$, $C_{mn}(\eta)$, appearing in Eq. (2a), are expressed in terms of the local vertical modes $\{Z_n\}_{n=-2,-1,0,1,..}$ and their derivatives, as

$$A_{mn}(\eta) = \langle Z_n, Z_m \rangle = \int_{z=-h(x)}^{z=\eta(x;t)} Z_n(z;h,\eta) Z_m(z;h,\eta)\, dz\,, \tag{3a}$$

$$B_{mn}(\eta) = 2\left\langle \frac{\partial Z_n}{\partial x}, Z_m \right\rangle + \frac{\partial h}{\partial x}\left[Z_n Z_m\right]_{-h} + \frac{\partial \eta}{\partial x}\left[Z_n Z_m\right]_{\eta}\,, \tag{3b}$$

$$C_{mn}(\eta) = \langle \Delta, Z_m \rangle + \left[\left(\frac{\partial h}{\partial x}\frac{\partial Z_n}{\partial x} + \frac{\partial Z_n}{\partial z}\right) Z_m\right]_{-h} + \left[\left(\frac{\partial \eta}{\partial x}\frac{\partial Z_n}{\partial x} - \frac{\partial Z_n}{\partial z}\right) Z_m\right]_{\eta} \tag{3c}$$

where $\Delta Z_n = \dfrac{\partial^2 Z_n}{\partial x^2} + \dfrac{\partial^2 Z_n}{\partial z^2}$. The matrix-coefficients $a_{mn}(\eta)$, $b_{mn}(\eta)$, $c_{mn}(\eta)$, appearing in Eq. (2b), are

$$a_{\ell n}^{(0,2)}(\eta) = \langle Z_n, W_\ell \rangle = \int_{z=-h(x)}^{z=\eta(x;t)} Z_n(z;h,\eta) W_\ell(z;h,\eta)\, dz\,, \tag{4a}$$

$$a_{\ell n}^{(1,1)}(\eta) = -\frac{1}{2}\left[Z_n Z_\ell\right]_{\eta} \tag{4b}$$

$$b_{\ell n}(\eta) = 2\left\langle \frac{\partial Z_n}{\partial x}, W_\ell \right\rangle + \frac{\partial h}{\partial x}\left[Z_n W_\ell\right]_{-h} - \left[Z_\ell \frac{\partial Z_n}{\partial x}\right]_{\eta}\,, \tag{4c}$$

$$c_{\ell n}(\eta) = \langle \Delta Z_n, W_\ell \rangle + \left[\left(\frac{\partial h}{\partial x}\frac{\partial Z_n}{\partial x} + \frac{\partial Z_n}{\partial z}\right) W_\ell\right]_{-h} - \frac{1}{2}\left[\frac{\partial Z_\ell}{\partial x}\frac{\partial Z_n}{\partial x} + \frac{\partial Z_\ell}{\partial z}\frac{\partial Z_n}{\partial z}\right]_{\eta}\,. \tag{4d}$$

The above coupled-mode system, Eqs. (2a,b), has been obtained without any simplifications concerning either the nonlinearity or the vertical structure of the wave potential. Thus, the coupled-mode system is equivalent with the initial (complete) formulation, Eqs. (2.4,5), and fully accounts for non-linearity and dispersion.

4.2 Comparison with Other Wave Theories

Various wave theories can be obtained by combining simplifications of the nonlinear equations expressing the physics of the problem, Eqs. (2.4,5), with simplifications of the vertical structure of the wave potential. Various simplifications introduced in the equations (such as linearisation or quadratisation), in conjunction with simplifications introduced in the vertical structure of the wave potential (mean-domain vertical modes or polynomial expansion), lead to various well-known simplified wave models.

A distinctive feature of the present theory is that no simplifications have been introduced for the construction of the nonlinear coupled-mode system. Thus, in principle, all simplified water-wave theories (wave models) are expected to be obtained as appropriate limiting forms of the coupled-mode system, Eqs. (2). For example, keeping only the propagating mode $Z_0(z)$ in the vertical representation and linearising the coupled-mode equations, the *classical mild-slope model,* Smith and Sprinks [21], is obtained. If the evanescent modes $Z_n(z), n=1,2,\ldots$, are also included, the *extended mild-slope model,* Massel [15], is obtained. If we keep only the two polynomial vertical modes $Z_{-2}(z)$, $Z_{-1}(z)$, Eqs. (3.3a,b), in the vertical structure of the wave potential, and retain up to second-order nonlinear terms in the coupled-mode system, the standard *Boussinesq models*, [14,16], are obtained. However, except of rederiving standard wave models, new enhanced ones can be constructed that include: (i) full dispersion and variable bathymetry effects, and (ii) better treatment of the free-surface nonlinearity. Some first examples of the latter category will be briefly presented in the following (sub)sections.

4.3 The Linearised Coupled-mode System

The linearisation of the above coupled-mode system is obtained by suppressing the explicit and implicit non-linearities appearing in Eqs (2), (3) and (4). In this case, the above system reduces to

$$\frac{\partial \eta}{\partial t} + \sum_{n=-2}^{\infty} \left(\tilde{A}_{mn} \frac{\partial^2 \varphi_n}{\partial x^2} + \tilde{B}_{mn} \frac{\partial \varphi_n}{\partial x} + \tilde{C}_{mn} \varphi_n \right) = 0, \qquad m = -2,-1,0,1,2..... \tag{5a}$$

$$g\eta + \sum_{n=-2}^{\infty} \frac{\partial \varphi_n}{\partial t} = 0 \ . \tag{5b}$$

The coefficients $\tilde{A}_{mn}, \tilde{B}_{mn}, \tilde{C}_{mn}$ of the linearised system, appearing in Eq. (5a), are independent from the free-surface elevation η. They are expressed in terms of the

local vertical modes $\{\tilde{Z}_n\}_{n=-2,-1,0,1,..}$, defined on the vertical interval $-h(x) \le z \le 0$. The detailed functional form of $\{\tilde{Z}_n\}_{n=-2,-1,0,1,..}$ is given by Eqs. (3.3), setting $\eta(x;t) = 0$. The specific expressions of the coefficients $\tilde{A}_{mn}$, $\tilde{B}_{mn}$, $\tilde{C}_{mn}$ are as follows

$$\tilde{A}_{mn} = \tilde{A}_{mn}(h) = \left\langle \tilde{Z}_n, \tilde{Z}_m \right\rangle_0 = \int_{z=-h(x)}^{z=0} \tilde{Z}_n(z;h) \cdot \tilde{Z}_m(z;h)\, dz, \qquad \textbf{(6a)}$$

$$\tilde{B}_{mn} = \tilde{B}_{mn}(h) = 2\left\langle \frac{\partial \tilde{Z}_n}{\partial x}, \tilde{Z}_m \right\rangle_0 + \frac{\partial h}{\partial x}\left[\tilde{Z}_n \tilde{Z}_m\right]_{z=-h(x)}, \qquad \textbf{(6b)}$$

$$\tilde{C}_{mn} = \tilde{C}_{mn}(h) = \left\langle \Delta \tilde{Z}_n, \tilde{Z}_m \right\rangle_0 + \left[\left(\frac{\partial h(x)}{\partial x}\frac{\partial \tilde{Z}_n}{\partial x} + \frac{\partial \tilde{Z}_n}{\partial z}\right)\tilde{Z}_m\right]_{z=-h} - \left[\frac{\partial \tilde{Z}_n}{\partial z}\tilde{Z}_m\right]_{z=0}, \qquad \textbf{(6c)}$$

where $h = h(x)$ is the local depth. That is, the coefficients $\tilde{A}_{mn}$, $\tilde{B}_{mn}$, $\tilde{C}_{mn}$, are dependent on the horizontal coordinate x, through the local depth function $h(x)$. By differentiating Eq. (5b) with respect to time it is possible to eliminate the unknown free surface elevation $\eta(x,t)$ from Eqs. (5), and obtain the following linearised coupled-mode system of differential equations with respect to the modal amplitudes $\varphi_n(x,t)$, $n = -2,-1,0,1,...$, alone:

$$\sum_{n=-2}^{\infty}\left(-\frac{1}{g}\frac{\partial^2 \varphi_n}{\partial t^2} + \tilde{A}_{mn}\frac{\partial^2 \varphi_n}{\partial x^2} + \tilde{B}_{mn}\frac{\partial \varphi_n}{\partial x} + \tilde{C}_{mn}\varphi_n\right) = 0, \quad m = -2,-1,0,1,2..... \qquad \textbf{(7)}$$

Two crucial questions concerning the theoretical value and practical effectiveness of the linearised coupled-mode system (LCMS), Eq. (7), (and thus, of the whole analysis presented herewith) are the following:

Q1: How many terms out of the infinite series expansion are enough for a satisfactory solution, or, alternatively, how fast does the infinite local-mode series converge?

Q2: How important are the two newly introduced modes, $\varphi_{-2}(x;t)$ and $\varphi_{-1}(x;t)$, in comparison with the other ones?

Although no rigorous mathematical results concerning the above questions are yet available, the extensive numerical experience of the authors suggests the following answers:

A1: A small number of modes, e.g., 5 to 7, are enough for numerical convergence, even in cases of very steep bathymetry. In fact, numerical results suggest that the following estimate should hold true

$$\max_{\substack{x_1 \le x \le x_2 \\ 0 \le t \le T}} \left|\varphi_n(x;t)\right| = O\left(n^{-4}\right)$$

A2: The first three modes in the series, i.e., the newly introduced ones $\varphi_{-2}(x;t)$ and $\varphi_{-1}(x;t)$, and the propagating mode $\varphi_0(x;t)$, are the most important terms in the series expansion, being one order of magnitude higher than the other modes $\varphi_n(x;t)$, $n = 1,2,3,\ldots$.

5 Applications to the Frequency Domain

5.1 The Time-Harmonic Case

Let us consider first the time-harmonic case, and seek for solutions of the form

$$\varphi_m(x,t) = Re\left\{\overset{o}{\varphi}_m(x,\omega)\cdot exp(-j\omega t)\right\}, \qquad m = -2,-1,0,1,\ldots, \tag{1}$$

where ω is a given angular wave frequency, $\overset{o}{\varphi}_m(x,\omega) \equiv \overset{o}{\varphi}_m(x)$ is the frequency-domain complex-valued modal amplitudes, and $j = \sqrt{-1}$. Differentiating (1) twice with respect to time and substituting to Eq. (4.7), the linearised coupled-mode system reduces to the equation

$$\sum_{n=-2}^{\infty}\left(A_{mn}\frac{\partial^2 \overset{o}{\varphi}_n}{\partial x^2} + B_{mn}\frac{\partial \overset{o}{\varphi}_n}{\partial x} + \left(C_{mn}+\omega^2\right)\overset{o}{\varphi}_n \right) = 0, \qquad m = -2,-1,0,1,2..... \tag{2}$$

If we select the parameter μ_0 (of the vertical eigenproblem) to be the wave frequency parameter $\mu_0 = \omega^2/g$, then, the free-surface mode $\varphi_{-2}(x,t)$ becomes identically

zero, i.e., $\overset{o}{\varphi}_{-2}(x,t) = 0$. Thus, the first row and the first column of the system (4.7) are eliminated. Furthermore, because of the normalization of the vertical eigenfunctions, the last term in the right-hand side of Eq. (4.6c) becomes:

$$\left[\frac{\partial \tilde{Z}_n}{\partial z}\tilde{Z}_m\right]_{z=0} = \left[\mu_0 \cdot \tilde{Z}_n \cdot \tilde{Z}_m\right]_{z=0} = \mu_0, \quad \text{for all } m,n = -1,0,1,2,\ldots \tag{4}$$

Taking into account all the above equations it can be easily seen that the system (2) reduces exactly to the corresponding frequency-domain coupled-mode system presented and studied in [1].

5.2 Second-Order Theories

Second-order versions of the nonlinear coupled-mode system in the frequency domain can be obtained by introducing the following expansion for the amplitudes of the modes $\varphi_m(x;t)$, m=-2,-1,0,... and for the free-surface elevation $\eta(x;t)$:

$$\varphi_m(x;t) = Re\left\{\varepsilon\,\varphi_m^{(1)}(\omega;t)\exp(-i\omega t) + \varepsilon^2\left(\varphi_m^{(20)}(\omega;t) + \varphi_m^{(22)}(\omega;t)\exp(-2i\omega t)\right) + \ldots.\right\}, \quad m\text{=-2,-1,0,..,} \tag{5}$$

$$\eta(x;t) = Re\left\{\varepsilon\eta^{(1)}(\omega;t)\exp(-i\omega t) + \varepsilon^2\left(\eta^{(20)}(\omega;t) + \eta^{(22)}(\omega;t)\exp(-2i\omega t)\right) + \ldots\right\}, \tag{6}$$

where ε is the usual non-linearity parameter (wave steepness). Substituting Eqs. (5) and (6) in the non-linear CMS (4.2) we obtain, at the first order, the linearised system in frequency domain, given by Eq. (2), and at the second-order the corresponding coupled-mode systems concerning the steady problem, for $\left\{\varphi_m^{(20)}, \eta^{(20)}\right\}$, and the double-frequency problem, for $\left\{\varphi_m^{(22)}, \eta^{(22)}\right\}$, respectively. The extension of Stokes theory to variable bathymetry by means of the coupled-mode system in the frequency domain has been studied in detail in [4]. Very satisfactory numerical results have been obtained by using only 6 modes $(m = -2,-1,0,1,2,3)$ in the representation. In Fig. 2 results obtained by the second-order CMS, shown by using crosses, are compared with the standard Stokes theory in constant depth. The comparison concerns the

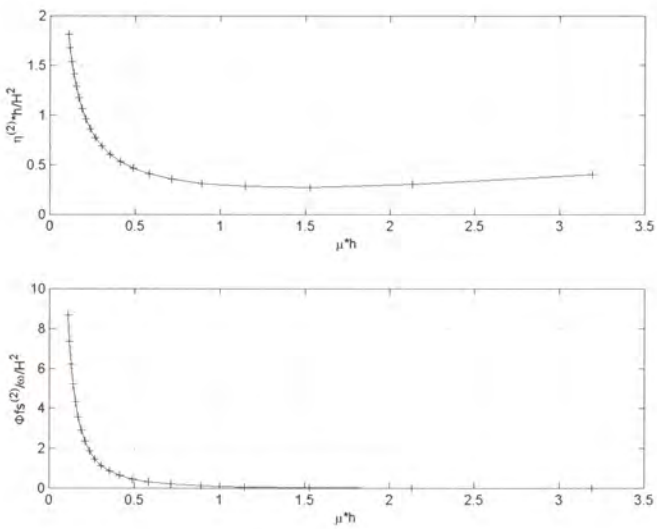

Fig. 2. Comparison of the amplitude of the second-order free-surface elevation and wave potential as obtained by means of the second-order CMS and the standard Stokes theory in constant depth.

second-order double-frequency free-surface elevation and the wave potential at the free surface, for values of the shallowness parameter μh ranging from very shallow to practically deep water.

6 Application to the Time Domain

6.1 Dispersion Characteristics of the Linearised Coupled-mode System

If we restrict ourselves to the constant-depth case, then the sloping-bottom mode $\varphi_{-1}(x,t)$ becomes identically zero, and the coefficient $\tilde{B}_{mn} = 0$. Thus, the time-domain linearised CMS (4.7) takes the form

$$\sum_{\substack{n=-2 \\ n\neq -1}}^{M}\left(-\frac{\partial^2\varphi_n}{\partial t^2}+A_{mn}(\mu_0)\frac{\partial^2\varphi_n}{\partial x^2}+C_{mn}(\mu_0)\varphi_n\right)=0\,,\qquad m=-2,0,1,2...,M\ . \tag{1}$$

In order to investigate the dispersion characteristics of this coupled-mode system, we have to examine if it admits of simple harmonic solutions of the form

$$\varphi_m(x,t)=Re\left\{\overset{o}{H}_m\cdot exp\left(jk\left(x\mp\hat{C}t\right)\right)\right\}, \tag{2}$$

and, to find out the functional dependence (in non-dimensional form) of the quantity $\hat{C}/\sqrt{gh}=\hat{\mathscr{C}}(kh)$, where $\hat{C}$ is the phase speed of this harmonic solution, and h is the constant depth considered. Recall that, in the case under examination, the exact form of the dispersion relation is $C/\sqrt{gh}=\mathscr{C}(kh)=\sqrt{tanh(kh)/kh}$. Thus, the question is how good the system (1), when applied in the frequency domain, can reproduce the exact dispersion relation. Clearly, the dispersion characteristics of the coupled-mode system are dependent on the choice of μ_0 and also are affected by the truncation of the infinite system. To emphasize this fact, we write $\hat{\mathscr{C}}(kh)=\hat{\mathscr{C}}(kh;\mu_0,M)$.

By introducing the representation (2) to the linearised CMS (1) we obtain the algebraic system

$$\sum_{\substack{n=-2 \\ n\neq -1}}^{M}\left(k^2A_{mn}(\mu_0)+\left(C_{mn}(\mu_0)+k^2\hat{C}^2\right)\right)\ =\ 0\,. \tag{3}$$

Nontrivial solutions of the latter are obtained by requiring its determinant to vanish, which can be then used for calculating $\hat{\mathscr{C}}(kh)$ and comparing with the analytical result $\mathscr{C}(kh)$. Fig. 3 presents such a comparison, for $\mu_0 h=0.25$, and various truncations of the infinite system. It is clearly shown that the inclusion of the free-surface mode in the representation dramatically improves the convergence to the exact solution. That is, if we include the propagating mode the free-surface mode and a small number (1 to 3) of evanescent modes, the dispersion curve $\hat{\mathscr{C}}(kh)$ is in fine agreement with the exact one. Thus, a few modes (≈ 6) are sufficient for modelling fully dispersive waves in variable bathymetry regions, without any mild-slope

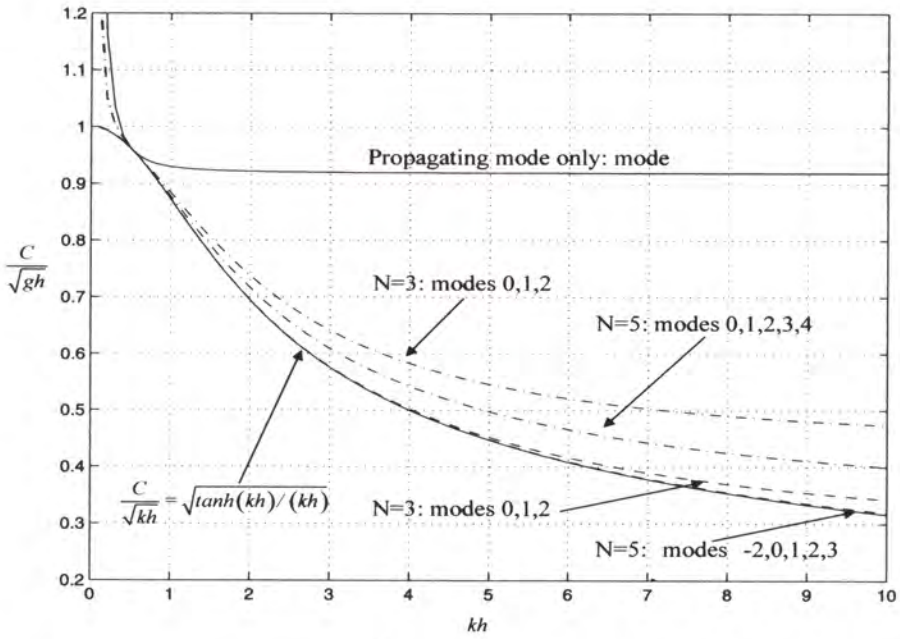

Fig. 3. Dispersion characteristics of the coupled mode system for $\mu_0 h = 0.25$, using the representation (3.2) without (dash-dot lines) and with (dashed lines) the free-surface mode.

assumptions. Let it be noted that this finding is compatible with the requirements concerning the convergence of the wave field at the bottom boundary, after the introduction of the sloping-bottom mode, for bottom slopes up to and above 100%!

6.2 Numerical Solution of the Linear Problem

As an example, we consider an environment characterised by the (monotonically varying) depth function shown in Fig. 4, which represents a smooth, but locally very steep, underwater shoaling (region 2), joining a water layer of 6m depth (region 1) with a shallower water layer of 2m depth (region 3). This bathymetry has also been studied in [1] in connection with the application of the linearised coupled-mode system in the frequency domain. The maximum bottom slope of the above shoaling is 95% and the mean bottom slope is 20%. Numerical results for this bottom geometry, and for an incident monochromatic wave of period T=3.14sec are presented in Fig. 4, at various instants.

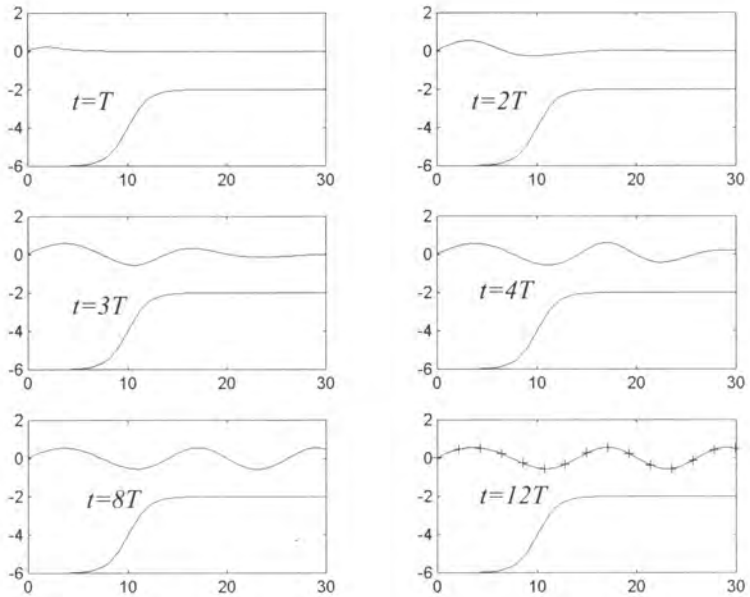

Fig. 4. Application of the linearised coupled-mode system to a smooth, but very steep shoaling. The continuous lines show the free surface elevation obtained by the direct numerical solution of the CMS (4.7) in the time domain, starting from rest, with harmonic forcing. In the last plot the crosses indicate the results obtained by the linearised CMS in the frequency-domain, Eq. (5.2).

In the examined case both shallowness ratios $h_1/\lambda_1 = 0.394$ and $h_3/\lambda_3 = 0.167$ fall well outside the limits of the deep or the shallow water theory. A total number of 6 modes have been retained in the local-mode representation (3.2) and the coupled-mode system has been discretised using finite differences. Starting from rest, the calculated wave after about 12 periods (t=12T), has fully converged to the harmonic solution [1], shown in the last plot by using crosses. In all cases examined the rate of decay of modal amplitudes φ_n in variable bathymetry regions is found (numerically) to exhibit a very rapid decay $\max|\varphi_n| = O\left(n^{-4}\right)$, fully justifying the inclusion of the two additional modes (the free-surface mode and the sloping-bottom mode) into the expansion. It is interesting to note that similar calculations without the two additional modes, i.e., keeping only the modes $\varphi_0, \varphi_1, ..., \varphi_M$, have shown that, in this case, $\max|\varphi_n| = O\left(n^{-2}\right)$. Thus, the additional modes make the convergence of the series

much faster, probably by summing the slowly convergent parts of the infinite series representation of the sought-for solution.

6.3 Applications to Nonlinear Problems

A direct numerical solution of the general nonlinear system (4.2) has not been tried yet. As a first step towards understanding the behaviour of this system, a weakly non-linear (second-order) time-domain variant, in variable bathymetry, has been constructed and studied. Numerical results and details will be presented elsewhere.

7 Conclusion

In the present work we consider the problem of non-linear gravity waves propagating over a general bathymetry. A complete local-mode series expansion of the wave potential has been developed and used, in conjunction with Luke's variational principle, to reformulate the original problem is as an infinite, coupled-mode system of equations in the propagation (horizontal) space. The present local-mode expansion represents exactly the vertical structure of the wave field. The series contains the usual propagating and evanescent modes, modelling the internal kinematics, plus two additional modes, the *free-surface mode* and the *sloping-bottom mode*, introduced in order to consistently treat the non-vertical end-conditions at the free-surface and the bottom boundaries, which model the boundary kinematics. The resulting coupled-mode system fully accounts for the effects of non-linearity and dispersion, in intermediate and shallow water depth.

References

1. Athanassoulis, G.A. & Belibassakis, K.A.: A Consistent Coupled-Mode Theory for the Propagation of Small-Amplitude Water Waves over Variable Bathymetry Regions. J. Fluid Mech. **389** (1999) 275-301
2. Athanassoulis, G.A. Belibassakis, K.A. & Gerostathis, Th.P.: A Coupled-Mode Theory for the Diffraction of Water Waves by Localized Scatterers Superimposed over a Parallel-Contour Bathymetry. Proc. 5th Int. Conf. on Mathematical and Numerical Models of Wave Propagation, SIAM (2000) 719-724.
3. Beji, S & Nadaoka, K.: A Time-Dependent Nonlinear Mild-Slope Equation for Water Waves. Proc. R. Soc. Lon. A **453** (1997) 319-332.
4. Belibassakis, K.A. & Athanassoulis, G.A.: Extension of Second-Order Stokes Theory to Variable Bathymetry (2000) submitted.
5. Friedman, A. & Shinbrot, M., The Initial Value Problem for the Linearized Equations of Water Waves. J. Math. And Mech. **17** (1967), 107-180.

6. Friedman, A. & Shinbrot, M., The Initial Value Problem for the Linearized Equations of Water Waves, II. J. Math. And Mech. **19** (1969), 1177-1193.
7. Huang, C.-J. & Dong, C.-M.: Wave Deformation and Vortex Generation in Water Waves Propagating over a Submerged Dike. Coastal Engng **37** (1999) 123-148
8. Kennedy, A.B. & Fenton, J.D.: A Fully Non-Linear Computational Method for Wave Propagation over Topography. Coastal Engng **32**, (1999) 137-161
9. Kirby, J.T.: Nonlinear, Dispersive Long Waves in Water of Variable Depth. In: Hunt, J.N. (ed.): Gravity Waves in Water of Finite Depth. Computational Mechanics Publications (1997)
10. Liu, P.L-F.: Model Equations for Wave Propagation from Deep to Shallow Water. In. Liu, P.L.-F (ed.): Advances in Coastal and Ocean Engineering. World Scientific (1995)
11. Longuet-Higgins, M.S. & Cokelet, E.D.: The Deformation of Steep Surface Waves on Water. I: A Numerical Method of Computation. Proc. R. Soc. Lon. A**350** (1976) 1-25
12. Luke, J.C.: A Variational Principle for a Fluid with a Free Surface. J. Fluid Mech. **27** (1967) 395-397
13. Madsen, P.A. & Sorensen, O.R.: A New Form of Boussinesq Equations with Improved Linear Dispersion Characteristics. 2. A Slowly Varying Bathymetry. Coastal Engng **18** (1992) 183-204
14. Massel, S.: Hydrodynamics of Coastal Zones. Elsevier, Amsterdam (1989)
15. Massel, S.: Extended Refraction-Diffraction Equations for Surface Waves. Coastal Engng **19** (1993) 97-126.
16. Mei, C.: The Applied Dynamics of Ocean Surface Waves, World Scientific (1986).
17. Nadaoka, K., Beji, S. & Nakagawa, Y.: A Fully Dispersive Weakly Nonlinear Model for Water Waves. Proc. R. Soc. Lon. A **453** (1997) 303-318
18. Nwogu, O.: Alternative Form of Boussinesq Equations for Nearshore Wave Propagation. J. Wtrwy., Port, Coast. and Oc. Engng. ASCE, **119** (1993) 618-638
19. Ohhyama T. & Nadaoka, K.: Development of a Numerical Wave Tank for Analysis of Nonlinear and Irregular Wave Field. Fluid Dyn. Res,. **8** (1991) 231-251-22.
20. Petrov, A.A.: Variational Statement of the Problem of Liquid Motion in a Container of Finite Dimensions. PMM, **28** (4), (1964) 917-922
21. Smith, R. & Sprinks, T.: Scattering of Surface Waves by a Conical Island, J. Fluid Mech. **72** (1975) 373-384.
22. Tang, Y. & Ouellet, Y.: A New Kind of Nonlinear Mild-Slope Equation for Combined Refraction-Diffraction of Multifrequency Water Waves. Coastal Engng., **31** (1997) 3-36
23. Tsai, W. & Yue, D.K.: Computation of Nonlinear Free-Surface Flows. Ann. Rev. Fluid Mech., **28** (1996) 249-278
24. Vinje, T. & Brevig, P.: Numerical Simulation of Breaking Waves. Adv. Water Resources, **4** (1981) 77-82
25. Wang, P., Mirie, R. & Tulin M.: An Efficient Numerical Tank for Nonlinear Water Waves, Based on the Multi-Subdomain Approach with BEM. Int. J. Numer. Meth. Fluids, **20** (1995) 1315-1336
26. Witham, G.B.: Linear and Nonlinear Waves. Wiley, New York (1974)
27. Zakharov, V.E.: Stability of Periodic Waves of Finite Amplitude on the Surface of a Deep Fluid. J. Appl. Math. Tech. Phys., **2** (1968) 190

Nonlinear Wave Interaction and Its Applications to the Analysis of Steep Ocean Waves

Jun Zhang

Ocean Engineering Program, Department of Civil Engineering, Texas A&M University, College Station, Texas 77843-3136, USA
Jzhang@civilmail.tamu.edu

Abstract. Interactions among free waves result in bound waves, which may significant affect resultant wave properties in a steep ocean wave field. Since the measurements actually record the resultant properties, the presence of bound waves makes it inaccurate to analyze the measurements of steep ocean waves based on linear spectral methods. To overcome this difficulty, Hybrid Wave Models (HWM) developed recently, separate bound waves from free waves in the decomposition of an irregular wave field as well as the prediction of its resultant properties. To ensure the convergence, the HWMs selectively use the conventional and phase modulation approaches to address the nonlinear interactions between free waves of different frequency ratios. The models are able to decompose a wave field accurately and hence can predict the wave properties accurately and deterministically based on the time-series measurements. Examples of their applications to the analyses of laboratory and field measurements are given to demonstrate the usefulness of HWMs.

1 Introduction

An ocean wave field consists of free (or linear) and bound waves. Free waves obey the dispersion relation. Due to the nonlinear nature of surface water waves, free waves interact among themselves and result in bound waves that do not obey the dispersion relation. Linear spectral methods assume ocean waves as a superposition of many free (or linear) waves. In applying them to the estimate of irregular wave properties based on measurements, bound waves are approximated as free waves of the same frequency in the decomposition of a measured wave field and then nonlinear interactions among free waves are ignored in the calculation of wave properties. When ocean waves are not steep, free waves are dominant in almost entire frequency range and a linear spectral method may offer a fairly good approximation. When they are steep, free waves near the spectral peak frequency still remain dominant but bound waves become dominant or comparable to free waves in the frequency ranges either much lower or higher than the peak frequency [21]. It is known that the relationship between the elevation and potential amplitudes of a free wave is quite different from that of a bound wave of the same frequency. The approximation of bound waves in linear spectral methods may result in large discrepancies.

Existing high-order nonlinear methods may accurately quantify high-order nonlinear effects based on free waves (e.g., [17], [3]). However, they do not address

the first approximation made in linear wave spectral methods, that is, to separate bound waves from free waves based on measurements. In reality, the records of a wave field are always related to resultant wave properties, that is, the superposition of free and bound waves. Hence, free waves of a wave field are usually unknown when the measurements are given. For accurate analysis of measurements, nonlinear wave effects have to be considered in the decomposition of a wave field into free waves. The focus of this paper is on wave models allowing for nonlinear wave interactions in the decomposition of ocean waves and their applications.

Before a measured wave field is decomposed into its free waves, the effects contributed from bound waves must be calculated and then subtracted from the corresponding measurements. However, in order to compute bound waves, free waves need to be known. Therefore, the process of decomposition is achieved through iterative processes and the convergence of the iteration is critical. When ocean waves are steep and of a broad-banded spectrum, the interactions may occur between free waves of either close frequencies or quite different frequencies. To ensure the truncated solutions are convergent, both conventional and phase modulation approaches are employed to derive the solutions for bound waves [21]. Since the wave models are based on two different perturbation approaches, they are named as Hybrid Wave Models (HWM). Once the free waves are known, the resultant wave properties in the vicinity of the measurements can be obtained as the superposition of free and bound waves. The most important nonlinear effects of wave-wave interactions are of second order in wave steepness. The HWMs are accurate up to second order at least. Their extension to include third-order nonlinear effects can be made although it is not trivial.

2 Numerical Scheme of HWM

A HWM was initially developed for unidirectional irregular waves. The water depth is assumed to be uniform and intermediate to free waves nearby the spectral peak frequency and deep to the free waves of frequencies significantly higher than the spectral peak frequency. The solutions for the interaction between two free waves were derived in deep water using both conventional and phase modulation perturbation approaches [20] and later extended to allow for water of intermediate depth [2]. These studies showed that the solutions obtained using the two different approaches are identical if the frequencies of the two interacting free waves are close. If their frequencies are quite different, the solution obtained using the conventional approach may diverge while that of the phase modulation approach remains convergent. Therefore, in an irregular wave field consisting of many free waves, the HWM calculates the interactions between free waves of close frequencies using the conventional solution and those between free waves of quite different frequencies using the phase modulation solution. The related formulations were given in [21] and are omitted here for brevity.

Nonlinear wave-wave interactions may become significant when both interacting free waves are of large wave steepness. To simplify the computation, only interactions of significant effects are considered. For the purpose of applying

conventional and phase modulation approaches, a spectrum is divided into three regions: a very-low frequency region, a ``powerful" region including all relatively large-amplitude free waves, and a high-frequency (tail) region, as sketched in Fig. 1. By the definition, free waves located in both very-low frequency and tail regions have relatively small amplitudes (or steepnesses), and any interactions involving one of these components are not significant and hence ignored. The powerful region is further divided into three (or more) bands: the long-wave band which usually includes the spectral peak, and short-wave bands 1 and 2. The frequencies of free waves within the same band are close and the interactions between them are computed using the conventional approach. The frequencies of free waves located in different bands are usually quite different and the interactions between them are computed using the phase modulation approach. It is known that the modulation of a short wave by a long wave is much more significant than the influence of the short wave on the long wave[20]. Therefore, the subtraction of the bound-wave effects from the measured wave properties is conducted in the order from low- to high-frequency bands.

At the beginning of the decomposition, the free-wave amplitude and initial phase spectra are approximated by the corresponding resultant wave spectra given based on the FFT of measured time-series. Bound waves resulting from the interactions among the free waves in the long-wave band are computed using the conventional approach and then subtracted from the resultant spectra. The modified spectra are closer to the free-wave spectra. If the maximum difference in the long-wave band of the two modified spectra of consecutive iterations is smaller than a prescribed error tolerance, the subtraction of nonlinear effects due to the interaction between the free waves in the long-wave band is accomplished and the decomposition of short-wave band 1 starts. Otherwise the interactions between the long-band free waves are re-computed based on the most recent modified spectra and then subtracted from the measured spectra.The procedure for the decomposition of the short-wave bands is different from that for the long-wave band. The modulation of the short-wave band 1 by the long-wave band is calculated first using the phase modulation approach and subtracted from the modified spectra. The interactions among the free waves of the short-wave band 1 are then computed using the conventional approach and subtracted from the modified spectra. The step-by-step subtraction of various nonlinear effects makes the

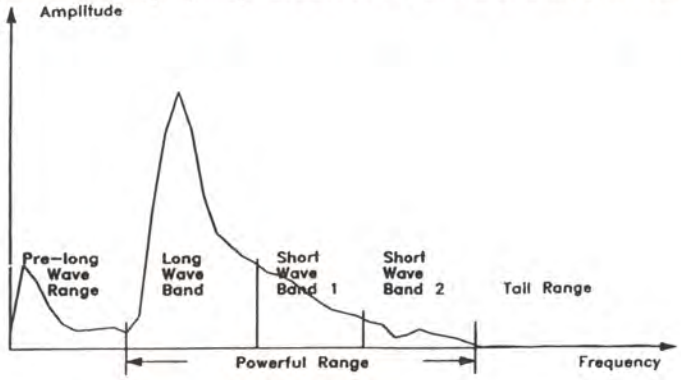

Fig. 1. Sketch of frequency band division

modified spectra closer and closer to the free-wave spectra. The decomposition of the short-wave band 2 is similar to that of the band 1. More detailed iterative procedures for the decomposition were described in [21].

Ocean waves are often directional or short-crested. Hence, a directional HWM (DHWM) was later developed to allow for wave directionality [22] and [23]. A straightforward linear decomposition of a directional sea is to apply two-dimensional FFT in wavenumber domain, but it needs numerous simultaneous wave records that are usually not available. As an alternative, linear wave theory and a cross-spectrum analysis are used to derive a directional frequency-amplitude or energy spectrum. Consequently, the initial phases of free waves are not retained. Different from a unidirectional wave field, the wave properties of short-crested ocean waves in general can not be deterministically recovered even within the scope of linear wave theory. That is probably the main reason why previous studies on the measurements of short-crested waves were dominated by statistical approaches either linear [1] or nonlinear [15], [16], [7].

To predict wave properties deterministically, the decomposition of a short-crested wave field should not only provide the amplitudes and directions of its free waves but also their initial phases. In addition, the DHWM also considers the effects of nonlinear wave-wave interactions in both decomposition and superposition as in the unidirectional HWH (UHWM). The DHWM thus includes three major steps: wave direction estimation, initial phase computation, and subtraction of the bound-wave effects from the measurements. To achieve relatively fine resolution in wave direction using as few as three simultaneous wave records, the estimate of wave energy spreading as a function of directional angle is based on data-adaptive methods, such as Maximum Likelihood Method (MLM) and Maximum Entropy Method (MEM). For deterministic decomposition, no smoothing or averaging is applied to the spectrum. According to a directional spectrum, a limited number of directional free waves are chosen at each frequency such that their amplitudes and directions conserve the total energy and resemble the energy spreading of the spectrum. The initial phases of the free waves are then determined by minimizing the square of the differences between the measurements and the resultant of predicted free and bound waves. Once the initial phases, amplitudes and directions of free waves are computed, the nonlinear interactions between them can be calculated and then subtracted from the corresponding measurements. Similar to the decomposition of long-crested irregular waves, the subtraction of bound-wave effects from the measurements is accomplished through iterative processes. Detailed descriptions were given in [22] and [23].

3 Applications

In typical storm seas, the frequencies of the free waves of significant amplitudes range from about 0.04 – 0.20 Hz. The nonlinear interactions among the free waves may result in bound waves of a much wider frequency band that may range from hundredth to several tenth Hz. Bound waves are in general much smaller in amplitude than free waves nearby the spectral peak. Nevertheless, they may be comparable to or even greater than free waves in the frequency bands far away from the peak

frequency, say from 0.20 to 0.4 Hz and below 0.05 Hz. In most engineering practices, the resultant wave properties are dictated by the free waves near the spectral peak. That is why linear spectral methods have been widely accepted. However, in certain cases, the contributions from waves in very low or relatively high frequency bands can be crucial to the resultant wave properties and structure responses to waves. Under these circumstances, distinguishing the bound waves from free waves in the computation is crucial, and the use of the HWMs can provide more accurate prediction than linear spectral methods or their improved modifications

3.1 Kinematics near Wave Crests

Predicted particle velocity near a steep wave crest based on linear spectral methods is significantly exaggerated. Many modifications to linear spectral methods, known as `stretching' and `extrapolation' techniques, were made to correct this error [18], [11]. Two of the most widely used modifications are Wheeler stretching and linear extrapolation methods. Because the modifications are based on empirical assumptions rather than sound hydrodynamic principles, they have two major shortcomings. First, in the case of extreme steep waves, based on the same measured wave elevation the predicted wave kinematics obtained using the two different modification methods can differ by more than 50 %, which greatly concerns the users in computing wave loads on offshore structures[14].

Secondly, the predictions made by either methods show very large discrepancies with respect to the corresponding measurements (see Fig. 2). In general, Wheeler stretching under-predicts horizontal velocities under wave crests while the linear extrapolation over-predicts them. However, relatively far away from the free surface, both predictions are close to the measurements [19], [21], [10]. Poor predicted wave kinematics obtained using the two modifications is not by accident. The contributions to the surface elevation from the free waves near the spectral peak are much greater than waves of relatively high frequencies. However, their respective contributions to wave kinematics, especially the acceleration near the free surface, may be comparable because the velocity induced by a free wave is roughly proportional to its frequency and the acceleration to the frequency squared. As mentioned before, bound waves are significant in the high-frequency band and their contribution to wave kinematics are quite different from that of the free waves of the same frequencies. The HWM distinguishes bound wave from the corresponding free waves in an irregular wave field and computes their contributions to wave kinematics accordingly. That is why the HWM is able to predict the kinematics more accurately than the modification methods, as demonstrated in Fig. 2.

3.2 Wave Elevation Predicted Based on Pressure Measurements

In using pressure transducers to record ocean waves, wave elevation is determined based on the measured dynamic pressure using a linear spectral method. Statistical analyses have shown that nonlinear effects, especially due to second-order wave interactions, are significant at very low frequencies and the frequencies about twice of

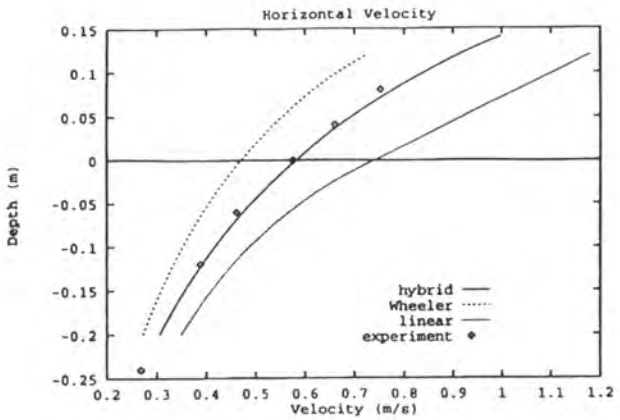

Fig. 2. Comparison of predicted (— HWM, ---- Wheeler stretching, and — · — Linear extrapolation) and measured (◊) horizontal velocities at time 16.58 sec

the spectral peak [4], [5]. Yet nonlinear effects on measured pressure in the time domain and their influence on the accuracy of predicted surface elevation have not received enough attention.

Fig. 3 shows the measured surface elevation of a transient wave train and its dynamic pressure recorded about 16 cm below the still water level. Both were measured at the same horizontal coordinate. The transient wave train generated in the wave flume at the Hydromechanic Laboratory of Texas A&M University was very steep but non-breaking at the location of measurements [8]. The measured elevation shows larger amplitudes at the crest than at the trough, while the corresponding pressure record shows larger pressure heads at the trough. At the first glance, the two records seem to indicate inconsistent measurements. The seemingly inconsistency between the two measurements, however, can be qualitatively explained by the interaction between high-frequency and dominant low-frequency free waves. Short (high-frequency) waves riding on the surface of long (low-frequency) waves may behave quite differently from themselves traveling alone. Short waves decrease in wavelength at the crests of long waves and increase at the troughs [6], [9]. In addition, as illustrated in Fig. 4, the vertical distance between the still water level with respect to short waves and the pressure transducer becomes greater at the crest of long waves and smaller at the trough. It is well known that the wave-induced dynamic pressure decays exponentially with the increase in the vertical distance from the surface. Thus, when the height of long waves is of the order of short wavelengths, the measured dynamic pressure induced by short waves at the pressure transducer will be much greater at long-wave trough than that at its crest. In a transient wave train, the large crests and troughs occur when the crests and troughs of short and long waves are in phase. At the crests of long waves, the pressure heads induced by short waves are much smaller than those at the trough of long waves. That is why the measured pressure heads are greater at the troughs than at the crests.

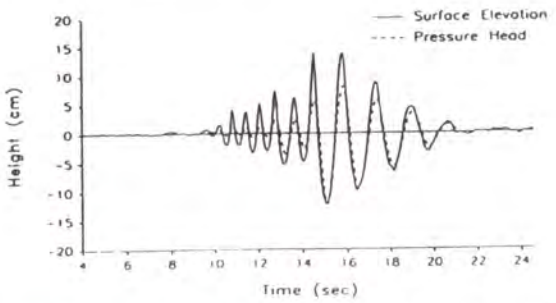

Fig. 3. Simultaneously measured surface elevation and pressure head time series. Pressure transducer was located 16 cm below the still water level

In using a linear spectral method, the surface elevation induced by each individual wave is computed as if it travels alone on otherwise calm water. As explained before, due to the presence of long waves, the dynamic pressure induced by the high-frequency waves depends on the phase of long waves. Therefore, the neglect of wave interactions in linear wave theory results in over-prediction in trough heights and under-prediction in crest heights. The comparison between the measured and predicted elevation obtained using linear wave theory (Fig. 5) confirms the over-prediction of trough height and under-prediction of crest height. The total wave height is also over-predicted but not as great as the trough height. On the other hand, the HWM considers the interactions among free waves and hence provides accurate predicted elevation as shown in Fig. 5. In ocean waves, large crests and troughs usually occur when waves of different frequencies are in phase. Therefore, the conclusion obtained based on the laboratory generated transient wave train is applicable to ocean waves in deep and intermediate-depth water.

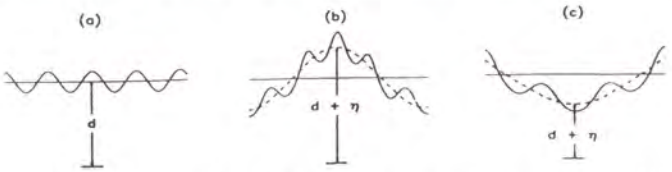

Fig. 4. Change in the still water level for a short wave due to the presence of a long wave: (a) no long wave, (b) at the crest of a long wave, (c) at the trough of a long wave

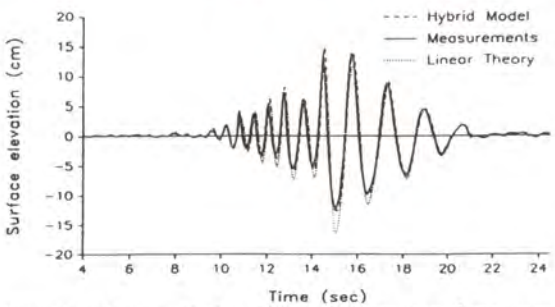

Fig. 5. Surface elevation predictions from pressure transducer measurements at 16 cm below the still water level

3.3 Decomposition of Directional Waves Based on Pressure Measurements

Pressure data were collected from an array of six pressure sensors mounted on the Texaco's Harvest offshore oil production platform. The pressure sensors were approximately 16 meters below the sea surface. The platform is a fixed structure located about 10 km west of Pt. Conception of the California coast in a water depth of 225 m. The location of the platform and local coordinates are sketched in Fig. 6. The coordinates of the six pressure sensors are listed in Table 1. The measured data were transferred to the Coastal Data Information Program (CDIP) at the Scripps Institution of Oceanography. The details of data acquisition are described in [12].

Table 1. Coordinates of the sensors installed on the HARVEST platform.

	111Sensor					
Coordinates	P1	P2	P3	P4	P5	P6
x (m)	0.0	22.9	22.9	0.0	59.4	59.4
y (m)	0.0	0.0	-22.7	-22.7	0.0	-22.7
z (m)	-16.0	-16.0	-16.0	-16.0	-16.0	-16.0

A set of data representing the sea states on May 7, 1993 was selected. It was a combination of a swell and local wind waves both coming from the northwest as indicated in Fig. 7. The peak frequencies of the swell and wind waves were around 0.066 and 0.11 Hz, respectively. The significant wave height was estimated to be 3.31 m. The sampling rate was 1 Hz. The duration of the time series used in the decomposition was limited to about 17 minutes assuming that within the duration wave properties such as wave amplitudes and directions were approximately stationary.

The measurements at P1, P2, and P3 were used as input to the decomposition, and the measurements at P4, P5, and P6 were reserved for examining the DHWM predi ctions. The measured signals at P1, P2, and P3 were filtered using a numerical low-pass filter of the cutoff frequency of 0.185 Hz before their input to the decomposition. The choice of the cut-off frequency at 0.185 Hz was because of low signal to noise ratio over this frequency. The cut-off frequency of free waves was also set at .185 Hz.

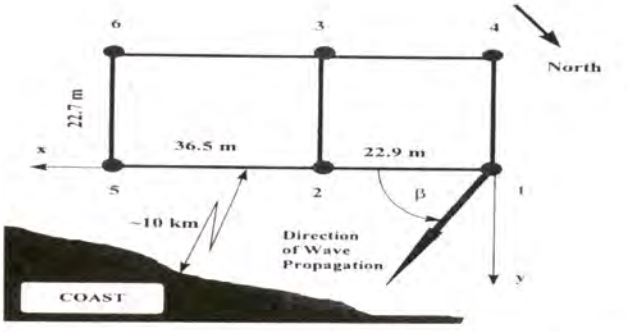

Fig. 6. Approximate location of the platform off the California coast and the local coordinates

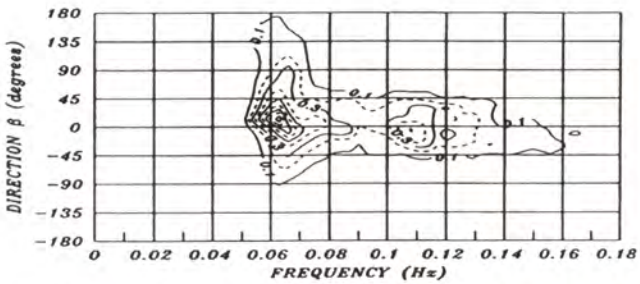

Fig. 7. Normalized directional pressure head spectrum near the Harvest Platform on May 7, 1993.

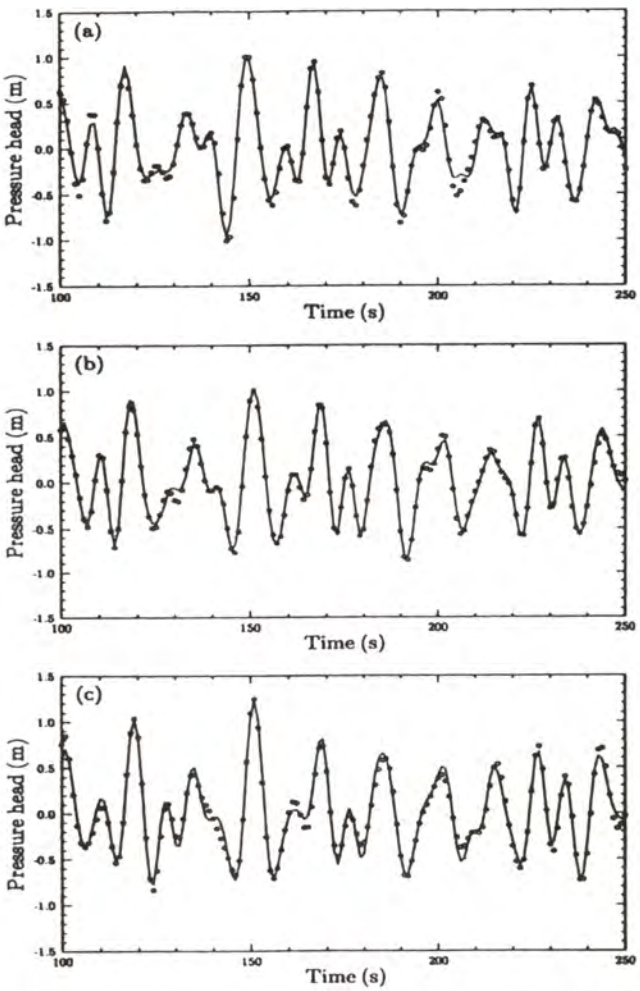

Fig. 8. Measured pressure heads (°) are compared with the corresponding predicted results (——) at: (a) P1, (b) P2, and (c) P3

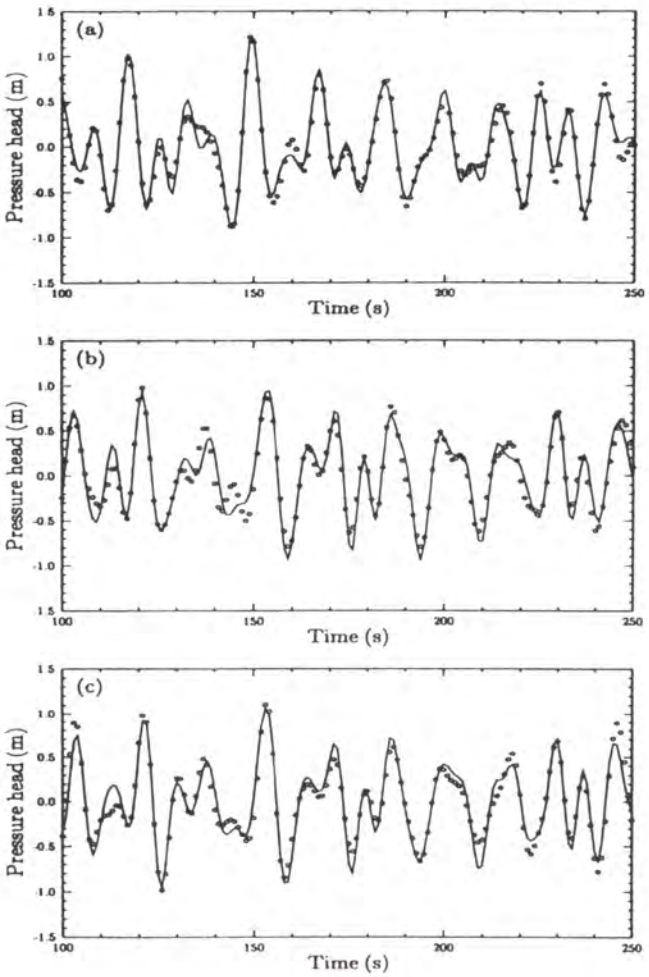

Fig. 9. Measured pressure heads (°) are compared with the corresponding predicted results (——) at: (a) P4, (b) P5, and (c) P6

After the decomposition, the free waves were used to predict the pressure heads at the locations of P1 to P6. The predicted pressure heads at P1, P2 and P3 are compared with the corresponding measurements in Fig. 8. The agreement between the predictions and measurements is excellent. It should be noticed that in the decomposition the initial phases of free waves were determined by matching the predictions with the corresponding input measurements. Since the measured pressure head at P1, P2 and P3 were used as the input, the excellent agreement between the predictions and measurements is expected. Hence, this type of comparison only divulges whether or not the iteration in the DHWM converges. To vindicate the

overall accuracy of the DHWM, the predicted pressure heads at P4, P5 and P6 are compared with the corresponding measurements in Fig. 9. The agreement between the predictions and the measurements remains satisfactory but is slightly deteriorated in comparison with the agreement shown in Fig. 8. Noticing that the measurements at P4, P5 and P6 had not been used in the decomposition, satisfactory agreement shown in Fig. 9 indicates that the DHWM is able to deterministically predict wave properties near the locations of measurements. More examples of applying the DHWM to the decomposition and prediction of other directional waves were presented in [23].

4 Conclusion

HWMs are unique and superior to most existing nonlinear wave theories in three respects. First, HWMs extract bound waves involved in the measurements before decomposing a measured wave field into its free waves. Secondly, the nonlinear interactions among free waves are modeled by two different perturbation methods, conventional and phase modulation approaches so that the truncated solutions converge quickly. Finally, the DHWM allows a deterministic analysis of short-crested ocean waves, which was not available previously, even in the scope of linear wave theory.

The effects of bound waves on measured wave properties can be more pronounced in a steep ocean wave field of a broader frequency range than in a periodic wave train. The use of HWMs can greatly improve the accuracy of predicted wave properties near the location of measurements. Some of these effects and their applications to wave predictions and measurements were demonstrated. In the future, it is hoped that more applications of HWMs will be made to ocean and coastal engineering and science.

5 Acknowledgements

This research was mainly supported by the OTRC and also supported by Texas Advance Technology Program and two Joint Industry Programs sponsored by Amoco Chevron, Exxon, Mobil, Shell, Statoil and Texaco.

References

1. Borgman, L. E.: Irregular Ocean Waves: Kinematics and Forces. In: Lemehaute and Hanes (eds.): The Seas. Ocean Engineering Science, Part A, Vol. 9.. J. Wiley and Sons (1990) 121-168
2. Chen, L. & Zhang, J.: On Interaction between Intermediate-Depth Long Waves and Deep-Water Short Waves. J. Ocean Engrg., Vol. 25 (1998) 395-423
3. Dommermuth, D. G. & Yue, D. K. P.: A High-Order Spectral Method for the Study of Nonlinear Gravity Waves. J. Fluid Mech., Vol. 184. (1987) 267-288

4. Herbers, T. H. C. & Guza, R. T.: Wind-Wave Nonlinearity Observed on the Seafloor: Part I. Forced Wave Energy. J. Phys. Oceanog., Vol. 21 (1991) 1740-1761
5. Herbers, T. H. C. & Guza, R. T.: Wind-Wave Nonlinearity Observed on the Seafloor: Part II. Wavenumbers and Third-Order Statistics. J. Phys. Oceanog., Vol. 22 (1992) 489-504
6. Longuet-Higgins, M. S. & Stewart, R. W.: Changes in the Form of Short Gravity Waves on Long Waves and Tidal Currents. J. Fluid Mech., Vol. 8 (1960) 565-583
7. Masuda, A., Kuo, Y. & Mitsuyasu, H.: On the Dispersion Relation of Random Gravity Waves: Part I. Theoretical Framework. J. Fluid Mech., Vol. 92: (1979) 717-730
8. Meza Conde, E., Zhang, J., & Seymour R. J.: Prediction of surface wave elevation based on the pressure measurements. J. Offshore Mech. & Arctic Engrg., Vol.121, No.4, (1999) 242-250
9. Philips, O. M.: The Dispersion of Short Wavelets in Presence of Dominant Long Wave. J. Fluid Mech., Vol. 107 (1981) 465-485
10. Randall, R. E., Zhang, J. & Longridge, J. K.: Laser Doppler Anemometer Measurements of Irregular Water Wave Kinematics. J. Ocean Engrg., Vol. 20 (1993) 541-554
11. Rodenbusch, G. & Forristall, G. Z.: An Empirical for Random Directional Wave Kinematics near the Free Surface. Offshore Technology Conference, OTC. Paper No. 5097 (1986)
12. Seymour, R. J., Castel, D., McGehee, D. Thomas, J. & O'Reilly, W.: New Technology in Coastal Wave Monitoring. In: Magoon & Hemsley (eds.): Ocean Wave Measurements & Analysis. ASCE, New York (1993) 105-123
13. Spell, C. A., Zhang, J. & Randall, R. E.: Hybrid Wave Model for Uni-Directional Irregular Waves: Part II. Comparison with Laboratory Measurements. Applied Ocean Res., Vol. 18 (1996) 93-110
14. Steele, K. M., Finn, L. D. & Lambrakos, K. F.: Compliant Tower Response Prediction Procedures. Offshore Technology Conf. OTC, Paper No. 5783 (1988)
15. Tick, L.J.: A Nonlinear Random Model for Gravity Waves. J. Maths & Mech., Vol. 8 (1959) 643-652
16. Weber,B. L. & Barrick, D. E.. On the Nonlinear Theory for Gravity Waves on the Ocean's Surface: Part I. Derivations. J. Geophys. Res., Vol. 100(C1) (1977) 773-778.
17. West, B. J., Brueckner, K. A. Janda, R. S., Milder, D. M. 7 Milton, R. L.: A New Numerical Method for Surface Hydrodynamics. J. Geophys. Res., Vol. 92, (1987) 11,803-11,804
18. Wheeler, J.D. Method for calculating forces produced by irregular waves. J. Petroleum Tech. 249: (1970) 359-367
19. Zhang, J., Randall, R.E. and Spell, C.A.: Component Wave Interactions and rregular wave kinematics. J. Wat., Port, Coastal and Ocean Engr., Vol. 118 (1991) 401-416
20. Zhang, J., Hong, K. & Yue, D. K. P. Effects of wavelength ratio on wave modeling. J. Fluid Mech. 248: (1993) 107-127.
21. Zhang, J., Chen, L., Ye, M. and Randall, R.E.:. Hybrid Wave Model for Unidirectional Irregular Waves, Part I. Theory and numerical scheme. Applied Ocean Res. Vol. 18 (1996) 77-92
22. Zhang, J., Yang, J., Prislin, I., Wen, J. and Hong, K.: Deterministic Wave Model for Short-Crested Ocean Waves, Part I. Theory and Numerical Scheme. Applied Ocean Res., Vol. 21 (1999a) 167-188
23. Zhang, J., Prislin, I., Yang, J., and Wen, J.: Deterministic Wave Model for Short-Crested Ocean Waves, Part II. Comparison with Laboratory and Field measurements. Applied Ocean Res., Vol. 21 (1999b) 189-206

Session 3

Observations and Measurements of Rogue Waves

Some Cases of Observed Rogue Waves and an Attempt to Characterize Their Occurrence Conditions

Michel Olagnon & Sylvie van Iseghem

IFREMER Centre de Brest
B.P. 70, F-29280 Plouzané, France
Michel.Olagnon@ifremer.fr, Sylvie.van.Iseghem@ifremer.fr
WWW home page: http://www.ifremer.fr/metocean/

Abstract. There is no consensus at present as to whether extreme waves are "normal" extremes in an homogeneous population of waves, or the results of totally different generation mechanisms, such as for instance non linear interaction and phase locking of wave trains. In a first stage of the present paper, we analyse a few selected extreme waves measured in the North Sea, and we verify, according to several criteria, that these waves can be classified as *Rogue Waves* according to the criteria commonly accepted. In addition, the occurrence of a very deep trough in front of the wave is verified by examination of the reconstructed instantaneous space profiles of the water surface at several time-steps before the maximum crest. In a second stage, the sea states where the selected extreme waves occurred are studied and characterized in terms of spectral bandwidth and multiple peakedness, of steepness, of non linearity, of wind conditions, and of the characteristics of the storm that contains them. These sea states are then compared with the other sea states of similar H_S where no rogue wave could be observed, with the intent to find some differences or trends that could then be used as forewarning signs of an increased risk of occurrence of rogue waves. Unfortunately, most of the differences are not significant enough to make a decisive step forward in the forecast of risks of rogue waves. Lastly, the individual rogue waves that were identified are analysed, both in the time domain and from the reconstructed shape that can be calculated in space. Special attention is given to the individual wave steepness and to its vertical and horizontal asymmetry. These parameters are compared to the same ones for "normal" maximum waves in other sea states.

Nomenclature

H_S Significant wave height
T_z Mean period estimated with $\sqrt{\frac{m0}{m2}}$
C_z Sea state steepness calculated using $\frac{H_s}{1.56T_z^2}$
H Down-zero-crossing wave height
A_C Crest height defined as the maximum height observed between an up-zero-crossing and the following downcrossing
T Wave period (by zero downcrossing counting)
T' Crest front period, see [3] for details
T" Crest rear period, see [3] for details
L Wave length
L' Crest front wave length, see [3] for details
L" Crest rear wave length, see [3] for details
μ_h Wave horizontal asymmetry, or height asymmetry, $\frac{A_c}{H}$
μ_{vs} Crest vertical asymmetry, or front/back asymmetry, in space $\frac{L''}{L'}$
μ_{vt} Crest vertical asymmetry, or front/back asymmetry, in time $\frac{T''}{T'}$
S_l Individual wave steepness by space domain analysis, $\frac{H}{L}$
S_t Individual wave steepness by time domain analysis, $\frac{H}{1.56T^2}$

1 Introduction

There is no lack of evidence that extreme and dangerous waves exist : their gigantic size has been testified by many shipmasters' reports and their dangerousness has been proven by damages on ships and offshore structures, some examples of which are described in [1] or [4].

However, the problem as to whether those waves are normal waves or abnormal ones in a statistical sense is still unsolved. The present paper intends to reach a better understanding of those waves by considering the extreme waves of the Frigg in situ data set, see [5] for details.

The first question raised in this paper is whether the waves selected in the Frigg data set are of the same kind as the extreme waves reported by meteocean engineers and shipmasters.

The problem of whether those waves can be called "rogue" (or "freak") is discussed in parts two and three. If they were "freak" or "rogue" waves, it should be possible to find characteristics that distinguish them from the "conventional" extreme waves. Two characteristics are studied: the individual shape of the individual waves, especially wave asymmetry and wave steepness, as presented in the second part; and the conditions in which those extreme waves occur, analysed in the last part.

2 Are We Talking about the Same Waves ?

2.1 Selection of Extreme Waves

Extreme waves analysed in this study have been selected according to two criteria, further named *Ch* and *Cc*.

$$Ch \equiv \frac{H}{H_S} > 2 \quad \text{and} \quad \mathrm{Cc} \equiv \frac{\mathrm{A_C}}{\mathrm{H_S}} > \mathrm{R_0} \tag{1}$$

The value 1.25 has be chosen for R_0 so that the number of waves selected with *Ch* would be similar to that of the ones selected with *Cc*. Examination of the dataset showed that the commonly used value of 1.1 was too frequently overpassed for a study that intends to deal with rare extremes. Only sea states with Hs larger than 2 m were considered.

We define a *maximal wave* as the wave corresponding to the highest crest of a given sea state. The set of maximal waves was then searched for extreme waves according to criteria (1). The numbers of waves selected in each set are presented in table 1.

Table 1. Description of the selected waves

	Number of waves				
	Total	selected by using criterion			
	$(Hs > 2m)$	Ch	Cc	$Ch \cap Cc$	$Ch \cup Cc$
Data set Frigg	1,600,000	79	74	25	128

Two sets of sea states are considered. The first one corresponds to all sea states with Hs>2 m and the second one to sea states for which Hs is larger than 2 m and the maximal wave crest higher than 5 m. Proportions of extreme waves are presented on table 2.

Table 2. Extreme waves among maximal waves

		Ch	Cc	$Ch \cup Cc$	
Sea state subset	# Maximal waves	# Extreme waves			% Extreme waves
$Hs > 2m$	9858	79	74	128	**1.3 %**
$Hs > 2m$ & $Ac > 5m$	780	22	35	46	**5.9 %**

Extreme waves have then been selected according to the criteria (1) commonly used to identify "freak" waves, but no justification of abnormality was made so far, so we will keep to naming them extreme waves.

A peculiarity of abnormal extreme waves for shipmasters is the "hole in the sea" that can been observed ahead of the wave. We investigate in the next part whether such a hole could have been observed ahead of the waves that we selected.

2.2 Is there a "hole in the sea" ahead of the selected waves ?

The analysis of the water surface elevation time history around the selected waves leads to the conclusion that the troughs ahead of high waves are benign. Observations from ships' bridges are however mostly relevant to spatial shapes of waves. To get an estimation of the wave shape in space, the following method is applied:

- The Fourier transform is applied to the time history, converting it into the frequency domain.
- A change of variables is performed to turn frequency into wavenumber, by use of the dispersion relationship.
- The values are multiplied by the appropriate complex phase to shift to the instant of interest.
- The inverse Fourier transform is then applied, thus providing the space shape.

It should be noted that with this method, waves are assumed to be all free waves propagating in a single direction.

Figure 1 presents an extreme wave recorded by the Frigg radar on 2 February 1988 in a sea state when Hs was 6.7m. Instantaneous space wave profiles have been computed every 0.5 s. The 40 wave profiles from T-20s to T, where T is the time at which the extreme crest is measured by the sensor, are presented on the top figure. The figure below shows the 20 profiles from T to T+10s.

It is interesting to note that the trough at time T is indeed not outstanding and that the wave crest-trough dissymmetry at that time is consequently very large. Such features are commonly observed with measurements from fixed platforms. If we consider now the wave profile at T-8s (yellow line), the crest is not so high but the trough, around 8m, is very deep.

If a sensor had been placed 30 m ahead (in the wave propagation direction) of the Frigg radar, a "hole in the sea" would have been recorded, but it would not necessarily have been matched with a maximal crest. The instantaneous profile about 5 seconds after T also shows a deep trough. Almost all extreme waves relative to Frigg data present similar profiles as the one presented above, i.e. the peculiarities described by shipmasters in reports of "rogue waves". Out of 46 extreme waves, 43 were also extremal in the sense of Podgórski *et al* (2000) [6], i.e. the crest was a maximum both in the time dimension and in the space dimension. Every single one of them exhibited a much deeper trough, about 0.25

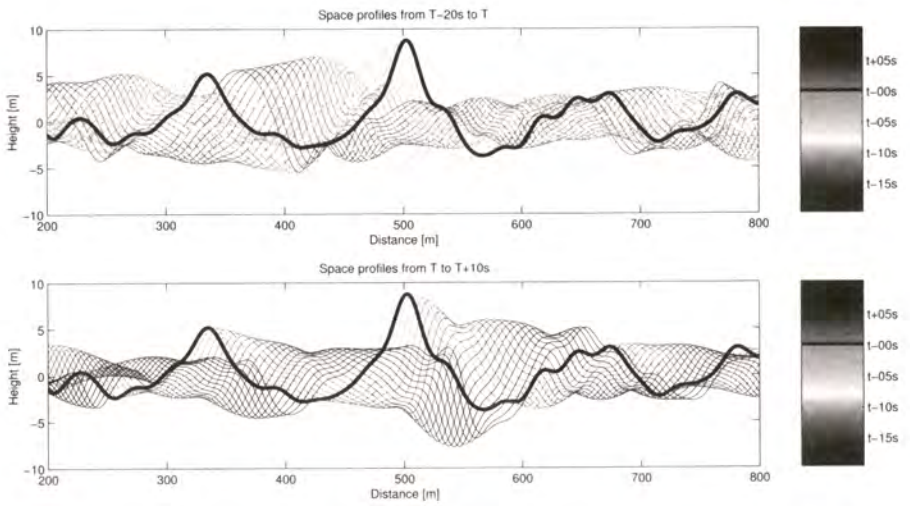

Fig. 1. Instantaneous space profiles [See also Appendix CP]

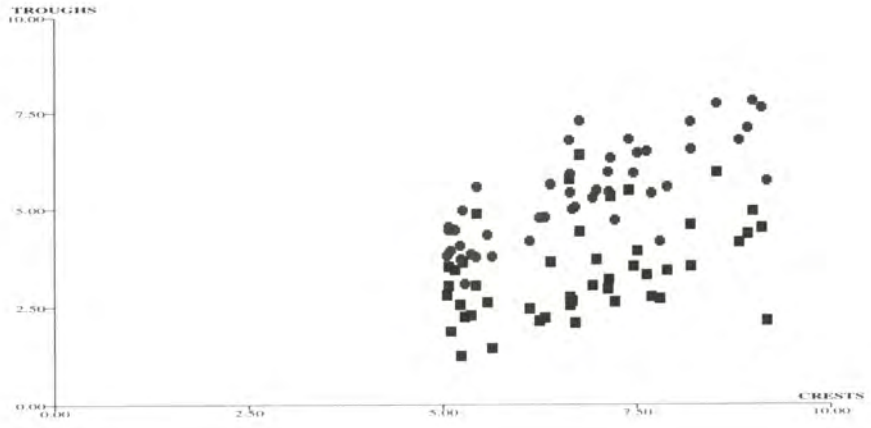

Fig. 2. Preceding trough versus crest [See also Appendix CP]

wave-length ahead of the maximal crest in space and 0.75 period ahead in time, with respect to the point measurement time-history.

Figure 2 shows the difference between the trough depths corresponding to the maximal waves in the time-history (blue squares) and the troughs at their deepest in space and time ahead of these waves (red circles).

Despite the fact that there might be a slight increase in the trough depth due to the assumptions used for estimation of the waves space shapes, there are many good reasons to believe that our selected extreme waves are of the same nature as the ones that were actually observed and identified as damaging giants.

Whether these selected waves are normal extremes is discussed in the next sections.

3 What Do Individual Extreme Waves Look Like?

If those selected waves are abnormal, it should be possible to find features to distinguish them from other normal large waves.

To check if it is the case, parameters relative to individual wave shapes have been chosen and their distributions have been compared for different subsets.

The subset of "conventional waves" (780 waves) corresponds to the "maximal waves" of each sea state for which the maximal crest is larger than 5m. The subset of extreme waves corresponds to the "conventional waves" identified as "extreme waves" with criteria of formula 1 (46 waves).

Parameters investigated are:

1. Wave horizontal asymmetry, or height asymmetry $\mu_h = \frac{A_c}{H}$
2. Crest vertical asymmetry, or front/back asymmetry, in space $\mu_{vs} = \frac{L''}{L'}$ and in time $\mu_{vt} = \frac{T''}{T'}$
3. Wave steepness in space $\frac{H}{L}$ and in time $\frac{H}{1.56T^2}$
4. Crest front steepness in space $\frac{A_c}{L'}$ and in time $\frac{A_c}{1.56(2T')^2}$

Parameters in space have been estimated from the reconstructed shape at the instant of the crest. To compare distributions, a Kolmogorov test is used to test hypothesis Ho: $F_T(x) = F(x)$ against H1: $F_T(x) \neq F(x)$. $F_T(x)$ is said to be significantly different from $F(x)$ with risk α if the statistic $D_n = sup|F_T(x) - F(x)|$ is higher than a value θ, with $(P(D_n > \theta) = \alpha$. The risk value used in the following of this paper is 5%.

3.1 Wave Asymmetry

Figure 3 shows a comparison of the crest front/back asymmetry distributions.

A distinction is made between extreme waves selected with the different conditions $Ch : \frac{H}{H_S} > 2$, $Cc : \frac{A_C}{H_S} > R_0$ and $Ch||Cc : \frac{H}{H_S} > 2 \cup \frac{A_C}{H_S} > R_0$.

The subset of the 780 maximal waves is denoted by FT on the following figures.

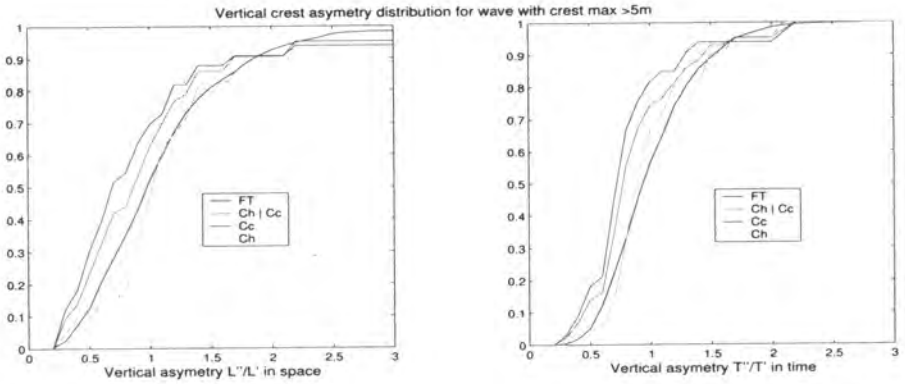

Fig. 3. Wave vertical (front/back) asymmetry [See also Appendix CP]

There is no significant difference between the crest vertical asymmetry distribution of all maximal waves and that relative to the selected extreme waves. A larger difference is observed for the extreme waves selected with *Cc* are considered: values of the vertical crest asymmetry parameter tend to be smaller for those extreme waves, $\mu_v < 1$ for 70% of them whereas $\mu_v < 1$ for only 50% of the maximal waves. Most of those extreme waves have thus a crest back period smaller than the front one. That result is unexpected but care has to be taken on the fact than it relies on only 35 waves and should be validated by an additional study not only on the crest period but on the trough to crest period.

Significant differences appear between maximal and extreme waves when considering wave height horizontal asymmetry parameter, see figure 4. The median of the maximal wave distribution equals 0.63 and the one relative to the extreme waves 0.68. Differences are most important when only the extreme waves selected with *Cc* are considered and become non significant if the extreme waves are restricted to the ones selected with *Ch*.

3.2 Wave and Crest Steepness

Comparisons of the individual wave or crest steepness are presented on figures 5 and 6.

Figure 5 shows differences between maximal and extreme waves in terms of individual wave steepness. Extreme waves are steeper than maximal ones, whatever criterion (*Ch* or *Cc*) is used to select them.

Results relative to crest front steepness are not so clear, see figure 6, crest front steepnesses relative to extreme waves are still larger than the ones relative to maximal waves but differences are much smaller and nearly not significant.

Differences have been found between extreme and maximal waves: larger height horizontal asymmetry, wave steepness more important but those differences are not always significant and depend on the criterion used to select the

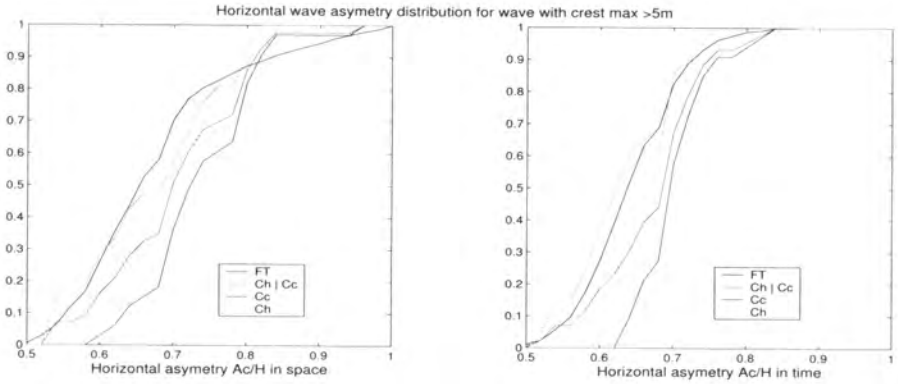

Fig. 4. Wave horizontal (height) asymmetry [See also Appendix CP]

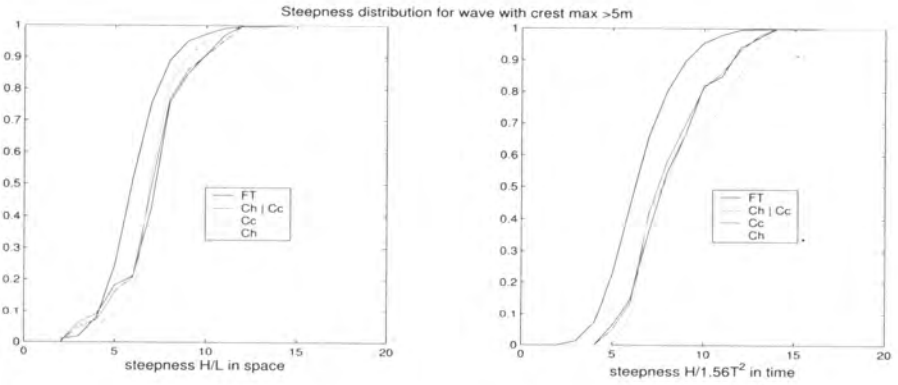

Fig. 5. Wave steepness [See also Appendix CP]

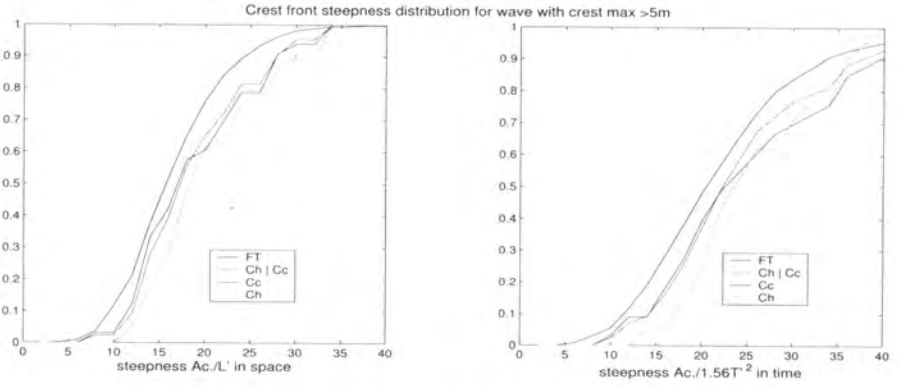

Fig. 6. Crest front steepness [See also Appendix CP]

extreme waves. It is thus not possible to assess the abnormality of extreme waves from this analysis.

4 What Are the Prevailing Sea Conditions when They Occur?

In order to check whether extreme waves are likely to occur in some special unusual conditions, we analyse several parameters describing the sea states where they were observed. For each of these parameters, we compare the distribution for sea states during which extreme waves have been detected (128 sea states) with the distribution relative to all sea states with Hs>2m (9850 sea states), called common marginal distribution.

4.1 Sea State Significant Height and Steepness

Figure 7 shows a comparison of the H_S distributions for Frigg data. The distribution relative to the sea states with extreme wave selected with Cc exhibits the largest differences from the common marginal one. Period distributions are identical in the extreme and common marginal cases.

Comparison of the steepness distributions leads to the same conclusions as the Hs distributions: extreme waves occur when sea states are steeper than the average. This increase in steepness is evenly observed over T_Z occurrences, and thus essentially the consequence of higher H_S.

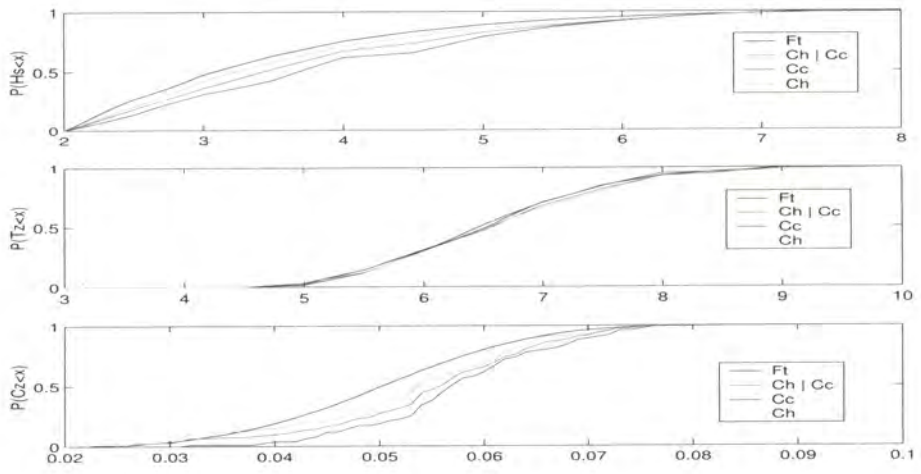

Fig. 7. Sea state Steepness [See also Appendix CP]

4.2 Multi- or Single-Peak Spectra

Double peaked sea states are identified by a modified version of the Guedes Soares criterion [2], for which details can be found in Van Iseghem *et al.* (2001) [8]. For several Hs classes, the occurrence probability of double peaks is calculated and used as a reference for the occurrence probability relative to the sea states where an extreme wave occurs.

The percentage of double peaks detected for sea states with extreme waves is smaller than when considering all sea states, see figure 8. It can be noted that there is no double peaked sea state at all for the 10 % 'most extreme' waves selected, as well with *Ch* as with *Cc*, but that significance of this fact is low since only 1 % of the sea states where a double peak was detected have H_S higher than 3m.

Yet one single wave coming at some significant angle from the direction of other waves, even the highest of the sea state, might not be sufficient to create a second peak in the spectrum.

4.3 Strong Winds

Wind distribution restricted to extreme wave cases is significantly different from the common marginal one. Wind speed is larger for extreme waves and the difference is at highest if we consider only the extremes waves selected with *Cc*. However, it may be noted that the largest values of wind speed do not correspond to the most extreme wave ratios.

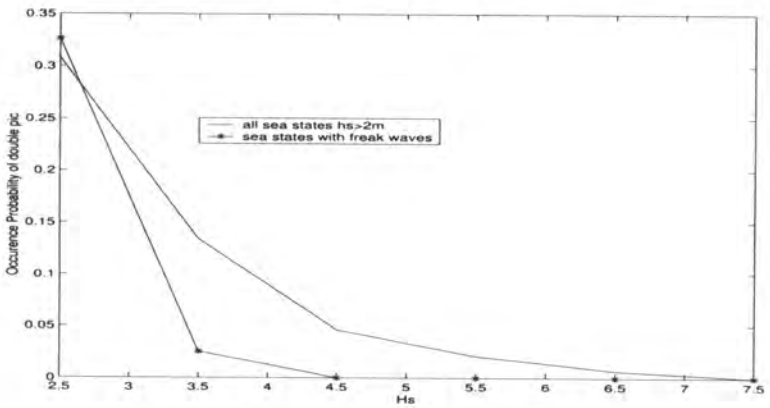

Fig. 8. Occurrence of double peak spectra

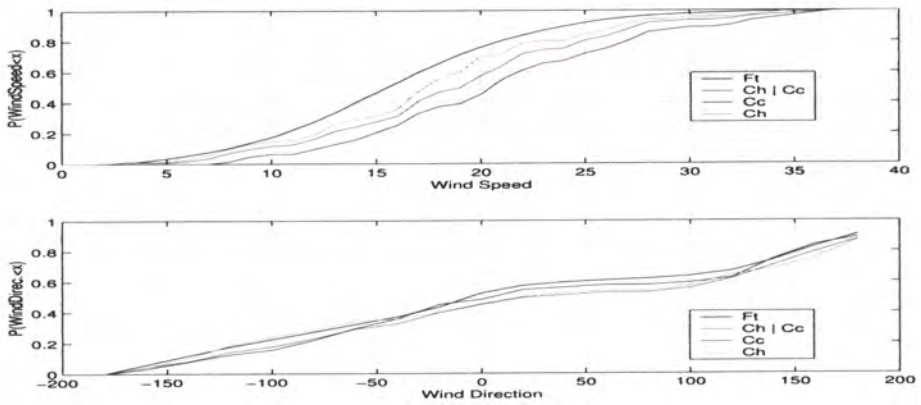

Fig. 9. Wind [See also Appendix CP]

4.4 Worsening Sea Conditions

Figure 10 shows the distribution of the three parameters $H_S - H_{S-2}$, $H_S - H_{S-1}$ and $H_S - H_{S+1}$, where H_{S-1} means the H_S of the previous sea state in the record history (3 hours earlier), and H_{S+1} that of the following one For 75 % of the selected sea states, we have $H_S > H_S - 2$ and for 80 % of the selected sea states, $H_S > H_S - 1$ whereas $H_S > H_S + 1$ occurs in half of the sea states. The probability of occurrence of extreme waves is thus slightly higher when sea conditions have been worsening in the previous hours.

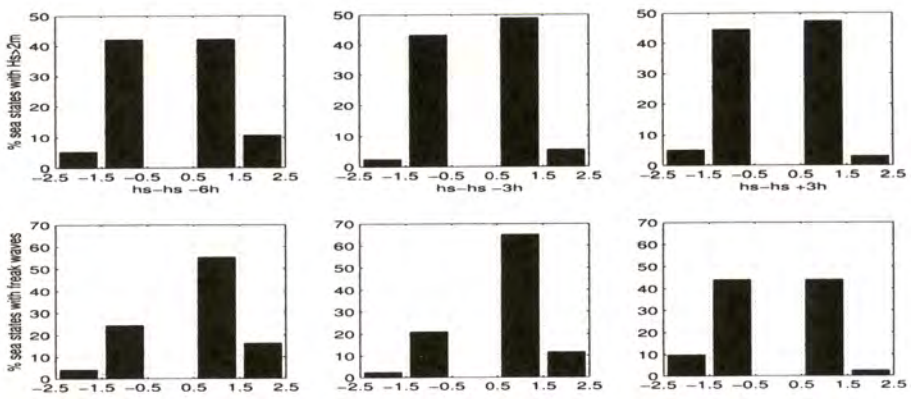

Fig. 10. Worsening sea conditions

5 Conclusion

It has been investigated whether "rogue waves" would be normal or abnormal. Characteristics of those waves have been proven to be consistent between measurements from a fixed platform and shipmasters'reports. Especially, the horizontal height asymmetry is very large at the time when the extreme wave occurs; but if the space wave profile at the instant a few seconds before is reconstructed, a deep trough a keen to a "hole in the sea" can be observed.

It is thus reasonable to assume that the selected extremes waves are of the same nature as the ones observed by mariners that have proven to be giant and dangerous.

A few hints have been provided to decide whether those waves are "normal" or not and tests have been made to try to distinguish them from the other common large waves. Some differences appear, relative to the individual wave shapes: larger horizontal wave height asymmetry, higher steepness, and to sea state conditions in which they occur: steeper sea states, worsening conditions. Nevertheless those differences are not significant enough to prove the belonging of those extreme waves to a different statistical population.

A recurrent problem with *in situ* data sets in the small number of identified extreme waves, which makes it difficult to conclude to any significant difference between extreme and common maximal waves.

We thus recommend that all available datasets be analysed in a similar fashion, and that further measurements be carried out in manners that would allow the identification of extreme waves, which is unfortunately not the case for many of the datasets currently recorded.

References

1. Ersdal, G. & Kvitrud, A.: Green Sea on Norwegian Production Ships. Proc. Airgap Workshop, HSE/E&P Forum London (1999)
2. Guedes Soares, C.: Spectral Modeling of Sea States with Multiple Wave Systems. Journal of Offshore Mechanics and Artics Engineering, vol.114 (1992)
3. International Association for Hydraulic Research: List of Sea State Parameters. *Supplement to bulletin*, No 52 (1986)
4. Kjeldsen, S.P.: Examples of Heavy Weather Damages Caused by Giant Waves. Bulletin of the Society of Naval Architects of Japan, 820, 1997-10 (1997) 744–748
5. Olagnon, M. & Krogstad, H.E.: Observed Short- and Long-Term Distributions of Wave Steepness. Proc. Int. Offshore and Polar Engineering Conf., Vol. 3. Montréal (1998) 63–70
6. Podgórski, K., Rychlik, I., Rydén, J & Sjö, E.: How Big Are the Big Waves in a Gaussian Sea ?. Int. J. of Offshore and Polar Engineering, Vol.10, No.3 (2000) 161–169
7. Robin, A. & Olagnon, M.: Occurrence of Extreme Waves with Respect to Significant Wave Height. Proc. Offshore Mechanics and Artic Engineering, OMAE, Vol.2a (1991) 1–9
8. van Iseghem, S., Deleuil, G. & Guerin, P.: Improved characterizattions for design waves. Proc. Int. Offshore and Polar Engineering Conf., ISOPE (2001)

Statistical Mechanics of the Frequency Modulation of Sea Waves

Hiroshi Tomita and Takafumi Kawamura

Ship Research Institute, Shinkawa 6-38-1, Mitaka, Tokyo 181-0004, Japan
tomita@srimot.go.jp

Abstract. Longtime stationary ocean wave data taken from the Sea of Japan are analyzed in particular for the stochastic properties of their wave periods. The probability density functions (PDF) of wave heights and periods are determined. A quasi-linear wave propagation model is examined to simulate the creation and annihilation of Rogue like waves. This simple model reproduces the actual feature of this phenomenon very well. It suggests that the frequency modulation in random sea waves is a possible cause of such abnormal a wave. A statistical mechanical technique is applied to the sequence of wave periods. The fluctuation of the wave period sequence has its spectrum inversely proportional to the frequency of the variation, which is a fairly common feature in many natural phenomena.

1 Introduction

The causes of Rogue (Freak) waves in actual ocean area have long been investigated by many researchers, and many hypothetical mechanisms of their occurrence have been proposed from different points of view and corresponding techniques. Those can be classified roughly as follows:

1. Non-linear effects of water waves.
2. External influences, varying current and/or bottom topography.
3. Superposition of wave systems, wave groups, multidirectional waves.

In this paper, we pay attention to the statistical properties of wave periods and to their role in the generation and annihilation of abnormal waves such as Rogue waves.

Firstly, actual ocean wave data from the Sea of Japan are reexamined in detail. Several existing formulae for the probability distribution of wave periods in stochastic processes are compared with the data of 14,227 waves, which were taken in almost identical sea conditions. The agreement in the distribution of wave periods is not as good as in the distribution of wave heights in general. However, for this large number of wave samples, classical Weibull distribution with index 4 is found to be in good agreement. The autocorrelation between successive wave periods is 0.35, which is slightly less than those of preceding results in a storm field.

Secondly, we attempt to predict the propagation characteristics of actually observed Rogue waves by assuming the non-linear dispersion relation for all wave

frequency components in a stochastic wave field. Referring to the results of this analysis, we perform a simple numerical simulation of generating and annihilating a Rogue wave by superposing a low frequency modulated wave group.

2 Distribution of Wave Period

Many types of probability density functions (PDF) have been proposed for sea waves. They were deduced from the assumption of a linear stochastic process, that is, a Gaussian process. The most typical formula is presented here as equation.

$$p(T)dT = \left(1+\frac{\nu^2}{4}\right)\frac{m_p}{2\nu T^2}\left\{1+\left(1-\frac{m_p}{T}\right)^2\frac{1}{\nu^2}\right\}^{-3/2} dT \qquad (1)$$

In this formula, spectrum of the process is also assumed narrow bandedand symbols ν and m_p represent the bandwidth and the mean value of the period respectively. Alternatively, we can make use of some empirical formula like

$$p(T)dT = c\left(\frac{1}{m_p}\right)^c T^{c-1} exp\left[-\left(\frac{T}{m_p}\right)^c\right] dT \qquad (2)$$

which is called the Weibull probability density distribution of index c, and m_p means the root mean square of the periods. Its excess distribution is integrated to be

$$P(T) = \int_T^\infty p(T)dT = exp\left[-\left(\frac{T}{m_p}\right)^c\right] \qquad (3)$$

3 Analysis of Data from the Sea of Japan

The most crucial condition for the statistics of sea waves is that we need to obtain enough long time data of stationary sea state to be compared with stationary random theory if non-linear effect of surface waves is not pronounced in actual ocean. In this paper, we deal with an available longtime (37 hours) wave data from the Sea of Japan on January 9th and 10th, 1988. The location of the observation site is shown in Fig. 1.

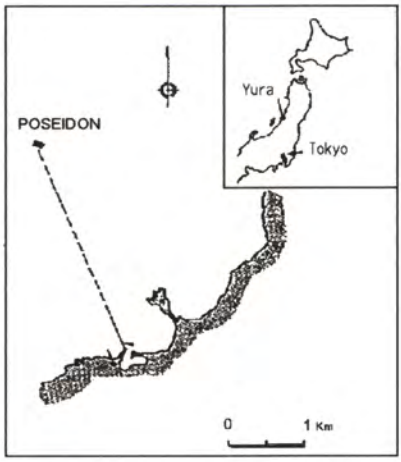

Fig. 1. Observation site at Yura

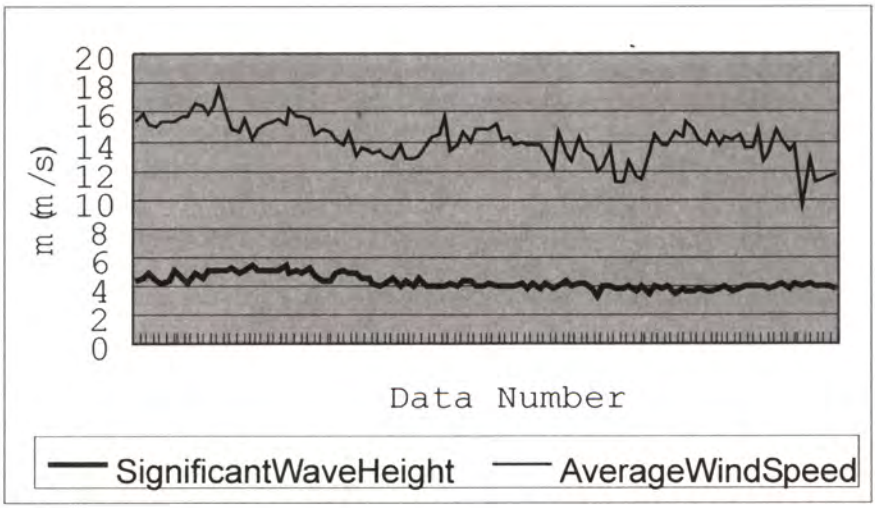

Fig. 2. Long term sea state of analyzed data

The sea condition during this observation period (average wind speed and significant wave height of every 20 minutes) is shown also in Fig. 2. Wind speed was around 15m/sec, and significant wave height was almost constant at 4m throughout.

This condition satisfies that of fully arisen sea and wind waves are to be found without swell. It is very rare case to have data for such many waves of amount to 140,000 under such a stationary sea condition. We can assume the law of large numbers in statistics of wave height and period analyzed by Zero Up Crossing method from these data.

At first, we examine the well-known result of wave height distribution with the well-established theoretical formula of Rayleigh distribution in equation (4).

$$p(H)dH = \frac{H}{4m_0} exp\left(-\frac{H^2}{8m_0}\right)dH \tag{4}$$

The result is shown in Fig. 3. The agreement of the observed PDF with that of the theory by the parameter m_0 is excellent as expected. Next, we examine the PDF of sea wave periods. A comparison is made with theoretical formula (1) [1] in Fig. 4. The agreement seems rather poor particularly in the longer periods region. It is not easy to explain this sort of discrepancy since it is not necessarily caused by the bandwidth effect.

Actually, the bandwidth parameter ε for every 20 minutes record is found to be between 0.6 and 0.7, a value that is commonly considered intermediate. On behalf of the unreliable theory, we adopt an empirical PDF of Weibull type of index c (2), which is an extension of the Rayleigh PDF. Actually it reduces to Rayleigh distribution when $c = 2$. For identification of the index c , we integrate it to have its excess probability distribution (3), which is described in Fig. 5.

Double logarithms of both sides of equation (3) are shown in Fig. 6. In this figure, we find the index c is very close to an integer value of 4 (actually 3.98). This result is in accordance with a formerly published result [2]. In Fig. 7, we confirm the excellent agreement of this formula with observed data. For reference, we show the joint PDF for normalized wave heights and periods of the whole 37 hour record in Fig. 8. The correlation of wave height and period seems high, which is mentioned in a latter section.

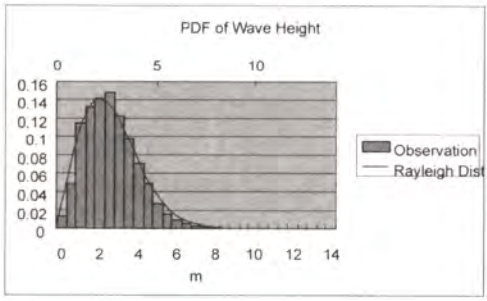

Fig. 3. Comparison of observed wave height with theory

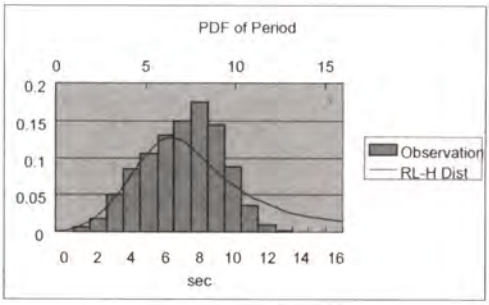

Fig. 4. Comparison of observed wave period with theory

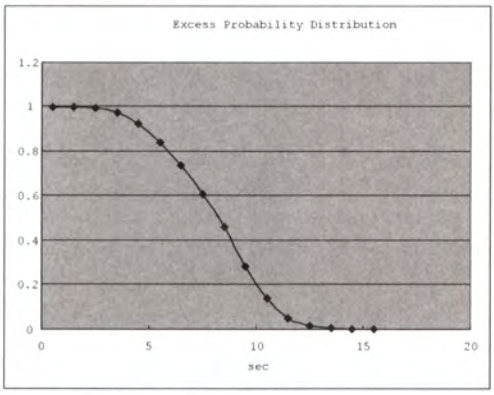

Fig. 5. Excess probability distribution of the period

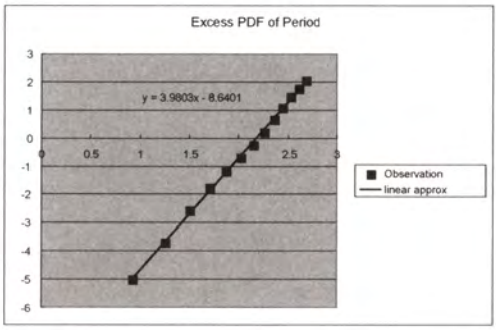

Fig. 6. Linear regression of the log-log plot

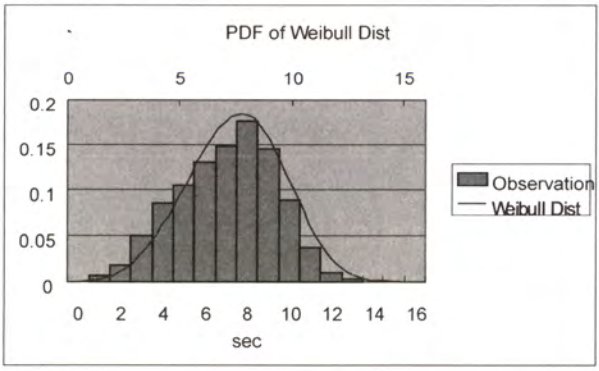

Fig. 7. Comparison of the observed period with Weibull distribution

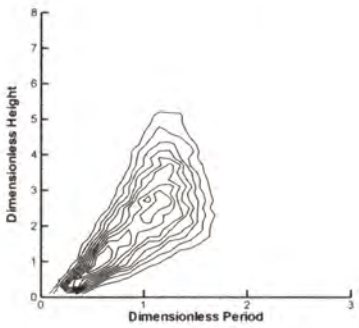

Fig. 8. Joint PDF of wave heights and periods

4 Transformation of Wave Record

Ocean wave data are acquired at a fixed position as time series. On the other hand, we can describe the wave elevation η in the following form.

$$\eta(x,t) = \int_0^\infty a(\omega)\cos\left(\omega t - \frac{\omega^2}{g}x\right)d\omega + \int_0^\infty b(\omega)\sin\left(\omega t - \frac{\omega^2}{g}x\right)d\omega \tag{5}$$

where the dispersion relation of deep water waves is taken into account. Moreover, we can consider the nonlinear dispersion relation of each component by replacing both sinusoidal terms as follows:

$$\cos\omega\left(t - \frac{x}{c_L}\right) \Rightarrow \cos\omega\left(t - \frac{x}{c_{NL}}\right) \tag{6}$$

$$\sin\omega\left(t - \frac{x}{c_L}\right) \Rightarrow \sin\omega\left(t - \frac{x}{c_{NL}}\right) \tag{7}$$

From equation (5), one can reproduce the observed time series simply by setting x=0.

$$\eta(0,t) = \int_0^\infty a(\omega)\cos(\omega t)d\omega + \int_0^\infty b(\omega)\sin(\omega t)d\omega \tag{8}$$

The Fourier coefficients $a(\omega)$ and $b(\omega)$ are determined easily from the observed record. We obtain the transformation of acquired record at x=0 to arbitrary point x by substituting $a(\omega)$ and $b(\omega)$ into equation (5) and integrating them along ω. If $x < 0$, $\eta(x, t)$ represents the wave record at x m upstream of the observed one.

Note that we neglect the bounded wave components and the directional spreading of random wind waves in the above quasi-linear model. The former is justified in the actual ocean however the latter is not always permissible.

5 Application to Rogue Waves

As was written in the preceding papers of the present authors [3], we found several cases of 20 minutes data in each of which a typical Rogue wave is included. We pick one of them up here and examine the transformation of its change of waveform at up and down-stream virtual observation sites. The original data is shown in Fig. 9 as x = 0. The transformation procedure explained in section 4 is applied to the data to provide the records each 80m up and down stream. It is clear that there is not such a pronounced peak at all in both calculated records.

It suggests that the rogue wave itself does not propagate as a crest preserved isolated wave. Instead, we can recognize that there is a comparatively small amplitude wave train, of which period is gradually increasing in time at x = -80m (see Fig. 10). Similarly, a gradually decreasing frequency modulated wave train appears at the record at x=80m (see Fig. 11). It means that one can experience the appearance of a large wave crest only within an interval a few times as long as the wavelength.

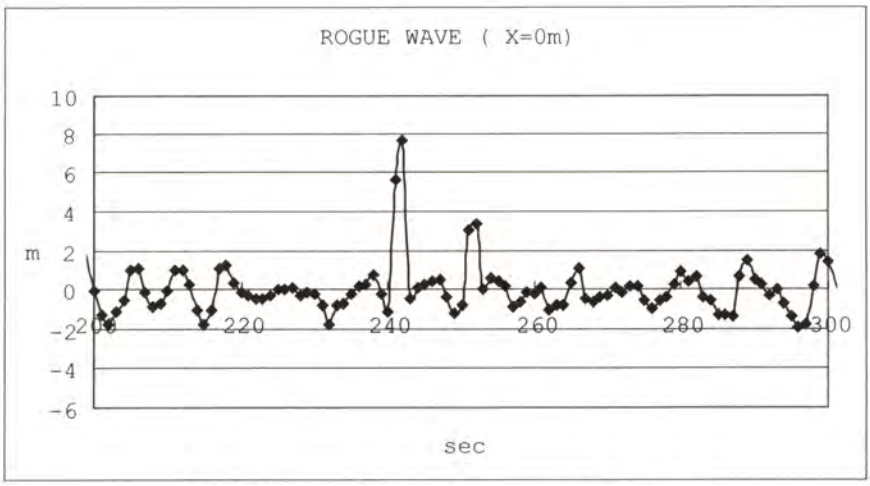

Fig. 9. Observed Rogue (Freak) wave at Yura site

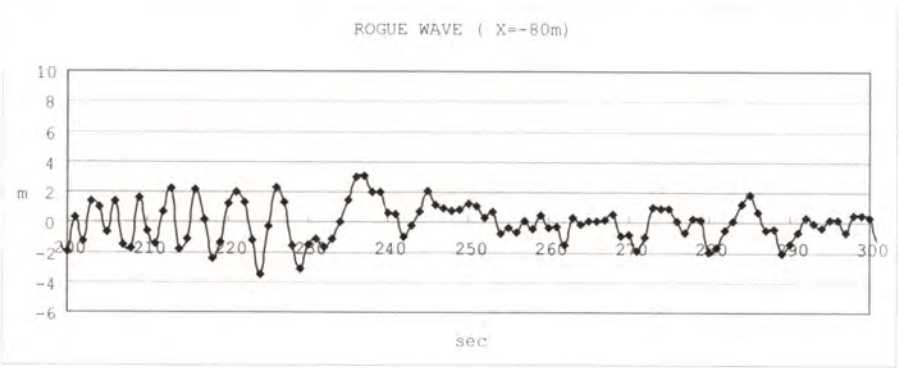

Fig. 10. Wave modulation at 80m upstream virtual site

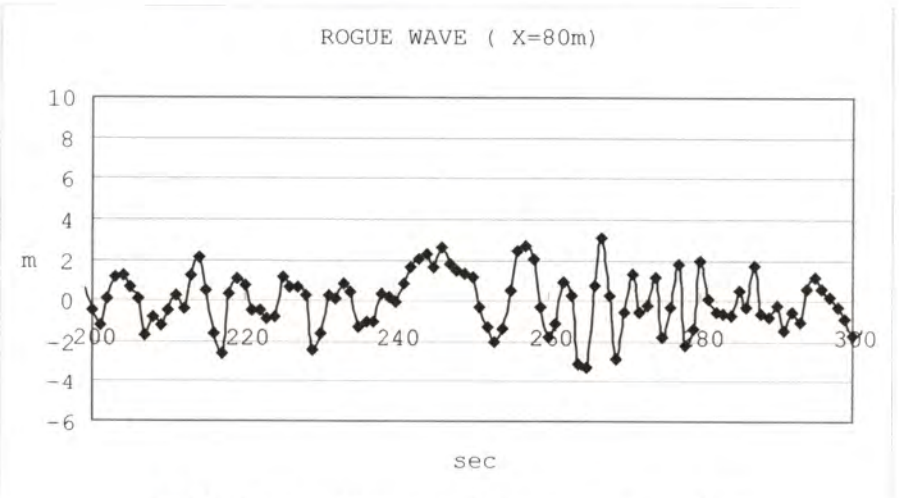

Fig. 11. Wave modulation at 80m downstream virtual site

6 Fluctuation Property of Sea Wave Period

In the statistical studies of ocean waves as random processes, PDF of wave height and period were investigated from various points of view. In contrast, the studies on the nature of time sequence of wave height and period are so far somehow scarce. So we present here briefly the time variation of these quantities and their stochastic natures.

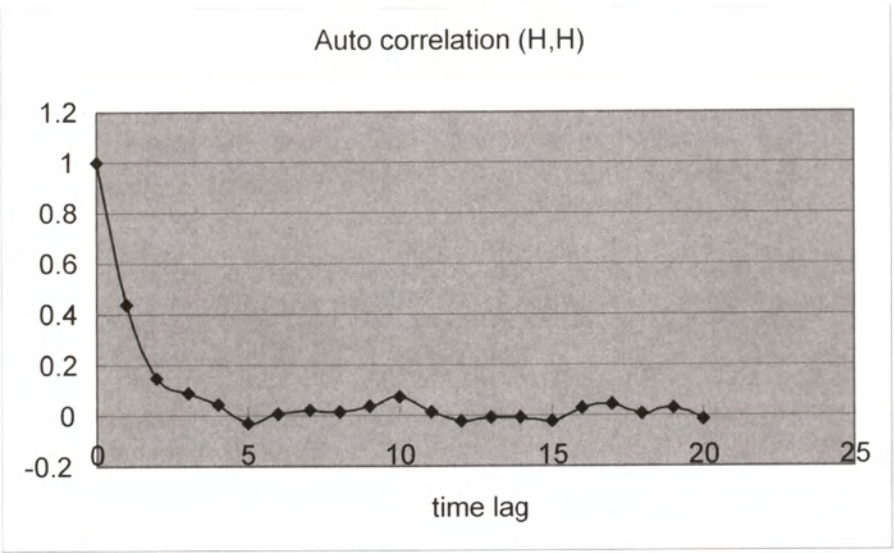

Fig. 12. Autocorrelation of the sequence of wave height

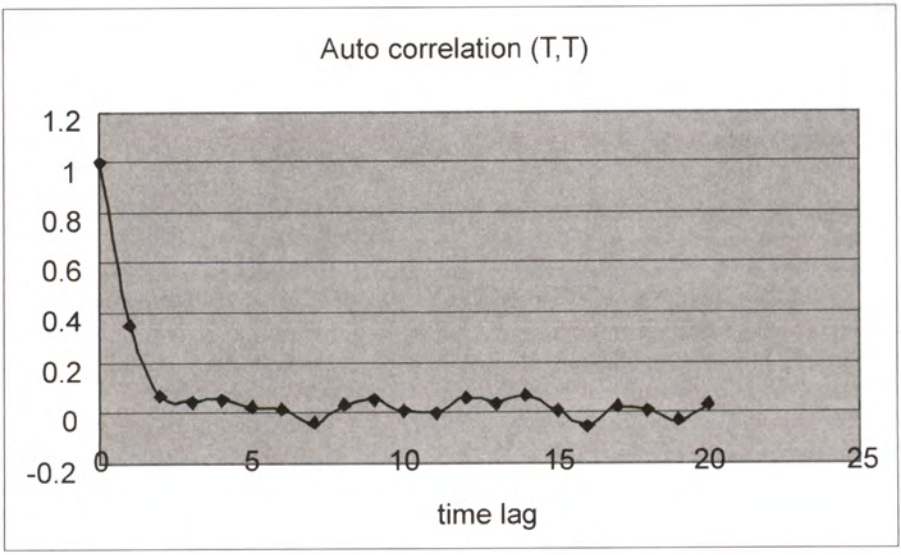

Fig. 13. Autocorrelation of the sequence of wave period

From the sequence of wave heights, we calculate their autocorrelation shown in Fig. 12.

In this figure, one can see that the correlation of successive wave heights is 0.43 , which lays almost at the middle of the values of actual measurements by Goda [4]. In his results, the values are 0.63 in swell and 0.26 in sea. For the sequence of wave periods, autocorrelation between successive periods is 0.35 as is seen in Fig. 13. The autocorrelation of wave height is slightly higher than that of wave period in a fully arisen sea. As for the wave period, the correlation of successive wave is rather lower than that mentioned in [2].

The discrepancy is partly explained by the fact that data adopted here is under the climatic condition of long lasting low atmospheric pressure in the winter season while their data were taken during a severe storm. In Fig. 14, we present the cross correlation of wave height to period.

At the origin of time lag, say for a same ZUC wave, correlation coefficient is 0.63 comparatively higher than those of non-stationary and is not discrepant to the result shown formerly in the contour lines from the contingency table of joint distribution. A closer study of the fluctuation of wave period is performed by the statistical mechanical technique. We calculated the power spectra of every sequence of 512 wave periods. Averaging 25 samples extracted from the stationary wind sea, the spectral density is obtained in Fig. 15 in log-log scale. Note that the ordinate S and abscissa f (recurrence frequency of periods) are in arbitrary scales. For the higher end of Fig. 15, we have the linear regression of the coefficient –0.98 shown in Fig. 16. This means the power law $S \propto 1/f$, which is the famous relation in many branches of science.

7 Conclusions

The nature of stochastic properties of a fully arisen wind sea are investigated by use of large number of wave data including up to 14,000 waves which were taken in almost stationary sea conditions. Precise analyses on PDF and temporal variation of wave period are performed. The results are considered to be statistically reliable because of the law of large numbers.

A simple quasi-linear method of wave record transformation is examined. It is applied to a typical example of Rogue wave in the actual ocean. The results suggest that the frequency-modulated wave train is a possible cause of creation and annihilation of such an abnormal wave in the ocean. Nevertheless, more observational data and more strict non-linear theory concerning wave period in a random seaway is needed. We must identify the isolated Rogue wave from the theoretical point of view and distinguish it from the Abnormal or Freak wave (wave height is 2 times larger than significant wave height), which has ever been defined for the convenience of practical use.

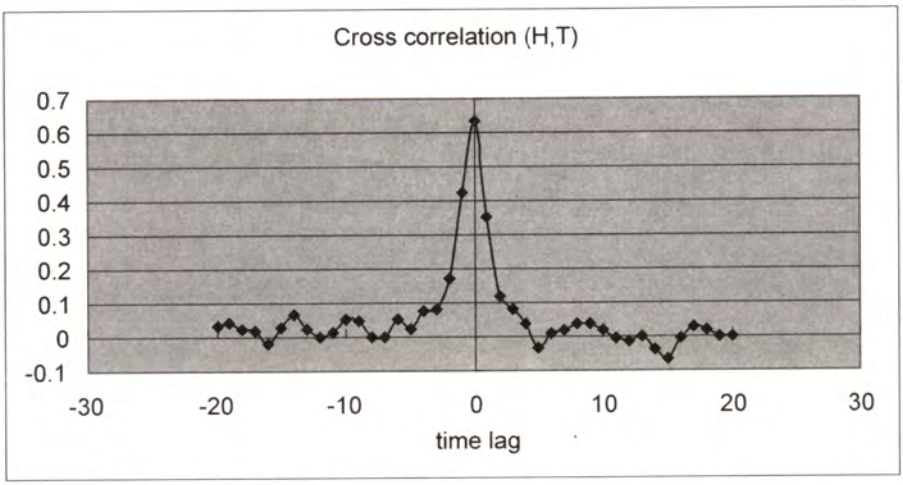

Fig. 14. Cross correlation of the sequence of wave height and period

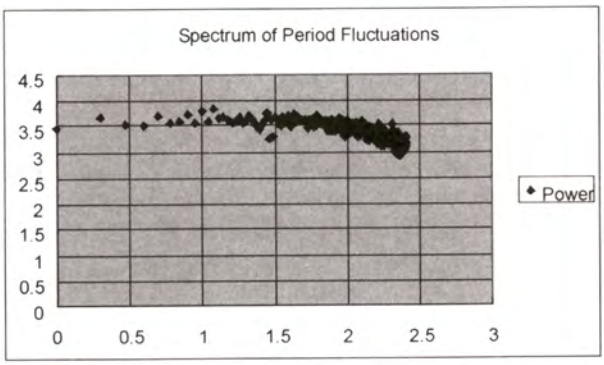

Fig. 15. Averaged power spectrum of the fluctuation of wave period

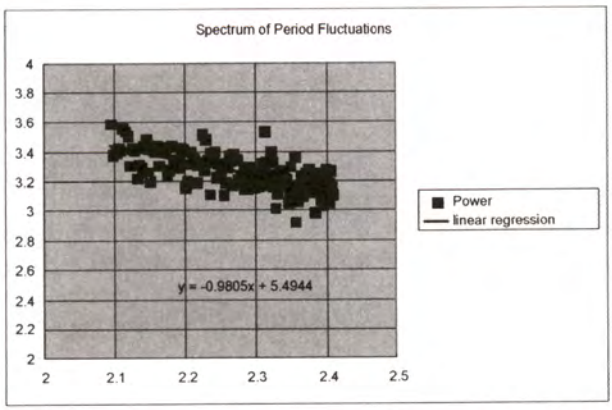

Fig. 16. Averaged power spectrum of the fluctuation of wave period and its linear regression

References

1. Longuet-Higgins M. S.: On the Joint Distribution of Wave Periods and Amplitudes in a Random Wave Field, Proc. Roy. Soc. London, Ser. A., Vol.389 (1983)
2. Myrhaug D. and H. Rue: Note on a Joint Distribution of Successive Wave Periods, J. Ship Research, Vol.37 (1993)
3. Tomita H. and T. Kawamura: Statistical Analysis and Inference from the In-Situ Data of the Sea of Japan with Reference to Abnormal and/or Freak Waves, Proceedings ISOPE2000, Vol.3 Seattle USA (2000)
4. Goda Y.: *Random Seas and Design of Maritime Structures*, University of Tokyo Press (1985)

Evidences of the Existence of Freak Waves

Sverre Haver

Statoil, E&P Norway, N-4035 Stavanger, Norway
svha@statoil.com

Abstract. As an extended introduction, the consequences of a possible existence of freak waves is discussed from a risk point of view, where focus is on the risk for loss of human lives. Herein freak waves are defined as wave events which are not captured by a second order model for the surface process, which as of today is the most advanced wave model for routine engineering. Finally, a major part of the paper is devoted to a review of literature which have presented wave events which may be examples of freak wave events.

1 Introduction

Over the last 2-3 decades major improvements are made regarding the modelling of environmental conditions for the purpose of designing offshore structures. This is the case both when it comes to the understanding of the underlying environmental processes and even more when it comes to the availability of good quality data which has made an empirical modelling of the environmental conditions rather accurate for a number of locations world-wide. Of course the models are not perfect and there are obviously rooms for improvements e.g.:

- Modelling of current in deep waters.
- Simultaneous modelling of wind sea and swell. This is mainly a question of more data of such events.
- Improved joint probabilistic modelling of wind waves water level and current.
- Closed form crest height model valid for various levels of sea state steepness and water depths.
- Improved predictions of the most extreme weather conditions (in terms of mean characteristics), i.e. so called 10^{-4} - weather.
- Kinematics (particle velocity and acceleration) associated with real ocean waves.

Although challenging from an environmental point of view, these short comings do not represent major problems from a design point of view. Doing some sensitivity studies, conservative choices can be made and together with the load factors used in the design process, a safe design should be achieved. More challenging from a design point of view is the wave - structure interactions - this topic is associated with very

large uncertainties and typically requires costly model tests in order to be solved properly.

One environmental problem, however, stands out as a possible major problem - freak waves - if it is proven that they exist as a separate population. There are a number of indications - more or less subjectively - indicating the existence of wave events which are much larger (either in terms of the wave height or in terms of the crest height) or much steeper than expected by the reporter. Of course - being realisations of a random process - there is always a possibility (although very small) that an unexpectedly large event is occurring. Assuming a 10-year storm is affecting an ocean area being so large that it can be divided into 100 sub areas between which extreme storm waves can be assumed to be statistically independent, one may well see a wave close to a 1000-year wave in one of these sub areas. If this is the reason for the observed unexpected large events, they do not represent a particular problem. The likelihood of occurrence are then baked into our standard design process.

For a structure to be designed for a site on the Norwegian continental shelf, the Norwegian authorities require that the following extreme load cases are controlled:

- Environmental loads corresponding to a return period of 100 years in combination with a load factor typically taken to be 1.3. No major damage are permitted for this load event. For a number of ocean structures the 100-year load is often reasonably well approximated by the loads caused by the 100-year wave.
- Environmental loads corresponding to a return period of 10000 years in combination with a load factor typically set to 1.0. Again - for a number of structures this load is reasonably well approximated with the load caused by the 10000-year wave. For this limit state local damage is accepted, but the situation shall not develop into a catastrophic event, i.e. the structure shall not collapse or sink. The latter is implemented by requiring that the structure in damaged condition (i.e. after being exposed to the 10000-year wave induced response) can withstand loads with a 100-year return period with the load factor typically set to 1.0.

When we are predicting 100-year and 10000-year loads, we account (at least within the Norwegian practise) for a certain deviation from a Gaussian surface process. And if observed unexpected large wave events can be concluded to be rare realisations of a slightly non-Gaussian surface process, an acceptable structural safety is tacitly assumed to be achieved by the limit states mentioned above.

It is, however, this authors point of view that we can not exclude the possibility that some of these observed unexpected large wave events are realisations from a separate freak wave population. The physical conditions that could onset such a population are not yet known and, accordingly, neither the relative frequency of occurrence of events. These events are most probably so rare that it is not likely to effect our predictions of 100-year wave induced loads. However, if existing, it may well impact our prediction of accidental wave induced loads, i.e. loads with a return period in the order of 10000 years. If this is the case, this means that the load we presently adopts as a load with an annual probability of occurrence of 10^{-4} actually

should be associated with an annual probability of occurrence of e.g. 10^{-3}. The load that should have been used as an accidental load, i.e. a load with an annual probability of occurring of 10^{-4}, could well be the load we (by excluding freak waves as a separate phenomenon) associate with a annual probability of 10^{-5}.

Let us illustrate the possible consequences of this by a simple but realistic example. At the Norwegian Continental Shelf, a jacket structure is usually designed such that the height from the still water surface to the deck level is so large that it is ensured that the wave crest height with an annual probability of occurrence of 10^{-4} does not reach the deck level. This means that the topside is not exposed to loading from the accidental wave, and, accordingly, the upper bay of the substructure is not designed to withstand major wave loading on the deck structure. If freak waves do exist for that particular site, one can well imagine that the actual 10000-year crest height is 10-20% larger than the accidental crest height according to which the necessary deck height is determined. This larger wave crest could submerge the lowest part of the deck structure with a couple of meters and this will result in an incredible horizontal load pulse. This load increase is not covered by our safety factors and a worst consequence is that the structure collapses in the upper bay. For a manned jacket this is a catastrophic scenario and the annual probability of such an event has to be extremely small.

A common measure for expressing the risk to people on board these platforms are the Fatal Accident Rate (FAR), which is defined as the expected number of fatalities per 10^8 exposed hours. For a given platform the FAR-value should in principle include all risks that represent a threat to the crew, i.e. explosions and fires, working accidents, collisions with other vessels, and structural failure due to weather and earthquakes. Let us for the sake of illustrations assume that an acceptable risk would be obtained by requiring $FAR < 5$. A good rule for a robust new structure would be to further require that structural failures due the environmental loading (wind, waves or earthquake) should represent a very small contribution to the FAR-value, say $FAR(environment) < 0.5$. There is a rather simple relation between the FAR-value and the annual probability of failure. Assuming all onboard lost due to the accidental environmental load, it is not too difficult to show:

$$\begin{aligned} p_f &= 10^{-5} \Rightarrow FAR \approx 0.1 \\ p_f &= 10^{-4} \Rightarrow FAR \approx 1 \\ p_f &= 10^{-3} \Rightarrow FAR \approx 10 \end{aligned} \quad . \tag{1}$$

Shall we fulfil the requirement above, it is seen from Eq. (1) that the resulting annual probability of structural failure has to fulfil:

$$p_f(environment) < 5 \cdot 10^{-5} . \tag{2}$$

This is to be implemented as an estimate of the actual failure probability. In carrying out a structural reliability analysis, effects of gross errors (human errors in a

broad sense) are usually not modelled explicitly. Referring to the failure probability estimated through a straight forward structural reliability analysis as a nominal failure probability, one can well imagine that gross errors could cause the actual (or true) failure probability to be $3-10$ times larger: This would of course depend on how sensitive the failure mode under consideration is to gross errors and/or the efforts done through procedures and training to minimise the impact of such failures. Taking 5 as a reasonable error factor accounting for gross errors, this means that a reasonable requirement to the nominal annual failure probability could be:

$$p_{f,nominal}\left(environment\right) \lesssim 10^{-5}. \tag{3}$$

As of today we will possibly have to interpret freak waves as some sort of a gross error. Ensuring that our structure fulfils Eq. (3) when excluding the freak wave phenomenon, one can hope that Eq. (2) is not too much violated if, in principle, freak waves could be consistently treated in a reliability assessment.

Eqs. (2 and 3) represent extremely rare events, but it is events at this probability that are of interest regarding structural failures. In order to verify that we actually can reach a target safety as low as indicated, we need to understand phenomena corresponding to such low annual probabilities of occurrence. If a freak wave population do exist, they will most probably affect our load predictions of such low probability events and, consequently, the risk exposure to crew and platform.

2 Definition of a Freak Wave

At present there is no broad consensus regarding what should be defined as a freak wave event. Over the years a ratio of wave height to significant wave height larger than 2 is taken as a definition of a freak wave. To this author this criterium is somewhat vague since nothing is said about the duration of the observation window, i.e. is it a 20min. time series, a 3-hour series, or is the observation window covering the whole storm event. Although the extremes are not extremely dependent of the time period, T, covered (roughly proportional with $\sqrt{ln\left(v_0^+\right)T}$, where v_0^+ is the expected zero-up crossing frequency of the wave process), the expected ratio will vary somewhat whether one look at 20-min. events or the full storm length.

To this author it seems reasonable to define freak waves as something that is beyond the knowledge available for routine design. This means that the criterium will evolve with time as our understanding is improved. If and when the freak phenomenon is fully understood, there is no reason to continue referring to these waves as freak waves. They will then be the extreme waves a structure is supposed to be designed against at a certain annual probability level.

As of today, the best we can do regarding the surface process is to describe it as a second order process, i.e.:

$$\Xi_2(t) = \Xi_1(t) + \Delta\Xi_2(t) \tag{4}$$

where, see e.g. [8]:

$$\Xi_1(t) = \sum_{k=1}^{N} A_k \cos(\omega_k t + \theta_k) = Re\left[\sum_{k=1}^{N} B_k \exp(i\omega_k t)\right]. \tag{5}$$

$Re[\cdot]$ denotes the real part of a complex number, and $B_k \exp(i\omega_k t)$ are the complex Fourier amplitudes. Furthermore, A_k and θ_k are Rayleigh distributed and uniformly distributed, respectively. The mean square of A_k is related to the underlying wave spectrum, $s_{\Xi\Xi}(\omega)$, through:

$$E\left[A_k^2\right] = 2 s_{\Xi\Xi}(\omega) d\omega_k, \quad d\omega_k = \omega_k - \omega_{k-1}. \tag{6}$$

The first order approximation to the surface process is given by Eq. (5), while the second order correction, $\Delta\Xi_2(t)$, can be written, see e.g. [13]:

$$\Delta\Xi_2(t) = Re\left[\sum_{m=1}^{N}\sum_{n=1}^{N} B_m B_n \left\{H_{mn}^{+} e^{i(\omega_m+\omega_n)t} + H_{mn}^{-} e^{i(\omega_m-\omega_n)t}\right\}\right]. \tag{7}$$

The functions H_{mn}^{+} and H_{mn}^{-} are usually referred to as quadratic transfer functions and should be evaluated for all frequency pairs (ω_m, ω_n). Closed form solutions for the quadratic transfer functions are available see e.g. [13].

A part of a second order simulation is shown in Fig. 1. The underlying first order process and the second order correction are also shown. It is seen that the main effect of the second order correction is to make the troughs slightly shallower, the crests slightly higher and the wave front slightly steeper.

Such a second order model is available in a number of computer codes for load calculations. The surface shown in Fig. 1 is obtained using Wavemaker, [18]. The surface represented by such a model seems to be broadly accepted as a rather accurate model for real waves. The empirical distribution functions of 20-min. maximum crest heights and 20-min. minimum trough depths of the storm data included in [6] are compared with the corresponding distribution functions obtained under a first and a second order assumption, respectively, in Figs. 2 and 3. It is seen that the second order simulation results in a reasonable fit, except for the largest observed crest height. This particular observation will be discussed later on.

Regarding the calculation of the corresponding kinematics, things are more complicated and there is no general agreement on how this should be done in order to be fully consistent with the simulated surface process.

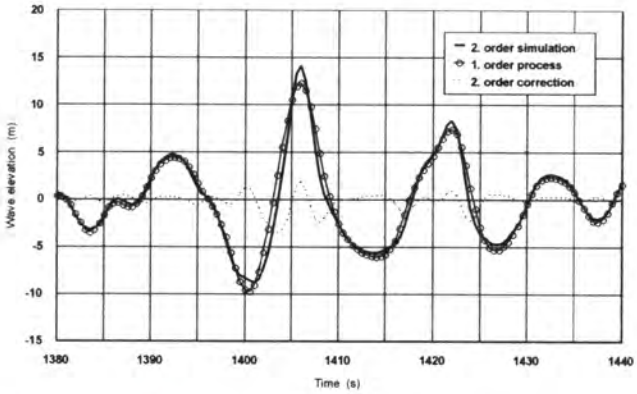

Fig. 1. Example of a simulated second order surface elevation process

Regarding crest heights, wave heights, and various measures of sea state steepness, a second order model is from this authors point of view today state-of-art. This is the background for suggesting the following definition of a freak wave event:

> *A freak wave event is an event (crest height, wave height, steepness, or group of waves) that represent an outlier when seen in view of the population of events generated by the second order model.*

If one is to look at freak waves in available data, one has to define the length of the observation window and a reasonably high fractile for the largest event in the actual window. This is discussed in [6]. There the length of the window is taken to be 20 min. since most available data series at least in Norway correspond to such a duration. In a second order process, the ratio of wave height to significant wave height that is likely to be exceeded in 1 out of 100 cases is about 2.0 while the same fractile for the crest height to significant wave height ratio is 1.25. Based on this, the following criterium is suggested as an indicator of possible freak wave events:

> *If for a 20-min time series,* $c_{max} / h_{m0} > 1.25$ *and/or* $h_{max} / h_{m0} > 2.0$, *the event is a possible freak wave. Further investigation will be necessary in order to finally conclude.*

Similar criteria can be established with respect to wave steepness and wave groupiness.

3 Some Observations of Possible Freak Waves

Over the years, a number of possible freak wave episodes are referred to in the literature. As a consequence of a number of episodes with significant wave induced damage on ships off the eastern South African coast during the fifties, sixties and early

seventies, the subject of freak or abnormal waves received some attention during the seventies, see e.g. [11], [12], [1] and [3]. The definition of a freak wave adopted by WMO (The World Meteorological Organisation) reads, [1]:

> *"A freak wave may be defined as a wave of a considerable height ahead of which there is a deep trough. Thus it is the unusual steepness of the wave which is its outstanding feature and makes it dangerous to shipping. Reports so far suggest that such waves have usually occurred where a strong current flows in the opposite direction to a heavy sea."*

A couple of actual observations supporting this deep trough is referred to in [11]. The first is due to the Master of the Edinburgh Castle describing an episode taking place off the eastern South African coast. The vessel was heading into a strong south-west wind and a heavy south-west swell, but being 750 feet long and of 28000 gross tonnage, these conditions presented no serious problems to her. According to the master: "Under these conditions she was very comfortable for three-quarters of an hour or so. The distance from one wave top to the next was about 150 feet and the ship was pitching and scending about 10-15 degrees to the horizontal. And then it happened. Suddenly, having scended normally, the wavelength appear to be double the normal, about 300 feet, so that when she pitched she charged, as it where, into a hole in the ocean at an angle of 30° or more, shovelling the next wave to a height of 15 or 20 feet before she could recover 'out of step'." (The wave lengths referred to above are surprisingly short. We will therefore question the unit feet - meter seems more likely.)

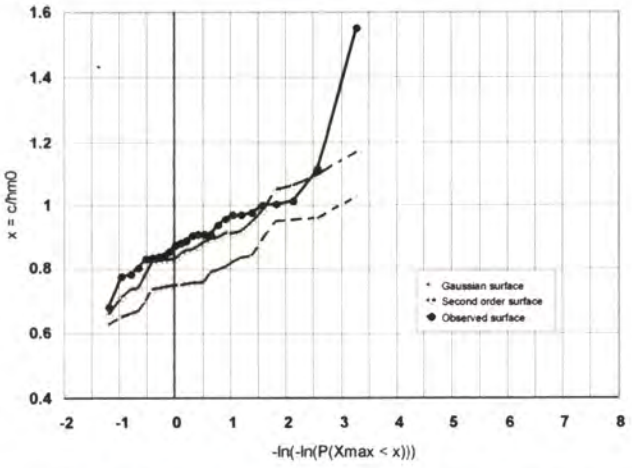

Fig. 2. Adequacy of the Gaussian - and second order assumption in representing observed 20-min. largest crest heights. (Normalised with the significant wave height, h_{m0}.)

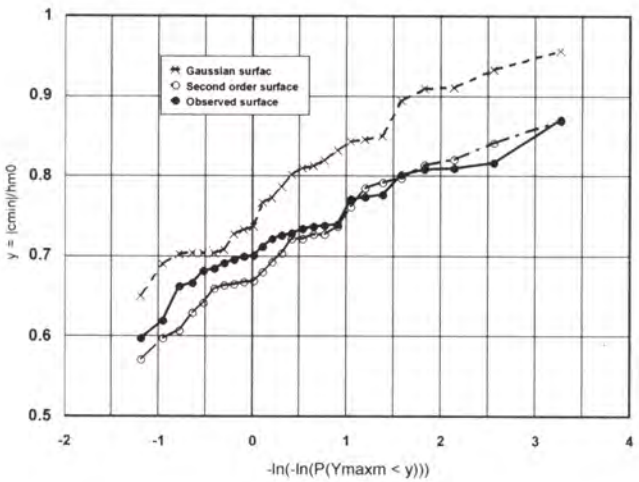

Fig. 3. Adequacy of the Gaussian - and second order assumption in representing observed 20-min. smallest trough depths. (Normalised with the significant wave height, h_{m0}.)

When this story reached the national press, it brought forward the following story from a second world war commander: "When I was serving at the cruiser Birmingham during the Second World War we had a similar experience in those waters one night which I recall the more vividly for being on watch at the time. We were about 100 miles south-southwest of Durban on our way to Cape Town, steaming fast but quite comfortably into moderate sea and swell when suddenly we hit the 'hole' and went down like a plummet into the next sea which came green over A and B turrets and broke over our open Bridge. I was knocked violently off my feet, only to recover and find myself wading around in 2 feet of water at a height 60 feet above normal sea level."

The idea of a long trough followed by a steep crest is elaborated in the paper by [12]. With a strong current opposing the waves, and the wave field built up by three sinusoidals of different lengths, such a scenario is illustrated within the framework of linear wave theory. For a sea state consisting of three pure swell systems, this model could possibly be representative. However, in most real sea systems, energy will be spread over a much broader range of frequencies and the probability for a very unfavourable phasing between the various components will be very small.

The early autumn of 1995, Queen Elisabeth II headed into a major storm, "Luis", off New Foundland, [2]. The maximum wave height from the ship's log was close to 30m. In a radio interview with the ship master after the storm, he refers to a particular episode where they from the bridge were looking at a wall of water for a "couple of minutes" before it hit the ship with some damage well above the water line. In the end of January 1995, a semi submersible, Veslefrikk B, operated by Statoil, was hit by a wave resulting in significant damage to the winch housing at the southern corner and the double bottom close to the western column. One of the crew members gave an oral description of this wave event that reminds very much of that of the QE II master. He

also referred "to wall of water they could see for a couple of minutes". In both these episodes, the wave conditions were rather severe, and the particular wave events will not necessarily be of a freak type. The reason for including these observations is the phrasing "a wall of water for a couple minutes". Whether the couple of minutes should be two minutes or, say, 30s, is not a major point, but these observations, although not very scientifically documented by this paper, suggest that these very extreme waves appear for the observers more or less as a frozen profile for some time. Such a situation could not be maintained for several wave periods within a second order frame work.

Some few measurements of possible freak waves have been made over the years. Concentrating on the Danish sector of the North Sea, [15] present a number of cases involving waves we according to the criteria above will consider as possible freak waves. They show several cases where the crest height is about twice the significant wave height, i.e. a factor 2 as compared to the factor 1.2 introduced in this paper as a definition of a possible freak crest height. Even if we consider these as the largest out of 2000-3000 waves, we would consider these realisations to be well outside of what we would expect within a second order framework. Increasing the number of underlying waves from 100 to 2500, would suggest that the body of the extreme value distribution is shifted some 30 - 50% towards higher values. As the crest heights referred to above are measured at a water depth of about 40m, it is most likely that the wave profiles under extreme conditions are significantly affected by the bottom. [15], however, do also refer to some few episodes from deeper water. Of particular interest is a case from the Ekofisk field, where significant damage was reported more than 20m above still water level. The significant wave height at the time of the damage is not known, but a value in the order of 10-12m is reasonable, suggesting a crest height close to twice the significant wave height. At this depth, the bottom is expected to influence the wave profile of the largest waves, but it is not likely to be a governing effect.

Kjeldsen, [9], has considered data recorded from the Frigg field in the North Sea. The water depth is about 100m, and limited depth is not expected to be an important parameter regarding the surface elevation process. Some few observations seem to belong to a possible freak wave class, in particular when attention is given to the crest height. Yasuda *et al.*, [20], have considered the occurrence of freak waves off Japan. They define a freak wave as a wave with a wave height being twice the significant wave height. A number of waves fulfilling this definition are included. An interesting example of a possible freak wave off Japan is shown by [19], but the measurements made off Japan correspond to rather shallow water, 43m, i.e. comparable to the depth of the cases from the Danish sector of the North Sea reported by [15]. We expect that results obtained for such water depths will not necessarily be representative for deeper waters, at least not if we consider sea states of a similar characteristic period.

A number of examples of heavy weather damages caused by giant waves are presented by [10]. In particular, he reefers to the capsizing of the semi-submersible, Ocean Ranger. The initiating event of this tragedy was according to [10] a giant wave that struck on the windows and flooded the control room. Over the years there has also been a number of ships disappearing without trace in stormy conditions with a considerable loss of human lives, an example being the Derbyshire disaster, see e.g.

[5] for some further references to this event. The 4-year old bulker being 965 feet long disappeared in a severe typhoon some 500 miles south of Japan. Since vessels are lost without trace, they must have been sinking very fast. In reasonable weather conditions this seems to suggest that the initiating event is a major explosion. In very severe weather conditions, the impact with a giant wave seems just as likely. The structural strength may in some cases have been significantly degraded due to age and, possibly, lack of proper maintenance. Some ship designs may also be somewhat more vulnerable to severe consequences of possible heavy weather damage. In spite of all this, one can still not exclude that the reason for the loss of some of these ships is that they unfortunately hit a wave well beyond the expected design waves.

Faulkner and Buckley, [5], do also refer a number of other episodes where massive damage to ships due to giant waves is reported. In 1943, the liner "Queen Elizabeth" hit a trough preceding a giant wave off the east coast of Greenland. The wave broke over the ship and was followed by a second wave. The wave impacts shattered the bridge windows about 90 feet above the normal water line. The fore deck was smashed 0.15m below its normal level. In a contribution to a HSE-study, [7], Prof. Faulkner, in addition to the episode referred to above, also mention an episode in 1942 where "Queen Mary", carrying 15000 US troops onboard, was close to capsizing in steep elevated seas in the north east Atlantic.

January 1 1995, a Statoil operated jacket platform, "Draupner", was hit by a giant wave, see Fig. 4. The meteorological conditions in connection with this event is discussed by [17]. The water depth in the area is about 70m. The wave was measured by a down-looking laser device and the significant wave height averaged over a 20-min. period was about 12m. The maximum wave height, see Fig. 5, was close to 26m, i.e. identified as a possible freak wave by the criterium established on basis of 20-min. measurements. The impressive thing about this wave, however, is its crest height which is measured to about 18.5m, well into the class of possible freak waves. This event is included in the data underlying Fig. 2 and it clearly deviates from the typical pattern. Within a second order frame work, Fig. 2 suggests that the probability of obtaining this value of the crest height to significant wave height ratio is 1:1000. The observed adjacent trough depth is less than 40% of the crest height. The conditional probability of having such a shallow trough following a major crest height is under the second order assumption most probably in the order of 1:100. Accordingly, the probability of observing an event like the event shown in Fig. 5 during a 20-min. window is in the order of 1:100000. For a typical North Sea site, the probability of observing a 20-min. sea state with a significant wave height of 10m or more is about $4 \cdot 10^{-4}$. Assuming 1 out of 10 to correspond to a steepness being necessary for producing the most extreme crest heights, we will expect about 1 event per year in at a given site. Due to the correlation between adjacent 20-min. events, a more proper interpretation may well be 10 events in a row every 10 years. No matter of interpretation, and in spite of the rather approximate probabilities presented in this paragraph, the observation of an wave event shown in Fig. 5 is rather unlikely event under the second order assumption. This author will take this event as an indication that the most extreme wave events are effected by phenomena not covered by our second order model.

The phenomena needed for explaining such a wave is not yet resolved. It could be an inherent energy fluctuation with a period much larger than 20 minutes (and a corresponding spatial distance) and thus destroyed by our assumption of stationarity. If that is the case, it will have major impacts on our fitting of probabilistic models since the ergodicity assumption will fail if the stationarity assumption fails. Another possibility is energy focusing as the wave system is travelling in space, see e.g. [16], [4], [14] or other disturbances suddenly make 3. and 4. order correction processes very important for a short time (maybe some few wave periods) and limited spatial area (of the order of some few wave lengths).

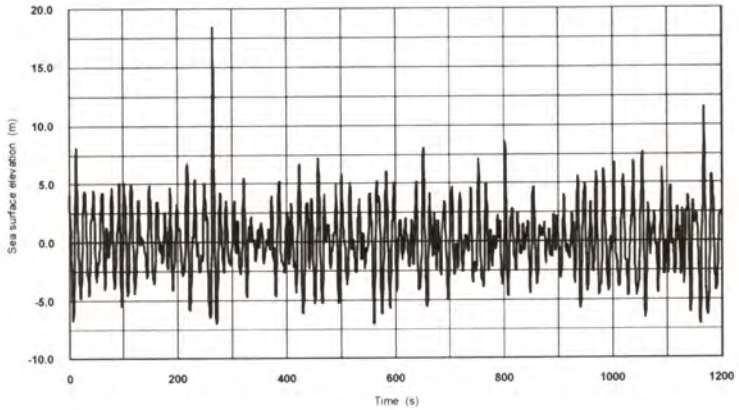

Fig. 4. A 20-min. wave recording at the "Draupner" platform, January 1, 1995 at 15:20

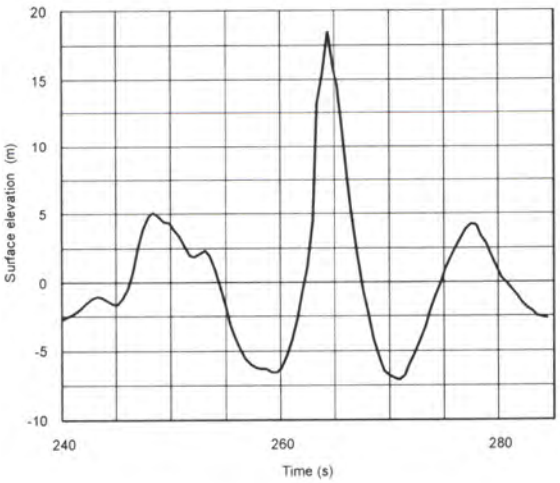

Fig. 5. The "New Year Wave" at "Draupner".

References

1. Atkins : Special Reports of Freak Waves. London Meteorological Office, London (1975). (The details on this reference is not known by the authors.)
2. Bigio : LUIS and the Buoys....and the Queen. 4th International Workshop on Wave Hindcasting and Forecasting", Banff (1995)
3. Dawson : Freak Ocean Waves Are Episodic. New Scientist (January 1977)
4. Dysthe, K.B., Trulsen, K.: Note on Breather Type Solutions of the NLS as Models for freak-waves. Physica Scripta, vol. T82 (1999)
5. Faulkner, D., Buckley, W.H.: Critical Survival Conditions for Ship Design. Proceedings for the International Conference; Design and Operation for Abnormal Conditions. Glasgow (1997)
6. Haver, S., Andersen, O.J.: Freak Waves - Rare Realisations of a Typical Population or Typical Realisations of a Rare Population?. Proceedings ISOPE-2000. Seattle (May 2000).
7. HSE: Review of Greenwater & Waveslam, Design & Specifications, Requirements for FPSO/FPU's, Offshore Technology Report - OTC 2000 004, Health & Safety Executive. Prepared by PAFA Consulting Engineering Ltd., London (March 2000)
8. Jha, A.K.: Nonlinear Stochastic Models for Loads and Responses of Offshore Structures and Vessels. PhD. Dissertation. Stanford University (1997)
9. Kjeldsen, S.P.: Breaking Waves. In: Tørum, A. and Gudmestad, O.T. (eds.): Water Wave Kinematics. Kluwer Academic Publishers, Dordrecht The Netherlands (1990)
10. Kjeldsen, S.P.: Examples of Heavy Weather Damage Caused by Giant Waves. Technomarine, no. 820 (1996)
11. London Meteorological Office:The One from Nowhere", Marine Observers, 35. London (1965)
12. Mallory : Abnormal Waves off the South African Coast - A Danger to Shipping. The Naval Architect (July 1975)
13. Marthinsen, T., Winterstein, S.R.: On the Skewness of Random Surface Waves. Proceedings ISOPE'92, San Francisco (1992)
14. Osborne, A.R.: The Random and Deterministic Dynamics of "Rogue Waves" in Unidirectional, Deep-Water Wave Trains. The Third International Workshop on Very Large Floating Structures (VLFS'99), Honolulu (1999)
15. Sand, S.E., Ottesen-Hansen, N.E., Klinting, P., Gudmestad, O.T. and Sterndorff, M.J.: Freak Wave Kinematics. In: Tørum, A. and Gudmestad, O.T. (eds.): Water Wave Kinematics. Kluwer Academic Publishers, Dordrecht The Netherlands (1990)
16. Stansberg, C.T.: Nonlinear Extreme Wave Evolution in Random Wave Groups. ISOPE'2000, Seattle (2000)
17. Sunde, A.: Kjempebølger i Nordsjøen (*in Norwegian*), Vær & Klima, vol. 18, no. 1 (1995)
18. Sweetman, B., Winterstein, S.R.: Second Order Random Ocean Waves: Prediction of Temporal and Spatial Variation from Fixed and Moving References - The Routine WAVEMAKER, , Version 3.2. Rep. No. RMS-37. Civil Engineering Dep., Stanford University, Stanford (1999)
19. Tomita, H, Sawada, H.: Statistics of Heavy Weather Actual Ocean Wave Data in North Sea and Japan Sea with Reference to Abnormal Waves. ISOPE'99, Brest France (1999)
20. Yasuda, T., Mori, N., Nakayama, S.: Characteristics of Giant Freak Waves Observed in the Sea of Japan. Proceedings Waves'97 Ocean Wave Measurements and Analysis, Vol. 2. Virginia Beach (1997)

Extremes from Evolved Waves Using Measurements from a Waverider Buoy and Vertical Lasers

Anne Karin Magnusson[1], Mark A. Donelan[2]

[1] Norwegian Meteorological Institute, Forecasting Division Western Norway,
Allegaten 70, 5007 Bergen, Norway
a.k.magnusson@dnmi.no
[2] RSMAS/Applied Marine Physics, University of Miami, 4600 Rickenbacker Causeway,
Miami, Florida 33149, USA
mdonelan@rsmas.miami.edu

Abstract. Extreme wave crests have been of special interest for fixed platforms, since the platform designs are directly connected to the statistics of extreme crest heights and the water velocities in such waves. Extreme statistics are usually made from point measurements, but waves often appear in wave groups. Due to the dispersive nature of the waves, these groups can have different maximum crests at different positions along the direction of travel. The probability of measuring the overall maxima from point measurements is quite low. Also, buoys, which are widely used for wave measurements, have a quasi-Lagrangian (qL) behaviour. In [1] a set of storm data measured with a waverider at Ekofisk (central North Sea) was analysed. The records were corrected for the qL behaviour and evolved up and down wave assuming unidirectionality. Maximum crest heights and forces were seen to increase. In this work we compare similar results using simultaneous waverider and vertical lasers measurements. The effect of buoy correction is discussed and some results of the comparison are shown. Evolution through dispersive propagation increases the number of waves with maximum height twice that of significant wave height (often used as the defining criterion for freak waves).

1 Introduction

On the 12th December 1990 a big storm swept through the North Sea, giving 13-15 meter significant wave heights and causing severe damage to platforms like those at the Ekofisk field (56.5°N, 3.2°E). It has been observed that extreme crest heights (or water damage on the lower deck on offshore platforms) occur in some storms but not in others, despite the significant wave height being the same in each of them. Since then, and also due to other situations with extremely high wave crests, research and development in forecasting of waves has been concerned with going a step further (than forecasting average parameters such as significant wave height and mean period) by also trying to predict the maximum crest heights in the different kinds of sea states.

The seafloor under the Ekofisk complex is subsiding due to the oil extraction. Besides other major safety actions like jack-ups and building of new platforms,

Phillips Petroleum Company of Norway (PPCON), operator for Ekofisk, and the Norwegian Meteorological Institute (DNMI) started developing a special forecasting service called EXWW (Ekofisk eXtreme Wave Warning), with well-defined procedures to ensure safety of operations. Experience proved very soon the importance of good instrumentation for the measuring of waves, and there are now 3 in-situ wave recorders (one waverider buoy and 2 vertical lasers) and a WAMOS radar (based on nautical radars) reporting wave data in real time to the forecaster in Bergen.

With such an extended database, we have the opportunity to analyse waves in detail and to sort out datasets subject to errors of any kind (lee effects - interaction effects with construction) that are often quite common in wave profile analysis. Earlier attempts have been made to find relations between extreme wave situations and weather phenomena [2], without much success. There are a number of reasons for this.

First, Waverider data were used. Buoys are 'wave followers': on the crest, they tend to move in the wave propagation direction and in the troughs they move the opposite way. The movement is restrained to some extent by the tethering. Therefore, typically, the buoy spends more time on crests and less in troughs than a fixed sensor.. Waves measured by buoys exhibit more vertical symmetry than when measured from a fixed position like vertical lasers. Also the apparent mean water level becomes displaced (higher), with the consequence that crest heights (above mean water level) become too low. Wave steepness measured with buoys are also generally lower than those measured from a fixed position. Longuet-Higgins ([3], [4]) describes this quasi-Lagrangian behaviour, and in [1] some storm data measured with a waverider at Ekofisk were corrected for this.

Secondly, waves come in groups, and their profiles change as they propagate due to different propagation speeds of different wave components forming the sea state. One way of producing extremes is by the 'coalescense' of the waves, when long waves overtake the shorter ones [5]. The chance of measuring at the coalescing point seems to be quite small. Looking for rare events in a dataset, even when using many years of data, must therefore result in very few 'captures'.

A statistical analysis of historic datasets is therefore unlikely to answer the question of what kind of extremes actually occur. It is a fact that water impacts (due to more than only sea spray) have occurred at very high levels above mean water, so high that it is reasonable to believe that extreme wave crest heights may occur outside the expectancies of Rayleigh distributions. Tank experiments are being done to find if certain spectral forms give such waves (see for example [6], [7]).

In [1] wave profile time series measured by a waverider during 4 storms have been corrected for the quasi-Lagrangian movement, thereafter propagated ('evolved') up- and down-wave assuming linear propagation and unidirectional waves. The new dataset showed that maximum wave crests could become considerably higher (25%) than in original datasets, in the average by 2.5%. Wave induced forces, proportional to the square of the particle velocity also analyzed in the paper using the method of Donelan et al [8], were seen to increase by up to 60%.

In this work we compare such calculations with the waverider with similar calculations with the laser measurements during 4 new storms from the winter season 1998-1999. The questions we ask are: do the corrections for quasi-Lagrangian

behaviour make the waverider data similar to the laser data? How does 'evolution' change the statistics for the 2 kinds of instruments? Some preliminary results are presented here.

2 Waverider and laser measurements

Wave profile time series from 3 in-situ instruments are used. The recording frequency for all three is 2 Hz and each wave record is 20 minutes long. The number of records used is dependent on the storm situation. We have sorted out time series with as constant wind and wave conditions as possible. The instruments are one waverider (heave-buoy) situated 1 nm NE of the Complex, and two lasers measuring the vertical height from their location (underside of a bridge between 2 platforms) to the sea surface. One laser is situated south of the northernmost platform of the complex ('Flare North'), the other one is north of the southernmost platform ('Flare South').

2. 1 Description of storm cases

Wind and wave data used in this study are from 25th October (storm no 1) and 27th December 1998 (storm no 2), and 4 to 5th (no 3) and 17th (no 4) February 1999. In the first storm wind and waves were from WNW. Wind speed was above 22m/s (10 min. - 10 m level). Significant wave height (Hs) in the period used in the analysis ranges from 4 to 10 m. In the second storm, waves at the Ekofisk location were produced by a strong wind (23-30m/s) with short fetch. Hs reached 12m. In the third storm, the waves and winds were taken in a period starting with WNW wind, veering NNW. In this case the laser at Flare South became located in a sector at the lee of the complex, so measurements from this location are disregarded. Wind speed reached at 27m/s from NW for a short time, but significant wave height was at the 9-10m level for a long time (from 17UTC the 4th to 04UTC the 5th). In the 4th storm, winds were from NNW, approximately 18m/s, and Hs values were between 7 and 8m for a period of about 5 hours.

2.2 Wave properties measured by different sensors

The difference in wave skewness (crest height relative to trough depth) recorded by a waverider compared to lasers is seen in Fig. 1, where time series of Hs, maximum crest and trough (absolute value) height in each 20 minute record from the 3 instruments at Ekofisk in the first storm are shown. For the waverider (WR, in the bottom panel) the crests and troughs (thin lines, stippled for the troughs) are about the same, while for the 2 laser time series the crests are mostly larger than the troughs, sometimes twice. The figure shows also how variable the sea state is measured from one location to another, with one or another sensor. Hs from laser at FN (Flare North) increases first, reaching 10m, WR crests one hour later at 10m, and FS (Flare South) 3 hours later than the WR at a slightly lower level (9m). Maximum crest height in the storm seems to occur at the same time for both lasers. It might be at that time that

significant wave height at Flare South is reduced because of lee-effects from the Ekofisk complex, but high crests do occur at this location anyway. There might be several explanations for this, for example can a high crest at the lee of the complex be a result of interaction between diffracted waves, but further discussion on this is beyond the scope of this paper. In the overall comparison of the wave measuring systems, only one of the lasers has been used in each storm: the one being free of lee effects of the platforms of the complex.

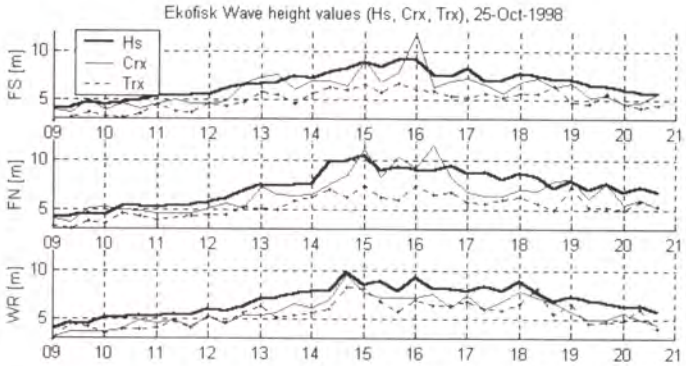

Fig. 1. Significant wave height (Hs, thick line), maximum crest height (Crx, thin line) and maximum trough depth (Trx, dotted line) during 25th october 1998 at Ekofisk, as measured by Waverider (WR, bottom panel) and lasers at Flare North (FN, center) and Flare South (FS, top).

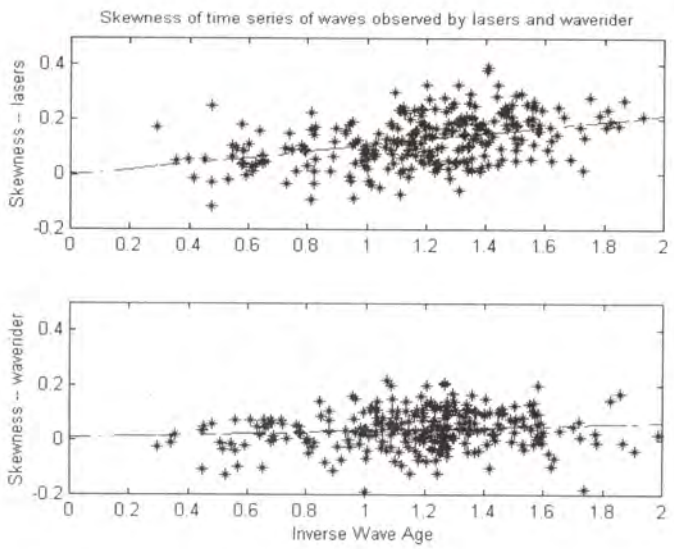

Fig. 2. Skewness (eq. 1) as function of inverse wave age (U_{10}/c_p) for Waverider (bottom panel) and laser measurements at Ekofisk during all 4 storms.

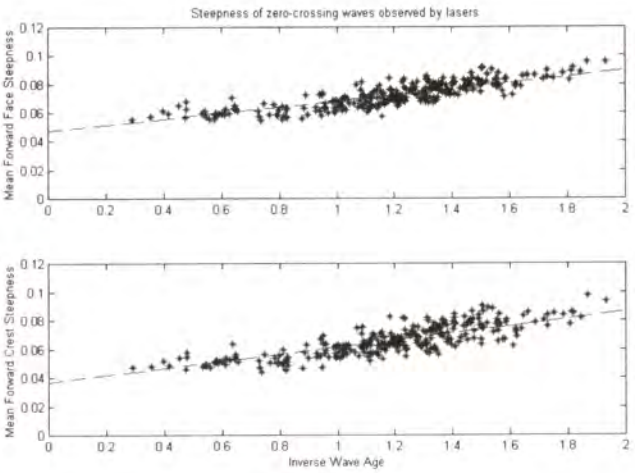

Fig. 3. Mean forward face steepness (FFS in eq. 2, top panel) and mean forward crest steepness (FCS, eq. 3, bottom panel) as function of inverse wave age as measured by lasers at Ekofisk.

Overall skewness versus wave age is shown in Fig. 2 for waverider (bottom panel) and laser data using data from all four storms. Average skewness ν is given by:

$$\eta = \left(\xi - \overline{\xi}\right)^3 \; > / \; std\left(\xi\right)^3 \tag{1}$$

where $\xi = \xi(t)$ is the time series of surface elevation. Inverse wave age is given by U_{10}/c_p, where U_{10} is the 10 meter height wind speed (10 min average) and c_p is phase velocity at the peak wave frequency. The figure shows that increasing the wind forcing increases the skewness for the waves measured with a laser, but such a relation is not at all obvious for waverider data, probably because the increasing nonlinearity of the surface with increasing forcing is to some extent suppressed by the quasi-Lagrangian behaviour of the buoy. This shows why searching for a better understanding of how and when extreme or rogue waves occur using buoy data is likely to fail. Buoys have been used widely (and are still), so it is worth finding a way to correct measurements for the quasi-Lagrangian behaviour that is the main cause of this discrepancy.

In the following, we have calculated different steepness parameters for waves measured by both type of instruments. These are *Forward Face Steepness* (FFS) and *Forward Crest Steepness* (FCS):

$$FFS \; = \; H \,/\, \left(\left(g \,/\, 2\pi\right).T.T'\right) \tag{2}$$

$$FCS \; = \; Cr \,/\, \left(\left(g \,/\, 2\pi\right).T.T''\right) \tag{3}$$

H is the trough to crest height, Cr is the crest height above mean water level. T is zero-crossing period including the trough followed by the crest, T′ is the period from trough to following crest, T′′ is the period from zero-crossing to crest.

Fig. 3 shows the mean steepness (FFS in upper panel, FCS in lower panel) measured with the lasers as a function of inverse wave age. Waverider measurements are shown in Fig. 4. Average values are comparable, but Waverider data show less variability. In Fig. 5 (laser data) and 6 (Waverider data) the maximum values in each 20 minute record are shown as a function of inverse wave age. The values have more variability than the average values, as can be expected. FFS values are similar for both instruments but forward crest steepnesses (FCS) are slightly less with the waverider.

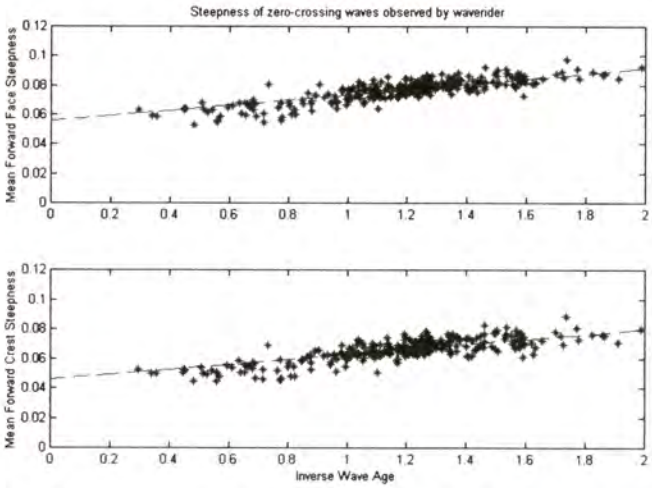

Fig. 4. Mean forward face steepness (FFS in eq. 2, top panel) and mean forward crest steepness (FCS, eq. 3, bottom panel) as function of inverse wave age, measured by the Waverider at Ekofisk.

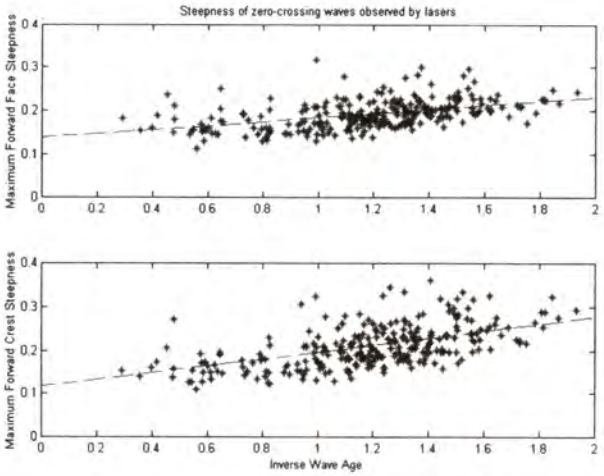

Fig. 5. Maximum forward face steepness (FFS in eq. 2, top panel) and forward crest steepness (FCS, eq. 3, bottom panel) from each 20 minute record used as function of inverse wave age as measured by lasers at Ekofisk.

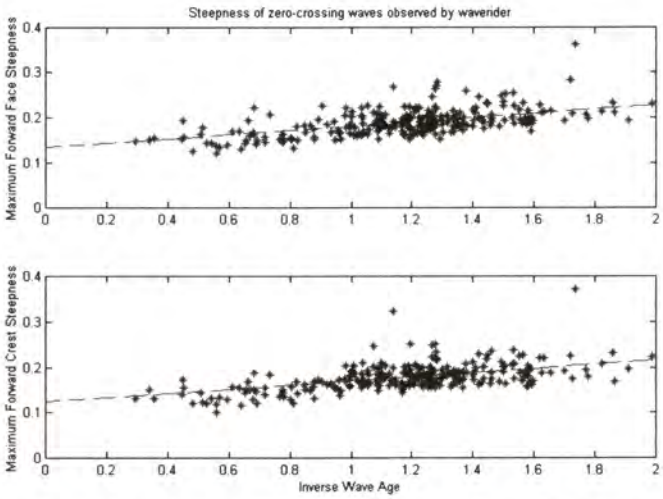

Fig. 6. Maximum forward face steepness (FFS in eq. 2, top panel) and forward crest steepness (FCS, eq. 3, bottom panel) from each 20 minute record used as function of inverse wave age as measured by the Waverider at Ekofisk.

3 Correcting for the quasi-Lagrangian behaviour

Following the method described in [1], the waverider data used in this study are corrected for the quasi-Lagrangian behaviour. We then see that the overall average of the FCS values over all 4 storms increases to be comparable to the laser value (0.18). But little difference is seen on other average values, i.e.: height factors like $\langle Hmax/Hs \rangle$ and $\langle Crx/Hs \rangle$, where *Hmax* is maximum wave height in a record, and Crx is maximum crest height above mean sea level. In Fig. 7 an example of the time series around the wave with the highest crest is shown. These are measurements from the storm no 2 (28. December 1998). The laser measures its highest crest at 06:40 UTC (top panel), while the Waverider (central panel) has a maximum crest in the 20 minute time series preceding the laser one - it is not the same wave passing by. The bottom panel shows this crest after correction for the quasi-Lagrangian behaviour. Compared to the laser crest, the waverider gives a much smoother one. QL-correction increases the skewness and steepness of this crest, as shown by the FFS and FCS numbers in the figures. We see that the Forward Crest Steepness especially increases by about 40% and becomes comparable to the laser data value.

4 Evolving wave groups

Evolving of wave time series using the linear method described in [1] has been applied to the waverider and laser time series. In [1] only waverider data was used to evaluate maximum crests, and horizontal velocities using the superposition method by

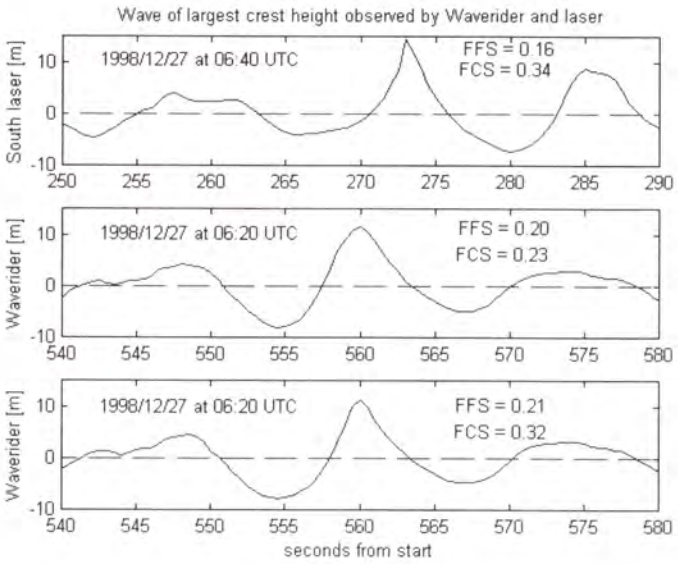

Fig. 7. Maximum crest in storm no 2 as measured by the laser at Flare South (top panel) and the waverider (center panel). Bottom panel shows the wave profile from the waverider after correction for quasi-Lagrangian behaviour.

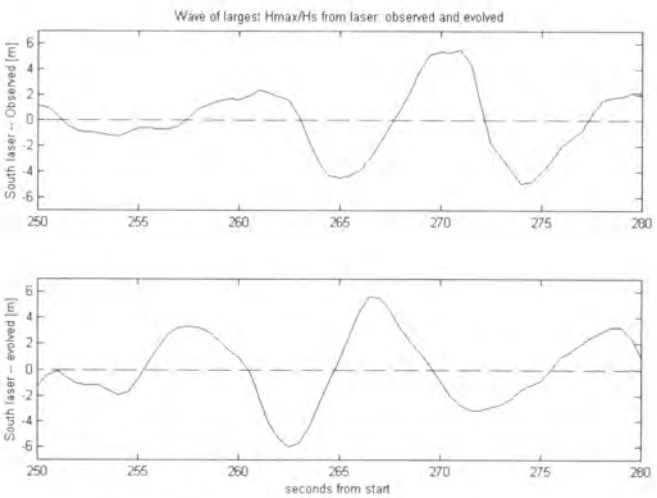

Fig. 8. Laser profile of the wave with highest Hmax/Hs factor; measured (top panel) and evolved (bottom panel).

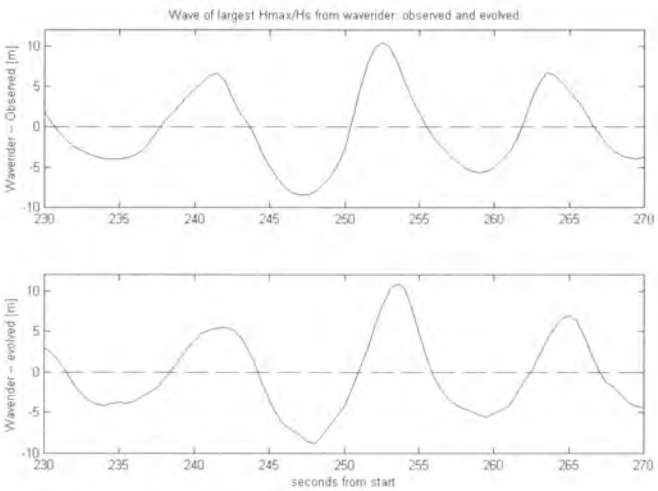

Fig. 9. Waverider profile of the wave with highest Hmax/Hs factor; measured (top panel) and evolved (bottom panel).

Donelan et al [8]. In summary it was found that evolving 150 original records increased the maximum crest to trough value in each record on average by about 10%, and the maximum crest height by 17%. But maximum increases were seen to be up to 30 and 50% respectively. Wave forces, being proportional to the horizontal velocity squared, were found to increase by 50%. Correcting for the quasi-Lagrangian behaviour of the buoy decreased the apparent mean water level by 8% of the standard deviation of surface elevation, increasing by this the skewness of the waverider data.

After evolving laser and waverider data from parts of the 4 storms in this study, we found that the number of 'freak' wave events (using the definition Hmax/Hs > 2.0) increased from 1 to 10 for the waverider, and from 0 to 8 for the laser data. Fig. 8 shows the crest with largest Hmax/Hs factor as measured with the laser in the first storm (upper panel) and how it appears after propagation to the point where the crest is highest (lower panel). The crest heights are very similar in this example, but the steepness is considerably larger. Fig. 9 shows the same comparison for the waverider (upper panel is the waverider record corrected for quasi-Lagrangian behaviour). The crest is 10% higher (10 vs 11m), but the steepness is less (70 % of original value).

5 Discussion and Conclusions

High singular waves (Hmax>2Hs) were not included in the laser records used in this study, but we did observe such waves in the time series. They occurred at or after the peak of the storms, or in the first period when wind increased suddenly. The records in this study were chosen to satisfy conditions of stationarity and unidirectionality, to satisfy conditions for evolving records using the linear dispersion relation. What we see in these records is that skewness and forward face steepness are strongly

correlated to wind forcing, while (not shown here) normalized height parameters (Hmax/Hs, Crx/Hs) seem not to be.

The requirements placed on the records discriminated against rapidly changing conditions when unusual wave records may have been obtained in the context of rogue waves. So meticulous studies of different weather situations and wave records one by one are needed to do proper statistics (or at least analysis since the number of occurences is low) on the occurrence of extreme waves. Observations of wave records from Ekofisk in real time give indications that high and steep crests occur when the wind is temporarily weakened, and also at the start of the storm when the waves are very steep. These are preliminary observations that need to be verified.

References

1. Magnusson, A.K., Donelan M.A., Drennan, W.M.: On estimating extremes in an evolving wave field. Coastal Eng. 36 (1999) 147-163
2. Magnusson, A.K.: High wave crests in the central North Sea. In Proceeding of the Symposium on The Air-Sea Interface. Radio and Acoustic Sensing, Turbulence and Wave Dynamics. Marseilles, France, 24-30 June 1993. ISBN 0-930050-00-2. University of Toronto Press Inc., Toronto. pp 289-295, 1996
3. Longuet-Higgins, M.S.: The effect of non-linearities on statistical distributions in the theory of sea waves. J. Fluid Mech. 17 (1963), 459-480
4. Longuet-Higgins, M.S.: Eulerian and Lagrangian aspects of surface waves. J. Fluid Mech. 173 (1986), 683-707
5. Pierson, W.J., M.A. Donelan, W.H. Hui: Linear and nonlinear propagation of water wave groups. J. Geophys. Res. 97 (1992), 5607-5621
6. Clauss, G.: Generation of task-related freak waves and critical wave groups. This publication
7. Stansberg, C.-T.: Random waves in the laboratory – What should be expected for the extremes?. This publication
8. Donelan, M.A., Anctil, F., Doering, J.C.: A simple method for calculating the velocity field beneath irregular waves. Coastal Eng. 16 (1992), 399-424

Characterizing Freak Waves with Wavelet Transform Analysis

Paul C. Liu[1] and Nobuhito Mori[2]

[1] NOAA Great Lakes Environmental Research Laboratory,
Ann Arbor, MI 48105-1593, USA
liu@glerl.noaa.gov
[2] Central Research Institution of Electric Power Industry,
Abiko, Chiba 270-1194 Japan
mori@criepi.denken.or.jp

Abstract. This paper presents an analysis of a set of available freak wave measurements gathered from several periods of continuous wave recordings made in the Sea of Japan during 1986 - 1990 by the Ship Research Institute of Japan. The analysis provides an ideal opportunity to catch a glimpse of the incidence of freak waves. The results show that a well-defined freak wave can be readily identified from the wavelet spectrum where strong energy density in the spectrum is instantly surged and seemingly carried over to the high frequency components at the instant the freak wave occurs. Thus for a given freak wave, there appears a clear corresponding signature shown in the time-frequency wavelet spectrum. Since freak waves are primarily transient events occurring unexpectedly, wavelet transform analysis on continuous, long duration wave measurements clearly represents the most ideal approach to discern the localized characteristics of freak waves for further exploration.

1 Introduction

Perhaps one of the weakest and most difficult aspects for the explorations of rogue or freak waves in the oceans is the ostensive scarcity of actual field measurements of rogue wave events. Because of the uncertain and unpredictable nature of the occurrence of rogue waves, the conventional, discrete kind of wave measurements at fixed time intervals have not been conducive in capturing actual freak wave episodes. A viable approach for making comprehensive rogue waves measurement does not seem to be presently available. The current literatures on rogue waves are predominantly comprised only with conjectured mechanisms such as those variously reported in [1], [11], [8], [2], [9], among others.

This paper presents an empirical analysis of available wave measurements collected during 1986 - 1990 in the Sea of Japan where freak waves are known to have observed. Since freak waves are primarily transient events, conventional frequency spectrum analysis is clearly incapable in effectively processing rogue waves in the frequency domain. We applied wavelet transform analysis here to analyze the time series and examine the localized freak wave characteristics in the generalized time-frequency domain.

2 The Wave Measurements

As freak waves are basically rare and unexpected occurrence, for the conventional wave measurements typically making 10 - 20 minutes recordings hourly, it would be entirely possible that an incidence of a freak wave be overlooked if it occurs in between recording times.Only through extended and continuous recordings would plausible expectations to capture an event of freak waves be realized. There are conspicuously fewer continuous wave measurements available, hence very few freak wave studies are based on actual measurement. Wave measurements used in this study were made from the Sea of Japan, at a location 3 km off the Yura fishery harbor in 43 m water depth. The instruments used in the measurement were ultrasonic type wave gages. Five sets of sea surface fluctuations data, recorded at 1 Hz sampling frequency, are used. Each of the data sets has over 20 to 40 hours of continuous recordings. Wind measurements were also available, which showed that the occurrence of freak waves are generally during steady wind conditions ([5], [11]). The measurement was originally made by the Ship Research Institute of the Ministry of Transport of Japan.

3 The Wavelet Spectrum

Wavelet transform analysis, developed during the last two decades, is an ideal tool for the study of the measured time series data of nonstationary, transient phenomenon such as freak waves. As the last decade marked an explosive publication of wavelet related books and articles, details on wavelet transform can now be found in many widely available introductory articles and texts (*e.g.* [3], [4]). Therefore we shall just present a very brief summarization of the formulation of continuous wavelet transform here.

For a given function or data signal $X(t)$, which is assumed to be square integrable, its Fourier transform, $\hat{X}(\omega)$, is given by

$$\hat{X}(\omega) = \int_{-\infty}^{\infty} X(t) e^{-i\omega t} dt, \tag{1}$$

which transforms the function in the time domain to the frequency domain. In order to examine the characteristics of the function in the frequency domain as well as the time domains, a direct approach of extending Eq.(1) to the time-frequency domain can be obtained by including a time windowing function $g(t)$ such that:

$$\hat{X}(\omega, \tau) = \int_{-\infty}^{\infty} X(t) g(t - \tau) e^{-i\omega t} dt. \tag{2}$$

Formulating analogously and replacing the window function with a new family of functions, and discretizing the time, t, and frequency, ω, with position, b, and scale, a, respectively, then it readily leads to the wavelet transform:

$$\tilde{X}(a, b) = \int_{-\infty}^{\infty} X(t) |a|^{-1/2} \psi^* \left(\frac{t - b}{a} \right) dt. \tag{3}$$

where $a > 0, -\infty < b < +\infty$, and the asterisk superscript indicates the complex conjugate.

Suffice to assert that the wavelet spectrum, based on the continuous wavelet transform, represents a natural extension of the familiar, conventional Fourier spectrum analysis. While Fourier transform is based on the concept of frequency, the wavelet transform is based on the concept of scale and time. As scale and frequency are inversely related, thus instead of results presented in a conventional plot of energy versus frequency for Fourier energy spectrum, the wavelet spectrum is known to be three-dimensional in nature and plotted in the time-frequency domain with the equivalent energy density appears in terms of contour levels. This provides an ideal opportunity to examine the process of energy variations where the freak waves occur locally and abruptly in time. Note that we present mainly the results of continuous wavelet transform using Morlet wavelet here, similar result of characteristic features shown here can in general also be obtained from using different mother wavelet, or with the application of discrete wavelet transforms.

Since there is presently no available studies examining the localized characteristics during the occurrence of freak waves, and neither is there any theoretical implications as to how a freak wave might have behaved in the time-frequency domain, our results are therefore necessarily exploratory and tentative. On the other hand, the qualitative nature of the results also presents challenging implications that are inviting for rational interpretation. From the five sets of continuously recorded surface wave data which comprise over 200 hours of measurement, only a few episodes of freak waves have been identified both in the field and by the time series data. These cases generally resembles the ideal freak wave time series case given by the North Sea measurement, [6]. Figure 1 presents such a characteristic freak wave time series and its corresponding wavelet spectrum. The freak wave episode shown in Figure 1 is represented by a plotting of 10 minutes time series segment that contains the occurrence of the freak wave along with a panel of corresponding contour plotting for the wavelet spectrum. It appears that for the well-defined freak wave as shown in the time series plot, it can also be readily identified from the wavelet spectrum where strong energy density in the spectrum appears instantly surged at the onset of the freak wave and the energy density seemingly carried over to the high frequency components at the freak wave instant. Therefore, for a given freak wave, there emerges a clear corresponding signature shown in the time-frequency domain of the wavelet spectrum.

However, for another similar characteristic freak wave time series shown in Figure 2, there is no corresponding instantaneous energy surge feature appear in the wavelet spectrum as those in Figure 1. So it is somewhat uncertain in this case whether a freak wave identified only in the time series can be really considered as a freak wave or not. On the other hand, it is of interest to note that the time series in Figure 1 at the onset of the freak wave its profile appeared rather asymmetric with respect to the mean level, whereas the freak wave profile in Figure 2 was generally symmetric[1]. So the difference in wavelet spectrum might also be a result

[1] We are indebted to Prof. Douglas Faulkner for pointing out this feature to us.

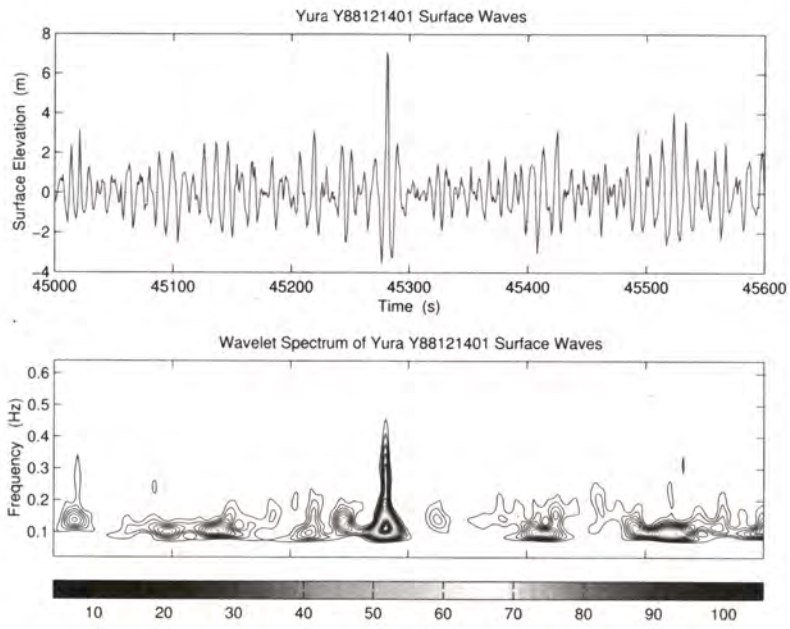

Fig. 1. Freak wave time series and its wavelet spectrum for data set Yura Y88121041 [See also Appendix CP]

of the difference in freak wave profiles. It is possible that the single large wave height shown in Figure 2 represents merely a maximum wave from the extreme statistics. Or alternatively it is indeed a freak wave but generated from a different process from the case shown in Figure 1. Just as various different conjectures all can be shown to produce freak waves, freak waves certainly can be generated from different physical processes. Time series alone clearly may or may not be relied on for distinguishing freak waves. While wavelet transform applied to the time series can provide further discernible features, it is still beyond the scope of the wavelet transform to readily comprehend the differences in possibly different processes. Undoubtedly more detailed measurements than just surface time series would be needed for proper and practical study of freak waves. At any rate, since the mechanism of freak wave formation is understandably diverse, it should not be surprising that different freak waves exhibit different qualitative features. Both cases in Figures 1 and 2 can be freak waves, or only the case in Figure 1 represent a freak wave. As idealized and more comprehensive measurements encompassing all possible relevant parameters are unavailable at the present, wavelet transform analysis is nevertheless the ideally suited approach to study the available freak wave time series that may be used to clarify the occurrence of the freak waves as well as their general characteristics and statistical properties.

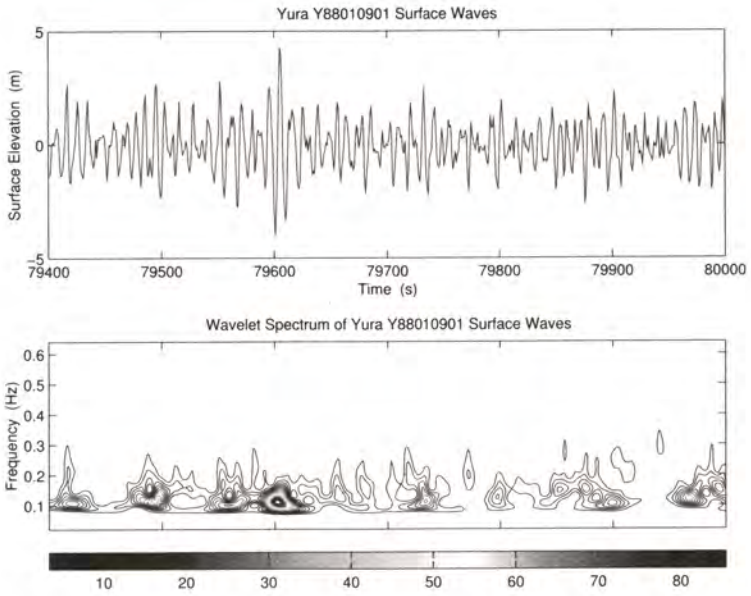

Fig. 2. Freak wave time series and its wavelet spectrum for data set Yura Y8010901 [See also Appendix CP]

4 Concluding Remarks

Rogue or freak waves have always been a fascinating subject for contemplation and speculation, but the hazard of severe damages it may inflect upon ships and mariners can not be over stated. While the existence of freak waves has been accepted by scientists and engineers, one can not overlook the fact that the existence of freak waves is basically only based on eyewitness accounts. It is of utmost importance that concerted field efforts should be implemented to provide actual detailed measurements and analysis and thus to ascertain its veritable existence. The working group on breaking and freak waves at the NATO Advanced Research Workshop (Torum and Gudmestad 1990, [7]) had recommended over 10 years ago that future research needs should be on full scale freak wave measurement, correlation of meteorological information and freak wave occurrence, and extended analysis of existing data. These recommendations are certainly well-founded, unfortunately none of the advices has been carried out since then. The continuous measurements of longer duration in time, made by the Ship Research Institute of Japan, which had led to possibly the only available field recordings of freak waves, are of extreme importance and usefulness. Analysis using wavelet transform would probably be the one of the versatile tools available that is truly ideal for the study of freak waves data. Hopefully the exploratory results presented in this paper may serve to demonstrate the

useful effects of wavelet transform and freak waves and thereby enticing more particularized freak wave measurements and wavelet transform applications.

5 Acknowledgement

The authors wish to express their gratitude to the Ship Research Institute of the Ministry of Transport of Japan for providing and allowing the use of their data.

References

1. Dean, R.G.: Freak waves: A possible explanation. In Torum, A. and Gudmestad, O.T. (eds.): Water Wave Kinematics. Kluwer (1990) 609-612
2. Lavrenov, I.V.: The wave energy concentration at the Agulhas current off South Africa. Natural Hazards, **17**, (1998) 117-127
3. Liu, P.C.: Wavelet spectrum analysis and ocean wind waves. In E. Foufoula-Georgiou and P. Kumar (Eds): Wavelets in Geophysics. Academic Press (1994) 151-166
4. Liu, P. C.: Wavelet transform and new perspective on coastal and ocean engineering data analysis. In P. Liu (Ed): Advances in Coastal and Ocean Engineering. World Scientific, Vol.6 (2000) 57-101
5. Mori, N., Yasuda, T. and Nakayama, S.: Statistical Properties of Freak Waves Observed in the Sea of Japan. ISOPE2000, **3**, (2000) 109-115.
6. Sand, S.E., Hansen, N.E.O., Klinting, P., Gudmestad, O.T. and Sterndorff, M.J.: Freak wave kinematics. In Torum, A. and Gudmestad, O.T. (eds.): Water Wave Kinematics. Kluwer (1990) 539-549
7. Torum, A. and Gudmestad, O.T. (eds.): Water Wave Kinematics. kluwer (1990) 771pp.
8. Trulsen, K. and Dysthe, K.: Freak waves – A Three-Dimensional Wave Simulation. Twenty-first Symposium on Naval Hydrodynamics, National Academy Press (1997) 550-558
9. White, B.S. and Fornberg, B.: On the Chance of Freak Waves at Sea. J. Fluid Mech., **355** (1998) 113-138
10. Yasuda, T., Mori, N. and Ito, K.: Freak Waves in a Unidirectional Wave Train and Their Kinematics. Proceedings 23rd International Conference on Coastal Engineering, ASCE (1992) 751-764
11. Yasuda, T., Mori, N. and Nakayama, S.: Characteristics of Giant Freak Waves Observed in the Sea of Japan. In B. Edge and M. Hemsley (Eds.): Ocean Wave Measurement and Analysis. ASCE (1997) 316-328

The Empirical Mode Decomposition and the Hilbert Spectra to Analyse Embedded Characteristic Oscillations of Extreme Waves

Torsten Schlurmann*

Hydraulic Engineering Section, Civil Engineering Department
University of Wuppertal, Pauluskirchstr. 7, 42285 Wuppertal, Germany
ph: +49 202 4394197, fax: +49 202 4394196, email: schlurma@uni-wuppertal.de

Abstract. This paper concerns the identification of characteristic oscillations of extreme waves based on the Hilbert-Huang Transformation (HHT) [7], [8]. The HHT decomposes any time-dependent signal into its individual embedded modes with the so-called Empirical Mode Decomposition (EMD). Applying the Hilbert Transformation (HT) to any of these disintegrated Intrinsic Mode Functions (IMF) subsequently generates distinct time-dependent Hilbert amplitude or energy spectra. This implies, in all probability, that the HHT is capable of revealing entirely new physical insights for any nonlinear and non-stationary data series and could also deduce dissimilar underlying dynamical processes of extreme waves.

1 Introduction

1.1 Fourier Transformation

Fourier analysis has become the most valuable tool in spectral data analysis and has consequently been applied to all kinds of data in many scientific or engineering disciplines. Although, it is strictly limited to linear systems and stationary data series [e. g. [19]]. Therefore, the Fourier spectrum can only be regarded as the coefficient function obtained by expanding a signal $x(t)$ into a family of an infinite number of waves generally in the form $exp(i\omega t)$, which are completely unlocalized in time – typifying the signal mathematically from a rather global point of view. Thus, the Fourier sprectrum essentially defines which spectral components, as well as their corresponding time-invariant amplitudes and phases, are embedded in the signal over the whole time span in which the signal was recorded.

1.2 Short-Time Fourier Transformation

In order to introduce a time-dependency in the Fourier transform technique, a simple and intuitive solution consists of pre-windowing the signal around a

* Dr.-Ing., Senior Research Assistant

particular instant in time, calculating its Fourier transform, and repeating that procedure for each time step – assuming the signal to be stationary in all windows. The resulting time-dependent spectrum (*spectrogram*) is called the short-time Fourier transformation (*STFT*) and was first introduced by Gabor, [6]. In order to localize an event precisely in time, the window width must be narrow, alternately the frequency resolution requires longer time spans. This leads to conflicting requirements (*Heisenberg-Gabor inequality*) and restrains this method from many practical applications, although it is still the most widely used technique in time-frequency analysis today.

1.3 Wavelet Transformation

To avoid these restrictions the wavelet analysis – in continuous and discrete representation – has been developed in the last decade [e. g., [5]]. Since it has an analytical form for the results, it has attracted extensive attention in the field of applied mathematics. The central idea of the wavelet transform is to correlate a signal *x(t)* with a family of zero-mean functions derived from an elementary function (*mother wavelet*), e. g. the complex-valued continuous Morlet mother wavelet derived from a plane wave modulated Gaussian envelope [14].

In principle, the wavelet transform provides an amplitude spectrum of the signal *x(t)* in time and frequency domain. But, even the wavelet analysis has certain limitations. Firstly, the chosen mother wavelet will significantly influence the result of the analysis, as the basic functions of wavelet transformation are fixed and do not necessarily match the shape of the considered data series in every instant in time. Moreover, spectral wavelet analysis certainly underlies an uncertainty principle, indicating that a time or a frequency dependent information cannot be classified by the same accuracy, simultaneously. A high frequency component is precisely resolved in time domain, but at the same time inexact in frequency domain and vice versa for low frequency components. Regardless of these restrictions the wavelet analysis has become a very popular tool to investigate non-stationary data series, although, it is basically a linear technique. Most recently, Liu, [11] a, [12] b] applied the continuous Morlet Wavelet Transformation to investigate the spectral energy content of coastal and ocean data series. Chien *et al.* [[3]] analysed nearshore observed extreme waves events east off the coast of Taiwan.

1.4 Hilbert-Huang Transformation

Empirical Mode Decomposition. Recently, Huang *et al.* [7], [8] developed the Hilbert-Huang transformation (HHT) to decompose a time-dependent data series into its individual characteristic oscillations with the so-called Empirical Mode Decomposition (EMD). This adaptive technique is derived from the simple assumption that any signal consists of different intrinsic mode functions (IMF) – each of them representing an embedded characteristic oscillation on a separated time-scale. An IMF is defined by two criteria: *i)* the number of extrema and of zero crossings must either equal or differ at most by one, and, *ii)* at any

instant in time, the mean value of the envelope defined by the local maxima and the envelope of the local minima is zero. The first criterion is almost similar to the narrow band requirement of a Gaussian process, while the latter condition modifies a global requirement to a local one, and, is necessary to ensure that the instantaneous frequency, which will be explained later, will not have unwanted fluctuations. In other words: the EMD is based on the direct extraction of energy associated with various intrinsic time scales. The following chart proposes an idea about the principle algorithm of the EMD.

1. **Initialize** $r_0(t) = x(t)$, $j = 1$
2. **Extract** the j-th IMF:
   (a) **Initialize** $h_0(t) = r_j(t)$, $k = 1$
   (b) Locate local **maxima** and **minima** of $h_{k-1}(t)$
   (c) Cubic **spline interpolation** to define **upper and lower envelope** of $h_{k-1}(t)$
   (d) Calculate **mean** $m_{k-1}(t)$ from upper and lower envelope of $h_{k-1}(t)$
   (e) **Define** $h_k(t) = h_{k-1}(t) - m_{k-1}(t)$
   (f) If **stopping criteria** are satisfied then $h_j(t) = h_k(t)$ else goto 2. (b) with $k = k + 1$
3. **Define** $r_j(t) = r_{j-1}(t) - h_j(t)$
4. If $r_j(t)$ still has at least two extrema then goto 2. (a) with $j = j + 1$ else the EMD is finished
5. $r_j(t)$ is the **residue** of $x(t)$

At the end of this numerical sifting process the signal *x(t)* can be expressed:

$$x(t) = \sum_{j=1}^{n} h_j(t) + r_n(t) \ , \tag{1}$$

where $h_j(t)$ indicates the j-th IMF, n as the number of sifted IMF and $r_n(t)$ denotes a residue which can be understood as the trend of the signal. Another way to explain how the EMD works is that it picks out the highest frequency oscillation that remains in the signal. Thus, locally, each IMF contains lower frequency components than the one extracted just before. This property can be very useful to detect rapid frequency changes, since a change will appear even more clearly at the level of an IMF. Completeness of this decomposition method is assured in princple and only dependent on the precision of the numerical sifting process. Orthogonality of the EMD is not guaranteed theoretically, but is satisfied in a practical sense that two IMF are orthogonal within a certain period of time. Additionally, the IMF *do not* guarantee a well-defined physical meaning and great caution is advised when attempting to interpret them. However, the IMF *do* carry physical significance in most cases as Huang *et al.* point out and since the EMD is a patented technique (US005983162A), they only introduce a rough overview of their decomposition method – allowing the reader sufficient room for adequate interpretation and realisation of their origin ideas.

Hilbert Transformation. In a next step, the Hilbert transformation (HT) is applied to each of the disintegrated IMF – subsequently providing the Hilbert amplitude spectra with significant instantaneous frequencies. Basically, the Hilbert transformation $H[x(t)] = y(t)$ of $x(t)$ is defined [see: Bendat & Piersol, [1]]:

$$H[x(t)] = y(t) = \lim_{\epsilon \to 0} \left[\int_{-\infty}^{0-\epsilon} \frac{x(u)}{\pi(t-u)} du + \int_{0+\epsilon}^{\infty} \frac{x(u)}{\pi(t-u)} du \right] , \tag{2}$$

assuming that $\int_{-\infty}^{\infty} (x(t))^2 \, dt < 0$, we can describe $H[x(t)] = y(t)$ of $x(t)$ as:

$$H[x(t)] = y(t) = \frac{1}{\pi} p.v. \int_{-\infty}^{\infty} \frac{x(u)}{(t-u)} du , \tag{3}$$

with $p.v.$ as the *Cauchy* principle value of the integral. Moreover, $z(t)$ is the analytical signal of $x(t)$:

$$z(t) = x(t) + iy(t) = A(t) \exp(i\Theta(t)) , \tag{4}$$

with: $A(t) = \sqrt{x(t)^2 + y(t)^2}$ and $\Theta(t) = \arctan(y(t)/x(t)) = \omega t$. We can then define the instantaneous frequency (IF) in *eq.* 5 as the rate of change of the phase of the analytical signal $z(t)$. The IF was first introduced by Ville [[21]]. The definition of an IF is highly controversially debated [2], [4], because a frequency is usually related with the number of cycles undergone during one time by a body in a periodic motion, so that there is an apparent paradox in associating the words 'instantaneous' and 'frequency'. However, in practice, signals are not truely sinusoidal, or even aggregates of sinusoidal components, representing the IF as an excellent discriptor of several physical phenomena. This concept was originally defined in the context of FM modulation in theory of communications.

$$\omega(t) = \frac{d\Theta(t)}{dt} . \tag{5}$$

The analytical signal $z(t)$ is the best local fit in time domain of an amplitude and phase varying trigonometric function to the data series $x(t)$. After having obtained the IMF and having generated the HT of each IMF, the data series $x(t)$ can be represented:

$$x(t) = \sum_{j=1}^{n} A_j(t) \exp\left(i \int \omega_j(t) dt \right) \tag{6}$$

This time-frequency distribution of the amplitude is designated as the Hilbert spectrum $H(\omega, t)$. The same data series $x(t)$ if expanded in conventional Fourier analysis representation would be: $x(t) = \sum_{j=1}^{\infty} a_j \exp(i\omega_j t)$. Physically, a definition of an IF has a true meaning only for monocomponent signals, where there's only one frequency or at least a narrow range of frequencies varying as a function of time. Most data series do not show these necessary characteristics, so that in former times a Hilbert transform only made little physical sense in most practical

applications. The real value of the Hilbert transform had to wait to be demonstrated until the EMD method was developed to separate a signal into its own characteristic oscillations each of them in a narrow-banded frequency range as Huang *et al.* further spotlight. Today, the HHT is applied in several scientific and engineering disciplines. E.g. in Geophysics or in Meteorology to study the nature of seismic, tidal and wind waves, to investigate the occurrences of tsunamis, or to examine the gravity wave characteristics in the middle atmosphere [Zhu *et al.*, [23]]. Moreover, the HHT is used in Medical Science & Engineering or in Physics to study the phenomema of physiological studies of the stomach [Liang *et al.*, [10]], heart beat irregularities, turbulences in blood flow, brain wave irregularities in epileptic seizures or to detect solar neutrino variations [*Details of last four research projects were communicated in personal correspondence with Dr. N. Huang, NASA Goddard Space Flight Center, USA*]. In addition, Schlurmann *et al.* [[17] a] investigate laboratory generated extreme waves with second order wavemaker theory and utilize a technically improved numerical algorithm of the HHT to decompose these data into their characteristic oscillations [18] b].

2 Embedded characteristic oscillations of extreme waves based on the HHT

Extreme waves – with a exceptional single waveheights – are defined as transient waves existing in one specific location in one particular instant in time. Extensive work has been carried out to study these phenomena either to examine their primary driving mechanics or to simulate these waves numerically [e. g.: [16], [15], [22], [20], or, [9].

Investigations in the present paper concentrate on the application of the HHT to analyse extreme wave events observed in the Sea of Japan. Water surface elevations were measured by three individual operating ultrasonic type wave gages mounted on the sea bottom ($d = 43$ m) approximately 3 km off the coast of Yura with a sampling frequency $\triangle f = 1$ Hz. Observations were carried out from 1986 to 1990 by the Ship Research Institute, Japan. Main results with emphasis on a statistical analysis were done by Yasuda *et al.*, [22]], and Mori *et al.*, [13] and conclude that most of the observed freak waves in this region occur in single peaked spectra sea conditions during seasonal winter storms, mainly without any multidirectional effects. Figure 1 presents one example of a freak wave measured at these three locations in a ten minute record on 24-Nov-1987. It is unmistakably defined by its transient character. Significant waveheights $H_{1/3}$ were derived from 30 minutes intervals and are practically constant for all three locations. Largest waveheight $H_{max} = 13.6$ m is measured at location ♯1 for this event. Figure 2 shows results of the EMD carried out for the signal from location ♯1. It is disintegrated into ten IMF in total, only the first seven IMF are shown here. This particular extreme wave event is separated into locally non-overlapping time scale components with altering amplitudes. The first three IMF carry most of the embedded energy. It is clearly identified that each IMF is dominated by an almost constant inter-wave component that rather represents a carrier wave

constituent. Only small intra-wave components are evident that modulate the carrier wave constituent in frequency domain. Figure 3 presents results from the Wavelet and Hilbert Transformation. The top panel *a* contains the recorded data series. Correspondingly, panel *b* shows the Wavelet (Morlet) spectrum and panel *c* presents the Hilbert spectrum, both in time domain. Horizontal colorbars beneath panel *b&c* denote the amplitude of each spectrum. Apparently, the Hilbert spectrum provides more distinct information on the time-frequency contents of this event – evidently showing that this extreme wave is the superimposition of selected characteristic embedded modes that are *in phase* at the concentration point.

3 Conclusion and Discussion

A conclusion that can be drawn from this very brief analysis of extreme wave events is, that the Hilbert-Huang Transformation gives the impression of being an extremely powerful tool to analyse nonlinear and non-stationary data series in the time-frequency plane. The EMD adaptively decomposes an extreme wave record into its embedded characteristic oscillations. The Hilbert spectra not only show no obvious constraints compared to other conventional analysing techniques in defining a more precise representation of particular events in time-frequency space, but also provide a more physically meaningful interpretation of the underlying dynamic processes. But, the Hilbert-Huang Transformation is not an undisputed analysing technique. Certain points are seriously debated in the moment:

1. technical improvements of EMD algorithm: e.g. spline fitting methods, boundary effects of splines, intermittency checks (merging of different IMF),
2. influence of sampling frequency (oversampling), minimum data length, weak oscillations embedded in strong oscillations, effects of noisy data,
3. derivation of further analytical characteristics: mean frequency spectrum (marginal spectrum), higher order moments, local frequency bandwidth,
4. closure of fragmentary theoretical mathematical background: final proof of orthogonality and completeness, IMF in closed analytical form.

Regardless of these obvious theoretical inadequacies the Hilbert-Huang Transformation is one of the most important discoveries in the field of applied mathematics in the last decades that is, in all probability, capable of determining entirely new physical insights of any nonlinear and non-stationary data series, and, therefore, could also presume different underlying dynamic processes of extreme waves.

"We've only begun to explore the fully physical interpretations of the Hilbert spectra for any complicated data series" [Huang *et al.*, [7]].

4 Acknowledgements

The author wants to express his deep appreciation to the Japanese Ship Research Institute for kindly providing the whole Yura dataset from the Sea of Japan.

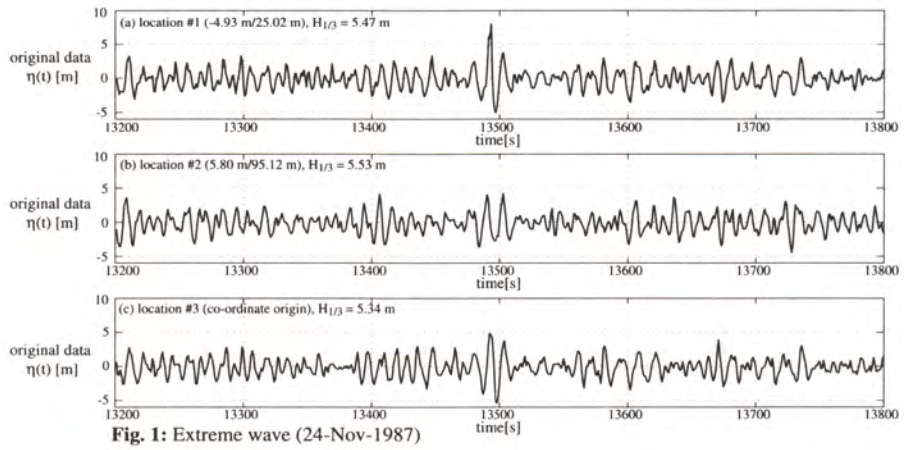

Fig. 1: Extreme wave (24-Nov-1987)

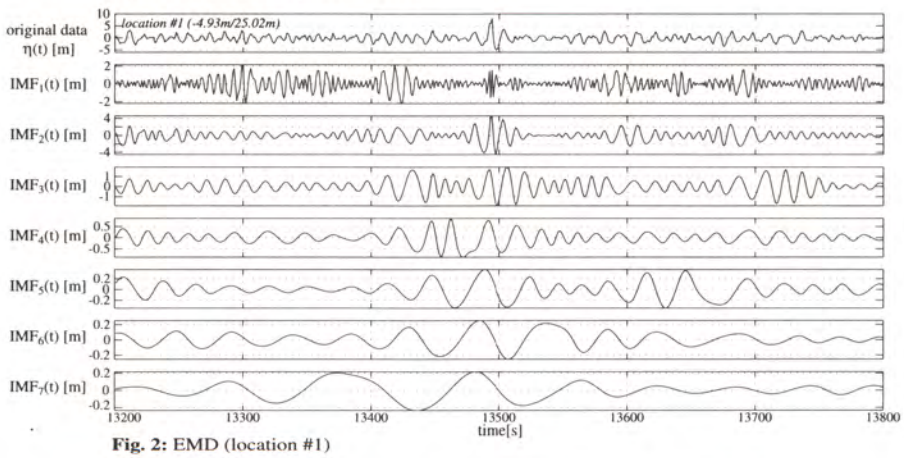

Fig. 2: EMD (location #1)

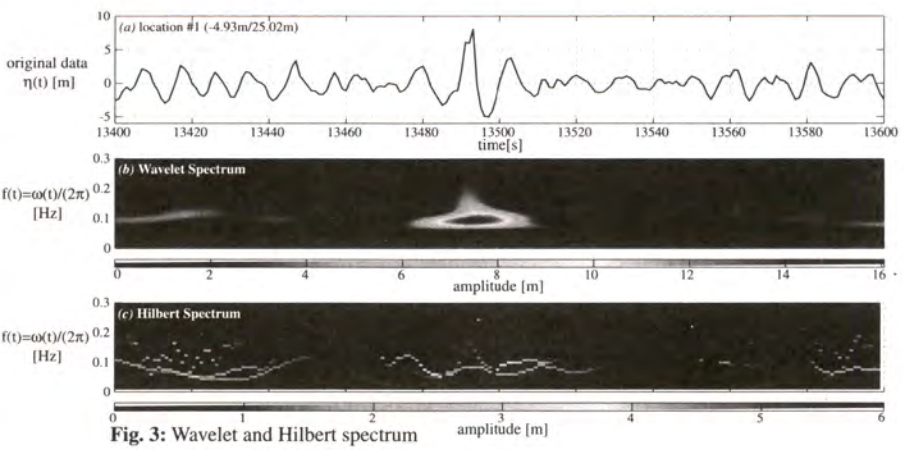

Fig. 3: Wavelet and Hilbert spectrum

[See also Appendix CP]

References

1. Bendat, J.S., Piersol, A.G.: Random Data: Analysis and Measurement Procedures. John Wiley & Sons, Inc. (1986)
2. Boashash, B.: Estimating and Interpreting the Instantaneous Frequency of a Signal - Part I: Fundamentals. Proc. IEEE, **80**, 4 (1992) 520-538
3. Chien, H., Chuang, L., Kao, C.C.: A Study on Mechanisms of Nearshore Rabid Waves. 2^{nd} German-Chinese J. Sem. on Rec. Dev. in C. Eng., China (1999) 469-483
4. Cohen, L., Loughlin, P., Vakman, D.: On an Ambiguity in the Definition of the Amplitude and Phase of a Signal. Sign. Proces., **79** (1999) 301-307
5. Daubechies, I.: Ten Lectures on Wavelets. Soc. f. Ind. & App. M. (1992) 357
6. Gabor, D.: Theory of Communication. IEE J. Comm. Eng. 93 429-457
7. Huang, N.E., Shen, Z., Long, S., Wu, M.C., Shih, H.H., Zheng, Q., Yen, N.-C., Tung, C. C., Liu, H. H.: The Empirical Mode Decomposition and Hilbert Spectrum for Nonlinear and Non-Stationary Time Series Analysis. Proc. R. Soc. London A, **454** (1998) 903-995
8. Huang, N. E., Shen, Z., Long, S.: A New View of Nonlinear Water Waves: The Hilbert Spectrum. Annual Review of Fluid Mechanics, **31** (1999) 417-457
9. Lavrenov, I. V.: The Wave Energy Concentration at the Agulhas Current off South Africa. Nat. Hazards, **17** (1998) 117-127
10. Liang, H., Lin, Z., McCallum, R. W.: Artifact Reduction in Electrogastrogram Based on Empirical Mode Decomposition Method. Med. Biol. Eng. C.,**38** (2000) 35-41
11. Liu, P. L.: Is the Wind Wave Frequency Spectrum Outdated. Oc. Eng., **27**, 5 (2000) 577-588
12. Liu, P. L.: Wave Ggrouping Characteristics in Nearshore Great Lakes. Oc. Eng., **27**, 11 (2000) 1221-1230
13. Mori, N., Yasuda, T., Nakayama, S. I.: Statistical Properties of Freak Waves Observed in the Sea of Japan. 10^{th} Int. Off. and P. Eng. Conf., **3** (2000) 109-115
14. Morlet, J., Arens, G., Fourgeau, I., Giard, D.: Wave Propagation and Sampling Theory. Geophysics, **47** (1982) 203-236
15. Rozario, J. B., Tromans, P. S., Taylor, P. H., Efthymiou, M.: Comparison of Loads Predicted using 'Newwave' and other Wave Models with Measurements on the Term Structure. Wave Kin. and Env. Forces, **29** (1993) 143-159
16. Sand, S. E., Ottesen Hansen, N. E., Klinting, P., Gudmestad, O. T., Sterndorf, M. J.: Freak Wave Kinematics. In Wat. W. K., Kluwer A. (1989) 535-549
17. Schlurmann, T., Lengricht, J., Graw, K.-U.: Spatial Evolution of Laboratory Generated Freak Wave in Deep Water Depth. 10^{th} Int. Off. and P. Eng. Conf., **3** (2000) 54-59
18. Schlurmann, T., Schimmels, S., Dose, T.: Spectral Frequency Analysis of Transient Waves Using Wavelet Spectra (Morlet) and Hilbert Spectra (EMD). 4^{th} Int. Conf. on Hyd. and Eng. (2000) (in press)
19. Titchmarsh, E. C.: Introduction to the Theory of Fourier Integrals. Ox. U. Pr. (1948)
20. Trulsen, K., Dysthe, K.: Freak Waves - A Three-Dimensional Wave Simulation. Proc. 21^{st} Symp. on Nav. Hydrodyn. (1997) 550-558
21. Ville, J.: Theorie et Application de la Notion de Signal Analytique. Cabl. et Transm., **2a** (1948) 61-74
22. Yasuda, T., Mori, N.: Occurrence Properties of Giant Freak Waves in Sea Area around Japan. J. of Wat., Port, Coast. and Oc. Eng., ASCE, **123**, 4 (1997) 209-213

23. Zhu, X., Shen, Z., Eckermann, S.D., Bittner, M., Hirota, I., Yee, J.-H.: Gravity Wave Characteristics in the Middle Atmosphere Derived from the Emirical Mode Decomposition Method. J. of Geoph. Res., **102**, D14 (1997) 16.545-16.561

Session 4

Possible Generation Mechanisms of Rogue Waves

Some Geometric and Kinematic Properties of Breaking Waves

Pierre Bonmarin[1] and Peter Kjeldsen[2]

[1] Institut de Recherche sur les Phénomènes Hors Equilibre (IRPHE), Laboratoire IOA, 163 Avenue de Luminy, Case 903, 13288 Marseilles, Cedex 9, France
Fax:++33(0)491419620, bonmarin@pollux.irphe.univ-mrs.fr
[2] Trondheim Maritime Academy, Ladehammerveien 6. – 7004 Trondheim, Norway
Fax: ++47 73528378, peter.kjeldsen@c2i.net

Abstract. Experiments were performed in a large wave-tank 40 meters long, in order to measure geometric and kinematic properties of waves breaking on deep water, especially of plunging breakers. Because the shape of waves approaching the breaking stage changes rapidly, we used a visualization technique associated to an image analysis process to make observations and measurements both in time and space. The asymmetry of the profile of wave breaking is in particular displayed. This asymmetry is an important parameter, which contributes to make breaking waves dangerous with regard to numerous marine activities.

1 Introduction

Among others, the knowledge of the geometric and kinematic properties of rogue waves is important from several practical points of view. It is in particular important with regard to the safety of ships and offshore structures.

The experimental study of this phenomenon is difficult for various reasons: the phenomenon is unsteady, it occurs suddenly and intermittently, and it can display three-dimensional aspects. In-situ experiments are especially difficult because the adverse conditions and the variability of the meteorological conditions. For these reasons, experiments in laboratory, in controlled conditions, are very useful.

The geometry and the kinematics of rogue waves occurring in ocean are practically unknown and the present paper tries to shed some light to this phenomenon by reporting on measurements in laboratory on deep-water breaking waves, which can be considered themselves as extreme waves. The experimental means used for these measurements could be easily applicable to the study of rogue waves.

In the present report, only plunging waves are considered because of their particularly dangerous aspect.

2 Experimental Method and Instrumentation

2.1 The Facility

Experiments were performed in the Air-Sea Interaction Simulation Facility of IRPHE. This facility is composed of two parts: a wave-tank 40m long, 1m deep and 2.6m wide, and a closed aerodynamic circuit 60m long, 1.5m high and 3.2m wide.

Waves can be generated either by wind (wind waves), blowing up to 14m/s, or by a complete immersed wave-maker (mechanical waves), working in the range 0.5 to 2 Hz. Adverse or following water-current up to 15cm/s in deep water condition can be generated by means of pumps.

2.2 The Visualization Technique

Wave breaking process is a non-stationary phenomenon. Therefore, visualization of the wave profile appears to be a privileged way for investigation. The principle of the technique is quite simple: a vertical thin sheet of light illuminates the water surface previously tinted by means of ink, so that the intersection between the water surface and the light sheet makes the wave profile visible. A video-camera perpendicular to the sheet of light takes pictures of the evolution of the wave profile. The camera and the sheet of light are put on a moving carriage allowing observations and pictures at different fetches (Fig. 1).

2.3 The Image Analysis Process

The video camera takes time series of pictures, which are then stored in a laser videodisc recorder. Selected pictures are then focused on an electronic tablet, in stop frame mode, where they are transformed into digital form for further quantitative analysis. At present, an operator follows the wave profile by means of an electronic stylus interacting with a computer. The digitalized pictures are finally stored in the memory of the computer. An automatic method of digitalization is currently in progress to allow "statistic" measurements. Fig. 2 shows a sample of plunging wave.

3 Application to Measurements of Plunging Waves

3.1 Geometric Properties

It is well known that breaking waves, especially plunging ones, display an asymmetric shape as they approach the breaking stage. Consequently, two parameters are no more sufficient to describe accurately the wave profile, as it is the case for sinusoidal waves (wavelength and wave height for example).

Among the most interesting parameters, four are of particular interest. These are (see Fig. 3):

- the horizontal asymmetry factor as μ; $\mu = \eta'/H$, where η' is the crest amplitude and H the full wave height. This parameter describes the asymmetry of the wave with respect to a horizontal axis, the still water level, taken as a reference.
- the slope of the front part of the crest, indicated as ε; $\varepsilon = \eta'/F_1$
- the slope of the rear part of the crest, indicated as δ; $\delta = \eta'/F_2$
- the vertical asymmetry fasctor, indicated as λ; $\lambda = F_2/F_1$; this parameter describes the asymmetry of the crest with respect to a vertical axis through this latter.

Evolution of the Geometry during the Breaking. Asymmetry increases as long as the wave approaches the breaking stage; see Figs. 4 and 5. These figures display the evolution of the horizontal asymmetry factor (μ), and of the factor (ε), related to the slope of the front part of the crest, respectively.

The horizontal asymmetry increases from an initial value about 0.5, corresponding to a symmetric wave, to about 0.9.

The slope of the front part of the crest increases, as expected, and reaches a maximum value at the breaking onset. Note that for a limiting second order Stokes wave, ε equals 0.282, which is significantly less than the present measured value of 0.5.

The present results are in good agreement with the ones by Kjeldsen and Myrhaug, [2].

The potential energy increases during breaking, as expected. However, it reaches a maximum value not at the breaking onset, as expected, but prior to this, see Fig. 6.

Geometry at the Breaking Onset. The asymmetry was measured at the breaking onset (see Table 1). The significant asymmetry with comparison to the case of a symmetric wave, and the relative good agreement, except perhaps for λ, between the results from different origins are noteworthy.

Table 1. Asymmetry properties of a plunging breaker at the breaking onset, [2]

Parameter	μ	λ	ε	δ
Computation (ak=0.25), [3]	0.77	1.83	0.59	0.32
Experiments (ak=0.28), [1]	0.76	1.87	0.54	0.30
Experiments (ak=0.24), [4]	0.76	1.43	0.50	0.35
Theory: symmetric (2^{nd} order Stokes limiting) wave, (ak=0.442)	0.50	1.00	0.28	0.28

It is clear that the asymmetry depends on the type of breaking; it is more pronounced for a plunging than for a spilling. Experimental results were classified into four families of breakers, from the fully spilling, or typical spilling, to the fully plunging, or typical plunging. Table 2 summarizes the results obtained.

Table 2. Relation between Asymmetry and Breaker Type

	μ	ε	δ	λ	α_1 / α_2	α_1' / α_2'
Fully spilling	0.69	0.39	0.33	1.20	0.97	0.99
Spilling	0.75	0.41	0.31	1.37	0.93	1.01
Plunging	0.76	0.47	0.30	1.60	0.88	1.01
Fully plunging	0.77	0.62	0.28	2.13	0.80	1.02
Symmetric (2^{nd} order Stokes limiting) wave	0.50	0.28	0.28	1.00	1.00	1.00

3.2 Kinematic Properties

Five regions of particular interest were investigated: the forward (or front) zero-crossing point, the rear zero-crossing point, the face of the falling water jet, the back of the overturning region and the crest of the wave.

The zero-crossing points are the points where the crest profile crosses the still water level taken as a reference: the forward (or front) crossing point is the upward zero-crossing ahead of the breaking crest, the rear crossing point is the downward zero-crossing after the crest. Fig. 7 shows that the breaking event concerns only a region located in the vicinity of the wave crest.

As about the face of the falling water and the back of the overturning region, their celerity is also constant as displayed on Fig. 8. The "breaking onset" corresponds to the time when the face of the crest becomes vertical, the plunge point, or touch-down point, corresponds to the time when the tip of the falling water jet hits the calm water surface ahead the breaking crest. Here again, it should be noticed that the breaking event does not affect the forward displacement of the back of the overturning region.

The face of the falling water jet moves forward with a constant celerity equal to the one of the crest before the breaking onset, as shown in Fig. 9. The crest celerity is constant in first approximation before the breaking onset, and then it decreases lightly.

The real (Langrangian) acceleration was measured on the surface of a plunging crest, and in the overturning region. Small floating tracers (respectively 15mm and 4mm in diameter) were used for these measurements. Acceleration up to 1.5g was measured when the plunging crest meets the floating tracer (see Fig. 10); maximum acceleration of the order of 2.2g was measured in the overturning region (see Fig. 11). These results are in relatively good agreement with the numerical predictions by Vinje and Brevig, [5], see Table 3. Here the numerical value 1.6g, resulting from the numerical simulation, takes into account the size of the tracer (15mm).

It should be noticed that because of their finite size, the tracers cannot be strictly equated to fluid particles, and consequently the present measurements are certainly lightly under valued.

3.3 Effect of an Adverse Current

The study of the effect of an adverse current is the subject of a cooperative work with the Japanese Ship Research Institute. Preliminary experiments were performed in the framework of this cooperation and some preliminary results are now presented. The experiments were performed both on a uniform weak current ($U/C = -0.10$), and on a shear current ($U_s/C = -0.27$), where U_s is the current velocity at the water surface.

Table 3. Action of an adverse current on the horizontal asymmetry factor and on the crest front steepness

Action on the Crest Front Steepness (ε)			
	Still water	Uniform current	Shear current
Kjeldsen and Myrhaug (1980)	0.70	-	0.70
Bonmarin (1999)	0.54	0.54	0.49

Action on the Horizontal Asymmetry Factor (μ)			
	Still water	Uniform current	Shear current
Kjeldsen and Myrhaug (1980)	0.80	-	0.75
Bonmarin (1999)	0.76	0.75	0.76

Effect on the Geometric Properties. The present results concern measurements made at the breaking onset. Table 3 summarizes the results obtained and compares them to previous results obtained by Kjeldsen and Myrhaug, [2].

It should be noticed that, at least at the breaking onset, the current does not significantly affect the wave asymmetry. On the contrary, Kjeldsen and Myrhaug, [2], have observed an amplification of about 13% of the crest front steepness, and of about 6% of the horizontal asymmetry factor on a weak adverse shear current (2% of the phase velocity), after the occurrence of the breaking stage. It is striking that a so weak adverse shear current can cause such drastic changes.

Effect on the Kinematic Properties. It was previously shown that, in the case of still water, the breaking event did not affect the displacement of the zero-crossing points; the same observation was made in the case of a current (Fig. 12). The celerity of these points depends nevertheless on the flow conditions as shown on Table 4: it decreases from still water to shear current.

When the wave profile is not sufficiently smooth, it is difficult to accurately locate the crest and, thus, to accurately measure the phase velocity. In this case, we suggest equating the phase velocity to the rear zero-crossing point one. Indeed, we have found out that the phase velocity, so estimated, is very close to the one deduced from the displacement of the crest. In addition, the zero-crossing points can be located with precision on the pictures.

Table 4 shows that the phase velocity is smaller on still water than on adverse current, as expected.

As previously observed on still water, the celerity of the face of the falling water jet and the one of the back of the overturning region are constant. Moreover, the celerity of the water jet is higher than the one of the back of the overturning region, as expected, (see Fig. 13).

Table 4. Action of the current on the celerity of the zero-crossing points and the phase velocity during the plunging (celerity scaled by the theoretical velocity $g / 2\pi f$)

Experimental condition	Forward Point	Rear point	"Phase velocity" 0.5 (Forward + Rear)
Still water	0.95	1.08	1.01
Uniform current	0.89	0.90	0.89
Shear current	0.82	0.82	0.82

4 Conclusions

A simple visualization technique and an associated image analysis process were developed in order to measure specific geometric and kinematic properties of breaking wave profile.

The following results should be mentioned:

- the wave profile becomes more and more asymmetric as the wave approaches the breaking stage
- the degree of asymmetry depends on the breaker type: it is more pronounced for plunging waves than for spilling ones
- because of this asymmetry, more than two parameters are needed to describe accurately the wave profile
- the potential energy concentrates into the crest, as approaching the breaking stage
- preliminary measurements on a relatively weak adverse current have not displayed any significant influence neither on geometric nor on kinematic properties of breaking waves at the breaking onset.

5 Prospects

(A) an automatic image analysis process is in progress in order to increase i) the number of measurements, ii) the reliability of the results
(B) the extension of the visualized field is considered
(C) further experiments are currently planed, to confirm the preliminary results
(D) from our point of view, the application of the present means to rogue waves could be helpful

6 Figures

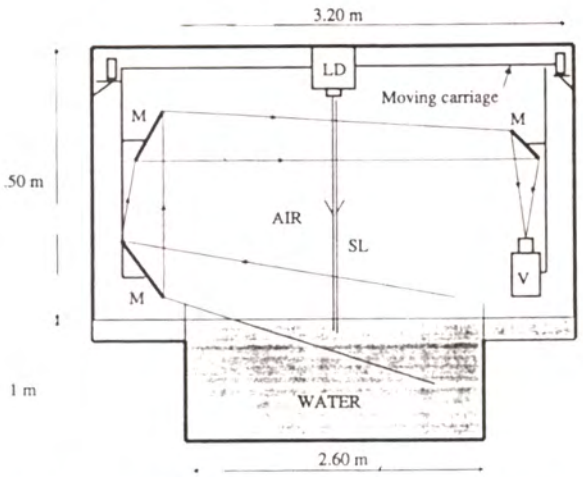

Fig. 1. Scheme of the Visualization Device. M: Plan Mirror; LD: Light Generator; SL: Light Sheet; V: Video Camera

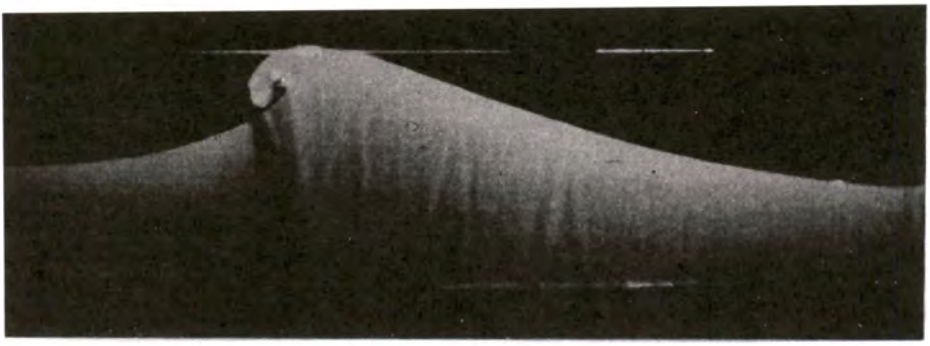

Fig. 2. Plunging wave in the large IRPHE Facility

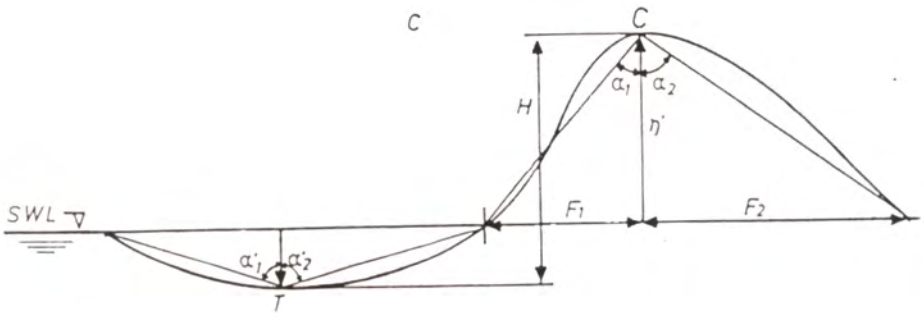

Fig. 3. Definition of Wave Parameters

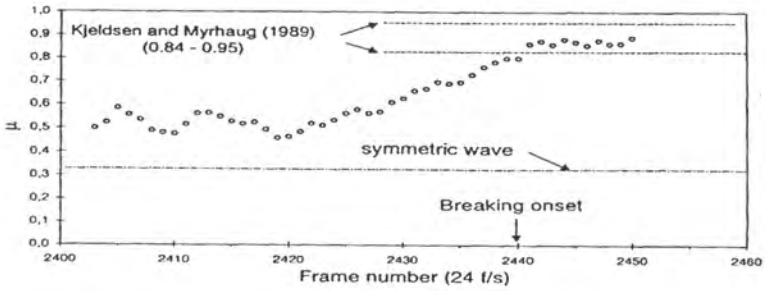

Fig. 4. Evolution of the horizontal asymmetry factor as a function of time, in the near-breaking region.

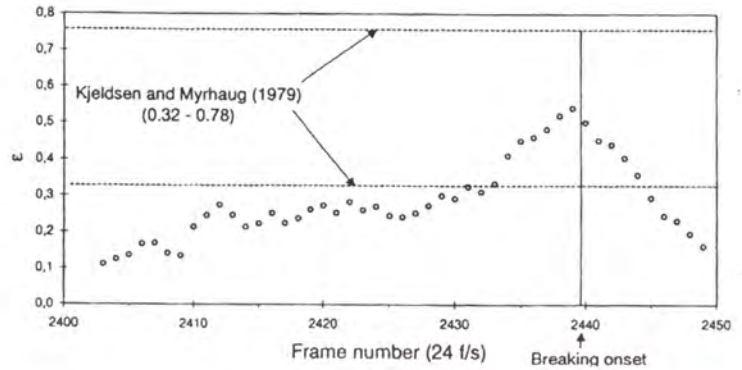

Fig. 5. Evolution of the crest front steepness as a function of time, in the near-breaking region.

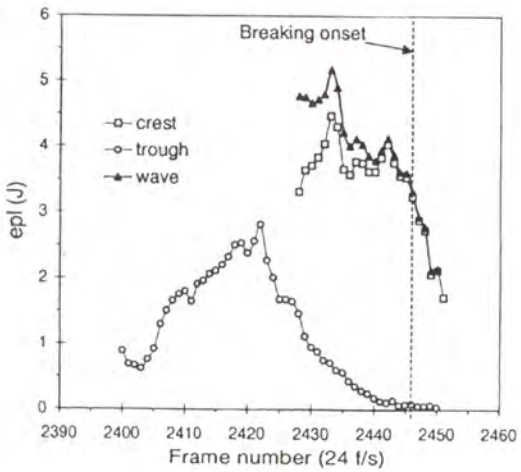

Fig. 6. Evolution of the potential energy in the near-breaking region

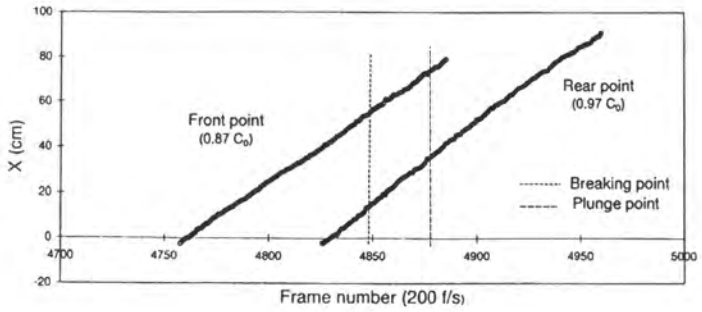

Fig. 7. Zero-crossing points position as a function of time (C_0: crest celerity before breaking onset, 144 cm/s)

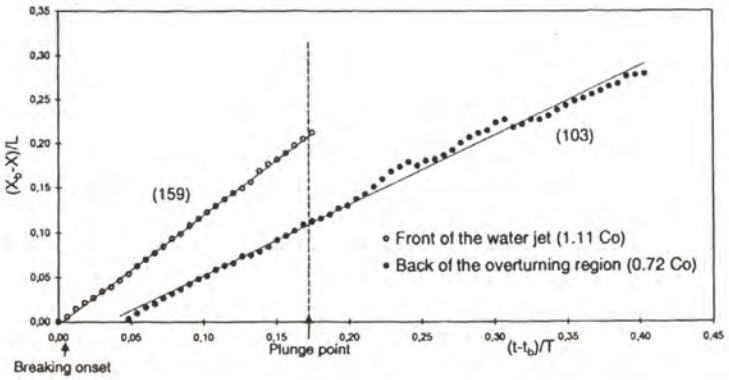

Fig. 8. Face of the water jet and back of the overturning region position as a funciton of time (in bracket: celerity in cm/s; C_0: phase velocity before the breaking onset)

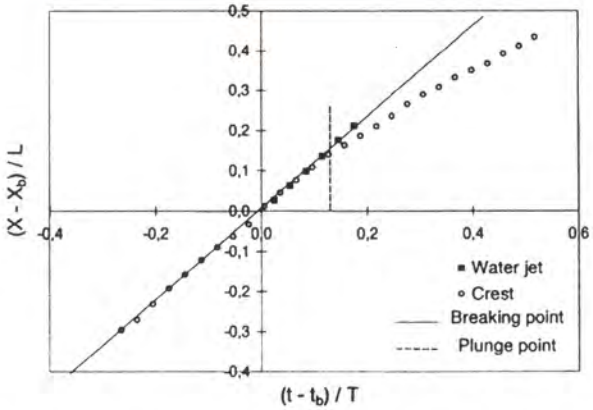

Fig. 9. Position of the crest and of the falling water jet as a funciton of time

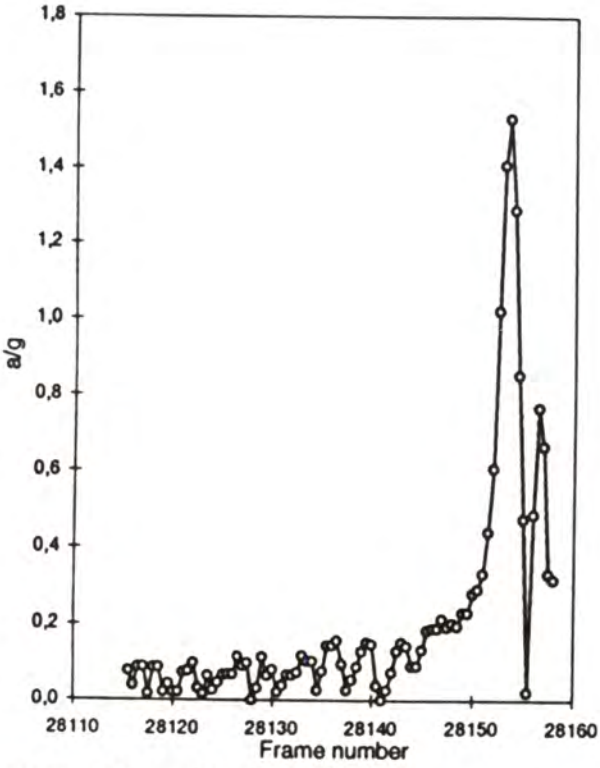

Fig. 10. Real acceleration at the surface of a plunging crest

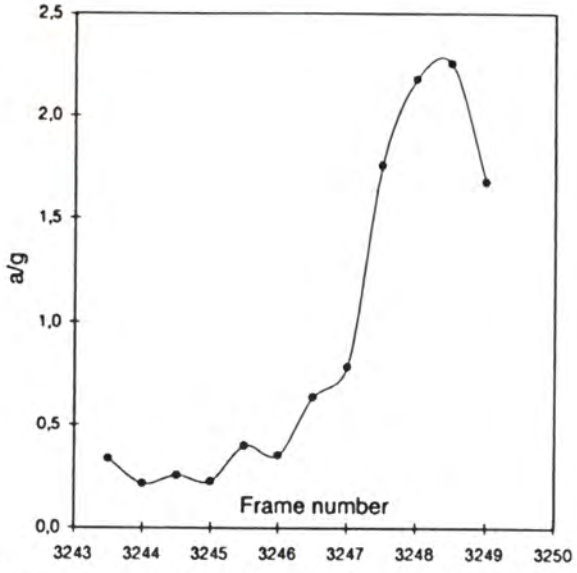

Fig. 11. Real acceleration at the water surface, in the overturning region

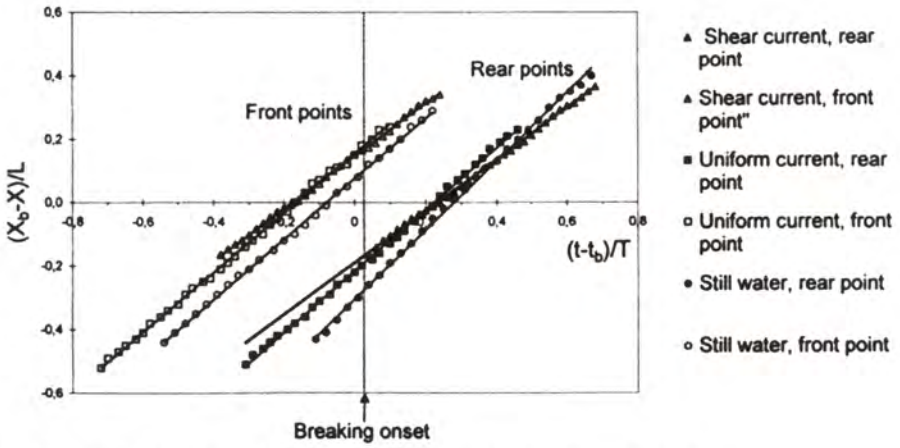

Fig. 12. Action of the current on the displacement of the zero-crossing points

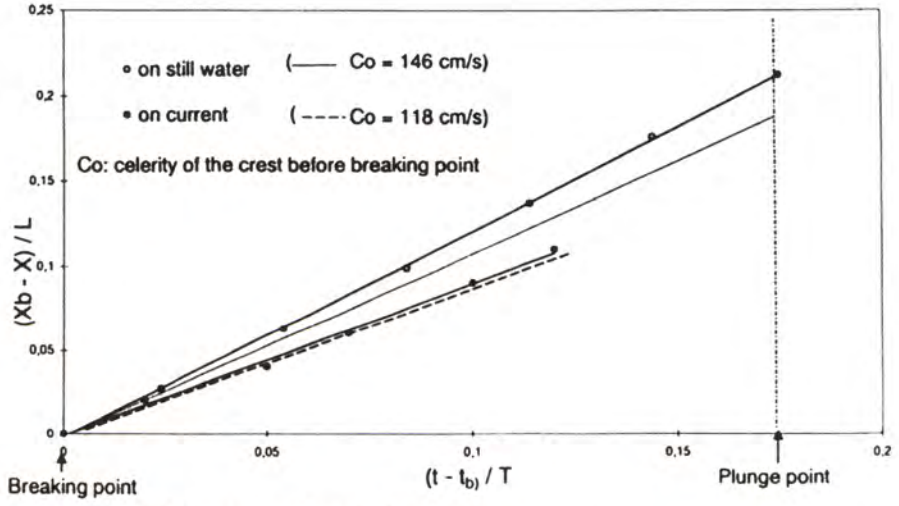

Fig. 13. Action of the current on the water jet displacement

Acknowledgments

We gratefully acknowledge the Japanese Ship Research Institute, which supported a part of the experiments. We would also like to express our gratitude to Pr. H. Tomita and Pr. S.P. Kjeldsen, for their helpful discussions and cooperation.

References

1. Bonmarin, P.: Geometric Properties of Deep-Water Breaking Waves. Journal of Fluid Mechanics, Vol. 209 (1989) 405
2. Kjeldsen, S.P. and Myrhaug, D.: Wave-Wave Interactions, Current-Wave Interactions and Resulting Extreme Waves and Breaking Waves. 17th ICCE (1980)
3. Longuet-Higgins, M.S. and Cokelet, E.d.: The Deformation of Deep Surface Waves on Water. II. Proc. R. Soc. Lond., A 364, 1 (1976)
4. Peltzer, R.d. and Griffin, O.M.: Spatial and Temporal Properties of Deep Water Breaking Waves. 45th APS Fluid Dyn. Meeting. Florida State Univ., Tallahassee, USA (1992)
5. Vinje, T. and Brevig, P.: Numerical Simulation of Breaking Waves. Adv. Water Res. (1981)

Occurrence of Freak Waves from Envelope Equations in Random Ocean Wave Simulations

Miguel Onorato, Alfred R. Osborne, Marina Serio, and Tomaso Damiani

Universitá di Torino, Via P. Giuria, 1 - 10125, Torino, Italy,
onorato@ph.unito.it

Abstract. The Nonlinear Schroedinger Equation (NLS) and higher order corrections (Dysthe equation) in the envelope-equation hierarchy are considered as simple models for explaining the generation of freak waves in 1+1 dimensions. We discuss a simple analytical formula that predicts the maximum wave amplitude as a function of wave steepness and number of waves under the envelope. We also perform numerical simulations using random-wave initial conditions characterized by the JONSWAP power spectrum: we find that the occurrence of freak waves is related to the initial steepness and to the correlation length of complex envelope of the initial time series. Cumulative probability density functions of wave heights from 1+1 numerical simulations are also reported.

1 Introduction

Freak waves are extraordinarily large water waves whose heights exceed by a factor of 2.2 the significant wave height of a measured wave train (see for example [1]). The mechanism of freak wave generation has become an issue of principal interest due to their potentially devastating effects on offshore structures and ships. In addition to the formation of such waves in the presence of strong currents [2] or as a result of a simple chance superposition of Fourier modes with coherent phases, it has recently been established that the weakly nonlinear envelope equations (Nonlinear Schroedinger (NLS) equation or higher order extensions) can describe many of the features of the dynamics of freak waves, which are thought to arise as a result of the nonlinear self-focusing phenomena [1, 3]. The self-focusing effect arises from the Benjamin-Feir instability [4] which causes a local exponential growth in the amplitude of a wave train. Moreover, it is known that small-amplitude instabilities are but a particular case of the much more complicated and general analytical solutions of the NLS equation obtained by exploiting its integrability properties via Inverse Scattering (IST) theory in the θ-function representation [5, 6] (see also [7]).

Herein we follow the pioneering work by Trulsen and Dysthe [1] and we investigate the generation of freak waves through the nonlinear self modulation of a slowly modulated wave train. An open question is how freak waves can be generated via the Benjamin-Feir instability in realistic oceanic conditions, i.e. in those characterized not by a simple monochromatic wave perturbed by two small

side-bands, but instead by a complex spectrum whose perturbation of the carrier wave cannot be viewed as being small. Therefore we have performed many numerical simulations starting from initial conditions that are characterized by the JONSWAP spectrum. Cumulative probability density functions (CPDF) of wave heights from very long numerical simulations have been computed for different JONSWAP spectra. It is found that as the "enhancement" parameter, γ, and the Phillips parameter, α, of the JONSWAP spectrum are increased, the CPDF manifest a right-hand tail which is higher than the one predicted from the Rayleigh distribution. The focus herein is not to attempt to model ocean waves but instead to study leading order effects using simple envelope equations. Research at higher order suggests that the results given herein are indicative of many physical phenomena in the primitive equations [3].

The paper is organized as follows: In Sec. (2) weakly nonlinear envelope equations are briefly reported, in Sec. (3) we give some theoretical prediction on the maximum wave amplitude from from small perturbation theory. Results from numerical simulations of the NLS and Dysthe equations in the case of JONSWAP random waves are reported in Sec. (4)

2 Envelope Equations

We consider the fluid inviscid, irrotational, on a horizontal bed, propagating in one direction, x. The envelope equations are obtained by employing an harmonic expansion of the velocity potential ϕ and the surface displacement η (for a formal and complete derivation of NLS equation see for example Ref. [8]). Since initial conditions for numerical simulations will be given starting from frequency spectra, the analysis is carried out by considering the so called time-like NLS equation (TNLS) (for the use of time-like equations in water waves see, e.g., [8, 9]) which describes the evolution of the nondimensional complex envelope $A(x,t)$ in deep water waves:

$$A_x + i\left(\frac{\Delta\omega}{\omega_0}\right)^2 A_{tt} + i\varepsilon^2 \mid A \mid^2 A = 0, \tag{1}$$

where ω_0 is the angular frequency of the carrier wave, $\varepsilon = k_0 A_0$ is the steepness and $1/\Delta\omega$ is a characteristic time scale. Here k_0 is the carrier wave number and A_0 is the amplitude of the carrier wave. Equation (1) solves a *boundary value problem*: given the temporal evolution $A(0,t)$ at some location $x = 0$, eq. (2) determines the wave motion over all space and time, $A(x,t)$.

It is instructive to introduce a parameter that estimates the influence of the nonlinearity in deep water waves. This parameter, which is a kind of "Ursell" number [9], can be obtained as the ratio between the nonlinear and the dispersive term in the TNLS equation:

$$Ur = \left(\frac{\varepsilon}{\Delta\omega/\omega_0}\right)^2. \tag{2}$$

When $Ur << 1$ waves are essentially linear and their dynamics can be expressed as a simple superposition of sinusoidal waves. For $Ur \geq 1$, the dynamics become nonlinear and the evolution of the wave train is likely dominated by envelope solitons or unstable mode solutions such as those studied by Yuen and coworkers [10].

Higher Order Envelope Equations. Dysthe, Trulsen and co-workers have done extensive research in trying to extend the NLS equation to higher order, especially for what concerns the spectral width (see [11–13]). In this paper we will perform numerical simulations of what we call the Dysthe-Lo-Mei (DLM) equation which is basically the equation originally written by Dysthe [11] in its time-like version. The transformation was first applied by Lo and Mei [14]. The equation reads as follows:

$$A_x + i\left(\frac{\Delta\omega}{\omega_0}\right)^2 A_{tt} + \varepsilon^2 i \mid A \mid^2 A + \frac{8\varepsilon^2 \Delta\omega}{\omega_0} \mid A \mid^2 A_t + 4i\varepsilon\left(\frac{\Delta\omega}{\omega_0}\right)^2 A\bar{\phi}_t = 0 \quad (3)$$

$$\bar{\phi}_z = \varepsilon \mid A \mid_t^2 \qquad z = 0. \quad (4)$$

$$4\left(\frac{\Delta\omega}{\omega_0}\right)^2 \bar{\phi}_{tt} + \bar{\phi}_{zz} = 0 \qquad -h < z < 0 \quad (5)$$

$$\bar{\phi}_z = 0 \qquad z = -h. \quad (6)$$

One motivation led us to use the variables and coordinate system as in Ref. [14]: the evolution of the waves can be directly compared with experimental time series from open-sea measurements or from wave tank facilities. For a discussion on the linear stability analysis of the Dysthe equation and an extended equation see Refs.[12, 13].

3 Predicting the maximum wave amplitude from small perturbation theory

It is well known that a monochromatic wave is unstable to sideband perturbations if the wave number of the perturbation, Δk, falls in the range:

$$0 \leq \Delta k \leq 2\sqrt{2} k_0 \varepsilon, \quad (7)$$

This result (which is the condition for the Benjamin-Feir instability to appear) has been obtained by a standard linear stability analysis of the NLS equation under the hypothesis of a small amplitude perturbation (see for example [10]). In this paragraph we complete this result by reporting a simple formula that we have recently obtained from Inverse Scattering Theory (for an outline of the derivation see [15]) which gives the maximum wave amplitude as a function of

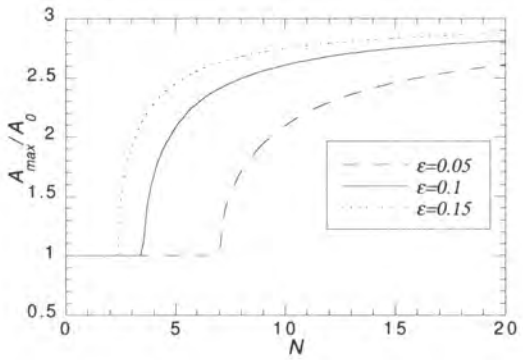

Fig. 1. Maximum wave amplitude as a function of N for ε=0.05, 0.1 and 0.15.

the wave steepness ε and $N = k_0/\Delta k$, that is the number of waves under the perturbation. The equation reads as follows:

$$\frac{A_{max}}{A_0} = 1 + 2\sqrt{1 - \left(\frac{1}{2\sqrt{2}\varepsilon N}\right)^2}. \tag{8}$$

In Fig. 1 we plot A_{max}/A_0 as a function of N for different values of the steepness. It is clear from the figure that as the steepness and the number of waves under the envelope increases, the wave can reach higher amplitudes: the maximum amplitude obtainable is 3 times the initial amplitude A_0. It has to be remembered that eq. (8) has been derived for a small amplitude perturbation: if the perturbation is larger, the waves can reach amplitudes greater than 3 (see [15]). Moreover, the NLS equation does not include breaking: physically some of the waves could indeed break before reaching their maximum amplitude. This last point definitely deserves more attention in further studies. For the TNLS equation which gives the evolution in space (instead of in time), it is straightforward to show that eq. (8) still applies (it has to be remembered that in deep water $k_0/\Delta k = f_0/(2\Delta f)$). In order to verify our results in Fig. 2 we show the maximum amplitude of the wave as a function of $2N = f_0/\Delta f$ with $\varepsilon = 0.1$ and from numerical experiments of the TNLS equation and from IST theory (eq. 8). The values of the amplitude of the perturbation were fixed at δ=10^{-4}. As expected, good agreement is achieved. In the same plot, the maximum amplitude from numerical simulations of the DLM equation (3) is also reported. We note that the maximum amplitude reached by the DLM equation is slightly smaller than that for the TNLS equation. Moreover, as anticipated, the region of instability for the DLM equation is restricted with respect to the TNLS equation: for example in Fig. 2, for $f_0/\Delta f$=8 the TNLS equation is unstable and the waves grow to a normalized amplitude of almost 2, while the DLM equation is stable and there is no growth.

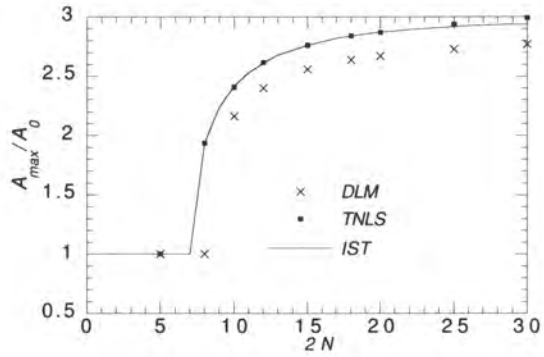

Fig. 2. Maximum wave amplitude from Inverse Scattering theory, numerical simulation of TNLS and DLM equation. The value of the initial steepness is ε=0.1.

4 The Jonswap Spectrum and Freak Waves

In this Section our attention is focused on freak wave generation in numerical simulations of the TNLS and DLM equation where we assume initial conditions described by the JONSWAP power spectrum [16]:

$$P(f) = \frac{\alpha}{f^5} \exp\left[-\frac{5}{4}\left(\frac{f_0}{f}\right)^4\right] \gamma^{\exp\left[-\frac{(f-f_0)^2}{2\sigma_0^2 f_0^2}\right]} \tag{9}$$

where σ_0=0.07 if $f \leq f_0$ and σ_0=0.09 if $f > f_0$. Our use of the JONSWAP formula is based upon the established result that developing storm dynamics are governed by this spectrum for a range of the parameters [16].

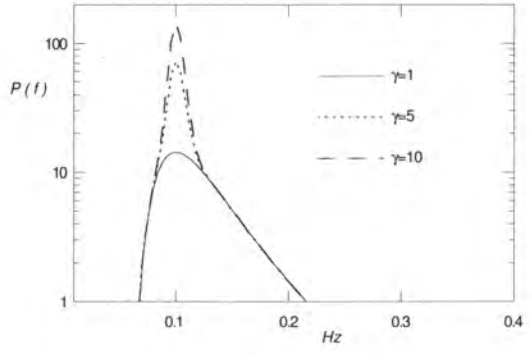

Fig. 3. The JONSWAP spectrum for γ=1 (dashed line), γ=5 (dotted line), γ=10 (solid line) with f_0=0.1 Hz and α=0.0081.

The constants α, γ and σ_0 were originally obtained by fitting experimental data from the international JONSWAP experiment conducted during 1968-69 in the North Sea. Here f_0 is the dominant frequency, γ is the "enhancement" coefficient and α is the Phillips parameter [16]. All of the JONSWAP parameters depend on the stage of wave development and probably are all interdependent on one another in a non trivial manner. For a recent description of these topics see [17] and references therein. In Fig. 3 we show the JONSWAP spectrum for different values of γ (γ=1, 5, 10) for f_0=0.1 Hz and α=0.0081: as γ increases the spectrum becomes narrower.

Many aspects of the importance of the nonlinearity can be addressed by computing Ur from the spectrum (9). In Fig. 4 we show the Ursell number as a function of the parameter γ for α=0.0081 and α=0.0162. In the construction of the plot an estimation of ε and $\Delta\omega/\omega_0$ needs to be given. The steepness ε has been estimated as the product of the wave number, k_0, of the carrier wave with a characteristic wave amplitude which we compute as the significant wave height (the mean of the highest 1/3 waves in a wave train), H_s, divided by 2. $\Delta\omega$ is a measure of the width of the spectrum and it has been estimated as the half-width at half-maximum of the spectrum. From the plot it is evident that for the Pierson-Moskowitz spectrum ($\gamma = 1$) the Ursell number is quite small: this indicates that dispersion dominates nonlinearity. Formally speaking the NLS equation is derived assuming that the spectrum is narrow banded and the steepness is small. When the spectral width is allowed to become large, the steepness becomes small; this in effect "linearizes" the NLS equation. Results of this type are evidently somewhat out of the range of applicability of the NLS equation, but are essentially linear.

As γ increases, the Ursell number increases rapidly reaching $Ur \sim 1$ for $\gamma \sim 10$. The influence of the parameter α consists in increasing the energy content of the time series and, therefore as α increases, the wave amplitude, and consequently the wave steepness, also increase. If α doubles, the steepness increases by a factor of $\sqrt{2}$ and the Ursell number by a factor of 2 since the spectral width remains constant. From this analysis we expect that large amplitude freak waves (large with respect to their significant wave height) are more likely to occur when γ and α are both large.

An additional aspect of this work that is rather important and gives a connection to what has been shown in the previous Section is the relationship of the "enhancement" parameter, γ, with the correlation length of the envelope of the time series generated via the JONSWAP spectrum. In Fig. 5 we show that the auto-correlation function of the complex envelope $A(t)$ computed from the JONSWAP spectrum for different values of γ. For small values of γ the correlation length is very small and therefore the field is more likely to be homogeneous. For high values of γ inhomogeneities such as wave grouping cannot be neglected: in this case wave groups could be unstable and develope into rogue waves.

We now verify our findings by numerical integration of eq. (1) which has been solved numerically using a standard split-step, pseudo-spectral Fourier method [14]. Initial conditions for the free surface elevation $\zeta(0,t)$ have been constructed

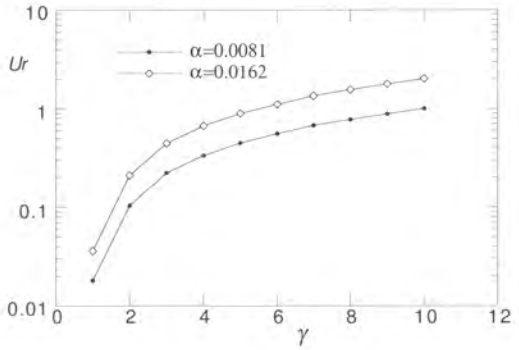

Fig. 4. The Ursell number as a function of γ for the JONSWAP spectrum.

as the following random process:

$$\zeta(0,t) = \sum_{n=1}^{N} C_n \cos(2\pi f_n t - \phi_n), \tag{10}$$

where ϕ_n are uniformly distributed random phases on the interval $(0, 2\pi)$, and $C_n = \sqrt{2P(f_n)\Delta f_n}$, where $P(f)$ is the JONSWAP spectrum given in (9). In order to give quantitative results we have performed more that 300 simulations of the TNLS equation. The simulations have been performed in dimensional units in the following way. An initial time series of 32768 seconds (about 9 hours) has been computed from the JONSWAP spectrum for different values of α and γ (from α=0.0081 to α=0.02 and from γ=1 to γ=10). Such a long time series has been computed in order to ensure a convergence of the tails of the probability density function. In many cases more than 10 different realizations (with different sets of random phases, ϕ_n) for each selected value of α and γ has been constructed. The time series were then allowed to evolve according

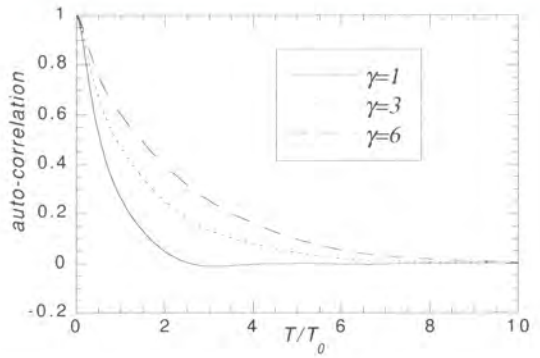

Fig. 5. Autocorrelation function of the complex envelope for γ=1,3 and 6.

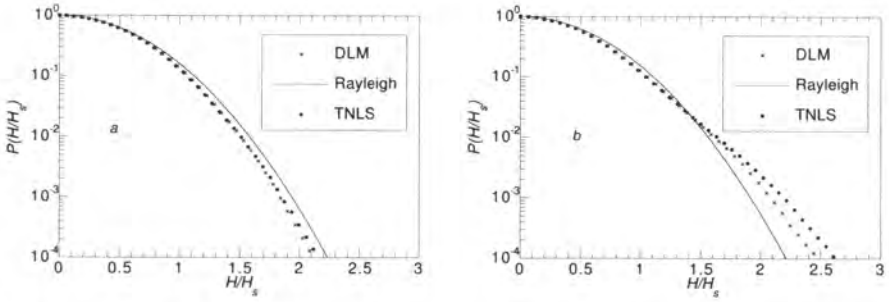

Fig. 6. Cumulative Probability Density Function from Rayleigh distribution and numerical simulations of TNLS, DLM. *a*: $\gamma = 2$ and $\alpha = 0.0081$, *b*: $\gamma = 6$ and $\alpha = 0.0081$.

to the periodic TNLS and DLM equations for a distance of 5 km, saving the output every 50 m. We have checked that during the space evolution the shape of the initial spectrum has been maintained in an average sense. We have then computed the CPDF of the wave heights normalized by the significant wave height, H_s, of the simulated $x - t$ field. In Fig. 6 we show CPDFs computed from a single realization of the TNLS and DLM equations for different values of γ and α. The CPDFs of the numerical simulations are also compared with the Rayleigh distribution which is theoretically obtained from a linear system in the case of small spectral width. For γ=2 and α=0.0081 (Fig. 6*a*) the numerical CPDF is below the linear prediction of Rayleigh. The CPDFs from TNLS and DLM numerical simulations are almost indistingushible. Fig. 6*b* refers to γ=6 and α=0.0081: in this case the linear prediction for extreme waves is well below our numerically obtained values; as previously mentioned the NLS equation over estimates the wave heights with respect to the DLM equation. Note further that in the same simulation, due to a sort of Fermi-Pasta-Ulam recurrence in a random field the same freak wave can appear with a certain periodicity in space, therefore contributing to the probability in the tail of the cumalive CPDFs.

In order to have more quantitative results we have computed the intersection between the CPDFs from the linear prediction and the numerical simulations for different values of α and γ. The results are shown in Fig. 7 in which we plot the the value of the probability at which linear theory and numerical experiment intersect, P_{cross}, as a function of γ for different values of α. The intersection point for each γ and α has been computed as the mean of the intersections of the different realizations. The figure clearly shows that as γ and α grow (increasing nonlinearity), the cumulative CPDFs from the numerical simulations cross the Rayleigh distribution at a higher probability and therefore at lower values of H/H_s.

5 Discussion and Conclusions

This work constitutes an attempt to study the influence of nonlinearity on the prediction of large amplitude waves in random sea states. Numerical simulations

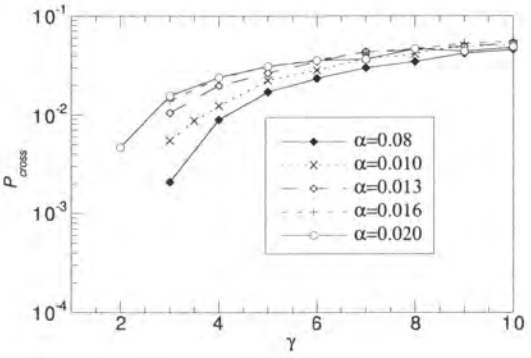

Fig. 7. Probability at which the Rayleigh distribution is crossed by numerical CPDFs as a function of γ for different values of α.

of random waves governed by the dynamics of the TNLS and DLM equations for the JONSWAP power spectrum have provided insight about this problem. We have shown that as γ and α increase the effects of nonlinearity become more important: therefore freak waves that result as a modulational instability are more likely to occur in a physical situation where γ and α are large. The local properties of the wave trains are presumably of fundamental importance for understanding the formation of freak waves. It may happen that the Benjamin-Feir instability mechanism is satisfied only in a small portion of the full wave train, giving raise to a local instability and therefore to the formation of a freak wave. We have shown that as γ increases the correlation length increases and therefore inhomogenities, such as wave packets that can evolve via the Benjamin Feir instability mechanism, are more likely to be encountered. The correlation length of the complex envelope is strictly related to the number of waves under the envelope, N, for the case of small-amplitude perturbation theory (see Sec. 3) and according to eq. (8) the maximum wave height, for a given steepness, increases as N increases. All these results can probably be better understood and explained in terms of the discrete unstable modes of the NLS equation whose integrability properties and the Inverse Scattering Transform provide a unique way of approaching the problem, the scope of a future paper.

We have found that the TNLS equation over estimates not only the region of instability but also the maximum wave amplitude with respect to the DLM equation. Furthermore it is well known that the NLS equation is formally derived from the Euler equations under the assumption of a narrow-banded process. Nevertheless, in spite of these deficiencies in the NLS equation, we believe that our results provide new important physical insight into the generation of freak waves. Simulations with the fully nonlinear equations of motion will be required in order to definitively confirm these results. Wave tank experiments will also be very useful in this regard.

Another important issue that has to be taken into account for future work is directional spreading: It is well known that sea states are not fully unidirectional and directionality can play an important role in the dynamics of ocean waves. In a recent paper [18] we have considered simple initial conditions in 2+1 dimensions using the NLS equation and we have demonstrated the ubiquitous occurrence of freak waves. Whether the additional directionality in the JONSWAP spectrum will drastically change our statistical results is still an open question. At the same time we are confident that our results can apply to the cases in which the spectrum is quasi-unidirectional. In particular, as suggested in a private communication [19], the so called "energetic swell", which corresponds to the early stages of a swell evolution, still characterized by a highly nonlinear regime, are described by high values of γ and α and are candidate sea states for the occurrence of freak waves. In such conditions the 1+1 TNLS or DLM equation could represent "good" evolution equations in this regards.

6 Acknowledgments

M. O. was supported by a Research Contract from the Universitá di Torino. This work was supported by the Office of Naval Research of the United States of America. Torino University funds (60 %) are also acknowledged.

References

1. Trulsen, K., Dysthe, K.: Freak Waves - A three-dimensional wave simulation. Proc. 21st Symp. on Naval Hydrodynamics, National Academy Press (1997) 550–560.
2. White, B. S., Fornberg, B.: On the chance of freak waves at sea. J. Fluid Mech. **335** (1998) 113–138.
3. Henderson, K. L., Peregrine, D. H., Dold, J. W.: Unsteady water wave modulations: fully nonlinear solutions and comparison with the nonlinear Schrodinger equation. Wave Motion **29** (1999) 341–361.
4. Benjamin, T. B., Feir, J. E.: The disintegration of wave trains on deep water. Part 1. Theory. J. Fluid Mech. **27**, 417-430, (1967).
5. Its, A. R., Kotljarov, V. P.: Dokl. Akad. Nauk. Ukain SSR Ser. A **11** (1976) 965.
6. Tracy, E. R.: *Topics in nonlinear wave theory with applications*, Ph.D. Thesis, University of Maryland (1984); Tracy, E. R., Chen, H. H.: Phys. Rev. A **37** (1988) 815–839.
7. Dysthe, K., Trulsen, K.: Note on Breather Type Solutions of the NLS as Models for Freak-Waves. Physica Scripta **T82** (1999) 48–52.
8. Mei, C. C.: *The Applied Dynamics of Ocean Surface Waves*, J. Wiley & Sons, New York (1983).
9. Osborne, A. R., Petti, M.: Laboratory-generated, shallow-water surface-waves - analysis using the periodic, inverse scattering transform. Phys. of Fluids **6** (1994) 1727–1744.
10. Yuen, H. C.: Nonlinear Dynamics of Deep-Water Gravity Waves. Adv. Appl. Mech. **22** (1982) 67–229.
11. Dysthe, K.: Note on a modification to the nonlinear Schroedinger equation for application to deep water waves. Proc. R. Soc. Lond. A **369** (1979) 105–114.

12. Trulsen, K., Dysthe, K.: A modified nonlinear Schrodeinger equation for broader bandwidth gravity waves on deep water. Wave Motion **24** (1996) 417–430.
13. Trulsen, K., Kliakhandler, I., Dysthe, K.B., Velarde, M.G.: On weakly nonlinear modulation of waves on deep water. Phys. Fluids **12** (2000), 2432–2437 .
14. Lo, E., Mei, C. C.: A numerical study of water-wave modulation based on a higher-order nonlinear Schroedinger equation. J. Fluid Mech. **150** (1985) 395–416.
15. Onorato, M., Osborne, A. R., Serio, M.: Nonlinear Dynamics of Rogue Waves. International Workshop on Wave Hindcasting and Forecasting, Monterey (2000) 470–479.
16. Komen, G. J., Cavaleri, L., Donelan, M., Hasselman, K., Hasselman, S., Janssen, P. A. E. M.: *Dynamics and modelling of ocean waves*, Cambridge University Press, (1994).
17. Babanin, A. V., Soloviev, Y. P.: Field investigation of transformation of the wind wave frequency spectrum with fetch and the stage of development. J. Phys. Oceanogr. **28** (1998) 563–576.
18. Osborne, A. R., Onorato, M., Serio, M.: The nonlinear dynamics of rogue waves and holes in deep water gravity wave trains. Phys. Lett. A **275** (2000) 386–393.
19. D. Resio, Private communication, Torino, October 2000.

Nonlinear Wave Focusing as a Mechanism of the Freak Wave Generation in the Ocean

Efim Pelinovsky[1], Christian Kharif[2], Tatiana Talipova[1], and Alexey Slunyaev[1]

[1] Laboratory of Hydrophysics and Nonlinear Acoustics, Institute of Applied Physics,
46 Ulianov Str., 603600 Nizhny Novgorod, Russia
enpeli@hydro.appl.sci-nnov.ru,
[2] Institut de Recherche sur les Phénomènes Hors Equilibre,
Parc Scientifique et Technologique de Luminy,
13288 Marseille, Cedex 9, France
kharif@pollux.univ-mrs.fr

Abstract. The mechanism of focusing of nonlinear wave field to explain the freak wave occurrence in the ocean is developed. First, the linear theory of amplitude-phase modulation is presented, and the conditions of the optimal focusing are obtained. Then, weak nonlinear theory of freak wave generation is given. For shallow water, the Korteweg – de Vries equation is used to demonstrate the features of the wave focusing. It is shown that large-amplitude abnormal impulse can be generated from the weak "invisible" deterministic (transient) component on the background of the random wind wave field. For deep water, the nonlinear Schroedinger equation for the complex amplitude of the wave envelope is applied. The mechanism of wave focusing is compared with the well-known mechanism of the Benjamin-Feir instability. It is shown that the preliminary phase modulation can amplify the process of appearance of large-amplitude abnormal waves.

1 Introduction

The rogue wave appearance is a phenomenon observed in many areas of the World Ocean. Several physical factors of the freak wave phenomenon are discussed in literature. First of all, the water wave interaction with an opposite current is considered as a mechanism of strong wave amplification. Historically, this effect has been taken into account due to large number of freak wave appearances in the Agulhas current off the south-east coast of South Africa (at least, 13 documented events since 1950). Significant wave amplification can be predicted as the blocking of water waves on current within the framework of 1D equations (modified nonlinear Schroedinger equation, energy action equation), as well as due to the formation of caustics in the wave field on the currents [1-5]. Many observations of abnormal were also made in the areas with no strong currents, for instance in the North Sea [6], including the famous "1995 New Year Wave" of 26 m at "Draupner", Statoil operated jacket platform, Norway [7]. For such areas two mechanisms are considered. The first one is the wave focusing related with the dispersion enhancement of water waves. It has been studied analytically within the framework of the linear theory only [8,9] and

also in laboratory tanks [10, 11]. The second one is the well-known effect of modulation instability (Benjamin – Feir instability) of nonlinear water waves in deep water [12-15]. This mechanism can explain the appearance of abnormal waves in the periodic weakly modulated wave field with heights exceeding 2-3 times unperturbed wave heights.

From our point of view, the mechanism of the focusing of nonlinear water wave packets related with phase (frequency) modulation should play significant role in the "short-lived" freak wave formation for both, deep and shallow water. This mechanism requires specific meteorological conditions. For instance, the increase of wind speed generates wave packets with large group velocities later than wave packets with lower group velocities, and due to the process of propagation, abnormal single waves can be formed by the superposition of many spectral components. The wind action far from the storm area can be ignored and the process of freak wave formation will be described within the framework of "free" hydrodynamic models.

The paper is organised as follows. Simple analytical theory demonstrating the focusing mechanism in the linear theory will be described in section 2. Then, it will be shown that the mechanism of wave focusing is applicable to the nonlinear theory of shallow water (section 3). A method to find possible forms of the wave trains evolving into the freak wave, including random background of wind waves will be suggested. Because of absence of the Benjamin - Feir instability for shallow water, the "focusing" mechanism seems to be major in shallow water for explanation of freak wave phenomenon. For deep water the mechanism of freak wave formation due to focusing of the nonlinear wave packets with phase modulation will be compared with the possible generation of giant waves due to the classical Benjamin - Feir instability of water waves (section 4). The main result here is that the frequency modulation of a nonlinear wave field leads to greatest amplification of the freak wave than the amplitude modulation usually studied in the theory of the Benjamin - Feir instability. Numerical simulations of the evolution equations for shallow water (Korteweg – de Vries equation) and for deep water (nonlinear Schroedinger equation) provide the details of the freak wave formation from deterministic and random wave fields.

2 Focusing of Linear Waves

To demonstrate the wave focusing effect, 1D linear theory of quasi-monochromatic wave packets can be applied. Considering the sea surface elevation in the form $\eta(x,t) = A(x,t) \exp(i\Theta)$with slowly varied amplitude $A(x,t)$, frequency $\omega(x,t) = \partial\Theta/\partial t$ and wave-number $k(x,t) = - \partial\Theta/\partial x$; its parameters satisfy the kinematic and energy balance equations [16-17]

$$\frac{\partial k}{\partial t} + c_{gr}(k)\frac{\partial k}{\partial x} = 0\,, \qquad \textbf{(1a)}$$

$$\frac{\partial A^2}{\partial t}+\frac{\partial}{\partial x}\left(c_{gr}(k)A^2\right)=0\,, \tag{1b}$$

where the group velocity $c_{gr}(k) = d\omega/dk$ is calculated using the dispersion relation of the water waves

$$\omega=\sqrt{gk\,tanh(kh)}\,. \tag{2}$$

Here h is water depth and g is the acceleration due to gravity. The solution of equation (1) satisfying the initial condition: $k(x,0) = k_0(x)$ and $A(x,0) = A_0(x)$ can be written in explicit form

$$c_{gr}(x,t)=c_0(\xi)=c_0\left(x-c_{gr}t\right), \tag{3a}$$

$$A(x,t)=\frac{A_0(\xi)}{\sqrt{1+t\left(dc_0/d\xi\right)}}, \tag{3b}$$

where $c_0 = c_{gr}(k_0)$. It describes the temporal evolution of initial spatial inhomogeneous wave field. An example of calculation for quasi-monochromatic waves having different values of wave-number outside of the transition zone is shown in Fig. 1. Packets with large values of the group velocity overtake the "low-speed" packets and the wave energy concentrates in the transition zone. Wave focusing occurs at the point where wave packets with different values of the wave-number meet together. The corresponding focusing time is

$$T_f=\frac{1}{max\left(-dc_{gr}/dx\right)}. \tag{4}$$

Optimal focusing with maximal amplification of the wave amplitude is achieved when all wave groups come to the focusing point simultaneously. As it can be shown, the optimal regime is realized for the following variation of wave parameters

$$c_{gr}=\frac{x-L_f}{t-T_f}. \tag{5}$$

In particular, for demonstration of this effect in the laboratory tank, the wavemaker should vary the wave frequency as (for deep water)

$$\omega(t)=\frac{g\left(T_f-t\right)}{2L_f}, \tag{6}$$

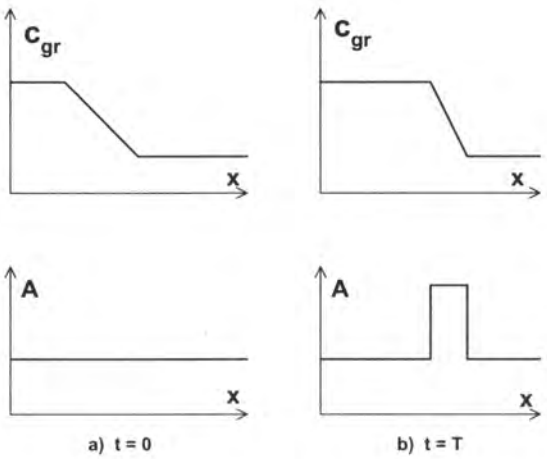

Fig. 1. Temporal evolution of the initial wave with phase modulation only.

and the wave of maximal amplitude will appear at the distance L_f from the wavemaker.

In the vicinity of the focusing point the approximation of slow variation of the parameters of quasi-monochromatic wave fails. To find the structure of the wave field there models of higher level should be used, for instance, the Fourier representation of sea surface elevation. In particular, wave impulses with Gaussian amplitude envelope will possess the Gaussian form [8, 9]

$$A(x,t) = \frac{A_0}{\sqrt[4]{1+4\left(t-T_f\right)^2 K_0^4}} exp\left(-\frac{K_0^2 x^2}{1+4\left(t-T_f\right)^2 K_0^4}\right), \tag{7}$$

if it has the phase modulation also

$$\Theta(x,t) = \frac{2\left(t-T_f\right)x^2 K_0^4}{1+4\left(t-T_f\right)^2 K_0^4} - \frac{atan\left(2\left(t-T_f\right)K_0^2\right)}{2}. \tag{8}$$

Here A_0 and $1/K_0$ are the amplitude and the length of the wave at the focusing point ($t = T_f$).

It is obvious that the random wind wave field in the linear theory cannot influence the process of the freak wave formation due to the well-known superposition of random and deterministic components, and an "invisible" (on the background of random field) wave train like (7) may transform into the "visible" peak [9]. Nonlinearity destroys the principle of wave superposition that leads to the dominant influence of one individual wave on the parameters of other individual waves. From the first point of view the focusing mechanism cannot amplify weak deterministic components on the background of a strong random field. As it will be shown in next

sections, the focusing mechanism is effective in the nonlinear case also, but it has specific features.

3 Nonlinear Wave Focusing in Shallow Water

To study wave processes in shallow water, the simplified nonlinear – dispersive theory based on the Korteweg – de Vries equation can be used

$$\frac{\partial \eta}{\partial t} + c\left(1 + \frac{3\eta}{2h}\right)\frac{\partial \eta}{\partial x} + \frac{ch^2}{6}\frac{\partial^3 \eta}{\partial x^3} = 0. \qquad (9)$$

Here $\eta(x,t)$ is the sea surface elevation and $c=(gh)^{1/2}$ is the linear wave speed propagation in shallow water. Equation (9) is valid for long waves of weak but finite amplitude. The Korteweg – de Vries equation is well studied. As it is known, the solution of the Cauchy problem for equation (9) with the impulse or periodic initial disturbances can be derived rigorously within the framework of the inverse scattering method [18]. In particular, if the initial disturbance represents a single crest of arbitrary amplitude (including very large amplitude), it evolves into a set of solitary waves (solitons) and an oscillating dispersive tail located in space according to the values of the speed for each component (solitons have large speed and they are in the front of the wave field). Due to invariance of the Korteweg – de Vries equation with respect to the reversal of time and coordinate, this wave field inverted in space should transform into the initial disturbance at fixed time, and then again transforms to solitons and dispersive tail. It means that there is no principal limitation on the formation of abnormal waves of large amplitude. Therefore, the wave focusing mechanism is applicable in the nonlinear case also but the wave field structure is more complicated, it includes solitons and amplitude-phase modulated wave packets. This process was investigated in detail in [19]. Fig. 2 displays the focusing of the initial wave field (containing the soliton and dispersive train) into the isolated crest and then its dispersion. The peak value of the wave field in the domain increases rapidly and then rapidly decreases, and this explains the rare and "short lived" character of the freak wave.

More important is to investigate the freak wave appearance in a nonlinear random wave field. First of all, we would like to mention that if an initial wave field has no significant phase (frequency) modulation, its evolution does not lead to the formation of the abnormal wave. The process of evolution of the initial amplitude modulated wave group (no phase modulation) is shown in Fig. 3. Due to absence of the Benjamin – Feir instability, the wave packet demodulates with time and this is confirmed by experimental data [20, 21].

Phase modulation cardinally influences the wave evolution. To investigate this effect, the invariance of the Korteweg – de Vries equation under the transformation $x \to -x$, $t \to -t$ can be used again, Equation (9) is solved for the initial disturbance containing superposition of irregular components and the large-amplitude crest, and then inverted in space. Its evolution is shown in Fig. 4. At short times the deterministic component is "invisible", but it became dominant at $t = 140$ and then

again invisible. Of course, due to interference of random waves sometimes, casual isolated peaks occur (for instance at $t = 40$), but usually they have no such large amplitude as the "expected" freak wave. These results correlate with the conclusions by Kriebel [22], who emphasizes that an energy of deterministic component about 10-20% of the energy of the random field may be able to produce freak waves.

The suggested method to find possible wave trains evolving into freak waves shows that many wave trains with different amplitude and phase spectra can generate the same freak wave. It means that the freak wave, being the rare event, is not an extremely rare one and, therefore, this should be forecast together with the wave climate. We would like to mention also that a relatively small deviation from the optimal conditions of the wave focusing, of course, decreases the amplitude of the freak wave (and change its form), but not cardinally, this effect is investigated in [19].

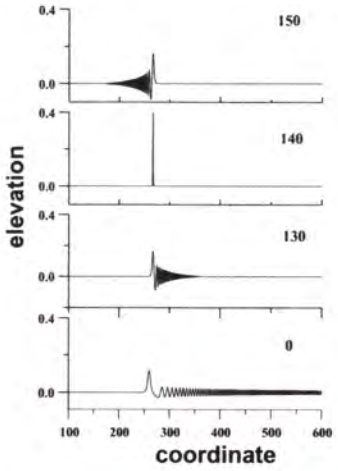

Fig. 2. The process of the large-amplitude isolated crest formation from the nonlinear-dispersive wave field for different times (all variables are dimensionless)

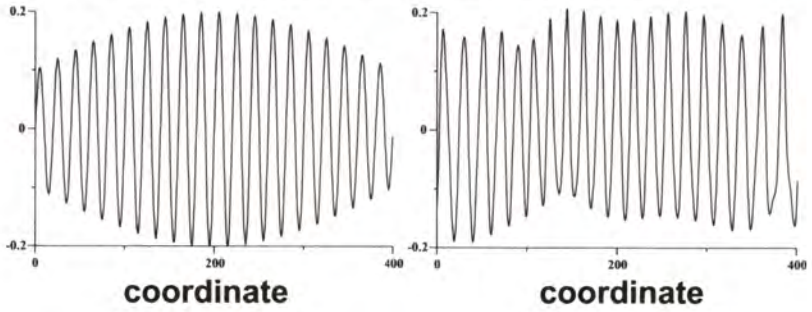

a) initial modulation b) large values of time

Fig. 3. The evolution of initial amplitude modulated wave group (no phase modulation) within the framework of the Korteweg – de Vries equation (all variables are dimensionless)

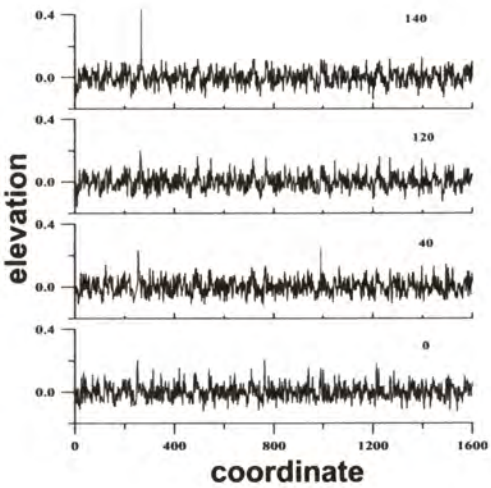

Fig. 4. The freak wave formation from the random field (all variables are dimensionless)

4 Wave Focusing in Deep Water

Wind waves in the first approximation can be considered as waves with narrow spectrum, and the complex envelope of sea surface elevation can be described by the nonlinear Schroedinger equation

$$i\frac{\partial A}{\partial t}+\frac{\partial^2 A}{\partial x^2}+2A|A|^2=0, \qquad \textbf{(10)}$$

written for dimensionless variables: wave steepness, $A=\sqrt{2k_0\eta}$, coordinate, $x' = 2k_0x - \omega_0t$, and time, $t' = \omega_0t/2$ ($'$ is omitted). Here k_0 and ω_0 are the wave-number and frequency of the carrier wave and i is the complex unit. The nonlinear Schroedinger equation is well studied too, and its exact solutions can be obtained by the inverse scattering method [18]. In particular, the solution of the Cauchy problem for equation (10) with impulse initial disturbances (including the large-amplitude impulse) represents a set of solitary waves (envelope solitons) and dispersive tail (last example of solution of the Cauchy problem for the rectangular disturbance is given in [23]). As it can be seen from (10), the nonlinear Schroedinger equation (as the Korteweg – de Vries equation) is invariant under the transformation: $x \to -x$, $t \to -t$, $i \to -i$. Due to this invariance, the solution of the Cauchy problem inverted in space should transform into the initial disturbance (including the large-amplitude impulse) at fixed time, and then again transforms into solitons and dispersive tail. It means that like the case of shallow water there is no principal limitation for the formation of an abnormal huge wave in deep water. More detailed information of the freak wave formation from the initial disturbances vanishing at infinity is contained in our paper [24].

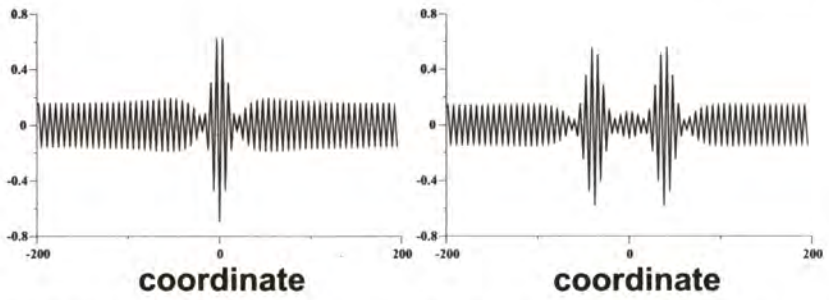

Fig. 5. High-energetic wave groups appeared in the initial amplitude modulated wave field

Periodic problem for the nonlinear Schroedinger equation is more complicated than for the Korteweg – de Vries equation due to well-known effect of modulation instability discovered for the water waves in deep water by Benjamin and Feir (see, for instance, [25]). Initial wave with weak amplitude modulation transforms into high-energy groups due to the Benjamin – Feir instability, and the examples of high-energetic groups (breathers) within the framework of the nonlinear Schroedinger equation is depicted in Fig. 5 for four values of time. Wave groups appear for relative short time and then – disappear. In the pure periodic problem the wave process is returned to the initial state (recurrence phenomenon). High-energetic wave groups correspond to the exact breather solutions of the nonlinear Schroedinger equation. These solutions are discussed in [12, 13]. There are three kinds of breathers, periodic in time (called sometimes as the Ma – soliton), periodic in space (Akhmediev's breather), and the algebraic breather. In particular, the algebraic breather is described by (its form is shown in Fig. 6):

$$q(x,t) = e^{2it}\left(1 - \frac{4(1+4it)}{1+4x^2+16t^2}\right). \qquad (11)$$

The maximal amplification in wave amplitude for breather solutions is $|q_{max}| = 3$. Therefore, possible peak amplitudes of the freak waves generated in the process of the Benjamin – Feir instability will not exceed more than three times unperturbed wave amplitude.

If the wave field contains transient waves with phase (frequency) modulation, generated abnormal waves have more energy. Results of wave transformation are de-

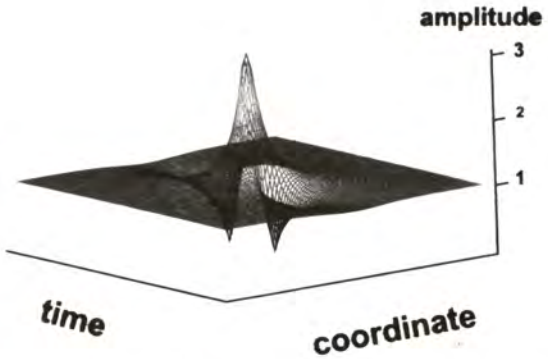

Fig. 6. Algebraic breather as a model of abnormal wave appeared in the periodic wave field [See also Appendix CP]

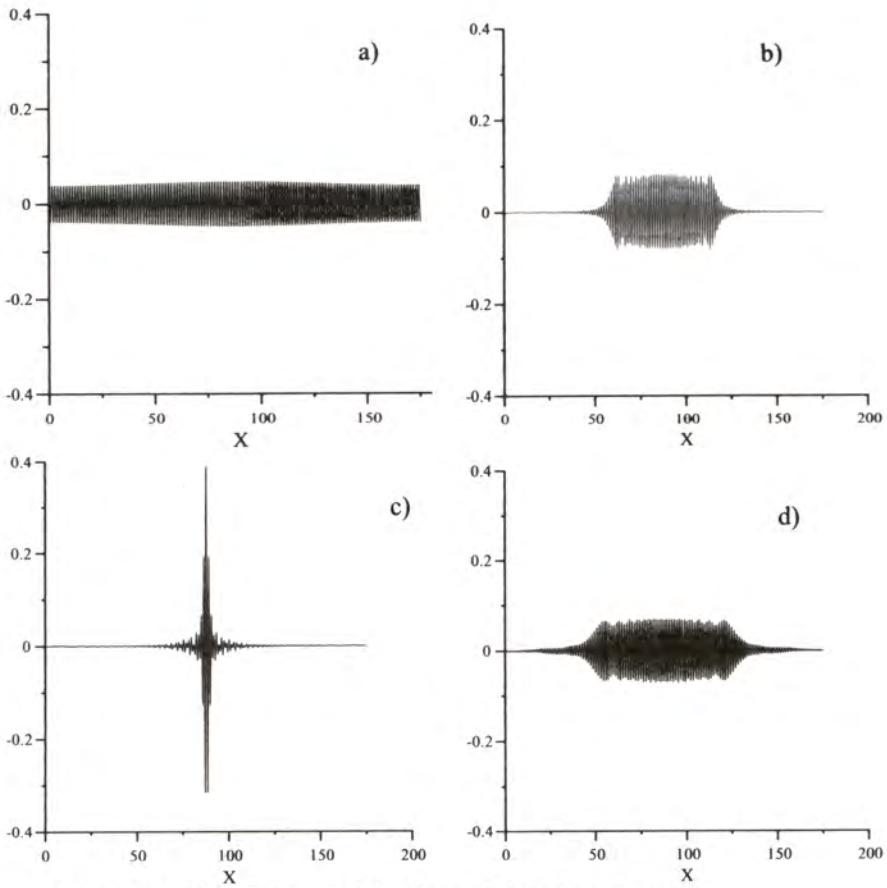

Fig. 7. Snapshot of initial phase modulated wave field in deep water

picted in Fig. 7. The wave packet focuses in a very narrow group (with a weak background), and then defocuses to the initial weakly modulated waves. The maximal wave amplitude is increased more than four times. Therefore, focusing mechanism can amplify the amplitude of the freak wave more than three times as it can be for Benjamin – Feir instability. It is important to mention also, that the phase modulation leads to decreasing of time of occurrence of the first freak wave. For large time, the influence of the periodic boundary conditions becomes dominant, as a result, the focusing of wave packets is possible several times. It leads to the complex picture of wave transformation with appearance and disappearance of large-amplitude waves.

Therefore, a freak wave in deep water can appear in the wave field due to nonlinear Benjamin – Feir instability and wave focusing. Phase modulation can amplify this process and an abnormal wave with larger amplitude can appear within shorter time.

5 Conclusion

From our point of view, the appearance of freak waves in the ocean is related mainly with the variable meteorological conditions generated the frequency modulated wind wave packets. Phase modulation leads to the focusing of wave energy in large-amplitude groups occurring within the short time. This mechanism is important for both, deep and shallow water. A simple analytical theory demonstrating the focusing mechanism in the linear theory was presented. It can predict the time and location of the appearance of large-amplitude waves. Also the optimal conditions of the wave focusing in the linear theory were formulated. Then it was shown that the mechanism of wave focusing is applicable in the weak nonlinear theory of shallow and deep water. For shallow water within the framework of the Korteweg – de Vries equation a method to find possible forms of the wave trains evolving into the freak wave, including random background of wind waves was suggested. Due to absence of the Benjamin - Feir instability for shallow water, the "focusing" mechanism seems to be major in shallow water for explanation of freak wave phenomenon. For deep water within the framework of the nonlinear Schroedinger equation for the wave envelope two possible mechanisms of large-amplitude wave appearance are discussed: the Benjamin – Feir instability of periodic waves and the mechanism of the nonlinear wave focusing. The main result here is that the frequency modulation of a nonlinear wave field leads to larger amplification of the freak wave than the amplitude modulation usually studied in the theory of the Benjamin - Feir instability. Numerical simulations point out the details of the freak wave formation from deterministic and random wave field.

6 Acknowledgements

The study was particular supported by INTAS grants (99-1537 and 99-1068) and RFBR grant (99-05-65576).

References

1. Lavrenov, I.: The Wave Energy Concentration at the Agulhas Current of South Africa. Natural Hazards **17** (1998) 117-127
2. Peregrine, D.H.: Interaction of Water Waves and Currents. Adv. Appl. Mech. **16** (1976) 9-117
3. Smith, R.: Giant Waves. J. Fluid Mech. **77** (1976) 417-431
4. White, B.S., Fornberg, B.: On the Chance of Freak Waves at Sea. J. Fluid Mech. 355 (1998) 113-138
5. Badulin, S.I., Tomita, H.: Effect of Vertical Shear Current on Appearance of Large-Amplitude Waves. PACON'99 Proceedings (June 23-25, 1999, Moscow), Moscow (2000) 380-390
6. Sand, S.E., Hansen, N.E.O., Klinting, P., Gudmestad, O.T., Sterndorf, M.J.: Water Wave Kinematics (Eds. Torum, O., Gudmestad, O.T.). Kluwer Academic Publ. (1990) 535-549
7. Haver, S., Andersen, O.: Freak Waves: Rare Realizations of a Typical Population or Typical Realization of Rare Population?. Proc. 10th Int. Offshore and Polar Engineering Conference. Seattle (May 28 – June 2, 2000) 123-130
8. Clauss, G.F., Bergman, J.: Gaussian Wave Packets - A New Approach to Seakeeping Tests of Ocean Structures. Applied Ocean Research, **8** N. 4 (1986)
9. Pelinovsky, E, Kharif, C.: Simplified Model of the Freak Wave Formation from the Random Wave Field. Proc. 15th Int. Workshop on Water Waves and Floating Bodies, Caesaria, Israel (February 27 – March 1, 2000) 142-145
10. Kjeldsen, S.P.: Breaking Waves. Water Wave Kinematics (Eds. Torum O., Gudmestad O.T.). Kluwer Academic Publ. (1990) 453-473.
11. Brown, M.G., Jensen, A.: Experiments on Focusing Unidirectional Water Waves. J. Geophys. Research (2001), submitted
12. Peregrine, D.H.: Water Waves, Nonlinear Schroedinger Equations and Their Solutions. J. Austral. Math. Soc., Ser. B **25** (1983) 16-43
13. Dysthe, K.B., Trulsen, K.: Note on Breather Type Solutions of the NLS as a Model for Freak-Waves. Physica Scripta **T82** (1999) 48-52
14. Henderson, K.L., Peregrine, D.H., Dold, J.W.: Unsteady Water Wave Modulations: Fully Nonlinear Solutions and Comparison with the Nonlinear Schroedinger Equation. Wave Motion **29** (1999) 341-361
15. Osborne, A.R., Onorato, M., Serio, M.: The Nonlinear Dynamics of Rogue Waves and Holes in Deep-Water Gravity Wave Train. Phys. Letters A **275** (2000) 386-393
16. Whitham, G.B.: Linear and Nonlinear Waves, Wiley, New York (1974)
17. Ostrovsky, L., Potapov, A.: Modulated Waves. Theory and Applications. John Hopkins Univ. Press, Baltimore-London (1999)
18. Drazin, P.G., Johnson, R.S.: Solitons: An Introduction. Cambridge Univ. Press (1996)
19. Pelinovsky, E., Talipova, T., Kharif, C.: Nonlinear Dispersive Mechanism of the Freak Wave Formation in Shallow Water. Physica D **147** (2000) 83-94
20. Pelinovsky, E., Talipova, T., Kit, E., Eitan, O.: Nonlinear Wave Packet Evolution in Shallow Water. Proc. Int. Symp. on Progress in Coastal Engineering and Oceanography, **2.** Seoul Korea (September 9 - 11, 1999) 53-62
21. Kit, E., Shemer, L., Pelinovsky, E., Talipova, T., Eitan, O., Jiao, H. Nonlinear Wave Group Evolution in Shallow Water. J. Waterway, Port, Costal, Ocean Eng. **126** (2000) 221-228.
22. Kriebel, D.: Efficient Simulation of Extreme Waves in a Random Sea. Abstract of Workshop "Rogue Waves'2000", Brest, France (November 29–30, 2000)
23. Clarke, S., Grimshaw, R., Miller, P., Pelinovsky, E., Talipova, T.: On the Generation of Solitons and Breathers in the Modified Korteweg – de Vries Equation. Chaos **10** (2000) 383-392

24.Kharif, C., Pelinovsky, E., Talipova, T., Slunyaev, A.: Focusing of Nonlinear Wave Group in Deep Water. JETP Letters (2001) accepted
25.Dias, F., Kharif, C.: Nonlinear Gravity and Capillary-Gravity Waves. Ann. Rev. Fluid Mech. **31** (1999) 301-346

Multi-wave Resonances and Formation of High-Amplitude Waves in the Ocean

Sergei Yu. Annenkov and Sergei I. Badulin

P.P.Shirshov Institute of Oceanology of Russian Academy of Sciences
36 Nakhimovsky pr, Moscow 117851, Russia
serge@wave.sio.rssi.ru; bsi@wave.sio.rssi.ru

Abstract. The problem of appearance of high-amplitude waves is considered within weakly nonlinear approach based on the Hamiltonian formulation for surface gravity waves. It is shown that the cooperative effect of four- and five-wave interactions with specific dispersion of wave components is likely to be responsible for the phenomena. The novel numerical approach for weakly nonlinear water wave equations without essential restrictions on spatio-temporal domain is proposed. Examples of numeric modelling are considered.

1 Introduction

Freak, rogue or extreme waves appear sporadically at the sea surface. Their emergence from 'nowhere' [1–4] is usually related to specific conditions of wind wave generation and propagation: bottom topography, mean current effect, strong wind effect *etc*. Besides these 'external agents', the extreme wave manifestations can be stimulated by the intrinsic wave dynamics itself.

In order to specify the role of wave packet dispersion and nonlinearity on the appearance of high-amplitude waves, the term 'nonlinear focusing' has been introduced recently [5–9]. The effect of dispersion on high-amplitude wave appearance corresponds to simple interference of different spectral components of the wave field. While these components have different wavelengths and propagate at different speeds, their interference leads to sporadic amplification of local (in space and time) wave amplitudes. On the other hand, the principal effect of nonlinearity is the energy redistribution between different wave components. While intrinsic frequencies and, hence, speeds of wave components are affected by their amplitudes, this sporadic amplification (focusing) is also modified by nonlinearity. Thus, it is not a trivial problem to predict the outcome of joint effects of nonlinearity and wave dispersion.

This paper is aimed at the analysis of the cooperative effect of nonlinearity and wave dispersion within a weakly nonlinear approach. The proper use of the approach, based on the Hamiltonian formulation for surface gravity waves proposed by Zakharov [10–13], allows the detailed physical analysis of the problem and enables one to elaborate an effective numerical algorithm with no essential restrictions on the dimension of spatio-temporal domain where a corresponding problem is considered [14–16].

The essence of the approach is the study of multi-wave resonant interactions responsible for energy exchange of water wave components. In Section 2, we consider arguments for the account of both four- and five-wave resonances in the problem. Details of numerical approach are given in Section 3. In the Discussion, examples of numerical modelling of freak waves emergence are presented.

2 Wave Resonances — Dynamics and Kinematics of Interacting Wave Components

2.1 Basics of Weakly Nonlinear Approach

Weakly nonlinear approach can be adequately used for the problem of freak waves as long as we are discussing the possibility of forecasting high-amplitude events but not their consequences. Normally, at rather heavy wind wave conditions wave steepness does not exceed magnitudes $ak = 0.2$. We use the Hamiltonian formulation for water wave equations proposed by Zakharov [10], which gives asymptotic expansions for the Hamilton function $\mathcal{H}$ in powers of the small parameter $\varepsilon = ak$, measuring wave steepness. Within the accuracy ε^4 of the corresponding equations, we have the so-called five-wave reduced Zakharov equation [10, 11]

$$\begin{aligned} \mathrm{i}\frac{\partial b_0}{\partial t} = \omega_0 b_0 &+ \int V^{(2)}_{0123} b_1^* b_2 b_3 \delta_{0+1-2-3} \mathrm{d}\mathbf{k}_{123} \\ &+ \int W^{(2)}_{01234} b_1^* b_2 b_3 b_4 \delta_{0+1-2-3-4} \mathrm{d}\mathbf{k}_{1234} \\ &+ \frac{3}{2} \int W^{(2)}_{43210} b_1^* b_2^* b_3 b_4 \delta_{0+1+2-3-4} \mathrm{d}\mathbf{k}_{1234}. \end{aligned} \tag{1}$$

In (1), only cubic and quartic nonlinear terms are present, corresponding to multi-wave resonances $2 \Leftrightarrow 2$ (four-wave resonances) and $2 \Leftrightarrow 3$ (five-wave resonances). Non-resonant quadratic terms, corresponding to processes $1 \Leftrightarrow 2$ are eliminated by the proper canonical transformation to normal variables $b(\mathbf{k})$. General form of this transformation from primitive physical variables (surface elevation and velocity potential at the surface) is discussed in a number of papers [11–13]. Such a transformation contains linear terms corresponding to linear approximation of the problem, and higher-order integral terms containing all their possible combinations. *Exact solutions* in the form of discrete set of δ-pulses in wavevector space

$$b(\mathbf{k}) = \sum_{i=1}^{L} b_i(t) \delta(\mathbf{k}_i - \mathbf{k}) \tag{2}$$

can be obtained with a special canonical transformation to normal variables $b(\mathbf{k})$ [12]. In the corresponding expansions for primitive variables these solutions are sums of L linear terms ('master harmonics') and a number of cross-terms

representing all their possible combinations [12, 13]. The proper canonical transformation, in fact, cumulates a great number of 'slave' (forced) harmonics into a small number of master modes, serving as nonlinear normal variables of the problem, and, thus, optimizes the dynamical description in weakly nonlinear approach. This description is two-stage. First, we have to solve the ordinary differential dynamical equations to obtain amplitudes and phases of master modes. Second, we have to unfold the relatively small set of master harmonics into a much richer set by means of a corresponding canonical transformation.

Formally, this technique can be considered as a truncation of primitive physical system by retaining a small number of elements (eigenfunctions), as it is done in commonly used spectral numerical methods. The essential feature of our approach lies in the use of the *master modes* as eigenfunctions. They cumulate the dynamically linked 'slave' (forced) harmonics automatically and, thus, all essential features of wave dynamics are preserved in the approach. In the case of five-wave Zakharov equation (1), this means the conservation of energy and momentum expressed by symmetry conditions for the kernels V_{0123} and W_{01234}. The truncation of the wave system within our approach implies a special choice of master modes. These modes have to be in resonances to provide non-trivial dynamics of the system and, thus, the corresponding 'grid' in wavevector space is not a trivial regular one, but is governed by resonance conditions. Different choices of the grid can affect (sometimes, significantly) the dynamics. Thus, numerical experiment within the proposed approach depends on the search for robust dynamical features.

Physically, the proposed approach facilitates dramatically the wave dynamics analysis. The first stage of the analysis is the solution of an ODE system. In fact, it gives a pure effect of energy exchange between relatively small number of dynamical master modes. The second stage is the canonical transformation from specially constructed variables $b(\mathbf{k})$ to the primitive variables. This transformation is a nonlinear superposition of a number of master modes with time-dependent amplitudes and phases. The effect of interference in the weakly nonlinear problem can be analyzed at this stage within plain algebraic transformation. Such a splitting of mathematical (ODE and canonical transformation) and physical (energy exchange and wave component dispersion) sides of the problem is very useful for the analysis.

2.2 The Simplest Models

In this subsection, nonlinear resonances, as the fundamental feature of nonlinear terms in (1), are briefly discussed. Details of quantitative and qualitative description of these resonances can be found in many papers [17, 18].

Dynamics of water wave resonances (energy exchange) are determined, first, by the order of resonances. Four-wave resonances are in general more efficient than higher-order five-wave ones. At the same time, kernels in (1) depend on the geometry of interacting wavevectors. The resonant curves for the simplest models of one dominant plane wave, as well as the values of the interaction coefficients, are shown in fig.1. It is seen that the interactions of waves of close wavevectors

are essential for the four-wave coupling associated with the Benjamin-Feir instability. Five-wave interactions are important (the corresponding kernels have relatively high magnitudes) for wave components of different scales. In the model discussed, this means different frequency ranges of interacting components that have important consequences for the model dynamics. The kinematical effect of this difference is of principal importance for our study: the components affected by five-wave coupling have different phase velocities and, thus, 'linearized' ideas of wave dispersion effects can be used in the problem. This qualitative hint is in contrast with the commonly used model of Benjamin-Feir modulations as a possible cause of freak wave appearance. In the latter case phase velocities of interacting components are close to each other and their dispersion is strongly affected by nonlinear dynamics [17].

The different role of four- and five-wave resonance in the energy exchange and wave dispersion (finally, on wave forms on the surface) brings up the question of how to model a wave field numerically. Within our approach we need to distribute wave harmonics in the wavevector space. Emphasizing four-wave resonances we tend to reinforce energy exchanges in the wave system, while the preference for quintet interactions weakens the exchanges but stimulates variations of wave forms due to interference of harmonics.

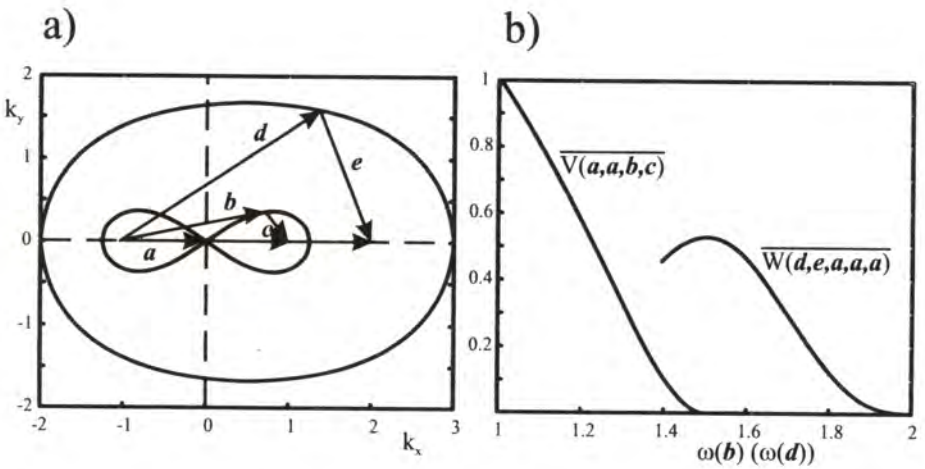

Fig. 1. Kinematical and dynamical features of water wave resonances. *a* — Resonant curves and corresponding wavevectors for the model geometry of four- ($\mathbf{2a} = \mathbf{b} + \mathbf{c}$) and five-wave ($\mathbf{3a} = \mathbf{d} + \mathbf{e}$) resonances; *b* — Normalized four- and five-wave kernels. Five-wave kernel is normalized on the amplitude factor corresponding to $\varepsilon = ak = 0.3$.

3 Numerical Approach

3.1 Approach Basics

Details of numerical approach are presented in recent papers [14–16]. Generally, we followed the same method in modelling of the effect of freak wave appearance. We tried to verify the basic features of freak wave events using the idea that the appearance of high-amplitude waves can be related to instantaneous coincidence of wave crests at quite ordinary wave field conditions. Since such coincidence is a rather rare event, we started with specific extreme-wave forms and solved time reversal problem observing the time behaviour of wave forms and wave spectra features. Time series, which are usually available as an input of numerical models, do not provide information on the spatial structure of water wave field and have to be supplemented by a priori conjectures. As the first point, we used a common concept of a wind wave field with narrow angular distribution and spectral amplitudes monotonically decreasing to high frequencies. Thus, we are going to show that high-amplitude waves can appear from initial conditions with no essential scale and angular preferences. We suppose that 'abnormal' appearance of oblique wave components from the 'stereotype' wave field is possible due to five-wave resonances at reasonable time scales.

The second hypothesis is based on our previous knowledge of nonlinear water wave dynamics. It has been shown [14, 16] that sporadic amplification of water wave components due to five-wave resonances is accompanied by the strong selection of water wave modes, so that in a generic case, only a small number of oblique components can grow due to five-wave resonances.

Thus, our method of numerical study can be summarized as follows:

- An initial wave field state is represented by a number of master modes in special canonical variables;
  - Amplitude distribution of master modes is taken as in conventional models of wind wave field (generally we use the simplest temporal Pierson-Moskowitz approximation for wave spectra);
  - Master modes are distributed mainly in along-wind direction. A small number of oblique wave components is placed in the vicinity of five-wave resonant curves in wavevector space;
  - Wave phases are chosen in such a way that the resulting wave profile has a characteristic pronounced amplitude;
- Calculations for initial conditions with different distributions of master modes in wavevector space but the same temporal spectra are performed in order to estimate characteristic time scales of transformation of wave forms and wave spectra.

In fact, in the study we meet a number of accompanying problems. While all these problems are solved in the simplest way, their correct resolution is necessary for the further progress.

3.2 Example. 'Draupner' Wave

As a numerical example, consider the case of the 'Draupner' wave [19]. The time series used in this example was provided by Dr Haver. The example allows to demonstrate the main physical results of the modelling as well as the possible difficulties.

The initial data of our numeric experiments is the 20 minutes time series with sample frequency 2.133 Hz. This data was used to construct the instantaneous Fourier amplitudes and then normal variables for the Hamiltonian equations. The normal variables can be related to temporal Fourier transform with the help of the dispersion relation. The problem of such a relation is that, first, it is a function of wavevector, second, it is amplitude-dependent for nonlinear waves. At present, we have no way to resolve correctly the arbitrariness of relation of frequency spectra to its spatial counterpart, and the simplest solution of the problem is accepted. In fig.2*a*, instantaneous amplitudes and phases of temporal Fourier transform and the profile of 'Draupner' wave are shown. The Fourier amplitudes have pronounced peaks at specific frequencies. Taking the frequency of the highest peak f_0 as a characteristic value, we see that almost all these peaks are in the range $f_0 \div 2f_0$. The next highest in magnitude peak is at $3/2f_0$, corresponding exactly to the symmetric five-wave resonance, whose specific role in wave dynamics has been discussed in recent papers [13, 14, 16].

The role of this resonance is the subject of the numeric experiment. The principal part of the initial wave field was modelled by a uni-directional distribution close to the 'reference' Pierson-Moskovitz spectrum (solid curve in fig. 1*a*). The excess of temporal Fourier amplitudes relative to the 'reference' wave field has been distributed in wavevector space close to the four-wave resonance curve in the range $f_0 \div 3/2f_0$, and close to the five-wave resonant curve for the range $3/2f_0 \div 2f_0$. Small noise of arbitrary distributed harmonics was added in the rest of the frequency range. A number of numerical experiments were performed with different distributions of the 'excess part' of such a wave field. The typical results of time evolution in terms of time series are presented in fig. 3 for the rather short time period of about 8 periods of dominant wave component. These results can be considered as unexpected. In the figure, the peak at $3/2f_0$ has disappeared! In fact the result is trivial: two spatial harmonics — the along-wind one and the oblique one from five-wave resonance contribute to the same linear frequencies but in different 'nonlinear' ones (with nonlinear corrections taken into account). This leads to the phase shift and effective interference between these two harmonics. Such a mixing of phases of different harmonics is a mechanism of disappearance of the freak wave which is a sum of harmonics with certain phases. As we see, this mechanism is nonlinear, due to the amplitude dependence of harmonics, but is not related to the energy exchange between harmonics.

The energy transfer in the problem under study has longer timescales. As we found in the example, this scale does not depend essentially on initial conditions and can be easily estimated in general case. In our experiments the oblique wave harmonics appear from (or 'disappear', in our time reversal approach) rather low 'noise' amplitude for about 1000 dominant wave periods.

4 Discussion

The study is the first attempt of the application of the novel numerical approach based on weakly nonlinear Hamiltonian formulation of water wave equations. This approach is very powerful because of the practical absence of limitations on time and space of the analysis. It has evident advantages for the modelling of different initial conditions as well, because the most expensive procedure is the solution of ODE systems. The possibility of effective qualitative analysis of the problem is extremely valuable in the approach. Thus, the approach represents a convenient tool to predict the results of a detailed study without large numerical and analytical difficulties.

The role of nonlinearity in the problem discussed is twofold. First, it is responsible for the transformation of temporal spectra. While in wavevector space the amplitudes of harmonics evolve slowly, in frequency space they can interfere effectively. Thus, frequency spectra appears to be inconvenient for the prediction of freak wave events.

Nonlinear energy exchange can provide the appearance of oblique waves of rather high amplitudes that can interfere effectively and stimulate sporadic high-amplitude events, creating conditions for their emergence. As we have seen, knowledge of spatial structure of wind wave field is of principal importance to estimate these conditions and the possibility of these events.

The work was supported by grants INTAS-97-575 and Russian Foundation for Basic Research N98-05-64714. Authors are grateful to the participants of Rogue 2000 workshop for fruitful discussion of the problem. Authors are especially grateful to Dr Sverre Haver (Statoil) for kindly providing the experimental data.

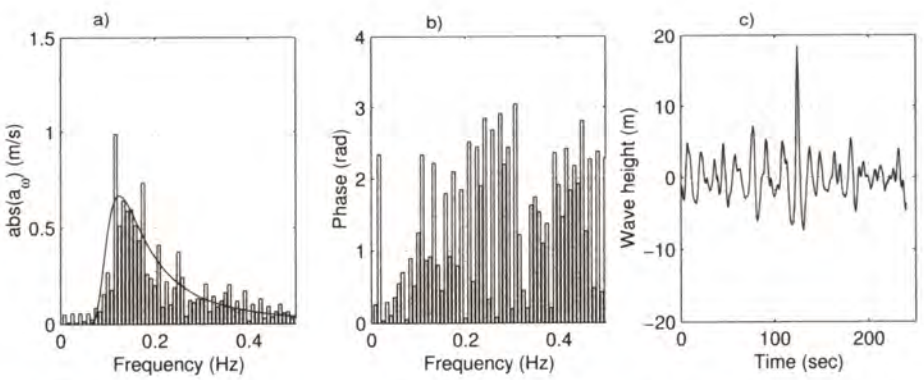

Fig. 2. Temporal characteristics of the 'Draupner' wave as a base for numeric modelling. *a,b* — Instantaneous Fourier amplitudes for 4 minutes period close to the highest wave amplitude. 'Reference' amplitude distribution corresponding to Pierson-Moskowitz spectra at wind speed approximately 10 m/s is shown, *c* — 4 minutes of time series.

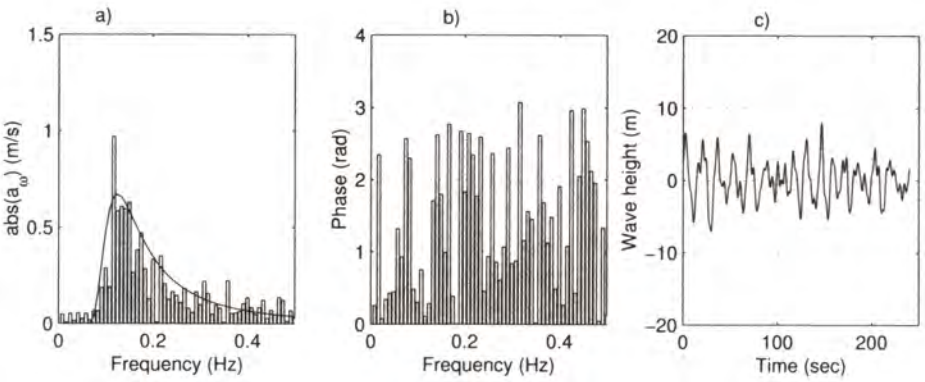

Fig. 3. Same as in previous figure at $t = 8/f_0$

References

1. Phillips, O.M.: Extreme waves and Breaking Wavelets, Theoretical and Applied Mechanics, ed. S.R.Bodher, J.Singer, A.Solan & Z.Hashin. Elsevier Science Publishers (1992).
2. Haver, S.,Anderson, O.: Freak Waves: Rare Realizations of a Typical Population or Typical Realization of Rare Population? Proc.10th Int.Offshore and Polar Engineering Conference (Seattle, May 28–June 2, 2000) (2000) 123–130.
3. Lavrenov, I.: The Wave Energy Concentration at the Aguihas Current of South Africa. Natural Hazards **17** (1998) 117–127
4. White, B.S., Fornberg B.: On the Chance of Freak Waves at Sea J.Fluid Mech., **355** (1998) 113–138
5. Peregrine, H.: Freak waves. 28th WEGEMT School 'Wave Modelling Applied to the Design of Offshore and Coastal Structures', 6–10 July 1998. (1998)
6. Pelinovsky E.N., Kharif Ch.: Dispersive Compression of Wave Packages as Mechanism of Occurence of Abnormal High Waves on a Surface of Ocean. Izvestia of Russian Academy of Engineering Sciences, Series: Applied Mathematics and Informatics, **1** (2000) 50–61 (in Russian)
7. Pelinovsky E., Talipova T., Kharif C.: Nonlinear Dispersive Mechanism of the Freak Wave Formation in Shallow Water. Physica D, **147** N 1-2 (2000) 83–94
8. Kharif C., Pelinovsky E., Talipova T., Slunyaev A.: Focusing of Nonlinear Wave Group in Deep Water. JETP Letters, (2001) (accepted)
9. Dysthe, C.B.: Modelling a 'Rogue Wave' — Speculations or a Realistic Possibility Abstracts for Rogue Waves 2000 workshops, Brest (2000)
10. Zakharov, V.E.: Stability of Periodic Waves of Finite Amplitude on the Surface of a Deep Fluid. J. Appl.Mech.Tech.Phys. (USSR) **9** (1968) 86–94
11. Krasitskii, V. P.: On Reduced Hamiltonian Equations in the Nonlinear Theory of Water Surface Waves. J. Fluid Mech. **272** (1994) 1–20
12. Badulin, S.I., Shrira, V.I., Kharif, C., Ioualalen, M.: On two Approaches to the Problem of Instability of Short-Crested Water Waves. J. Fluid Mech. **303** (1995) 297–326
13. Shrira, V.I., Badulin, S.I., Kharif, C.: A Model of Water Wave 'Horse-Shoe' Patterns. J. Fluid Mech. **318** (1996) 375–404

14. Annenkov, S.Yu., Shrira, V.I.: Physical Mechanisms for Sporadic Wind Wave Horse-Shoe patterns. European Journal of Mechanics, B/Fluids **18** N3 (1999) 463–474
15. Annenkov, S.Yu., Shrira, V.I.: Sporadic Wind Wave Horse-Shoe Patterns. Report 99-001. Institute for Nonlinear Science, National University of Ireland, University College, Cork (1999) 43 pp.
16. Annenkov, S.Yu., Shrira, V.I.: Numerical Modelling of Water Waves Evolution Based on the Zakharov Equation. J. Fluid Mech. (2001) (submitted)
17. Stiassnie, M., Kroszynski, U.I.: Long-time Evolution of an Unstable Water-Wave Train. J. Fluid Mech. **116** (1982) 207–225
18. Stiassnie, M., Shemer, L.: Energy Computations for Evolution of Class I and II nstabilities of Stokes Waves. J. Fluid Mech. **174** (1987) 299–312
19. Haver, S.: Some Evidence of the Existence of So-Called Freak Waves Abstracts for Rogue Waves 2000 Workshops, Brest (2000)

Modulational Interactions of Broad-Band Gravity Waves Observed during North Sea Storms

Brian Linfoot, Julian Wolfram, and Paul Stansell

Heriot-Watt University, Edinburgh EH14 4AS, UK
b.t.linfoot@hw.ac.uk

Abstract. The conjecture explored in this paper is that the interference of 'latent' wave groups evolving in different directions at differing group celerities might provide a (partial) explanation for 'freak' waves and correlated large 'riding' waves, with associated phase loops, observed in extreme seas. The S-transform, a form of wavelet transform, provides a time-frequency matrix directly related to the time evolution of the conventional water surface power spectral density. The interpretation of this matrix is illustrated by applying the S-transform to single point and three probe wave array data, obtained at the North Alwyn platform in the North Sea. These time-frequency contour plots of typical wave packet energy may be interpreted as representing both wave packet evolution and interaction. In addition the decomposition of single-point wave records into 'latent' wave groups is described using the inverse S-transform.

1 Introduction

A series of papers describing experimental measurements of the evolution of wave groups by Stansberg (e.g. [1]) demonstrate the hypothesis that freak waves result from the natural process of evolution of wave groups in accordance with the predictions of the nonlinear Schrödinger equation (NLS). Similar experiments were undertaken by Clauss and Kühnlein [2] in order to determine the response characteristics of scale model offshore structures. Their experiments give a valuable insight into possible mechanisms of freak wave causation in the laboratory which can also be studied by numerical simulations based on the NLS equation.

Papers by Mollo-Christenson and coworkers [3, 4] argued that similar evolutionary behaviour of the envelope modulations also occurs in deep water storm waves. Recently Magnusson *et al.* [5] have provided further observational support using measurements in the North Sea. They have used both the linear and nonlinear evolution equations to obtain estimates of the effect of local wave packet evolution on wave height statistics.

Storm waves observed by Linfoot *et al.* [6] at the North Alwyn platform in the North Sea [7] exhibit the familiar modulational characteristics and wave group statistics expected from narrow band theory (Longuet-Higgins [8]). However,

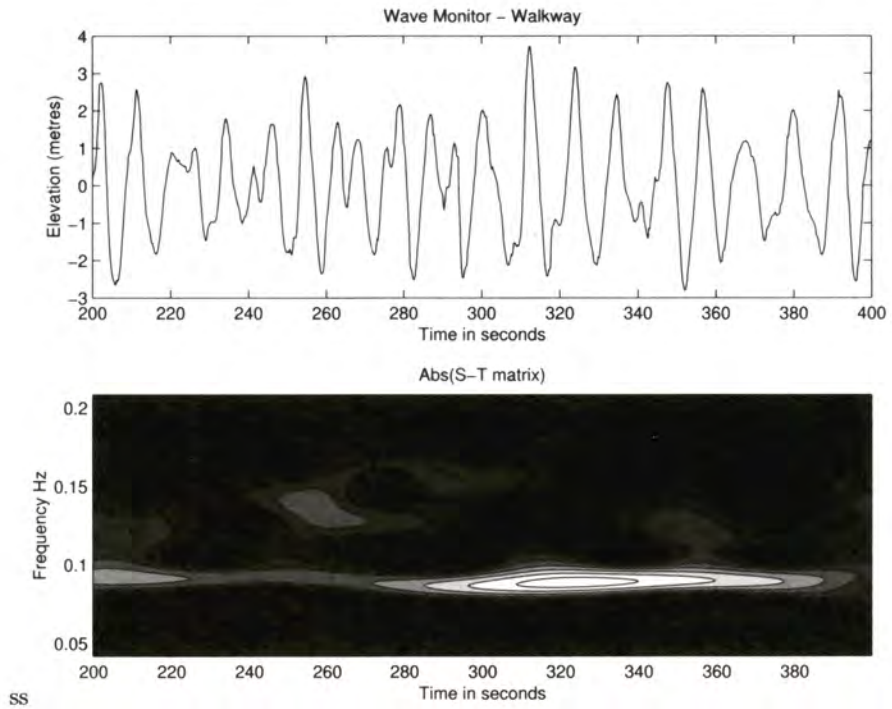

Fig. 1. : Wave record during storm: (a - upper) large amplitude 'riding' waves 240 to 300 seconds (b - lower) time -frequency plot showing main group modulation at 0.9 hz and a secondary group splitting at 0.13Hz to 0.15 Hz at 240 to 300 seconds [See also Appendix CP]

close inspection of group profiles, sampled at high-rate (5Hz), shows instances of carrier frequencies which are noticeably different from their neighbours while others show locally correlated 'riding' waves (Figure 1a) which appear as secondary loops in the instantaneous phase-time plot. These features are not explained by narrow-band processes.

It is our contention that these features provide observational support for arguments originally made by Mollo-Christensen and cited recently by Donelan *et al.*[9] that the sea surface during broad-banded storms may be represented by the interaction of independent evolving wave packets which may be travelling in different directions at different wave group celerities- even in circumstances when the directional spectrum is unimodal.

2 Techniques for Time-Frequency Analysis and Time Series Decomposition

In the last few decades a range of techniques have been developed to study the frequency distribution of time series over short time spans (e.g. [10]) including

the recent development of the S-transform due to Stockwell [11]. The Stockwell transform output is a complex matrix which is directly related to the amplitude and phase spectra of the fourier transform. A time-frequency energy distribution is obtained directly from the square of the absolute values of the complex S-matrix while time averaging the S- matrix gives the unwindowed complex fourier spectrum. This property allows the S-matrix to be inverted to recover the original signal: an adaptive filter based on this has been developed which constructs 'latent' time series from the dominant ridges in the time-frequency contour plot (Fig.2 (b)) effectively decomposing the original time series into a small number of components and a residual as shown in Fig. 2(c). The large wave at 350 seconds and the distortions in the surface profile at 330 seconds and 360 to 380 seconds are shown to be a possible consequence of the interaction of two wave packets. The residual component at the peak (350 seconds)is the non-linear contribution to the second higher-frequency wave packet.

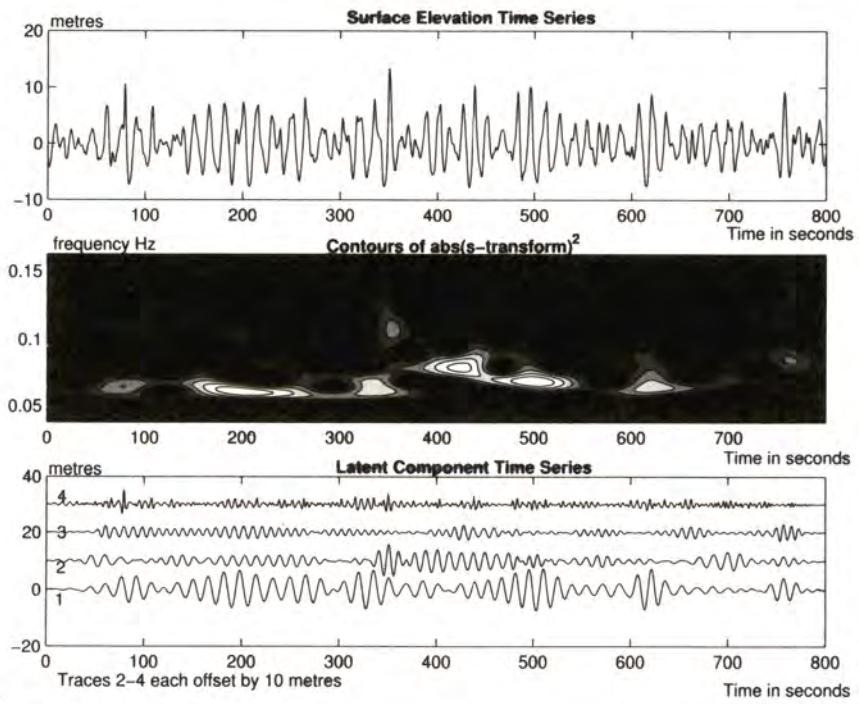

Fig. 2. 800 seconds of wave data from North Sea storm (1 Jan 1995): (a -upper) water surface elevation time series (b - middle) Time-frequency contour plot derived from S-transform matrix: light patches indicate high energy concentrations (c - lower) component time series produced by adaptive inversion of S-transform matrix with a 5% Hanning taper applied to ends of time series in plots (b) and (c) [See also Appendix CP]

A number of other time-series decomposition algorithms published recently have been tested to provide representations of the 'latent' wave groups. These include the time-varying autocorrelation method (TVAR) of Prado and West [12] and the Empirical Mode Decomposition (EMD) of Huang *et al.*[13]. We have found the S-transform method to be successful in effectively separating 'riding' wave components, as shown above, while preliminary exploration of the same time series using the TVAR method shows promising agreement. The corresponding results from *our* coding of the EMD algorithm show discrepancies and physical inconsistences which require further investigation.

3 Simultaneous S-T Matrix Plots Derived from Wave Probe Array

The array of three wave altimeters at North Alwyn has allowed us to produce synchronous time-frequency plots from each time series. Representative time series are shown in Fig.3 while the corresponding time-frequency contour plots are in Fig.4, with light tones indicating energy peaks.

Figures 3 and 4 show similar large energy packets at around 100-150 seconds and at 1080-1180 seconds at each probe. At 670, 780 and 850 seconds the T-F plots in Fig.4 (upper) show packet interactions which are almost absent in the lower plot: we interpret this as clear evidence that the interacting packets are moving independently with no significant higher frequency component appearing on the lower plot. In Fig.4 (lower) two, or possibly three, packets appear to be interacting at 500 seconds while in the upper plot the two component packets are not quite synchronous. We are currently investigating these features to establish the directions of the components and comparing the results with data obtained from experiments in a short-crested wave basin.

4 Conclusions

We conclude that

1. the S-transform provides a useful analysis tool for constructing time-frequency plots of wave packet evolution and interaction; and,
2. mixing and evolution of independently propagating wave groups may contribute to the explanation of 'rogue' waves; and,
3. locally correlated 'riding' waves may also be explained by group interactions.

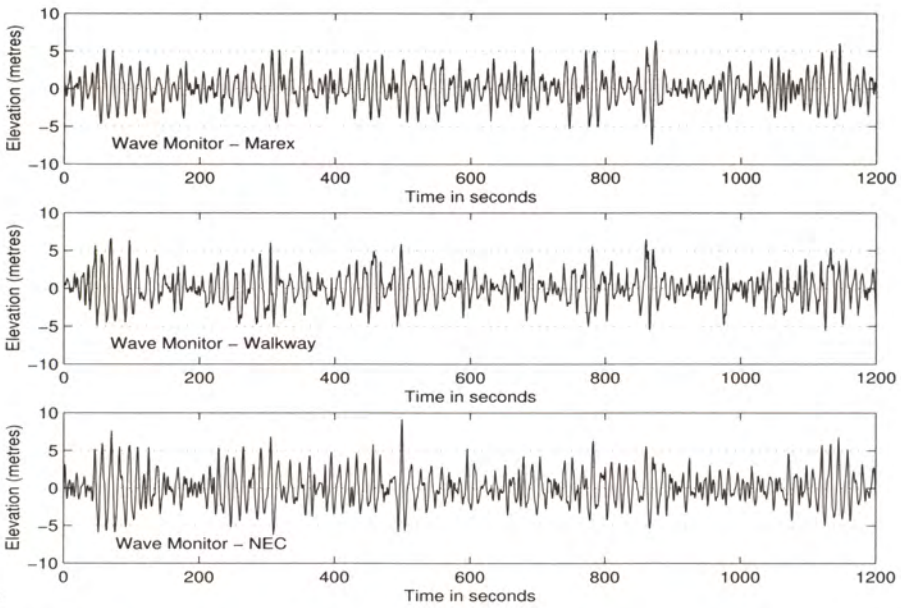

SS

Fig. 3. : Wave synchronous records from three wave altimeters

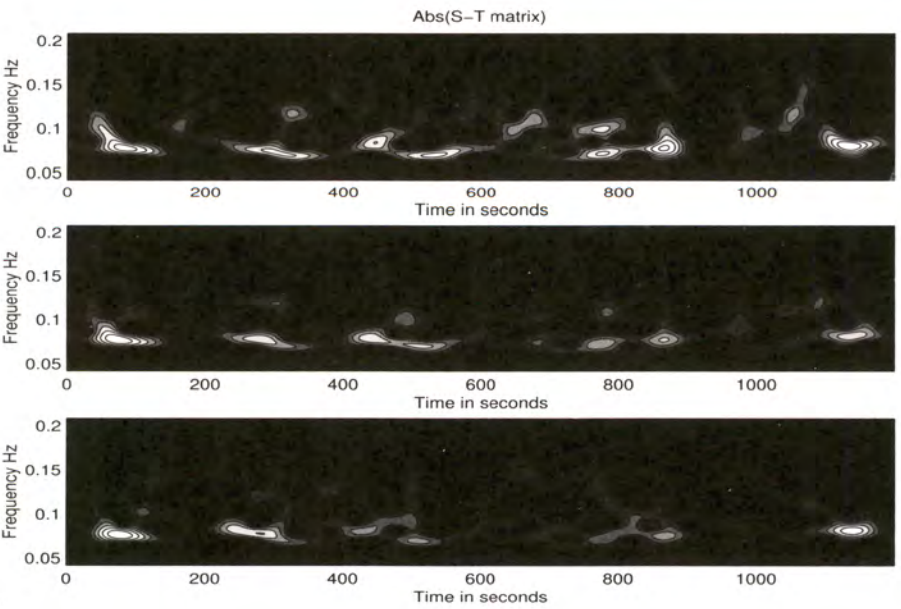

SS

Fig. 4. : Time-frequency contour plots of abs(S-matrix) corresponding to the wave records in Fig.3 [See also Appendix CP]

References

1. Stansberg, C.T.: Nonlinear extreme wave evolution in random wave groups. Proc. 10^{th} I. Offshore and Polar Eng. Conf., ISOPE, Vol III (2000) 1-8
2. Clauss, G.F., Kühnlein, W.L.: Simulation of design storm conditions with tailored wave groups. Proc. 7^{th} I. Offshore and Polar Eng. Conf., ISOPE, Vol III (1997) 228-237.
3. Mollo-Christensen, E., Ramamonjiarisoa, A.: Subharmonic transitions and group formation in a wind wave field. J. of Geophysical Research, **87**(C8)(1982) 5699-5717.
4. Chereskin, T.K., Mollo-Christensen, E.: Modulational development of nonlinear gravity-wave groups. J.Fluid Mech. **151** (1985) 337-365.
5. Magnusson, A.K. Donelan, M.A., Drennan, W.M.: On estimating extremes in an evolving wave field. Coastal Engineering, **36** (1999) 147-163
6. Linfoot, B.T., Stansell, P., Wolfram, J.: On the Characteristics of Storm Waves. Proc. 10^{th} I. Offshore and Polar Eng. Conf., ISOPE, Vol III (2000)74-77.
7. Wolfram, J., Feld, G., Allen, J.: A new approach to estimating extreme environmental loading using joint probabilities. In: Behaviour of Offshore Structures. BOSS'94,(ed: C. Chryssostomidis) Pergamon,Vol 2 (1994) 701-713
8. Longuet-Higgins, M.S.: On the statistical distribution of the heights of sea waves. J. Marine Research,**11** (1952) 245-266
9. Donelan, M.A., Drennan,W.M., Magnusson, A.K.: Nonstationary analysis of the directional properties of propagating waves. J. Physical Oceanography, **26**(9)(1996) 1901-1914
10. Auger,F., Flandrin, P. Gonalvs, Lemoine, O.: Time -frequency toolbox for use with Matlab. Centre National de la Recherche Scientifique, France, (1997)
11. Stockwell , R.G., Mansinha, L., Lowe, R.P.: Localization of the Complex Spectrum: The S Transform. IEEE, T. Sig. Pro., **44**(1996) 998-1001
12. Prado,R., West,M.: Exploratory modelling of multiple non-stationary time series: Latent process structure and decompositions. In: Modelling Longitudinal and Spatially Correlated Data, (ed: T. Gregoire), Springer-Verlag (1997)
13. Huang, N.E., *et al.*: The empirical mode decomposition and the Hilbert spectrum for nonlinear and non-stationary time series analysis. Proc. R. Soc. Lond. A **454,**(1998) 903-995

Geometrical and Kinematic Properties of Breaking Waves in the Framework of a Stationary Flow Approximation

Alastair D. Jenkins

DNMI Marine Forecasting Centre, Allégaten 70, 5007 Bergen, Norway,
Alastair.Jenkins@dnmi.no, http://www.dnmi.no/

Abstract. In view of the potentially devastating consequences of the impact of rogue waves, it is necessary to make predictions of the geometry and kinematics of such severe wave events, as well as calculating their occurrence probability.

In spite of the fact that steep and breaking waves come in many different forms: spilling or plunging breakers, for example, it appears that very many of these wave forms can be related to a particular potential flow geometry which is stationary in a frame of reference moving with the wave crest. This flow field has a geometrical scale which has a fixed relation to the amount of fluid which is expelled forwards in a jet emanating from the wave crest.

Comparison with relevant laboratory investigations indicate that some aspects of the observed breaker geometry, such as the orientation of the loop structure under the breaking crest, are correctly predicted by the quasi-stationary theory. The length and velocity scales, however, are highly variable, but it may be possible to make quantitative predictions by analogy with already-established relationships for the characterization of waves breaking on beaches. Waves which are initially steeper tend to generate smaller-scale 'spilling' breaker structures.

1 Introduction—What Happens during a Rogue Wave Event?

The extreme loading on structures caused by the impact of breaking waves has long been known, and has recently been brought into focus again as a result of the occurrence of unexpectedly high or steep waves around both fixed and floating offshore facilities. The probability of occurrence of such waves can be determined by statistical analysis [4, 12] and long-term simulation studies [15]. However, In view of the potentially devastating consequences of severe wave impact, it is also necessary to know the wave form and kinematics in order to predict their effects on vessels, floating and fixed structures. It is also very likely that such rogue waves will have breaking crests, so a quantitative understanding of the dynamics of breaking is necessary.

2 Quasi-Stationary Flow Approximation for Breaking Crest

Wave breaking is a complicated nonlinear time-dependent process, and has been investigated in numerous studies, involving field and laboratory experiments, and analytical and numerical modelling studies [2, 13, 14, 16, 18]. Although there are many different possible forms of breaking wave which can occur under different circumstances, there is one 'classical' form (the plunging breaker) which is very common, in which a jet projects forward from the wave crest and descends in a parabolic trajectory down to the forward face of the wave.

The 'plunging' breaker geometry can appear at many different length scales, but with essentially the same shape, and it can be argued that the 'spilling' breakers which are common in the open ocean and on gently-shelving shorelines are in fact a short-lengthscale form of plunging breaker.

A steady-state irrotational flow which satisfies the necessary boundary conditions and which tends to 120° Stokes corner flow at large distances from the crest [5, 6] may be a useful approximation, to estimate impact velocities, for example. In this flow:

- The length scale depends on the flux of fluid through the jet: the length of the loop under the jet is $\approx 8g^{-\frac{1}{3}}\Psi^{\frac{2}{3}}$
- The acceleration is scale-independent, with a maximum of $\approx 5.4g$
- The velocity scale $V = (g\Psi)^{\frac{1}{3}}$; the relative speed of the fluid in the jet and the main body of water at the 'impact point' is $\approx 6.9V$

This quasi-stationary flow is illustrated in the upper part of Fig. 1, and the velocity of the flow with respect to the stagnation point at the crest is shown in Fig. 2.

Comparison with laboratory measurements Figure 3 shows the dimensions of the width (minor axis) of the interior of the loop under the breaking crest jet, during breaking events in two laboratory investigations: those of Bonmarin [1] and of Tomita and Sawada [14]. During the later stages of the breaking events (but before the breaker loop collapses) the spatial dimensions of the breaking structure are fairly constant, and the loop orientation is reasonably close to that in the quasi-stationary flow ($\approx 51°$ from the horizontal). The behaviour is more complex and variable in the initial stages of breaking.

3 Plunging or Spilling Breakers?—Relation to the Rest of the Flow Field

The quasi-stationary flow approximation is only useful if we can determine the length scale which is applicable during a typical 'rogue wave' event. This is not straightforward, as we may need to 'patch' the stationary flow on top of a complicated, time-dependent flow. However, we can perhaps find some simple rules by reviewing the criteria for when plunging and spilling breakers are observed in

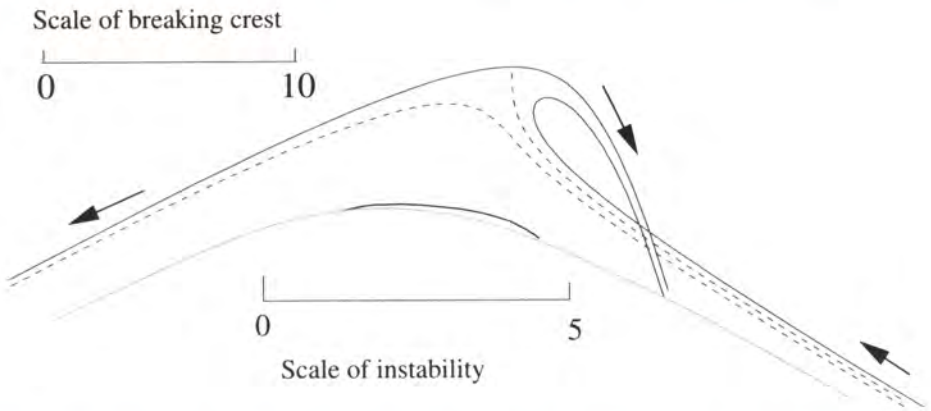

Fig. 1. The upper graph shows the quasi-stationary breaking-crest flow field of Jenkins [5]. The lower graph shows the superharmonic instability which grows on the crest of an 'almost-highest' wave crest according to Jillians, Longuet-Higgins and Cleaver [7–9]. The jet emanating from the crest of the quasi-stationary breaker may be thought of as a fully-developed form of this instability. The scale units are as in the papers cited.

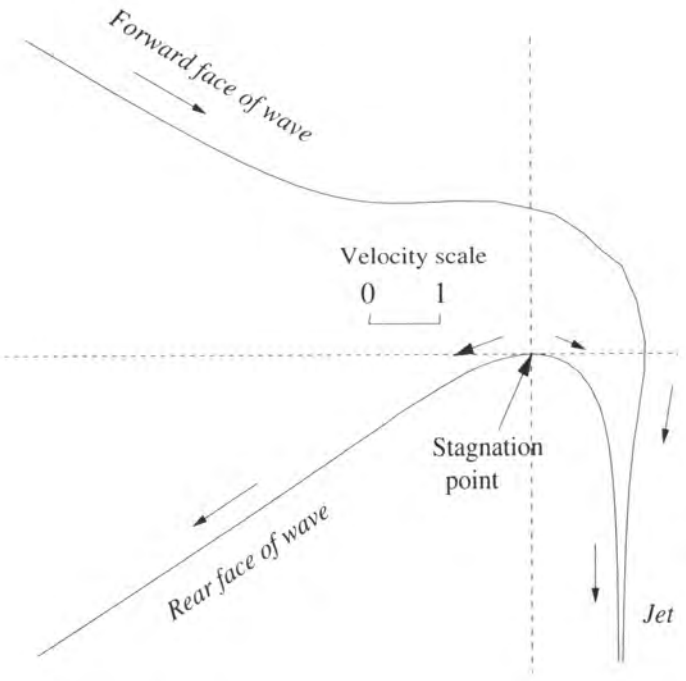

Fig. 2. A hodograph of the velocity of the fluid in upper graph of Fig. 1.

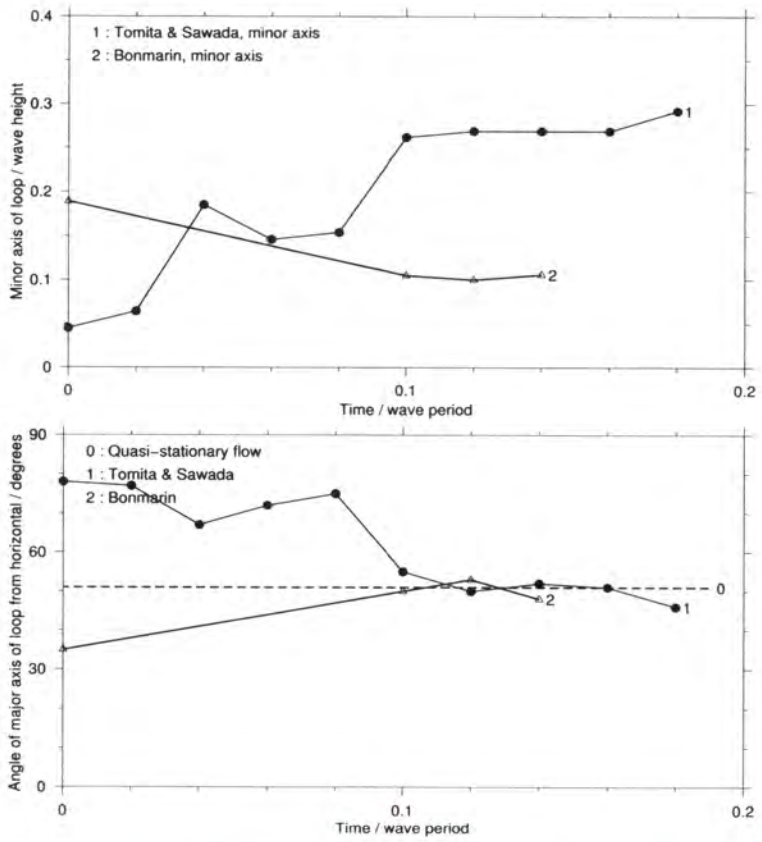

Fig. 3. Analysis of two laboratory investigations: those of Bonmarin [1] and of Tomita and Sawada [14]. The upper curve shows the width (minor axis) of the interior of the loop under the breaker jet, and the lower curve shows the orientation of the major axis of the loop with respect to the horizontal plane.

the field. Given the paucity of systematic observations (and the rarity of plunging breakers) in the open sea, it is necessary to refer to observations of breakers in coastal areas. The rule seems to be:

- Spilling breakers are observed on gently-shelving shorelines
- Plunging breakers are observed when the shoreline shelves more steeply, particularly when large-amplitude long-wavelength swell waves propagate onto the coast from offshore.

On further investigation ([17] Fig. 4, after [3]), it actually appears that:

- the transition from spilling to plunging breakers, and also the transition from plunging to the more violent 'surging' breakers, is most strongly determined by the ratio $H_b/H_0^{'}$, where $H_0^{'}$ is the wave height offshore, before it has been

affected by depth-dependent refraction, and H_b is the height of the wave when it breaks. The dependence on incident wave steepness H_0'/gT^2, where T is the wave period, is considerably weaker. The transition from spilling to plunging is at $H_b/H_0' \approx 1.2$

Hence it may be the case that the geometrical scale of the breaker is more-or-less proportional to $H_b - H_0'$, the amount that bottom refraction has increased the wave height above its original value. This may also be the case where the wave height has been increased by refraction by variable currents, and by focusing. This is confirmed by the fact that e.g. focusing can be used to generate plunging breakers in the laboratory.

A general explanation of how we get a breaker length scale which is proportional to the increase in wave height before breaking is probably that the initial waves have smooth crests if they are not steep, but in general have sharper crests, with a smaller radius of curvature, if they are steeper and thus initially closer to breaking. An idealized example of this would be the almost-highest periodic waves of Longuet-Higgins and Fox [11]. The superharmonic instability mechanism of Jillians, Longuet-Higgins, Cleaver and Fox [7, 10], depicted in Fig. 1, will generate a more rapidly-growing instability of a smaller length scale, in the case where the crest radius of curvature is smaller, and thus will generate a breaking structure with a smaller scale in this case.

4 Conclusion

The quasi-stationary breaking crest flow field described in this paper may be useful in predicting the geometry and kinematics of breaking crests in rogue wave events, provided that the length scale of the flow field can be predicted. Certain aspects of the geometry, such as the orientation of the breaking-crest loop, are approximated reasonably well. The length scale, and thus the velocity scale, are more variable and need to be determined by other means. There is empirical evidence, from the behaviour of breakers on shorelines, that the relevant length scale is proportional to the increase in wave height above that of the surrounding 'undisturbed' waves. This height increase may be due to bottom refraction, refraction by currents, or wave focusing, and an explanation for the relation can be that the length scale of a superharmonic instability at the wave crest is smaller for waves which are steeper and initially closer to breaking.

References

1. Bonmarin, P.: Geometric properties of deep-water breaking waves. J. Fluid Mech. **209** (1989) 405–433
2. D. G. Dommermuth, D. G., D. K. P. Yue, Lin, W. M., Rapp, R. J., Chan, E. S., Melville, W. K.: Deep-water plunging breakers: A comparison between potential theory and experiments. J. Fluid Mech. **189** (1988) 423–442
3. Goda, Y.: A synthesis of breaker indices. Trans. J. Soc. Civ. Engrs **2** (part 2) (1970)

4. Haver, S., Andersen, O. J.: Freak waves: Rare realization of a typical population or typical realization of a rare population? Proc. ISOPE 2000, Seattle, WA, USA, May 28—June 2 (2000), volume 3, pp. 123–130
5. Jenkins, A. D.: A stationary potential-flow approximation for a breaking-wave crest. J. Fluid Mech. **280** (1994) 335–347
6. Jenkins, A. D.: A quasi-stationary irrotational solution for a breaking wave crest. In M. A. Donelan, W. H. Hui, and W. J. Plant, editors, The Air–Sea Interface. Proceedings of the Symposium on the Air–Sea Interface, Radio and Acoustic Sensing, Turbulence and Wave Dynamics, Marseilles, France, June 24–30, 1993, pages 247–252, Miami, Florida, U.S.A. The Rosenstiel School of Marine and Atmospheric Sciences, University of Miami (1996)
7. Jillians, W. J.: The superharmonic instability of Stokes waves in deep water. J. Fluid Mech. **204** (1989) 563–579
8. Longuet-Higgins, M. S.: The crest instability of steep gravity waves, or how do short waves break? In M. A. Donelan, W. H. Hui, and W. J. Plant, editors, The Air–Sea Interface. Proceedings of the Symposium on the Air–Sea Interface, Radio and Acoustic Sensing, Turbulence and Wave Dynamics, Marseilles, France, June 24–30, 1993, pages 237–246, Miami, Florida, U.S.A. The Rosenstiel School of Marine and Atmospheric Sciences, University of Miami (1996)
9. Longuet-Higgins, M. S., Cleaver, R. P.: Crest instabilities of gravity waves. Part 1. The almost-highest wave. J. Fluid Mech. **258** (1994) 115–129
10. Longuet-Higgins, M. S., Cleaver, R. P., Fox, M. J. H.: Crest instabilities of gravity waves. Part 2. Matching and asymptotic analysis. J. Fluid Mech. **259** (1994) 333–344
11. Longuet-Higgins, M. S., Fox, M. J. H.: Theory of the almost-highest wave. Part 2. Matching and analytic extension. J. Fluid Mech. **85** (1978) 769–786
12. Magnusson, A. K., Donelan, M. A., Drennan, W. M.: On estimating extremes in an evolving wave field. Coastal Engng **36** (1999) 147–163
13. Rapp, R. J., Melville, W. K.: Laboratory measurements of deep-water breaking waves. Phil. Trans. R. Soc. Lond. **A331** (1990) 735–800
14. Tomita, H., Sawada, H.: On the dynamical properties of plunging breakers in deep water. In M. A. Donelan, W. H. Hui, and W. J. Plant, editors, The Air–Sea Interface. Proceedings of the Symposium on the Air–Sea Interface, Radio and Acoustic Sensing, Turbulence and Wave Dynamics, Marseilles, France, June 24–30, 1993, pages 269–276, Miami, Florida, U.S.A. The Rosenstiel School of Marine and Atmospheric Sciences, University of Miami (1996)
15. Trulsen, K., Dysthe, K. B.: A modified nonlinear Schrödinger equation for broader bandwidth gravity waves on deep water. Wave Motion, **24** (1996) 281–289
16. Tulin, M. P., Yao, Y., Wang, P.: The simulation of the deformation and breaking of ocean waves in wave groups. In Proc. 7th Intl Conf. on Behaviour of Offshore Structures (BOSS'94), MIT (1994)
17. US Army Corps of Engineers: Shore Protection Manual. US Army Corps of Engineers, Washington D.C., 4th edition (1984)
18. Vinje, T., Brevig, P.: Breaking waves on finite water depths: A numerical study. Technical report, Ship Research Institute of Norway, Report R-111.81 (1981).

Session 5

Numerical Modelling of Rogue Waves

Effects of High-Order Nonlinear Wave-Wave Interactions on Gravity Waves

Nobuhito Mori[1] and Takashi Yasuda[2]

[1] Department of Hydraulics, Abiko Research Laboratory,
Central Research Institute of Electric Power Industry(CRIEPI),
1646 Abiko, Abiko, Chiba 2701194, JAPAN,
mori@criepi.denken.or.jp.
[2] Graduate Course of Environ. and Renew. Energy System,
Gifu University, Yanagido 1-1, Gifu, JAPAN,
coyasuda@cc.gifu-u.ac.jp.

Abstract. Numerical simulations of gravity waves with high-order nonlinearities in two and three dimensional domains are performed by using a pseudo spectral method. High-order nonlinearities higher than third-order excite apparently chaotic evolutions of the Fourier energy in deep-water random waves. The high-order nonlinearities increase kurtosis, wave height distribution and $H_{max}/H_{1/3}$ in deep-water and decrease these wave statistics in shallow water. They, moreover, can generate a single extreme high wave with an outstanding crest height in deep-water. The high-order nonlinearities more than third-order can be regarded as one of the reasons that may cause a freak wave in deep-water.

1 Introduction

Since the discovery of the Benjamin-Feir instability in the Stokes wave train, much attention has been paid to the behavior of nonlinear deep-water waves. In the last two decades, the instability of the gravity waves has been studied by many researchers by using nonlinear Schrödinger type equations[1][2][3], mode-coupling equations[4], pseudo-spectral methods[5] and experiments[6]. However, most of them are concentrated on amplitude modulations of the Stokes wave for the purpose of scientific interest. The rest of studies are related to energy transfer of random waves for the purpose of prediction of ocean wave spectra[7][8]. Little is known about the high-order resonant interaction effects on random wave statistics in deep and shallow-water.

Alber mathematically demonstrated that randomness of waves leads wave trains to stabilize[9] and others stated that the instability is confined within an initially unstable range and becomes weaker when the spectral bandwidth becomes broader[10]. However, it is not clear how stability and instability of the gravity waves are connected between Stokes waves and random waves having broad band spectra. It is found that relatively broad banded spectrum waves can transfer the Fourier mode energy in deep-water[11][12].

On the other hand, freak waves recently became an important topic and are sometimes featured by a single and steep crest giving severe damage to offshore structures and ships. There is no doubt on the occurrence of freak waves from many reports[13] and the mechanisms and detailed statistical properties of the freak wave are getting clearer[14][15]. The state of the art on freak waves was summarized at a *NATO Advanced Research Workshop* in the last decade. It was concluded that both nonlinearity and directionality effects are primary possible causes of the freak waves[16]. Experimental studies demonstrate that the freak-like waves can be generated in a two-dimensional wave flume without current, refraction and diffraction[17]. Numerical studies also indicate that freak waves having a single and steep crest can be generated by third-order nonlinear interaction in deep-water[11]. It is, however, not clear what statistical properties, occurrence probabilities and effects of spectrum shape and water depth are for the instability generated freak waves.

The purpose of this study is to investigate influence of spectrum bandwidth and water depth on the stability of random waves, solving highly nonlinear equations of a potential flow by a pseudo spectrum method. On the basis of the numerical results, the importance of the high-order nonlinearities is evaluated in comparison with the second-order solution. Moreover, the stability of the Stokes wave in the three dimensional domain is demonstrated.

2 Numerical Method

2.1 Governing Equations

Two types of nonlinear equations for gravity waves are numerically solved in this study. One is high-order nonlinear equations which can completely take into consideration nonlinear interactions at higher than third-order[18] and another one is the second-order approximated equations which exclude nonlinear terms higher than the 3rd order[11].

A periodic boundary condition is assumed and is assigned to spatial coordinates $(\boldsymbol{x}, z)$; the origin is located at the mean water level, $\boldsymbol{x} = (x, y)$ the horizontal axis and z the upward vertical axis. Kinematic and dynamic boundary conditions on the free surface are rewritten into the evolution equations as a function of the free surface profile $\eta(\boldsymbol{x}, t)$ and of the velocity potential on the surface $\phi^s(\boldsymbol{x}, t)$=$\phi(\boldsymbol{x}, \eta, t)$[19];

$$\eta_t + \nabla_{\boldsymbol{x}}\phi^s\eta_{\boldsymbol{x}} - (1 + \nabla_{\boldsymbol{x}}\eta\cdot\nabla_{\boldsymbol{x}}\eta)\phi_z = 0, \qquad (z = \eta) \qquad (1)$$

$$\phi_t + g\eta + \frac{1}{2}\nabla_{\boldsymbol{x}}\phi^s\cdot\nabla_{\boldsymbol{x}}\phi^s - \frac{1}{2}(1 + \nabla_{\boldsymbol{x}}\eta\cdot\nabla_{\boldsymbol{x}}\eta)\phi_z^2 = 0, \qquad (z = \eta) \qquad (2)$$

where $\nabla\boldsymbol{x}$=$(\partial/\partial x, \partial/\partial y)$, the subscript t denotes the partial differentiation with t, ϕ_z is the vertical gradient of the velocity potential ϕ, t the time and g the acceleration due to the gravity. Dommermuth & Yue[18] directly solved eqs.(1) and (2) for quasi-monochromatic waves by using a pseudo-spectral method. They considered an approximation ϕ_z up to the order M in relative wave steepness. To

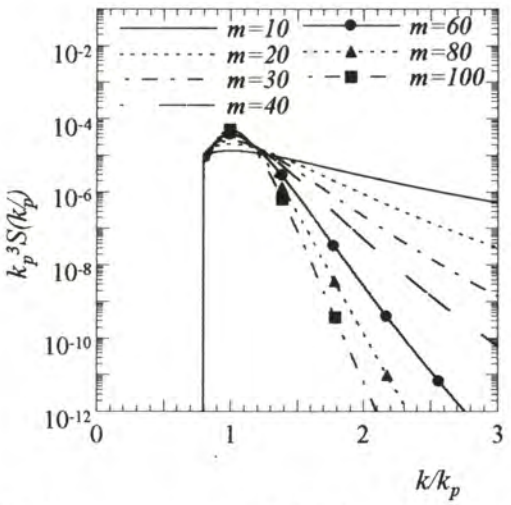

Fig. 1. Initial profiles of wavenumber spectra for 2D simulations given by Wallops type spectra as a function of spectrum bandwidth m.

skip the detail of the formulation, finally, it is formulated the vertical gradient of velocity potential on the surface as

$$\phi_z(x,\eta,t) = \sum_{l=1}^{M} \sum_{\kappa=0}^{M-l} \frac{\eta^\kappa}{\kappa!} \sum_{n=0}^{N} \phi_n^{(l)}(t) \frac{\partial^{\kappa+1}}{\partial z^{\kappa+1}} \psi_n(x,0), \tag{3}$$

where M is the order of nonlinearity.

As a result, the eqs.(1) and (2) can be solved with the approximated ϕ_z in the Fourier space by using a pseudo-spectral method. The spatial derivations of $\nabla_{\boldsymbol{x}}\phi^s$ and $\nabla\eta$ are evaluated in the Fourier space, the nonlinear products are calculated in the physical space. Therefore, this approach is useful to simulate the long time evolution of random waves having broad band spectra because it requires CPU time of the order of $N \log N$, whereas the mode-coupling equation consumes the CPU time as order of N^3. All aliasing errors generated in the nonlinear terms are deleted. The time integration of the Fourier modes of η and $\nabla_{\boldsymbol{x}}\phi^s$ is evaluated in the Fourier space with a fourth-order Runge-Kutta-Gill method. The order of nonlinearity M is fixed to four for all cases, that is the fourth-order nonlinear interactions were taken into consideration for the high-order nonlinear simulation.

The accuracy and convergence of the numerical model are verified by propagating the exact solution of a Stokes wave. The maximum error of the total energy leak and the surface profile change were 2.39×10^{-5} and 6.70×10^{-4}, respectively. It is hence expected sufficient accuracy from the high-order nonlinear wave propagation in solving eqs.(1), (2) and (3).

2.2 Initial Conditions: Random Waves in 2D

The amplitudes of initial waves are taken from a Wallops type spectrum in wavenumber space transformed through the linear dispersion relation.

$$S(k)\,dk = \frac{\alpha}{2} H_{1/3}^2 \kappa^{-\frac{m}{2}} \exp\left(-\frac{m}{4}\kappa^{-2}\right) \sqrt{\frac{4\pi^2}{k k_p \mathrm{th}kh \mathrm{th}k_p h}} \left[1 + \frac{2kh}{\mathrm{sh}2kh}\right] dk \quad (4)$$

$$\kappa = k\mathrm{th}kh / k_p \mathrm{th}k_p h \quad (5)$$

where m is the spectral bandwidth parameter, k_p the peak wavenumber of the spectrum, h the water depth and α is a constant satisfying the following relation with $H_{1/3}$:

$$H_{1/3} = 4.004\sqrt{\int_0^\infty S(k)dk}. \quad (6)$$

Eq.(4) with m=5 and $k_p h$=∞ is equivalent to the Pierson-Moskowitz spectrum and the shape of the spectrum is getting narrower as the value of m increases. The Wallops spectrum is a function of spectral bandwidth m only. The phase constants of the initial waves are assumed to follow the random phase approximation. This assumption is very important simulating random wave propagation representatively. A further important point is that if the phase is chosen factitiously(*e.g.* frequency wave focusing), it is then possible to generate a freak-like surface profile at any arbitrary time and location. However, such an approach is out of our intention.

The computations are made in a periodic space having the length of $256L_p$. Initial wave statistics are chosen with a fixed characteristic wave steepness: $k_p a$=0.14 and spectrum band widths:m=10, 20, 30, 40, 60, 80 and 100 as shown in Figure 1. Here, a is half of $H_{1/3}$, and L_p and T_p are the wave length and wave period at the spectral peak (mode), respectively. The water depth was chosen as $k_p h$=∞(deep-water), 3.0, 2.0, 1.36, 1.0. The total time integration was calculated up to t=$100T_p$.

2.3 Initial Conditions: Stokes Wave in 3D

An initial wave profile and a potential energy on the surface for three dimensional simulation were taken as the Stokes exact solution[20] for 3D simulation. The relative amplitude ka was fixed at 0.15. The amplitudes of the perturbations for the Stokes wave were taken as 1/100 of the carrier wave amplitude and the angles as θ=5, 15, 30 degree, respectively. The number of Fourier modes were taken as 64X64 in wavenumber space. The total time integration was carried out up to t=$250T_p$.

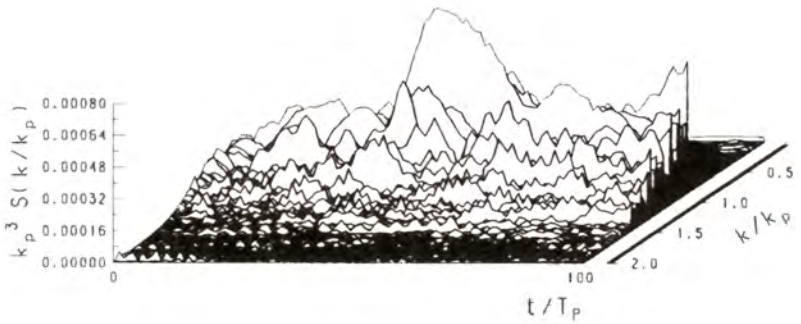

(a)High-order solution.

(b)Second-order solution.

Fig. 2. Temporal evolutions of the Fourier spectra of the simulated wave train which initially has steepness $k_{pa} = 0.14$ and spectrum bandwidth $m = 10$

3 Numerical Results and Discussions

3.1 High-order Nonlinear Effects on Random Wave Trains in 2D

Spectral Evolutions and Dispersion Relations. Figure 2 shows the time evolutions of the wavenumber spectra for m=10 and $k_p h$=∞ for both the high-order and the second-order solution. Although both simulations were started with the same initial conditions, there are significant differences in the spectrum evolution between them. It is found that the Fourier modes actively exchange their energy and the Fourier mode amplitudes are strongly modulated during the propagation process for the high-order solution, while the second-order solution seems to remain stable. These differences between the high-order solution and the second-order one in Figure 2 suggest that the Fourier modes can transfer

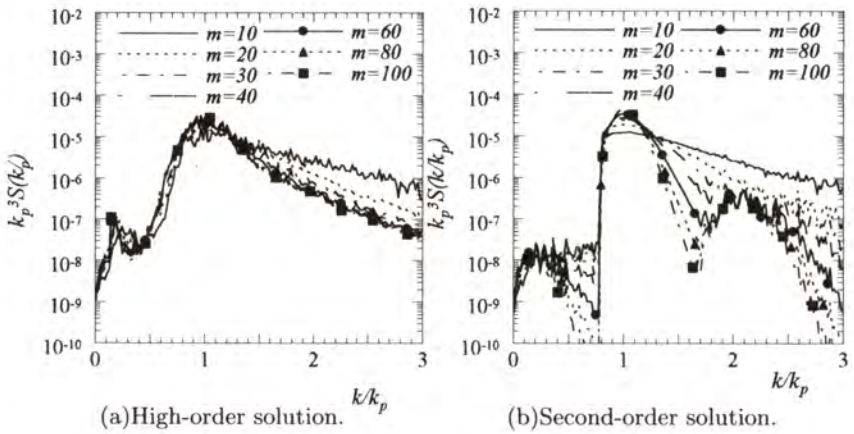

Fig. 3. The spectra time-averaged over t/T=30 to 100, and their relations to the initial bandwidth m.

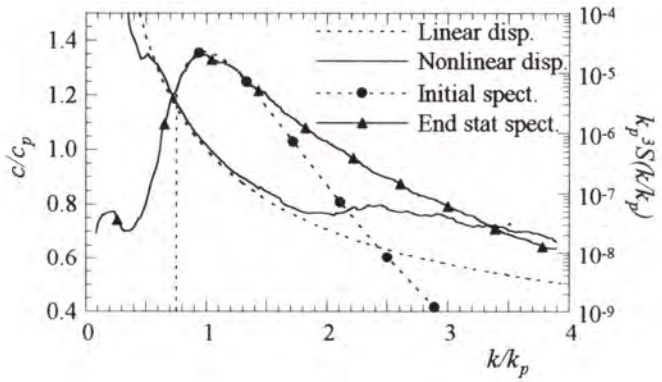

Fig. 4. Relationship between the relative phase velocity c/c_p and the relative wavenumber k/k_p for the high-order and linear solutions.

the energy due to the high-order nonlinear interactions even when the spectrum bandwidth is relatively broad. A similar relation was observed for various spectrum bandwidths in deep-water conditions. However, the intensity of energy transfer becomes weaker as the initial spectrum bandwidth becomes broader. The amplitude modulation-like behavior becomes weaker with decreasing water depth and finally disappears if the characteristic water depth $k_p h$ is shallower than 1.36.

Figure 3 shows the time averaged wavenumber spectra for both the high-order and the second-order solution in deep-water conditions. The second-order solution shows a secondary peak in the higher harmonics when the initial spectrum bandwidth is narrow. On the contrary, there is no significant difference amongst

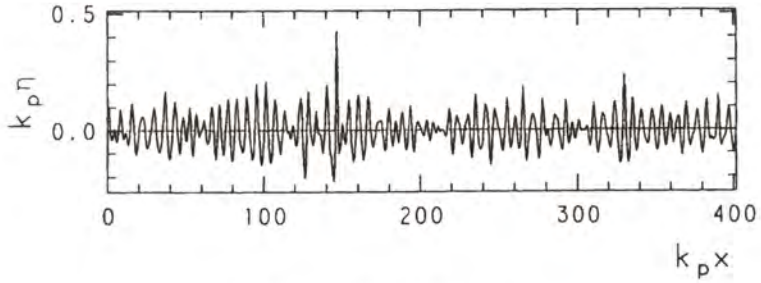

(a) High-order solution

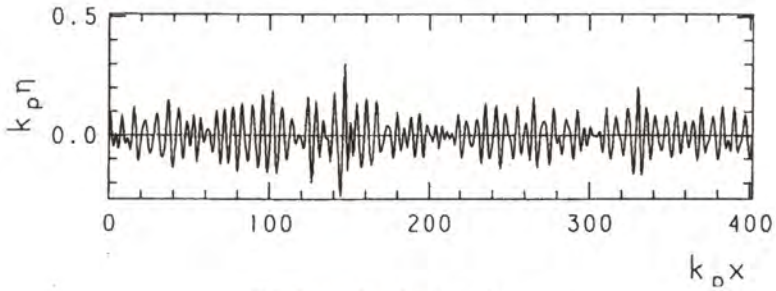

(b) Second-order solution

Fig. 5. Examples of simulated water surface profiles for both the high-order and the second-order solution at time t/T_p=25.

the time averaged wavenumber spectra of the high-order solution. This result demonstrates that spectra of random wave trains in deep-water transform their profiles through high-order nonlinear resonant interaction and it is equivalent to phase averaged high-order equation (*e.g.* Hasselmann's eq.)

It appears that the shapes of time averaged spectra of the high-order solution are similar and independent from the initial spectrum bandwidth. However, effects of the initial spectrum bandwidth are not seen in the shape of the time averaged spectra but are found out in dispersion relations. The phase of the nonlinear wave is given by

$$\psi(k,t) = kx - \omega(k,t)t + \delta(k), \tag{7}$$

where $\delta(k)$ is the phase constant and ω the angular frequency as a function of x and t. Then the nonlinear dispersion relation ω=$\omega(k,t)$ can be calculated numerically through finite differentiation of the phase $\psi(k,t)$:

$$\omega(k,t) \simeq \frac{\psi(k,t) - \psi(k,t+\Delta t)}{\Delta t}. \tag{8}$$

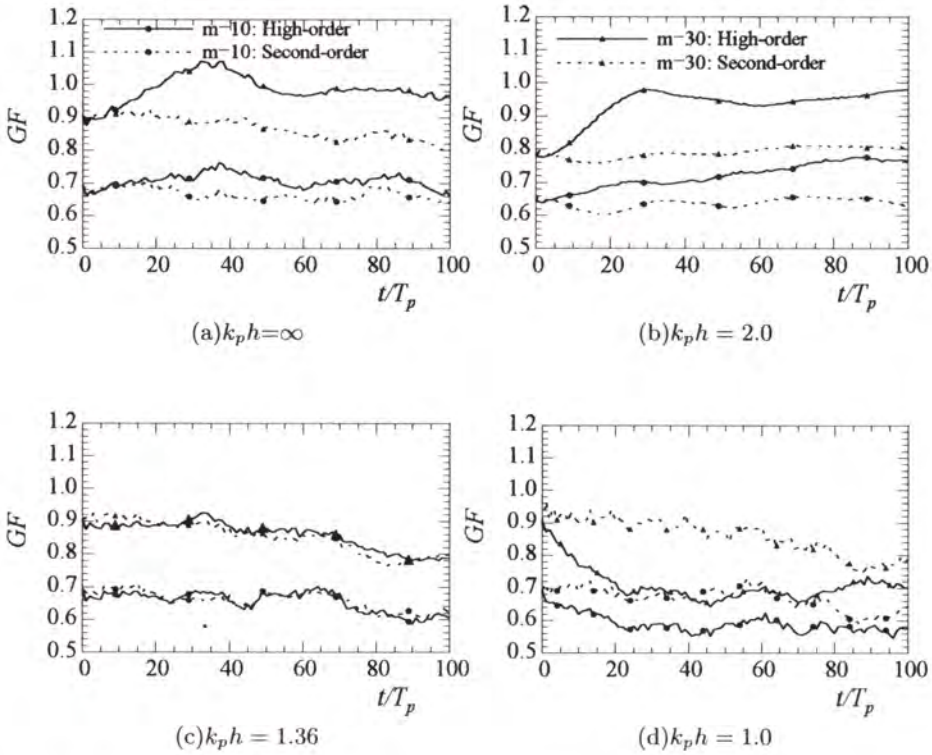

Fig. 6. Temporal histories of GF of a simulated wave train for the high-order solution (solid line) and the second-order one (dashed line), filled circle:m=10, filled triangle:m=30.

Figure 4 shows the relationship between phase speed c/c_p and wavenumber k of the high-order nonlinear solution for m=10 and k_ph=∞. The solid line in the figure denotes the nonlinear dispersion relation calculated by Eqn.(8), the dashed line denotes the linear dispersion relation, the dashed line with filled circles and the solid line with filled triangles denote wavenumber spectra at t/T_p=0 and 100, respectively. The nonlinear dispersion relation is distinct from the linear dispersion relation at high wavenumbers $k/k_p > 2.0$. The separation points from the linear dispersion relation depend on the initial spectrum bandwidth and are shifted to the low wave number side in the initially narrow banded spectrum case. The fact that a nonlinear wave grouping becomes dominant for narrow banded spectrum waves suggests that the nonlinear components of the spectrum are important to describe the nonlinear characteristics of the wave train.

Surface Wave Profile and Wave Statistics. It is important for engineering practice to make clear the high-order nonlinear effects on water surface elevations and their statistics, because understanding of the wave characteristics/statistics

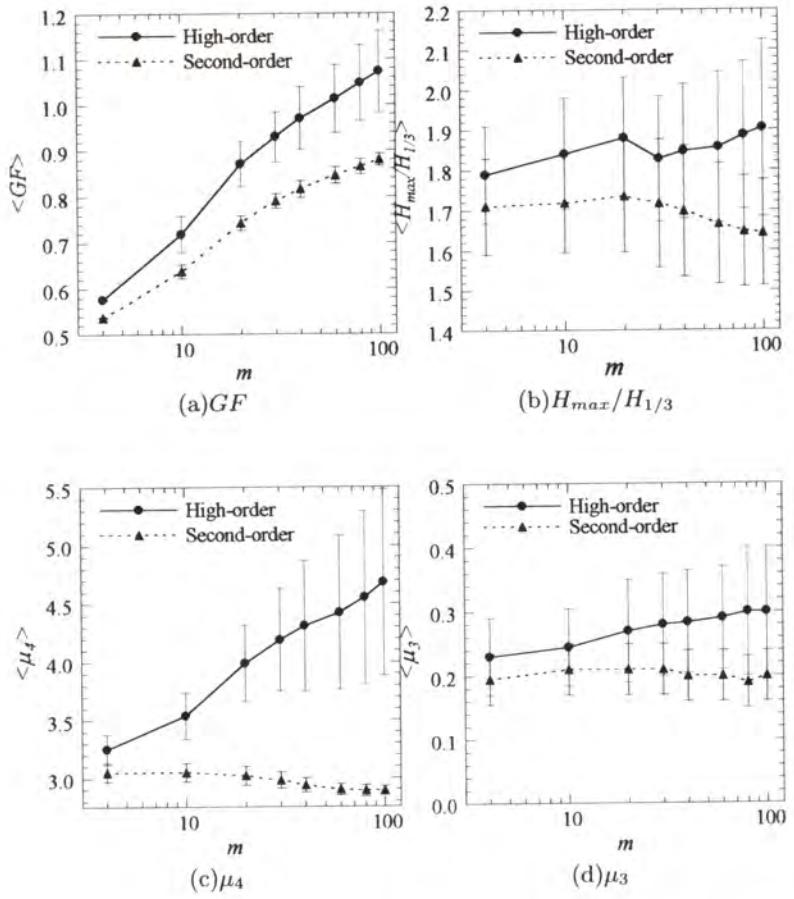

Fig. 7. Time averaged wave statistics as a function of spectral bandwidth m in deep-water conditions (solid line: high-order solution, dashed line: second-order solution).

is of high value for engineering. Figure 5 are plotted the spatial wave profiles of the high-order and 2nd order solutions at the evolution time of t/T_p=25 for m=10 and $k_p h$=∞. The whole of the surface profiles of the high-order and second-order solution are quite similar, however, a giant and steep wave, freak wave-like, can be observed at $k_p x$=140 of the high-order solution. It is found that the high-order nonlinear interactions are strongly related to the occurrence of a single extreme wave having an outstanding crest height, because such a wave can be never observed in the second-order nonlinear solution. The occurrence of the steep wave is related to wavenumber components higher than $2k/k_p$, particularly $3k/k_p$[12] and has high velocity near the surface[21].

The fact that the high-order nonlinear interactions generate a steep wave suggests that such high-order nonlinearities also affect wave statistics. GF (Groupi-

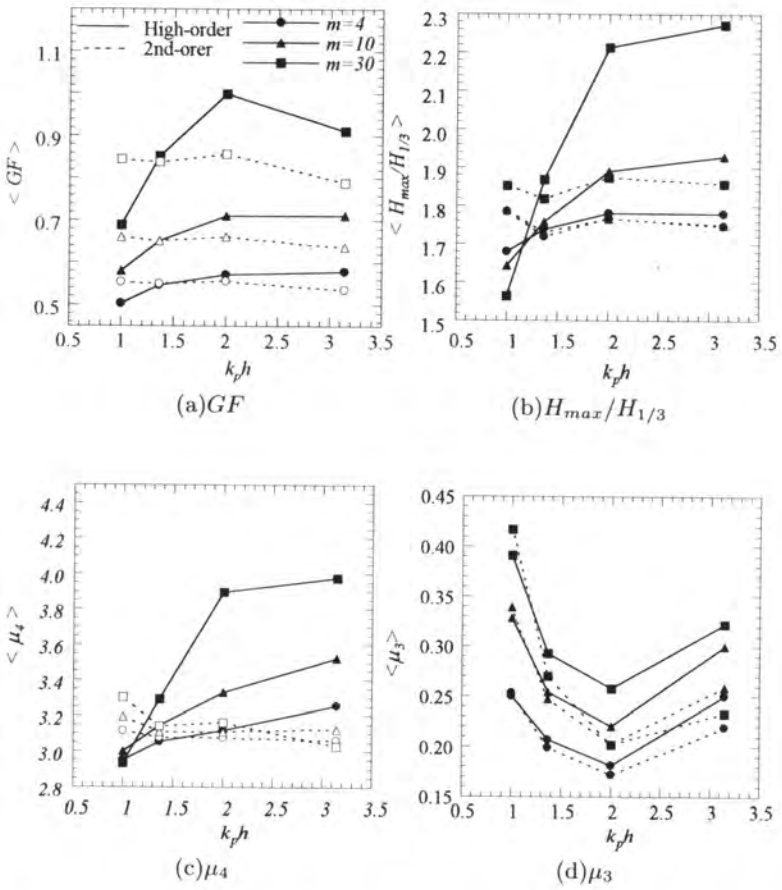

Fig. 8. Time averaged wave statistics as a function of relative water depth k_ph for m=4, 10, 30 (solid line: high-order solution, dashed line: second-order solution, filled circles: m=4, filled triangles: m=10, filled squares: m=30).

ness Factor) is thus picked up to describe the characteristics of the wave train. The time histories of GF during the propagating process are shown in Figure 6 for m=10, 30 and 100. GF of the high-order non-linear solution is always larger than that of the second order solution, and the high-order effects are stronger for initially narrow banded spectrum waves in deep-water conditions. Moreover, if the water depth becomes shallower, differences between the high-order and the second-order solution become smaller. And finally they are almost same in the case of k_ph=1.36 that corresponds to a saddle node point of the stability of the nonlinear Schrödinger equation.

To verify quantitatively the effects of the high-order nonlinearities on wave statistics, time averaged GF, $H_{max}/H_{1/3}$, kurtosis μ_4, and skewness μ_3, are plotted in Figure 7 and Figure 8 as a function of initial spectral bandwidth m

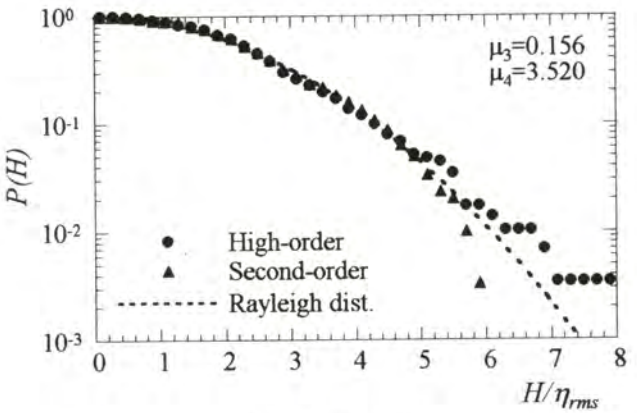

(a) $m = 4$, $k_p h = \infty$

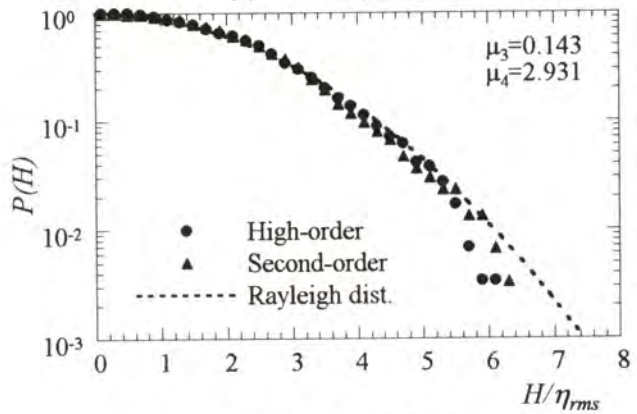

(b) $m = 4$, $k_p h = 1.36$

Fig. 9. Comparison of exceedance probabilities of wave heights for high-order and second-order solutions with the Rayleigh distribution.

and water-depth $k_p h$. The vertical bars in the figures indicate variance of the statistics and brackets $<>$ indicate time averaged values. The difference of $<\mu_3>$ between the high-order and the second-order solution is small. However, $<GF>$, $< H_{max}/H_{1/3} >$ and $< \mu_4 >$ of the high-order solution are larger than those of the second-order solution, and the differences between the high-order solution and the second-order one decrease when the spectrum bandwidth becomes broader in deep-water. These differences are reduced for $k_p h$=2.0 and vanish when $k_p h$=1.36. Moreover, they become opposite when $k_p h$=1.0. This implies that the high-order nonlinear effects play an important role to stabilize the waves in shallow-water. The effects of the high-order nonlinearities are most remarkable in μ_4. The reason why μ_4 is outstanding is that μ_4 statistically depends on

the third-order nonlinearities[22]. Therefore, the value of μ_4 is necessary step to check the influence of the high-order nonlinearities of an observed wave train.

Wave Height Distribution. High-order nonlinearities increase $H_{max}/H_{1/3}$, kurtosis and GF. Another significant aspect of the high-order nonlinear effects is the exceedance probability of wave heights. Figure 9 shows a comparison of exceedance probabilities of wave heights for the high-order nonlinear solution (filled circles), second-order one (filled triangles) and the Rayleigh distribution (dashed line) for $k_ph=\infty$ and 1.36. The exceedance probabilities of wave heights for the second-order solution are independent from the water depth and are slightly below the Rayleigh distribution. On the other hand, the exceedance probabilities of wave heights of the high-order solution exceed the Rayleigh distribution in deep-water and are the same as for the second-order solution when k_ph=1.36. This tendency of the exceedance probability of wave heights is the same as for kurtosis. The results of numerical simulation clearly show that the wave heights distribution is not constant and varies as a function of kurtosis. The authors studied the nonlinear wave heights distribution as a function of kurtosis in [23][24].

3.2 High-order Nonlinear Effects for a Stokes Wave in 3D

Numerical simulations in three dimensional domain were performed for a Stokes wave. Figure 11 shows the temporal evolutions of spatial surface profiles of the wave at t/T_p=0, 100 and 200 with the perturbations making angles 5 and 30 degree to the carrier wave. The horizontal and vertical axes denote respectively the x and y axss normalized by the carrier wave length L_p. The Stokes wave trains become unstable due to five wave resonances at t/T_p=200. Figure 12 shows temporal evolutions of two dimensional wavenumber spectra for the same case of Figure 11. The horizontal and vertical axis denote two dimensional wavenumber space normalized by carrier wavenumber k_p, respectively. The energy of the carrier wave spreads out on wavenumber space for both θ=5 and 30. There is no significant difference between θ=5 and 30 at t/T_p=200, although the influence of the initial conditions still remains at t/T_p=100. Finally the temporal evolution of the wavenumber spectra in the x direction is shown in Figure 12. There is no regular motion such as the FPU recurrence of the two dimensional case.

4 Conclusion

It is found that the high-order nonlinear interactions play a very important role in the long time evolutions of gravity waves both in deep and shallow-water when solving the hydrodynamic equations for gravity waves having narrow to broad banded spectra. It is concluded as follows:

- The high-order nonlinear interactions can transfer energy between the Fourier modes and excite apparently chaotic mode evolutions even if waves have a broad band spectrum in deep-water.

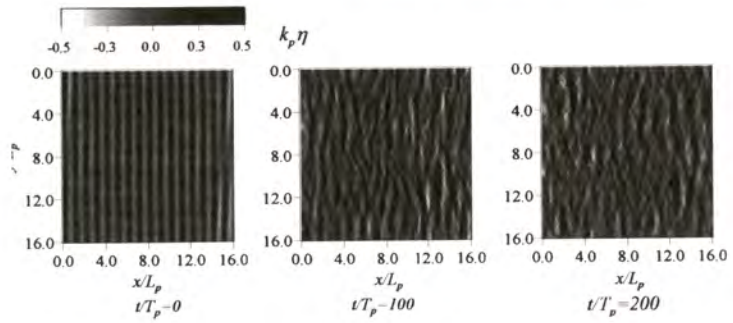

(a) θ=5[deg]

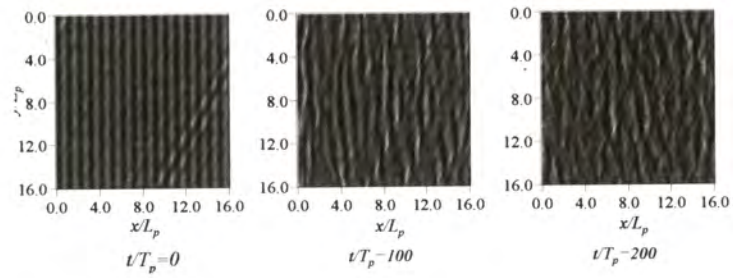

(b) θ=30[deg]

Fig. 10. Temporal evolutions of spatial surface profiles for a 3D monochromatic wave train with perturbations from different initial angles.

- The high-order nonlinear interactions can generate a single extreme high wave having outstanding crest height such as a freak wave.
- The high-order nonlinear interactions affect H_{max}, kurtosis and GF remarkably.
- The high-order nonlinear interactions increase the occurrence probability of large wave heights in deep-water and decrease it in shallow-water in comparison with the Rayleigh theory.

Consequently, the high-order nonlinear effects should be taken into account independently of the spectral bandwidth to predict the maximum wave and the freak wave generation.

5 Acknowledgement

We would like to thank Shinichi Ohmiya and Atsushi Kawai for their supports.

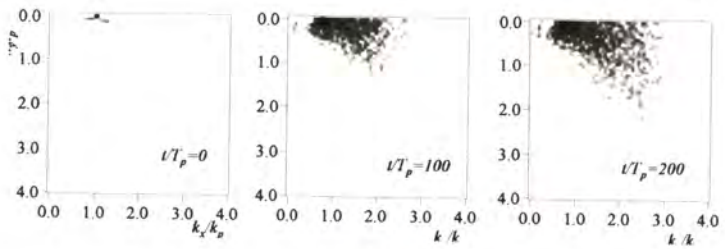

(a) θ=5[deg]

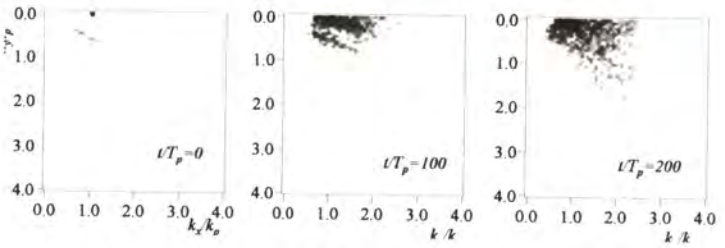

(b) θ=30[deg]

Fig. 11. Temporal evolutions of wavenumber spectra for a 3D monochromatic wave train with perturbations from different initial angles (same as Figure 10).

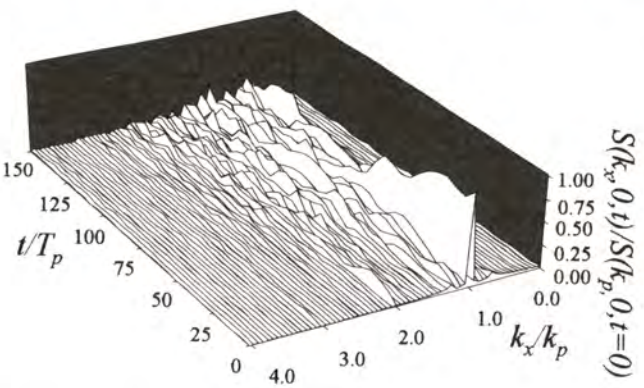

Fig. 12. Temporal evolutions of the Fourier spectra (x direction only) of a 3D monochromatic wave train (θ=5).

References

[1] H.C. Yuen and B.M. Lake. Nonlinear dynamics of deep-water gravity waves. *Advances in Applied Mech.*, 22:67–327, 1982.

[2] E.A. Caponi, P.G. Saffman, and H.C. Yuen. Instability and confined chaos in a nonlinear dispersive wave system. *Phys. Fluids*, 25(12):2159–2166, 1982.

[3] K.B. Dysthe. Note on modification to the nonlinear Schrödinger equation for application to deep water waves. *Proc. Roy. Soc. Lond.*, A369:105–114, 1979.

[4] M. Stiassnie and L. Shemer. Energy computations for evolution of class I and II instabilities of Stokes waves. *J. Fluid Mech.*, 174:299–312, 1987.

[5] T. Yasuda and N. Mori. Roles of sideband instability and mode coupling in forming a water wave chaos. *Wave Motion*, 26(2):163–185, 1997.

[6] M.Y. Su. Three-dimensional deep-water waves. part.1, experimental measurement of skew and symmetric patterns. *J. Fluid Mech.*, 124:73–108, 1982.

[7] K. Hasselmann. On the nonlinear energy transfer in gravity-wave spectrum. I.gerenral theory. *J. Fluid Mech.*, 12:481–500, 1962.

[8] A. Masuda. Nonlinear energy transfer between wind waves. *J. Phys. Oceanogr.*, 10:2082–2092, 1980.

[9] I.E. Alber. The effects of randomness of the stability of two-dimensional surface wavetrains. *Proc. Roy. Soc. Lond.*, A363:525–546, 1978.

[10] H.C. Yuen and W.E. Ferguson Jr. Relationship between Benjamin-Feir instability and recurrence in the nonlinear Schrödinger equation. *Phys. Fluids*, 21(8):1275–1278, 1978.

[11] T. Yasuda, N. Mori, and K. Ito. Freak waves in a unidirectional wave train and their kinematics. In *Proc. of the 23th Int. Conf. on Coastal Eng.*, volume 1, pages 751–764, Venice, 1992. ASCE.

[12] T. Yasuda and N. Mori. High order nonlinear effects on deep-water random wave trains. In *International Symposium: Waves-Physical and Numerical Modelling*, volume 2, pages 823–332, Vancouver, 1994.

[13] T. Yasuda and N. Mori. Occurrence properties of giant freak waves the sea area around Japan. *J. Waterway, Port, Coast. and Ocean Eng.*, 123(4):209–213, 1997.

[14] T. Yasuda, N. Mori, and S. Nakayama. Characteristics of giant freak waves observed in the sea of Japan. In *Waves97*, pages 482–495, Virginia, VA, 1997.

[15] N. Mori, T. Yasuda, and S. Nakayama. Statistical properties of freak waves observed in the sea of Japan. In *Proc. International Offshore and Polar Engineering Conference*, volume 3, pages 109–115, Seattle, 2000. ISOPE.

[16] R.G. Dean. Freak waves: a possible explanation. In A. Tørum and O.T. Gudmestad, editors, *Water wave kinematics*, pages 609–612. Kluwer Academic Pub., 1990.

[17] C.T. Stansberg. Extreme waves in laboratory generated irregular wave trains. In A. Tørum and O.T. Gudmestad, editors, *Water wave kinematics*, pages 573–590. Kluwer Academic Pub., 1990.

[18] D.G. Dommermuth and D.K.P. Yue. A high-order spectral method for the study of nonlinear gravity waves. *J. Fluid Mech.*, 184:267–288, 1987.

[19] V.E. Zakharov. Stability of periodic waves of finite amplitude on the surface of a deep fluid. *J. Appl. Tech. Phys.*, 9:190–194, 1968.

[20] M. Tanaka. The stability of steep gravity waves. *J. Phys. Soc. Japan*, 52(9):3047–3055, 1983.

[21] T. Yasuda, N. Mori, and S. Nakayama. Freak wave kinematics in unidirectional deep water waves. In *Proc. of the 4th Int. Offshore and Polar Eng. Conf.*, volume 3, pages 43–50, Osaka, 1994.

[22] M.S. Longuet-Higgins. The effect of non-linearities on statistical distributions in the theory of sea waves. *J. Fluid Mech.*, 17:459–480, 1963.

[23] N. Mori and T. Yasuda. Weakly non-gaussian model of wave height distribution for random waves. In *Proc. of the 24th Int. Conf. on Coastal Eng.*, volume 1, pages 412–426, Orlando, 1996. ASCE.

[24] N. Mori and T. Yasuda. Maximum wave height distributions of nonlinear narrow banded random waves. In *Proc. International Offshore and Polar Engineering Conference*, volume 3, pages 9–13, Seattle, 2000. ISOPE.

NewWaves, Solitons and Spreading

Paul H. Taylor[1] and Christopher Swan[2]

[1]Department of Engineering Science, University of Oxford, Parks Road,
Oxford OX1 3PJ, U.K.
paul.taylor@eng.ox.ac.uk
[2]Department of Civil and Environmental Engineering, Imperial College,
London SW7 2UB, U.K.
c.swan@ic.ac.uk

Abstract. The simplest model for random waves is based on Gaussian statistics. The idea of an average shape for an extreme wave crest in a linear sea, due to Lindgren and subsequently known as NewWave, is used as a starting point for a review of the effects of non-linearity in the production of extreme waves in random seas. Both experiments and numerical simulations show that the physics of the evolution of directionally spread wave fields is different to that of unidirectional waves. Thus, efforts to explain the occurrence of rogue waves should reflect the wave spreading obvious in nature.

1 Introduction

What is a rogue wave? A possible definition might be

> *"An extreme wave event which apparently occurs on average more often than would be predicted using the tail of the Rayleigh distribution for statistics of linear waves - even after allowing for the obvious 2nd order crest-trough asymmetry of steep waves".*

Let us start by assuming that the possible occurrence of rogue waves can be explored by means of solutions to the full Euler equations of potential flow for an ideal incompressible and constant density fluid. There is no dissipation or energy input into the fluid domain. Hence, the fluid remains irrotational. Further, we shall assume that there are no ocean currents and that the water is deep. The free-surface boundary conditions neglect any influence of the air above the surface and surface tension is ignored. Since our models cannot calculate beyond wave breaking, we further assume that wave overturning does not occur and that white water is not important. Although these assumptions represent an enormous simplification of reality in the open ocean during severe storms, the prediction of the evolution of surface water waves still remains challenging.

If rogue waves exist, they must be inherently non-linear. If they are defined to be more severe than a 2nd order model would predict, then they must arise from 3rd and

higher order interactions – if such a perturbation expansion is meaningful. This contribution attempts a partial, somewhat personally biased review of the literature on steep wave focussing.

2 Second Order Models and NewWave

A Stokes 2nd order model for steep waves represents the 1st non-linear term in a perturbation expansion for surface waves in terms of wave steepness. As such, it can only weakly be non-linear – the kinematics at the free surface are different for crests and troughs and there is the radiation-stress driven return flow beneath localized wave steep groups. However, the underlying dynamics are still assumed to be linear – the position of the dominant linear Fourier components for any time can be predicted using simple linear dispersion.

So long as only a 2nd order accurate model is used, then the properties of extremes in an underlying effectively linear random Gaussian process are simple to describe. The average shape of a tall crest tends to the scaled auto-correlation function, Lindgren [1]. Tromans [2] introduced this idea into offshore engineering where it has become known as NewWave. One of the reasons why this is an attractive model is that it connects the (averaged) properties of the largest extremes in a sea-state to the properties of all the waves in that sea-state. The auto-correlation function is simply the Fourier transform of the power spectrum. This model is convenient for both physical experiments and computation as it gives a localized wave group consistent with the broad-banded and directional spread nature of real sea-states.

Second order corrections to an underlying linear model are consistent with much field data. The average shapes of large deep-water waves measured during severe winter storms at Tern, a northern North Sea platform in 170m of water, are entirely consistent with the NewWave model [3]. Both the simple case of a single point measurement of surface elevation in time and the more complex case of the simultaneous time history at a second location given a wave crest of given size at an adjacent point were studied. The prediction of this latter case required directional sea-state information obtained from a directional wave-rider buoy. For small waves, the full solution by Lindgren [1] for the average shape of waves is required. However, in the limit of a large event ($A > 2\sigma$, where A is the individual wave amplitude and σ is the rms surface elevation), this exact Lindgren solution tends to the shape of the auto-correlation function. As well as being a good model for the average shape of large wave crests on deep water, analysis of wave data measured in 17m water depth during the recent WACSIS joint industry project confirms the validity of this approach for steep waves on intermediate water depth in winter storms.

At second order, all the terms quadratic in wave amplitude are slaved to the (assumed) underlying linear components which move in a manner consistent with simple linear dispersion. Thus, brute force simulation of random sea-states can provide benchmark statistics on crest elevations etc. (Forristall [4], Prevosto in this workshop). A more elegant method of obtaining the same short-term wave statistics is the re-

sponse surface (FORM) approach of Tromans. This approach has been applied to the statistics of crest elevation for deep-water uni-directional waves [5].

The apparent consistency between field data in severe storms and 2nd order models implies that rogues are rare – perhaps requiring a special set of circumstances that we don't yet understand.

3 Beyond Second Order for Wave Evolution

Theoretical models of steep waves beyond 2nd order in wave steepness must account for non-linear dispersion if they are to be accurate over long distance and time scales. The simplest example of non-linear dispersion is the amplitude dependent Stokes correction to the phase speed of regular waves arising at 3rd order in the theory.

The idea of having shorter, slower waves overtaken by longer, faster ones - frequency-based focussing – pre-dates the derivation of the non-linear Schrödinger equation and the derivation of a general solution method by inverse scattering, Zakharov and Shabat [6]. The interaction of linear dispersion and wave non-linearity was first studied by Lighthill [7] and is briefly discussed in his book [8], p.462.

At 3rd order for narrow-banded wave groups, non-linear evolution equations (NLEEs) can be used to explore the effects of wave amplitude in the dynamics. The consequences are profound – and different for group structure in a longitudinal down-wave direction or structure laterally along the wave crests. The simplest NLEE is the non-linear Schrödinger equation, Zakharov and Shabat [6], Yuen and Lake [9] and Peregrine [10]. For isolated uni-directional wave groups on deep water described by the positive (NLS+) version of the equation, there are soliton solutions where linear dispersion is balanced by 3rd order amplitude dispersion to produce permanent and robust localized groups.

Both one-dimensional physical experiments, Baldock, Swan and Taylor [11], and numerical and analytic modelling [12] show that non-linearity co-operates with linear focussing, when an extreme event is produced by having long wave components overtake short ones. The following simple argument, originally due to Lighthill, shows how this co-operation can occur. Consider a wave group with shorter waves ahead and longer ones behind. Due to linear dispersion the longer waves will slowly catch up with the shorter ones. In the centre of the group the waves are higher than those at the edges. Since high waves move faster than small waves of the same wavelength, the waves in the centre of the group will catch up with those ahead – amplitude dispersion. The waves ahead will be compressed, the local wavelength is reduced, and those behind stretched, leading to further linear dispersive changes to the focus event. A simple approximation for this physical process is captured by the NLS equation.

Although the NLS equation is the lowest order NLEE for deep-water waves, it is not quantitatively accurate for isolated wave groups. Dysthe [13], Stiassnie [14] and Lo and Mei [15] include other terms to improve both the dispersive and non-linear aspects of the physics.

Probably the most important piece of the physics not captured by the NLS equation is the dynamical consequence of the return flow beneath the wave group. Any

finite size deep-water wave transports fluid forwards in the direction of wave advance – Stokes drift. However, an isolated wave group rides on a quiescent ocean. Thus, there must be a continuous return flow beneath the wave group balancing the Stokes drift. The length-scales associated with this flow are those of the whole group, not those of individual waves. In a perturbation expansion for a wave group, this return flow occurs at 2nd order and is associated with the set-down beneath the group. To this order there is no effect on the wave dynamics. However, there is a physical effect at 3rd order. The large waves in the centre of the group ride on a locally opposing current – the return flow. Thus, the full dynamics to 3rd order are weaker than predicted by the NLS equation. The relative importance of the return flow depends on the length of the group. If the group is compact (the spectrum broad-banded), this effect is important.

In an engineering context, the direction and magnitude of this return flow is important, both for waves on deep and shallow water. Being backwards in direction, the horizontal fluid velocity subtracts from the usual in-line kinematics beneath the wave crests but adds to the backward flow beneath wave troughs. Thus, for steep waves the magnitude of the net horizontal kinematics at elevations below the level of the deepest trough can be larger beneath a deep trough than beneath tall crests. Of course, the highest kinematics occur in the in-line direction within the crests above mean-sea-level.

One result, clear from experiment [11], is the fast rate at which non-linear energy transfer between spectral components can occur in uni-directional wave groups. Starting 10 periods before focus, a wave group could become $O(25\%)$ higher than predicted by linear theory at focus, even after allowing for 2nd order effects. Such a localized wave group is formed which is more compact, taller and longer lasting than would be predicted by simple linear theory (even if 2nd order corrected). Indeed, if the spectral components in the converging group are chosen suitably, a group is formed which at least locally closely approximates a solitary wave group. Perhaps such a soliton might be a good candidate for a model of rogue waves.

The discussion thus far has concentrated on isolated wave groups on quiescent water. In reality, every large event in a random sea emerges and presumably disperses back into a random background. Does the presence of this background have any effect on the coalescence properties of a large wave event? Yuen and Lake [9] discuss the work of Albers and Saffman on this problem. For sufficiently narrow-banded problems so that the NLS equation is valid, they conclude that the modulational (Benjamin-Feir) instability of a Stokes wave train is weakened and can be eliminated if the background is sufficiently strong. This can be understood as phase randomization of the 3rd order wave-wave interactions (which feed back to the principal dynamics only when the 3rd order difference terms remain in phase with the otherwise dominant linear components). Both recent experiments by Stansberg [16] in a long wave tank and full simulations of the Euler equations by Mori and Yasuda (this workshop) show that the statistical properties of a uni-directional random wave field do change with distance and or time. Hence, some cumulative non-linear effects survive randomization.

In contrast to 1-D waves with group structure along the mean wave direction but crests running transversely to infinity, variation in the height of a wave group along the wave crest direction leads to the NLS– or defocusing version of the equation. Non-linearity is still important but the focussing of components to produce an extreme

event is weakened –the group is now lower but longer-crested. Consistent with this, there are now no soliton solutions propagating in isolation. Thus, group structure in the mean wave and transverse directions has different consequences for the production of extreme events.

4 Wave Focussing for Directionally Spread Components

Real waves on the open ocean are directionally spread. The wave crests do not run at constant height from horizon to horizon. Instead, a strongly two-dimensional pattern is obvious. A simple argument indicates that non-linearity could well be less important for a spread sea than it is for the 1-D case. A wave group can be built up from many individual Fourier components, each with its own phase speed and group velocity. The group velocity is defined as the speed of propagation of energy of that component. Due to the range of wavelengths present, the length of the group will increase with time away from the instant of focus when all the components are in phase. Thus, the length of the group increases asymptotically with time as $L \sim O(t)$. As the group lengthens, the wave height drops to satisfy conservation of total energy. The total energy of the group is constant as $E \sim O(A^2 L)$, where A is the amplitude of a linearly dispersing wave group. Thus, the amplitude decays asymptotically as $A \sim O(t^{-1/2})$ as the energy becomes more and more spread out along a line. This simple asymptotic behaviour is consistent with the linear part of the NLS equation. Now, the NLS equation contains both linear and cubic terms in the wave amplitude. The net effect of the cubic term in the NLS equation on the amplitude over long times is $O(A^3 t) \sim O(A)$, assuming the effect is cumulative. Thus, there are long-term consequences for the evolution of the group in 1-D.

The situation is quite different for directionally spread wave groups. A localized wave group now disperses out over a plane rather than along a line. The wave amplitude decays asymptotically as t^{-1}. Over long times, the long-term contribution to the amplitude from the cubic NLS term is $O(A^3 t) \sim O(A^2)$, being negligible compared to linear behaviour which is $O(A)$. Thus, wave-wave interactions are more localized - needing a large wave group close to the linear focus to produce significant effects.

Both versions (NLS+ and NLS-) of the Schrödinger equation in 1-D are solvable by inverse-scattering techniques. The combined spread sea (x, y, t) version is not. The spread sea (x, y, t) version of the NLS equation also suffers from a catastrophic defect – energy is predicted to leak to higher and higher wavenumber. This leakage is non-physical and implies that long-time simulations in 2-D using the NLS equation would be severely flawed. In an exciting development described at this workshop, Trulsen presented an improved version of the wave evolution equation with this energy leakage problem cured. This work may represent an elegant starting point to study the statistics of the freak wave problem with a realistic amount of computer resources. However, benchmarking against fully non-linear schemes will be required as the range of free wavelengths that any evolution equation can simulate is restricted and real ocean wave spectra are broad-banded. Note also that NLEEs are usually studied nu-

merically with pseudo-spectral numerical schemes, with the computational effort scaling as *O(N Log N)*, where *N* is the number of points on the surface.

As discussed above, the standard NLS equation does not include the dynamic effects of the return current beneath the wave group, which is driven by the Stokes drift. For a directional spread wave group, the return flow still exists, as the Stokes drift is still transporting fluid forwards to the lead edge of the group. However, this flow is now locally considerably weaker - it is able to spread out sideways horizontally as well as penetrating downwards underneath the centre of the group. Thus, the backward advection velocity of the tall waves in the centre of the group is significantly reduced, and the effect on the wave dynamics at 3rd order is smaller. There is a NLEE with this effect included – the Davey-Stewartson equation. For deep water spread seas, the Davey-Stewartson equation is not solvable by inverse scattering, Ablowitz and Clarkson [17].

Overall, we have two opposing effects – the directionally spread groups are compact and tall for a shorter time than uni-directional groups, simply due to linear dispersion. This reduces the time over which 3rd order non-linear effects are able to act. However, the dynamical consequences of the return flow (opposing non-linear focussing) are also weaker. Further, it is known that new physics enters with the extra spatial dimension – the resonant interactions of Phillips [18] and Hasselmann [19], which permanently transfer energy from 3 components to a 4th.

All of this suggests that the behaviour of directional spread wave groups is likely to be both qualitatively as well as quantitatively different to uni-directional wave groups. Thus, it is probably inappropriate to base the analysis of field data on one-dimensional models. However, this discussion has been based on known properties of solutions to the non-linear evolution equations. Whether, these approximate equations capture enough of the behaviour of solutions to the full Euler equations for water waves remains to be seen.

5 Fully Non-Linear Simulations

Many different computational approaches have been proposed for the solution of the full water wave equations. For uni-directional problems perhaps the best is the boundary integral technique used by Dold [20] and others.

For directionally spread waves, there are several pseudo-spectral methods in the literature. These are attractive as the main computational task is taking Fourier transforms, for which efficient FFT algorithms exist. Thus, the computational effort scales as *O(N Log N)*, where *N* is the number of points on the surface. This is the same scaling, albeit with a larger coefficient in front, as nonlinear evolution equations – which are considerably more restricted in the range of wavelengths that can be accurately represented. Although Fenton and Rienecker presented the first full non-linear Fourier scheme [21], a more recent one devised by Dommermuth and Yue [22] is widely used. In work presented at this workshop, Mori and Yasuda used it in their study of the statistics of random realizations of sea-states. They conclude that 3rd order interactions are important both for uni-directional and directionally spread waves.

A new, efficient and robust numerical scheme for the solution for the full Euler equations for water waves has recently been derived [23]. This is based on the Dirichlet-Neumann (G-) operator of Craig and Sulem [24]. This operator permits the accurate conversion of the velocity potential on the free surface into the normal gradient of this velocity potential, even with a large range of wavenumber components represented. This step is essential in any time-integration scheme for water waves based on the exact dynamic and kinematic boundary conditions. In common with all pseudo-spectral schemes, this approach is restricted to non-overturning waves: the surface elevation is assumed to be a single-valued function of the horizontal co-ordinates. Thus, only the early stages of wave breaking can be studied. However, the main advantages of this new scheme are its efficiency and robustness. It can be run on a PC and is sufficiently robust that it can be used to predict the time histories and local kinematics of near breaking waves. The results are in excellent agreement with the high quality wave basin data recently reported by Johannessen and Swan [25] and discussed at this workshop by Swan in a separate contribution.

6 Results from Steep Wave Simulations

A fundamental difficulty with numerical modelling is the choice of suitable initial conditions to start the simulation. With random initial conditions, considerable computer resources are required to represent a large enough patch of ocean surface evolving over a long enough time to generate useful statistics. The average shape of an extreme wave crest helps here. This defines an isolated NewWave group, which in some sense is typical of the occurrence of large events in a random sea-state. Away from the focus point, such a localized wave group would disperse. If the group is isolated, it arises from and presumably disperses back to a linear background state. Such a NewWave group well before the focus time provides a suitable initial condition for numerical simulation. The non-linear physics of steep waves can then be explored with a 'clean' calculation. At a later stage, the presence of the random background could be included.

Although numerical work is still in progress, examples of fully non-linear focussed wave groups on deep water show that the introduction of a realistic degree of directional spreading has dramatic consequences for the focussing of a steep wave group [26]. Using a realistic wave spectrum and directional spreading to define a NewWave well before focus, Bateman at Imperial College in London has followed the fully non-linear evolution in time. The wave-wave interactions, which are so important for uni-directional wave groups, are considerably modified by directional spreading. In particular, the peak surface elevations arising in directional spread focussed wave groups are similar to those predicted by simple 2nd order theory if the spreading is as large as that commonly observed in severe winter storm waves. However, the underlying dynamics of spread group focussing are not close to linear – in the vicinity of the focus event, the group becomes more compact in the mean wave direction but wider in the along-crest direction and the position of the occurrence of the highest surface elevation is shifted. Thus, the shape of the wave group is modified – and for engineer-

ing applications the local factor on in-line wave kinematics to allow for spreading would be closer to unity than expected from linear theory. Furthermore, this localization of the total energy into a small area of sea for a relatively short time has a permanent effect even as the group subsequently diverges to infinity - the directional spreading of the group far downstream is different to that far upstream.

One clear result from the numerical runs is that the same net directionality changes arise whether the input groups are designed to create a tall crest or inverted to give a deep trough. This symmetry property is obeyed even for waves only a few per cent lower than the breaking limit for that spectral shape. Thus, only the shape and amplitude of the group are important, not the relative phasing of the 'wiggles' within the group. This observation implies that these large-scale group changes can only be only consistent with odd order non-linear interactions. Presumably these global changes are examples of the 3rd order resonant interactions of Phillips [18] and Hasselmann [19]. To date, this part of the physics has only been incorporated into wavefield prediction and hindcast via perturbation interaction equations [27]. The adequacy of these interaction equations is yet to be assessed for events typical of extremes in a random sea.

7 Conclusion

It is apparent that most waves in a random sea behave for most of the time in a manner consistent with simple 2nd order models based on linear dynamics. As a consequence, the average shape of a large wave crest, the scaled auto-correlation function New-Wave, becomes a useful model. It captures considerable information about the overall statistical properties of the sea-state into a single isolated wave group.

Beyond 2nd there is interesting non-linear dynamics to be explored. Both experiments and numerical simulations show that the evolution of directionally spread wave fields is qualitatively different to that of uni-directional waves. The important role played by soliton-type non-linear wave groups in uni-directional wave evolution seems to be absent from the physics of directionally spread seas. Thus, efforts to explain the occurrence of rogue waves should reflect the directional spreading of waves obvious in nature.

Although the possible implications of wave dynamical non-linearity on the likelihood of the occurrence of rogue waves is still not resolved, the study of steep wave groups arising by frequency focussing appears to be a useful area of research. Even if the true explanation for rogue waves lies elsewhere, improved models for the statistics of wave crests and the associated wave kinematics would be an important contribution to oceanography and offshore engineering.

It is a great pleasure to acknowledge the major contributions to this work made by William Bateman and others at Imperial College, Peter Tromans, Philip Jonathan and George Forristall.

References

1. Lindgren G. Some Properties of a Normal Process near a Local Maximum. The Annals of Mathematical Statistics 41, no.6, (1970) 1870-1883
2. Tromans P.S., Anaturk A.R. and Hagemeijer P. A New Model for the Kinematics of Large Ocean Waves. ISOPE-91 Conference, Edinburgh (1991)
3. Jonathan P. and Taylor P.H. Irregular, Nonlinear Waves in a Spread Sea. ASME Transactions J. of Offshore Mechanics and Arctic Engineering 119, no.1 (1996), 37-41
4. Forristall, G.Z. 2000 Wave Crest Distributions: Observations and Second Order Theory, J. Phys. Oceanogr., 30 (2000) 1931-1943
5. Tromans P.S. and Taylor P.H. 1998 The Shapes, Histories and Statistics of Non-Linear Wave Crests in Random Seas. Proc. 17th Int. Conf. On Offshore Mechanics and Arctic Engineering. OMAE98-1206
6. Zakharov V.E. and Shabat A.B. Exact Theory of Two-Dimensional Self-Focussing and One-Dimensional Self-Modulation in Nonlinear Media. Sov. Phys. JETP 34 (1972), 62-9
7. Lighthill M.J. Contributions to the Theory of Waves in Non-Linear Dispersive Systems. Jn. Inst. Maths Applic. 1, (1965) 269-306
8. Lighthill M.J. Waves in Fluids. 1st edn. Cambridge University Press (1978)
9. Yuen H.C. and Lake B.M. Nonlinear Dynamics of Deep-Water Gravity Waves. In Chia-Shun Yih (ed.): Advances in Applied Mechanics vol.22, 153-180. Academic Press (1992)
10. Peregrine D.H. Water Waves, Nonlinear Schrodinger Equations and Their Solutions. J. Austral. Math. Soc. B25, (1983) 16-43
11. Baldock T.E., Swan C. and Taylor P.H. A Laboratory Study of Non-Linear Surface Waves on Water. Phil.Trans. Roy. Soc. Lond. A 354, (1996) 649-676
12. Taylor P.H. and Haagsma Ij. Focussing of Steep Wave Groups on Deep Water. Proc. Int. Symp. Waves – Physical and Numerical Modelling, Vancouver, Canada, Vol.2 (1994), 862-870
13. Dysthe K.B. Note on a Modification to the Nonlinear Schrodinger Equation for Application to Deep Water Waves. Proc. Roy. Soc. A 269 (1979), 105-114.
14. Stiassnie M. Note on the Modified Nonlinear Schrodinger Equation for Deep Water Waves. Wave Motion 6 (1984), 431-433
15. Lo E and Mei C.C. A Numerical Study of Water-Wave Modulation Based on a Higher Order Nonlinear Schrodinger Equation. J. Fluid Mech. 150 (1985), 395-416
16. Stansberg C-T Nonlinear Extreme Wave Evolution in Random Wave Groups. Paper Presented at ISOPE2000, May 28-June 2, 2000. Held in Seattle, Washington, USA
17. Ablowitz M.J. and Clarkson P.A. 1991 Solitons, Nonlinear Evolution Equations and Inverse Scattering. 1st edn. Cambridge University Press, publ. as London Mathematical Lecture Note Series, 149
18. Phillips O.M. The Dynamics of Unsteady Gravity Waves of Finite Amplitude, part 1. J. Fluid Mech. 4 (1960), 426-434
19. Hasselmann K. On the Non-Linear Energy Transfer in a Gravity-Wave Spectrum, part 1: general theory. J. Fluid Mech. 12 (1967), 481
20. Dold J.W. An Efficient Surface-Integral Algorithm Applied to Unsteady Gravity Waves. J. Comput. Phys. 103 (1992), 90-115
21. Fenton J.D. and Rienecker M.M A Fourier Method for Solving Nonlinear Water Wave Problems: Application to Solitary Wave Interactions. J. Fluid Mech. 118 (1982), 411-443
22. Dommermuth D.G. and Yue D.K.P. A Higher-Order Spectral Scheme for the Study of Nonlinear Gravity Waves. J. Fluid Mech. 184 (1987), 267-288
23. Bateman W.J.C., Swan C. and Taylor P.H. On the Efficient Numerical Simulation of Directional-Spread Water Waves. Submitted to Journal of Comput. Phys. (2001)

24. Craig W. and Sulem C. Numerical Simulation of Gravity Waves. J. Comput. Phys. 108 (1993), 73-83
25. Johannessen T.B. and Swan C. A Laboratory Study of the Focusing of Transient and Directionally Spread Surface Water Waves. Proc. Roy. Soc. Lond. A 457 (2001), 1-36
26. Bateman W.J.C., Swan C. and Taylor P.H. Steep Multi-Directional Waves on Constant Depth. Proc. 18th Int. Conf. on Offshore Mechanics and Arctic Engineering. OMAE99-6463 (1999)
27. WAMDI Group (13 authors, including V. J. Cardone and J. A Greenwood) The WAM Model - A 3rd Generation Ocean Wave Prediction Model. J. Phys. Oceanog., 18 (1988), 1775-1810

Modelling a "Rogue Wave" - Speculations or a Realistic Possibility?

Kristian B. Dysthe

Dep.Math.University of Bergen, Norway
kristian.dysthe@mi.uib.no

Abstract. The findings of Skourup et.al., [13], who analyzed 89 storms over a 12 year period at the Gorm field in the central North Sea is interpreted to indicate that the freak- or rogue waves generally belongs to very short groups. We examine three basic physical mechanisms that may be responsible for the formation of such groups. In each case, however, there seems to be some special preparation or coherens that is needed for the effect to work. The data indicates that nonlinear effects are important. One possibility is that the weak coherence introduced by four-wave interactions may influence the probability of the rare events of constructive interference. This is presently being investigated by simulating an ocean area of approximately 100x100 wavelengths using a nonlinear numerical model (Trulsen et.al., [15]).

1 Introduction.

There is growing evidence that wave records may under certain conditions have occurrences of extreme waves in excess of those predicted by the Rayleigh distribution (e.g.[13]). The occurrences of dangerous wave conditions in coastal waters may possibly be explained by focussing (or caustics) due to refraction by bottom topography or current gradients, and even reflection from land. Well documented in that respect are the giant waves sometimes found in the Aguhlas current on the eastern coast of South Africa, [7].

It seems, however, that this kind of freak- or rogue waves exist even in the open ocean far away from strong current gradients, e.g. [12], [13]. In the following I shall concentrate on this latter case.

Skourup et.al., [13], analyzed more than 12 years of wave records from the central north sea (the Gorm field). They used the following criteria to select candidates for their rogue wave collection: Single waves with cam heights, $a_c > 1.1H_s$,[1] or wave heigts larger than $2H_s$, where H_s is the significant wave height of the surrounding 20 min. wave record. They find the expected extreme value of the ratio a_c/H_s to be approximately 1.8, which is outside the range of Gaussian waves.

[1] The probability $P(a_c > 1.1H_s)$ for such an event to happen according to the Rayleigh distribution is roughly $\simeq 6 \cdot 10^{-5}$.

Warren et.al., [17], analyzed some other North Sea data. Comparisons were made with the modified Rayleigh distribution of Tung and Huang, [16], which take into account second order nonlinear effects. For the case of deep water waves (see their figure 11) the data is not easily reconciled with the theoretical distribution.

Ratios of $a_c/H_s > 2$ and $H_{\max}/H_s > 2.5$ has been reported, [6], [12]. Although years of wave data from numerous buoys have been analyzed, the number of freak wave events recorded are still modest. The chances that such a wave hits a buoy is even lower than was previously expected, as pointed out in [8].

Interest in these waves is not only because of our rather limited knowledge of their statistical probability of occurrence. We need to know more about their dynamics, what they look like, how long they last and so on.

2 The Freak Character of Extreme Waves.

The rogue wave is often described as a freak, "the one out of nowhere". The paper in [13] sheds some light on the form of a rogue wave event. They found that the expected ratio between the crest height and the corresponding wave height of their rogue waves was approximately 0.7. This large ratio can clearly not be explained by the nonlinear crest asymmetry of Stokes waves, as pointed out by the authors. It is, however, rather easily explained as the effect of a

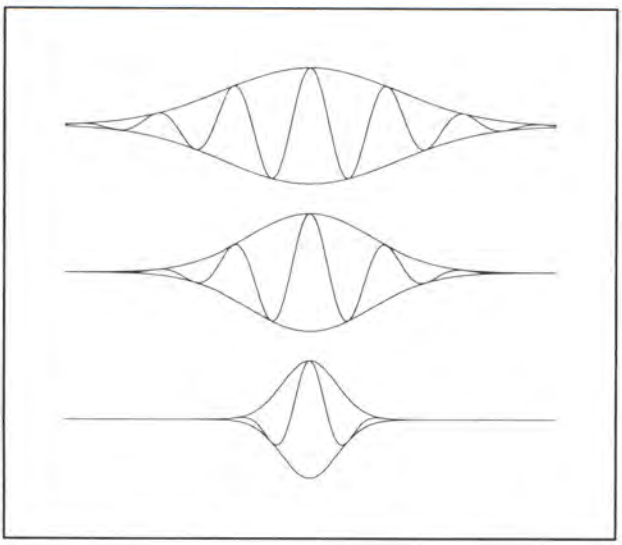

Fig. 1. Shows the ratio a_c/H to increase with decreasing group length.

very short group as demonstrated in Figure 1 by comparing groups of different lengths.

Boccotti, [2] (see also [11]) have investigated the expected configuration in space and time surrounding extremely high crests in a random Gaussian wave field. The most likely configuration was found to have approximately the form of the auto-correlation function for the wave field. A real test of this result need more data than is presently available. The findings, [11], seem to indicate that the variability of the extreme event configuration is rather large.

3 The Physics of Rogue Wave Events.

What about the physics behind rogue waves? Clearly they represent a very high concentration of wave energy compared to the average[2]. A number of mechanisms are known that produce large waves from moderately small ones by focusing the energy. Basically there are three types of effects:

Spatial Focusing. This is due to refraction by bottom topography or current gradients and is a well known reason for dangerous waves in coastal waters. An example of the effect of current refraction is the giant waves reported in the Agulhas current off the African south-east coast (see e.g. [7]). Far offshore on the open ocean only very small current velocities (less than 20cm/s say) it would seem that these effects are negligible. White and Fornberg, [18], have pointed out, however, that even small random current fluctuations with rms values of the order 10cm/s can give focussing provided their scale is sufficiently large (of the order of 10km). Thus they maintain that even the very weak refraction found in the open ocean may produce "hotspots" of wave energy. In their numerical ray-tracing calculations the incoming wave field is unidirectional, and they get caustics after some distance into the fluctuating wave field. Further "downstream" the rays appear rather random.

From experience with similar refraction calculations, [14], we suggest that even a small directional distribution of the incoming wave field will "smear out" the caustics and thus reduce the effect of weak refraction to minor fluctuations in energy density. This effect is illustrated by the refraction calculations shown in Figure 2. In Figure2 (a) three neighboring rays (note the different scales on the two axis) enter in the same direction, and a caustic forms after some distance into the weak current area. In Figure 2(b) each of the three original rays have got two companions starting in slightly different directions ($\backsim 1^o, 2^o$). The location of the caustic is seen to depend strongly on the angular direction of the incoming waves.

It is demonstrated elsewhere, [4], that the curvature $\varkappa$ of the refracted rays is given by the simple formula

[2] For a wave with $a_c = 1.5H_s$ the concentration is roughly a factor 18, if the energy density in the rogue wave is estimated by $\rho g a_c^2/2$.

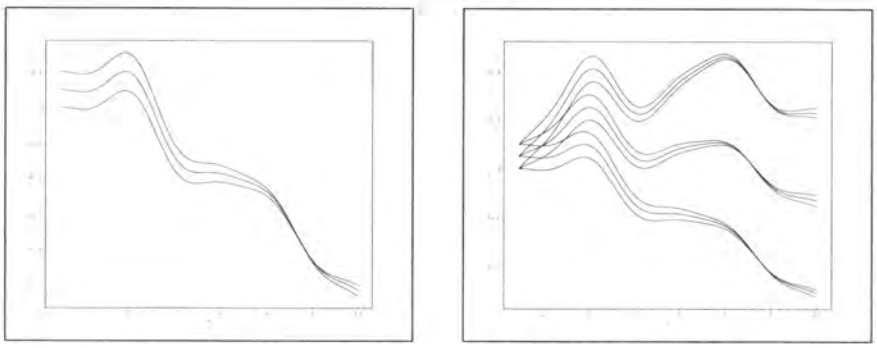

Fig. 2. (a) Caustic formed by three initially parallel rays. (b) Shows how the caustic move sideways by slight changes (1^o, 2^o) of the initial ray direction.

$$\varkappa = \frac{\zeta}{v_g} + O(\mu^2) \tag{1}$$

where $\zeta = \frac{\partial v}{\partial x} - \frac{\partial u}{\partial y}$ is the vertical component of vorticity of the (horizontal) current velocity $\mathbf{u} = (u, v)$ and v_g is the group velocity, provided that $\mu \equiv |\mathbf{u}| / v_g \ll 1$. For a zero mean, random vorticity field which is statistically homogeneous and isotropic it is shown in the appendix that rays moving through such an area of the ocean experience an angular diffusion i.e. $\langle \Delta\theta^2 \rangle = 4Ds$ where s is the arclength and $\Delta\theta$ the angular deviation from some reference point on a ray, and the diffusion coefficient is given by

$$D = \frac{1}{2} \frac{\langle \zeta^2 \rangle}{v_g^2} L_{int} \tag{2}$$

The integral length scale L_{int} is given in terms of the normalized vorticity auto-correlation function $R(|\mathbf{x} - \mathbf{y}|) = \langle \zeta(\mathbf{x}) \zeta(\mathbf{y}) \rangle \, / \, \langle \zeta^2 \rangle$ as $L_{int} = \int_0^\infty R(x) dx$. As an example we use parameters roughly corresponding to those used in Figure 6a in Ref. [18] with $\langle \zeta^2 \rangle^{1/2} = 2 \cdot 10^{-5} s^{-1}$, $v_g = 8m/s$ and $L_{int} = 3km$. We then get $D \simeq 0.94 \cdot 10^{-5} km^{-1}$. To produce a rms angular spread of $\pm 5^o$ to initially mono-directional rays will then require a propagation distance of $\simeq 270km$, which seems in reasonable agreement with their result (Figure 6a). For swell this tendency towards angular spreading will counteract the tendency towards "directional filtering" due to distance from the storm area that created it. The initial mono directional wave field of White and Fornberg therefore appears rather unrealistic.

Temporal-Spatial Focusing. This is the result of dispersion and a chirped spatial distribution of frequencies. The effect is used in a well-known technique

for producing short groups of large waves at a given position in a wave tank. It is done by producing a long and chirped wave group (with steadily decreasing frequency) by the wave maker. With proper design of the frequency chirp, dispersion brings this group to contract to a few wavelengths at a given position. This type of focussing has been suggested in [10] (see also their article in this book) as a possible explanation for freak waves. They show (using the KdV equation for shallow water waves) that if a given chirped wavetrain produces strong focusing in the absence of other waves, it will still do so (although somewhat weaker) when a random wave field is added. If the amplitude of the deterministic chirped wavetrain is below the rms value of the random waves it will remain "invisible" until it focuses.

For the temporal-spatial focussing to work, however, a spatial ordering of frequencies in a chirped wavetrain is needed. So far the question of how such a situation may develop spontaneously has not been answered.

Nonlinear Focusing. The so-called Benjamin Feir (BF) instability of regular wavetrains is well-known. Henderson et.al., [5], have investigated what they call steep wave events (SWE) by simulating the evolution of a periodically perturbed regular wavetrain. Due to the BF instability the wavetrain breaks up into periodic groups. Within each group a further focusing takes place producing a very large wave having a steepness roughly 3 times the initial steepness of the wavetrain. For narrow band waves centered around the wave number k, the lowest order evolution equation accounting for both nonlinearity and dispersion is the Non-Linear Schroedinger equation (NLS). The surface elevation ζ can be represented as

$$\zeta = A(x,t)e^{i(kx-\omega(k)t)} + A_2(x,t)e^{i2(kx-\omega(k)t)} + ..c.c$$

and a similar expression for the velocity potential. Here the complex amplitude functions A and A_2 (of the first and second harmonic) are slowly varying in space and time compared to the wavelength and wave period. The ratio $A_2/A = O(\epsilon)$ where ϵ is a typical wave steepness. To lowest significant order the amplitude function A of the first harmonic satisfies the NLS equation

$$i(A_t + v_g A_x) - \frac{\omega}{8k^2} A_{xx} = \frac{\omega k^2}{2} A\,|A|^2$$

By the transformation to non-dimensional variables

$$x \to k(x - v_g t)$$
$$t \to \frac{1}{2}\omega t$$
$$A \to \frac{k^2}{\sqrt{2}\omega} A^*$$

this equation attains the canonical form

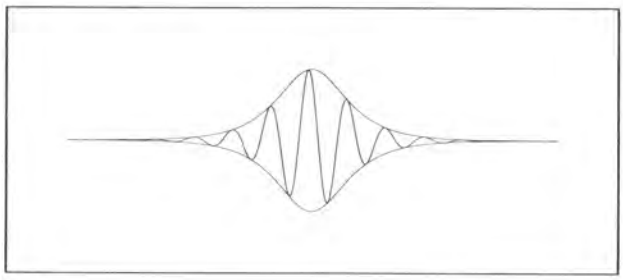

Fig. 3. Envelope soliton.

$$iA_t + A_{xx} + 2A|A|^2 = 0 \tag{3}$$

There are two types of solutions of (3) associated with a group of large waves. The first is the envelope soliton solution

$$\frac{e^{it}}{\cosh(x)}$$

whose first harmonic envelope $|A|$ does not change its form (see Figure 3). The second are the so-called breather solutions, a one parameter family of solutions that can be written

$$e^{2it}\frac{\cosh(\Omega t - 2i\varphi) - \cos\varphi\cos(px)}{\cosh(\Omega t) - \cos\varphi\cos(px)} \tag{4}$$

where

$$p = 2\sin\varphi \qquad \text{and} \qquad \Omega = 2\sin(2\varphi)$$

For real φ the solution is space-periodic. It evolves from a nearly uniform wavetrain to space-periodic soliton-like groups, and back to a uniform wavetrain.

For imaginary φ the solution (4) is time-periodic, "breathing" itself up from a nearly uniform wavetrain to a soliton-like group and back to a uniform wavetrain during one period (see [3] and the references therein).

As a limiting case for these two solutions (i.e. when $\varphi \to 0$) (4) tends to the Peregrine solution, [9],

$$e^{2it}\left[1 - \frac{4(1+4it)}{1+4x^2+16t^2}\right] \tag{5}$$

which is illustrated in Figure 4(a) and 4(b). In [5], ([3]) it is suggested that the SWE they observe in their simulations can be approximately modelled by this breather solution. A Peregrine type breather at its maximum is shown in Figure 5. Here the second order term A_2 is taken into account and the initial uniform

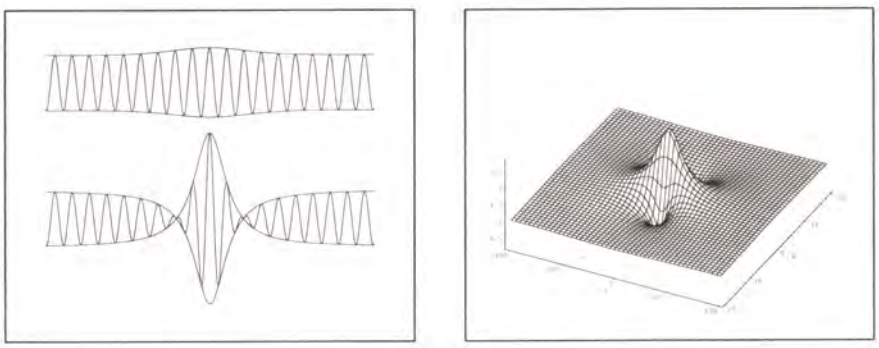

Fig. 4. (a) The Peregrine breather solution (equation (5)) at two different times. (b) Space-time illustration of the Peregrine breather envelope.

wavetrain had a steepness of 0.12 . While the solution (5) is in the frame of reference moving with the group velocity, Figure 5 is a breather "time-series" as it would have been observed by buoys at three slightly different horizontal locations (the envelope of the first harmonic is also shown).

It was shown in [1] that if the bandwidth exceeds some small critical value, there is no BF instability. The natural wind wave spectra seems to always exceed this critical value. Thus the nonlinear focussing as described by Henderson et. al., [5], is not likely to work. This does not mean, however, that the form and dynamics of the SWE they observe may not have a close relation to the rogue wave phenomena.

Thus it seems that all the above mechanisms for producing large waves need some special preparation or coherence to work.

Does this leave us with the old idea that the rogue waves are simple (and unlikely) constructive interference phenomena that can be explained by linear- or slightly (second order) nonlinear theory? This seems to be a rather popular assumption, and serves as a basis for the statistical estimates.

Another possibility, however, is that weak (third order) nonlinear wave interactions may play a role. Although these interactions are slow they are known to produce large waves under special conditions. The correlation they introduces between the interacting waves may change the probability of constructive interference.

I think it is fair to say that nobody knows the answer to these questions yet. To test this latter idea, a project funded by The Norwegian Research Council is presently starting up. The idea is to simulate a piece of the ocean surface of dimensions approximately 100x100 wavelengths. Starting with a wave field based on a suitably truncated empirical spectrum (like JONSWAP) we will use the numerical model described in [15] to follow the evolution of the wave field.

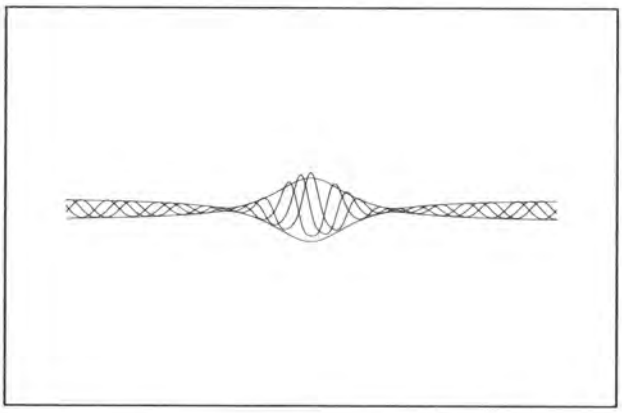

Fig. 5. Time series of a passing Peregrine breather from three slightly different horizontal locations. Here the full second order expression for the elevation ζ is used. Also shown is the first harmonic envelope. The steepness of the initial wavetrain is 0.12.

The probability of seeing a freak wave event in a simulation is estimated to be more than 10^4 times higher than for a corresponding point measurement (buoy) over the same period of time.

References

1. Alber, I.E. : The effect of randomness on the stability of two-dimensional surface wave trains. Proc.Roy.Soc. A 363 (1978) 528
2. Boccotti, P.: On the highest waves in a stationary Gaussian process. Atti.Acc.Lig. 38 (1981) 45-73
3. Dysthe, K.B. and Trulsen, K.: Note on breather type solutions of the NLS as model for freak waves. Phys.Scripta T82 (1999) 48-52
4. Dysthe, K.B.: Refraction of gravity waves by weak current gradients. Submitted to J.Fluid Mech.
5. Henderson, K.L., Peregrine, D.H. and Dold, J.W.: Unsteady water wave modulations: fully nonlinear solutions and comparison with the NLS equation. Wave Motion 29 (1999) 341-361
6. Kjeldsen, S.P. : Dangerous wave groups. Norvegian Maritime Reseach. 12 (1984) 4-16
7. Lavrenov, I.: The wave energy concentration at the Agulhas current of South Africa. Nat. Hazards 17 (1998) 117-127
8. Magnusson, A.K., Donelan, M.A. and Drennan, W.M.: On estimating extremes in an evolving wavefield. Coastal Engineering 36 (1999) 147-163
9. Peregrine, D.H.: J. Austral. Math. Soc. Ser.B 25, (1983)
10. Pelinovsky, E., Talipova, T. and Kharif, C.: Physica D 145 (2000) 83-94

11. Phillips, O.M., Gu, D. and Donelan, M.: Expected structure of extreme waves in a Gaussian sea. Part I: Theory and SWADE buoy measurements. J.Phys.Oceanogr. 23 (1993) 992-1000
12. Sand, S.E., Hansen, N.E.O., Klinting, P., Gudmestad, O.T. and Sterndorff, M.J.: Freak wave kinematics. Water Wave Kinematics. (Eds. A. Torum and O.T. Gudmestad) (1989) 535-549
13. Skourup, J., Andreasen, K.K. and Hansen, N.E.O.: Non-Gaussian extreme waves in the central North Sea. 1996 OMAE, Vol I, part A, Offshore Technology, ASME (1996)
14. Trulsen, G.N., Dysthe, K.B. and Trulsen J.: Evolution of a gravity wave spectrum through a current gradient. J.Geophys.Res. 95 (1990) 22141-22151
15. Trulsen, K., Kliakhandler, I., Dysthe, K.B. and Velarde, M.G.: On weakly nonlinear modulation of waves on deep water. Phys.Fluids 12 (2000) 2432-2437
16. Tung and Huang, N.: Peak and trough distributions of nonlinear waves. Ocean Engng. 12 (1985) 201-209
17. Warren, S.J., Bole, J.B. and Driver, D.B.: Measured wave crest distributions in central and southern North Sea storms. Proc. of the 8th International Offshore and Polar Engeneering Conference (1998)
18. White, B.S. and Fornberg, B.: On the chance of freak waves at sea. J.Fluid Mech. 355 (1998) 113-138

Appendix

We shall now consider angular diffusion of rays moving through a random eddy field. For simplicity we shall assume this vorticity field ζ to be statistically homogeneous and isotropic with zero mean.

We denote by $\Delta\theta$ the angular change of direction over an arclength s of the ray path from some reference starting point. From the formula (1) we have to order ϵ

$$\Delta\theta = \frac{1}{v_g}\int_0^s \zeta(\mathbf{x}(s'))ds'$$

It follows that

$$\langle \Delta\theta^2 \rangle = \frac{1}{v_g^2}\int_0^s \int_0^s \langle \zeta(\mathbf{x}(s'))\zeta(\mathbf{x}(s'')) \rangle \, ds'ds''$$

and by the assumption of homogeneity and isotropy we have

$$\langle \Delta\theta^2 \rangle = \frac{\langle \zeta^2 \rangle}{v_g^2}\int_0^s \int_0^s R(|\mathbf{x}(s')-\mathbf{x}(s'')|)ds'ds'' \tag{6}$$

where the normalized vorticity auto-correlation function R is given by

$$R(|\mathbf{x}-\mathbf{y}|) = \frac{\langle \zeta(\mathbf{x})\zeta(\mathbf{y}) \rangle}{\langle \zeta^2 \rangle}$$

Let L be a characteristic correlation distance for ζ, i.e. $R(|\mathbf{x}-\mathbf{y}|)$ is small when $|\mathbf{x}-\mathbf{y}| > L$. If we assume that $\varkappa L << 1$, then the ray $\mathbf{x}(s)$ can be

approximated by a straight line in the integral (6). Doing this we obtain for $s >> L$

$$\langle \Delta\theta^2 \rangle = \frac{\langle \zeta^2 \rangle}{v_g^2} \int_0^s \int_0^s R(|s' - s''|) ds' ds''$$
$$\cong 2 \frac{\langle \zeta^2 \rangle}{v_g^2} \int_0^\infty R(x)(s - x) dx \cong 2s \frac{\langle \zeta^2 \rangle}{v_g^2} \int_0^\infty R(x) dx \equiv 4Ds$$

where D is the diffusion coefficient of angular diffusion given by

$$D = \frac{1}{2} \frac{\langle \zeta^2 \rangle}{v_g^2} L_{int}$$

and L_{int} is the integral lengthscale

$$L_{int} = \int_0^\infty R(x) dx$$

Simulating the Spatial Evolution of a Measured Time Series of a Freak Wave

Karsten Trulsen

SINTEF Applied Mathematics, P.O.Box 124 Blindern
N-0314 Oslo, Norway
Karsten.Trulsen@math.sintef.no, http://www.math.sintef.no/

Abstract. The measured time history of the "New Year" freak wave that hit the "Draupner" platform is simulated forward and backward in space to find the time histories at neighboring locations. The impression that could have been seen by an observer is reconstructed. The freak wave likely did not suddenly appear from nowhere. Instead, the simulation suggests that a short and tall wave group approached the platform for at least a minute or so.

1 Introduction

In many cases it is more useful to perform space-domain simulation than time-domain simulation. Conventional methods for quantitative field observations usually yield time series of the surface displacement at one or a few selected locations. Spatial evolution is implied between the selected locations, or between the instrumented locations and other locations of interest. A time-domain simulation tool would likely not be very useful for application to such data, or at best it would be quite difficult to initialize since knowledge of the entire sea surface at initial time is not known. A better approach is to interchange the role of space and time in the evolution equations in order to obtain a space-domain simulator; initialization with the measured time history at a point then becomes trivial.

We have cast the modified nonlinear Schrödinger equation as a space domain simulator, and have "initialized" it with the measured time series of the freak wave that hit the Statoil operated "Draupner" platform, January 1, 1995 at 15:20. Figure 1 shows a 20 minute wave recording measured by a down-looking laser device (see [2]). The measured response of the platform was found to be unidirectional ([3]), therefore it is reasonable to assume that the waves were long-crested. The sea floor is flat at 70 m depth.

The desired model should obey the empirical scaling laws that are observed in the field. We have earlier reported [10] that characteristic values for steepness and bandwidth for this wave train is $k_c a_c \sim 0.12$, $\Delta\omega/\omega_c \sim 0.24$ and $\Delta k/k_c \sim 0.4$, where k_c, a_c, ω_c, $\Delta\omega$ and Δk are the characteristic wavenumber, amplitude, frequency, modulation frequency and modulation wavenumber, respectively. Therefore, we have previously argued that the modulation should be

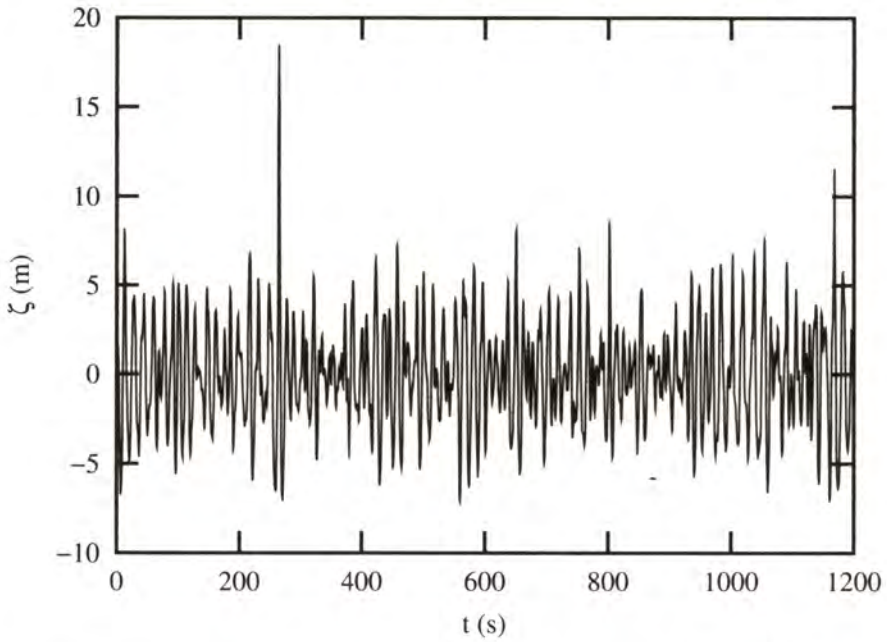

Fig. 1. Freak wave measured at the Statoil Draupner platform, January 1, 1995 at 15:20.

scaled as the square root of the steepness; we thus derived a modified nonlinear Schrödinger equation for this purpose [9]. Recently, we have further taken the consequence of the importance of linear dispersion by enhancing the modified nonlinear Schrödinger equation with exact linear dispersion, [11]. Our approach is based on the assumption that the spectrum to leading order of approximation is narrow-banded. The remaining part of the spectrum is reconstructed only to the extent that it is nonlinearly forced by, and thus coherent with, the linear waves near the spectral peak. Special care must be taken for proper initialization to distinguish between linear free waves and nonlinearly forced waves. To this end we have developed an iterative technique by which the extracted spectrum of linear free waves is refined until exact reconstruction of the most energetic part of the measured complex spectrum has been achieved.

Early attempts to simulate the ocean surface in two horizontal dimensions with the nonlinear Schrödinger equation were only partially successful due to energy leakage that broadened an initially narrow spectrum such that the model eventually violated its own bandwidth constraint, [6]. The higher-order modified nonlinear Schrödinger equation reduced the leakage such that 2D simulations became feasible. As of the new equation with exact linear dispersion, the leakage is completely eliminated, [11]. Numerical integration can be done as efficiently as for the conventional nonlinear Schrödinger equation through operator splitting

methods. In this paper we limit consideration to simulation in one horizontal dimension.

The natural spatial scale of nonlinear modulation is $\eta = \epsilon^2 k_c x$, where $\epsilon = k_c a_c$ is the wave steepness, k_c and a_c are characteristic scales for wavenumber and amplitude, and x is the fetch. Results presented elsewhere [12] comparing simulations with laboratory experiments suggest that the modified nonlinear Schrödinger equation predicts the evolution of individual wave crests quite well at least up to $\eta = 3$, while it becomes poor for $\eta > 5$. In the present paper we present simulations over 500 m, which corresponds to $\eta = 0.26$.

In [5] Lo & Meifirst presented comparisons between experiments and the space evolution predicted by the modified nonlinear Schrödinger equation, and obtained good results. Similar work with the cubic nonlinear Schrödinger equation was done by Shemer et al. [8] for deep water and with the Korteweg de-Vries equation for shallow water by Kit et al. [4]. The Zakharov equation, which in its original form is a time-domain equation, has been discretized for application to measurements, [7]); it can likely be cast as a space domain simulator and be used for the same purpose as in the present paper.

2 Mathematical Model for Space-Domain Simulation

Starting from the inviscid equations for potential flow, normalized with the characteristic wavenumber k_c and frequency ω_c, we make an assumption that the velocity potential ϕ and surface displacement ζ of the wave field can be expanded in harmonic expansions

$$\phi = \bar{\phi} + \frac{1}{2}\left(A\mathrm{e}^{\mathrm{i}(x-t)+z} + A_2\mathrm{e}^{2\mathrm{i}(x-t)+2z} + A_3\mathrm{e}^{3\mathrm{i}(x-t)+3z} + \cdots + \text{c.c.}\right), \quad (1)$$

$$\zeta = \bar{\zeta} + \frac{1}{2}\left(B\mathrm{e}^{\mathrm{i}(x-t)} + B_2\mathrm{e}^{2\mathrm{i}(x-t)} + B_3\mathrm{e}^{3\mathrm{i}(x-t)} + \cdots + \text{c.c.}\right). \quad (2)$$

Here x and y are horizontal coordinates, z is the vertical coordinate, t is time, $\bar{\phi}$ and $\bar{\zeta}$ are the mean fields (zeroth harmonic), A and B are the linear first harmonics, and A_n and B_n are the higher order nonlinear harmonics. We limit consideration to a constant depth h and assume that the linear dispersion relation can be approximated by the deep water assumption, while the induced flow will be affected by the depth.

Trulsen et al. ([11]) enhanced the modified nonlinear Schrödinger equation with exact linear dispersion by introducing a pseudo-differential operator for the linear part. In two horizontal dimensions it reads

$$\frac{\partial B}{\partial t} + L(\partial_x, \partial_y)B + \frac{\mathrm{i}}{2}|B|^2 B + \frac{3}{2}|B|^2\frac{\partial B}{\partial x} + \frac{1}{4}B^2\frac{\partial B^*}{\partial x} + \mathrm{i}\frac{\partial \bar{\phi}}{\partial x}B = 0 \quad \text{at} \quad z = 0, \quad (3)$$

$$\frac{\partial \bar{\phi}}{\partial z} = \frac{1}{2}\frac{\partial}{\partial x}|B|^2 \quad \text{at} \quad z = 0, \quad (4)$$

$$\nabla^2\bar{\phi} = 0 \quad \text{for} \quad -h < z < 0, \quad (5)$$

$$\frac{\partial \bar{\phi}}{\partial z} = 0 \quad \text{at} \quad z = -h. \tag{6}$$

The pseudo-differential operator L is

$$L(\partial_x, \partial_y) = \mathrm{i}\left\{\left[(1 - \mathrm{i}\partial_x)^2 - \partial_y^2\right]^{1/4} - 1\right\}. \tag{7}$$

These equations can be inverted with respect to space and time to yield a space-domain formulation

$$\frac{\partial B}{\partial x} + \mathcal{L}(\partial_t, \partial_y)B + \mathrm{i}|B|^2 B - 8|B|^2 \frac{\partial B}{\partial t} - 2B^2 \frac{\partial B^*}{\partial t} - 4\mathrm{i}\frac{\partial \bar{\phi}}{\partial t} B = 0 \quad \text{at} \quad z = 0, \tag{8}$$

$$\frac{\partial \bar{\phi}}{\partial z} = -\frac{\partial}{\partial t}|B|^2 \quad \text{at} \quad z = 0, \tag{9}$$

$$4\frac{\partial^2 \bar{\phi}}{\partial t^2} + \frac{\partial^2 \bar{\phi}}{\partial y^2} + \frac{\partial^2 \bar{\phi}}{\partial z^2} = 0 \quad \text{for} \quad -h < z < 0, \tag{10}$$

$$\frac{\partial \bar{\phi}}{\partial z} = 0 \quad \text{at} \quad z = -h. \tag{11}$$

Here we have used the fact that $\partial\bar{\phi}/\partial x = -2\partial\bar{\phi}/\partial t$ to the leading order. The pseudo-differential operator becomes

$$\mathcal{L}(\partial_t, \partial_y) = -\mathrm{i}\left\{\left[(1 + \mathrm{i}\partial_t)^4 + \partial_y^2\right]^{1/2} - 1\right\}. \tag{12}$$

By expanding the linear pseudo-differential operators L or $\mathcal{L}$ in power series expansions and truncating at appropriate orders, we recover the previous modified nonlinear Schrödinger equation of Dysthe ([1]) and the broader bandwidth equation of Trulsen & Dysthe ([9]). Furthermore by truncating the nonlinear part to retain only the leading cubic nonlinear term, we recover the standard cubic nonlinear Schrödinger equation.

The reconstruction of the surface displacement (2) is achieved by the formulas

$$\bar{\zeta} = -\frac{\partial \bar{\phi}}{\partial t}, \tag{13}$$

$$B_2 = \frac{1}{2}B^2 + \mathrm{i}B\frac{\partial B}{\partial t}, \tag{14}$$

and

$$B_3 = \frac{3}{8}B^3. \tag{15}$$

3 Initialization

The complex spectrum of the first harmonic B is first tentatively assigned by bandpassing the most energetic part of the desired complex spectrum of ζ. Then the first harmonic B is adjusted in an iterative manner until the desired spectrum of ζ is exactly reconstructed within the bandpass part of the frequency domain.

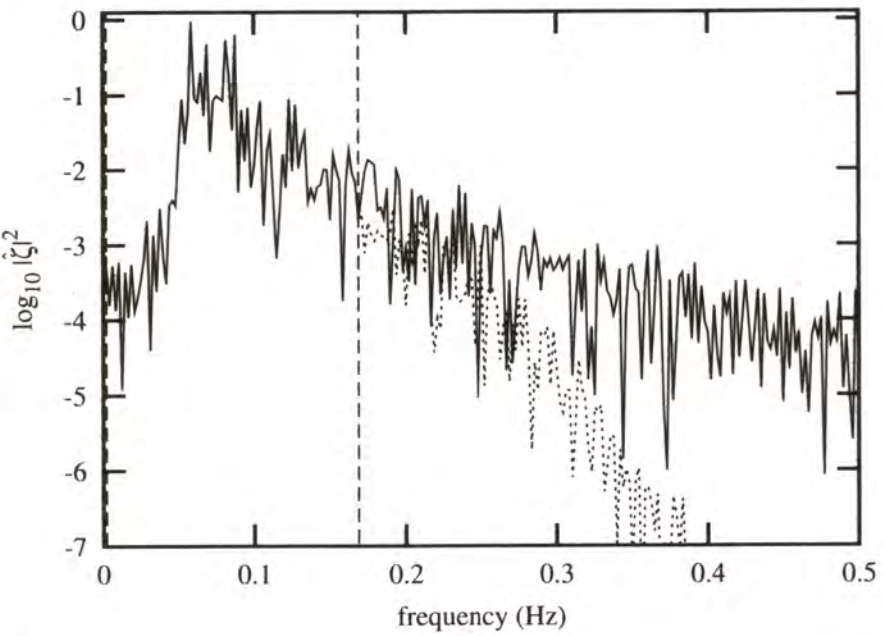

Fig. 2. Power spectrum: —, measured; ···, reconstructed. The vertical dashed lines indicate the bandpass filter used to define the domain of the first harmonic.

Figure 2 shows the measured and the reconstructed power spectrum of the surface displacement ζ. The full complex spectrum is reconstructed exactly within the bandpass region bounded by the vertical dashed lines (the figure only shows the reconstruction of the power spectrum). The reconstruction of the high frequency tail includes contributions that are coherent with the energetic part near the peak. The mismatch in reconstruction in the tail is to a large extent due to uncorrelated noise and incoherent waves, which are assumed to be unimportant for the evolution of the main features of the wave train.

The reconstruction of the freak wave is compared with the desired surface displacement in figure 3. The consequence of the mismatch in the spectrum seen in the previous figure is that the most rapid wave disturbances are smoothed out.

4 Forward and Backward Propagation in Space

The predicted time histories at 50 meter intervals upstream and downstream are shown in figures 4 and 5, respectively. At 500 m upstream of "Draupner" there appears to be a large wave group passing by about one minute before the freak wave hits the platform. This wave group appears to split up into a short and large leading group that runs away from a longer and smaller trailing group

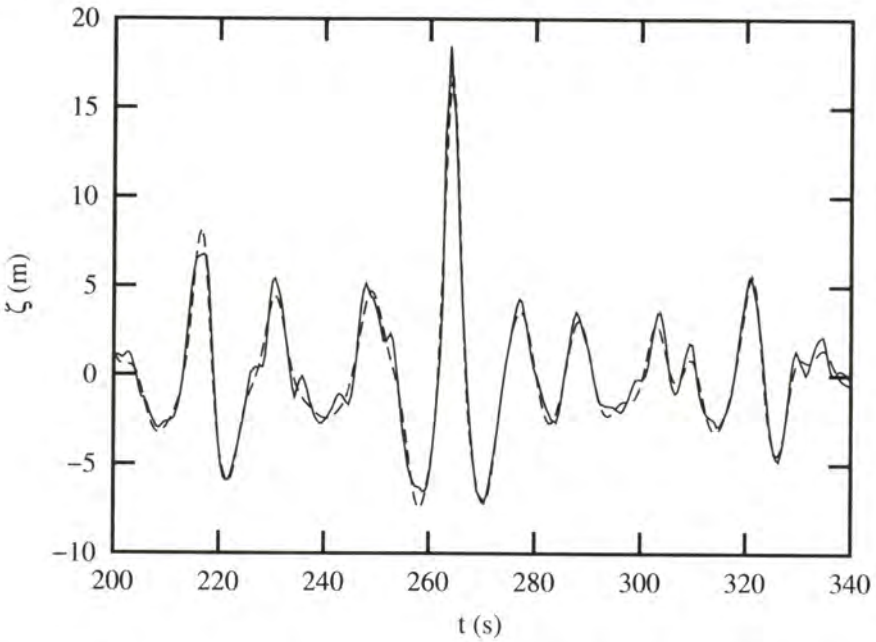

Fig. 3. Measured (—) and reconstructed (- - -) surface displacement.

that becomes rather diffuse as it approaches the platform. The freak wave that hits the platform is in the middle of the short leading group. After the impact with the platform, this wave group broadens, becomes less steep, and slows down slightly. A large trough (a "hole" in the ocean) can be observed slightly upstream of the platform.

Since the platform is of jacket type, it is not expected to have modified the waves.

5 Conclusion

We have presented a model for weakly nonlinear spatial evolution of waves, and have shown how a measured time history of a freak wave can be used for initialization and be propagated forward and backward in space.

As far as the "New Year" freak wave that hit "Draupner" is concerned, the most important conclusion is probably that it did not occur suddenly and unexpectedly. There is rather reason to believe that large waves approached the platform for at least a minute or so, and would likely have been an impressive view for a daring observer.

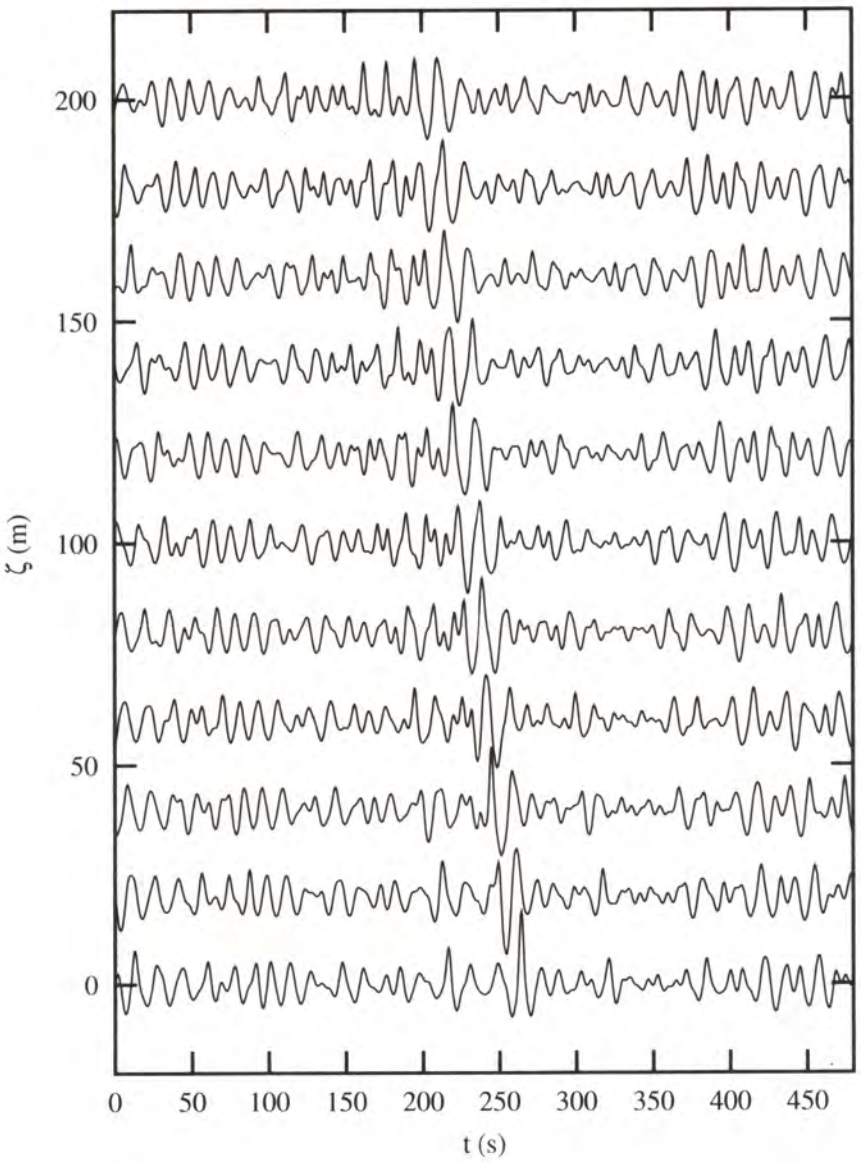

Fig. 4. Time histories at 50 meters intervals upstream (bottom to top).

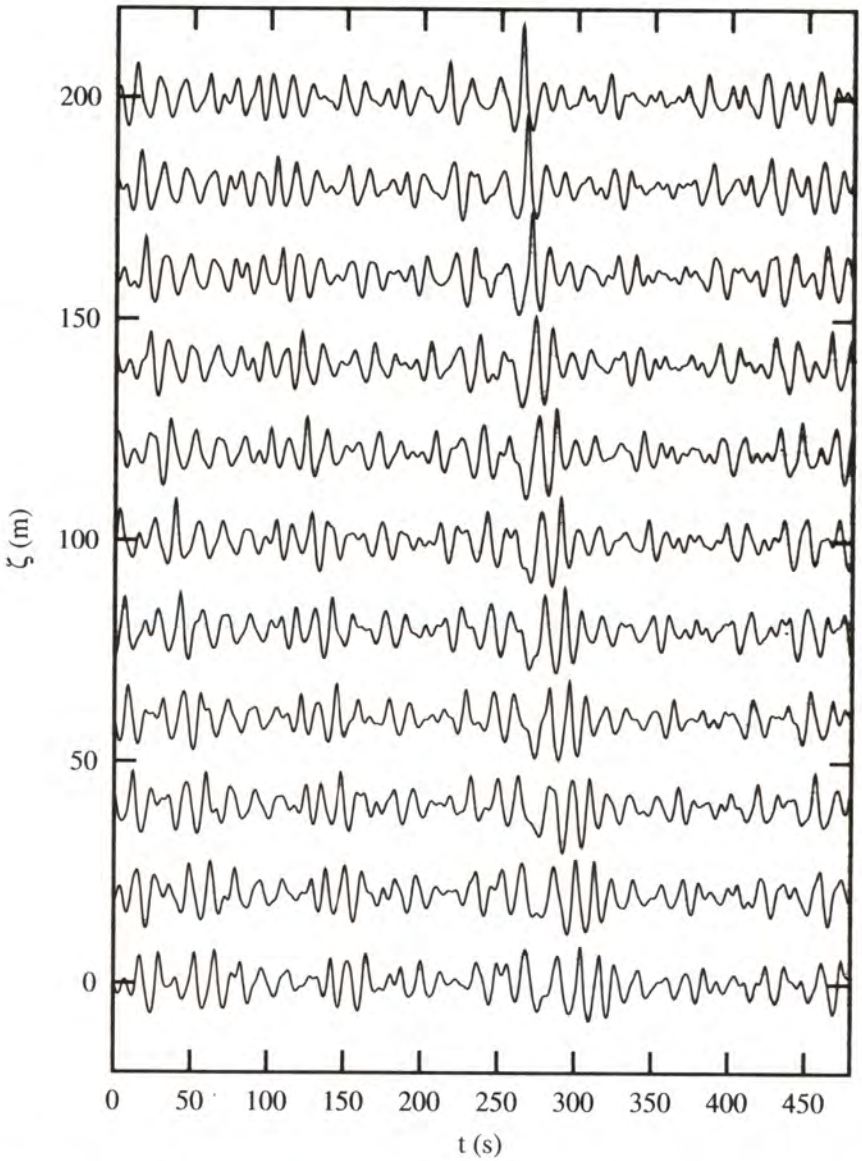

Fig. 5. Time histories at 50 meters intervals downstream (top to bottom).

6 Acknowledgments

This work has been supported by the Norwegian Research Council through the project "Modeling of extreme ocean waves and ocean wave climate on mesoscale" (139177/431). The data was made available from Statoil.

References

1. Dysthe, K. B.: Note on a modification to the nonlinear Schrödinger equation for application to deep water waves. Proc. R. Soc. Lond. A, **369** (1979) 105–114
2. Haver, S. & Andersen, O. J.: Freak waves: Rare realizations of a typical population or typical realizations of a rare population? In Proc. 10th International Offshore and Polar Engineering Conference, volume III (2000) 123–130
3. Karunakaran, D., Bærheim, M., & Leira, B. J.: Measured and simulated dynamic response of a jacket platform. In C. Guedes-Soares, M. Arai, A. Naess, & N. Shetty (Eds.): Proceedings of the 16th International Conference on Offshore Mechanics and Arctic Engineering, ASME, volume II (1997) 157–164
4. Kit, E., Shemer, L., Pelinovsky, E., Talipova, T., Eitan, O., & Jiao, H.-Y.: Nonlinear wave group evolution in shallow water. J. Waterway, Port, Coastal and Ocean Engineering, **126** (2000) 221–228
5. Lo, E. & Mei, C. C.: A numerical study of water-wave modulation based on a higher-order nonlinear Schrödinger equation. J. Fluid Mech., **150** (1985) 395–416
6. Martin, D. U. & Yuen, H. C.: Quasi-recurring energy leakage in the two-space-dimensional nonlinear Schrödinger equation. Phys. Fluids, **23** (1980) 881–883
7. Rasmussen, J. H. & Stiassnie, M.: Discretization of Zakharov's equation. Eur. J. Mech. B/Fluids, **18** (1999) 353–364
8. Shemer, L., Kit, E., Jiao, H.-Y., & Eitan, O.: Experiments on nonlinear wave groups in intermediate water depth. J. Waterway, Port, Coastal and Ocean Engineering, **124** (1998) 320–327
9. Trulsen, K. & Dysthe, K. B.: A modified nonlinear Schrödinger equation for broader bandwidth gravity waves on deep water. Wave Motion, **24** (1996) 281–289
10. Trulsen, K. & Dysthe, K. B.: Freak waves — a three-dimensional wave simulation. In Proceedings of the 21st Symposium on Naval Hydrodynamics, National Academy Press (1997) 550–560
11. Trulsen, K., Kliakhandler, I., Dysthe, K. B., & Velarde, M. G.: On weakly nonlinear modulation of waves on deep water. Phys. Fluids, **12** (2000) 2432–2437
12. Trulsen, K. & Stansberg, C. T.: Spatial evolution of water surface waves: Numerical simulation and experiment of bichromatic waves. In Proc. 11th International Offshore and Polar Engineering Conference (2001)(submitted)

Evolution of Three-Dimensional Unsteady Wave Modulations

Carlo Brandini[1] and Stéphan Grilli[2]

[1] Dipartimento di Ingegneria Civile, Università degli Studi di Firenze
Via di Santa Marta 3, 50139 Firenze (Italy)
brandini@dicea.unifi.it
[2] Ocean Engineering Department, University of Rhode Island
Narragansett, RI 02882, USA
grilli@oce.uri.edu
http://www.oce.uri.edu/~grilli

Abstract. A numerical investigation of nonlinear interaction mechanisms producing large wave energy concentrations, which lead to episodic transient waves, is performed using both a Higher Order Spectral (HOS) model and a three-dimensional (3D) fully nonlinear Numerical Wave Tank (NWT). Self-focusing of wave energy is achieved through modulating a periodic wave train along two orthogonal directions. Nonlinear unsteady 3D wave groups are obtained, which show a curved wavefront structure, with focusing of wave energy in both the directional and the frequency domains. Breaking would ultimately occur in such groups. This, however, cannot be described by the HOS model but, based on the HOS solution, both breaking and non-breaking freak waves may be simulated in the NWT, and their shape and kinematics can be studied.

1 Introduction

A number of attempts have been reported in the literature to produce freak waves by nonlinear self-modulation of a two-dimensional slowly modulating wave train. Both solutions based on the (weakly) nonlinear Schrödinger equation (NLS), or its modifications [4], and numerical models solving fully nonlinear free surface flows, have been proposed [5, 17]. Freak waves have been observed to be essentially three-dimensional (3D) phenomena. McLean [8] theoretically predicted a type of wave instability (called type II), which is predominantly 3D, in contrast with the 2D instability (type I; i.e., the side-band instability) identified by Benjamin and Feir (BF) [7], which leads to the formation of wave groups in quasi-2D swells, through a self-focusing mechanism. Su *et al.* [10] experimentally confirmed this prediction by showing how a steep 2D wave train can evolve into 3D spilling breakers. Hence, 3D modulational instabilities cannot be neglected when describing the steepest ocean waves. Two-dimensional nonlinear wave instabilities have been simulated in a few numerical studies, by slow self-modulations of a 2D periodic wave train (Dysthe and Trulsen [4]; Henderson *et al.*, [5]). In such studies, an initially periodic wave train of moderate steepness

is perturbed by a small periodic perturbation. After a large time of propagation (typically over 100 wave periods), it is observed that a large steep wave, i.e., a freak wave, may emerge from the initial wave train, and break or recede and periodically reappear. In these studies, 3D effects were not usually addressed because, either it was not possible to generalize the method of solution to 3D, or the computational effort in a 3D model was too high. Nevertheless directional effects are of prime importance. Breaking may occur, when waves reach a sufficient size, at some stage of the modulation. Nepf *et al.* [14], for instance, experimentally showed that curved wave fronts lead to 3D breaking in ocean waves, and that the shape and kinematics of 3D breaking waves greatly differ from those of two-dimensional (2D) breakers (see also She *et al.* [15]; and Johannessen and Swan [19]). The degree of angular spreading is found to have large effects on wave breaking characteristics and kinematics, and non directional wave theories are demonstrated to be insufficient to describe the kinematics of 3D waves.

Since many extreme (freak) waves are expected (and have been observed) to be 3D, modulational instabilities occurring in three dimensions cannot be neglected when describing the steepest waves.

2 Three-dimensional modulations

The computationally efficient Higher Order Spectral (HOS) method [17, 18] is used in the present computations, assuming doubly periodic boundary conditions in the computational domain. Extreme waves are produced through the evolution of 3D wavetrains subjected to both longitudinal and lateral modulations. Modulations of this type are characterized by the initial steepness of the wave train (ak), and by two characteristic wavelengths, for the longitudinal and transverse modulations, respectively.

A transverse modulation is superimposed to the longitudinal one. For the free surface elevation, this leads to expressions of the form,

$$\eta_p = 2\mu\,(ka)\cos\left(2\pi\frac{y'}{\lambda_y}\right)\cos\left(2\pi\frac{x'}{\lambda_x}\right)\cos\left(kx-\omega t\right) \tag{1}$$

where a is the wave amplitude, k the wavenumber, ω the circular frequency of the initial 2D wave train (which, here, for sake of illustration, is simply sinusoidal), and λ_x and λ_y are the longitudinal and transverse wavelengths of the perturbations, respectively (in terms of the longitudinal wavelength $\lambda = 2\pi/k$ of the initial 2D wavetrain; dashes indicate nondimensional variables).

A systematic study of such kinds of modulations, would require, for each wave steepness, the evaluation of the influence of both the longitudinal and the transverse wavelengths, on the evolution of initially slowly modulated wavetrains.

The evolution of a modulated wavetrain having $ak = 0.14$, $\lambda_x = 5$ and $\lambda_y = 10$ (hence with a lateral modulational wavelength that is two times the longitudinal one) is described in Figs. 1-4. The initial regime shown in Fig. 1 is composed of nearly uniform Stokes waves. At these early stages of the evolution, waves are essentially 2D while, at later stages, the growth of transverse

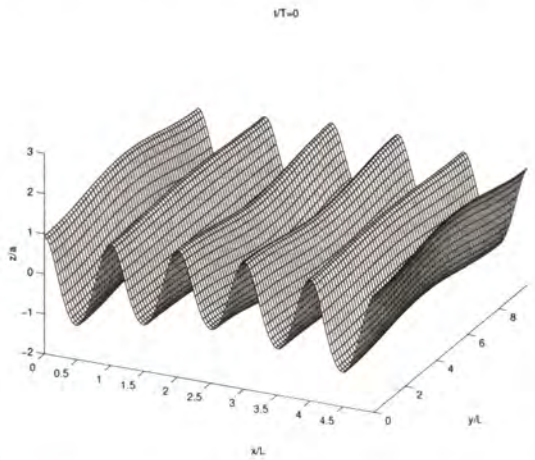

Fig. 1. Initial condition for a 3D wave train modulated in both the longitudinal and the transverse direction

perturbations causes a 3D structure to develop. At final stages of evolution, both a longitudinal and a transverse growth of modulations are observed. Fig. 2, for instance, shows the evolution of the wavetrain at time $t/T = 90$. This evolution results from the combination of two effects :

1. In the longitudinal direction a BF-like mechanism causes the wave group to shorten ahead and to lengthen behind, with a wave energy concentration in the middle of the wave envelope.
2. In the lateral direction the growth of transverse perturbations affects the highest wave and its first predecessor. Lateral features in the form of standing waves across the (periodic) wavetank appear.

The combination of these two effects gives rise to a fully three-dimensional structure of the wave group. Fig. 3 shows the evolution after just one more wave period, hence at time $t/T = 91$; we see that a large crest elevation is produced. This clarifies the evolution as a truly directional self-focusing process. The 3D structure of this doubly modulated wave is more evident in planview (Fig. 4), where an identical wavefield has been placed at one of the lateral sides (this is possible because of the lateral periodicity assumed for the computational domain). The appearance of curved wave fronts is an important feature of such 3D waves. These wave groups, as shown in Figs. 2-4, are also characterized by skewed wave patterns that qualitatively agree with Su's experiments. In particular :

1. The system of oblique wave groups, which is seen to radiate symmetrically from the primary wave direction, seems similar to that observed in the experiments. The angle, locally measured in these oblique wave fronts, approaches the 30^o value which was found experimentally.
2. A shifting of the lateral wave forms between two consecutive rows.

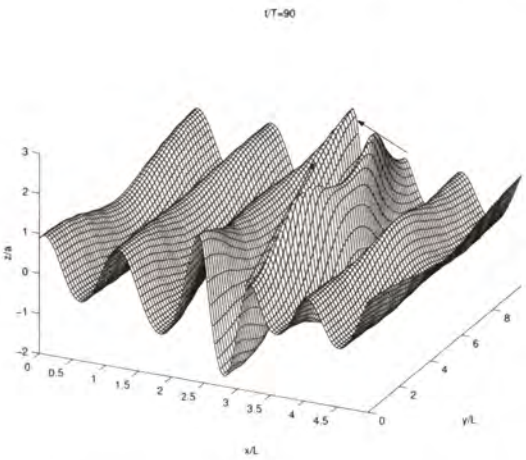

Fig. 2. Evolution of the wave train in Fig. 1 after $t/T = 90$

Our interpretation of these observations is that the BF-like mechanism produces a short wave group of increasing height and steepness, and it is within such a group that the lateral instability manifests itself, if the modulational wavelength in the lateral direction is long enough. For instance, the evolution of a modulated wavetrain having the same initial steepness $ak = 0.14$ and $\lambda_x = 5$ $\lambda_y = 4$ (so that the lateral modulational wavelength is only 0.8 times the longitudinal one) is shown in Fig. 5. In this case, only the longitudinal modulation grows according to a classical BF modulational mechanism. More details can be found in [3].

The growth of perturbations leads, for the steepest initial waves, to a rapid development of high wavenumber instabilities. A few time steps later, the model fails to converge. Using the HOS method, it is not possible to conclude whether this would be a case leading to wave breaking, but the range of wave steepness over which such numerical instabilities occur is consistent with typical values of steepness, relative to the occurrence of spilling breakers observed in laboratory experiments ($ak > 0.25$).

To be able to follow the evolution of this system further in time, after numerical breaking occurs, an ideal filter, removing all high frequency components and producing a loss of energy, has been applied. In this case, the loss of one or two wave crests may occur after the wavetrain has reached the maximum stage of modulations. This effect is the equivalent of the downshifting observed in physical experiments. A similar tendency to lateral energy transfer is also reported by Trulsen and Dysthe [11], who suggested that the full explanation of this downshift probably involves the combined effects of 3D nonlinear modulations, dissipation, and wave breaking.

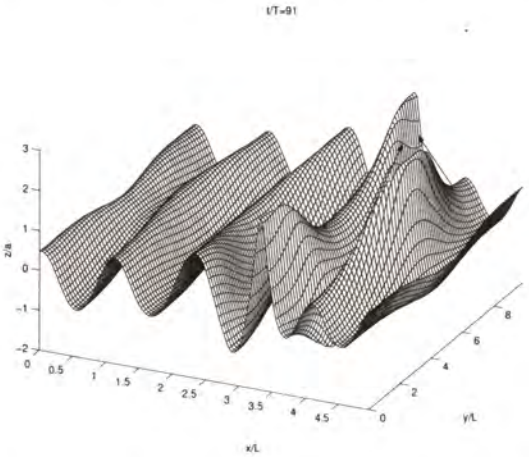

Fig. 3. Evolution of the wave train in Fig. 1 after $t/T = 91$

3 Three-dimensional breaking waves

The modulation growth observed in 3D modulations should be limited by wave breaking, which cannot be modeled using a method describing the free surface as single-valued, such as the HOS method. Breaking will not happen uniformly along a wave crest, and a 3D self-focused breaking wave is expected to appear at some stage of the modulation. A 3D fully nonlinear potential flow model, with an Eulerian-Lagrangian flow representation, recently developed by Grilli et al. [16], has been extended to represent 3D directional and wave focusing, including the additional possibility of frequency focusing such as studied in earlier 2D nonlinear models. To do so a "snake" wavemaker similar to those used in laboratory facilities is modeled at one extremity of a 3D Numerical Wave Tank (NWT), while a snake absorbing piston is modeled at the other extremity of the NWT to minimize the effect of wave reflection. Details can be found in [2]. In directional focusing, waves are focused in front of the wavemaker. For instance Fig. 5 shows an example of directional wave focusing where waves are focused at a distance $x_f = 2\lambda$ in front of the wavemaker. In Fig. 6 a case with more intense directional energy focusing is shown, producing a giant steep wave a short distance away from the wavemaker, whose crest is starting to break by spilling breaking.

Very large, possibly breaking (i.e., overturning), 3D transient waves could be modeled in this 3D-BEM model, by using the HOS method to compute the first stages of growth of wave modulations (the longer ones, on the order of 100 wave periods) as initial condition for the model. In this case the initial wave elevation and velocity potential are specified at time t on the free surface, based on the HOS solution. This will be the object of further studies.

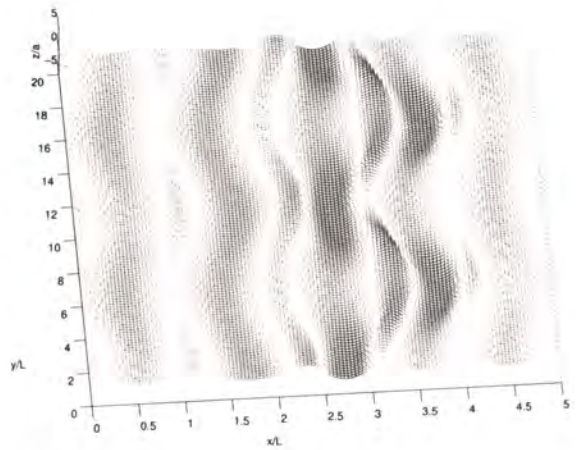

Fig. 4. Planview of the situation depicted in Fig. 3 clearly showing the appearance of curved wave fronts.

4 Conclusions

Three-dimensional self-focusing of wave energy is achieved through modulating a periodic wave train along two orthogonal directions. Both the well known Benjamin-Feir instability (essentially 2D) and 3D instability mechanisms are found to be important for describing the evolution of nonlinear waves. Nonlinear wave interactions produce an instability which transforms an initially two-dimensional wavetrain into a three-dimensional unsteady wave pattern, with short-crestedness in the lateral direction. When the transverse modulation wavelength is sufficiently large, one can observe the growth of the lateral modulation through the absorption of part of the longitudinal wave energy. The model not only predicts the initial stages of instability, but also the evolution of unsteady modulations of 3D finite amplitude waves in a fully nonlinear sense. Three dimensional effects lead to the natural formation of locally curved wave fronts which spread energy from the primary (longitudinal) motion to the secondary (transverse) one. This curved structure of 3D wave groups produces a self-focusing mechanism in both the directional and the frequency domain. Ultimately, this would lead to wave breaking, which cannot be described by the HOS model. However this 3D self-focusing case can be studied in the NWT, which has the capability of modeling both breaking and non-breaking freak waves. Such as study would be very difficult to achieve in a laboratory tank, due to the long distances of propagation required for both the 2D and 3D instabilities to grow.

References

1. Baldock, T.E., Swan, C.: Numerical calculations of large transient water waves. Applied Ocean Research **16** (1994) 101-112.

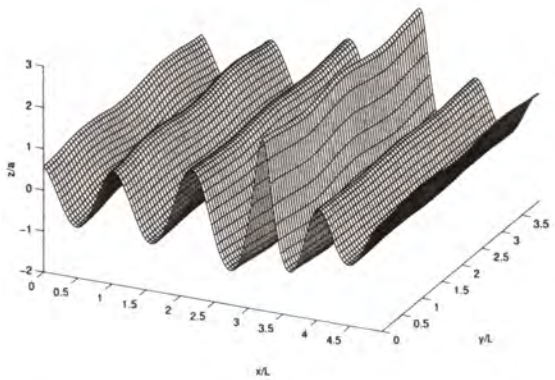

Fig. 5. Evolution of a 3D wave train ($ak = 0.14$, $\lambda_x = 5$, $\lambda_y = 4$) after $t/T = 90$. Note the differences with the corresponding evolution of the wavetrain ($ak = 0.14$, $\lambda_x = 5$, $\lambda_y = 10$ represented in Fig. 2, at the same stages

2. Brandini, C., Grilli, S.: Modeling of freak wave generation in a 3D-NWT. Submitted to 11th ISOPE Conf. (2001).
3. Brandini, C.: Nonlinear Interaction Processes in Extreme Wave Dynamics. Ph.D. Dissertation. University of Firenze (2001).
4. Dysthe, K.B., Trulsen, K.: Note on breather type solutions of the NLS as model for freak waves. Phys. Scripta. **T82** (1999) 45-73.
5. Henderson, K.L., Peregrine, D.H., Dold, J.W.: Unsteady water wave modulations: fully non linear solutions and comparison with the non linear Schrödinger equation. Wave motion **9** (1999) 341-361.
6. Trulsen, K., and Dysthe, K.B.: Freak waves: a 3D wave simulation. Proc. 21st Intl. Symp. on Naval Hydrodynamics. Trondheim, Norway. (1996) 550-558.
7. Benjamin, T.B., Feir, J.E.: The disintegration of wave trains on deep water. Part 1. Theory. J. Fluid Mech. **27** (1967) 417-430.
8. McLean, J.W.: Instabilities and breaking of finite amplitude waves I. J. Fluid Mech. **114** (1982ab) 315–341.
9. Su, M.Y., Bergin, M., Marler, P., Myrick, R.: Experiments on nonlinear instabilities and evolution of steep gravity-wave trains. J. Fluid Mech. **124** (1982) 45-72.
10. Su, M.Y.: Three-dimensional deep-water waves Part 1. Experimental measurements of skew and symmetric wave patterns. J. Fluid Mech. **124** (1982) 73-108.
11. Trulsen, K., and Dysthe, K.B.: Frequency downshift in three dimensional wave trains in deep basin. J. Fluid Mech. **352** (1997) 359-373.
12. Tulin, M.P., Waseda, T.: Laboratory observations of wave group evolution, including breaking effects. J. Fluid Mech. **378** (1999) 197-232.
13. Chaplin, J.R.: On frequency-focusing unidirectional waves. Intl. J. Offshore and Polar Engng. **6** (1996) 131-137.
14. Nepf, H.M., Wu, C.H., Chan, E.S.: A comparison of two- and three-dimensional wave breaking. Journal of Physical Oceanography. **28** (1998) 1496-1510.
15. She, K., Greated, C.A., Easson, W.J.: Experimental study of three-dimensional breaking wave kinematics. Applied Ocean Research. **19** (1997) 329-343.

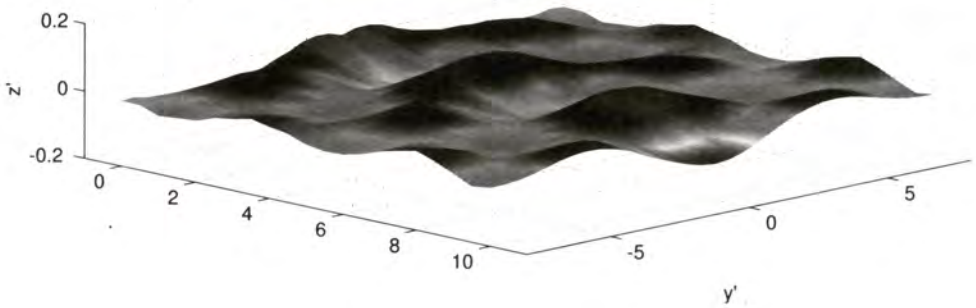

Fig. 6. Directional wave energy using a snake wavemaker in a 3D-NWT. Non breaking case

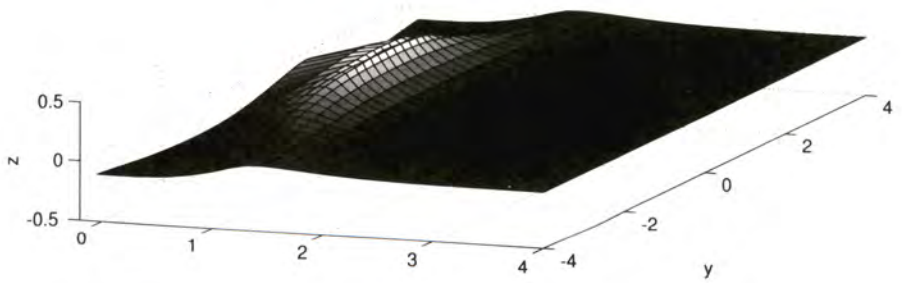

Fig. 7. Directional wave energy using a snake wavemaker in a 3D-NWT. Breaking case

16. Grilli, S.T., Guyenne, P. and Dias, F.: A fully nonlinear model for three-dimensional overturning waves over arbitrary bottom. Intl. J. Numer. Methods in Fluids. **34** (2001) 39 pps. (in press)
17. Dommermuth, D.G., Yue, D.K.P.: A higher-order spectral method for the study of non linear gravity waves. J. Fluid Mech. **184** (1987) 267-288.
18. West, B.J., Brueckner, K.A., Janda, R.S., Milder, D.M., Milton, R.L.: A new numerical method for surface hydrodynamics. J. Geophys. Res. **92** (1987) 11803-11824.
19. Johannessen, T.B., and Swan, C.: Extreme multi-directional waves. Proc. 26th Intl. Conf. Coast. Engng., ASCE, (1998) 1110-1123.

On the Use of Smoothed Particle Hydrodynamics to Model Breaking Waves and Their Interaction with a Structure

Emmanuel Fontaine

Institut Français du Pétrole, Division Mécanique Appliquée,
1 et 4 av. de Bois Préau, 92852 Rueil Malmaison. FRANCE.
Emmanuel.Fontaine@ifp.fr, http://www.ifp.fr

The evolution of wave groups in the ocean can be modeled with high accuracy using the classical Mixed Eulerian Lagrangian approach based on Boundary Element Method (see e.g. [1], [2]). Nevertheless, this method which relies on the fact that the flow is irrotationnal and the fluid is incompressible fails when breaking occurs. Indeed, as the jet re-enters the front face of the wave, vorticity is created in the fluid. To pursue the simulation, a suitable method should allow for (i) the modeling of rotational flow and, (ii) an easy treatment of discontinuities since the free surface experiences extremely large deformations. Among the different possibilities, the Smoothed Particle Hydrodynamics (SPH) method has been choosen by several authors [3], [4], [5].

The key concept of the method is to give a local approximation of a generic physical variable $f(\boldsymbol{x},t)$ in terms of the values $f_i(t)$ carried by a finite number of particles, i.e.

$$f(\boldsymbol{x},t) = \iint f(\boldsymbol{x}',t)\,\delta(\boldsymbol{x}-\boldsymbol{x}')\,ds \simeq \iint f(\boldsymbol{x}',t)\,W(\boldsymbol{x}-\boldsymbol{x}')\,ds \qquad (1)$$

$$\simeq \Sigma_j \frac{m_j}{\rho_j} f(\boldsymbol{x_j},t)\,W(\|\boldsymbol{x}_j-\boldsymbol{x}\|) \qquad (2)$$

where the smoothing kernel $W(\boldsymbol{x})$ is an approximation to the Dirac δ function, m_i and ρ_i are the mass and density of the fluid particle. Upon identifying f with the variables ρ and $\boldsymbol{U}$, Euler's equation reduces to a set of ODEs that are integrated with respect to time to give the evolution of the fluid dynamic system. Spatial derivatives of the quantities are obtained by differentiating eq. (2), i.e. using analytical kernel derivatives. The compact support of the kernel leads each particle to interact only with its close neighbors. Mass and momentum conservation are explicitly enforced by requiring each particle to have a constant mass and symmetric interactions between them, respectively. The pressure is computed by using the density and a suitable equation of state for water which is considered a weakly compressible fluid. Simulations are performed at a low Mach number (typically $M = 0.1$), leading to non essential perturbations in density during the simulation (typically of the order of $O(M^2) = 0.01$). As in most numerical methods, artificial viscosity is introduced to stabilize the scheme. Changes in the total energy, typically within a few percent, are representative of

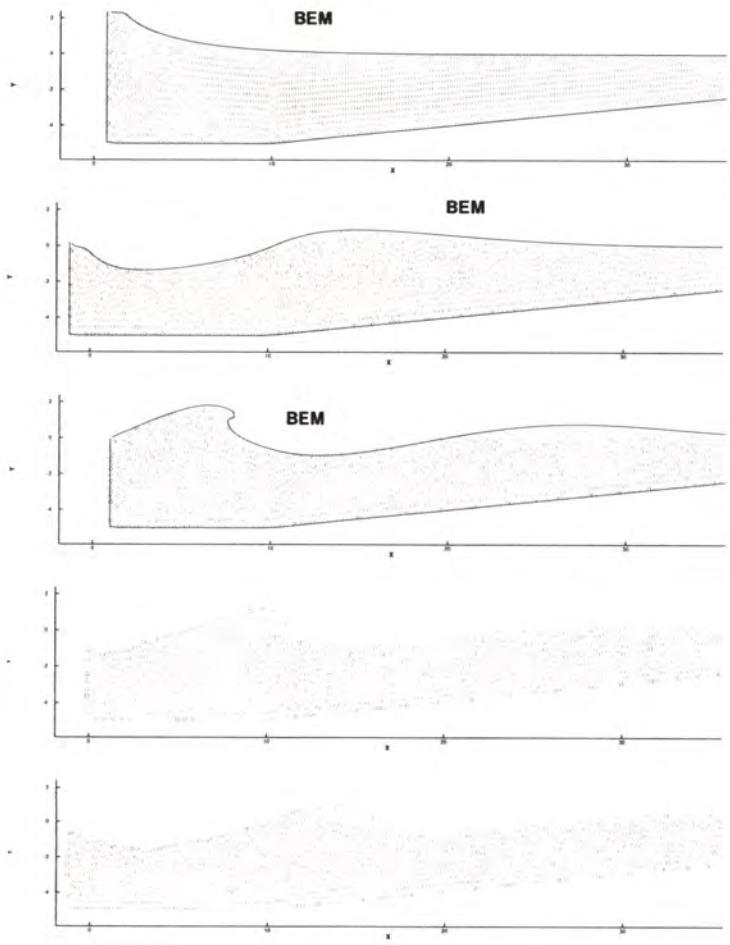

Fig. 1. Comparison between BEM and SPH simulation for a breaking wave in shallow water [See also Appendix CP]

the global accuracy of the simulations. Although individual time stepping algorithm can be use to speed-up the computations, the method remains demanding in term of CPU time so that most applications have been performed assuming two dimensional flow. The accuracy of the initial algorithms is also enhanced using Reproducing Kernel Method [6].

Recent studies have proven the ability of the resulting method to reproduce most of the physical features observed in the flow, such as the occurrence of breaking in shallow water, fluid fragmentation of some parts of the fluid and creation of vortices during the post-breaking phase. The qualitative agreement between computations and experiments has been clearly demonstrated despite

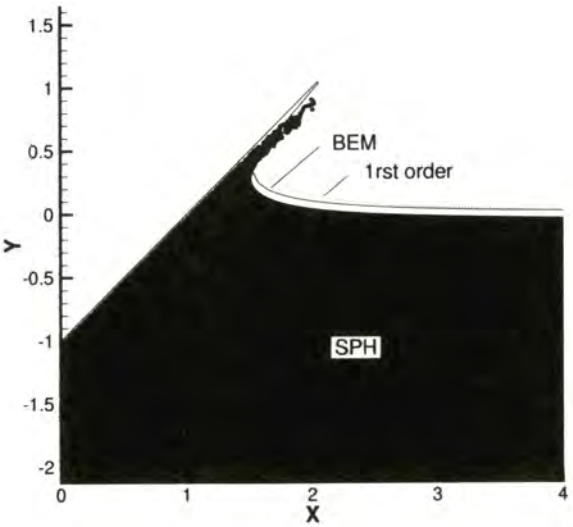

Fig. 2. Comparison between BEM and SPH simulation for the vertical entry of a 45 degrees wedge

the complexity of the physical processes involved during breaking. The next stage in developing the method is to perform quantitative comparisons.

Detailed comparisons between SPH and BEM simulations of a propagating wave before breaking occurs are presented in fig. 1. As expected, the two methods give similar results for the wave elevation until the BEM simulation breaks down as the jet re-enters the front face of the wave. For this simulation, a total of 10.000 particles were used. Clearly, this is not sufficient to model accurately the jet. A local modeling of the so called splashing and ploughing phase is presented [4].

Breaking wave leads to impulsive loads on structures. To test the ability of the method to predict these loads, the classical water entry problem of a wedge is considered (see fig. 2). For this simulation, 100.000 particules were used although this number could have been reduced by a factor of 10 using of particules with different sizes. The SPH simulation is compared to both fully nonlinear BEM and first order (linear) asymptotic solution. Although, compressibility effects affect the free surface position, good agreement is recovered for the loads on the body.

These two test case problems allow to conclude that SPH would seem to be a good choice for simulation complex free surface flows where breaking and fluid-structure interaction occur. More work is nevertheless needed to improve the algorithms which allow to consider boundary conditions on the structure and far away, together with a systematic validation of the method against experiments.

References

1. Cointe, R. : Numerical Simulation of a Wave Channel. Engineering Analysis with Boundary Elements. (1990), **7**, No. 4, pp. 167-177.
2. Tulin, M.P., Waseda, T. : Laboratory Observations of Wave Group Evolution, Including Breaking Effects. (1999) J. Fluid Mech, **378**, pp. 197-232.
3. Monaghan, J.: Simulating Free Surface Flows with SPH. Journal of Computational Physics, (1994), **110**, pp. 399-406.
4. Fontaine, E., Landrini, M. and Tulin, M.: Breaking : Splashing and Ploughing Phases. Intl. Workshop on Water Waves and Floating Bodies (2000) 4 pp.
5. Tulin M.P., Landrini M. (2000) Breaking Waves in the Ocean and Ships 23. Symp. Naval Hydrodynamics, Val de Reuil, France, Vol. 4, pp. 1-32.
6. Liu, W.K., Jun, S., Zhang, Y.F. : Reproducing kernel particle methods. International Journal for Numerical Methods in Engineering, **20**, 1081-1106.

Session 6

Physical Simulation of Rogue Waves

Random Waves in the Laboratory – What is Expected for the Extremes?

Carl Trygve Stansberg
Norwegian Marine Technology Research Institute A/S (MARINTEK)
P.O.Box 4125 Valentinlyst, N-7046 TRONDHEIM, Norway
CarlTrygve.Stansberg@marintek.sintef.no

Abstract. The generation and interpretation of extreme waves in physical model testing is discussed. A list of relevant wave parameters describing the extremes is outlined. A probabilistic approach is considered, with extremes occurring randomly in a wave train synthesized for the test. Statistical reference models based on linear and second-order wave theory are applied. Comparisons to model test results show that the second-order model predicts reasonably well in most cases, although with a slight under-prediction of steep extremes, possibly due to unidirectional wave conditions in the laboratory. Under particular conditions, with narrow-banded unidirectional spectra propagating more than 12 – 15 wavelengths, special modulation effects may occur in energetic wave groups, leading to very high extremes that are clearly beyond second order. This may one possible explanation of "freak waves" observed in the real ocean. The effect is reflected in the 4^{th} order statistical moment (kurtosis), and a prediction formula taking this into account is suggested.

1 Introduction

The prediction and reproduction of extreme ocean waves is a complex task, since they are rare events, and therefore hard to observe in the real ocean. Trying to understand all the underlying mechanisms, and the resulting physics, can be confusing, since there may be a number of various conditions leading to the different events actually observed. Ideally, perfect theoretical and physical models should therefore be able to cover a broad range of situations. A discussion of the occurrence and prediction of extreme waves has been given in [1]. Fully nonlinear theoretical models for random extreme waves do still not exist, although there are several theoretical approaches that include essential linear and nonlinear components and properties. Thus the challenge in present day-to-day applications is to sort out which are the most relevant properties to be modelled, and how to model them. This may vary from application to application, but there are also general patterns. In the present paper, the generation and interpretation of wave extremes in physical model testing is discussed.

The laboratory generation of waves has been reviewed in [2]. There are still a number of questions to be handled in connection with reproduction and use of extreme wave generation. One of them is: What should we expect – or, in other words, what is our reference? This question may be two-fold: 1) What is required from the application?, and 2) what is actually possible, given the laboratory frame?

And furthermore, can we learn something about the wave physics itself from the experiment? Some key words in this process are:

Parameters selected for reproduction
Input from full scale or theory
Methodology (Stochastic vs. deterministic approach; Synthesisation etc.)
Basic physics vs. laboratory effects
Simplifications

Some practical examples from the experience in an offshore model test basin are discussed in the paper, on basis of previous presentations in [3], [4]. Here a stochastic approach is followed, with the synthesisation and physical generation of random storm records (typically of 3-hours duration, full scale). Thus, the extremes occur as random events in the scaled wave field, as the result of the random summation of a large number (thousands) of independent input components. Nonlinear effects observed in the records are then mainly interpreted as results from nonlinear couplings in the actual propagation of the laboratory wave field, although one has to be aware of possible laboratory defined effects. Another approach which has been suggested and applied in the literature, is the design and use of single deterministic, transient wave groups specified with particular extreme value properties [5]. The two different approaches may in certain situations be considered as alternatives to each other, but it is perhaps more fruitful to treat them as complementary, since they are based on quite different background philosophies.

The present experimental results are seen in relation to linear and second-order random wave prediction models, with a particular discussion of deviations from the models. Thus one possible way of defining "freak waves" may be considered as waves and crests clearly higher than second-order. A possible connection between such extremes and nonlinear wave grouping is considered.

2 Background: Critical Wave Events and Parameters

2.1 Some Critical Wave Situations in Offshore Engineering

The design and operation of FPSO's in extreme weather exposed areas must take into account the effects from steep and energetic individual wave events. The wave impact on bow and deck structures can be serious, such as the bow slam experienced on the Schiehallion FPSO [6], as well as the water on deck problems reported on Norwegian production vessels [7]. New design tools are being developed as a result of this [8]. The impact loads and possible damages are certainly a combined effect from the wave properties and the interaction with the vessel, but knowledge about the incoming energetic waves is very helpful in the further development in the area.

For floating platforms, such as semisubmersibles, TLPs and Spars, the deck clearance (air-gap) is critical. Thus the ability to properly predict the extreme wave crests and their kinematics, in 100-year storms is essential, not only for the prediction of the probability of impact, but also for the prediction of resulting loads. Other direct

results from extreme waves interacting with platforms include the ringing problem on TLP's and GBS's (see e.g. [9], as well as the possible capsizing of platforms with compliant mooring.

Extreme waves or wave groups can also induce particular vessel motions, as a result of particularly large slow-drift forces. For FPSO's, this may lead to large head angles and, consequently, even larger offset and high nonlinear mooring line loads (static as well as dynamic). Large slow-drift is critical also for the extreme loads of platform moorings.

2.2 Critical Wave Parameters

The detailed description of dangerous waves is complex, since the different problems such as described above may depend on different wave properties. A list of possible parameters or characteristics may be as follows:

Individual waves

Crest height:	A_{max}	or	A_{max}/σ
Wave height:	H_{max}	or	H_{max}/σ
Steepness:	$(\partial\eta/\partial x)_{max}$	or	$(kA)_{max}$
Particle velocity:	U_{max}		
Particle acceleration:	$(dU/dt)_{max}$		
Grouping (succeeding waves);			
Energy envelope:	E(t); Group spectrum – relative to linear model		
Breaking			

Short-term sea state properties

Skewness: $\gamma_1 = 1/(M\sigma^3) \cdot \Sigma\,[\eta_i - E(\eta)]^3$ **(1)**

Kurtosis (grouping parameter): $\gamma_2 = 1/(M\sigma^4) \cdot \Sigma\,[\eta_i - E(\eta)]^4$ **(2)**

Probability of given extreme levels

where η is the elevation, σ is the standard deviation of the elevation record, and M is the number of record samples. In addition, there may also be other parameters relevant for particular problems.

2.3 Extreme Waves: Possible Physical Mechanisms

For a proper prediction of extreme and rare waves, it is also important to keep in mind that there may be a range of different physical mechanisms leading to the events. Some of these are:

Phase combination of harmonic components
Steepness-induced crest increase ("Stokes effects")
Nonlinear self-focusing of energetic wave groups
Multi-directional effects
Bottom effects (finite water depth; refraction)

Current effects (wave-current interaction: refraction)
Wind influence
Storm age and duration
Several storm systems?

Thus the description of real cases may be complex. In offshore engineering applications, the first two mechanisms listed are perhaps those with most attention. It may be a reasonable choice to consider them as basic conditions, and then add the effects from the others when appropriate. Later in this paper, effects from nonlinear wave grouping are discussed in particular, on basis of some laboratory results.

3 Specification and Limitations of Laboratory Waves

The reproduction of wave conditions in a laboratory must be based upon a chosen specification, which can be essential for the generated extremes. Thus the reproduced conditions will be simplified with regard to some properties, while others are emphasised. Parameters of a specification may include some of the following:

In a *probabilistic* approach:
Significant wave height H_s ; H_{mo}
Spectral peak period (or equivalent) T_p ; T_z
Spectrum shape (e.g. JONSWAP, 2-peaked etc.)
Storm duration
Additional requirements?
(H_{max} ; A_{max} ; γ_1 ; γ_2 ; wave grouping; others ?)

In a *deterministic* transient wave approach:
Specific properties of single wave (or wave group)

Some laboratory simplifications may typically (but not necessarily) be:
Uni-directional waves
Horizontal bottom or deep water
Stationary sea state
Mechanical wave generator - no wind influence
If "transient wave" : Specific parameters of event

Specific laboratory-defined effects:
Reflections & diffraction
"Parasitic waves" due to imperfect boundary conditions
Size & shape of basin / distance from wave generator
Repeatability
Scale effects (viscous effects; breaking)
Synthesization method

4 Probabilistic Modelling of Linear and Nonlinear Waves

Based on the specification, the synthesisation of a random laboratory signal input to the wave-maker is typically made as a linear sum of a large number of independent harmonic components. Nonlinear corrections may also be made [10]. As an example, a 3-hours storm duration may be simulated by inverse Fast Fourier Transform (FFT) with 16000 frequency components. Extreme waves are then a result of this random combination, plus nonlinear interactions during the propagation from the wavemaker to the actual location. The statistical behaviour is observed through parameters like the skewness γ_1 and kurtosis γ_2 of the wave record, and probability distributions and extremes of the crests and wave heights.

The results can then be compared to reference models. In particular there are two models in use: Linear waves, with Gaussian statistics and Rayleigh distributed peaks, and second-order waves [11], [12], with a non-Gaussian correction on the statistics, and with extreme crests deviating from the Rayleigh model. The effect from second-order contributions on an extreme wave is shown in a numerical example in Fig. 1. One should also take into account the sampling scatter of a finite record [12]. The estimation of extremes from a given 3-hours record can be improved by use of e.g. fitting the tail of the peak distribution to a Weibull distribution, and predict the extreme from that.

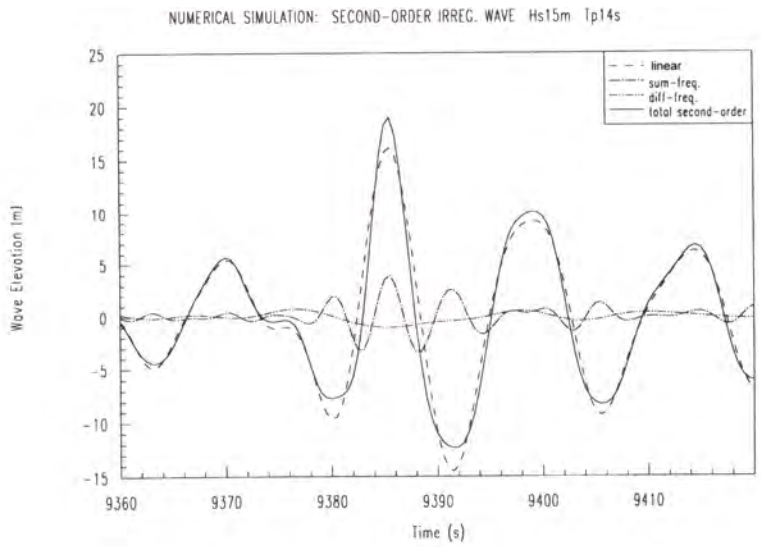

Fig. 1. Time series sample from numerically generated second-order random wave

Based on the reference models, we can derive expectations for the measured statistics, and the extremes in particular. For a simple linear model, the expected skewness and kurtosis are $\gamma_1 = 0$; $\gamma_2 = 3.0$, respectively, and extreme crests and wave heights are expected to be Rayleigh distributed with the following commonly used relations:

$$E[A_{max}] \equiv A_R = \sigma \left[\sqrt{(2 \ln (M))} + 0.577/\sqrt{(2 \ln (M))}\right] \quad (3)$$

$$E[H_{max}] = 2 A_R \quad (4)$$

In a second-order model, the skewness γ_1 increases linearly with the steepness. Models for γ_1 and γ_2 have been derived in [13]:

$$\gamma_1 = 5.41 (H_{m0} / L_p) \quad (5)$$

$$\gamma_2 - 3 = 3 \gamma_1^2 \quad (6)$$

where L_p is the wavelength corresponding to the peak wave period. For extreme crests a simplified formula has been proposed by [14]:

$$E[A_{max}] = A_R \ (1 + \tfrac{1}{2} k_p A_R) \quad (7)$$

where k_p is the wave number corresponding to L_p, and A_R is given in Eq. (3) above. The wave heights are still Rayleigh distributed as in the linear model.

The experience from [11] is that the second-order model generally agrees quite well with deep water full scale measurements of crests. Thus the linear model will underpredict extreme crests but not the wave heights. Laboratory measurements in [3] more or less confirm this (see the next chapter), but a slight under-prediction is observed. In special conditions, even higher extremes have been observed [4]. Higher-order models can also predict this [15]. Such events may possibly be seen in relation to full-scale observations of so-called "freak waves", and will be discussed later in this paper.

5 Observed Nonlinear Behaviour of Random Extremes

Observations from a range of model test studies in scales 1:55 – 1:70, with random wave generation in a large wave basin [3], have shown that the largest *crest* heights deviate systematically from Rayleigh model predictions derived for linear waves. In general, a second-order description fits reasonably well, as concluded from the full-scale study in [11], although it slightly under-predicts the most extreme cases, typically by 5% of the total crests. See Fig. 2. The deviation may be partly due to the fact that most of the results in this figure were obtained with unidirectional waves, while field data are expected to be more or less muliti-directional. There is a also a considerable sampling scatter, as expected from theory. Extreme *peak-to-peak* wave heights are normally reasonably well predicted by Rayleigh theory. The same results are also reflected in probability distributions (Fig. 3).

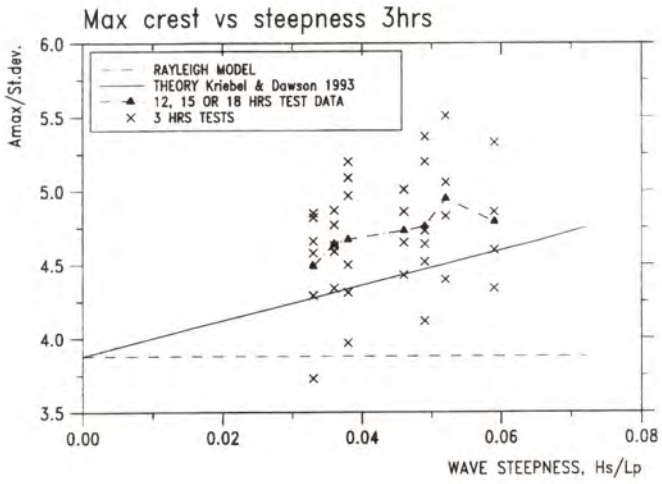

Fig.2. Measured extreme crests from laboratory tests, compared to second-order and Rayleigh predictions. 3-hours as well as 12 – 18-hours storm duration models (from Stansberg, 2000a)

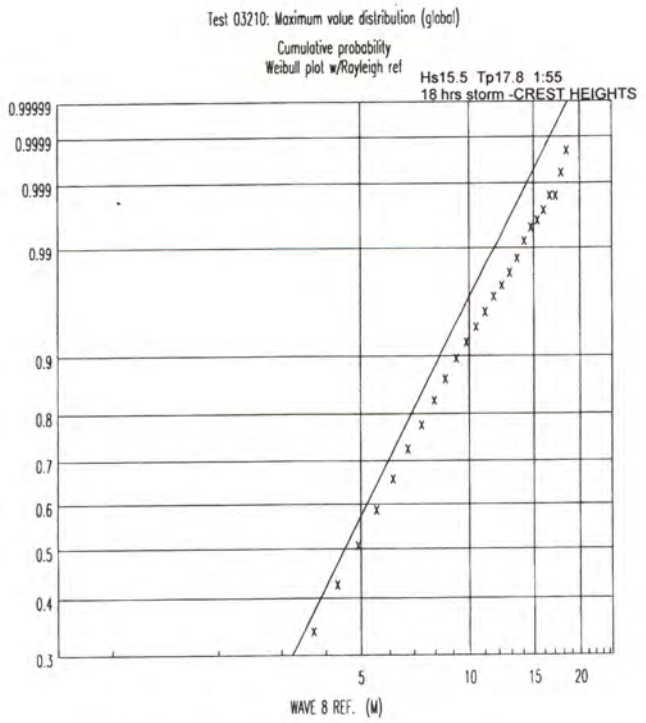

Fig.3a. Probability distributions of crests in 1:55 scaled 18-hours storm model test

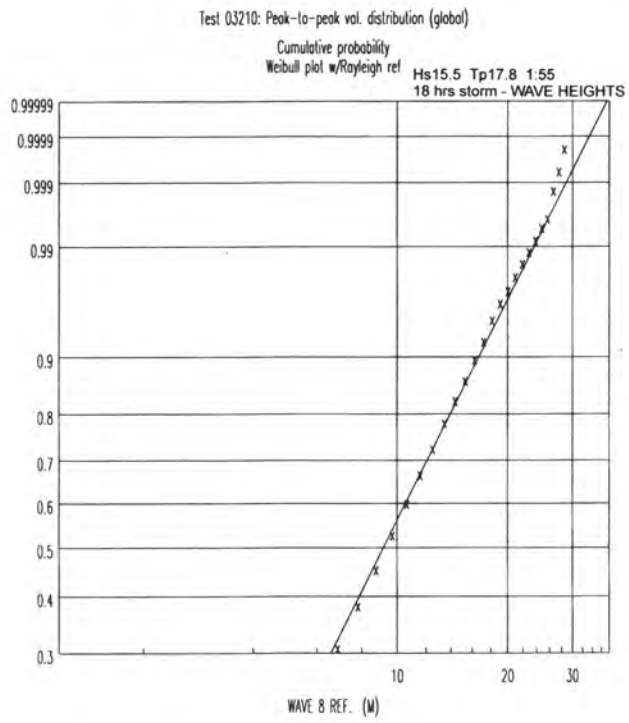

Fig. 3b. As Fig. 3a, but for wave heights.

Under certain conditions, extremes in random wave trains may be observed to be significantly higher than second-order predictions, even for moderately steep wave conditions [4]. This occurs when unidirectional, narrow-banded spectra propagate over large distances, that is, more than about 12-15 wavelengths, in which case higher-order wave group amplification may take place, leading to particularly high crests and wave heights. This is illustrated by an example from a 1:200 scaled laboratory experiment shown in Fig.4. We may interpret it as a so-called "freak wave" event. However, the results in [4] also show that it can be a result of systematic behaviour under these particular conditions. A reasonable physical explanation is the self-focusing casued by amplitude dispersion in energetic wave groups, which can be related to the modulational instabilities commonly referred to as the Benjamin-Feir effect [16]. The physics is studied experimentally in [17]. Results from tests with different scales indicate that the phenomenon is not scale dependent. For bi-chromatic wave trains, observations have been found to agree very well with a higher-order Schrödinger formulation [18]. Probability crest and height distributions from a case where the effect is particularly strong are shown in Fig 5. The difference from Fig. 3 above is clearly seen, also for the peak-to-peak wave heights.

The 4th-order statistical moment parameter γ_2 (kurtosis) reflects, on an average, the increased groupiness, although it is also statistically unstable [12]. An empirical relation has been derived on basis of the experimental data above, with very

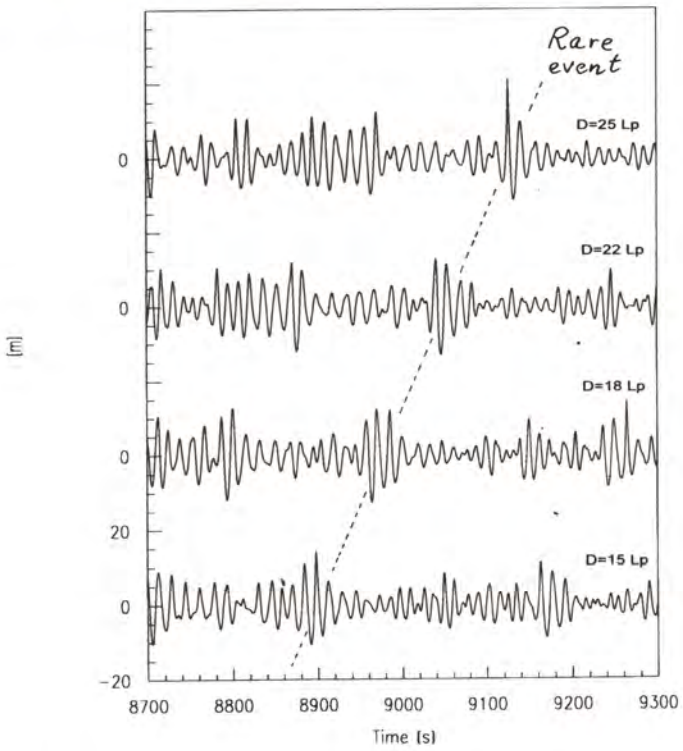

Fig. 4. Space and time evolution of energetic wave group into extreme wave – example from model tests. (*D = distance from wave-maker, in wavelengths)*)

long records corresponding to 12, 15, 18 and 36 hour storm models. Thus the kurtosis has been correlated with the corresponding 3-hours extreme crest and wave height estimates A_{max} , H_{max}. The result is shown in Fig. 6, where deviations from the second-order and Rayleigh models (for A_{max} and H_{max} , respectively) are plotted against the kurtosis. The values are normalised by the standard deviation σ of the record. From this, the following simplified formulae are proposed for extreme crests and wave heights, taking into account the second-order term for A_{max} [16] as well as an empirical higher order correction for A_{max} and for H_{max}:

$$A_{max}/\sigma = (A_{max,R}/\sigma)\cdot(1 + \tfrac{1}{2} k_p A_{max,R}) + 1.3\cdot(\gamma_2 - 3.0) \quad \textbf{(8)}$$

$$H_{max}/2\sigma = (H_{max,R}/2\sigma) + (\gamma_2 - 3.25) \quad \textbf{(9)}$$

We sees that for the extreme wave heights, the Rayleigh model overpredicts the measurements when the kurtosis approaches 3.0 (that is, Gaussian waves). This is an expected result in linear waves, due to the de-correlation between crests and neighbouring troughs in a finite-bandwidth spectrum.

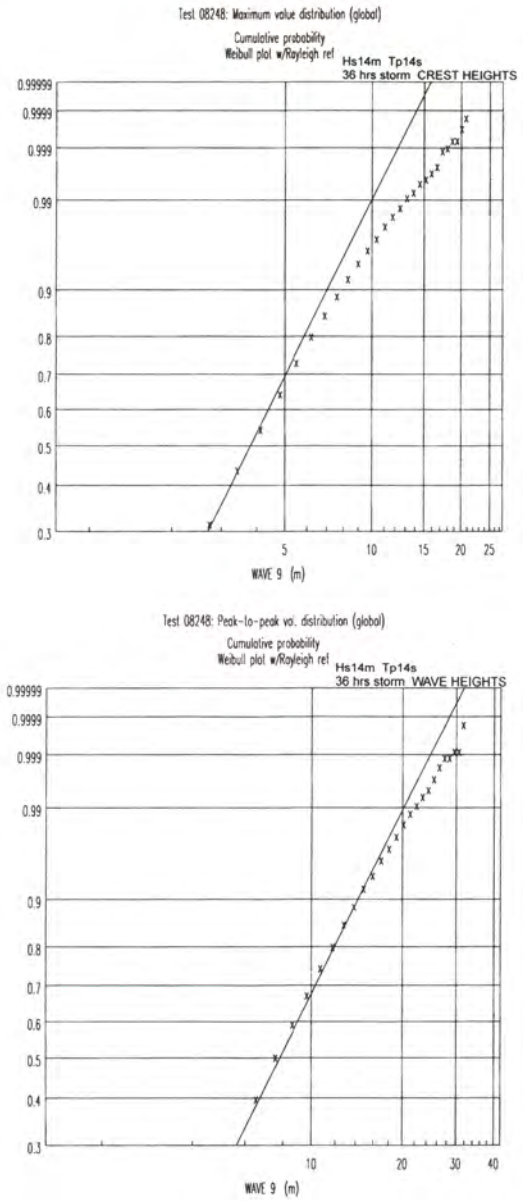

Fig. 5. Probability distributions of crests and wave heights, after 25 wavelengths

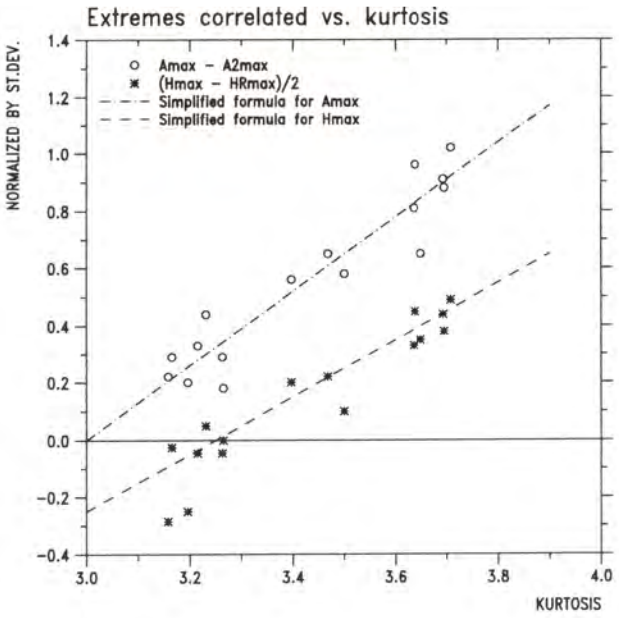

Fig. 6. Measured extreme crests and wave heights in 12 – 36 hours storm tests: Deviations from second-order and Rayleigh models, respectively, vs. kurtosis

Another, more general alternative to this empirical formula is the Hermite transformation method in [19]), where the extremes are estimated directly on basis of the statistical moments γ_1 and γ_2.

The kurtosis γ_2 will have to be determined for the actual case. Thus there is a task for the future: How do we know when to assume γ_2 clearly larger than 3.0 , and how do we predict it?

The typical time domain behaviour of the most extreme ("freak") events is shown in Fig. 7. It normally results from an energetic wave group of 4-6 waves, which after some propagation is focused into a narrower group of of 1-2 waves. Most of the energy is then concentrated in the front wave. Until this point, only little energy has been dissipated from the original wave group. Thus the occurrence of such "freak" events may possibly be caused by the time and space development of wave groups with a duration sufficient to contain a large amount of integrated energy.

6 Conclusions

Probabilistic modelling of storm sea states in a laboratory wave basin, with particular emphasis on the resulting extreme wave events, has been discussed and demonstrated. The results are seen in light of what is expected from linear and second

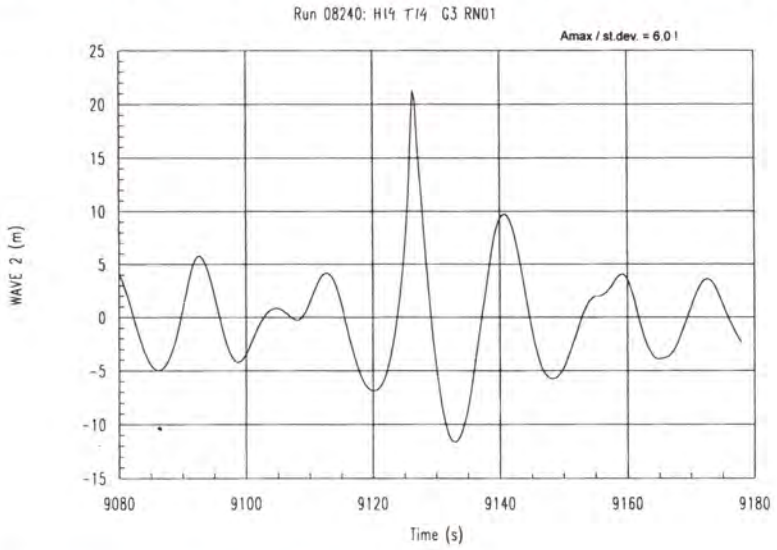

Fig. 7. Particularly extreme wave event.

order models. Main findings are:

An empirically adjusted formula for extremes is suggested. For the crests, this is based on a second-order model plus an empirical correction for kurtosis values larger than 3.0. For the wave heights, a Rayleigh model with a similar kurtosis correction is proposed.

The kurtosis is closely connected with the average "groupiness" of the sea state. Normally it is 3.0 – 3.2, but it can under certain conditions, such as narrow-banded, unidirectional sea on deep water, grow significantly higher.

Nonlinear group amplification (focusing) can generate strongly nonlinear, rare wave events – clearly beyond second order

There is a considerable sampling variability in a randomly chosen 3-hours realisation, as expected from theory.

References

1. ISSC, Report from the 23rd International Ships and Structures Conference - Environment Committee, Nagasaki, Japan (2000).
2. ITTC, Report from the 22nd International Towing Tank Conference - Environment Committee, Seoul, Korea and Shanghai, China (1999).

3. Stansberg, C.T.: Laboratory Reproduction of Extreme Waves in a Random Sea, Proc., Wave Generation'99 (International Workshop on Natural Disaster by Storm Waves and Their Reproduction in Experimental Basin), Kyoto, Japan, (2000).
4. Stansberg, C.T.: Nonlinear Extreme Wave Evolution in Random Wave Groups, Proc., Vol. III, the 10th ISOPE Conf., Seattle, WA, USA, (2000).
5. Clauss, G.: Task-Related Wave Groups for Seakeeping Tests or Simulation of Design Storm Waves, Appl. Ocean Res., Vol. **21**, (1999), pp. 219-234.
6. MacGregor, J.R., Black, F., Wright, D. and Gregg, J.: Design and Construction of the FPSO Vessel for the Schiehallion Field, Trans., Royal Inst. of Naval Architects, London, UK, (2000).
7. Ersdal, G. and Kvitrud, A.: Green Water on Norwegian Production Ships, Proc., the 10th ISOPE Conf., Seattle, WA, USA, (2000).
8. Hellan, Ø., Hermundstad, O.A. and Stansberg, C.T.: Design Tool for Green Sea, Wave Impact and Structural Responses on Bow and Deck Structures, OTC Paper No. 13213, OTC 2001 Conference, Houston, TX, USA, (2001).
9. Davies, K.B., Leverette, S.J. and Spillane, M.W.: Ringing Response of TLP and GBS Platforms, Proc. Vol. II, the 7th BOSS Conf., Cambridge, Mass., USA, (1994).
10. Schäffer, H.A.: Second-Order Wavemaker Theory for Irregular Waves, Ocean Engr, **23**, No. 1, (1996), 47-88.
11. Forristall, G.: Wave Crest Distributions: Observations and Second-Order Theory, Proc., Conf. On Ocean Wave Kinematics, Dynamics, and Loads on Structures, Houston, TX, USA, (1998), 372-382.
12. Stansberg, C.T.: Non-Gaussian Extremes in Numerically Generated Second-Order Random Waves in Deep Water, Proc., Vol. III, the 8th ISOPE Conf., Montreal, Canada, (1998), 103-110.
13. Vinje, T. and Haver, S.: On the Non-Gaussian Structure of Ocean Waves, Proc., Vol. 2, the 7th BOSS Conf., MIT, Cambridge, Mass., USA. (Published by Pergamon, Oxford, UK, (1994).
14. Kriebel, D.L. and Dawson, T.H.: Nonlinearity in Wave Crest Statistics, Proc., 2nd Int Symp on Wave Measurement and Analysis, New Orleans, LA, USA, (1993), 61-75.
15. Yasuda, T. and Mori, N.: High Order Nonlinear Effects on Deep-Water Random Wave Trains, Proc., Vol. II, Int Symp on Waves – Phys. and Num. Modelling, Univ. of British Columbia, Vancouver, Canada, (1994), 823 – 832.
16. Benjamin, T.B. and Feir, J.E.: The Disintegration of Wave Trains on Deep Water, J. Fluid Mech., Vol. **27**, (1967), 417-430.
17. Stansberg, C.T.: On the Nonlinear Behaviour of Ocean Wave Groups, Proc. WAVES 1997 Symposium (ASCE), Virginia Beach, VA, USA, (1998).
18. Trulsen, K. and Stansberg, C.T.: Spatial Evolution of Water Surface Waves: Numerical Simulation and Experiment of Bichromatic Waves, Proc., the 11th ISOPE Conf., Stavanger, Norway, (2001).
19. Winterstein, S.R.: Nonlinear Vibration Models for Extremes and Fatigue, J. Eng. Mech., Vol. **114**, (1988), 1772-1790.

Generation of Task-related Freak Waves and Critical Wave Groups

Günther F. Clauss

Institute of Naval Architecture and Ocean Engineering, Technical University Berlin,
Sekr. SG 17, Salzufer 17-19, D-10587 Berlin, Germany
Clauss@ism.tu-berlin.de,
WWW home page: http://www.ism.tu-berlin.de/MT/index.html

Abstract. In this paper a new procedure is proposed to generate predetermined nonlinear wave sequences in random seaways. These tailored wave trains are simulated numerically in time domain using the finite element method. Modern nonlinear programming methods are applied to fit the two dimensional wave field to global parameters defined in terms of significant wave height and peak period as well as local target parameters like wave height, crest height, and period of individual waves. Firstly, a linear approximation of the desired wave train is computed by optimizing an initially random phase spectrum for given variance spectrum. This initial guess is further improved by fitting the fully nonlinear wave evolution simulated in a numerical wave tank to the target characteristics. The discrete wavelet transform of the wave board motion allows to identify the relevant signal information efficiently, as only a small number of wavelet coefficients needs to be considered in the fitting problem. Results are presented for a steep and high transient wave within a tailored group of three successive waves embedded in random seaway.

As an alternative to the numerical optimization of the wave generation control signal an experimental simulation technique is also presented. In this case nonlinear free surface effects, even wave breaking are naturally included in the fitting process since the simulation of the physical wave evolution under laboratory conditions is an integral part of the new technique. This feature is especially important for simulating experimentally wave/structure interactions in rogue waves and critical wave groups. As an application of the deterministic transient wave technique the paper presents

- the generation of a 3.2 m freak wave in a dedicated wave tank
- a typical seakeeping test with a high speed catamaran
- a RANSE/VOF analysis of the interaction of a wave and an artificial reef (including viscous effects).

In conclusion it is shown that the deterministic transient wave technique is a powerful tool for evaluating the cause/reaction chain of wave/structure interactions.

For the design of safe and economic offshore structures and ships the knowledge of the extreme wave environment and related wave/structure interactions

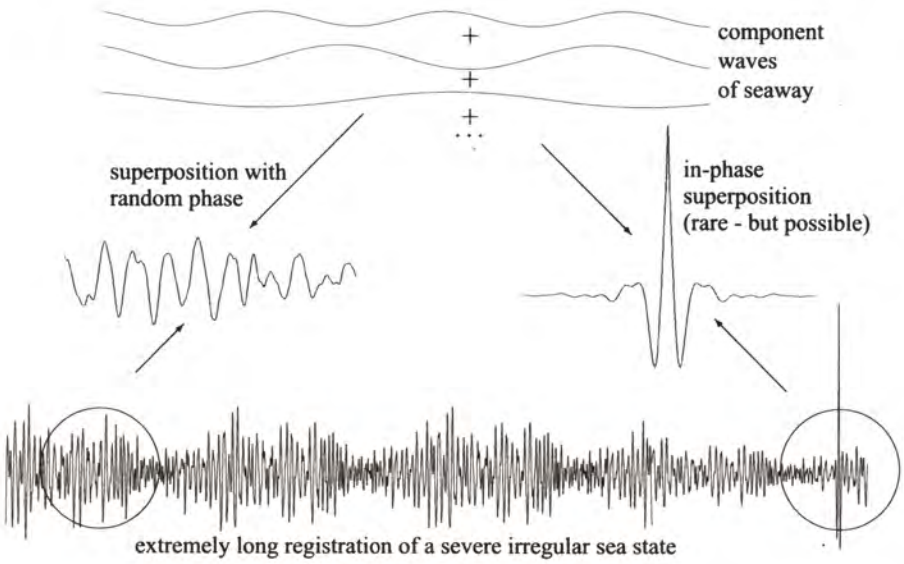

Fig.1. Design wave as rare event of a severe irregular sea state

is required. A stochastic analysis of these phenomena is insufficient as local characteristics in the wave pattern are of great importance for deriving appropriate design criteria. This paper describes techniques to synthesize deterministic task-

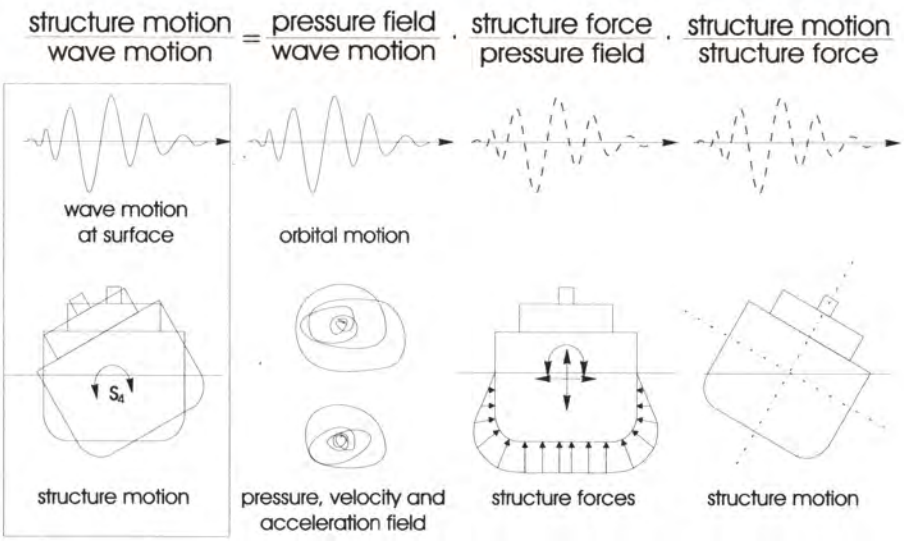

Fig.2. Wave/structure interaction as a cause-reaction chain

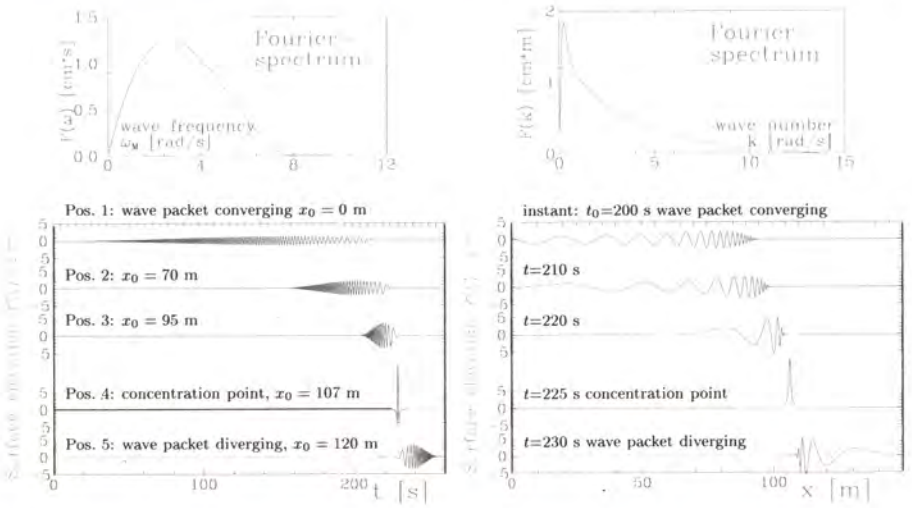

Fig.3. Wave packet registration at different positions (left) as well as instantaneous wave profiles at selected instances (right) (water depth $d = 4.2$ m)

related 'rogue' waves or critical wave groups for engineering applications. These extreme events, characterized by local parameters like tailored design wave sequences, are integrated in a random or deterministic seaway with a defined energy spectrum, and can be generated deterministically (Fig.l). If a strictly deterministic process is established, cause and effect are clearly related: at any position the non-linear surface elevation and the associated pressure field as well as the velocity and acceleration fields can be determined. Also the point of wave/structure interaction can be selected arbitrarily, and any test can be repeated deliberately. Wave-structure interaction is decomposable into subsequent steps (Fig.2): surface elevation - wave kinematics and dynamics - forces on structure components and the entire structure - structure motions [1].

Firstly, the generation of linear wave groups is presented. The synthesis and up-stream transformation of arbitrary wave packets is developed from its so-called concentration point where all component waves are superimposed without phase-shift. For a target Fourier wave spectrum a tailored wave sequence can be assigned to a selected position.

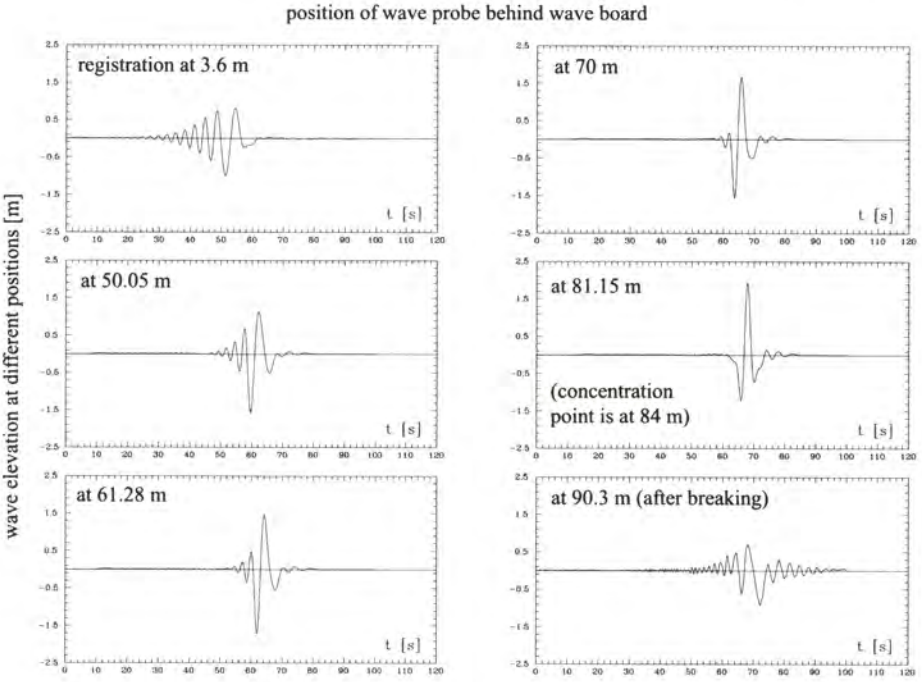

Fig. 4. Genesis of a 3.2 m rogue wave by deterministic superposition of component waves (water depth $d = 4$ m)

This wave train is linearly transformed back to the wave maker and - by introducing the electro-hydraulic transfer function of the wave generator - the associated control signal is calculated. Fig. 3 shows a linear wave packet converging at the concentration point $x_c = 107$ m. It illustrates registrations at different positions as well as instantaneous wave profiles at selected instances.

The generation of steeper and higher wave groups requires a more sophisticated approach as propagation velocity increases with height. With a semi-empirical procedure the control signal of extremely high wave groups is determined, and the propagation of the associated wave train is calculated by iterative integration of coupled equations of particle positions. With this deterministic technique "freak" waves up to 3.2 m high have been generated in a wave tank [5] (Fig. 4).

Based on the linear wave packet technique the seakeeping behaviour of ships or offshore structures is efficiently determined with just one single model test [4] (Fig. 5). With higher wave trains this technique is used to analyze the capsizing mechanism of ships in tailored transient wave packet sequences [3].

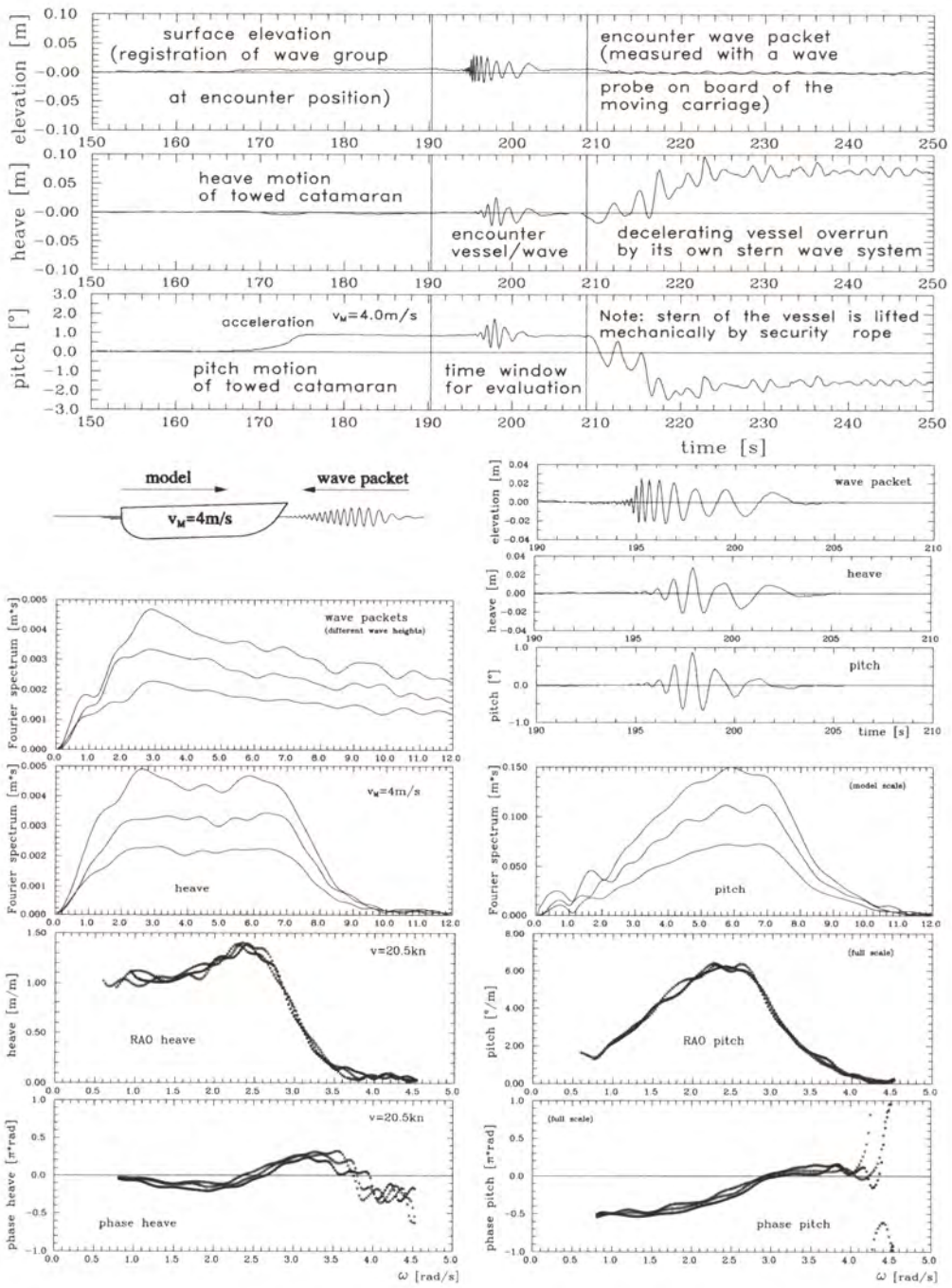

Fig. 5. Registrations, Fourier spectra, and transfer functions of a typical seakeeping test with a high-speed catamaran in transient wave trains (model scale: 1:7, V_m = 4.0 m/s; full scale: V = 20.5 kN; Fn = 0.56)

In many applications the detailed knowledge of the nonlinear characteristics of the flow field is required, i.e. wave elevation, pressure field as well as velocity and acceleration fields. In this case a finite element method developed by G. Wu and R. Eatock Taylor [12,13] is used to determine the velocity potential, which satisfies the Laplace equation for Neumann and Dirichlet boundary conditions. The Neumann boundary condition at the wave generator is introduced in form of the first time-derivative of the measured wave board motion. To develop the solution in time domain the forth order Runge-Kutta method is applied [7]. Starting from a finite element mesh with 8000 triangular elements (401 nodes in x-direction, 11 nodes in -direction, i.e. 4411 nodes) a new boundary-fitted mesh is created at each time step. Lagrangian particles concentrate in regions of high velocity gradients, leading to a high resolution at the concentration point. This mixed Eulerian-Langrangian approach has proved its capability to handle the singularities at intersection points of the free surface and the wave board. Fig. 6 and Fig. 7 show wave profiles with associated velocity potential as well as registrations at different positions. Excellent agreement of numerical and experimental results is observed. Note that the pressure distribution as well as velocity and acceleration fields including particle tracks at arbitrary locations are deduced from the velocity potential.

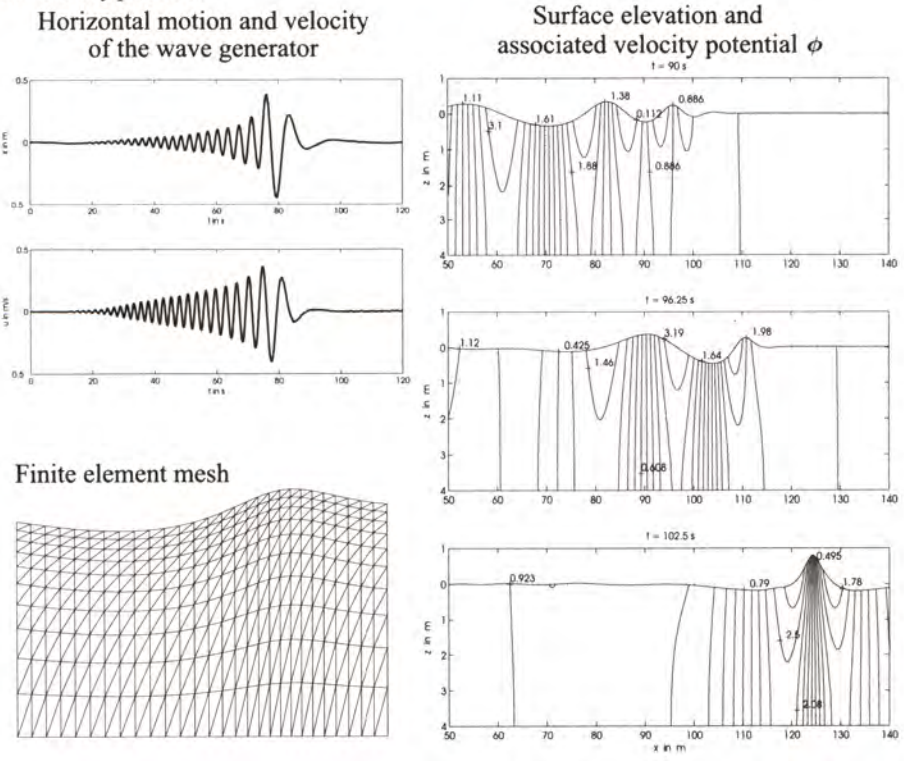

Fig.6. Nonlinear numerical simulation of transient waves

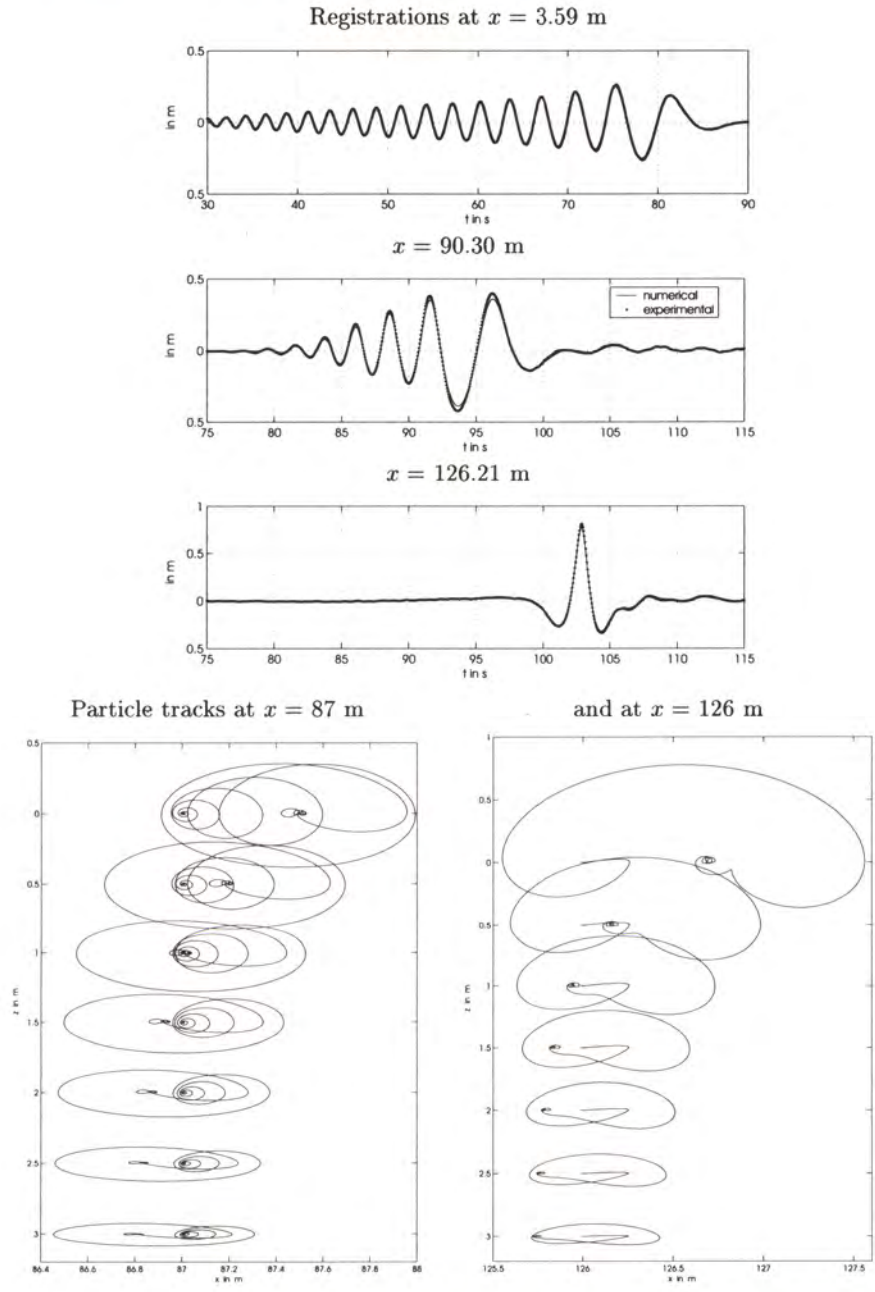

Fig.7. Nonlinear numerical simulation of transient waves and its experimental validation

So far, nonlinear wave groups is an ideal fluid have been discussed. If viscous effects are also considered an approach of transient viscous free surface flow

computation with RANSE/VOF solver is used. As an application, an artificial reef - modeled as a submerged permeable wall - has been investigated: Using an unstructured grid, the dissipation loss is explained by overtopping phenomena and subsequent recirculation of the flow locked in chambers between filter elements (Fig. 8). Jet flow between filter components is also fostering high energy loss. Due to non-linear wave/filter interactions long low-frequency incident waves with substantial erosive impact are transformed into irregular wave trains with high-frequency wave energy components, which cause less erosion to the sea floor [2].

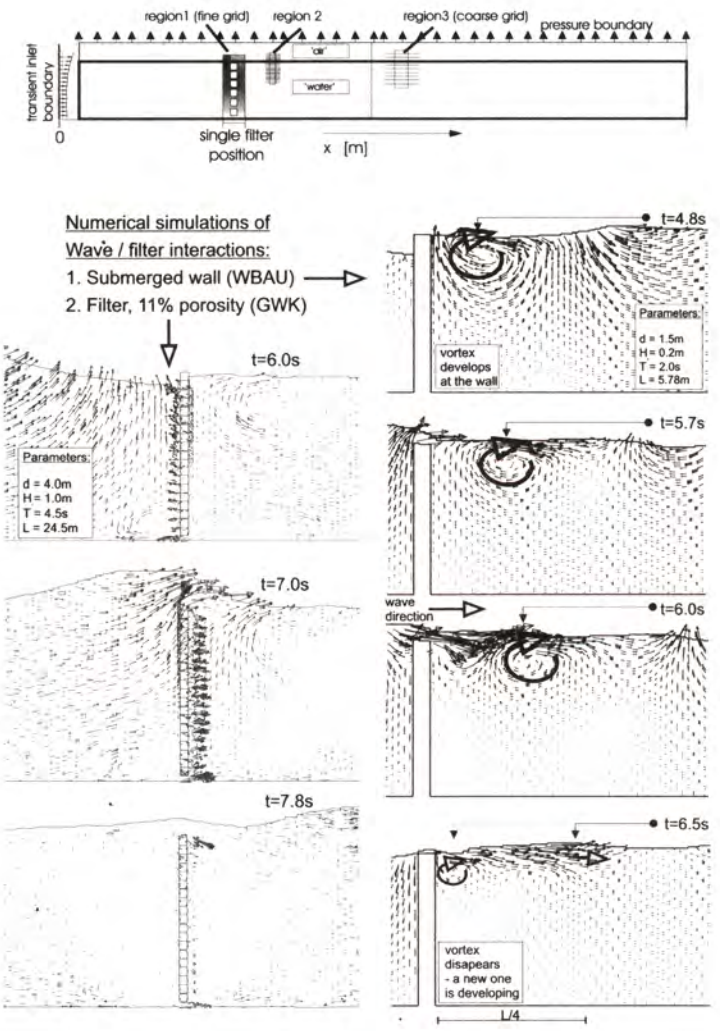

Fig.8. Transient viscous computation of artificial reefs (RANSE/VOF)- velocities due to wave/filter interaction for submerged wall and 11% filter

In general, extremely high "rogue" craves or critical wave groups are rare events embedded in a random seaway. The most efficient and economical procedure to simulate and generate such a specified wave scenario for a given design variance spectrum is based on the appropriate superposition of component waves or wavelets. As the method is linear, the wave train can be transformed down-stream and up-stream between wave board and target position. The desired characteristics like wave height and period as well as crest height and steepness are defined by an appropriate objective function. The subsequent optimization of the initially random phase spectrum is solved by a Sequential Quadratic Programming method (SQP) (Fig. 9) [8]. The linear synthetization of critical

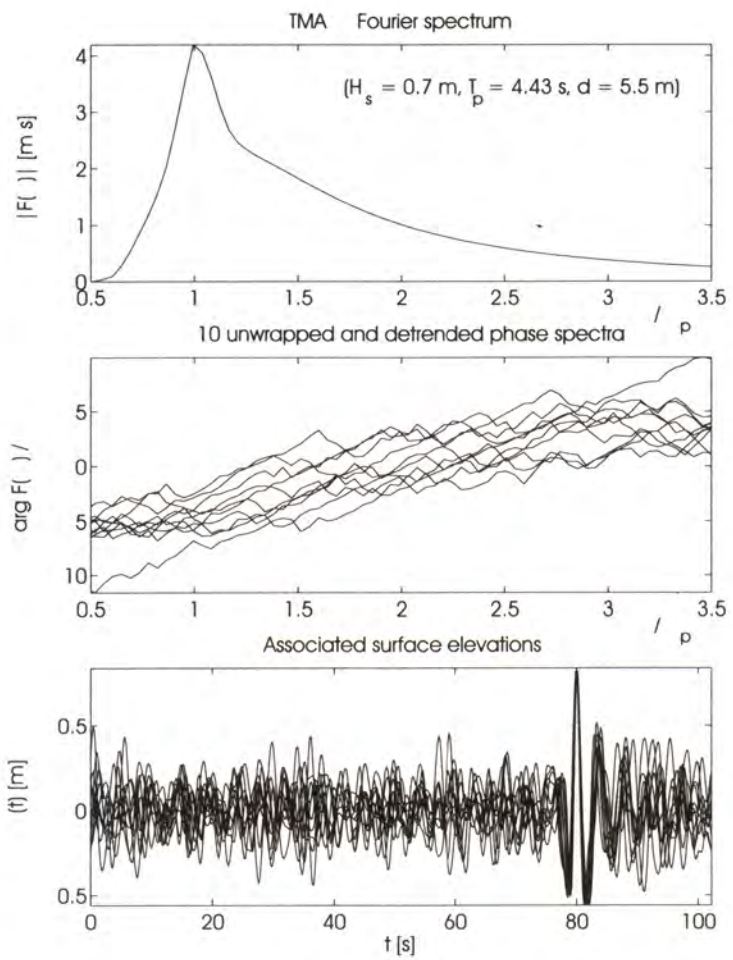

Fig.9. Optimized phase spectra and associated wave trains resulting from different initial phase distributions.

wave events is expanded to a fully nonlinear simulation by applying the subplex method, developed by T. Rowan [11]. The domain space is decomposed into smaller subdomains which are minimized by the Nelder and Mead simplex method [10]. Improving the linear SQP-solution by the nonlinear subplex expansion results in realistic 'rogue'-waves embedded in random seas [8]. In case of extremely high 'rogue' waves, however, embedded in irregular seas at target position we may observe local differences in wave characteristics if the resulting wave sequence is compared to the target wave train. Consequently, a subsequent optimization process is required to obtain the design wave sequence. This fully nonlinear calculation of wave elevation is based on a linear initial guess which is iteratively improved to fit the target characteristics. The discrete wavelet transform of the wave board motion allows to identify the relevant signal efficiently, as only a small number of wavelet coefficients need to be considered. Fig. 10 presents results for a steep and high transient wave within a tailored group of three successive waves embedded in a random seaway [9].

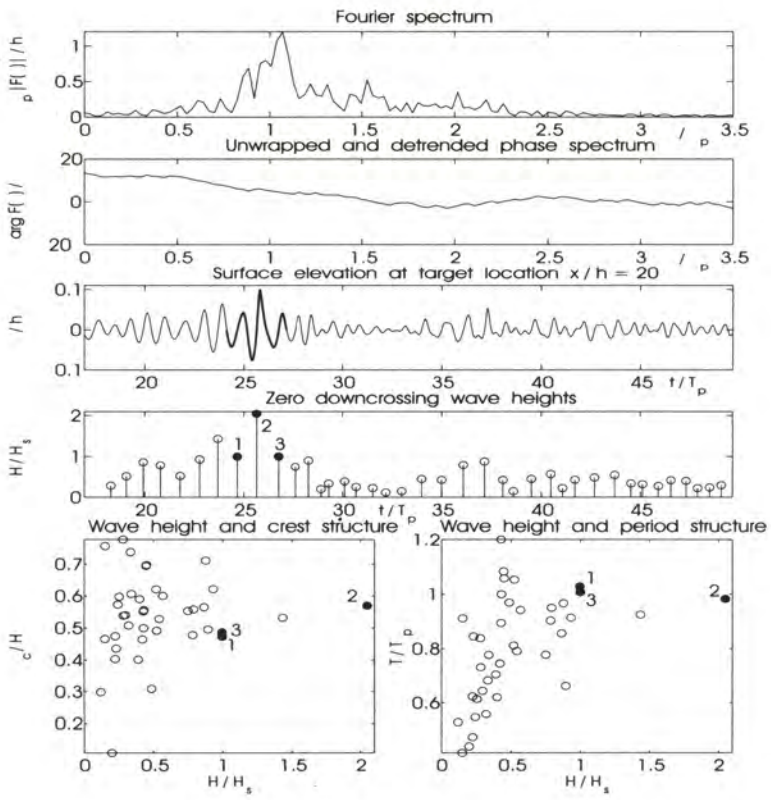

Fig.10. Nonlinear wave train simulated with tailored wave sequence - wave board motion optimized with subplex method

As an alternative to the numerical optimization of the wave generation control signal by the nonlinear subplex method an experimental simulation technique has been developed (Fig. 11) [6]. For a given design variance spectrum, the SQP-method yields an optimized phase spectrum which corresponds to the desired wave characteristics at target position. The wave generator control signal is determined by transforming this wave train in terms of the complex Fourier transform to the location of the wave generator. The measured wave train at target position is then iteratively improved by systematic variation of the wave board control signal which is based on the linear SQP-optimization with subsequent non-linear subplex improvement. To synthesize the control signal wavelet coefficients are used. The number of free variables is significantly reduced if this signal is compressed by low-pass discrete wavelet decomposition, concentrating on the high energy band. Based on deviations between the measured wave sequence and the design wave group at target location the control signal for generating the seaway is iteratively optimized in a fully automatic computer-controlled model test procedure. As this new experimental technique can cope with breaking waves it is a promising procedure for synthesizing model rogue waves or critical wave groups for wave/structure interactions. Fig. 11 illustrates the experimental procedure, and demonstrates the improvement of the linear SQP solution by nonlinear subplex fitting. It also shows registrations at different locations as well as the Fourier spectra of the target wave, the linear SQP solution and the finally obtained subplex fitting.

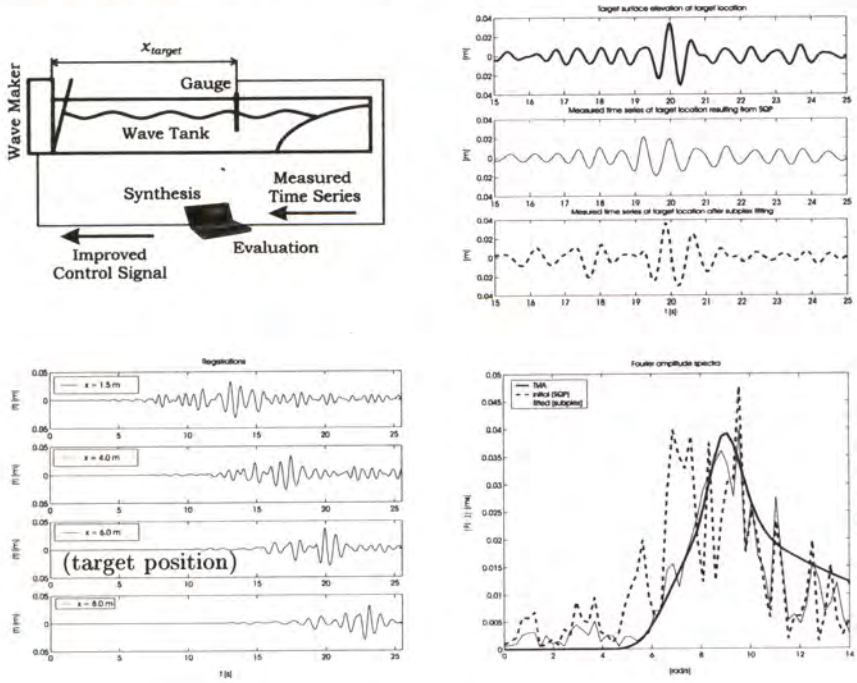

Fig.11. Experimental simulation of tailored design wave sequences in extreme seas

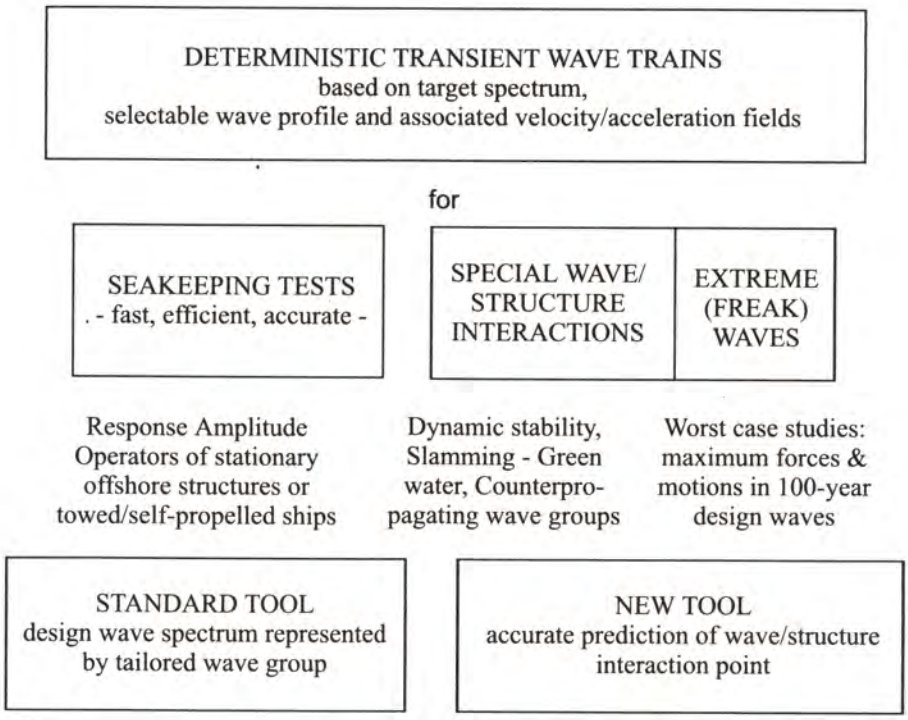

Fig. 12. Applications of the transient wave technique

In conclusion, it has been demonstrated that the transient wave technique is capable to generate tailored wave sequences with high accuracy

- for standard seakeeping tests
- for special wave/structure interactions
- for worst-case studies in extreme waves (Fig. 12).

The simulation technique is based on a computer controlled nonlinear procedure: at any position we can determine the (non-linear) surface elevation as well as the associated pressure, velocity and acceleration fields. Also the point of wave/structure interaction can be selected arbitrarily, and any test can be repeated deliberately. Consequently, cause-reaction chains can be identified to reveal the mechanism of wave/structure interactions.

References

[1] Clauss, G. (1999). Task-related wave groups for seakeeping tests or simulation of design storm waves. *Applied Ocean Research* (21):219-234.

[2] Clauss, G. and Habel, R. (2000). Artificial reefs for coastal protection - transient viscous computation and experimental evaluation. In *Proceedings of the 27th International Conference on Coastal Engineering (ICCE)* Sydney, Australia.

[3] Clauss, G. and Hennig, J. (2001). Tailored transient wave packet sequences for computer-controlled capsizing tests. In *Proceedings of the 20th OMAE Symposium,* Rio de Janeiro. (to be published).

[4] Clauss, G. and Kühnlein, W. (1995). Transient wave packets - an efficient technique for seakeeping tests of self-propelled models in oblique waves. In *Third International Conference on Fast Sea Transportation,* pages 1193-1204, Vol. 2, Lübeck-Travemünde, Germany.

[5] Clauss, G. and Kühnlein, W. (1997). Simulation of design storm wave conditions with tailored wave groups. In *Proceedings of the 7th Int. Offshore and Polar Engineering Conference (ISOPE),* pages 228-237, Honolulu, Hawaii, USA.

[6] Clauss, G., Pakozdi, C., and Steinhagen, U. (2001). Experimental optimization of transient waves in extreme seas. In *Proceedings of the 11th International Offshore and Polar Conference (ISOPE),* Stavanger. Paper No: 2001-MP-05.

[7] Clauss, G. and Steinhagen, U. (1999). Numerical simulation of nonlinear transient waves and its validation by laboratory data. In *Proceedings of 9th International Offshore and Polar Engineering Conference (ISOPE),* volume III, pages 368-375, Brest, France.

[8] Clauss, G. and Steinhagen, U. (2000). Optimization of transient design waves in random sea. In *Proceedings of 10th International Offshore and Polar Engineering Conference (ISOPE),* volume III, pages 229-236, Seattle, USA.

[9] Clauss, G. and Steinhagen, U. (2001). Generation and numerical simulation of predetermined nonlinear wave sequences in random seaways. In *Proceedings of the 20th OMAE Symposium,* Rio de Janeiro. Paper No: OMAE2001/OFT-1230.

[10] Nelder, J. and Mead, R. (1965). A simplex method for function minimization. *Computer Journal,* (7):308-313.

[11] Rowan, T. (1990). *Functional Stability Analysis of Numerical Algorithms.* PhD thesis, University of Texas at Austin.

[12] Wu, G. and Eatock Taylor, R. (1994). Finite element analysis of two-dimensional non-linear transient water waves. *Applied Ocean Research,* (16):363-372.

[13] Wu, G. and Eatock Taylor, R. (1995). Time stepping solutions of two-dimensional non-linear wave radiation problem. *Ocean Engineering,* 22(8): 785-798.

Observations of Extreme 3-D Surface Water Waves

Swan, C.[1], Johannessen, T.B.[2], and Bateman, W.J.D[1]

[1] Department of Civil & Environmental Engineering
Imperial College, London. SW7 2UB.UK.
{c.swan, w.bateman}@ic.ac.uk
[2] Now at: Kværner Oil and Gas a.s.
P.O. Box 222, N-1326 Lysaker, Norway.
Thomas-B.Johannessen@kvaerner.com

Abstract. In a deep-water ocean environment wind waves are characterised by a spread of energy in both frequency and direction. In such circumstances wave focusing provides a likely mechanism for the occurrence of an extreme wave event. This arises when the phasing and direction of freely propagating wave components is such that a large number of wave crests arise at one point in space and time, thereby producing a large transient wave group. The present paper concerns the characteristics of such waves, providing both laboratory data and numerical calculations. The principle findings arising from this work are two-fold. First the importance of directionality in defining the characteristics of extreme waves is clearly highlighted. In particular, if a constant energy level (or input amplitude sum, $A = \sum a_n$) is maintained an increase in directionality leads to reduced nonlinearity and hence lower crest elevations. Conversely, if the energy levels are increased until the onset of wave breaking, an increase in the directional spread allows larger limiting waves to evolve. Secondly, the frequency-amplitude spectra in the vicinity of the extreme highlight some new and unexpected energy shifts. These are consistent with the widening of the free wave regime in the vicinity of the extreme and, as such, provide a possible mechanism for the occurrence of rogue or freak waves.

1 Introduction

Throughout this workshop the definition of a *rogue* or *freak* wave received much attention. Although no consensus was reached, the most frequently adopted definitions were based upon $\eta_{max} > 1.25H_s$ or $H > 2H_s$, where η_{max} defines the maximum crest elevation, H the wave height and H_s the significant wave height. Irrespective of the precise value employed, it is clear that rogue waves correspond to extreme events that are either larger than is statistically predicted or occur more often than is expected, given the underlying characteristics of the sea state. From an engineering perspective such events are of enormous practical importance. In particular, they are believed to be associated with the loss of an effective airgap leading to wave impacts on the underside of fixed structures, the

occurrence of wave slamming on both fixed and floating structures, and green-water inundation on the decks of floating vessels. Such problems are relevant to both offshore engineers and naval architects.

Field observations (see, for example [9]) confirm that large ocean waves do not arise as part of a regular or 'steady' wave train, but occur as isolated events within a random or irregular sea, involving a significant spread of wave energy in both frequency and direction. Furthermore, since rogue waves are large they will, inevitably, involve steep water surface elevations implying that both the wave shape and the underlying wave motions are highly nonlinear. The combination of nonlinearity, unsteadiness and directional spreading makes for a highly complex phenomena, the description of which is well beyond the scope of the commonly applied design wave solutions. Furthermore, if such waves genuinely lie outside accepted statistical predictions, and this remains an open question, it perhaps implies that their evolution involves new or unexpected physical processes that are not generally applicable to the wavefield as a whole.

The present paper considers the description of extreme water waves and seeks to define their underlying characteristics. Experimental data from a new series of laboratory observations are combined with supporting numerical calculations based upon a state-of-the-art fully nonlinear, three-dimensional, wave model. The combination of these results suggests that the evolution of large wave groups is characterised by rapid energy transfers, occurring in the vicinity of the extreme, leading to the generation of new high-frequency wave components resulting in a widening of the free-wave regime. This effect leads to a local increase in the energy density and therefore allows larger maximum crest elevations to evolve. The present paper argues that these energy transfers correspond to the 'new physics' that is necessary to explain the occurrence of rogue waves. Indeed, it is perhaps not surprising that statistical predictions, based on the original (underlying) frequency spectrum, cannot model the largest water surface elevations if, as a consequence of the evolution of large waves, the spectrum itself undergoes significant change. The present paper will also demonstrate that the directionality of a wavefield plays a crucial role in determining the effectiveness of these processes.

2 Experimental Observations

The initial motivation behind these observations was the apparent contrast between field data [9] and laboratory observations describing the focusing of unidirectional waves [1]. A typical example of the latter observations is provided in Figure 1a. This contrasts the time-history of the water surface elevation, $\eta(t)$, with a linear and a second-order theory based on the wave components generated at the paddle. It is clear from these results that the nonlinear interactions lead to a huge increase in the maximum water surface elevation, with the maximum measured crest elevation 40% larger than the linear predictions and 30% larger than second-order theory. An explanation for this lies in the nature of the nonlinear wave-wave interactions clearly identified in the frequency-amplitude

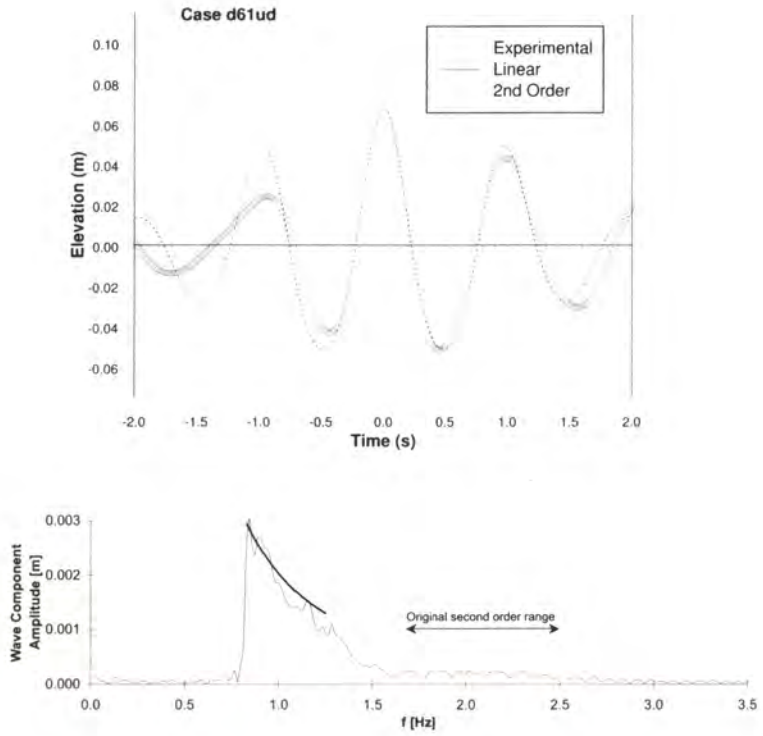

Fig. 1. Uni-directional waves: a comparison with established theory (a) Time-history of the water surface elevation, $\eta(t)$, and (b) Frequency-amplitude spectrum.

spectra given on Figure 1b. In this case the input spectrum (denoted by the thick solid line) is both narrow-banded and truncated at $f = 1.25Hz$. As a result, there is a clear division between the input range and the corresponding second-order range, defining the frequency-sum terms first identified in [10]. According to second-order theory there should be no energy within this interlying region. Furthermore, if it is assumed that any energy present is of third or higher order, it should be very small. However, Figure 1b shows that this is not, in fact, the case. Indeed, there appears to be a large transfer of energy from frequencies within the input range to those lying immediately outside. Although detailed analysis of field observations clearly identifies nonlinear effects, they are typically much smaller than those identified in Figure 1. An obvious explanation for this difference lies in the directionality (or three-dimensional character) of real ocean waves. For example, [9] shows that in the northern North Sea wind waves arising in large storms have a typical directional spread corresponding to a normal distribution with a standard deviation of 30°.

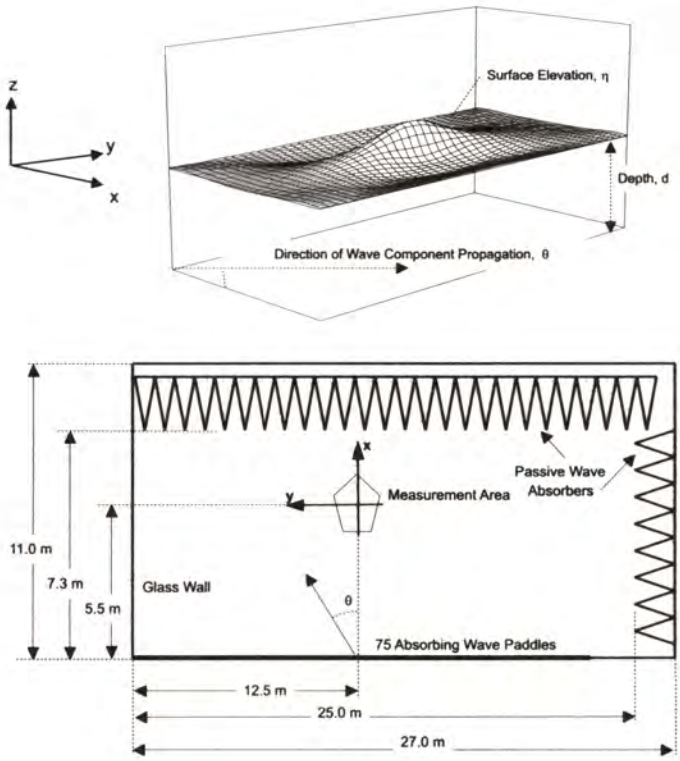

Fig. 2. a) Definition sketch. b) Wave basin

To investigate the influence of directionality laboratory observations were undertaken in which wave components, involving a spread of energy in both frequency and direction, were focused at one point in space and time. Depending on the directional spread this produces a wave form similar to that indicated in Figure 2a, where x defines the mean wave direction and d the constant water depth. These observations were undertaken in the wide wave basin at Edinburgh University. This facility has a plan area of $25m \times 11m$, a uniform depth of $1.2m$, and is equipped with 75 numerically controlled wave paddles, each $0.3m$ wide. (Figure 2b).

The test programme incorporated three frequency spectra: Case B, corresponding to a broad-banded frequency spectrum ($0.17 \leq f \leq 1.66Hz$); Case D, a narrow-banded spectrum ($0.83 \leq f \leq 1.25Hz$); and Case C of intermediate bandwidth ($0.77 \leq f \leq 1.42$). For each case, six directional spreads were considered ranging from uni-directional (or $s = \infty$), to a very short-crested sea with a large directional spread ($s = 4$), where s is the Mitsuyasu [12] spreading parameter. For each of these combinations, a range of input amplitudes were considered so that the characteristics of the focused wave event could be considered from

a near-linear condition ($A = 20mm$, where A represents the linear sum of the component wave amplitudes) to the limit of incipient wave breaking. Full details of this experimental study are given in [7].

A typical set of surface elevation measurements is presented on Figures 3a & 3b. These concern the narrow-banded frequency spectrum addressed in Figure 1a (Case D), but with directional spreads of $s = 45$ (relatively long-crested) in Figure 3a and s=4(very short-crested) in Figure 3b. In each of these three cases (Figure 1a, Figure 3a & Figure 3b) the focused waves are very close to the limit of wave breaking, and comparisons are made with both a linear and a second-order theory (where the latter model is based on [11] for the directionally-spread cases in Figures 3a & 3b). Comparisons between these results suggests that as the directionality of the wavefield increases, the second-order solution appears to provide an improved description of the maximum crest elevation. This is consistent with the field observations discussed earlier.

Further evidence of this effect is given in Figure 4a. This provides data corresponding to each of the three frequency spectra (cases B, C & D) and describes the variation in the maximum crest elevation with the directional spread (expressed as $1/s$, where $1/s = 0$ corresponds to a uni-directional wave). In each test case the input amplitude was set at $A = 55mm$. The reduction in the maximum crest elevation with increasing directionality is clearly observed. Indeed, it appears that the introduction of even a small directional spread ($s = 150$ or $1/s = 0.0067$) leads to a large reduction in the nonlinear crest elevation. If this effect is interpreted as a real reduction in the nonlinearity of a wave group (having a constant energy input: $A = 55mm$) it may, perhaps, be explained by a reduction in the absolute wave-front steepness. This arises due to the fact that as the directionality increases the wave steepness is no longer constrained within a single plain, as is the case in a uni-directional wave, but spread over a number of intersecting plains. The larger the directional spread, the smaller the wave-front steepness. The reduced nonlinearity and therefore the lower crest elevations follow as a logical consequence.

Further evidence of the reduced nonlinearity is provided by the frequency-amplitude spectra, $a(\omega)$, presented on Figure 5a. These results are derived from a Fourier transform of the water surface elevation, $\eta(t)$, recorded at the position of the maximum crest. Four data records are considered, each corresponding to the narrow banded spectrum (Case D) with an input amplitude of $A = 55mm$, but with differing directional spreads defined by $s = \infty$ (or uni-directional), $s = 150$, $s = 45$ and $s = 4$. A comparison between these traces highlights significant differences in the transfer of energy to the high-frequency wave components that lie immediately outside the input range. This transfer is largest in the uni-directional case, and progressively reduces as the directionality increases. These results appear to be consistent with the nonlinearity of a large wave being strongly dependent upon the directionality of a sea state.

Although, at first sight, the arguments noted above appear 'positive' from a design perspective, the reduced nonlinearity has wider implications. If it is assumed that the limiting condition, corresponding to the onset of wave-breaking,

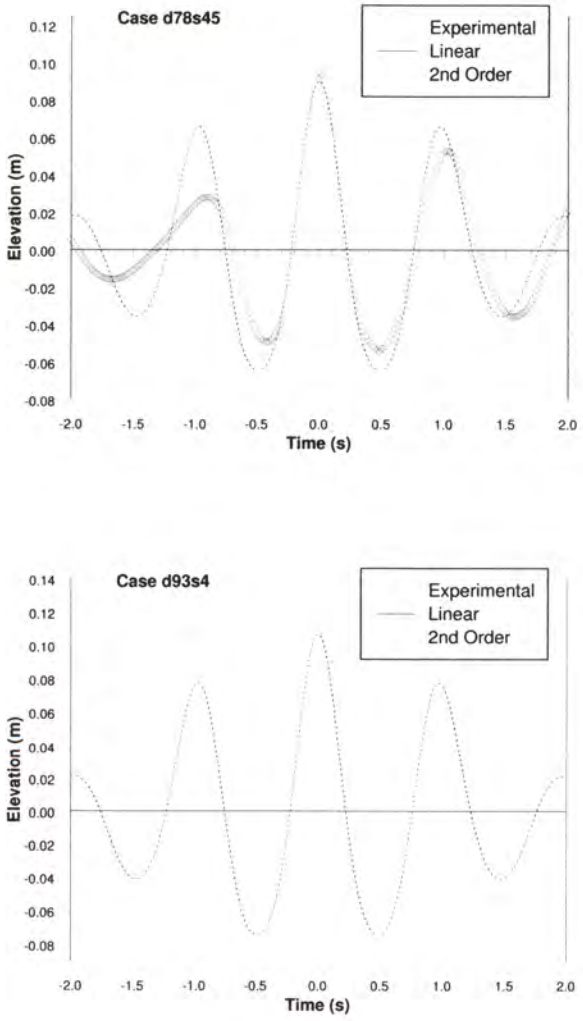

Fig. 3. Time-history of the water surface elevation, Case D. (a) $A = 78mm, s = 45$. b) $A = 93mm, s = 4$.

is largely determined by the wave steepness ($H/2k \approx 0.44$ in uni-directional regular waves), an increase in directionality should allow larger limiting wave heights and hence larger limiting crest elevations. Figure 4b again concerns each of the three underlying frequency spectra (Cases B, C & D), with the directionality specified in term of $1/s$. For each combination, the input amplitude, A, was increased until the onset of incipient wave breaking (determined visually) and

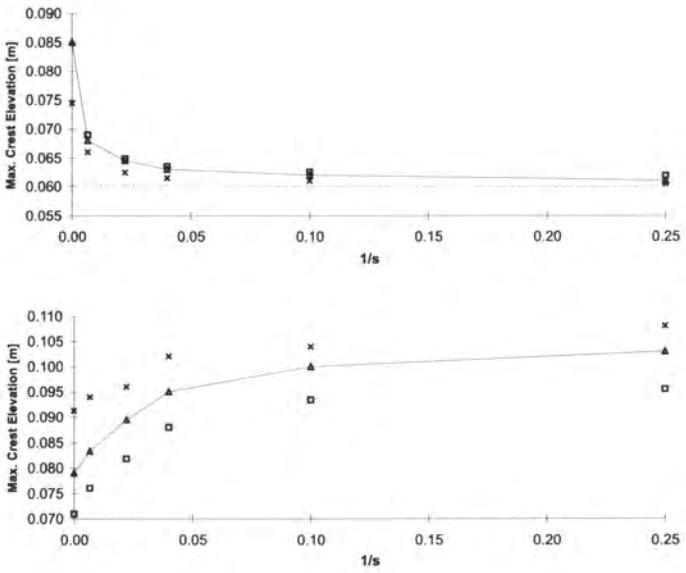

Fig. 4. Maximum crest elevation vs. directional spread. (a) Constant input amplitude, $A = 55mm$. (b) At the breaking limit. □ Case B, △ Case C & × Case D.

the maximum limiting crest elevation recorded. The data presented on Figure 4b confirms that an increase in the directional spread allows larger limiting wave crests to evolve prior to the onset of wave breaking.

Further analysis of the limiting wave profiles recorded in the narrow-banded spectrum (Case D) is given on Figure 5b. Comparisons between these results confirms that the input energy required to achieve a limiting wave increases with the underlying directionality. However, at this limiting condition the energy transferred to the high-frequency components, immediately outside the input range, appears to be independent of the directional spread. One possible explanation for these results is that the limiting wave conditions are largely dependent upon the generation of sufficient nonlinear wave components (involving both free and bound waves) arising outside the initial input range. Once this threshold is reached the wave breaks. This condition may perhaps be defined in terms of some limiting in-line crest-front steepness. In the case of a directional wave, the reduction in crest-front steepness means that more energy is required in the input range to achieve this threshold value. Accordingly, the limiting wave height and therefore also the limiting crest elevation increases with the directionality of the sea state.

Having demonstrated the importance of the energy transfers immediately outside the input range, attempts were made to determine whether these wave components were bound or freely propagating. Unfortunately, although there

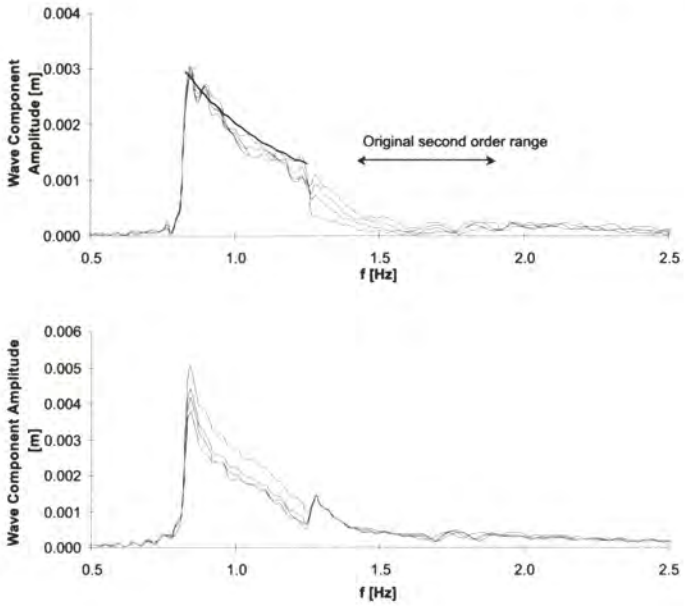

Fig. 5. Frequency-amplitude spectra (Case D). (a) Constant input amplitude, $A = 55mm$. (b) At the breaking limit.

was considerable evidence to suggest the latter, this could not be rigorously proven on the basis of the laboratory data alone.

3 Numerical Calculations

To further our understanding of extreme ocean waves recent work has sought to provide a fully nonlinear numerical wave model capable of describing the evolution of waves which are spread in both frequency and direction. This work has progressed in two stages. The first was undertaken by Johannessen [6] in which he developed a three-dimensional scheme based upon the uni-directional model proposed in [5]. This was the first fully nonlinear three-dimensional wave model of its kind. As with other (uni-directional) time-marching procedures this solution is essentially exact and very good agreement was achieved with the previously-noted laboratory data [7]. However, the nature of this solution, involving large matrix inversion, is such that it is computationally intensive. As a result, the solution is limited when it comes to the description of realistic ocean waves, involving a large range of length-scales in two horizontal directions (x, y).

To overcome this difficulty a second solution has been proposed by Bateman [2]. This model extends a uni-directional scheme proposed in [4] to describe directionally spread waves. The principal advantage of this solution lies in its computational efficiency, achieved by the application of a new three-dimensional

G-operator. This represents an approximation of the Dirichlet-Neuman operator the purpose of which is to transform boundary values of the velocity potential, ϕ, at the water surface into values of ϕ_z. This allows an initial spatial representation of the water surface elevation and the velocity potential on this surface to be time-marched using fast Fourier transforms, thereby avoiding the need for large matrix inversion.

The elegance of this approach is such that the computational effort required to run the scheme increases as $NlogN$, where N is the number of surface points at which calculations are undertaken. This is in stark contrast to the original scheme, proposed in [6] and further explained in [8], where the computational effort increases as N^3. This difference is of fundamental importance when seeking to provide accurate calculations of extreme ocean waves, involving broad-banded frequency spectra and realistic directional spreads. In its present form the model is appropriate to waves propagating in water of constant depth. It runs on a standard PC, and is sufficiently stable to predict the evolution of near-breaking waves. Indeed, the only significant restriction arises due to the Fourier series representation. This requires the water surface elevation, $\eta(x, y)$, to be a single-valued function of the horizontal coordinates and therefore limits the model to non-overturning waves. Full details of this solution are given in [3].

4 Discussion of Results

To highlight the success of the numerical modelling Figures 6a-6c provide a typical example of the agreement between the laboratory data and the numerical calculations. This case concerns the narrow-banded spectrum (Case D), with a large directional spread ($s = 4$) and an input amplitude of $A = 93mm$ giving rise to a highly nonlinear, near-breaking, wave event. This case will subsequently be referred to as Case D93S04.

In this and all subsequent comparisons, the numerical model is simply based upon the underlying linear wave spectrum, $S_{\eta\eta}(\omega, \theta)$, or the wave components generated at the wave paddles, together with the assumption that their phasing and/or direction of propagation, θ, are such that they will come into phase at one point in space and time. (This latter assumption also forms the basis of the NewWave model [16] used to describe the average or most-probable shape of an extreme wave event). The initial or starting conditions, from which the time-marching process commences, are specified using a linear wave theory applied at some initial time $t = t_0$, well in advance of the extreme event so that the wave energy is widely distributed across the computational domain. Using this approach no prior knowledge is required concerning the shape of the extreme water surface elevation and consequently the method is genuinely 'predictive'. This is in marked contrast to the second-order, or quasi second-order, solutions given in [15] and [17]. These are based upon either a recorded time-history of the extreme wave event, $\eta(t)$, or a power spectrum describing the energy distribution associated with such an event, $S_{\eta\eta}(\omega)$, where the latter implies the same prior description of the extreme water surface elevation.

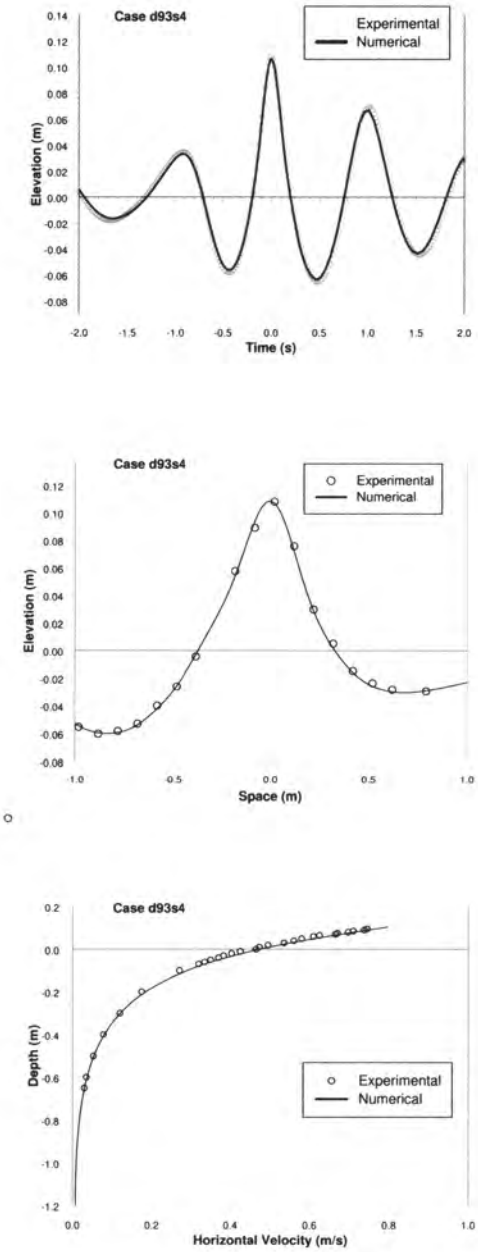

Fig. 6. Comparison with the numerical model. (a) Time-history of the water surface elevation, $\eta(t)$. (b) Spatial history of the water surface elevation, $\eta(x)$. (c) Horizontal velocity profile beneath the largest crest, $u(z)$

Figure 6a contrasts the measured and predicted time-history of the water surface elevation, $\eta(t)$, at the focal position; Figure 6b the spatial description of the water surface profile, $\eta(x)$, at the instant of wave focusing; and Figure 6c the in-line (or x-component) of the wave induced horizontal velocity directly beneath the largest wave crest, $u(z)$. In each of these figures the agreement between the experiment and the theory is near perfect.

To clarify the nature of the nonlinear interactions associated with the evolution of an extreme, directionally spread, wave group the distribution of energy in the vicinity of the extreme must be considered. Such an investigation is best conducted in the absolute wavenumber-frequency domain, or $|k|$ vs ω, where $|k| = \sqrt{k_x^2 + k_y^2}$ and (k_x, k_y) are the wavenumbers in the x and y directions respectively. Figure 7 concerns Case D93S04 and provides a contour plot outlining the energy distributions within this domain. In effect, this figure may be viewed as a sequence of diagonal 'patches', where the second patch from the left incorporates the highest energy levels and corresponds, at least in part, to the linear input range. Within this dominant energy, the solid black line defines the linear dispersion equation, the boundaries of which (denoted by a vertical line) correspond to the range of freely propagating wave components generated at the wave paddles.

Immediately to the left of this dominant energy there is a relatively indistinct 'patch' involving small energy distributions. These correspond to the low frequency, or frequency-difference, terms representing the set-down beneath the wave group. This energy distribution will be dominated by second-order effects [11, 13] which are not expected to be large in deep water. Further discussion of these terms and, in particular, their increasing importance as the water depth reduces is given in [14]. To the right of this dominant energy lies a sequence of 'patches' representing the second, third, and fourth-order interactions, where the second-order terms correspond to the two-wave frequency-sum terms, again investigated in [11, 13]. As expected, the frequency-sum terms involve larger energy distributions than the frequency-difference terms. Furthermore, within the high-frequency range the energy levels rapidly decline with increasing order.

The most significant aspect of this figure arises within the dominant or first-order range. Comparisons between the contour lines and the linear input range confirms that there is significant energy arising in frequencies that are immediately adjacent to the upper limit of the input range i.e. $1.25 \leq f \leq 2.25Hz$. This corresponds to the additional wave energy identified in the frequency-amplitude spectra given in Figures 5a & 5b. If the line representing the linear dispersion equation is extended beyond the input range, defining the wave components generated at the wave paddle, the dashed line included on Figure 7 results. Comparison between this line and the new high-frequency energy distributions suggests that much of this energy is freely propagating. This result suggests that in the vicinity of an extreme wave event there is a local, and rapid, widening of the free wave regime. This is consistent with several other aspects of the laboratory study reported in [7]. In particular, quantitative observations of the velocity of the largest wave crest suggests that as it evolves, and grows in size, its velocity

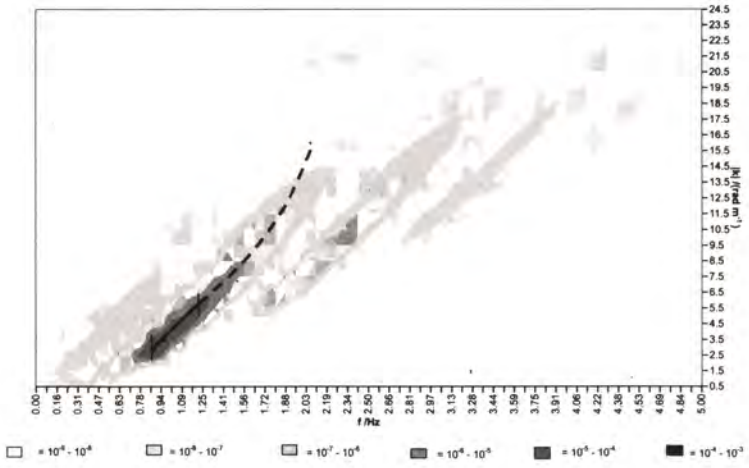

Fig. 7. Energy distribution in f vs $|k|$ space.

initially increases and then, in the vicinity of the extreme, actually reduces. The initial increase undoubtedly represents the nonlinear increase in the phase velocity and is consistent with the notion that larger waves travel faster. However, the subsequent decrease can only come about due to changes in the free-wave regime. Indeed, the bound-wave structure cannot produce such a change since it is, by definition, tied to its associated free waves and therefore has no impact on the crest velocity.

This apparent widening of the free wave regime is important from the perspective of rogue waves since it implies the potential for increased crest elevations. This effect can easily be demonstrated by considering a simple linear argument. If a focused wavefield consists of N linear wave components defining a top hat amplitude spectrum, the maximum crest elevation is given by the linear amplitude sum, A:

$$A = \sum_{n=1}^{N} a_n = Na \tag{1}$$

where $a_n = a$ is the constant amplitude of the wave components. The energy associated with such a system is proportional to:

$$M_0 = \sum_{n=1}^{N} \frac{1}{2} a_n^2 = \frac{1}{2} N a^2 \tag{2}$$

If this is compared to a second focused wave group consisting of $2N$ wave components each with an amplitude of a', twice the band width, but an identical

energy we obtain:

$$M_0 = \sum_{n=1}^{2N} \frac{1}{2} a'^2 \text{or} a' = \frac{1}{\sqrt{2}^a} \tag{3}$$

As a result, it is easily shown that the amplitude sum, and hence the maximum crest elevation, arising in the second wave field is larger than that of the first by a factor of $\sqrt{2}$:

$$A' = \sum_{n=1}^{2N} a' = 2Na' = \sqrt{2}A \tag{4}$$

5 Concluding Remarks

The present paper has provided both laboratory observations and numerical calculations appropriate to the description of extreme, near-breaking, waves arising due to the focusing of wave components involving a spread of energy in both frequency and direction. The results have shown that if the energy associated with the wavefield is held constant (in a laboratory context this corresponds to a constant input amplitude sum, A) an increase in the directional spread leads to lower maximum crest elevations. It is believed that this arises due to a reduction in the in-line crest-front steepness, thereby causing the reduced nonlinearity. This explains the apparent mismatch between uni-directional laboratory studies and recent field observations of large waves, where the latter appear to be less nonlinear. In contrast, if one considers the limiting characteristics of focused waves an increase in the directional spread allows larger limiting crest elevations to evolve.

More significantly, the present results have shown that as a large wave event evolves, the nonlinear interactions lead to a transfer of energy to the higher-frequency wave components lying immediately outside the input range. This is quite distinct from the second-order frequency-sum terms originally identified in [10]. Indeed, numerical calculations suggest that much of this transferred energy is freely propagating. In the context of rogue waves this is an important result since it implies a local and rapid widening of the free wave regime in the vicinity of the extreme event. This, in turn, has the potential to allow increases in the maximum crest elevation. Indeed, if the underlying spectrum defining the freely propagating wave components can change in both space and time, it is perhaps not surprising that local extremes may differ significantly from the results of statistical predictions based on the underlying linear spectrum. Although further work is undoubtedly required, the energy transfers identified within this study may provide at least a partial explanation for the occurrence of rogue waves.

References

1. Baldock, T.E., Swan, C. and Taylor, P.H.: A Laboratory Study of Non-Linear Surface Waves on Water. Phil. Trans. Roy. Soc. London. Ser. A, 354, (1996) 649–676

2. Bateman, W.J.D.: A Numerical Investigation of Three Dimensional Extreme Water Waves. PhD Thesis, Imperial College, University of London (2000)
3. Bateman, W.J.D., Swan, C. and Taylor, P.H.: On the Efficient Numerical Simulation of Directionally-Spread Surface Water Waves Submitted to J.Comp.Phys. (2001)
4. Craig, W. and Sulem, C.: Numerical Simulation of Gravity Waves. J. Comp. Physics, **108** (1993) 73–83
5. Fenton, J.D. and Rienecker, M.M.: A Fourier Method for Solving Nonlinear Water-Wave Problems: Application to Solitary-Wave Interactions. J.Fluid Mechanics, **118** (1982) 411–443
6. Johannessen, T.B.: The Effect of Directionality on the Nonlinear Behaviour of Extreme Transient Ocean Waves. PhD Thesis, Imperial College, University of London (1997)
7. Johannessen, T.B. and Swan, C.: A Laboratory Study of the Focusing of Transient and Directionally Spread Surface Water Waves. Proc. R. Soc., Ser. A, **457** (2001) 1–36
8. Johannessen, T.B. and Swan, C.: The Nonlinear Dynamics of Focussed Wave Groups in Two and Three Dimensions. Submitted to Proc. R. Soc., Ser A (2001)
9. Jonathan, P. and Taylor, P.H.: Irregular Nonlinear Waves in a Spread Sea. ASME Transactions J. of Offshore Mechanics and Arctic Engineering, **119** (1996) 37–41
10. Longuet-Higgins, M.S. and Stewart, R.W.: Changes in the Form of Short Gravity Waves on Long Waves and Tidal Currents. J.Fluid Mechanics, **8** (1960) 565–583
11. Longuet-Higgins,M.S.: The Effect of Non-Linearities on Statistical Distributions in the Theory of Sea Waves. J.Fluid Mechanics, **17** (1963) 459–480
12. Mitsuyasu, H.: Observation of Directional Spectrum of Ocean Waves Ua Cloverlead Buoy. J.Phys. Oceanography, **16** (1975) 459–482
13. Sharma, J.N. and Dean, R.G.: Second-Order Directional Seas and Associated Wave Forces. Society of Petroleum Engineering Journal, **4**, (1981) 129–140
14. Smith S.F. and Swan C.: Extreme Two-Dimensional Water Waves: An Assessment of Potential Design Solutions. To appear: J. Ocean Engng. (2001)
15. Stansberg, C.T.: Second-Order Numerical Reconstruction of Laboratory Generated Random Waves. Proc. 12th Offshore Mech. and Arctic Eng. Conf. (OMAE),**2** (1993) 143-151
16. Tromans, P.S., Anaturk, A.R. and Hagemeijer, P.: A New Model for the Kinematics of Large Ocean Waves. Submitted to ISOPE-91 Conference in Edinburgh. (1991)
17. Zhang, J., Yang, J. and Wen, J.: Hybrid Wave Models and Their Application. Proc. Int. Symp. Ocean Wave Kinematics Dynamics and Loads on Structures. ASCE, Ed. J. Zhang. Houston, Texas. **1** (1998) 25-33

Session 7

Statistics for Extreme Waves

Statistics of Second-Order Stokes Waves and of Their Extremes

Ulla Machado

Lund University, Centre for Mathematical Sciences, Box 118,
SE-22100 Lund, Sweden
ullam@maths.lth.se

Abstract. A general method is presented for estimating distributions of the characteristic wave parameters of second-order Stokes waves. The second-order Stokes waves are expressed as a sum of a linear part (Gaussian process), and a non-linear part (quadratic transformation of a Gaussian process). Using Rice's formula the mean up-crossing intensities are estimated for different sea levels. The Transform Gaussian Process Method is then used to obtain the distributions. A numerical example is shown where the distributions of crest period vs crest amplitude are estimated.

1 Introduction

In safety analysis of offshore structures and marine vessels there are mainly two types of problems we need to consider: the estimation of the probability for waves to exceed a critical level, and the estimation of the variability of the stresses that causes fatigue. Most research has been carried out under the assumption that both the wave loads and the responses of the offshore structures are Gaussian processes. However, statistical analyses of real sea data show that the high and steep waves deviate from this assumption. Moreover, it is well known that most of the offshore structures are non-linear systems, and accordingly their response processes are also non-Gaussian.

In this study we consider the non-linear process of the second-order description of the sea, the so called Stokes waves. We apply Rice's formula in order to estimate the mean up-crossing intensities of different sea levels. The numerically computed intensities are then used to determine approximately the distributions of the characteristic wave parameters of the non-Gaussian sea surface elevation.

2 The Stochastic Process

We approximate the random free surface elevation by the second-order Stokes wave, $\eta(t)$. From a probabilistic point of view this is a stochastic process which can be expressed as a sum of a linear part (Gaussian process), and a non-linear part (quadratic transformation of a Gaussian process). More precisely,

$$\eta(t) = \eta_g(t) + \eta_{so}(t) = \sum_{j=1}^{2N} \beta_j Z_j(t) + \lambda_j Z_j(t)^2 \qquad (1)$$

where Z_j are independent Gaussian processes, and β_j and λ_j are coefficients computed based on the information provided by the sea spectrum $S(\omega_n)$, which is chosen for a given sea state (H_S, T_Z). More precisely, these coefficients β_j and λ_j are obtained following a procedure first proposed by Langley in [1], a brief review is presented in the Appendix.

Other processes interesting to engineers can be represented as in eq. (1), such as the motion response of a linear structure subjected to a Gaussian wind velocity, and the excursion response of a moored floating offshore platform in a random sea. Some research has been done, see for instance [3] or [4].

3 The Narrow-Band Approximation

In case of the narrow-band approximation the interaction coefficients $E^-_{n,m}$ and $E^+_{n,m}$ (see the Appendix), become

$$E^+_{n,m} \approx \frac{\omega_p^2}{2g} \qquad \text{and} \qquad E^-_{n,m} \approx 0 \tag{2}$$

where ω_p is the peak frequency. Introducing this information into the formulation presented in the Appendix we can verify that eq. (1) becomes much simpler

$$\eta(t) = \beta_1 Z_1(t) + \lambda_1 Z_1(t)^2 + \lambda_2 Z_2(t)^2 \tag{3}$$

where

$$\beta_1 = \sqrt{\sum_{i=1}^{N} S(\omega_i)\,\Delta\omega} \qquad \lambda_1 = \frac{\omega_p^2}{2g} \sum_{i=1}^{N} S(\omega_i)\,\Delta\omega \qquad \lambda_2 = -\lambda_1. \tag{4}$$

In general, when the narrow-band approximation is considered in the literature, the process is written as

$$\eta(t) = X(t) + \frac{\omega_p^2}{2g}(X(t)^2 - Y(t)^2) \tag{5}$$

where $X(t)$ is a zero mean Gaussian process with one side spectral density $S(\omega)$ and $Y(t)$ is its Hilbert transform. It is easy to see that eqs. (3 and 5) are equivalent.

4 Distributions of the Characteristic Wave Parameters

In order to develop practical models for use in the offshore-industry it is necessary to 'obtain' statistics of waves. There are different ways to obtain these statistics, either from direct measurements, or from different models which take the wave spectrum as input. Although, direct measurements appear to be straight forward they have a great disadvantage: the measurements are never long enough to provide valid information concerning the extremes. In addition, the data are not

'clean', i.e. they need processing which leads to a loss of information, increasing costs and time. Thus, there is a great need for mathematical models that enable us to obtain statistics of waves from a selected sea spectrum.

We can say that there exists mainly two types of models: models based on Monte Carlo techniques and development of simulators, and models derived from theoretical considerations. Here, we use a model of the second type, more precisely the *Transform Gaussian Process Method*, which was first presented in Rychlik et al. [7]. The main idea is as follows: once we have written the sea elevation process as in eq. (1), and computed the intensity of up-crossings for the different sea levels $\mu^+(u)$, we consider a transformed Gaussian process which has the same intensity of up-crossings as our initial process. For this last process we compute then the different distributions of the characteristic wave parameters (statistics of waves).

In this way, the problem of estimating the distributions of the characteristic wave parameters of the process $\eta(t)$ is reduced to that of estimating distributions of the characteristic wave parameters of a Gaussian process as in [5]. More precisely, these distributions are obtained using a MATLAB toolbox WAFO-Wave Analysis in Fatigue and Oceanography [1], which was developed by the department of Mathematical Statistics in Lund, and contains a comprehensive package of numerical subroutines and programs for statistical analysis of random waves.

5 Numerical Procedures

5.1 The Mean Up-Crossing Intensity

For a given water level u the mean up-crossing intensity $\mu^+(u)$ of the process $\eta(t)$ is given by Rice's formula

$$\mu^+(u) = \int_0^{+\infty} z\, p_{\eta\dot{\eta}}(u, z) dz \tag{6}$$

where $p_{\eta\dot{\eta}}(u, z)$ denotes the joint probability density function of η and $\dot{\eta}$. This density is very difficult (if possible) to compute. In contrary, the characteristic function of η and $\dot{\eta}$, $M(\theta_1, \theta_2)$ can be evaluated by a closed form. By definition, $M(\theta_1, \theta_2) = \mathrm{E}\left[e^{i\theta_1\eta + i\theta_2\dot{\eta}}\right]$ and is the Fourier transform of $p_{\eta\dot{\eta}}(u, z)$. Introducing this fact and using the Fourier transform properties, the formula above can be written in a more compact form (which replaces the triple integration by a double one, and introduces an extra derivative). As shown by Naess in [2], (for a stationary process)

$$\mu^+(u) = -\frac{1}{2\pi} \int_{-\infty}^{+\infty} \left[\frac{1}{2\pi} \int_{-\infty}^{+\infty} \frac{1}{\theta_2} \frac{\partial M(\theta_1, \theta_2)}{\partial \theta_2} e^{-iu\theta_1} d\theta_1 \right] d\theta_2 \tag{7}$$

[1] Available for free of charge at `http:/www.maths.lth.se/matstat/wafo/`.

where the outer integral is interpreted as a principal value integral in the sense that $\int_{-\infty}^{+\infty} = \lim_{\epsilon \to 0}\left(\int_{-\infty}^{-\epsilon} + \int_{+\epsilon}^{+\infty}\right)$. The characteristic function $M(\theta_1, \theta_2)$ in the present case can be evaluated as

$$M(\theta_1, \theta_2) = \exp\left\{ -\frac{1}{2}\ln(\det(\mathbf{A})) - \frac{1}{2}\theta_2^2\,\boldsymbol{\beta}'\,\mathbf{V}\,\boldsymbol{\beta} + \frac{1}{2}\mathbf{t}'\,\mathbf{A}^{-1}\,\mathbf{t}\right\} \tag{8}$$

where

$$\begin{aligned} \mathbf{A} &= \mathbf{I} - 2i\theta_1\boldsymbol{\Lambda} - 2\,i\,\theta_2\,(\boldsymbol{\Lambda}\,\boldsymbol{\Sigma}_{21} + \boldsymbol{\Sigma}_{12}\,\boldsymbol{\Lambda}) + 4\,\theta_2^2\,\boldsymbol{\Lambda}\,\mathbf{V}\,\boldsymbol{\Lambda} \\ \mathbf{t} &= (i\,\theta_1\,\mathbf{I} + i\,\theta_2\,\boldsymbol{\Sigma}_{12} - 2\,\theta_2^2\,\boldsymbol{\Lambda}\,\mathbf{V})\boldsymbol{\beta} \\ \mathbf{V} &= \boldsymbol{\Sigma}_{22} - \boldsymbol{\Sigma}_{21}\boldsymbol{\Sigma}_{12} \end{aligned} \tag{9}$$

and $\boldsymbol{\Lambda}$ is a diagonal matrix with the parameters $\lambda_1, \lambda_2, \cdots \lambda_{2N}$ on the main diagonal. The correlation structure between the Gaussian variables $Z_i(t), Z_j(t)$ and $\dot{Z}_i(t), \dot{Z}_j(t)$ is given by the following covariance matrix

$$\boldsymbol{\Sigma} = \begin{pmatrix} \boldsymbol{\Sigma}_{11} & \boldsymbol{\Sigma}_{12} \\ \boldsymbol{\Sigma}_{21} & \boldsymbol{\Sigma}_{22} \end{pmatrix} \tag{10}$$

where

$$\boldsymbol{\Sigma}_{11}(i,j) = \mathrm{E}[Z_i Z_j] \qquad \boldsymbol{\Sigma}_{12}(i,j) = \mathrm{E}[Z_i \dot{Z}_j] \tag{11}$$

$$\boldsymbol{\Sigma}_{21}(i,j) = \mathrm{E}[\dot{Z}_i Z_j] \qquad \boldsymbol{\Sigma}_{22}(i,j) = \mathrm{E}[\dot{Z}_i \dot{Z}_j]. \tag{12}$$

In order to solve the integral inside brackets in eq. (7) we use a method similar to the Saddle Point Method. It is a generalization of the numerical method first proposed by Rice in [6].

6 Numerical Example

The input spectrum selected for the present example is a JONSWAP spectrum (deep waters) with significant wave height $H_S = 7$ [m], peak period $T_P = 11$ [sec] and peak-shape parameter $\gamma = 2.3853$. The spectrum is evaluated in 257 bands of frequency, ranging from 0 to 3 [rad/sec], see figure (1) on the *Left*.

To evaluate the accuracy of our theoretical model we simulate the process represented by the spectrum above, and compute the empirical up-crossings intensity for it. Hence, eq. (13) with the interaction coefficients evaluated for the deep water conditions, is used to perform 100 non-linear simulations, each of them with a duration of $T = 10000$ [sec] ≈ 2.8 [hours] where $\Delta t = 0.5$ [sec].

We define crest Period Tc, as the period between an up-crossing and the next down-crossing, and crest Amplitude Ac the amplitude of the crest. In the *Right* graph of figure (1) we can see the empirical distribution (Tc, Ac) obtained from the simulation described above. Notice that the dots represent only part of the simulated waves. The continuous lines (level curves) are obtained using a

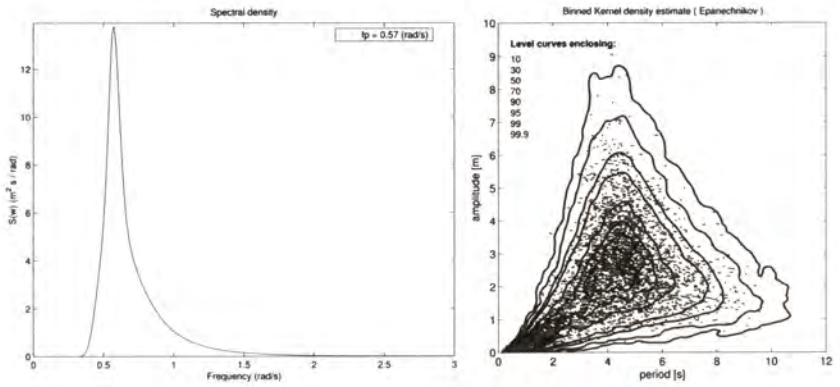

Fig. 1. *Left*: JONSWAP spectrum used in the example. *Right*: Kernel density estimate of Tc and Ac, using circa 100000 non-linear simulated waves.

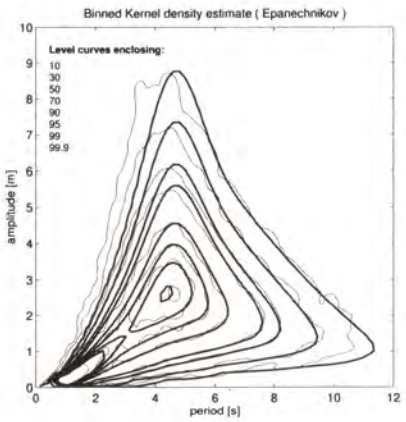

Fig. 2. Theoretical method (bold line) and Kernel estimate (thin line).

Kernel density estimate (WAFO toolbox). Each of the level curves encloses the percentage of waves mentioned in the legend of the plot. For example, if we look to the outer curve; it means that 99.9 % of the simulated waves are inside this curve, and 0.1 % are outside. In the present case this corresponds to have about 100 waves outside this level curve.

To apply the method here proposed we proceed as follows: We compute the coefficients β_j and λ_j as explained in the Appendix, and then we estimate the mean up-crossing intensity $\mu^+(u)$ according to eq. (7) using a numerical method. Next we use $\mu^+(u)$ as input to the *Transform Gaussian Process Method* in order to obtain a transformation function and finally get the distribution (Tc, Ac). The results obtained are presented using bold line in Fig. 2. When comparing them with the Kernel density estimate (thinner line), we notice that the steepest

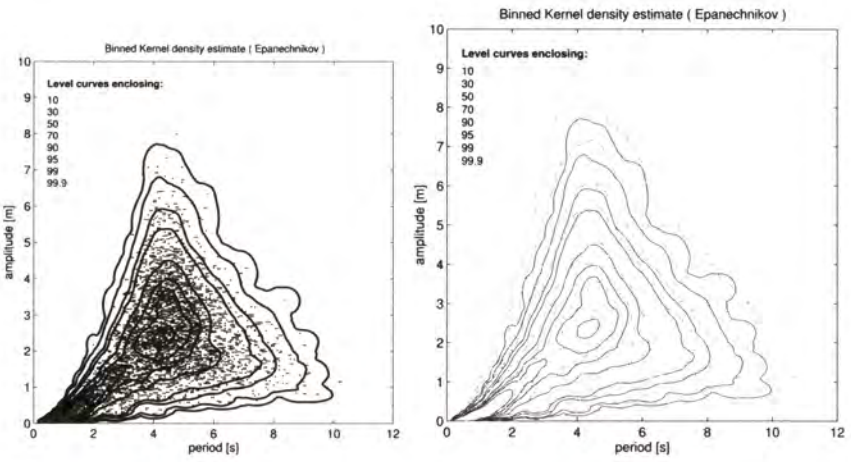

Fig. 3. *Left*: Kernel density estimate of Tc and Ac, in the case of the narrow band approximation. *Right*: Comparison of the Kernel density estimates; broad band (dashed line) and narrow band (solid line).

waves are 'missing'. The distributions fit well each other in the areas with larger number of waves, however in the case of waves of short (Tc) and high (Ac) the curves are not agreeing so well.

6.1 Narrow-Band Approximation

To the *Left* in figure (3), we have the Kernel density estimate of Tc and Ac in the case of the

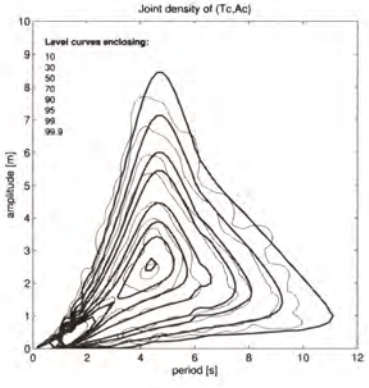

Fig. 4. Theoretical method (bold line) and Kernel estimate (thin line).

narrow-band approximation, and to the *Right* we compare it (solid line) to the Kernel estimate in the broad-band case (dashed line). We notice that we obtain smaller waves when we assume a narrow band spectrum.

In figure (4) we apply the theoretical method (bold line) to the narrow-band case and compare it to the empirical distribution. In this case it seems that the theoretical distribution fits well with the empirical distribution in all the regions. Although, since narrow-band is assumed we have already excluded the very steep waves.

7 Conclusions and Further Developments

We have applied the Transform Gaussian Process Method to obtain distributions of the characteristic wave parameters of the second-order Stokes waves. A case study where we used the JONSWAP spectrum as input has been presented. We have found that the simulations of the complete second-order Stokes waves model contains steeper waves then the waves obtained when applying the Transform Gaussian Method. However, for larger values of crest period there is a good agreement between the simulated values and the values produced by the theoretical model. When we consider narrow-band approximation the simulations and the theoretical model give similar results which shows that the theoretical model works well under this assumption.

Currently we investigate if the same tendencies appear when we consider other types of wave spectra as input, namely bi-modal spectra and measured spectra.

References

1. Langley, R. S.: A Statistical Analysis of Non-Linear Random Waves. Ocean Eng. Offshore Structures Group, College of Aeronautics, Cranfield Institute of Technology, Cranfield, Beds. MK43 0AL, U.K. (1986) 389–407
2. Naess, A.: Crossing Rate Statistics of Quadratic Transformations of Gaussian Processes. Technical Report R-2-00, Norwegian University of Science and Technology, Department of Structural Engineering (2000)
3. Naess, A., Machado U.: Response Statistics of Large Compliant Offshore Structures. In *Proceedings 8th ASCE Specialty Conference on Probabilistic Mechanics and Structural Reliability* New York: ASCE (2000)
4. Naess, A., Machado U.: Response Statistics of Linear Dynamic Systems Subjected to Quadratic Transformations of Gaussian Processes. In *Proceedings of the Euromech Colloquium 413: Stochastic Dynamics of Nonlinear Mechanical Systems* Palermo, Italy (2000)
5. Podgórski, K., Rychlik, I., Machado, U.: Exact Distributions for Apparent Waves in Irregular Seas. Ocean Eng **27** (2000) 979–1016
6. Rice, S. O.: Distribution of Quadratic Forms in Normal Random Variables - Evaluation by Numerical Integration. Siam Journal Sci. Stat. Comput. **1** (1980) 438–448
7. Rychlik, I., Johannesson, P., Leadbetter, M.R.: Modeling and Statistical Analysis of Ocean Wave Data Using Transformed Gaussian Processes. Marine Structures **10** (1997) 13–47

Appendix

Computation of β_j and λ_j in the Case of the Second-Order Description of the Sea

The second-order sea elevation can be expressed as

$$\eta(t) = \mathbf{s}^T\mathbf{X}(t) + \mathbf{X}(t)^T(\mathbf{Q}+\mathbf{R})\mathbf{X}(t) + \mathbf{Y}(t)^T(\mathbf{Q}-\mathbf{R})\mathbf{Y}(t) \tag{13}$$

where $\mathbf{s}$ is a vector with components $\sqrt{S(\omega_n)\,\Delta\omega}$, $\mathbf{X}(t)$ and $\mathbf{Y}(t)$ are vectors for each t, and $\mathbf{Q}$ and $\mathbf{R}$ are real symmetric matrices with components $\mathbf{Q}(n,m) = \sqrt{S(\omega_n)\,S(\omega_m)}\,\Delta\omega\,E^-_{n,m}$ and $\mathbf{R}(n,m) = \sqrt{S(\omega_n)\,S(\omega_m)}\,\Delta\omega\,E^+_{n,m}$. The interaction coefficients $E^-_{n,m}$ and $E^+_{n,m}$, are obtained from a second-order perturbation analysis. In the case of deep waters they assume the following form

$$E^+_{n,m} \approx \frac{1}{4g}(\omega_n^2+\omega_m^2) \qquad \text{and} \qquad E^-_{n,m} \approx -\frac{1}{4g}|\omega_n^2-\omega_m^2|. \tag{14}$$

Introducing an eigenvalue decomposition, eq. (13) becomes

$$\eta(t) = \mathbf{s}^T\mathbf{X}(t) + \mathbf{X}(t)^T\mathbf{P}_1^T\Delta_1\mathbf{P}_1\mathbf{X}(t) + \mathbf{Y}(t)^T\mathbf{P}_2^T\Delta_2\mathbf{P}_2\mathbf{Y}(t) \tag{15}$$

where Δ_i is a diagonal matrix with the eigenvalues in the respective diagonal and $\mathbf{P}_i$ contains the corresponding eigenvectors per row. Introducing a new set of Gaussian random variables $Z_j(t)$, such that

$$\mathbf{Z}(t) = \begin{bmatrix} \mathbf{P}_1 & 0 \\ 0 & \mathbf{P}_2 \end{bmatrix} \begin{bmatrix} \mathbf{X}(t) \\ \mathbf{Y}(t) \end{bmatrix} \tag{16}$$

we can write the stochastic process $\eta(t)$ as in eq. (1), with the coefficients computed as follows

$$\beta = \begin{bmatrix} \mathbf{P}_1\mathbf{s} \\ 0 \end{bmatrix} \qquad \lambda = \begin{bmatrix} (\Delta_1)^d \\ (\Delta_2)^d \end{bmatrix} \tag{17}$$

where $(\Delta_i)^d$ denotes a column vector formed by the diagonal elements of Δ_i.

Long- and Short-Term Extreme Wave Statistics in the North Sea: 1994-1998

Julian Wolfram, Brian Linfoot, and Paul Stansell

Heriot-Watt University, Edinburgh EH14 4AS, UK
b.t.linfoot@hw.ac.uk

Abstract. The results of probability analysis of rogue waves recorded at North Alwyn between August, 1994 and June, 1998 are presented as a bivariate distribution of normalised $H' = H/H_{mo}$ vs. $S' = gST_{zu}^2/2\pi H_{mo}$ for rogue waves defined as $H' > 2.0, S' > 0.5$. The probability distribution is the extreme tail of the bivariate distribution formed from the overall population of H' and S'. The rogue waves exhibited a marginal exponential distribution of normalised height, the marginal distribution of normalised steepness was Weibull and the joint distribution showed that the maxima of the conditional distribution of normalised steepness were constant at 1.5. The rogue waves were generally 50% steeper than the significant steepness and the preceding and succeeding waves had steepness values around half the corresponding significant values while their heights were around the significant height. Tentatively we propose that a more logical definition for rogue waves would be those where $H' > 2.3$ since the probability distribution of these waves appears to depart from that of their neighbours from this point.

1 Introduction

The conventional definition of rogue waves as all waves exceeding twice the significant wave height (e.g. Ochi [1],page 253) provides a conveniently precise criterion for the automated analysis of field data records; although it can be argued, Ochi, *op. cit.*, that such waves would occur fairly frequently in the natural record of extended duration storms. The approximate asymptotic formula due to Longuet-Higgins [2] for the expected value of the maximum wave height for the number of zero-crossing waves, assuming stationary conditions, is

$$\frac{H_{\max}}{H_{mo}} = \frac{1}{\sqrt{2}}\left((\ln N)^{1/2} + 0.2886(\ln N)^{-1/2}\right) \tag{1}$$

which leads to $N = 1655$ with $H_{\max}/H_{mo} = 2$.

For T_z ranging between 8 and 16 seconds the corresponding durations in hours are:

T_z (s)	8	10	12	14	16
Duration (h)	3.68	4.60	5.52	6.44	7.36

The duration of quasi-stationary conditions at the storm peak, with H_{mo} varying within ± 0.5m, typically falls in the range between 2 to 5 hours. Total storm durations commonly exceed these values - two data sets collected in the North Sea in 1997 had lengths of 159 hours and 139 hours during which H_{mo} exceeded 3.5m. For the purposes of this paper we have adopted this definition of rogue waves and applied it to data collected over four years in the northern North Sea in order to provide a probabilistic measure of rogue wave occurrence based on the joint distribution of normalised wave height and steepness. The height and steepness of these extreme waves has been compared with corresponding values for neighbouring waves in order to determine if the extreme waves are singular isolated events in the wave record or if they belong to groups.

The paper begins with a summary of the data collection systems at North Alwyn and procedures adopted to process this data to obtain joint H', S' distributions conditional on H_{mo}, T_z. This data set has been reprocessed to provide a bivariate H', S' distribution for rogue waves. Finally, the height and steepness characteristics of the rogue waves and their immediate neighbours are compared to provide a context for the occurrence of rogue events.

2 North Alwyn Metocean data collection station

The metocean observation system at North Alywn was set up in 1994 and includes three wave altimeters and two anemometers. It records waves and wind continuously at 5Hz when the significant wave height exceeds 3.5m; at other times 20-minute summary statistics only are recorded. Wolfram, *et al.* [3] have documented full details of the instrumention and analysis procedures. Detailed results of data analysis of six severe storms, recorded by the system, were reported by Linfoot, *et al.* [4].

3 Statistics of Wave Height and Steepness at N Alwyn

All the data collected between 1994 and 1998 have recently been analysed to determine bivariate Weibull probability models for individual wave height and steepness conditional on H_{mo} and T_z (Wolfram *et al.*, [5]). The bivariate distribution is

$$p(H', S') = \frac{\gamma H'^{\gamma-1}}{\eta^{\gamma}} \exp\left(-\left(\frac{H'}{\eta}\right)^{\gamma}\right) \frac{\beta S'^{\beta-1}}{\alpha^{\beta}} \exp\left(-\left(\frac{S'}{\alpha}\right)^{\beta}\right) \qquad (2)$$

where α, β and γ are dimensionless parameters, and $\eta = \tau S^{\lambda}$ where τ and λ are also dimensionless parameters. Data analysis involved aggregating the individual wave data for each twenty-minute observation period into the corresponding H_{mo}, T_z bin . Bivariate Weibull models were then fitted to the aggregated data in individual bins as shown in Table 1 and regression models were determined for the parameters of the bivariate distributions over H_{mo}, T_z space. Predictions of the bivariate parameters based on these regression models were then tested

against observations for two bins which were not included in the regression analysis and found to give reasonable correspondence [5].

Table 1. Coefficients for bivariate Weibull distribution for normalised waveheight H' and steepness S' for various H_{mo}, T_z bins

H_{mo}	T_z	α	β	γ	τ	λ	Total waves	No. waves analysed	20 minute periods
6.5	7.5	0.729	1.9491	1.8215	0.701	0.0894	48298	46848	302
6.5	8.5	0.768	1.9383	1.9771	0.739	0.1346	154708	151651	1096
7.5	8.5	0.748	1.9752	1.9083	0.742	0.1686	35729	35078	253
8.5	8.5	0.707	1.8762	1.7610	0.760	0.2902	4823	4699	34
6.5	9.5	0.810	1.8387	2.0911	0.739	0.1038	20154	19833	160
7.5	9.5	0.782	1.9496	2.0333	0.762	0.1787	41897	41297	331
8.5	9.5	0.764	1.9855	1.9905	0.768	0.2134	26715	26343	211
9.5	9.5	0.730	2.0648	1.9318	0.774	0.2768	4613	4581	37
7.5	10.5	0.817	1.8392	2.1285	0.735	0.0855	5160	5083	45
8.5	10.5	0.798	1.9444	2.1189	0.773	0.1912	14226	14052	124
9.5	10.5	0.775	2.0545	2.0977	0.774	0.2154	10032	9969	88
10.5	10.5	0.719	1.9869	1.9495	0.781	0.3279	4362	4305	38
11.5	10.5	0.692	1.8412	1.8169	0.761	0.3457	2751	2697	24
11.5	11.5	0.753	2.0382	2.0415	0.754	0.2215	1939	1926	19
	mean	0.756	1.9487	1.9763	0.754	0.2031			
	s.d.	0.038	0.0771	0.1184	0.021	0.0845			
	c.o.v.	0.050	0.0396	0.0599	0.028	0.4160			

4 Bivariate distribution of Height and Steepness of Normalised Rogue Waves

In the study reported here the individual binned wave data has been reanalysed for the occurrence of rogue wave events in terms of the number of exceedences. Table 2 shows the total number of waves in each bin together with the number of rogue wave events.

The complete unbinned data have also been analysed to determine the bivariate H', S' distribution of the rogue waves. These data represent the combined extreme right-hand tails of the H', S' distributions for $H' > 2$ in the study referred to above. The best fit simplified distribution was found to be

$$p(H', S'|H' > 2.0, S' > 0.5) = \frac{C}{\eta} \exp\left(-\frac{H'-2}{\eta}\right) \frac{\beta S'^{\beta-1}}{\alpha^{\beta}} \exp\left(-\left(\frac{S'}{\alpha}\right)^{\beta}\right) \tag{3}$$

Table 2. Total number of waves (upper) and number of rogue waves (lower) in each H_{mo}, T_z bin

	Mid-points of H_{mo} bins (m)							
T_z(s)	6.5	7.5	8.5	9.5	10.5	11.5	12.5	13.5
7.5	48298	1865	1928	337	962	160		
	21	3	8	0	0	0		
8.5	154708	35729	4823	979	703	1001	429	
	38	10	6	0	0	0	0	
9.5	20154	41897	26715	4613	1607	1019	123	
	1	15	5	4	0	0	0	
10.5	953	5160	14226	10032	4362	2751	1371	221
	0	0	2	1	0	0	0	0
11.5	106		856	1394	1169	1939	1062	
	0		0	0	0	0	0	
12.5			94		390	391	391	
			0		0	0	0	
All T_z	224219	84651	48642	17355	9193	7261	3376	221
	60	28	21	5	0	0	0	0

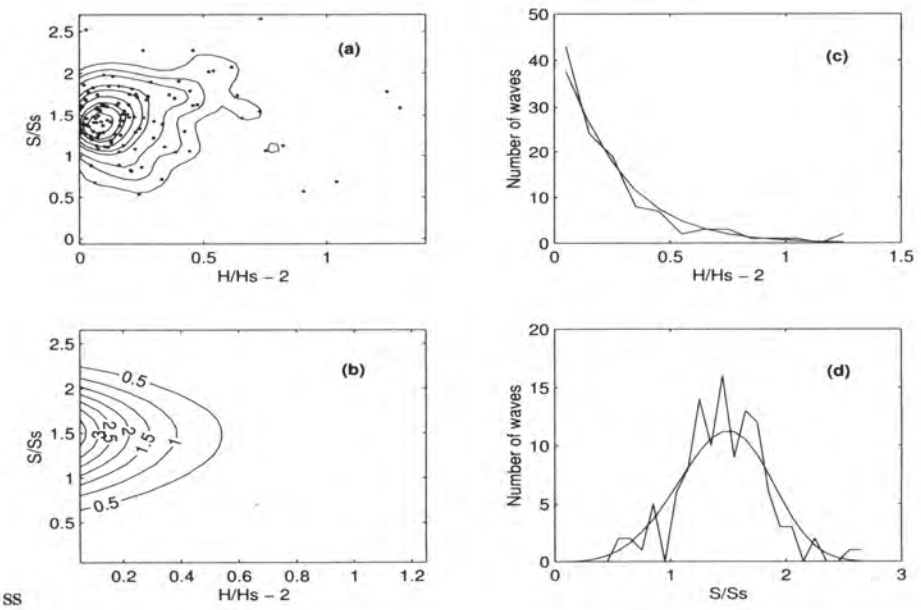

SS

Fig. 1. : Bivariate distribution of normalised waveheight H' and steepness S' for rogue waves. (a) scatterplot and kernel density estimate contours at 90% to 10%. (b) fitted distribution (c) marginal distribution of waveheight and (d) marginal distribution of steepness showing fitted model (smooth curve) and data

since log likelihood fitting gave $\gamma \approx 1$ and where C is a normalising constant. The other parameters were $\alpha = 1.60, \beta = 4.18, \tau = 0.25$ and $\lambda = -0.089$.

5 Comparison of rogue waves with their immediate neighbours

Joint probability models have also been fitted for the height and steepness of the waves immediately before and after the rogue wave events.

Kernel density estimates were made for the scatterplots for the height and steepness of the rogue waves against the waves immediately preceding and succeeding them. Quantile-quantile plots were also constructed to determine if the rogue waves departed from the expected distributions of wave height and steepness of their immediate neighbours. The KDE and QQ plots show that the normalised largest waves occur in groups where approximately 50% of the immediately preceding and/or succeeding waves exceed H_{mo} and 90% exceed $H_{mo}/2$. The QQ plots show that the highest 20% of the rogue waves, i.e those with $H' > 2.3$, follow a different distribution of normalised height to their neighbours.

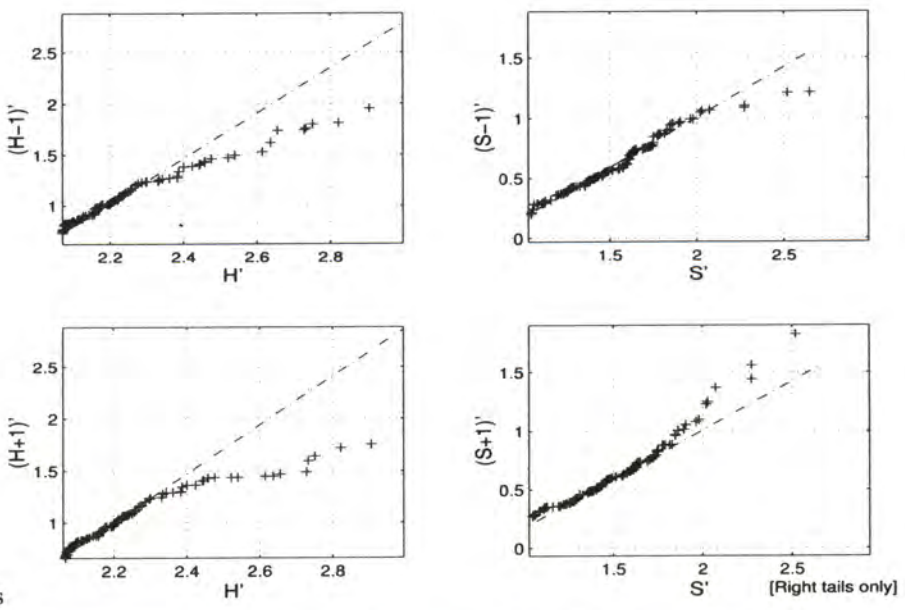

Fig. 2. : Quantile-Quantile plots of normalised height and steepness of preceding and succeeding waves. Deviation from straight line indicates samples from differing distributions

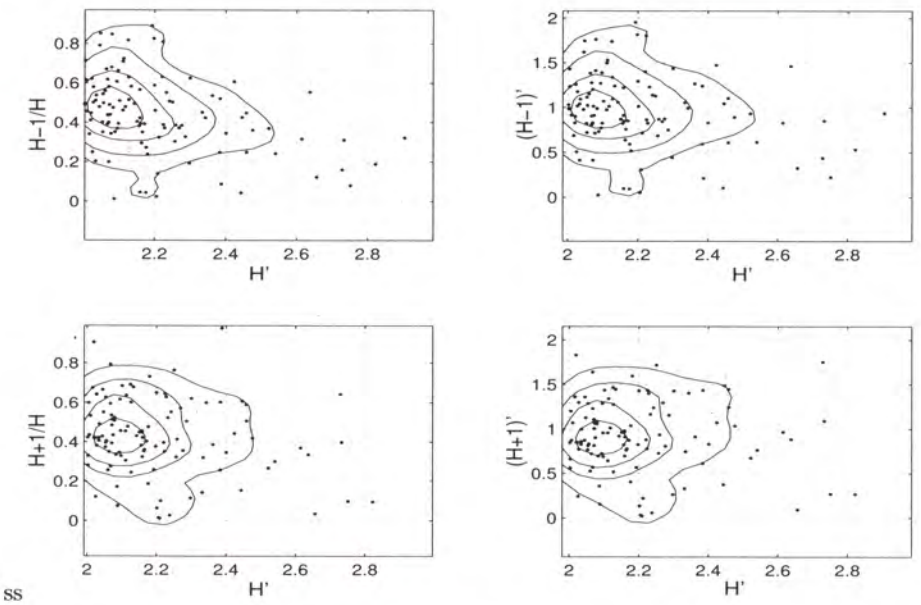

Fig. 3. : Relative and normalised heights of waves preceding $(H-1)$ and succeeding $(H+1)$ the rogue waves H; kernel density estimate contours at 80% to 20%

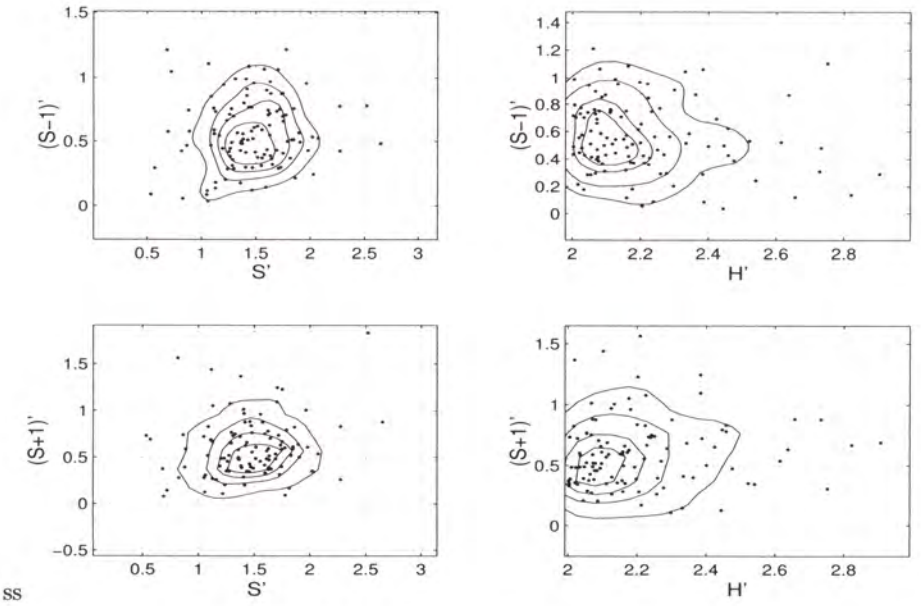

Fig. 4. : Normalised steepness of waves preceding $(S-1)'$ and succeeding $(S+1)'$ the rogue waves against normalised rogue wave steepness S' and height H'; kernel density estimate contours at 80% to 20%

6 Conclusions

We conclude that the rogue waves were generally 50% steeper than the significant steepness and that the preceding and succeeding waves had steepness values around half the corresponding significant values while their heights were around the significant height. The rogue waves exhibited a marginal exponential distribution of normalised height, the marginal distribution of normalised steepness was Weibull and the joint distribution showed that the maxima of the conditional distribution of normalised steepness were constant at 1.5. Tentatively we propose that a more logical definition for rogue waves would be those where $H' > 2.3$ since the probability distribution of these waves appears to depart from that of their neighbours from this point.

References

1. Ochi, M.K.: Ocean Waves: The stochastic approach. Cambridge University Press. (1998) 319
2. Longuet-Higgins, M.S.: On the statistical distribution of the heights of sea waves. J. Marine Research. **11** (1952) 245-266
3. Wolfram, J., Feld, G., Allen, J.: A new approach to estimating extreme environmental loading using joint probabilities. In: Behaviour of Offshore Structures. BOSS'94, (ed: C. Chryssostomidis) Pergamon, Vol 2 (1994) 701-713
4. Linfoot, B.T., Stansell, P.,Wolfram J.: On the characteristics of storm waves. Proc. 10th I. Offshore and Polar Eng. Conf., ISOPE, Vol III (2000) 74–77
5. Wolfram, J., Linfoot, B., Venugopal,V.: Some results from the analysis of metocean data collected during storms in the northern North Sea. Underwater Technology. **24**(4) (2000) *in press*

Collective Reference List

HSE, *Review of Greenwater & Waveslam, Design & Specifications, Requirements for FPSO/FPU's,* Offshore Technology Report - OTC 2000, 004, Health & Safety Executive, Prepared by PAFA Consulting Engineering Ltd., London, March 2000

Ifremer, *Rogue Waves 2000*, Proceedings of International Workshop, Brest, France, Nov. 29-30 2000

International Association for Hydraulic Research (I.A.H.R./P.I.A.N.C), *List of Sea State Parameters*, Supplement to Bulletin, **No. 52**, 1986

International Ship and Offshore Structure Congress (ISSC), Report from the 23rd International Ships and Structures Conference - Environment Committee, Nagasaki, Japan, 11, 2000

International Towing Tank Conference, Report from the 22nd International Towing Tank Conference -Environment Committee, Seoul, Korea and Shanghai, China, 11, 1999

London Meteorological Office, *The One from Nowhere,* Marine Observers, London, **35**, 1965

US Army Corps of Engineers, *Shore Protection Manual*, US Army Corps of Engineers, Washington D.C., 4th edition, 1984

WAMDI Group (13 authors, including Cardone, V. J., Greenwood, J. A), *The WAM Model - A 3rd Generation Ocean Wave Prediction Model,* J. Phys. Oceanog., **18**, 1775-1810, 1988

World Meteorological Organization, *Provision and Engineering/Operational Application of Ocean Wave Data,* Conf. Report WMO/TD-No.938, Marine Meteorology and related Oceanographic Activities, Report No. 42, UNESCO, 1998

Ablowitz M.J., Clarkson, P.A., *Solitons, Nonlinear Evolution Equations and Inverse Scattering,* 1st edn., Cambridge University Press, publ. as London Mathematical Lecture Note Series, **149**, 1991

Alber, I.E., *The effect of randomness on the stability of two-dimensional surface wave trains*, Proc. Roy. Soc., **A 363**, 528, 1978

Annenkov, S.Yu., Shrira, V.I., *Numerical Modelling of Water Waves Evolution Based on the Zakharov Equation*, J. Fluid Mech., 2001, submitted

Annenkov, S.Yu., Shrira, V.I., *Physical Mechanisms for Sporadic Wind Wave Horse-Shoe patterns*, European Journal of Mechanics, B/Fluids, **18 No.3**, 463-474, 1999

Annenkov, S.Yu., Shrira, V.I., *Sporadic Wind Wave Horse-Shoe Patterns*, Report 99-001, Institute for Nonlinear Science, National University of Ireland, University College, Cork, **43**, 1999

Athanassoulis, G.A., Belibassakis, K.A., *A Consistent Coupled-Mode Theory for the Propagation of Small-Amplitude Water Waves over Variable Bathymetry Regions*, J. Fluid Mech., **389,** 275-301, 1999

Athanassoulis, G.A., Belibassakis, K.A., Gerostathis, Th.P., *A Coupled-Mode Theory for the Diffraction of Water Waves by Localized Scatterers Superimposed over a Parallel-Contour Bathymetry*, Proc. 5th Int. Conf. on Mathematical and Numerical Models of Wave Propagation, SIAM, 719-724, 2000

Atkins, *Special Reports of Freak Waves,* London Meteorological Office, London, 1975

Auger, F., Flandrin, P.G., Lemoine, O., *Time -frequency toolbox for use with Matlab*, Centre National de la Recherche Scientifique, France, 1997

Babanin, A.V., Soloviev, Y.P., *Field investigation of transformation of the wind wave frequency spectrum with fetch and the stage of development*, J. Phys. Oceanogr., **28**, 563-576, 1998

Badulin, S.I., Shrira, V.I., Kharif, C., Ioualalen, M., *On two Approaches to the Problem of Instability of Short-Crested Water Waves*, J. Fluid Mech. **303**, 297-326, 1995

Badulin, S.I., Tomita, H., *Effect of Vertical Shear Current on Appearance of Large-Amplitude Waves,* PACON'99 Proceedings, 380-390, June 23-25, 1999, Moscow, Moscow 2000

Baldock T.E., Swan, C., Taylor, P.H., *A Laboratory Study of Non-Linear Surface Waves on Water,* Phil.Trans. Roy. Soc. London, **A 354**, 649-676, 1996

Baldock, T.E., Swan, C., *Numerical calculations of large transient water waves*, Applied Ocean Research, **16**, 101-112, 1994

Bateman W.J.C., Swan, C., Taylor, P.H., *On the Efficient Numerical Simulation of Directional-Spread Water Waves,* Submitted to Journal of Comput. Phys., 2001

Bateman W.J.C., Swan, C., Taylor, P.H., *Steep Multi-Directional Waves on Constant Depth,* Proc. 18th Int. Conf. on Offshore Mechanics and Arctic Engineering, OMAE99-6463, 1999

Bateman, W.J.D., *A Numerical Investigation of Three Dimensional Extreme Water Waves*, PhD Thesis, Imperial College, University of London, 2000

Beji, S., Nadaoka, K., *A Time-Dependent Nonlinear Mild-Slope Equation for Water Waves,* Proc. R. Soc. Lon., **A 453**, 319-332, 1997

Belenky, V.L., *Seventh International Conference on the Stability of Ships and Ocean Vehicles (STAB' 2000) - A Review*, Marine Technology, **Vol. 38 No. 1**, 1-8, Jan. 2001

Belibassakis, K.A., Athanassoulis, G.A., *Extension of Second-Order Stokes Theory to Variable Bathymetry,* 2000, submitted.

Bendat, J.S., Piersol, A.G., *Random Data: Analysis and Measurement Procedures*, John Wiley & Sons Inc., 1986

Benjamin, T.B., Feir, J.E., *The Disintegration of Wave Trains on Deep Water Part I*, J. of Fluid Mech., **27**, 417-430, 1967

Bigio, R., *Luis and the Buoys....and the Queen,* 4th International Workshop on Wave Hindcasting and Forecasting, Banff, Alberta, Canada, 1995

Bird, H., Morrall, A., *Research Towards Realistic Stability Criteria*, Proceedings of the International Conference on the Safeship Project: Ship Stability and Safety, RINA, London, 9-10 June 1986

Blume, P., *On Capsize Model Testing,* Proceedings of the U. S, Coast Guard Vessel Stability Symposium, New London, CT, 15-17 March, 1993

Boashash, B., *Estimating and Interpreting the Instantaneous Frequency of a Signal - Part I: Fundamentals*, Proc. IEEE, Series 80, **4**, 520-538, 1992

Boccadamo, G., Cassella, P., Russo Krauss, G., Scamardella, A., *Analysis of I.M.O. Stability Criteria by Systematic Hull Series and by Ship Disasters*, Proceedings of the 5th International Conference on Stability of Ships and Ocean Vehicles (STAB 94), Melbourne, Fl., USA, 1994

Boccadamo, G., Cassella, P., Scamardella, A., *Stability, Operability and Working Conditions on Board Fishing Vessels,* Proceedings of the 7th International Conference on Stability of Ships and Ocean Vehicles (STAB 2000), Launceston, Tasmania, Australia, 7-11 February 2000

Boccotti, P., *On the highest waves in a stationary Gaussian process*, Atti. Acc. Lig, **38**, 45-73, 1981

Bonmarin, P, Kjeldsen, S.P., *Some Geometric and Kinematic Properties of Breaking Waves*, Proc. Int. Workshop ROGUE WAVES 2000, Brest, France, 2000

Bonmarin, P., *Geometric Properties of Deep-Water Breaking Waves,* Journal of Fluid Mechanics, **209**, 405-433, 1989

Bonmarin, P., Ramamonjiarisoa, A., *Deformation to Breaking of Deep Water Gravity Waves*, Experiments in Fluids, **2**, 1-6, 1984

Borgman, L. E., *Irregular Ocean Waves: Kinematics and Forces*, In: Lemehaute and Hanes (eds.): *The Seas, Ocean Engineering Science Part A*, J. Wiley and Sons, **9**, 121-168, 1990

Brandini, C., Grilli, S., Modeling of freak wave generation in a 3D-NWT, Submitted to 11th ISOPE Conf., 2001

Brandini, C., Nonlinear Interaction Processes in Extreme Wave Dynamics, Ph.D. Dissertation, University of Firenze, 2001

Brown, M.G., Jensen, A., *Experiments on Focusing Unidirectional Water Waves,* J. Geophys. Research, 2001, submitted.

Buckley, W.H., *Design Wave Climates for the Worldwide Operation of Ships – Part 1: Establishment of Design Wave Climates,* (being published as a SNAME T&R Report)

Buckley, W.H., *Extreme and Climatic Wave Spectra for Use in Structural Design of Ships,* Naval Engineers J., September 1988

Buckley, W.H., *Hull Girder Structural Design – The Case for New Loading Conditions for Extreme Waves*, Nav. Eng. J., Feb. 1978

Buckley, W.H., *Stability Criteria: Development of a First Principles Methodology,* 5th Int. Conf. Stability of Ships and Ocean Vehicles STAB '94, **3**, Nov. 7-11 1994

Caponi, E.A., Saffman, P.G., Yuen, H.C., *Instability and confined chaos in a nonlinear dispersive wave system*, Phys. Fluids, **25** (12), 2159-2166, 1982

Chaplin, J.R., *On frequency-focusing unidirectional waves*, Intl. J. Offshore and Polar Engng., **6**, 131-137, 1996

Chen, L., Zhang, J., *On Interaction between Intermediate-Depth Long Waves and Deep-Water Short Waves,* J. Ocean Engrg., **25**, 395-423, 1998

Chereskin, T.K., Mollo-Christensen, E., *Modulational development of nonlinear gravity-wave groups*, J. Fluid Mech., **151**, 337-365, 1985

Chien, H., Chuang, L., Kao, C.C., *A Study on Mechanisms of Nearshore Rabid Waves*, German-Chinese J. Sem. on Rec. Dev. in C. Eng., China, 469-483, 1999

Clarke, S., Grimshaw, R., Miller, P., Pelinovsky, E., Talipova, T., *On the Generation of Solitons and Breathers in the Modified Korteweg – de Vries Equation,* Chaos, **10**, 383-392, 2000

Claughton, A., Handley, P., *An Investigation into the Stability of Sailing Yachts in Large Breaking Waves*, University of Southampton Ship Science Report, **No. 15,** January 1984

Clauss, G, *Generation of task-related freak waves and critical wave groups,* This publication, 2001

Clauss, G., Habel, R., *Artificial reefs for coastal protection – transient viscous computation and experimental evaluation*, In Proc. of the 27th Intern. Conf. on Coastal Eng. (ICCE), Sydney, Australia, 2000

Clauss, G., Hennig, J., *Tailored transient wave packet sequences for computer – controlled capsizing tests*, In Proc. of the 20th OMAE Aymposium, Rio de Janeiro, 2001, to be published

Clauss, G., Kuhnlein, W., *Transient wave packets- an efficient technique for seakeeping tests of self-propelled tests*, In 3rd Intern. Conf. on Fast Sea Transportation, Lubeck- Travemunde, Germany, **2**, 1193-1204, 1995

Clauss, G., Pakozdi, C., Steinhagen, U., *Experimental Optimization of Transient Waves in Extreme Seas*, In Proc. of the 11th Intern. Offshore and Polar Conference (ISOPE), Stavanger, Paper No.: 2001-MP-05, 2001

Clauss, G., Steinhagen, U., Generation and Numerical Simulation of Predetermined Nonlinear Wave Sequences in Random Seaways, In Proc. of the 20th OMAE Symposium, Rio de Janeiro, Paper No.: OMAE2001/OFT-1230, 2001

Clauss, G., Steinhagen, U., *Numerical Simulation of Nonlinear Transient Waves and its Validation by Laboratory Data*, In Proc. of the 9th Intern. Offshore and Polar Engineering Conference (ISOPE), Brest, France, **3**, 368-375, 1999

Clauss, G., Steinhagen, U., *Optimization of Transient Design Waves in Random Seas*, In Proc. of the 10th Intern. Offshore and Polar Engineering Conference (ISOPE), Seattle, USA, **3**, 229-236, 2000

Clauss, G., *Task-Related Wave Groups for Seakeeping Tests or Simulation of Design Storm Waves,* Appl. Ocean Res., **21**, 219-234, 1999

Clauss, G.F., Bergman, J., *Gaussian Wave Packets - A New Approach to Seakeeping Tests of Ocean Structures*, Applied Ocean Research, **8 No. 4**, 1986

Clauss, G.F., Kuhnlein, W.L., *Simulation of design storm conditions with tailored wave groups*, Proc. 7th Int. Offshore and Polar Eng. Conf. ISOPE, **3**, 228-237, 1997

Cleary, W., *The Regulation of Ships Stability Reserve*, Proceedings of the U. S. Coast Guard Vessel Stability Symposium, New London, CT, 15-17 March 1993

Cohen, L., Loughlin, P., Vakman, D., *On an Ambiguity in the Definition of the Amplitude and Phase of a Signal Sign*, Proces., **79**, 301-307, 1999

Cointe, R., *Numerical simulation of a wave channel,* Engineering Analysis with Boundary Elements, **7 No. 4**, 167-177, 1990

Cokelet, E.D., *Steep Gravity Waves in Water of Arbitrary Uniform Depth*, Philosophical Transactions of the Royal Society of London, **286 No. 1335**, 183-230, 1977

Coles, K. A., *Heavy Weather Sailing,* 4th edn revised by Peter Bryce, Adlard Coles Nautical, 1991

Colman, A.D., *Report on the Re-Opened Formal Investigation into the Loss of the MV DERBYSHIRE,* Treasury Solicitors Office publication, 2000

Craig W, Sulem, C., *Numerical Simulation of Gravity Waves,* J. Comput. Phys., **108**, 73-83, 1993

Creamer, D.B., Henyey, F.S., Schult, R., Wright, J., *Improved Linear Representation of Ocean Surface Waves,* J. Fluid Mech., **205**, 135-161, 1989

Dahle, E.A., Myrhaug, D., *Risk Analysis Applied to Capsize of Fishing Vessels*, Marine Technology, **32 No. 4,** 245-257, October 1995

Daubechies, I., *Ten Lectures on Wavelets*, Soc. F. Ind. & App. M., 357, 1992

Davies, K.B., Leverette, S.J., Spillane, M.W., *Ringing Response of TLP and GBS Platforms*, Proc. of the 7th BOSS Conf., Cambridge, Mass., USA, **2**, 1994

Dawson, T.H., *Freak Ocean Waves Are Episodic,* New Scientist, Jan. 1977

Dawson, T.H., *Rayleigh Law and Stokes Correction for High Waves in Heavy Seas*, US Naval Academy Report, **11**, 2000

Deakin, B., *Model Tests to Study Capsize and Stability of Sailing Multihulls*, Proceedings of the 15th Chesapeake Sailing Yacht Symposium, Annapolis, MD, 26-27 January 2001

Dean, R.G., *Freak waves: A possible explanation*, In Torum, A. and Gudmestad, O.T. (eds.): *Water Wave Kinematics*, Kluwer, 609-612, 1990

deKat, J.O., *Dynamics of Vessel capsizing in Critical Wave Conditions*, Workshop on Safety of Ocean Racing Yachts, Sydney, 28 March 1999

Dias, F., Kharif, C., *Nonlinear Gravity and Capillary-Gravity Waves,* Ann. Rev. Fluid Mech., **31**, 301-346, 1999

Dold J.W., *An Efficient Surface-Integral Algorithm Applied to Unsteady Gravity Waves,* J. Comput. Phys., **103**, 90-115, 1992

Dommermuth, D.G., Yue, D.K.P., *A High-Order Spectral Method for the Study of Nonlinear Gravity Waves*, J. Fluid Mech., **184**, 267-288, 1987

Dommermuth, D.G., Yue, D.K.P., Lin, W.M., Rapp, R.J., Chan, E.S., Melville, W.K., *Deep-water plunging breakers: A comparison between potential theory and experiments*, J. Fluid Mech., **189**, 423-442, 1988

Dommermuth, D.G., Yue, D.K.P., *Numerical Simulations of Nonlinear Axisymmetric Flows with a Free Surface*, J. Fluid Mech., **178**, 195-219, 1987

Donaldson, L., *Assessment (DERBYSHIRE), Annex*, Cm 3120, London: HMSO, 37-60, 1995

Donelan, M.A., Anctil, F., Doering, J.C., *A simple method for calculating the velocity field beneath irregular waves*, Coastal Eng., **16**, 399-424, 1992

Donelan, M.A., Drennan, W.M., Magnusson, A.K., *Nonstationary analysis of the directional properties of propagating waves*, J. Physical Oceanography, **26**, 1901-1914, Sept. 1996

Draper, L., *Freak Ocean Waves*, Oceanus, London, **10 No. 4 + 35**, 1964+1965

Drazin, P.G., Johnson, R.S., *Solitons: An Introduction,* Cambridge Univ. Press, 1996

Duncan, J.H., Wallendorf, L. A., Johnson, B., *An Experimental Investigation of the Kinematics of Breaking Waves*, Proceedings of the IAWR Seminar on Wave Analysis in Laboratory Basins, 411-422, 1-4 Sept. 1987

Dyer, M.G., *Hazard and Risk in the New England Fishing Fleet*, Marine Technology, **37 No. 1**, 30-49, 2000

Dysthe K.B., *Note on a Modification to the Nonlinear Schroedinger Equation for Application to Deep Water Waves*, Proc. Roy. Soc., **A 269**, 105-114, 1979

Dysthe, C.B., *Modelling a "Rogue Wave" - Speculations or a Realistic Possibility*, Abstracts for Rogue Waves 2000 workshops, Brest, 2000

Dysthe, K.B., Trulsen, K., *Note on Breather Type Solutions of the NLS as a Model for Freak-Waves*, Physica Scripta, **T82**, 48-52, 1999

Ersdal, G., Kvitrud, A., *Green Sea on Norwegian Production Ships*, Proc. Airgap

Workshop, HSE/ E&P Forum London, 1999

Ersdal, G., Kvitrud, A., *Green Water on Norwegian Production Ships,* Proc. of the 10th ISOPE Conf., Seattle, WA, USA, 2000

Faulkner, D., *An Independent Assessment of the Sinking of the M.V. DERBYSHIRE*, SNAME, 1999

Faulkner, D., Buckley, W.H., *Critical Survival Conditions for Ship Design*, RINA Proceedings of the 1st International Conference: Design and Operation for Abnormal Conditions, Glasgow, 1-25, 21-22 Oct. 1997

Faulkner, D., Corlett, B.J., Romeling, J.U., *Design of Hatch Covers and Coamings for Abnormal Waves,* RINA Int. Conf., Watertight Integrity and Ship Survivability, London, 21-22 Nov. 1996

Faulkner, D., *Reliability Based Design and Assessment of FPSO structures,* HSE OTO 98164, November 1998

Fenton, J.D., Rienecker, M.M., *A Fourier Method for Solving Nonlinear Water Wave Problems: Application to Solitary Wave Interactions*, J. Fluid Mech., **118**, 411-443, 1982

Fontaine, E., Landrini, M., Tulin, M., *Breaking: splashing and ploughing phases,* Intl. Workshop on Water Waves and Floating Bodies, 4, 2000

Forristall, G.Z., *Wave Crest Distributions: Observations and Second-Order Theory,* Journal of Physical Oceanography, **30**, 1931-1943, Aug. 2000

Forristall, G.Z., *Wave Crest Distributions: Observations and Second-Order Theory,* Conf. On Ocean Wave Kinematics, Dynamics, and Loads on Structures, Houston, TX, USA, 372-382, 1998

Friedman, A., Shinbrot, M., *The Initial Value Problem for the Linearized Equations of Water Waves*, J. Math. And Mech, **17,** 107-180, 1967

Friedman, A., Shinbrot, M., *The Initial Value Problem for the Linearized Equations of Water Waves II,* J. Math. And Mech. **19**, 1177-1193, 1969

Gabor, D., *Theory of Communication*, IEE J. Comm. Eng., **93**, 429-457

Goda, Y., *A synthesis of breaker indices*, Trans, J. Soc. Civ. Engrs, **2**, part 2, 1970

Goda, Y., *Random Seas and Design of Maritime Structures,* University of Tokyo Press, 1985

Grilli, S.T., Guyenne, P., Dias, F., *A fully nonlinear model for three-dimensional*

overturning waves over arbitrary bottom, Intl. J. Numer. Methods in Fluids, **34**, 39 2001, in press

Grochowalski, S., *Investigation into the Physics of Ship Capsizing by Combined Captive and Free-Running Model Tests*, SNAME Transactions, 169-212, 1989

Guedes Soares, C., *Spectral Modeling of Sea States with Multiple Wave Systems*, Journal of Offshore Mechanics and Artics Engineering, **114**, 1992

Haring, R.E., Heideman, J.C., *Gulf of Mexico Rare Wave Return Periods,* Proc. Offshore Technology Conference, OTC 3230, 1537-1550, 1978

Hasselmann, K., *On the Non-Linear Energy Transfer in a Gravity-Wave Spectrum, part 1: General Theory,* J. Fluid Mech., **12**, 481-500, 1962

Haver, S., Andersen, O., *Freak Waves: Rare Realizations of a Typical Population or Typical Realization of Rare Population?*, Proc. 10th Int. Offshore and Polar Engineering Conference ISOPE2000, Seattle, **3**, 123-130, May 28 – 2 June, 2000

Haver, S., *Some Evidence of the Existence of So-Called Freak Waves*, Abstracts for Rogue Waves 2000 Workshops, Brest, 2000

Hellan, O., Hermundstad, O.A., Stansberg, C.T., *Design Tool for Green Sea,* Wave Impact and Structural Responses on Bow and Deck Structures, OTC Paper No. 13213, Offshore Technology Conference, Houston, TX, USA, 2001

Henderson, K.L., Peregrine, D.H., Dold, J.W., *Unsteady Water Wave Modulations: Fully Nonlinear Solutions and Comparison with the Nonlinear Schroedinger Equation,* Wave Motion, **29**, 341-361, 1999

Herbers, T.H.C., Guza, R.T., *Wind-Wave Nonlinearity Observed on the Seafloor: Part II: Wavenumbers and Third-Order Statistics,* J. Phys. Oceanog., **22**, 489-504, 1992

Herbers, T.H.C., Guza, R.T., *Wind-Wave Nonlinearity Observed on the Seafloor: Part I: Forced Wave Energy,* J. Phys. Oceanog., **21**, 1740-1761, 1991

Hogben, N., Dachuna, N.M.C., Oliver, G.F., *Global Wave Statistics,* Unwin Brothers, 1986

Houghton, D., Wolf, J., *Waves of Destruction,* Yachting World, Jan. 2001

Huang, C.-J., Dong, C.-M., *Wave Deformation and Vortex Generation in Water Waves Propagating over a Submerged Dike,* Coastal Engng, **37**, 123-148, 1999

Huang, N.E., Shen, Z., Long, S., *A New View of Nonlinear Water Waves: The Hilbert Spectrum*, Annual Review of Fluid Mechanics, **31**, 417-457, 1999

Huang, N.E., et al., *The empirical mode decomposition and the Hilbert spectrum for nonlinear and non-stationary time series analysis*, Proc. R. Soc. London, **A454**, 903-995, 1998

Huang, N.E., Shen, Z., Long, S., Wu, M.C., Shih, H.H., Zheng, Q., Yen, N.-C., Tung, C.C., Liu, H.H., *The Empirical Mode Decomposition and Hilbert Spectrum for Nonlinear and Non-Stationary Time Series Analysis*, Proc. R. Soc. London, **A454**, 903-995, 1998

Isaacson, M., *Nonlinear Wave Effects on Fixed and Floating Bodies*, J. Fluid Mech., **120**, 267-281, 1982

Its, A.R., Kotljarov, V.P., *Dokl. Akad. Nauk.*, Ukain SSR, **A11**, 965, 1976

Jahns, H.O., Wheeler, J.D., *Long-Term Wave Probabilities Based on Hindcasting of Severe Storms*, J. Pet. Technol., 473-486, 1973

Jenkins, A.D., *A quasi-stationary irrotational solution for a breaking wave crest*, In Donelan, M.A., Hui, W.H., Plant, W.J., (eds.), *The Air-Sea Interface*, Proceedings of the Symposium on the Air--Sea Interface, Radio and Acoustic Sensing, Turbulence and Wave Dynamics, Marseilles, France, June 24-30, 1993, Miami, Florida, U.S.A. The Rosenstiel School of Marine and Atmospheric Sciences, University of Miami, 247-252, (1996)

Jenkins, A.D., *A stationary potential-flow approximation for a breaking-wave crest*, J. Fluid Mech., **280**, 335-347, 1994

Jha, A.K., *Nonlinear Stochastic Models for Loads and Responses of Offshore Structures and Vessels*, PhD. Dissertation, Stanford University, 1997

Jillians, W.J., *The superharmonic instability of Stokes waves in deep water*, J. Fluid Mech., **204**, 563-579, 1989

Johannessen, T.B., Swan, C., *A Laboratory Study of the Focusing of Transient and Directionally Spread Surface Water Waves,* Proc. Roy. Soc. Lond., **A457**, 1-36, 2001

Johannessen, T.B., Swan, C., *Extreme multi-directional waves*, Proc. 26th Intl. Conf. Coast. Engng., ASCE, 1110-1123, 1998

Johannessen, T.B., Swan, C., The Nonlinear Dynamics of Focussed Wave Groups in Two and Three Dimensions, Submitted to Proc. R. Soc., Ser A, 2001

Johannessen, T.B., The Effect of Directionality on the Nonlinear Behaviour of Extreme Transient Ocean Waves, PhD Thesis, Imperial College, University of London, 1997

Jonathan, P., Taylor, P.H., *Irregular, Nonlinear Waves in a Spread Sea,* ASME

Transactions J. of Offshore Mechanics and Arctic Engineering, **119 No.1,** 37-41, 1996

Karunakaran, D., Baerheim, M., Leira, B.J., *Measured and simulated dynamic response of a jacket platform*, In C. Guedes-Soares, M. Arai, A. Naess, & N. Shetty (Eds.), Proceedings of the 16th International Conference on Offshore Mechanics and Arctic Engineering ASME, **2**, 157-164, 1997

Kennedy, A.B., Fenton, J.D., *A Fully Non-Linear Computational Method for Wave Propagation over Topography,* Coastal Engng, **32**, 137-161, 1999

Kharif, C., Pelinovsky, E., Talipona, T., Slunyaev, A., *Focusing of Nonlinear Wave Group in Deep Water,* JETP Letters accepted, 2001

Kirby, J.T., *Nonlinear, Disersive Long Waves in Water of Variable Depth,* In: Hunt, J.N. (ed.): *Gravity Waves in Water of Finite Depth*, Computational Mechanics Publications, 1997

Kirkman, K., *On the Avoidance of Inverted Stable Equilibrium*, AIAA/SNAME Ancient Interface XIII, 1983

Kit, E., Shemer, L., Pelinovsky, E., Talipova, T., Eitan, O., Jiao, H., *Nonlinear Wave Group Evolution in Shallow Water,* J. Waterway, Port, Costal, Ocean Eng., **126**, 221-228, 2000

Kjeldsen, S.P, Bonmarin, P., Skafel, M.G., Drennan, W.M., *Lagrangian Measurements of Accelerations in the Crest of Breaking and Broken Waves,* Proc. 26th International Conference on Coastal Engineering, Copenhagen, Denmark, 1998

Kjeldsen, S.P, *The Practical Value of Directional Ocean Wave Spectra*, in Beal, R.C. (ed): *Measuring, Modeling, Predicting and Applying Directional Ocean Wave Spectra*, The Johns Hopkins University Press, Baltimore, London, 1991

Kjeldsen, S.P, Vinje, T., Myrhaug, D., Brevig, P., *Kinematics of Deep Water Breaking Waves,* Proc. of the 12th Offshore Technology Conference, Paper No. 3714, Houston, Texas, 1980

Kjeldsen, S.P., *2- and 3-Dimensional Deterministic Freak Waves,* Proc. 18th Int. Conf. on Coastal Engineering, Cape Town, South Africa, 1982

Kjeldsen, S.P., Bonmarin, P., *Development of a Numerical Ocean Basin for Simulation of Ringing Effects on Monotower Platforms ISOPE 2001,* Conference, Stavanger, Norway, 2001

Kjeldsen, S.P., *Breaking Waves. Water Wave Kinematics,* Kluwer Academic Publ., (Eds.): Torum O., Gudmestad O.T., Dordrecht The Netherlands, 1990

Kjeldsen, S.P., *Dangerous Wave Groups,* Norwegian Maritime Research, **12 No. 2,** 4-16, 1984

Kjeldsen, S.P., Drennan, W.M., Skafel, M.G., *Modelling of Velocities in Giant Waves,* The ISOPE-Journal, **10 No. 3**, 170-172, 2000

Kjeldsen, S.P., *Examples of Heavy Weather Damage Caused by Giant Waves,* Technomarine, **820**, 1996

Kjeldsen, S.P., *Examples of Heavy Weather Damages Caused by Giant Waves*, Bulletin of the Society of Naval Architects of Japan, **828**, 744-748, 10/ 1997

Kjeldsen, S.P., Myrhaug, D., *Breaking Waves in DeepWaters and Resulting Wave Forces,* Proc. 11th Offshore Technology Conference, Paper No. 3646, Houston, Texas, 1979

Kjeldsen, S.P., Myrhaug, D., *Wave-Wave Interactions, Current-Wave Interactions and Resulting Extreme Waves and Breaking Waves,* 17th ICCE, 1980

Kobylinski, L., *Methodology of the Development of Stability Criteria on the Basis of Risk Evaluation*, Proceedings of the 5th International Conference on Stability of Ships and Ocean Vehicles (STAB 94), Melbourne, Fl. USA, 1994

Kobylinski, L., *Stability Standards - Future Outlook*, Proceedings of the 7th International Conference on Stability of Ships and Ocean Vehicles (STAB 2000), Launceston, Tasmania, Australia, 7-11 February 2000

Komen, G.J., Cavaleri, L., Donelan, M., Hasselmann, K., Hasselmann, S., Janssen, P.A.E.M., *Dynamics and Modelling of Ocean Waves,* CUP, 1994

Krasitskii, V.P., *On Reduced Hamiltonian Equations in the Nonlinear Theory of Water Surface Waves*, J. Fluid Mech., **272**, 1-20, 1994

Kriebel, D.L., Alsina, M.V., *Simulation of Extreme Waves in a Background Random Sea*, Proceedings of the 10th International Offshore and Polar Engineering Conference, Seattle, USA, 28 May - 2 June, 2000

Kriebel, D.L., Dawson, T.H., *Nonlinear Effects on Wave Groups in Random Seas,* J. Offshore Mech. Arctic Eng., No. 113, 142-147, 1991

Kriebel, D.L., Dawson, T.H., *Nonlinearity in Wave Crest Statistics,* Proc. 2nd Int. Symp. Ocean Wave Measurement and Analysis, New Orleans, USA, 61-75, 1993

Kriebel, D.L., *Efficient Simulation of Extreme Waves in a Random Sea,* Abstract of Workshop "Rogue Waves 2000", Brest, France, 29–30 November, 2000

Langley, R.S., *A Statistical Analysis of Non-Linear Random Waves*, Ocean Eng.

Offshore Structures Group, College of Aeronautics, Cranfield Institute of Technology, Cranfield, Beds, MK43 0AL, U.K., 389-407, 1986

Lavrenov, I., *The Wave Energy Concentration at the Agulhas Current of South Africa,* Natural Hazards, **17**, 117-127, 1998

Liang, H., Lin, Z., McCallum, R.W., *Artifact Reduction in Electrogastrogram Based on Empirical Mode Decomposition Method*, Med. Biol. Eng. C., **38**, 35-41, 2000

Lighthill, M.J., *Contributions to the Theory of Waves in Non-Linear Dispersive Systems*, J. Inst. Maths Applic., **1**, 269-306, 1965

Lighthill, M.J., *Waves in Fluids*, 1st edn., Cambridge University Press, 1978

Lin, W.-M., Salvesen, N., *Nine Years of Progress with LAMP – The Large Amplitude Motion Program,* Report SAIC-97/1079, of the Science Applications International Corp., 134 Holiday Court, Annapolis, MD, 21401, USA, Dec. 1979

Lindgren, G., *Some Properties of a Normal Process near a Local Maximum*, The Annals of Mathematical Statistics, **41 No. 6**, 1870-1883, 1970

Linfoot, B.T., Stansell, P., Wolfram, J., *On the Characteristics of Storm Waves*, Proc. 10th Int. Offshore and Polar Eng. Conf. ISOPE, **3**, 74-77, 2000

Liu, P.C., *Wavelet transform and new perspective on coastal and ocean engineering data analysis*, In P. Liu (Ed): *Advances in Coastal and Ocean Engineering*, World Scientific, **6**, 57-101, 2000

Liu, P.L., *Is the Wind Wave Frequency Spectrum Outdated*, Oc. Eng., **27**, 5, 577-588, 2000

Liu, P.L., *Wave Grouping Characteristics in Nearshore Great Lakes*, Oc. Eng., **27**, 1221-1230, Nov. 2000

Liu, P.C., *Wavelet spectrum analysis and ocean wind waves*, In E. Foufoula-Georgiou and P. Kumar (Eds): *Wavelets in Geophysics*, Academic Press, 151-166, 1994

Liu, P.L-F., *Model Equations for Wave Propagation from Deep to Shallow Water,* In. Liu, P.L.-F (ed.): *Advances in Coastal and Ocean Engineering*, World Scientific, 1995

Liu, W.K., Jun, S., Zhang, Y.F., *Reproducing kernel particle methods*, International Journal for Numerical Methods in engineering, **20**, 1081-1106

Lo, E., Mei, C.C., *A Numerical Study of Water-Wave Modulation Based on a Higher Order Nonlinear Schroedinger Equation,* J. Fluid Mech., **150**, 395-416, 1985

Longuet-Higgins, M.S, *Eulerian and Lagrangian Aspects of Surface Waves,* J. Fluid Mech., **173**, 683-707, 1986

Longuet-Higgins, M.S., Cleaver, R.P., *Crest instabilities of gravity waves Part 1: The almost-highest wave*, J. Fluid Mech., **258**, 115-129, 1994

Longuet-Higgins, M.S., Cleaver, R.P., Fox, M.J.H., *Crest instabilities of gravity waves Part 2: Matching and asymptotic analysis*, J. Fluid Mech., **259**, 333-344, 1994

Longuet-Higgins, M.S., Cokelet, E.D., *The Deformation of Deep Surface Waves on Water II,* Proc. R. Soc. Lond., **A364**, 1, 1976

Longuet-Higgins, M.S., Cokelet, E.D., *The Deformation of Steep Surface Waves on Water I: A Numerical Method of Computation,* Proc. R. Soc. Lon., **A350**, 1-25, 1976

Longuet-Higgins, M.S., Fox, M.J.H., *Theory of the almost-highest wave Part 2: Matching and analytic extension*, J. Fluid Mech., **85**, 769-786, 1978

Longuet-Higgins, M.S., *On the Joint Distribution of Wave Periods and Amplitudes in a Random Wave Field,* Proc. Roy. Soc. London, **A389**, 1983

Longuet-Higgins, M.S., *On the statistical distribution of the heights of sea waves*, J. Marine Research, **11**, 245-266, 1952

Longuet-Higgins, M.S., Stewart, R. W., *Changes in the Form of Short Gravity Waves on Long Waves and Tidal Currents,* J. Fluid Mech., **8**, 565-583, 1960

Longuet-Higgins, M.S., *The crest instability of steep gravity waves, or how do short waves break?,* In M.A. Donelan, W.H. Hui, and W.J. Plant, (eds), *The Air-Sea Interface,* Proceedings of the Symposium on the Air-Sea Interface, Radio and Acoustic Sensing, Turbulence and Wave Dynamics, Marseilles, France, June 24-30, 1993, Miami, Florida, U.S.A. The Rosenstiel School of Marine and Atmospheric Sciences, University of Miami, 237-246, 1996

Longuet-Higgins, M.S., *The Effect of Non-Linearities on Statistical Distributions in the Theory of Sea Waves,* J. Fluid Mech, **17**, 459-480, 1963

Luke, J.C., *A Variational Principle for a Fluid with a Free Surface,* J. Fluid Mech., **27**, 395-397, 1967

MacGregor, J.R., Black, F., Wright, D., Gregg, J., *Design and Construction of the FPSO Vessel for the Schiehallion Field,* Trans. Royal Inst. of Naval Architects, London, UK, 2000

Madsen, P.A., Sorensen, O.R., *A New Form of Boussinesq Equations with Improved Linear Dispersion Characteristics. 2: A Slowly Varying Bathymetry,* Coastal Engng, **18**, 183-204, 1992

Magnusson, A.K., Donelan M.A., Drennan, W.M., *On estimating extremes in an evolving wave field,* Coastal Eng., **36**, 147-163, 1999

Magnusson, A.K., *High wave crests in the central North Sea*, In Proceeding of the Symposium on The Air-Sea Interface. Radio and Acoustic Sensing, Turbulence and Wave Dynamics, Marseilles, France, 24-30 June, 1993, Univiversity of Toronto Press Inc, Toronto, 289-295, 1996

Mallory, *Abnormal Waves off the South African Coast - A Danger to Shipping,* The Naval Architect, July 1975

Marthinsen, T., Winterstein, S.R., *On the Skewness of Random Surface Waves,* Proceedings ISOPE'92, San Francisco, 1992

Martin, D.U., Yuen, H.C., *Quasi-recurring energy leakage in the two-space-dimensional nonlinear Schrodinger equation*, Phys. Fluids, **23**, 881-883, 1980

Massel, S., *Extended Refraction-Diffraction Equations for Surface Waves,* Coastal Engng, **19,** 97-126, 1993

Massel, S., *Hydrodynamics of Coastal Zones,* Elsevier, Amsterdam, 1989

Masuda, A., Kuo, Y., Mitsuyasu, H., *On the Dispersion Relation of Random Gravity Waves Part I: Theoretical Framework,* J. Fluid Mech., **92**, 717-730, 1979

Masuda, A., *Nonlinear energy transfer between wind waves*, J. Phys. Oceanogr., **10**, 2082-2092, 1980

McLean, J.W., *Instabilities and breaking of finite amplitude waves I*, J. Fluid Mech., **114**, 315-341, 1982ab

Mei, C., *The Applied Dynamics of Ocean Surface Waves*, J. Wiley & Sons World Scientific, New York, 1983+1986

Meza Conde, E., Zhang, J., Seymour, R. J., *Prediction of surface wave elevation based on the pressure measurements,* J. Offshore Mech. & Arctic Engrg., **121 No. 4,** 242-250, 1999

Mitsuyasu, H., *Observation of Directional Spectrum of Ocean Waves*, Ua Cloverlead Buoy. J.Phys. Oceanography, **16**, 459-482, 1975

Mollo-Christensen, E., Ramamonjiarisoa, A., *Subharmonic transitions and group formation in a wind wave field*, J. of Geophysical Research, C8, **87**, 5699-5717, 1982

Monaghan, J., *Simulating Free Surface Flows with SPH*, Journal of Computational Physics, **110**, 399-406, 1994

Mori, N., Yasuda, T., *Maximum wave height distributions of nonlinear narrow banded random waves*, In Proc. International Offshore and Polar Engineering Conference, ISOPE, Seattle, **3**, 9-13, 2000

Mori, N., Yasuda, T., *Weakly non-gaussian model of wave height distribution for random waves*, In Proc. of the 24th Int. Conf. on Coastal Eng., Orlando ASCE, **1**, 412-426, 1996

Mori, N., Yasuda, T., Nakayama, S., *Statistical Properties of Freak Waves Observed in the Sea of Japan*, Proc. of the 10th Int. Off. & P. Eng. Conf. ISOPE 2000, Seattle, **3**, 109-115, 2000

Morlet, J., Arens, G., Fourgeau, I., Giard, D., *Wave Propagation and Sampling Theory*, Geophysics, **47**, 203-236, 1982

Morrison, W.D.M., Millar, J., Buchner, B., *Green Water Susceptibility of North Sea FPSO/FSUs,* IBC's 15th Conf. on Floating Production Systems, London, Dec. 11-12 2000

Mundle, R., *Fatal Storm: The Inside Story of the Tragic Sydney-Hobart Race*, International Marine/McGraw-Hill, 1999

Myrhaug, D., Kjeldsen, P., *Parametric Modeling of Joint Probability Density Distributions for Steepness and Asymmetry in Deep Water Waves*, Journal of Coastal Engineering, Amsterdam, 1983

Myrhaug, D., Kjeldsen, S. P., *Prediction of occurrences of steep and high waves in deep water,* J. Waterways, Port, Coastal and Ocean Engineering, ASCE, **113, No. 2**, 128-138, 1987

Myrhaug, D., Rue, H., *Note on a Joint Distribution of Successive Wave Periods,* J. Ship Research, **37**, 1993

Nadaoka, K., Beji, S., Nakagawa, Y., *A Fully Dispersive Weakly Nonlinear Model for Water Waves,* Proc. R. Soc. London, **A453**, 303-318, 1997

Naess, A., *Crossing Rate Statistics of Quadratic Transformations of Gaussian Processes*, Technical Report R-2-00, Norwegian University of Science and Technology, Department of Structural Engineering, 2000

Naess, A., Machado U., *Response Statistics of Large Compliant Offshore Structures*, In Proceedings 8th ASCE Specialty Conference on Probabilistic Mechanics and Structural Reliability, New York, ASCE, 2000

Naess, A., Machado U., *Response Statistics of Linear Dynamic Systems Subjected to Quadratic Transformations of Gaussian Processes*, In Proceedings of the Euromech Colloquium 413 Stochastic Dynamics of Nonlinear Mechanical Systems, Palermo,

Italy, 2000

Nelder, J., Mead, R., *A Simplex Method for Function Minimization*, Computer Journal, **7**, 308-313, 1965

Nepf, H.M., Wu, C.H., Chan, E.S., *A comparison of two- and three-dimensional wave breaking*, Journal of Physical Oceanography, **28**, 1496-1510, 1998

Nickersen, J.W., *"Three Sisters" Marine Historic Voyage,* Mariners Weather Log, No. 30, 190-196, 1986

Nickersen, J.W., *Freak Waves!*, Mariners Weather Log, **37 No. 2**, 13-27, 1993

Nickersen, J.W., *Marine Observation Program, Freak Waves and Extreme Storm Waves,* Mariners Weather Log, Washington, **29**, 13-17, 1985

Nitta, A., Arai, H., Magaino, A., *Basis of IACS Unified Longitudinal Strength Standard,* Int. J. Marine Structures, **5 No 1**, 1992

Nwogu, O., *Alternative Form of Boussinesq Equations for Nearshore Wave Propagation,* J. Wtrwy., Port, Coast. and Oc. Engng. ASCE, **119**, 618-638, 1993
Ochi, M. K., *Ocean Waves – The Stochastic Approach,* Ocean Technology Series 6, Cambridge University Press, 1998

Ohhyama T., Nadaoka, K., *Development of a Numerical Wave Tank for Analysis of Nonlinear and Irregular Wave Field,* Fluid Dyn. Res, **8**, 231-251-22, 1991

Ohhyama T., Nadaoka, K., *Transformation of a Nonlinear Wave Train Passing over a Submerged Shelf Without Breaking,* Coastal Engng., **24**, 1-22, 1994

Olagnon, M., Krogstad, H.E., *Observed Short- and Long- Term Distributions of Wave Steepness,* Proc. Int. Offshore and Polar Engineering Conf., Montreal, **3**, 63-70, 1998

Olagnon, M., van Iseghem, S., *Some cases of observed rogue waves and attempts to characterize their occurrence conditions*, Proceedings of the Rogue Waves 2000 Workshop, Brest, France, 29-30 November 2000

Onorato, M., Osborne, A.R., Serio, M., *Nonlinear Dynamics of Rogue Waves*, International Workshop on Wave Hindcasting and Forecasting, Monterey, 470-479, 2000

Osborne, A.R., Onorato, M., Serio, M., *The Nonlinear Dynamics of Rogue Waves and Holes in Deep-Water Gravity Wave Train,* Phys. Letters, **A275**, 386-393, 2000

Osborne, A.R., Petti, M., *Laboratory-generated, shallow-water surface-waves–analysis using the periodic, inverse scattering transform*, Phys. of Fluids, **6**, 1727-1744, 1994

Osborne, A.R., *The Random and Deterministic Dynamics of "Rogue Waves" in Unidirectional, Deep-Water Wave Trains,* The 3rd International Workshop on Very Large Floating Structures (VLFS'99), Honolulu, 1999

Ostrovsky, L., Potapov, A., *Modulated Waves, Theory and Applications,* John Hopkins Univ. Press, Baltimore-London, 1999

Pelinovsky E.N., Kharif Ch., *Dispersive Compression of Wave Packages as Mechanism of Occurence of Abnormal High Waves on a Surface of Ocean*, Izvestia of Russian Academy of Engineering Sciences, Series: Applied Mathematics and Informatics, **1**, 50-61, 2000, in Russian

Pelinovsky, E., Kharif, C., *Simplified Model of the Freak Wave Formation from the Random Wave Field,* Proc. 15th Int. Workshop on Water Waves and Floating Bodies, Caesaria, Israel, 142-145, February 27 – 1March 2000

Pelinovsky, E., Talipova, T., Kharif, C., *Nonlinear Dispersive Mechanism of the Freak Wave Formation in Shallow Water,* Physica, **D147**, 83-94, 2000

Pelinovsky, E., Talipova, T., Kit, E., Eitan, O., *Nonlinear Wave Packet Evolution in Shallow Water,* Proc. Int. Symp. on Progress in Coastal Engineering and Oceanography, Seoul Korea, **2**, 53-62, 9 - 11 September 1999

Peltzer, R.D., Griffin, O.M., *Spatial and Temporal Properties of Deep Water Breaking Waves*, 45th APS Fluid Dyn. Meeting, Florida State Univ., Tallahassee, USA, 1992

Peregrine, D.H., *Interaction of Water Waves and Currents,* Adv. Appl. Mech., **16**, 9-117, 1976

Peregrine, D.H., *Water Waves, Nonlinear Schroedinger Equations and Their Solutions,* J. Austral. Math. Soc., Ser. B25, 16-43, 1983

Peregrine, H., *Freak waves*, 28th WEGEMT School "Wave Modelling Applied to the Design of Offshore and Coastal Structures", 6-10 July 1998

Petrov, A.A., *Variational Statement of the Problem of Liquid Motion in a Container of Finite Dimensions,* PMM, **28** (4), 917-922, 1964

Philips, O.M., *The Dispersion of Short Wavelets in Presence of Dominant Long Wave,* J. Fluid Mech., **107**, 465-485, 1981

Phillips, O.M., *Extreme waves and Breaking Wavelets*, Theoretical and Applied Mechanics, S.R.Bodher, J.Singer, A.Solan & Z.Hashin (ed.), Elsevier Science Publishers, 1992

Phillips, O.M., Gu, D., Donelan, M., *Expected structure of extreme waves in a*

Gaussian sea Part I: Theory and SWADE buoymeasurements, J.Phys.Oceanogr., **23**, 992-1000, 1993

Phillips, O.M., *The Dynamics of Unsteady Gravity Waves of Finite Amplitude Part 1*, J. Fluid Mech, **4**, 426-434, 1960

Pierson, W.J, Donelan, M.A., Hui, W.H., *Linear and nonlinear propagation of water wave groups,* J. Geophys. Res., **97**, 5607-5621, 1992

Podgorski, K., Rychlik, I., Machado, U., *Exact Distributions for Apparent Waves in Irregular Seas*, Ocean Eng, **27**, 979-1016, 2000

Podgorski, K., Rychlik, I., Ryden, J., Sjo, E., *How Big Are the Big Waves in A Gaussian Sea?*, Int. J. of Offshore and Polar Engineering, **10 No. 3**, 161-169, 2000

Prado,R., West,M., *Exploratory modelling of multiple non-stationary time series: Latent process structure and decompositions*, In: Modelling Longitudinal and Spatially Correlated Data, (ed: T. Gregoire), Springer-Verlag, 1997

Prevosto, M., *Effect of Directional Spreading and Spectral Bandwidth on the Nonlinearity of the Irregular Waves*, Proc. 8th ISOPE Conf., **3**, 119-123, 1998

Prevosto, M., Forristall, G.Z., *Results of the WACSIS project*, to be published

Prevosto, M., Krogstad, H.E., Robin, A., *Probability Distributions for Maximum Wave and Crest Heights,* Coastal Engineering, **40**, 329-360, 2000

Randall, R. E., Zhang, J., Longridge, J.K., *Laser Doppler Anemometer Measurements of Irregular Water Wave Kinematics,* J. Ocean Engrg., **20**, 541-554, 1993

Rapp, R.J., *Melville, W.K., Laboratory measurements of deep-water breaking waves*, Phil. Trans. R. Soc. Lond., **A331**, 735-800, 1990

Rasmussen, J.H., Stiassnie, M., *Discretization of Zakharov's equation*, Eur. J. Mech. B/Fluids, **18**, 353-364, 1999

Renilson, M., Binns, J. R., Tuite, A., *The Re-Righting of Sailing Yachts in Waves - A Comparison of Different Hull Forms*, Proceedings of the 15th Chesapeake Sailing Yacht Symposium, Annapolis, MD, 26-27 January 2001

Rice, S.O., *Distribution of Quadratic Forms in Normal Random Variables - Evaluation by Numerical Integration*, Siam Journal Sci. Stat. Comput., **1**, 438-448, 1980

Robin, A., Olagnon, M., *Occurrence of Extreme Waves with Respect to Significant Wave Height*, Proc. Offshore Mechanics and Artic Engineering OMAE, **2a**, 1-9, 1991

Rodenbusch, G., Forristall, G.Z., *An Empirical for Random Directional Wave Kinematics near the Free Surface,* Offshore Technology Conference OTC, Paper No. 5097, 1986

Rowan, T., *Functional Stability Analysis of Numerical Algorithms*, PhD Thesis, University of Texas, Austin, 1990

Rozario, J.B., Tromans, P.S., Taylor, P.H., Efthymiou, M., *Comparison of Loads Predicted using "Newwave" and other Wave Models with Measurements on the Term Structure*, Wave Kin. and Env. Forces, **29**, 143-159, 1993

Rychlik, I., Johannesson, P., Leadbetter, M.R., *Modeling and Statistical Analysis of Ocean-Wave Data Using Transformed Gaussian Processes,* Marine Structures, **10**, 13-47, 1997

Salsich, J., Zseleczky, J.J., *Experimental Studies of Capsizing in Breaking Waves*, AIAA/SNAME Ancient Interface XIII, 1983b

Salsich, J.O., Johnson, B., Holton, C., *A Transient Wave Generation Technique and Some Engineering Applications*, Proceedings of the 20th American Towing Tank Conference, 1983

Sand, S.E., Hansen, N.E.O., Klinting, P., Gudmestad, O.T., Sterndorf, M.J., *Freak Wave Kinematics*, (Eds.): Torum, O., Gudmestad, O.T.: *Water Wave Kinematics*, Kluwer Academic Publ., 539-549, 1990

Sand, S.E., Ottesen-Hansen, N.E., Klinting, P., Gudmestad, O.T., Sterndorff, M.J., *Freak Wave Kinematics*, In: Torum, A. and Gudmestad, O.T. (eds.): *Water Wave Kinematics,* Kluwer Academic Publishers, Dordrecht, The Netherlands, 1990

Schäffer, H.A., *Second-Order Wavemaker Theory for Irregular Waves,* Ocean Engr, **23 No. 1,** 47-88, 1996

Schlurmann, T., Lengricht, J., Graw, K.-U., *Spatial Evolution of Laboratory Generated Freak Wave in Deep Water Depth*, 10th Int. Off. and P. Eng. Conf., **3**, 54-59, 2000

Schlurmann, T., Schimmels, S., Dose, T., *Spectral Frequency Analysis of Transient Waves Using Wavelet Spectra (Morlet) and Hilbert Spectra (EMD)*, 4th Int. Conf. on Hyd. and Eng., 2000, in press

Seymour, R. J., Castel, D., McGehee, D., Thomas, J. & O'Reilly, W., *New Technology in Coastal Wave Monitoring,* In Magoon & Hemsley (eds.): *Ocean Wave Measurements & Analysis,* ASCE, New York, 105-123, 1993

Sharma, J.N., Dean, R.G., *Second-Order Directional Seas and Associated Wave Forces*, Society of Petroleum Engineering Journal, **4**, 129-140, 1981

She, K., Greated, C.A., Easson, W.J., *Experimental study of three-dimensional breaking wave kinematics*, Applied Ocean Research, **19**, 329-343, 1997

Shemer, L., Kit, E., Jiao, H.-Y., Eitan, O., *Experiments on nonlinear wave groups in intermediate water depth*, J. Waterway, Port, Coastal and Ocean Engineering, **124**, 320-327, 1998

Shrira, V.I., Badulin, S.I., Kharif, C., *A Model of Water Wave "Horse-Shoe" Patterns*, J.Fluid Mech., **318**, 375-404, 1996

Smith S.F., Swan C., *Extreme Two-Dimensional Water Waves: An Assessment of Potential Design Solutions*, To appear: J. Ocean. Engng., 2001

Smith, R., *Giant Waves,* J. Fluid Mech, **77**, 417-431, 1976

Smith, R., Sprinks, T., *Scattering of Surface Waves by a Conical Island*, J. Fluid Mech., **72,** 373-384, 1975

Spell, C.A., Zhang, J., Randall, R.E., *Hybrid Wave Model for Uni-Directional Irregular Waves Part II: Comparison with Laboratory Measurements,* Applied Ocean Res., **18**, 93-110, 1996

Stansberg, C.T., *Extreme waves in laboratory generated irregular wave trains*, In Torum, A. and Gudmestad, O.T., (eds): *Water wave kinematics*, Kluwer Academic Pub., 573-590, 1990

Stansberg, C.T., *Laboratory Reproduction of Extreme Waves in a Random Sea,* Proc., Wave Generation'99 (International Workshop on Natural Disaster by Storm Waves and Their Reproduction in Experimental Basin), Kyoto, Japan, 2000

Stansberg, C.T., *Non-Gaussian Extremes in Numerically Generated Second-Order Random Waves in Deep Water,* Proc. the 8th ISOPE Conf., Montreal Canada, **3,** 103-110, 1998

Stansberg, C.T., *Nonlinear Extreme Wave Evolution in Random Wave Groups,* Proc., the 10th ISOPE Conf., Seattle, WA, USA, **3**, May 28-2 June 2000

Stansberg, C.T., *On the Nonlinear Behaviour of Ocean Wave Groups,* Proc. WAVES 1997 Symposium (ASCE), Virginia Beach, VA, USA, 1998

Stansberg, C.T., *Random waves in the laboratory – What should be expected for the extremes?*, This publication

Stansberg, C.T., *Second-Order Numerical Reconstruction of Laboratory Generated Random Waves*, Proc. 12th Offshore Mech. and Arctic Eng. Conf. (OMAE), **2**, 143-151, 1993

Steele, K. M., Finn, L.D., Lambrakos, K.F., *Compliant Tower Response Prediction Procedures,* Offshore Technology Conf. OTC, Paper No. 5783, 1988

Stiassnie, M., *Note on the Modified Nonlinear Schroedinger Equation for Deep Water Waves,* Wave Motion, **6**, 431-433, 1984

Stiassnie, M., Shemer, L., *Energy Computations for Evolution of Class I and II Instabilities of Stokes Waves*, J.Fluid Mech., **174**, 299-312, 1987

Stockwell, R.G., Mansinha, L., Lowe, R.P., *Localization of the Complex Spectrum: The S Transform*, IEEE, T. Sig. Pro., **44**, 998-1001, 1996

Stokes, G.G., *Supplement to a Paper on the Theory of Oscillatory Waves,* Mathematical and Physical Papers, Cambridge University Press, London, **1**, 314-326, 1880

Su, M.Y., Bergin, M., Marler, P., Myrick, R., *Experiments on nonlinear instabilities and evolution of steep gravity-wave trains*, J. Fluid Mech., **124**, 45-72, 1982

Su, M.Y., *Three-dimensional deep-water waves Part 1: Experimental measurements of skew and symmetric wave patterns*, J. Fluid Mech., **124**, 73-108, 1982

Sunde, A., *Kjempebolger i Nordsjoen,* (in Norwegian), Vaer & Klima, **18 No. 1,** 1995

Sweetman, B., Winterstein, S.R., *Second Order Random Ocean Waves: Prediction of Temporal and Spatial Variation from Fixed and Moving References - The Routine WAVEMAKER*, Version 3.2. Rep. No. RMS-37, Civil Engineering Dep., Stanford University, Stanford, 1999

Tanaka, M., *The stability of steep gravity waves*, J. Phys. Soc. Japan, **52** (9), 3047-3055, 1983

Tang, Y., Quellet, Y., *A New Kind of Nonlinear Mild-Slope Equation for Combined Refraction-Diffraction of Multifrequency Water Waves,* Coastal Engng., **31**, 3-36, 1997

Tayfun, M.A., *Narrow-Band Nonlinear Sea Waves,* J. Geophys. Res., **85 No. C3**, 1548-1552, 1980

Taylor P.H., Haagsma, Ij., *Focussing of Steep Wave Groups on Deep Water,* Proc. Int. Symp, Waves – Physical and Numerical Modelling, Vancouver, Canada, **2**, 862-870, 1994

Tick, L.J., *A Nonlinear Random Model for Gravity Waves,* J. Maths & Mech., **8**, 643-652, 1959

Titchmarsh, E.C., *Introduction to the Theory of Fourier Integrals*, Oxford University

Press, 1948

Tomita H., Kawamura, T., *Statistical Analysis and Inference from the In-Situ Data of the Sea of Japan with Reference to Abnormal and/or Freak Waves,* Proceedings ISOPE2000, Seattle, USA, **3**, 2000

Tomita, H., Sawada, H., *On the dynamical properties of plunging breakers in deep water*, In Donelan, M.A., Hui, W.H. and Plant, W.J. (eds): *The Air-Sea Interface,* Proceedings of the Symposium on the Air-Sea Interface, Radio and Acoustic Sensing, Turbulence and Wave Dynamics, Marseilles, France, June 24-30, 1993, 269-276, Miami, Florida, U.S.A. The Rosenstiel School of Marine and Atmospheric Sciences, University of Miami, 1996

Tomita, H., Sawada, H., *Statistics of Heavy Weather Actual Ocean Wave Data in North Sea and Japan Sea with Reference to Abnormal Waves,* ISOPE '99, Brest France, 1999

Torum, A., Gudmestad, O.T. (eds.), *Water Wave Kinematics*, Kluwer, 771, 1990

Tracy, E.R., *Topics in nonlinear wave theory with applications*, Ph.D. Thesis, University of Maryland (1984), Tracy, E.R., Chen, H.H., Phys. Rev., **A37**, 815-839, 1988

Tromans, P.S., Anaturk, A.R., Hagemeijer, P., *A New Model for the Kinematics of Large Ocean Waves,* Proc. of ISOPE '91 Conference, Edinburgh, 1991

Tromans, P.S., Taylor, P.H., *The Shapes, Histories and Statistics of Non-Linear Wave Crests in Random Seas,* Proc. 17th Int. Conf. On Offshore Mechanics and Arctic Engineering, OMAE98-1206, 1998

Trulsen, G.N., Dysthe, K.B., Trulsen J., *Evolution of a gravity wave spectrum through a current gradient*, J.Geophys.Res., **95**, 22141-22151, 1990

Trulsen, K., Dysthe, K., *A modified nonlinear Schroedinger equation for broader bandwidth gravity waves on deep water*, Wave Motion, **24**, 417-430, 1996

Trulsen, K., Dysthe, K., *Freak waves - A Three-Dimensional Wave Simulation*, Proc. 21st Symposium on Naval Hydrodynamics, National Academy Press, 550-560, 1997

Trulsen, K., Dysthe, K.B., *Frequency downshift in three dimensional wave trains in deep basin*, J. Fluid Mech., **352**, 359-373, 1997

Trulsen, K., Kliakhandler, I., Dysthe, K.B., Velarde, M.G., *On weakly nonlinear modulation of waves on deep water*, Phys. Fluids, **12**, 2432-2437, 2000

Trulsen, K., Stansberg, C.T., *Spatial Evolution of Water Surface Waves: Numerical Simulation and Experiment of Bichromatic Waves,* Proc., the 11th ISOPE Conf.,

Stavanger, Norway, 2001

Tsai, W., Yue, D.K., *Computation of Nonlinear Free-Surface Flows*, Ann. Rev. Fluid Mech., **28**, 249-278, 1996
Tucker, M.J., Pitt, E.G., *Waves in Ocean Engineering,* Elsevier, 2001

Tulin M.P., Landrini M., *Breaking waves in the ocean and ships 23*, Symp. Naval Hydrodynamics, Val de Reuil, France, **4**, 1-32, 2000

Tulin, M.P., Waseda, T., *Laboratory Observations of Wave Group Evolution*, Including Breaking Effects, J. Fluid Mech,, 1999

Tulin, M.P., Yao, Y., Wang, P., The simulation of the deformation and breaking of ocean waves in wave groups, In Proc. 7th Intl Conf. on Behaviour of Offshore Structures BOSS'94, MIT, 1994

Tung, C.C., Huang, N.E., *Peak and Trough Distributions of Nonlinear Waves,* Ocean Eng., **12 No. 3,** 201-209, 1985

Umeda, N., Ikeda, Y., *Rational Examination of Stability Criteria in the Light of Capsizing Probability*, Proceedings of the 5th International Conference on Stability of Ships and Ocean Vehicles (STAB 94), Melbourne, Fl. USA, 1994

Umeda, N., Matsuda, A., *Broaching in Following and Quartering Seas - Theoretical Attempts and New Prevention Device*, Proceedings of the 7th International Conference on Stability of Ships and Ocean Vehicles (STAB 2000), Launceston, Tasmania, Australia, 7-11 February 2000

Umeda, N., Matsuda, A., Hamamoto, M., Suzuki, S., *Stability Assessment for Intact Ships in the Light of Model Experiments,* J. of Marine Science and Technology, SNAJ, Japan, **4**, 45-57, 1999

van Iseghem, S., Deleuil, G., Guerin, P., *Improved Characterizations for Design Waves*, Proc. Int. Offshore and Polar Engineering Conf., ISOPE, 2001

Vassalos, D., Maimun, A., *Broaching-To: Thirty Years On*, Proceedings of the 5th International Conference on Stability of Ships and Ocean Vehicles (STAB 94), Melbourne, Fl. USA, 1994

Ville, J., *Theorie et Application de la Notion de Signal Analytique*, Cabl. et Transm., **2a**, 61-74, 1948

Vinje, T., Brevig, P., *Breaking waves on finite water depths: A numerical study, Technical report*, Ship Research Institute of Norway, Report R-111, **81**, 1981

Vinje, T., Brevig, P., *Numerical Simulation of Breaking Waves,* Adv. Water Resources, **4**, 77-82, 1981

Vinje, T., Haver, S., *On the Non-Gaussian Structure of Ocean Waves,* Proc., the 7th BOSS Conf., MIT, Cambridge, Mass., USA. (Published by Pergamon, Oxford, UK), **2**, 1994

Wang, P., Mirie, R., Tulin M., *An Efficient Numerical Tank for Nonlinear Water Waves, Based on the Multi-Subdomain Approach with BEM,* Int. J. Numer. Meth. Fluids, **20**, 1315-1336, 1995

Warren, S.J., Bole, J.B., Driver, D.B., *Measured wave crest distributions in central and southern North Sea storms*, Proc. of the 8th International Offshore and Polar Engeneering Conference, 1998

Weber, B.L., Barrick, D.E., *On the Nonlinear Theory for Gravity Waves on the Ocean's Surface: Part I. Derivations,* J. Geophys. Res., **100(C1)**, 773-778, 1977

West, B.J., Brueckner, K.A., Janda, R.S., Milder, D.M., Milton, R, *A New Numerical Method for Surface Hydrodynamics,* J. Geophys. Res., **92** (11), 803-11, 804, 1987

Wheeler, J.D., *Method for Calculating Forces Produced by Irregular Waves,* J. Petroleum Tech., **249**, 359-367, 1970

White, B.S., Fornberg, B., *On the Chance of Freak Waves at Sea,* J. Fluid Mech., **355**, 113-138, 1998

Winterstein, S.R., *Nonlinear Vibration Models for Extremes and Fatigue,* J. Eng. Mech., **114**, 1772-1790, 1988

Witham, G.B., *Linear and Nonlinear Waves*, Wiley, New York, 1974

Wolfram, J., Feld, G., Allen, J., *A new approach to estimating extreme environmental loading using joint probabilities*, In: Behaviour of Offshore Structures BOSS'94, (ed: C. Chryssostomidis), Pergamon, **2**, 701-713, 1994

Wolfram, J., Linfoot, B., Venugopal,V., *Some results from the analysis of metocean data collected during storms in the northern North Sea*, Underwater Technology, **4** (4), 2000, in press

Wu, G., Eatock T.R., *Finite Element Analysis of Two-Dimensional Non-Linear Transient Water Waves*, Applied Ocean Research, **16**, 363-372, 1994

Wu, G., Eatock T.R., *Time Stepping Solutions of Two-Dimensional Non-Linear Wave Radiation Problem*, Ocean Engineering, **22** (8), 785-798, 1995

Yasuda, T., Mori, N., *High Order Nonlinear Effects on Deep-Water Random Wave Trains,* Proc. of the Int. Symp. on Waves – Physical and Numerical Modelling, Univ. of British Columbia, Vancouver, Canada, **2**, 823-832, 1994

Yasuda, T., Mori, N., Ito, K., *Freak Waves in a Unidirectional Wave Train and Their Kinematics*, Proceedings 23rd International Conference on Coastal Engineering, ASCE, Venice, 751-764, 1992

Yasuda, T., Mori, N., Nakayama, S., *Characteristics of Giant Freak Waves Observed in the Sea of Japan,* Proceedings Waves'97 Ocean Wave Measurements and Analysis, Virginia Beach, **2**, 482-495, 1997

Yasuda, T., Mori, N., Nakayama, S., *Characteristics of Giant Freak Waves Observed in the Sea of Japan*, In B. Edge and M. Hemsley (Eds.): *Ocean Wave Measurement and Analysis*, ASCE, 316-328, 1997

Yasuda, T., Mori, N., Nakayama, S., *Freak wave kinematics in unidirectional deep water waves*, In Proc. of the 4th Int. Offshore and Polar Eng. Conf., Osaka, **3**, 43-50, 1994

Yasuda, T., Mori, N., *Occurrence Properties of Giant Freak Waves in Sea Area around Japan*, J. of Wat., Port, Coast. and Oc. Eng. ASCE, **123**, 209-213, March 1997

Yasuda, T., Mori, N., *Roles of sideband instability and mode coupling in forming a water wave chaos*, Wave Motion, **26** (2), 163-185, 1997

Yuen, H. C., *Nonlinear Dynamics of Deep-Water Gravity Waves*, Adv. Appl. Mech., **22**, 67-229, 1982

Yuen, H.C., Ferguson, Jr., W.E., *Relationship between benjamin-feir instability and recurrence in the nonlinear Schrodinger equation*, Phys. Fluids, **21** (8), 1275-1278, 1978

Yuen, H.C., Lake, B.M., *Nonlinear Dynamics of Deep-Water Gravity Waves,* In Chia-Shun Yih (ed.): *Advances in Applied Mechanics,* Academic Press, **22**, 153-180, 1992

Zakharov, V.E., Shabat, A.B., *Exact Theory of Two-Dimensional Self-Focussing and One-Dimensional Self-Modulation in Nonlinear Media,* Sov. Phys. JETP, **34**, 62-9, 1972

Zakharov, V.E., *Stability of Periodic Waves of Finite Amplitude on the Surface of a Deep Fluid,* J. Appl. Math. Tech. Phys., (USSR), **2+9**, 190+86+94, 1968

Zhang, J., Chen, L., Ye, M., Randall, R.E., *Hybrid Wave Model for Unidirectional Irregular Waves Part: Theory and numerical scheme,* Applied Ocean Res., **18**, 77-92, 1996

Zhang, J., Hong, K., Yue, D. K. P., *Effects of wavelength ratio on wave modeling,* J. Fluid Mech., **248**, 107-127, 1993

Zhang, J., Prislin, I., Yang, J., Wen, J., *Deterministic Wave Model for Short-Crested Ocean Waves Part II: Comparison with Laboratory and Field measurements,* Applied Ocean Res., **21**, 189-206, 1999b

Zhang, J., Randall, R.E., Spell, C.A., *Component Wave Interactions and Irregular Wave Kinematics,* J. Wat., Port, Coastal and Ocean Engr., **118**, 401-416, 1991

Zhang, J., Yang, J., Wen, J., *Hybrid Wave Models and Their Application*, Proc. Int. Symp. Ocean Wave Kinematics Dynamics and Loads on Structures ASCE, J. Zhang (ed.), Houston, Texas, **1**, 25-33, 1998

Zhang, J., Yang, J., Wen, J., Prislin, I., Hong, K., *Deterministic Wave Model for Short-Crested Ocean Waves Part I: Theory and Numerical Scheme,* Applied Ocean Research, **21,** 167-188, 1999a

Zhu, X., Shen, Z., Eckermann, S.D., Bittner, M., Hirota, I., Yee, J.-H., *Gravity Wave Characteristics in the Middle Atmosphere Derived from the Emirical Mode Decomposition Method*, J. of Geoph. Res., **102**, D14, 16.545-16.561, 1997

Zseleczky, J.J., Cohen, S.H., *Model Tests to Evaluate the Capsize Resistance of a Motor Lifeboat in Breaking Waves*, 22nd American Towing Tank Conference, St. Johns, Newfoundland, 1989

Zseleczky, J.J., *Evolving Methods for Estimating Capsize Resistance in Breaking Waves*, SNAME New England Sailing Yacht Symposium, New England, March 1988

Recent Additional References *(added in proof)*

Athanassoulis, G.A., Belibassakis, K.A., *Nonlinear Water Waves Over a General Bathymetry: A Unified Variational Approach*, in Proceedings of "Progress in Nonlinear Science" International Conference, Nizhny Novgorod, July 2-6, 2001, to be published

Brandini, C., Grilli, S.T., *Modelling of Freak Wave Generation in a 3D-NWT*, in Proceedings of ISOPE, Stavanger, Vol. 3, pp. 124-131, 2001

Brown, M.G., *Space–time surface gravity wave caustics: structurally stable extreme wave events*, Wave Motion, **33**, pp 117-143, 2001

Clamond, D., Grue, J., On an efficient Numerical Model for Freak Wave Simulations, in Proceedings of ISOPE, Stavanger, Vol. 3, pp. 54-57, 2001

Conteto, G., Codiglia, R., D' Este, F., *Nonlinear effects in 2D transient nonbreaking waves in a closed flume*, Applied Ocean Research, **23**, pp 3-13, 2001

Dysthe, K.B., Trulsen, K., *On the Evolution of Evolution Equations for Surface Gravity Waves*, in Proceedings of "Progress in Nonlinear Science" International Conference, Nizhny Novgorod, July 2-6, 2001, to be published

Grilli, S.T. Guyenne, P., Dias, F., *A fully nonlinear model for three-dimensional overturning waves over an arbitrary bottom*, Int. Journal Numerical Methods in Fluids, **35**, pp 829-867, 2001

Jakobsen, J.B., Haver, S., Odegard, J.E., *Study of Freak Waves by Use of Wavelet Transform*, in Proceedings of ISOPE, Stavanger, Vol. 3, pp. 58-64, 2001

Onorato, M., Osborne, A.R., Serio, M., Bertone, S., *Freak Waves in Random Oceanic Sea States*, Phys. Rev. Lett., **86**, 25, pp.5831-5834, 2001

Osborne, A.R., *The random and deterministic dynamics of "rogue waves" in unidirectional, deep-water wave trains*, Marine Structures, **14**, pp 275-293, 2001

Osborne, A.R., Onorato, M., Serio, M., *The nonlinear dynamics of rogue waves and holes in deep-water gravity wave trains*, Physics Letters, **A 275**, pp 386-393, 2000

Pelinovsky, E.N., Talipova, T., Slunyaev, A., *Ocean Rogue Wave Phenomenon as Nonlinear-dispersive Wave focusing*, in Proceedings of "Progress in Nonlinear Science" International Conference, Nizhny Novgorod, July 2-6, 2001, to be published

Author's Index

Appendix CP: Coloured Plates

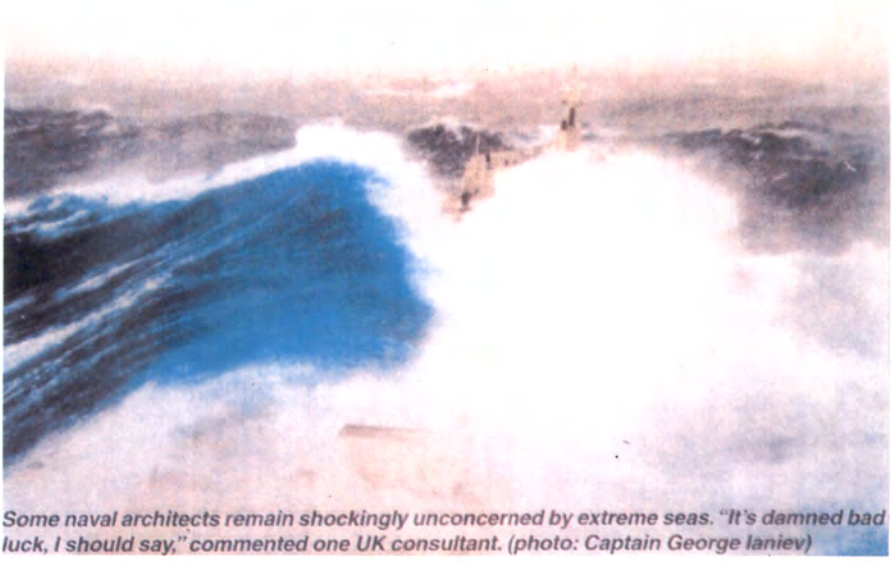

Fig. 10. MV SELKIRK SETTLER encounters a beam on rogue wave in 1977

Fig. 11. Container ship plunging into moderate seas

CAPSIZE RESISTANCE AND SURVIVABILITY WHEN SMALLER VESSELS ENCOUNTER EXTREME WAVES

by Bruce Johnson

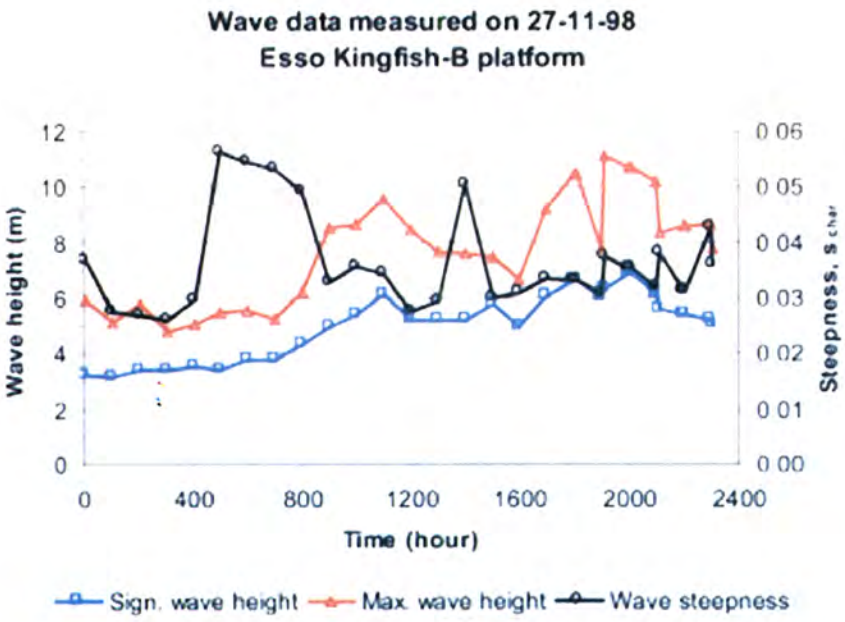

Fig. 1. Wave height (significant and maximum) and direction in eastern Bass Strait

STATISTICS OF WAVE CRESTS FROM SECOND ORDER IRREGULAR WAVE 3D MODELS

by Marc Prevosto

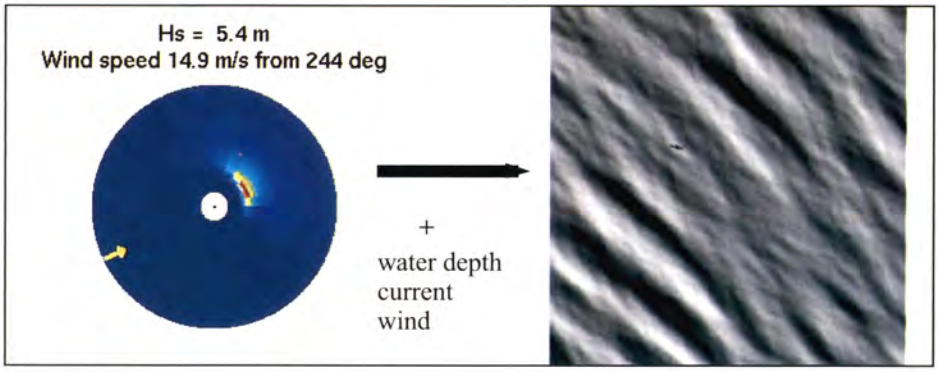

Fig. 1. From directional spectra to wave kinematics

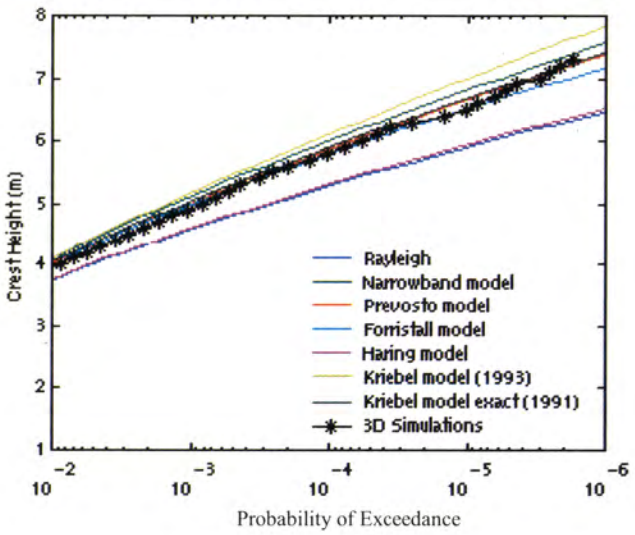

Fig. 2. Water depth 1000 meters

STATISTICS OF WAVE CRESTS FROM SECOND ORDER IRREGULAR WAVE 3D MODELS

by Marc Prevosto

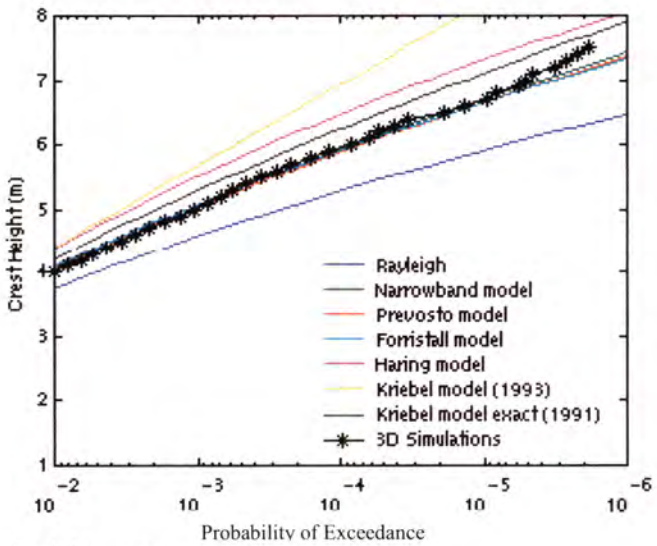

Fig. 3. Water depth 30 meters

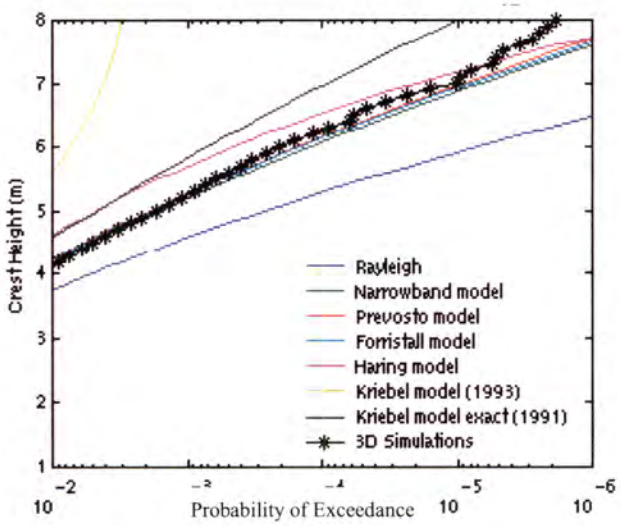

Fig. 4. Water depth 20 meters

STATISTICS OF WAVE CRESTS FROM SECOND ORDER IRREGULAR WAVE 3D MODELS

by Marc Prevosto

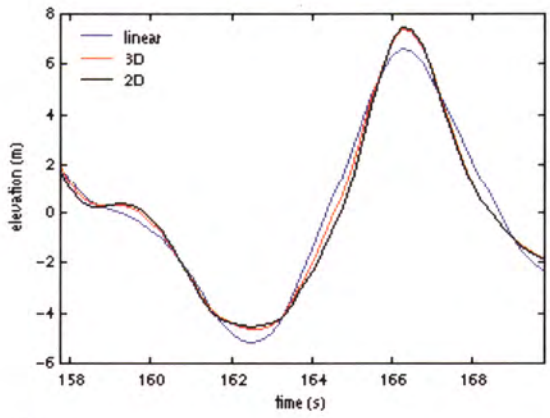

Fig. 5. The biggest crest

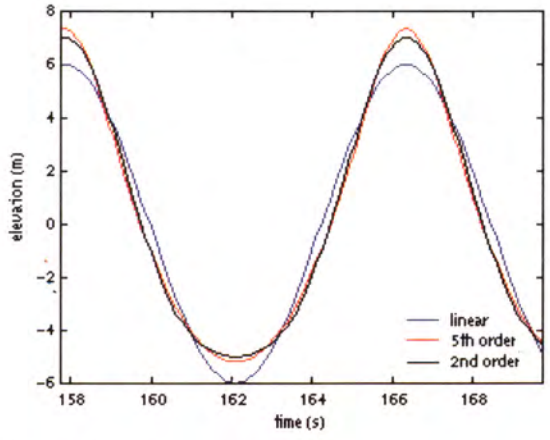

Fig. 6. The equivalent regular wave

Fig. 7. 3D view of the biggest crest

SOME CASES OF OBSERVED ROGUE WAVES AND AN ATTEMPT TO CHARACTERIZE THEIR OCCURRENCE CONDITIONS

by Michel Olagnon and Sylvie van Iseghem

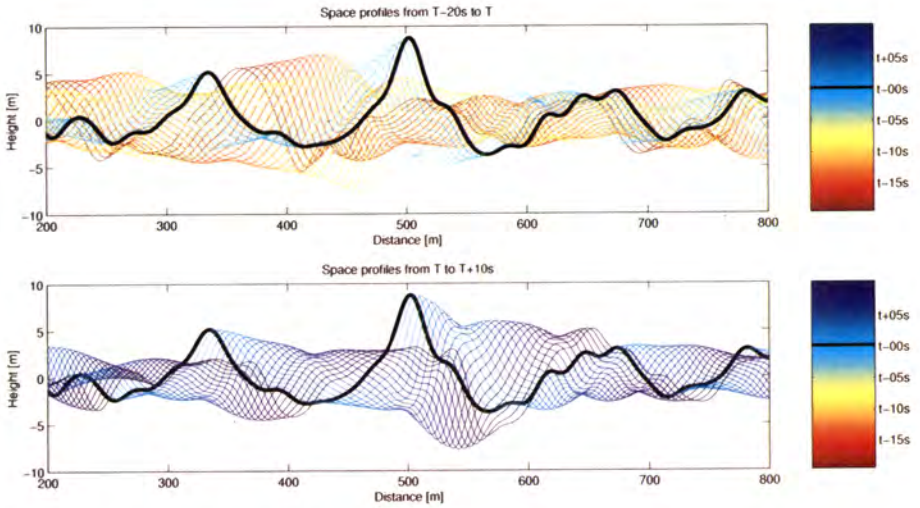

Fig. 1. Instantaneous space profiles

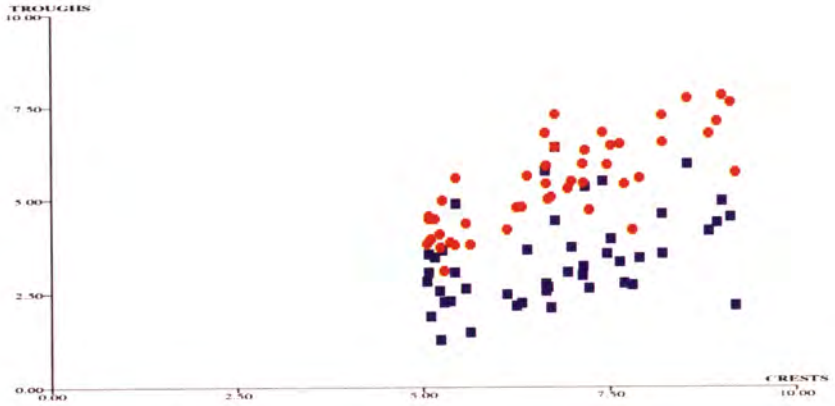

Fig. 2. Preceding trough versus crest

SOME CASES OF OBSERVED ROGUE WAVES AND AN ATTEMPT TO CHARACTERIZE THEIR OCCURRENCE CONDITIONS

by Michel Olagnon and Sylvie van Iseghem

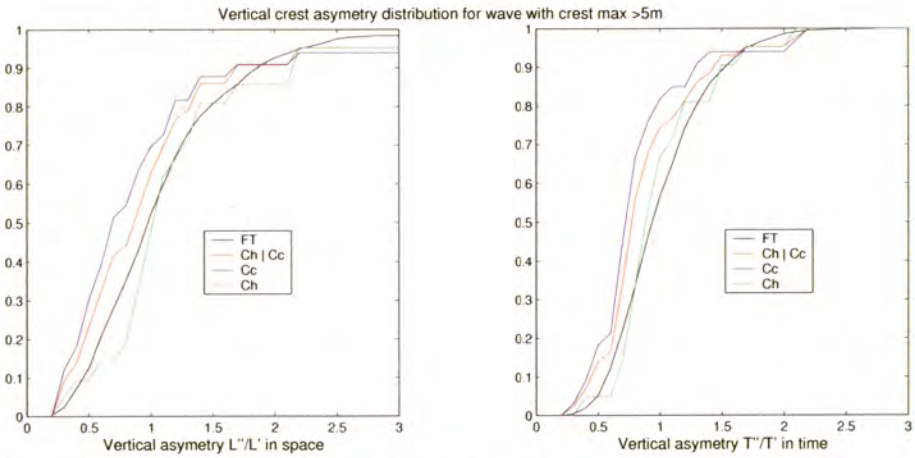

Fig. 3. Wave vertical (front/back) asymmetry

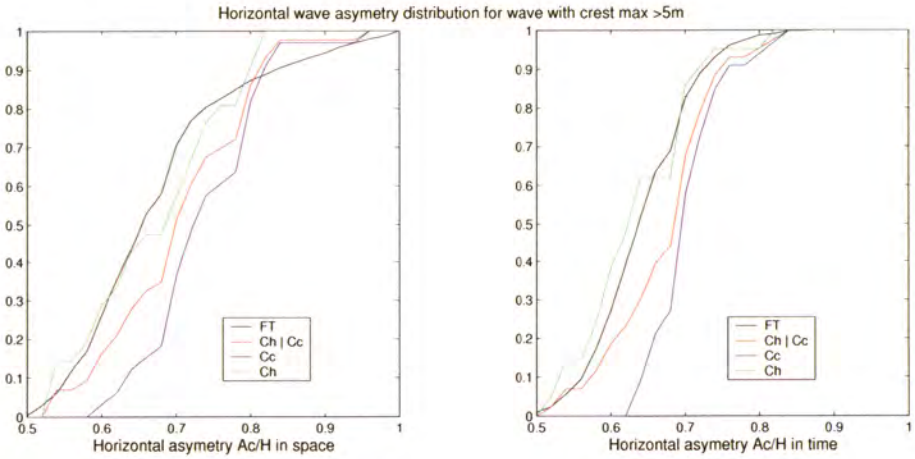

Fig. 4. Wave horizontal (height) asymmetry

SOME CASES OF OBSERVED ROGUE WAVES AND AN ATTEMPT TO CHARACTERIZE THEIR OCCURRENCE CONDITIONS

by Michel Olagnon and Sylvie van Iseghem

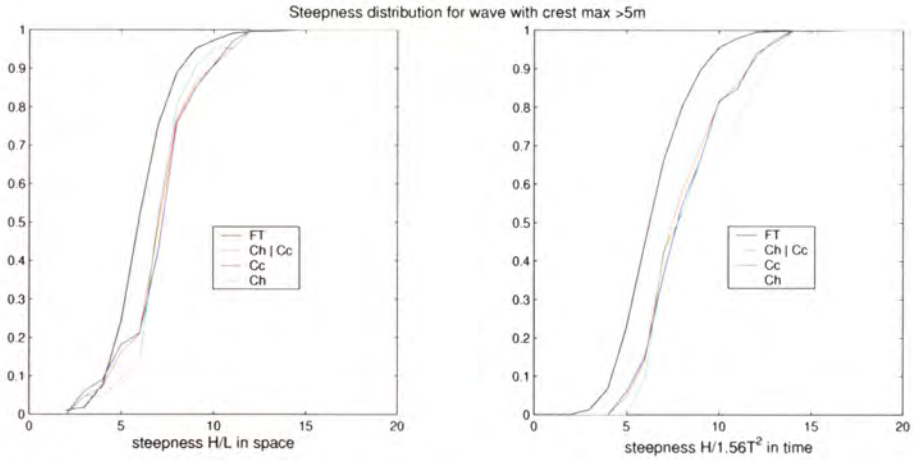

Fig. 5. Wave steepness

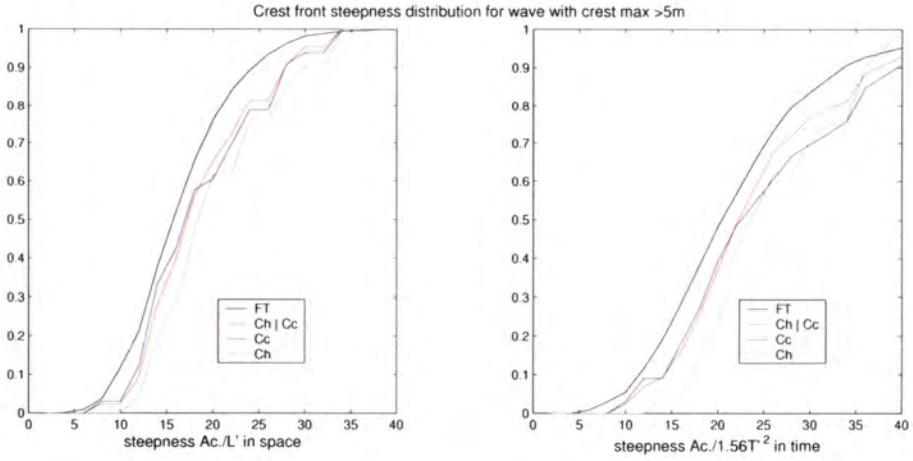

Fig. 6. Crest front steepness

SOME CASES OF OBSERVED ROGUE WAVES AND AN ATTEMPT TO CHARACTERIZE THEIR OCCURRENCE CONDITIONS

by Michel Olagnon and Sylvie van Iseghem

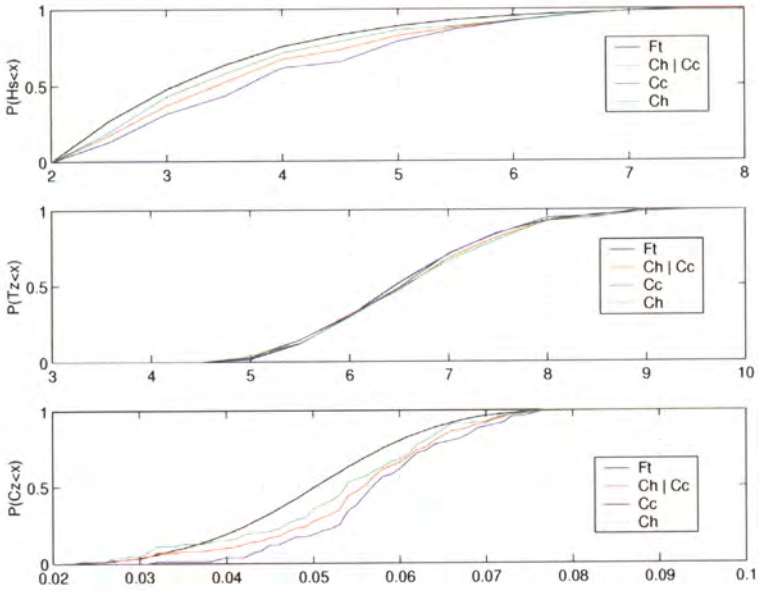

Fig. 7. Instantaneous space profiles

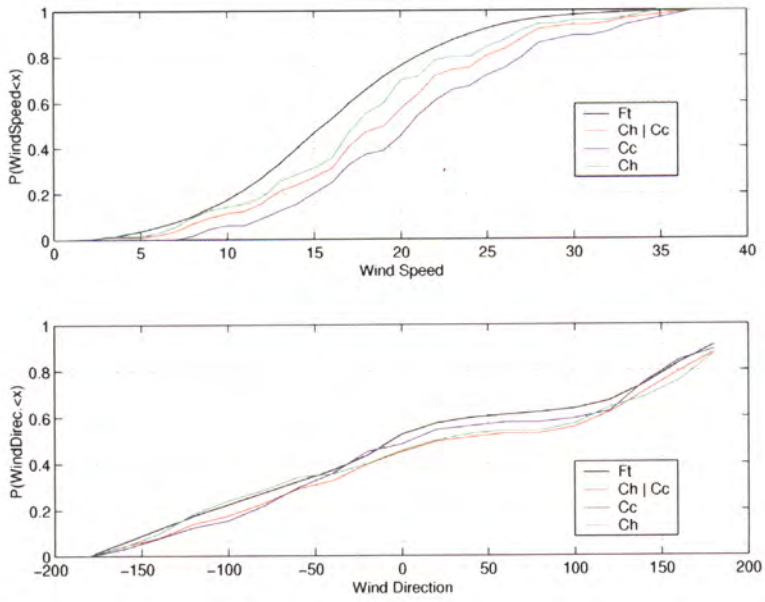

Fig. 9. Wind

CHARACTERIZING FREAK WAVES WITH WAVELET TRANSFORM ANALYSIS

by Paul C. Liu and Nobuhito Mori

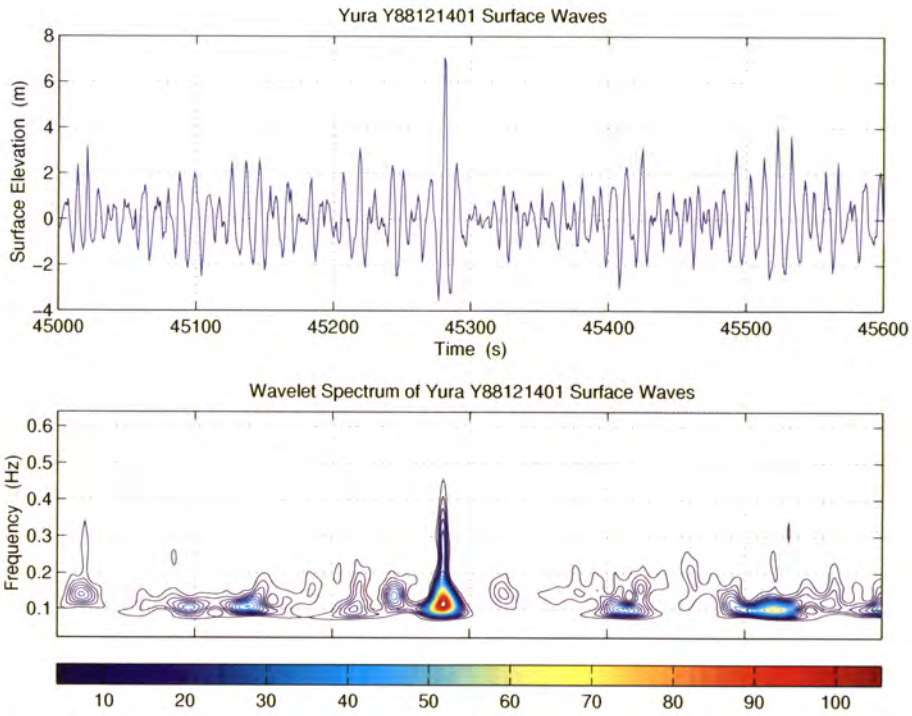

Fig. 1. Freak wave time series and its wavelet spectrum for data set Yura Y88121041

CHARACTERIZING FREAK WAVES WITH WAVELET TRANSFORM ANALYSIS

by Paul C. Liu and Nobuhito Mori

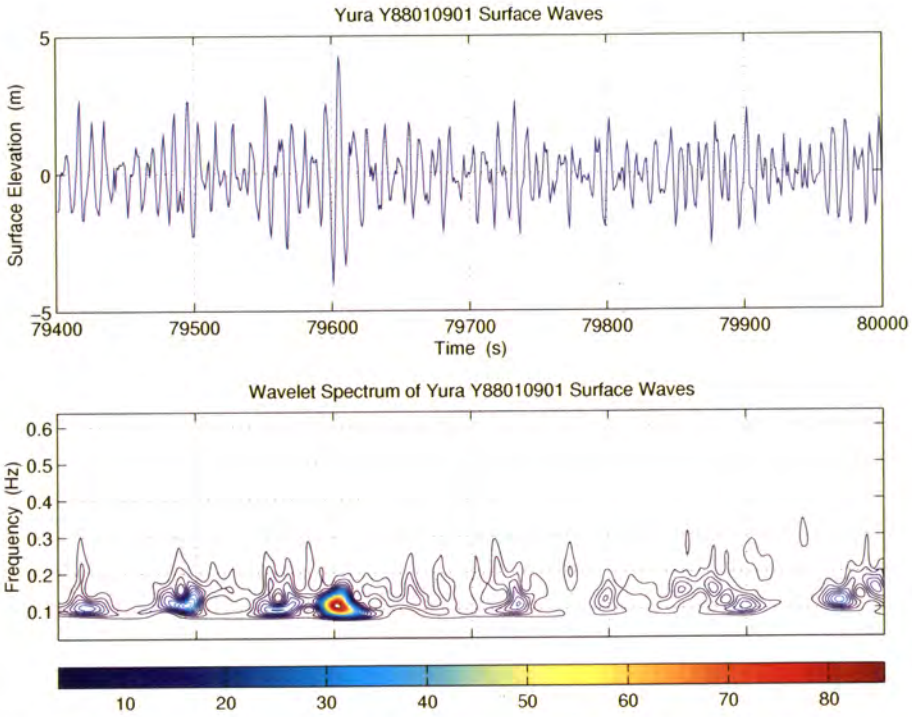

Fig. 2. Freak wave time series and its wavelet spectrum for data set Yura Y8010901

THE EMPIRICAL MODE DECOMPOSITION AND THE HILBERT SPECTRA TO ANALYSE EMBEDDED CHARACTERISTIC OSCILLATIONS OF EXTREME WAVES

by Torsten Schlurmann

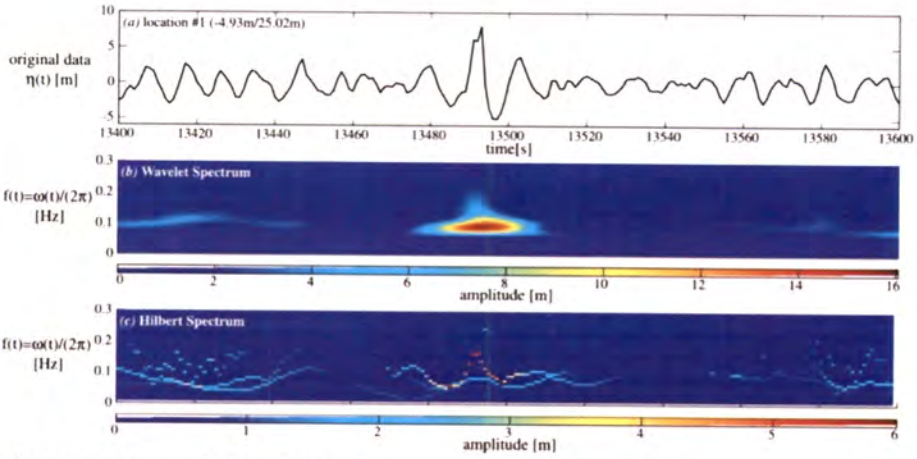

Fig. 3. Wavelet and Hilbert Spectrum

NONLINEAR WAVE FOCUSING AS A MECHANISM OF THE FREAK WAVE GENERATION IN THE OCEAN

by Efim Pelinovsky et al.

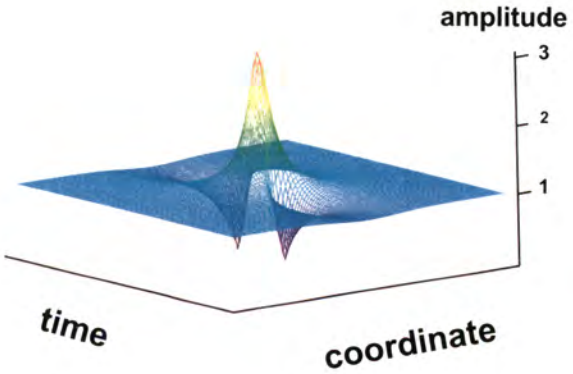

Fig. 6. Algebraic breather as a model of abnormal wave appeared in the periodic wave field

MODULATIONAL INTERACTIONS OF BROAD-BAND GRAVITY WAVES OBSERVED DURING NORTH SEA STORMS

by Brian Linfoot et al.

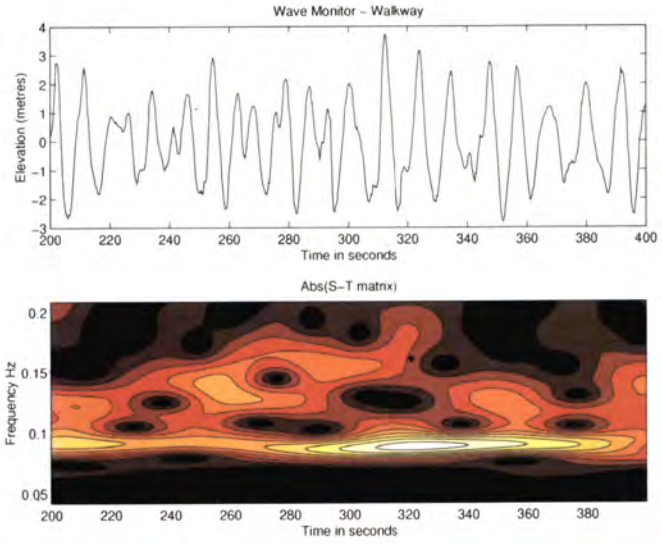

Fig. 1. Wave record during storm: (*a - upper*) large amplitude "riding" waves 240 to 300 seconds (*b - lower*) time -frequency plot showing main group modulation at 0.9 Hz and a secondary group splitting at 0.13Hz to 0.15 Hz at 240 to 300 seconds

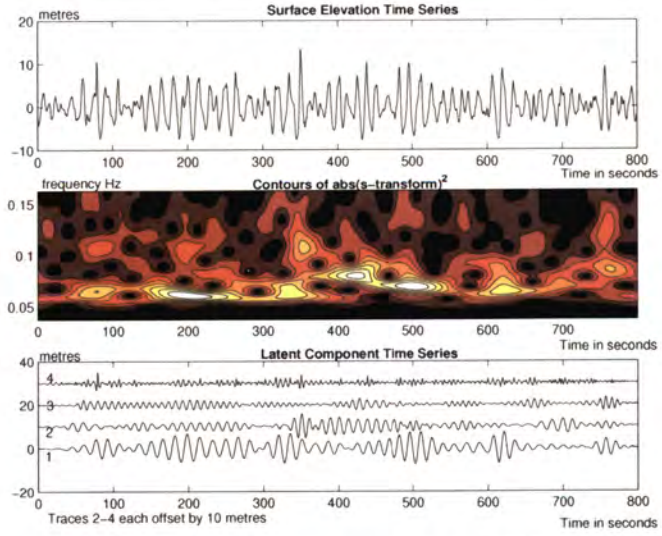

Fig. 2. 800 seconds of wave data from North Sea storm (1 Jan 1995): (*a -upper*) water surface elevation time series (*b - middle*) Time-frequency contour plot derived from S-transform matrix: light patches indicate high energy concentrations (*c - lower*) component time series produced by adaptive inversion of S-transform matrix with a 5% Hanning taper applied to ends of time series in plots (b) and (c)

MODULATIONAL INTERACTIONS OF BROAD-BAND GRAVITY WAVES OBSERVED DURING NORTH SEA STORMS

by Brian Linfoot et al.

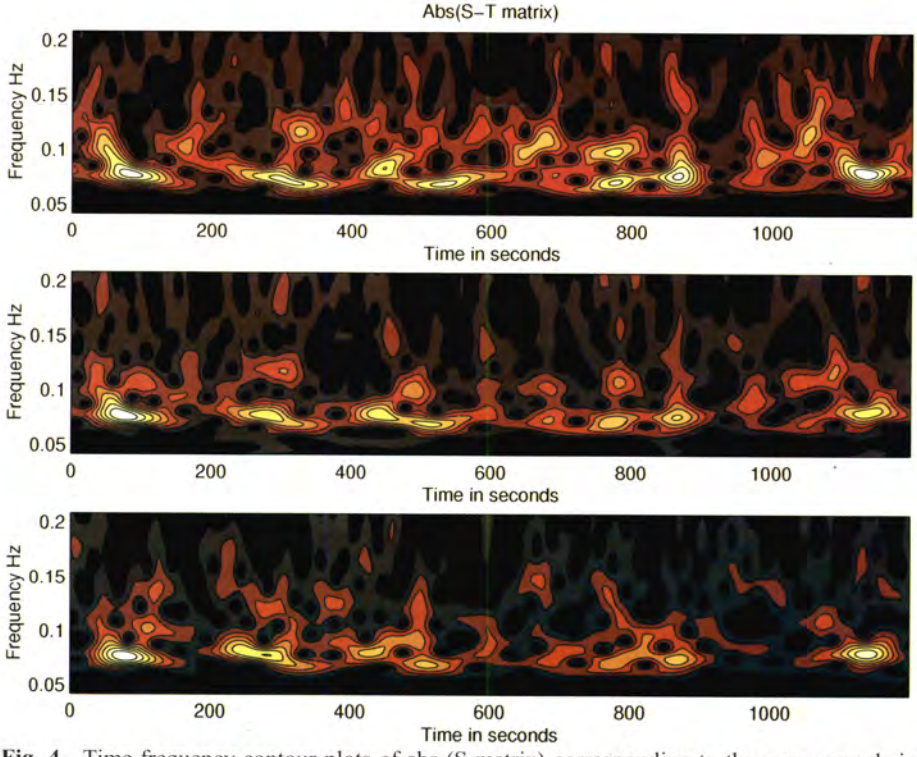

Fig. 4. Time-frequency contour plots of abs (S-matrix) corresponding to the wave records in Fig. 3

ON THE USE OF SMOOTHED PARTICLE HYDRODYNAMICS TO MODEL BREAKING WAVES AND THEIR INTERACTION WITH A STRUCTURE

by E. Fontaine

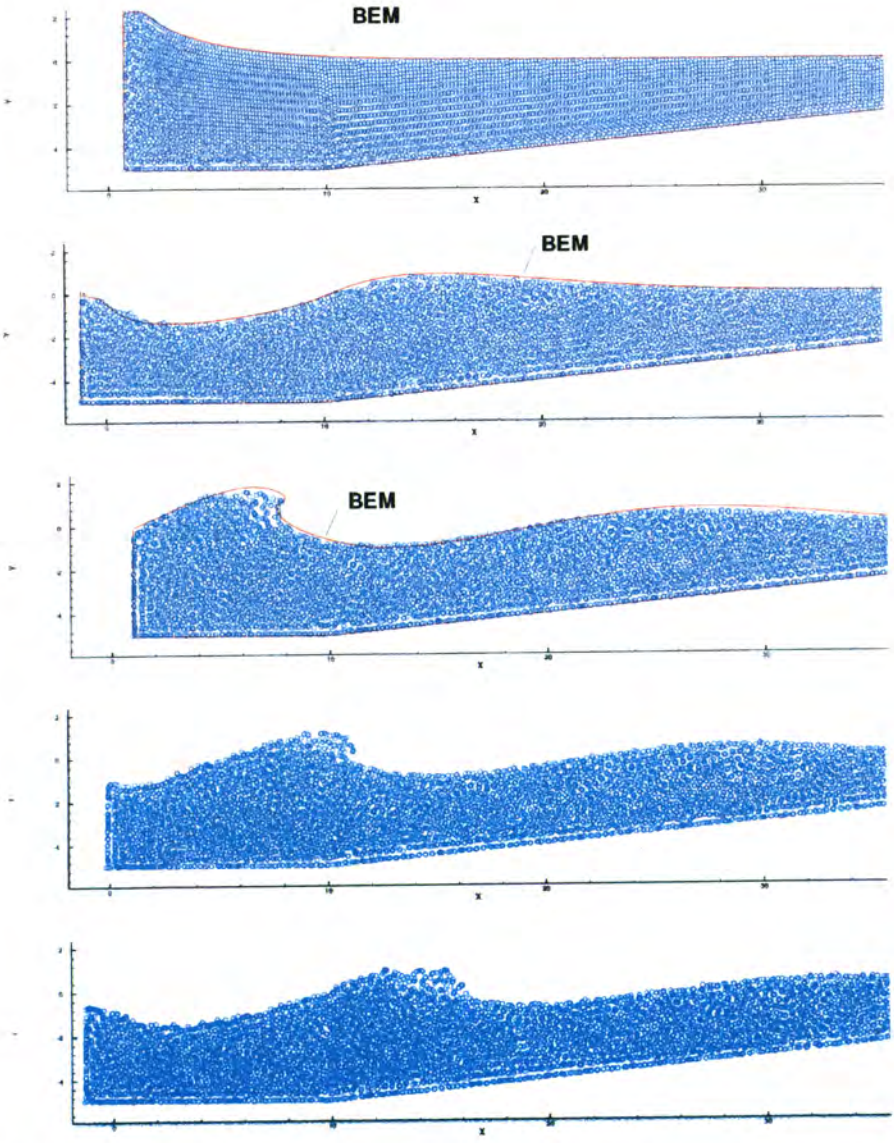

Fig. 1. Comparison between BEM and SPH simulation for a breaking wave in shallow water

Éditions Ifremer
BP 70, 29280 Plouzané, France
tel. ++33 (0)2 98 22 40 13
fax ++33 (0)2 98 22 45 86
editions@ifremer.fr
http://www.ifremer.fr

ISSN: 0761-3962
ISBN: 2-84433-063-0

Printed in Greece

actes de colloques

Rogue waves 2000
Brest, 29-30 november 2000

There are now many evidences that some waves do significantly exceed the common height and steepness expectations that can be derived from existing models. A better understanding of why, how, and when these huge waves occur should thus be a research priority. The Brest ROGUE WAVES 2000 workshop gathered many of the scientists and engineers actively working on the subject to an opportunity to confront and discuss their most recent advances concerning the definition, statistics, modeling and prediction of those abnormal waves.

Keywords: ocean waves, non-linear waves, extremes, rogue waves, freak waves.

Vagues scélérates
Brest, 29-30 novembre 2000

C'est aujourd'hui une certitude que certaines vagues outrepassent en hauteur et en cambrure les prédictions fondées sur les modèles courants. L'amélioration de la compréhension des raisons, des mécanismes, et des circonstances de leur apparition se doit donc d'être une priorité de recherche. Le colloque Rogue Waves 2000 a rassemblé à Brest nombre des scientifiques et ingénieurs actifs sur le sujet, qui y ont trouvé l'occasion de confronter et discuter leurs avancées les plus récentes en termes de définition, de statistiques, de modélisation et de prédiction de ces vagues anormales.

Mots-clés : vagues, extrêmes, non-linéarités, vagues anormales, vagues scélérates.

32

Editions Ifremer
BP 70, 29280 Plouzané, France
tél. 02 98 22 40 13
fax 02 98 22 45 86
mél : editions@ifremer.fr

Diffusion : ALT Brest
Service Logistique
3, rue Edouard Belin - BP 23
29801 Brest Cedex 9
tél. 02 98 02 42 34
fax. 02 98 02 05 84
mél : alt.belin@wanadoo.fr

ISSN 0761-3962
ISBN 2-84433-063-0

38,11 € - 250 F